NATIONAL TECHNICAL UNIVERSITY OF ATHENS

SCHOOL OF CIVIL ENGINEERING
DEPARTMENT OF STRUCTURAL ENGINEERING
INSTITUTE OF STRUCTURAL ANALYSIS & ANTISEISMIC RESEARCH

DYNAMIC VIBRATION ABSORBERS IN CIVIL ENGINEERING STRUCTURES

DOCTORAL DISSERTATION

for the title of Doctor of Philosophy in Engineer submitted in
the School of Civil Engineering, National Technical University of Athens

KAPASAKALIS A. KONSTANTINOS

Diploma in Civil Engineering N.T.U.A.
Master of Science in Civil Engineering N.T.U.A.

ATHENS 2020

ΕΘΝΙΚΟ ΜΕΤΣΟΒΙΟ ΠΟΛΥΤΕΧΝΕΙΟ

ΣΧΟΛΗ ΠΟΛΙΤΙΚΩΝ ΜΗΧΑΝΙΚΩΝ
ΤΟΜΕΑΣ ΔΟΜΟΣΤΑΤΙΚΗΣ
ΕΡΓΑΣΤΗΡΙΟ ΣΤΑΤΙΚΗΣ & ΑΝΤΙΣΕΙΣΜΙΚΩΝ ΕΡΕΥΝΩΝ

ΔΥΝΑΜΙΚΑ ΣΥΣΤΗΜΑΤΑ ΑΠΟΡΡΟΦΗΣΗΣ ΤΑΛΑΝΤΩΣΕΩΝ ΣΕ ΚΑΤΑΣΚΕΥΕΣ ΠΟΛΙΤΙΚΟΥ ΜΗΧΑΝΙΚΟΥ

ΔΙΔΑΚΤΟΡΙΚΗ ΔΙΑΤΡΙΒΗ

για τον Επιστημονικό Τίτλο του Διδάκτορα Μηχανικού υποβληθείσα στη
Σχολή Πολιτικών Μηχανικών του Εθνικού Μετσόβιου Πολυτεχνείου

ΚΑΠΑΣΑΚΑΛΗΣ Α. ΚΩΝΣΤΑΝΤΙΝΟΣ

Διπλωματούχος Πολιτικός Μηχανικός Ε.Μ.Π.
Μεταπτυχιακό Δίπλωμα Ειδίκευσης Ε.Μ.Π.

ΑΘΗΝΑ 2020

NATIONAL TECHNICAL UNIVERSITY OF ATHENS

SCHOOL OF CIVIL ENGINEERING

DEPARTMENT OF STRUTURAL ENGINEERING

INSTITUTE OF STRUCTURAL ANALYSIS & ANTISEISMIC RESEARCH

DYNAMIC VIBRATION ABSORBERS IN CIVIL ENGINEERING STRUCTURES

DOCTORAL DISSERTATION

for the title of Doctor of Philosophy in Engineer submitted in
the School of Civil Engineering, National Technical University of Athens

KAPASAKALIS A. KONSTANTINOS

M.Sc., Diploma in Civil Engineering N.T.U.A.

ADVISORY COMMITTEE:

1. Sapountzakis J. Evangelos, Professor N.T.U.A. (Supervisor)
2. Antoniadis A. Ioannis, Professor N.T.U.A.
3. Gazetas George, Professor Emeritus N.T.U.A.

EXAMINATION COMMITTEE:

1. Sapountzakis J. Evangelos, Professor N.T.U.A. (Supervisor)
2. Antoniadis A. Ioannis, Professor N.T.U.A.
3. Gazetas George, Professor Emeritus N.T.U.A.
4. Karabalis L. Dimitrios, Professor University of Patras
5. Psycharis N. Ioannis, Professor N.T.U.A.
6. Lagaros D. Nikos, Associate Professor N.T.U.A.
7. Spitas Vasilis, Associate Professor N.T.U.A.

ATHENS 2020

The research for this dissertation was co-financed by Greece and the European Union (European Social Fund- ESF) through the Operational Programme «Human Resources Development, Education and Lifelong Learning» in the context of the project “Strengthening Human Resources Research Potential via Doctorate Research” (MIS-5000432), implemented by the State Scholarships Foundation (IKY).

To my family …

Acknowledgments

First and foremost, I would like to express my sincere gratitude to my teacher and advisor, Professor Evangelos Sapountzakis, for the exemplary guidance and constant encouragement throughout the course of this study. His continuous support, motivation and dedicated involvement in every step of the way extend beyond his academic role and for that I am deeply thankful.

I would also like to express my deep gratitude and thanks to Professor Ioannis Antoniadis, for serving at my doctoral advisor committee. From the beginning of my doctoral dissertation, Professor Antoniadis guided me and provided me with the chance to work in a plethora of exciting subjects in the field of Mechanical Engineering and many others. I feel grateful for sharing his expertise and experience with me and helping me to grow both as an engineer and as a person.

Moreover, I would also like to express my most sincere gratitude to Professor Emeritus George Gazetas for serving on my doctoral advisory committee. His beneficial comments, as well as his illuminating lectures have contributed the most to the accomplishment of this dissertation and are highly appreciated. My sincere gratitude also goes to Professor Dimitrios Karabalis, Professor Ioannis Psycharis, Associate Professor Nikos Lagaros and Associate Professor Vasilis Spitas for serving on my doctoral examination committee and for their constructive comments which enriched this dissertation.

My sincere gratitude goes to my friends and schoolmates Antonis Gikakis, Antonis Mastropetros, Christos Chatzakis, Dimitris Psarrakis, Dimitris Christidis, Giannis Politis, Giorgos Koroniotis, Kimonas Sapantzoglou and Lena Papoutsi for being next to me for nearly my entire life.

To the very special person of my life Maria, my companion, I will always be grateful for her love, patience and support. Thank you for encouraging me and always believing in me.

Most of all, I would like to thank my parents Anestis and Rania and my brother Spyros. My deepest appreciation is expressed to them for being a constant source of inspiration. Their

unconditional love, unwavering support and constant encouragement will follow me throughout my life.

This research was co-financed by Greece and the European Union (European Social Fund-ESF) through the Operational Programme «Human Resources Development, Education and Lifelong Learning» in the context of the project “Strengthening Human Resources Research Potential via Doctorate Research” (MIS-5000432), implemented by the State Scholarships Foundation (IKY).

Περίληψη

Διδακτορική Διατριβή του Καπασακάλη Α. Κωνσταντίνου

ΔΥΝΑΜΙΚΑ ΣΥΣΤΗΜΑΤΑ ΑΠΟΡΡΟΦΗΣΗΣ ΤΑΛΑΝΤΩΣΕΩΝ ΣΕ ΚΑΤΑΣΚΕΥΕΣ ΠΟΛΙΤΙΚΟΥ ΜΗΧΑΝΙΚΟΥ

Το ευρύτερο πεδίο της παρούσας διατριβής αφορά περιβαλλοντικές διεγέρσεις, όπως σεισμικές διεγέρσεις και φορτία ανέμου, σε κατασκευές πολιτικού μηχανικού. Συγκεκριμένα, εξετάζονται τρία επιστημονικά πεδία. Το πρώτο αφορά την προστασία κατασκευών από οριζόντιες σεισμικές διεγέρσεις, το δεύτερο αφορά προστασία από κατακόρυφες σεισμικές διεγέρσεις, ενώ το τρίτο αφορά στην μόνωση ταλαντώσεων πυλώνων ανεμογεννητριών.

Τα προτεινόμενα δυναμικά συστήματα απορρόφησης ταλαντώσεων είναι βασισμένα στον ταλαντωτή KDamper. Ο KDamper είναι ένα καινοτόμο σύστημα παθητικής μόνωσης ταλαντώσεων και απόσβεσης, βασισμένο στον βέλτιστο συνδυασμό στοιχείων στιβαρότητας, συμπεριλαμβανομένου και ενός στοιχείου αρνητικής στιβαρότητας. Ο σχεδιασμός των συστημάτων με βάση τον KDamper ακολουθεί πρόβλημα βελτιστοποίησης βασισμένο σε τεχνικά κριτήρια, ανάλογα με την εκάστοτε κατασκευή. Οι εξωτερικές διεγέρσεις επιλέγονται με βάση τις διατάξεις του εκάστοτε κανονισμού, που αφορά την υπό εξέταση εφαρμογή. Τέλος, προτείνονται δύο εναλλακτικές διατάξεις για την υλοποίηση του στοιχείου αρνητικής στιβαρότητας, σε μια και δυο διαστάσεις, αντίστοιχα.

Η απόδοση του KDamper αξιολογείται με αντιπροσωπευτικά αριθμητικά παραδείγματα, και η αποτελεσματικότητά του επιβεβαιώνεται μέσα από συγκρίσεις με υπάρχοντα συστήματα μόνωσης ταλαντώσεων. Με βάση τις αριθμητικές αναλύσεις, τα προτεινόμενα δυναμικά συστήματα απορρόφησης ταλαντώσεων προσφέρουν μια ρεαλιστική εναλλακτική στις υπάρχουσες διατάξεις για οριζόντια και κατακόρυφη σεισμική μόνωση, καθώς και βιώσιμες επιλογές για ενίσχυση υφιστάμενων κατασκευών. Επιπρόσθετα, επεκτείνεται η απόδοση ανεμογεννητριών μέσω της αύξησης της ισοδύναμης απόσβεσης των πυλώνων τους.

Πίνακας Περιεχομένων Εκτενούς Περίληψης

Εκτενής Περίληψη

Δυναμικά Συστήματα Απορρόφησης Ταλαντώσεων σε Κατασκευές Πολιτικού Μηχανικού

I. Εισαγωγή

Το αντικείμενο της παρούσας διδακτορικής διατριβής αφορά την προστασία κατασκευών Πολιτικού Μηχανικού από περιβαλλοντικές διεγέρσεις. Η έρευνα εστιάζει στην απορρόφηση ταλαντώσεων που οφείλονται σε περιβαλλοντικές διεγέρσεις, όπως σεισμικές διεγέρσεις και αεροδυναμικά φορτία, με σκοπό την ενίσχυση της δυναμικής συμπεριφοράς του εκάστοτε δομικού συστήματος, και κατ' επέκταση την αποφυγή της κατάρρευσής του λόγω ακραίων εντατικών καταστάσεων, που προκύπτουν από υπέρβαση της φέρουσας ικανότητας (σεισμικές διεγέρσεις), ή από κόπωση (αεροδυναμικά φορτία).

Τα τελευταία χρόνια, λόγω των καταστροφών από σεισμικές διεγέρσεις, ιδιαίτερα σε πυκνοκατοικημένες περιοχές, οι αντισεισμικοί κανονισμοί για κτίρια, γέφυρες και έργα υποδομής άλλαξαν, στοχεύοντας προς τον σχεδιασμό των κατασκευών με καλύτερη σεισμική συμπεριφορά. Αναφορικά με την οριζόντια συνιστώσα των σεισμικών διεγέρσεων, η σεισμική μόνωση φαίνεται να αποτελεί την καλύτερη εναλλακτική έναντι των συμβατικών αντισεισμικών τεχνικών, καθώς βασίζεται στην ιδέα της μείωσης των σεισμικών φορτίων αντί της αύξησης της φέρουσας ικανότητας της κατασκευής. Η σεισμική μόνωση βασίζεται στην παρεμβολή μιας πλευρικά εύκαμπτης στρώσης μεταξύ της κατασκευής και της βάσης της. Με αυτόν τον τρόπο, η θεμελιώδης ιδιοπερίοδος του σεισμικά μονωμένου συστήματος μεγαλώνει σημαντικά, με συνέπεια τη μείωση των επιταχύνσεων που «φτάνουν» / καταπονούν την κατασκευή. Προς αυτήν την κατεύθυνση, πλήθος συσκευών μόνωσης από απλά ελαστικά εφέδρανα μέχρι πιο σύνθετες διατάξεις έχουν αναπτυχθεί και εξελιχθεί μέσα στα χρόνια. Ωστόσο, η σεισμική μόνωση που εφαρμόζεται στην βάση κατασκευών οδηγεί αναπόφευκτα στην ανάπτυξη μεγάλων μετακινήσεων κατά τη διάρκεια του σεισμικού κραδασμού. Το γεγονός αυτό δεν είναι αποδεκτό σε όλες τις περιπτώσεις για διάφορους λόγους, όπως η

ευαισθησία των σεισμικά μονωμένων κατασκευών σε φορτία ανέμου, οι ειδικές διατάξεις που απαιτούνται για τα συστήματα ύδρευσης, θέρμανσης και αποχέτευσης στις κατασκευές, αλλά και η αναγκαιότητα για ικανού μεγέθους αντισεισμικό αρμό ώστε να αποφευχθεί η σύγκρουση μεταξύ γειτονικών κτιρίων. Οι παραπάνω απαιτήσεις καθιστούν την προσέγγιση της σεισμικής μόνωσης ακατάλληλη για υφιστάμενες κατασκευές. Παρόλα αυτά, συσκευές που παρέχουν προστασία έναντι της οριζόντιας σεισμικής συνιστώσας έχουν εφαρμοσθεί επιτυχώς σε κατασκευές.

Αντίθετα, η προστασία κατασκευών από την κατακόρυφη συνιστώσα της σεισμικής διέγερσης βρίσκεται ακόμα σε ερευνητικό επίπεδο, καθώς δεν έχει φτάσει ακόμα στο στάδιο ρεαλιστικής υλοποίησης. Μάλιστα, τα τελευταία χρόνια έχουν καταγραφεί πολλές σεισμικές διεγέρσεις των οποίων η κατακόρυφη συνιστώσα είναι σχεδόν 1 g ή και περισσότερο. Για την προστασία των κτιρίων, όπως επίσης και των μη δομικών στοιχείων τους, όπως εύθραυστα αντικείμενα, μηχανολογικός εξοπλισμός και έργα τέχνης, από αυτές τις μεγάλου μεγέθους σεισμικές διεγέρσεις, χρειάζεται μόνωση ταλαντώσεων όχι μόνο στην οριζόντια διεύθυνση αλλά και στην κατακόρυφη. Ο κύριος λόγος για την δυσκολία υλοποίησης συστημάτων κατακόρυφης μόνωσης είναι η απαίτηση του συστήματος για επαρκή στιβαρότητα μόνωσης. Πιο συγκεκριμένα, ένα κατακόρυφα σεισμικά μονωμένο σύστημα πρέπει να έχει επαρκή κατακόρυφη ακαμψία για να μπορεί να παραλάβει τα κατακόρυφα φορτία λόγω του ιδίου βάρους, διατηρώντας παράλληλα τις στατικές κατακόρυφες παραμορφώσεις του σε αποδεκτά επίπεδα. Από την άλλη, ένα σεισμικά μονωμένο σύστημα πρέπει να έχει αρκετή ευκαμψία ώστε να μπορεί να μονώσει τις επιταχύνσεις που φτάνουν στην κατασκευή.

Ένα άλλο είδος δυναμικής διέγερσης που μπορεί να προκαλέσει αστοχία λόγω κόπωσης ή υπέρβασης της φέρουσας ικανότητας στις κατασκευές Πολιτικού Μηχανικού είναι τα φορτία ανέμου. Καθώς η αιολική ενέργεια αναπτύσσεται διαρκώς σε παγκόσμιο επίπεδο, τα αιολικά πάρκα είναι πιθανό να αποτελέσουν σημαντικό μέρος της συνολικής παραγωγής αιολικής ενέργειας, και να συνεισφέρουν σημαντικά στην συνολική παραγωγή ενέργειας σε ορισμένες χώρες. Ωστόσο, ο ετήσιος ρυθμός εγκατάστασης ανεμογεννητριών μειώνεται τα τελευταία χρόνια, σε σύγκριση με την αρχή της βιομηχανικής τους ανάπτυξης. Επιπλέον, πολλές αστοχίες έχουν καταγραφεί σε υπάρχουσες ανεμογεννήτριες λόγω δομικών βλαβών. Έτσι, κύρια προτεραιότητα είναι η προστασία των δομικών στοιχείων ανεμογεννητριών (πυλώνας, θεμελίωση) μέσω συστημάτων ελέγχου.

Τα παραπάνω δεδομένα έχουν παρακινήσει την ανάπτυξη εναλλακτικών συστημάτων μόνωσης ταλαντώσεων, στα οποία μεταξύ άλλων συγκαταλέγονται: (i) αποσβεστήρες συντονισμένης μάζας (TMD), (ii) inerters (στοιχεία αδράνειας), (iii) μονωτές αρνητικής

στιβαρότητας και ταλαντωτές «μηδενικής στιβαρότητας» (QZS), και (iv) συστήματα απορρόφησης ταλαντώσεων με στοιχεία αρνητικής στιβαρότητας (KDampers).

Έχοντας υπόψη όλα τα παραπάνω, κρίνεται απαραίτητη η ανάπτυξη δυναμικών συστημάτων απορρόφησης ταλαντώσεων, τα οποία συνδυάζουν τα ευεργετικά χαρακτηριστικά των προαναφερθέντων συστημάτων, χωρίς να παρουσιάζουν τα αντίστοιχα μειονεκτήματά τους.

Κύριος στόχος της παρούσας διδακτορικής διατριβής είναι η ανάπτυξη καινοτόμων δυναμικών συστημάτων απορρόφησης ταλαντώσεων, βασισμένα στον ταλαντωτή KDamper, για την προστασία κατασκευών Πολιτικού Μηχανικού από εξωτερικές περιβαλλοντικές διεγέρσεις. Ο ταλαντωτής KDamper είναι προϊόν της ερευνητικής δραστηριότητας του εργαστηρίου Δυναμικής & Κατασκευών της σχολής Μηχανολόγων Μηχανικών ΕΜΠ, και αποτελεί ουσιαστικά μια επέκταση της αρχής του κλασσικού ταλαντωτή ελέγχου δονήσεων TMD. Η διαφορά έγκειται στην εισαγωγή ενός στοιχείου αρνητικής στιβαρότητας. Εξ ορισμού, ο όρος «στοιχείο αρνητικής στιβαρότητας», συνεπάγεται ότι ο ρυθμός μεταβολής της δύναμης που ασκεί το στοιχείο συναρτήσει της παραμόρφωσής του εκατέρωθεν μιας θέσης ισορροπίας είναι αρνητικός. Η γενική ιδέα του KDamper βασίζεται στην τοποθέτηση του ασταθούς στοιχείου αρνητικής στιβαρότητας μέσα σε ένα ευσταθές περιβάλλον. Με την προσθήκη αυτή, ενισχύεται η αδρανειακή επίδραση της πρόσθετης μάζας του TMD, με την ελαστική δύναμη του εν λόγω στοιχείου. Αυτό οδηγεί στη βελτίωση των χαρακτηριστικών απόσβεσης του ταλαντωτή, χωρίς να είναι απαραίτητη η αύξηση της πρόσθετης μάζας.

Για τον βέλτιστο σχεδιασμό των προτεινόμενων συστημάτων απορρόφησης ταλαντώσεων με βάση τον KDamper, διατυπώθηκε πρόβλημα βελτιστοποίησης βασισμένο σε τεχνικά κριτήρια, ώστε να ληφθούν υπόψη γεωμετρικοί και κατασκευαστικοί περιορισμοί. Πιο συγκεκριμένα, προτείνονται δύο εναλλακτικές διατάξεις για την υλοποίηση του στοιχείου αρνητικής στιβαρότητας με προ-συμπιεσμένα συμβατικά στοιχεία θετικής ελαστικής σταθεράς (ελατήρια), παράγοντας αρνητική στιβαρότητα σε μία και δύο διαστάσεις αντίστοιχα. Τα δυναμικά φορτία, σεισμικά αλλά και ανέμου, επιλέχθηκαν ώστε να ακολουθούν τις διατάξεις του εκάστοτε κανονισμού. Στη συνέχεια, αναπτύχθηκαν ρεαλιστικά μοντέλα για την εισαγωγή των προτεινόμενων δυναμικών συστημάτων απορρόφησης ταλαντώσεων σε κατασκευές Πολιτικού Μηχανικού για την σεισμική προστασία υφιστάμενων αλλά και νέων κατασκευών στην οριζόντια και στην κατακόρυφη διεύθυνση, αλλά και την προστασία πυλώνων ανεμογεννητριών από αεροδυναμικά φορτία.

Η έρευνα που παρουσιάζεται στην παρούσα διατριβή είναι καινοτόμα και πρωτότυπη. Τα κύρια στοιχεία πρωτοτυπίας συνοψίζονται στα ακόλουθα:

i. Ο ταλαντωτής KDamper διερευνάται ως ένα δυναμικό σύστημα απορρόφησης ταλαντώσεων σε κατασκευές Πολιτικού Μηχανικού, ξεπερνώντας τα μειονεκτήματα των υφιστάμενων συστημάτων απορρόφησης/μόνωσης ταλαντώσεων.
ii. Εξετάστηκαν εναλλακτικές διευρυμένες διατάξεις του KDamper, με στόχο την βελτιστοποίηση της απόδοσής του, ανάλογα με το δομικό σύστημα στο οποίο εφαρμόζεται κάθε φορά.
iii. Σε κάθε εφαρμογή ακολουθείται μέθοδος βελτιστοποίησης με βάση τεχνικά κριτήρια για την επιλογή των παραμέτρων των διατάξεων βασισμένων στο KDamper, λαμβάνοντας υπόψη τους γεωμετρικούς και κατασκευαστικούς περιορισμούς της εκάστοτε εφαρμογής.
iv. Προτείνονται δύο εναλλακτικές διατάξεις για την υλοποίηση του στοιχείου αρνητικής στιβαρότητας, παράγοντας αρνητική στιβαρότητα σε μια και δύο διαστάσεις, αντίστοιχα.
v. Τα συστήματα μόνωσης με βάση τον ταλαντωτή KDamper έχουν εφαρμοσθεί επιτυχώς μέσα από πλήθος αριθμητικών εφαρμογών στις βάσεις κατασκευών για οριζόντια σεισμική προστασία, ως πιθανό συμπλήρωμα των συμβατικών προσεγγίσεων σεισμικής μόνωσης.
vi. Παρουσιάζεται μια εναλλακτική εφαρμογή των προτεινόμενων συστημάτων για οριζόντια σεισμική προστασία, η οποία αποτελεί ουσιαστικά μια στιβαρή βάση απορρόφησης ταλαντώσεων τόσο σε υπάρχουσες, αλλά και σε νέες κατασκευές.
vii. Διερευνώνται διάφοροι τύποι επέμβασης σε υφιστάμενες κατασκευές, με βάση τις διευρυμένες εκδοχές του KDamper, χωρίς να επιδρούν δυσμενώς στη φέρουσα ικανότητα της κατασκευής ή να εισάγουν βαριές επιπρόσθετες μάζες.
viii. Τα προτεινόμενα δυναμικά συστήματα απορρόφησης ταλαντώσεων εφαρμόζονται αποτελεσματικά (μέσω αριθμητικών εφαρμογών) για κατακόρυφη σεισμική προστασία, αντιμετωπίζοντας τα μειονεκτήματα των υφιστάμενων συστημάτων κατακόρυφης σεισμικής μόνωσης, όπως οι μεγάλες στατικές παραμορφώσεις.
ix. Οι διατάξεις βασισμένες στα διευρυμένα KDamper εφαρμόζονται σε πυλώνες ανεμογεννητριών με στόχο τη βελτίωση της δυναμικής τους συμπεριφοράς μέσω της αύξησης της ισοδύναμης απόσβεσης των πυλώνων τους.

Τέλος, αξίζει να αναφερθεί ότι από την παρούσα ερευνητική προσπάθεια προέκυψαν δημοσιεύσεις σε έγκριτα επιστημονικά περιοδικά διεθνούς κυκλοφορίας, σε πρακτικά επιστημονικών διεθνών και εθνικών συνεδρίων, καθώς και σε σεμινάρια και ημερίδες.

II. Προτεινόμενα Δυναμικά Συστήματα Απορρόφησης Ταλαντώσεων Βασισμένα στην Αρνητική Στιβαρότητα

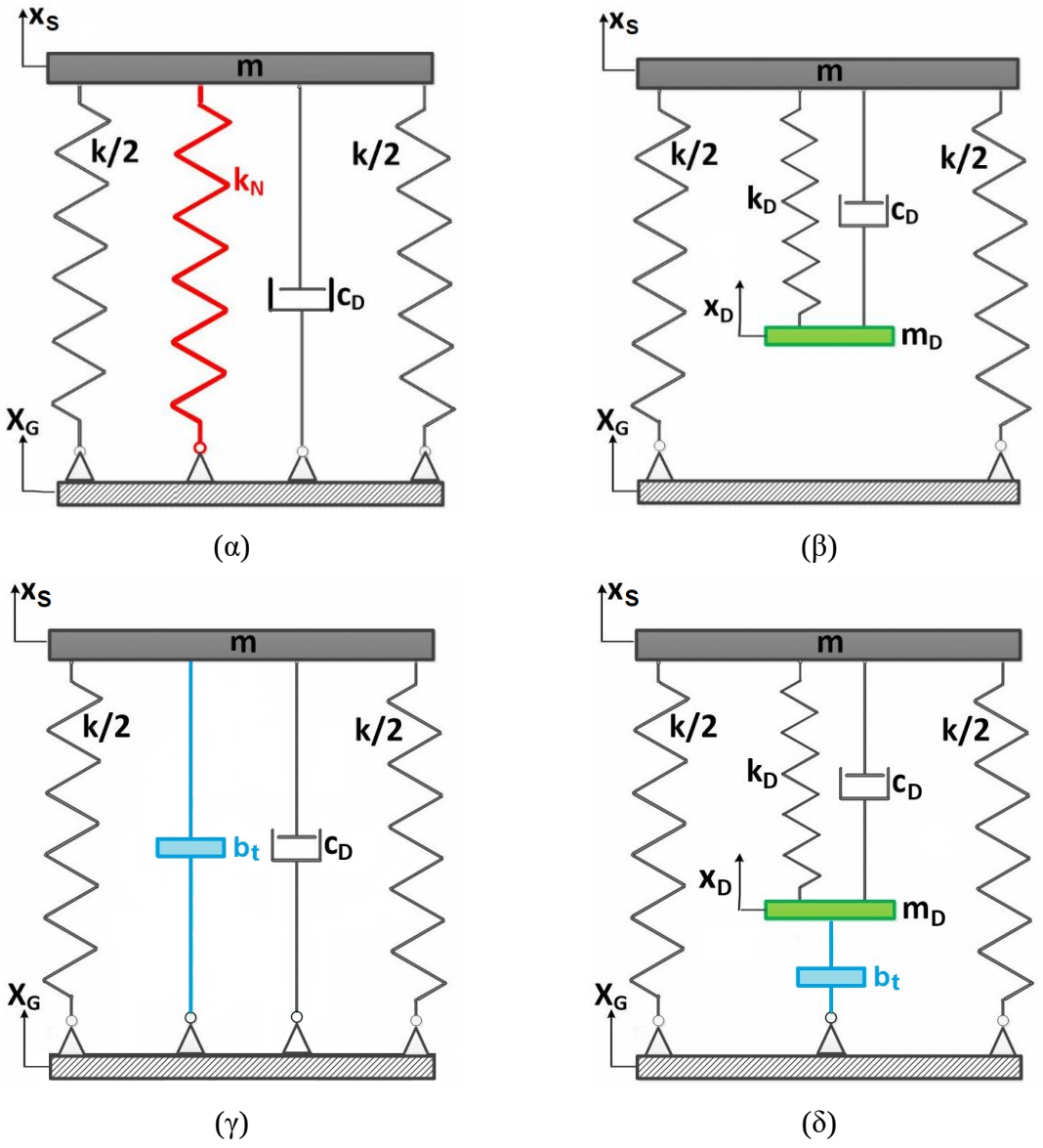

Σχήμα 1: *Σχηματική αναπαράσταση συστημάτων απορρόφησης ταλαντώσεων: (α) ταλαντωτής «μηδενικής στιβαρότητας» (QZS), (β) αποσβεστήρας συντονισμένης μάζας (TMD), (γ) Inerter (JDamper), και (δ) Tuned Mass Damper Inerter (TMDI).*

Η ιδέα της εισαγωγής στοιχείων αρνητικής στιβαρότητας (ή 'anti-springs') για απορρόφηση ταλαντώσεων έχει μακρά ιστορία στον τομέα της αεροναυπηγικής, καθώς είχε αρχικά προταθεί στην πρωτοποριακή δημοσίευση του (Molyneaux, 1957), όπως επίσης και στην μελέτη του (Platus 1992). Η προσέγγιση αυτή βασίζεται στην επίτευξη δραματικής μείωσης της στιβαρότητας του μονωτή και συνεπώς στην μείωση της ιδιοσυχνότητας του συστήματος σε πολύ μικρές τιμές, οριακά μηδενικές. Τα συστήματα αυτά ονομάζονται ταλαντωτές 'Οιονεί'

Μηδενικής Στιβαρότητας (Quazi Zero Stiffness, QZS). Κατά αυτόν τον τρόπο, μειώνεται η απόκριση του συστήματος για όλες τις μεγαλύτερες συχνότητες διέγερσης από τις φυσικές ιδιοσυχνότητες του συστήματος, έχοντας σαν αποτέλεσμα την επίτευξη σημαντικής μόνωσης (έναντι δυναμικών φορτίων).

Η αρνητική στιβαρότητα επιτυγχάνεται κυρίως μέσω ειδικού μηχανολογικού σχεδιασμού που συμπεριλαμβάνει συμβατικά προεντεταμένα ελαστικά στοιχεία θετικής στιβαρότητας, όπως δοκοί, πλάκες, κελύφη (σε μεταλυγισμική διαμόρφωση) καθώς επίσης και προ-συμπιεσμένα ελατήρια, τοποθετημένα με κατάλληλη γεωμετρική διαμόρφωση. Το κύριο μειονέκτημα των ταλαντωτών 'Οιονεί' Μηδενικής Στιβαρότητας (QZS), προκύπτει λόγω της θεμελιώδους απαίτησης για δραστικά μειωμένη στιβαρότητα της κατασκευής, σχεδόν σε μηδενικά επίπεδα. Το γεγονός αυτό περιορίζει την φέρουσα ικανότητα της κατασκευής σε στατικά φορτία. Η σχηματική αναπαράσταση ενός απλού (QZS) ταλαντωτή παρουσιάζεται στο Σχήμα 1.α, όπου ένα στοιχείο αρνητικής ελαστικής σταθεράς τοποθετείται παράλληλα στο συμβατικό στοιχείο θετικής στιβαρότητας. Η εξίσωση κίνησης του συστήματος αυτού είναι:

$$m\ddot{u}_S + c_D\dot{u}_S + (k + k_N)u_S = m\ddot{u}_S + c_D\dot{u}_S + k_{QZS}u_S = -m\ddot{X}_G \tag{1}$$

όπου η ιδιοσυχνότητα και ο λόγος απόσβεσης του ταλαντωτή QZS εκφράζονται ως:

$$\omega_{QZS} = 2\pi f_0 = \sqrt{k_{QZS}/m} \tag{2.α}$$

$$\zeta_{QZS} = c_D / \left(2\sqrt{k_{QZS}/m}\right) \tag{2.β}$$

Αφού το στοιχείο στιβαρότητας k_N είναι αρνητικό, η συνολική στιβαρότητα του συστήματος μειώνεται, $k_{QZS}=k+k_N$, όπως φαίνεται στην Εξίσωση (1). Συνεπώς, η φέρουσα ικανότητα του συστήματος μειώνεται και κατ' επέκταση και η ιδιοσυχνότητα του συστήματος, Εξίσωση (2.α). Με αυτόν τον τρόπο, μειώνονται τα σεισμικά φορτία, και ακολούθως οι μέγιστες επιταχύνσεις της κατασκευής, όπως στην περίπτωση ενός σεισμικά μονωμένου συστήματος. Ωστόσο, μειώνοντας την φέρουσα ικανότητα της κατασκευής, δημιουργούνται ποικίλα προβλήματα, ειδικά στην περίπτωση της κατακόρυφης σεισμικής μόνωσης. Για παράδειγμα, εάν X_{SVD} υποδηλώνει την στατική παραμόρφωση ενός τέτοιου συστήματος λόγω του ιδίου βάρους του στην κατακόρυφη διεύθυνση:

$$X_{SVD} = \frac{mg}{k} = \frac{g}{\left(2\pi f_0\right)^2} \tag{3}$$

Βασική αρχή λειτουργίας των TMDs είναι η μείωση των μετατοπίσεων μιας κατασκευής μέσω της μεταφοράς ενέργειας σε ένα σύστημα ταλάντωσης μιας πρόσθετης μάζας, σχεδιασμένο με κατάλληλα χαρακτηριστικά και προσαρμοσμένο σε κατάλληλη θέση στην κατασκευή. Το TMD, αποτελείται συνήθως από μία πρόσθετη μάζα (η οποία αποτελεί ένα μικρό ποσοστό της συνολικής μάζας) και ένα ελατήριο σε συνδυασμό με έναν τεχνητό αποσβεστήρα. Οι τιμές και τα μεγέθη που αφορούν στο σχεδιασμό τέτοιων συσκευών εξαρτώνται τόσο από τα επιθυμητά αποτελέσματα στην τελική δυναμική απόκριση της κατασκευής, όσο και από την ρύθμιση της συχνότητας του TMD με την θεμελιώδη ιδιοσυχνότητα της αρχικής κατασκευής. Η τελευταία αυτή ιδιότητα έχει σαν αποτέλεσμα μία μεγάλη ποσότητα της ενέργειας ταλάντωσης της κατασκευής λόγω του σεισμού να περνά από την κατασκευή στην πρόσθετη μάζα της συσκευής και στη συνέχεια να αναλίσκεται μέσω του αποσβεστήρα. Η ιδέα του TMD εφαρμόστηκε για πρώτη φορά από τον Frahm (1909), και η θεωρία για τα TMD παρουσιάστηκε αργότερα από τους Ormondroyd και Den Hartog (1928). Τέτοιες συσκευές έχουν πλήθος εφαρμογών στο πεδίο του Πολιτικού Μηχανικού.

Παρά το γεγονός ότι οι συσκευές αυτές είναι γνωστές για την αποτελεσματικότητα και την αξιοπιστία τους, το βασικό μειονέκτημα που παρουσιάζουν είναι η ευαισθησία των παραμέτρων που τις χαρακτηρίζουν. Περιβαλλοντικοί και άλλοι εξωτερικοί παράγοντες μπορούν εύκολα να απορρυθμίσουν τις παραμέτρους αυτές, επηρεάζοντας αρνητικά την απόδοση της συσκευής και κατ' επέκταση την απόκριση της κατασκευής . Η δυσκολία στην κατασκευή και τοποθέτηση των μεγάλων πρόσθετων μαζών που απαιτούνται, προκειμένου να επιτευχθεί σημαντική μείωση των επιβαλλόμενων σεισμικών ταλαντώσεων, αποτελεί έναν επιπλέον περιορισμό στη χρήση τους. Η ιδέα του TMD παρουσιάζεται στο Σχήμα 1.β. Οι εξισώσεις κίνησης που προκύπτουν είναι:

$$m\ddot{u}_S + c_D(\dot{u}_S - \dot{u}_D) + k_D(u_S - u_D) + ku_S = -m\ddot{X}_G \tag{4.α}$$

$$m_D\ddot{u}_D - c_D(\dot{u}_S - \dot{u}_D) - k_D(u_S - u_D) = -m_D\ddot{X}_G \tag{4.β}$$

και τα χαρακτηριστικά που διέπουν το σύστημα αυτό είναι:

$$\omega_D = \sqrt{k_D / m_D} \tag{5.α}$$

$$\zeta_D = c_D / \left(2\sqrt{k_D / m_D}\right) \tag{5.β}$$

$$\mu = m_D / m \tag{5.γ}$$

Αναφορικά με τον βέλτιστο σχεδιασμό του TMD, ποικίλες προσεγγίσεις βρίσκονται στην βιβλιογραφία, ανάλογα με το εκάστοτε πρόβλημα. Κοινή πρακτική είναι ο συντονισμός του TMD με την θεμελιώδη ιδιοσυχνότητα του αρχικού συστήματος, και στη συνέχεια ο λόγος απόσβεσης υπολογίζεται αριθμητικά.

Σε μια προσπάθεια να μειωθούν οι απαιτήσεις για μεγάλη επιπλέον μάζα, εισήχθη στις αρχές της δεκαετίας του 2000 από τον Smith (2002) η αρχή του inerter. Ο inerter είναι ένα στοιχείο δύο τερματικών που έχει την ιδιότητα, η δύναμη που παράγεται στα άκρα του να είναι ανάλογη της σχετικής επιτάχυνσης των τερματικών του. Αυτή η σταθερά της αναλογίας ονομάζεται "inertance" και μετράται σε χιλιόγραμμα. Το κύριο πλεονέκτημα του inerter είναι ότι δεν χρειάζεται να έχει μεγάλη μάζα για να επιτύχει το ίδιο αδρανειακό αποτέλεσμα με την πρόσθετη μάζα του TMD. Ωστόσο, σύμφωνα με τους (Chen and Smith, 2009) δεδομένου ότι οι inerters, οι αποσβεστήρες και τα ελατήρια μπορούν να συνδεθούν σε διάφορες διαμορφώσεις, η σύγκριση της κατασκευής των συναρτήσεων απόκρισης-συχνότητας του inerter και του TMD γίνεται πολύ περίπλοκη.

Μια ενδεικτική εφαρμογή του inerter παρουσιάζεται στο Σχήμα 1.γ. Στην συγκεκριμένη διάταξη, ο inerter συνδέει την μάζα της κατασκευής κατευθείαν με την βάση. Με αυτόν τον τρόπο, μειώνεται η ιδιοσυχνότητα του συστήματος, και κατ' επέκταση τα σεισμικά φορτία, χωρίς την μείωση της φέρουσας ικανότητας της κατασκευής ή την εισαγωγή επιπλέον μαζών. Η εξίσωση κίνησης του συστήματος αυτού είναι:

$$(m + b_t)\ddot{u}_S + c_D\dot{u}_S + ku_S = -m\ddot{X}_G \tag{6}$$

και τα χαρακτηριστικά που διέπουν το σύστημα αυτό είναι:

$$\omega_t = 2\pi f_t = \sqrt{k / (m + b_t)} \tag{7.α}$$

$$\zeta_t = c_D / \left(2\sqrt{k / (m + b_t)}\right) \tag{7.β}$$

$$\mu_t = b_t / m \tag{7.γ}$$

Πρόσφατα έχει προταθεί ο συνδυασμός του TMD με inerter (TMDI) (De Domenico and Ricciardi, 2018a; Lazar et al., 2014). Σε αυτήν την διάταξη, η πρόσθετη μάζα του TMD

συνδέεται με την βάση μέσω ενός inerter. Κατ' αυτόν τον τρόπο, η αδρανειακή δύναμη της πρόσθετης μάζας αυξάνεται, χωρίς να αυξηθεί η ίδια η μάζα. Ο TMDI παρουσιάζεται στο Σχήμα 1.δ, και οι εξισώσεις κίνησης του είναι:

$$m\ddot{u}_S + c_D(\dot{u}_S - \dot{u}_D) + k_D(u_S - u_D) + ku_S = -m\ddot{X}_G \quad (8.\alpha)$$

$$(m_D + b_t)\ddot{u}_D - c_D(\dot{u}_S - \dot{u}_D) - k_D(u_S - u_D) = -m_D\ddot{X}_G \quad (8.\beta)$$

και τα χαρακτηριστικά που διέπουν το σύστημα αυτό είναι:

$$\omega_D = \sqrt{k_D / (m_D + b_t)} \quad (9.\alpha)$$

$$\zeta_D = c_D / \left(2\sqrt{k_D / (m_D + b_t)}\right) \quad (9.\beta)$$

$$\mu = m_D / m \quad (9.\gamma)$$

$$\mu_t = b_t / m \quad (9.\delta)$$

$$\mu_{eff} = \mu + \mu_t = \frac{m_D + b_t}{m} = \frac{m_{eff}}{m} \quad (9.\varepsilon)$$

Οι αποσβεστήρες KDampers με ενσωματωμένα στοιχεία αρνητικής στιβαρότητας είναι μία νέα πρωτοποριακή ιδέα μόνωσης κραδασμών και απόσβεσης (Antoniadis et al., 2018), που βασίζεται κυρίως στον βέλτιστο συνδυασμό των κατάλληλων στοιχείων στιβαρότητας, ένα από τα οποία στοιχεία έχει αρνητική σταθερά στιβαρότητας (Negative Stiffness). Οι αποσβεστήρες με βάση την αρχή του KDamper δεν απαιτούν μείωση της συνολικής δομικής στιβαρότητας της κατασκευής, ξεπερνώντας έτσι το αντίστοιχο εγγενές μειονέκτημα των γνωστών μονωτών ταλαντώσεων «μηδενικής δυσκαμψίας» ("Quazi Zero Stiffness" - QZS), οι οποίοι απαιτούν δραστική μείωση της στιβαρότητας και κατά συνέπεια της αντοχής του φέροντος οργανισμού της κατασκευής. Σε σύγκριση με τους παραδοσιακούς αδρανειακούς αποσβεστήρες (Tuned Mass Dampers-TMD), ο KDamper μπορεί να επιτύχει καλύτερα χαρακτηριστικά μόνωσης και απόσβεσης, χωρίς την ανάγκη επιπρόσθετων βαρών μαζών, όπως απαιτεί ο TMD. Σε αντίθεση με τον TMD και τις παραλλαγές του, ο KDamper αντικαθιστά τις απαραίτητες υψηλές δυνάμεις αδράνειας της προστιθέμενης μάζας με τη δύναμη από το αρνητικό στοιχείο στιβαρότητας. Μεταξύ άλλων, αυτό μπορεί να προσφέρει συγκριτικά πλεονεκτήματα στην περιοχή πολύ χαμηλών συχνοτήτων. Επιπλέον, γνωρίζοντας ότι οι ιδιότητες μόνωσης και απόσβεσης του KDamper είναι ουσιαστικά αποτέλεσμα των στοιχείων στιβαρότητας του συστήματος, περαιτέρω τεχνολογικά πλεονεκτήματα μπορούν να

προκύψουν, όσον αφορά το βάρος, την πολυπλοκότητα και την αξιοπιστία. Τέλος θα πρέπει ειδικά να σημειωθεί, ότι ο KDamper προσφέρει ουσιαστικές δυνατότητες για την απόσβεση της κατακόρυφης συνιστώσας των σεισμικών διεγέρσεων, όπου δεν υπάρχει δόκιμη μέθοδος, η οποία λειτουργεί αποτελεσματικά σήμερα.

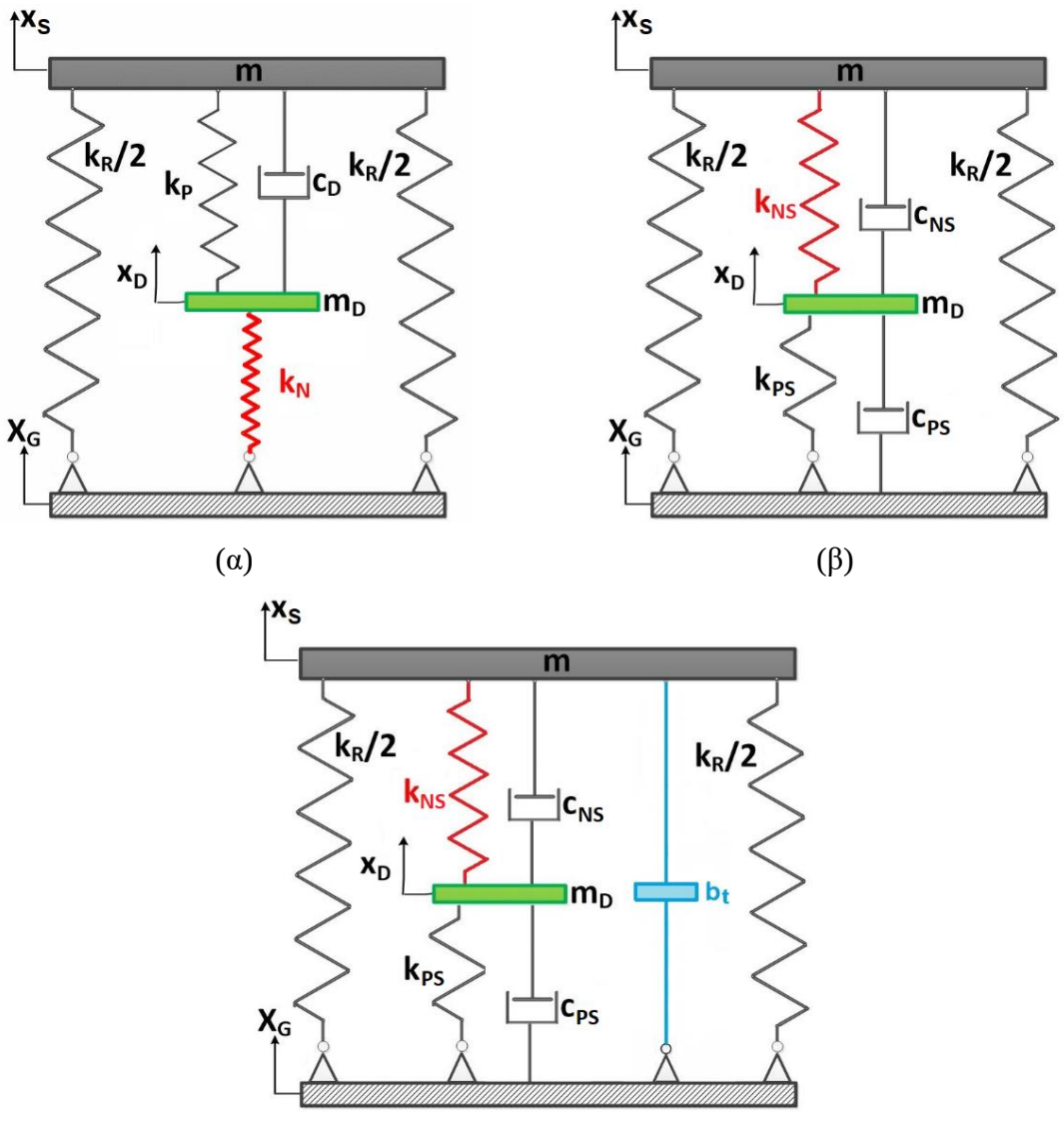

Σχήμα 2: *Σχηματική αναπαράσταση δυναμικών συστημάτων απορρόφησης ταλαντώσεων βασισμένα στον KDamper: (α) ταλαντωτής KDamper, (β) διευρυμένη έκδοση του KDamper, και (γ) διευρυμένη έκδοση του KDamper με inerter.*

Ο KDamper παρουσιάζεται στο Σχήμα 2.α. Όμοια με τον ταλαντωτή QZS εισάγεται ένα στοιχείο αρνητικής στιβαρότητας. Σε αντίθεση με τον QZS, η πρώτη βασική προϋπόθεση του KDamper είναι η διατήρηση της συνολικής στατικής στιβαρότητας:

$$k_R + \frac{k_P k_N}{k_P + k_N} = k = (2\pi f_0)^2 (m + m_D) \tag{10}$$

Έτσι, ο KDamper ξεπερνά το αντίστοιχο εγγενές μειονέκτημα των γνωστών μονωτών ταλαντώσεων «μηδενικής στιβαρότητας». Συγκριτικά με τον TMD ή τον TMDI, ο KDamper εισάγει ένα στοιχείο αρνητικής στιβαρότητας, το οποίο συνδέει την προστιθέμενη μάζα με την βάση του συστήματος. Οι εξισώσεις κίνησης που προκύπτουν είναι:

$$m\ddot{u}_S + c_D(\dot{u}_S - \dot{u}_D) + k_P(u_S - u_D) + k_R u_S = -m\ddot{X}_G \tag{11.α}$$

$$m_D\ddot{u}_D - c_D(\dot{u}_S - \dot{u}_D) - k_P(u_S - u_D) + k_N u_D = -m_D\ddot{X}_G \tag{11.β}$$

όπου, u_S=X_S-X_G και u_D=X_D-X_G. Υποθέτοντας αρμονική διέγερση στην βάση της κατασκευής, της μορφής:

$$\ddot{X}_G(t) = A_G \exp(j\omega t) \tag{12}$$

και αποκρίσεις σταθερής κατάστασης της μορφής:

$$u_S(t) = \tilde{U}_S \exp(j\omega t) \tag{13.α}$$

$$u_D(t) = \tilde{U}_D \exp(j\omega t) \tag{13.β}$$

Οι εξισώσεις του KDamper προκύπτουν ως:

$$-\omega^2 m\tilde{U}_S + j\omega c_D(\tilde{U}_S - \tilde{U}_D) + k_P(\tilde{U}_S - \tilde{U}_D) + k_R\tilde{U}_S = -mA_G \tag{14.α}$$

$$-\omega^2 m_D\tilde{U}_D - j\omega c_D(\tilde{U}_S - \tilde{U}_D) - k_P(\tilde{U}_S - \tilde{U}_D) + k_N\tilde{U}_D = -m_D A_G \tag{14.β}$$

Ένας προσεκτικός έλεγχος των Εξισώσεων (14.α, β) δείχνει πως το πλάτος F_{MD} της αδρανειακής δύναμης της προστιθέμενης μάζας και το πλάτος F_N της δύναμης του στοιχείου αρνητικής στιβαρότητας είναι σε φάση λόγω της αρνητικής τιμής του k_N:

$$F_{MD} = -\omega^2 m_D \left|\tilde{U}_D\right| \tag{15.α}$$

$$F_N = k_N \left|\tilde{U}_D\right| \le 0 \tag{15.β}$$

Έτσι, παρόμοια με τον TMDI, ο KDamper μπορεί να θεωρηθεί ως μια έμμεση προσέγγιση για την αύξηση της δύναμης της αδρανειακής μάζας χωρίς την αύξηση της ίδιας της μάζας. Τα χαρακτηριστικά που διέπουν τον KDamper είναι:

$$\mu = m_D/m \tag{16.α}$$

$$k_D = k_N + k_P \tag{16.β}$$

$$\omega_D = \sqrt{k_D / m_D} = \sqrt{(k_N + k_P)/m_D} \tag{16.γ}$$

$$\zeta_D = c_D / 2\omega_D m_D = c_D / 2\sqrt{(k_N + k_P)m_D} \tag{16.δ}$$

$$m_{tot} = m + m_D \tag{16.ε}$$

$$f_0 = \sqrt{k / m_{tot}} / 2\pi = \sqrt{\left(k_R + k_P k_N / k_P + k_N\right) / \left(m + m_D\right)} / 2\pi \tag{16.η}$$

όπου μ είναι ο λόγος της προστιθέμενης μάζας προς την μάζα της κατασκευής, ζ_D είναι ο λόγος απόσβεσης του τεχνητού αποσβεστήρα, και f_0 είναι η ονομαστική συχνότητα του KDamper.

Η διευρυμένη έκδοση του KDamper (extended KDamper-EKD) παρουσιάζεται στο Σχήμα 2.β. Η συγκεκριμένη διάταξη συνίσταται στην εναλλαγή θέσεων του θετικού και αρνητικού στοιχείου στιβαρότητας, k_P, k_N, και στην προσθήκη ενός τεχνητού αποσβεστήρα παράλληλα σε κάθε ένα από αυτά τα στοιχεία. Αρχικά, η εναλλαγή αυτή γίνεται για τεχνικούς λόγους. Πρώτον, με αυτή τη διάταξη, στο στοιχείο αρνητικής στιβαρότητας δεν ασκείται καμία εξωτερική δύναμη, όπως στην περίπτωση του KDamper όπου ασκείται το ίδιο βάρος της m_D. Αντίθετα, στον EKD, το ίδιο βάρος της m_D παραλαμβάνεται από το στοιχείο θετικής στιβαρότητας k_P, το οποίο μπορεί εύκολα να παραλάβει δυνάμεις τέτοιας τάξης μεγέθους, όντας πρακτικά άκαμπτο στην κατακόρυφη διεύθυνση (πχ. απλά ελαστικά εφέδρανα). Δεύτερον, με την προσθήκη τεχνητών αποσβεστήρων παράλληλα σε κάθε στοιχείο στιβαρότητας, επιτυγχάνεται περεταίρω βελτίωση της δυναμικής συμπεριφοράς του αρχικού συστήματος, καθώς επίσης και μείωση στη σχετική μετατόπιση μεταξύ των δύο τερματικών του στοιχείου αρνητικής στιβαρότητας, κάτι που είναι εξαιρετικής σημασίας για τον ρεαλιστικό σχεδιασμό του.

Τέλος, ο EKD με inerter παρουσιάζεται στο Σχήμα 2.γ. Η προσθήκη του inerter έγκειται στην μείωση της θεμελιώδους ιδιοσυχνότητας της κατασκευής χωρίς την προσθήκη επιπλέον μαζών ή μείωση της συνολικής στιβαρότητας, με αποτέλεσμα την μείωση των επιταχύνσεων. Στην συνέχεια, οι μεγάλες σχετικές μετατοπίσεις που θα αναπτυσσόντουσαν, περιορίζονται σημαντικά με τις εξαιρετικές ιδιότητες απόσβεσης του προσφέρει ο EKD, όταν σχεδιαστεί κατάλληλα. Περαιτέρω πληροφορίες σχετικά με τον βέλτιστο σχεδιασμό των προτεινόμενων

δυναμικών συστημάτων απορρόφησης ταλαντώσεων βασισμένα στον KDamper βρίσκονται στην επόμενη ενότητα.

III. Βέλτιστος Σχεδιασμός Προηγμένων Συστημάτων Απορρόφησης Ταλαντώσεων με Στοιχεία Αρνητικής Στιβαρότητας

Η βέλτιστη προσέγγιση σχεδιασμού για τον ταλαντωτή KDamper ακολουθεί ακριβώς τα ίδια βήματα όπως στο (Den Hartog, 1956). Αρχικά, μορφώνονται οι συναρτήσεις μεταφοράς του KDamper, για αρμονική διέγερση στη βάση, από τις Εξισώσεις (14):

$$\tilde{H}_{US} = \frac{\tilde{U}_S}{A_G} = -\frac{\tilde{N}_{US}}{\tilde{D}} \tag{17.α}$$

$$\tilde{H}_{UD} = \frac{\tilde{U}_D}{A_G} = \frac{(j\omega c_D + k_P)H_{US} - m_D}{(-\omega^2 m_D + j\omega c_D + k_p + k_N)} = \frac{\tilde{N}_{UD}}{\tilde{D}} \tag{17.β}$$

$$\tilde{H}_{AS} = \frac{\tilde{A}_S}{A_G} = 1 - \omega^2 \tilde{H}_{US} = \frac{\tilde{N}_{AS}}{\tilde{D}} \tag{17.γ}$$

όπου:

$$\tilde{N}_{US} = -\omega^2 m m_D + j\omega c_D (m + m_D) + m(k_P + k_N) + m_D k_P \tag{18.α}$$

$$\tilde{N}_{UD} = -\omega^2 m m_D + j\omega c_D (m + m_D) + m k_P + m_D (k_R + k_P) \tag{18.β}$$

$$\tilde{N}_{AS} = -\omega^2 m_D k_R + j\omega c_D (k_R + k_N) + k(k_P + k_N) \tag{18.γ}$$

$$\begin{aligned} \tilde{D} = {} & \omega^4 m m_D - \omega^2 [m(k_P + k_R) + m_D (k_P + k_R)] \\ & - j\omega^3 (m + m_D) c_D + j\omega c_D (k_R + k_N) + k(k_P + k_N) \end{aligned} \tag{18.δ}$$

Ακολούθως εισάγονται οι ακόλουθες παράμετροι για την διάταξη του KDamper:

$$\kappa = -k_N / (k_P + k_N) \tag{19.α}$$

$$\mu = m_D / m \tag{19.β}$$

$$\rho = \omega_D / \omega_0 \tag{19.γ}$$

$$q = \omega / \omega_0 \tag{19.δ}$$

$$\omega_0 = \sqrt{k / m} \tag{19.ε}$$

$$\omega_D = \sqrt{k_D / m_D} \tag{19.ζ}$$

$$\zeta_D = c_D / 2\sqrt{k_D m_D} \tag{19.η}$$

Οι ελεύθερες παράμετροι σχεδιασμού του KDamper είναι ο λόγος μάζας μ και στιβαρότητας κ, όπως ορίζονται στις Εξισώσεις (19.α, β). Η βέλτιστη τιμή του λόγου συχνοτήτων ρ (Εξίσωση 19.γ) προκύπτει ως συνάρτηση των μ και κ, αφού επιλεχθεί η συνάρτηση μεταφοράς προς ελαχιστοποίηση. Ο λόγος απόσβεσης ζ_D μπορεί να υπολογισθεί αριθμητικά έτσι ώστε να ελαχιστοποιεί την αντίστοιχη συνάρτηση μεταφοράς. Όταν προσδιορισθούν οι παράμετροι κ, μ, ρ, και ζ_D, οι τιμές των επιμέρους στοιχείων του KDamper προκύπτουν ως:

$$k_N / k = \kappa_N = -\kappa\mu\rho^2 \tag{20.α}$$

$$k_P / k = \kappa_P = (1+\kappa)\mu\rho^2 \tag{20.β}$$

$$k_R / k = \kappa_S = 1+\kappa(1+\kappa)\mu\rho^2 \tag{20.γ}$$

$$m_D = \mu m \tag{20.δ}$$

$$c_D = 2\zeta_D\sqrt{(k_P + k_N)m_D} \tag{20.ε}$$

Η συνάρτηση μεταφοράς που επιλέγεται προς ελαχιστοποίηση είναι εκείνη της απόλυτης επιτάχυνσης της κατασκευής H_{AS}. Αντίστοιχη διαδικασία με αυτήν που θα παρουσιαστεί παρακάτω, ακολουθείται και στην περίπτωση που επιλεχθεί εκείνη της σχετικής μετατόπισης της κατασκευής H_{US}. Η Εξίσωση (17.γ) γίνεται:

$$\tilde{H}_{AS} = -\frac{A+(j2\zeta_D)B}{C+(j2\zeta_D)D} \tag{21}$$

Και κατ' επέκταση:

$$H_{AS} = \frac{\left|\tilde{A}_S\right|}{A_G} = \frac{A_S}{A_G} = \sqrt{\frac{A^2+(2\zeta_D)^2 B^2}{C^2+(2\zeta_D)^2 D^2}} \tag{22}$$

όπου:

$$A = -q^2[1+\kappa(1+\kappa)\mu\rho^2]+\rho^2 \tag{23.α}$$

$$B = \rho q(1+\kappa^2\mu\rho^2) \tag{23.β}$$

$$C = q^4 - q^2[1+\rho^2+(1+\kappa^2)\mu\rho^2]+\rho^2 \tag{23.γ}$$

$$D = \rho q[(1+\kappa^2\mu\rho^2) - q^2(1+\mu)] \tag{23.δ}$$

Για την οριακή συνθήκη όπου $\zeta_D = 0$ ή $\zeta_D \to \infty$, η H_{AS} της Εξίσωσης (22) γίνεται:

$$H_{AS}(0) = \left|\frac{A}{C}\right| \tag{24.α}$$

$$H_{AS}(\infty) = \left|\frac{B}{D}\right| \tag{24.β}$$

Η διαδικασία που περιγράφεται στο (Den Hartog, 1956), και επίσης χρησιμοποιείται και στην παρούσα διδακτορική διατριβή βασίζεται στην ταυτοποίηση ενός ζεύγους συχνοτήτων q_L <1 και q_R>1, όπου οι τιμές $H_{AS}(q_L)$ και $H_{AS}(q_R)$ γίνονται ανεξάρτητες της τιμής ζ_D. Το πρώτο στάδιο της διαδικασίας βελτιστοποίησης εστιάζεται στη συνθήκη που αναφέρει ότι οι τιμές των συναρτήσεων μεταφοράς σε αυτά τα σημεία είναι ίσες:

$$H_{AS}(q_L) = H_{AS}(q_R) = H_{ASI} = H_{AS}(\infty) \tag{25}$$

Προκειμένου να υπάρξει λύση για αυτό το ζευγάρι συχνοτήτων πρέπει να επαληθεύεται μία από τις εξής συνθήκες:

Περίπτωση I: $AD = BC$ (26.α)

Περίπτωση II: $AD = -BC$ (26.β)

Όπως μπορεί πολύ εύκολα να αποδειχθεί, δεν υπάρχει λύση της Εξίσωσης (26.α) για θετικό q^2, όταν οι τιμές των κ, μ, και ρ είναι θετικές. Μετά από πράξεις στην Εξίσωση (26.β) προκύπτει ότι:

$$(A_2D_2 + B_0)q^4 + (A_0D_2 + A_2D_0 + B_0C_2)q^2 + (A_0D_0 + B_0C_0) = 0 \tag{27}$$

Από την Εξίσωση (27) προκύπτει ότι για το ζευγάρι των ριζών της πρέπει να ισχύει:

$$q_L^2 + q_R^2 = -\frac{(A_0 D_2 + A_2 D_0 + B_0 C_2)}{(A_2 D_2 + B_0)} \tag{28}$$

Επιπλέον, και οι δύο ρίζες q_L και q_R πρέπει να ικανοποιούν την Εξίσωση (24.β), και άρα προκύπτει ότι:

$$\frac{B_0}{D_0 + D_2 q_L^2} = -\frac{B_0}{D_0 + D_2 q_R^2} \Rightarrow q_L^2 + q_R^2 = -\frac{2D_0}{D_2} \tag{29}$$

Ο συνδυασμός των εξισώσεων (28) και (29) οδηγεί στην βέλτιστη τιμή για την παράμετρο ρ, ως συνάρτηση των κ και μ:

$$A_\rho \rho^4 + B_\rho \rho^2 + C_\rho = 0 \tag{30}$$

Η βέλτιστη τιμή της παραμέτρου ρ επιλέγεται ως η ελάχιστη από τις δύο ρίζες της Εξίσωσης (30). Ο λόγος απόσβεσης ζ_D υπολογίζεται αριθμητικά έτσι ώστε να ελαχιστοποιεί τις μέγιστες τιμές της συνάρτησης μεταφοράς $H_{AS}(q,\zeta_D)$. Στο Σχήμα 3 παρουσιάζεται η μεταβολή της $H_{AS}(q,\zeta_D)$ λόγω μεταβολής του ζ_D. Παρατηρείται πως για την βέλτιστη τιμή του $\zeta_{Dopt}=\zeta_{min}$, τα δύο μέγιστα της $H_{AS}(q,\zeta_D)$ είναι ίσα και ελάχιστα.

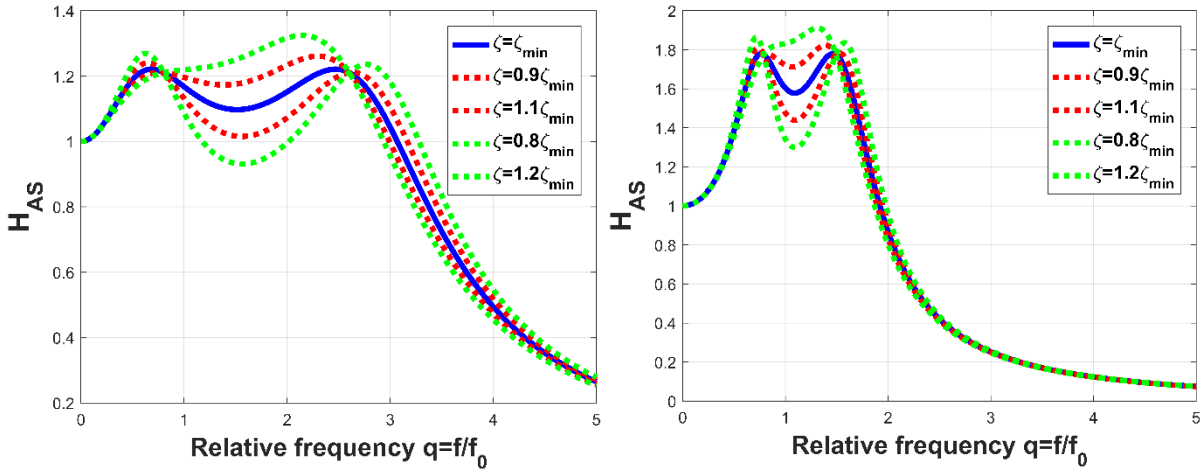

(α) (β)

Σχήμα 3: *Επίδραση του λόγου απόσβεσης ζ_D στην συνάρτηση μεταφοράς H_{AS} για (α) μ=0.05, κ=3.41, και (β) μ=0.05, κ=2.56.*

Η πρώτη θεμελιώδης ιδιότητα του KDamper είναι πως με την προσθήκη του στοιχείου αρνητικής στιβαρότητας μειώνεται η μέγιστη τιμή της συνάρτησης μεταφοράς H_{AS}, σε σύγκριση με τον TMD για ίδιο λόγο προστιθέμενης μάζας μ, όπως φαίνεται στο Σχήμα 4. Επιπρόσθετα, αυξάνοντας την τιμή της παραμέτρου κ, μειώνεται το μεγαλύτερο κομμάτι της H_{AS}, η οποία γίνεται πιο 'επίπεδη'. Αυτό έχει σαν συνέπεια ο KDamper να είναι λιγότερο ευαίσθητος σε φαινόμενα αποσυντονισμού συγκριτικά με τον TMD. Ωστόσο, η αύξηση του κ είναι άνω φραγμένη από την τιμή κ_{max}. Όπως παρατηρούμε στο Σχήμα 5.α, όταν η τιμή του κ προσεγγίζει την τιμή κ_{max}, ο λόγος ιδιοσυχνοτήτων ρ τείνει στο άπειρο. Την ίδια στιγμή, η μέγιστη τιμή της συνάρτησης μεταφοράς H_{AS} τείνει στην μονάδα (ελάχιστη τιμή).

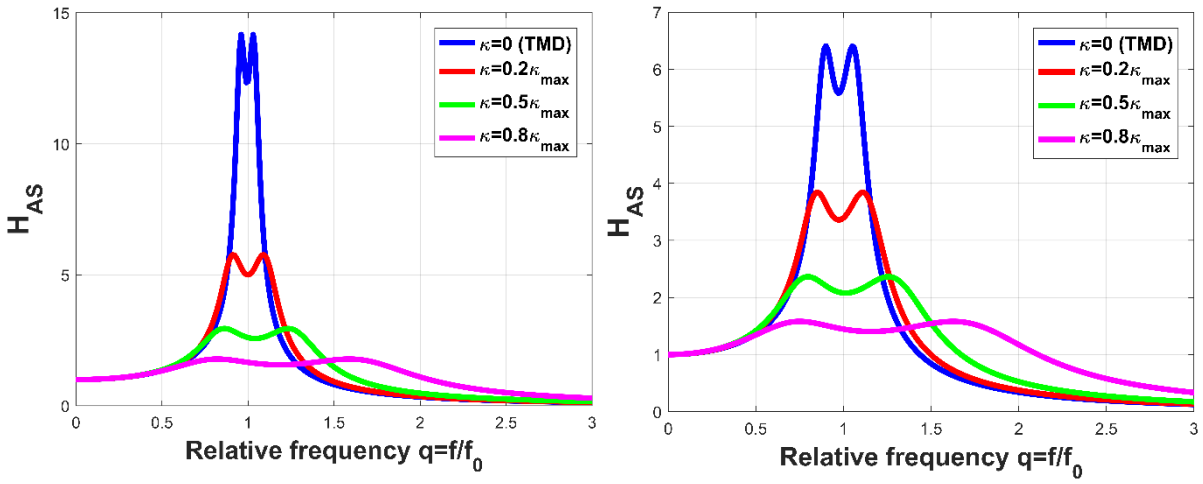

(α) (β)

Σχήμα 4: *Επίδραση του λόγου στιβαρότητας κ στην συνάρτηση μεταφοράς H_{AS} του KDamper για (α) μ=0.01, και (β) μ=0.05.*

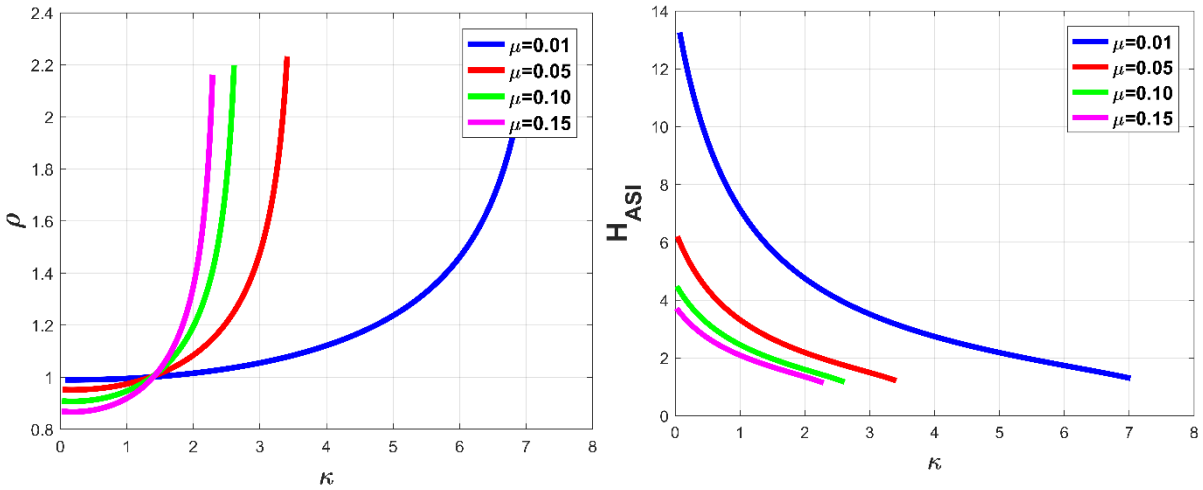

(α) (β)

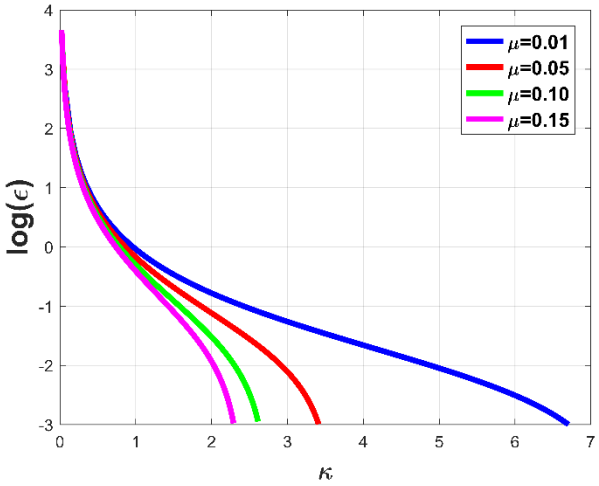

(γ)

Σχήμα 5: *Επίδραση των παραμέτρων κ και μ του KDamper σε: α) την παράμετρο $\rho=\omega_D/\omega_0$, β) στην τιμή (μέγιστη) H_{ASI} της συνάρτησης μεταφοράς H_{AS} στα σημεία q_L, q_R, και γ) τον δείκτη στατικής ευστάθειας ε.*

Ωστόσο, αυξάνοντας την παράμετρο *κ* οι τιμές των στοιχείων στιβαρότητας αυξάνουν σημαντικά, όπως φαίνεται στο Σχήμα 6. Επιπρόσθετα, αυξάνοντας την τιμή του στοιχείου αρνητικής στιβαρότητας k_N, ενδέχεται το σύστημα να γίνει ασταθές. Παρόλο που θεωρητικά η τιμή του k_N επιλέγεται μέσω της Εξίσωσης (10) για να εξασφαλίσει την στατική ευστάθεια του συστήματος, μεταβολές στην τιμή του στοιχείου αρνητικής στιβαρότητας αναμένεται να προκύψουν. Συνεπώς, μία αύξηση στην τιμή του k_N κατά *ε* οδηγεί σε μία νέα τιμή k_{NL} όπου το σύστημα είναι ασταθές:

$$k_S + \frac{k_P k_{NL}}{k_P + k_{NL}} = 0 \Leftrightarrow k_{NL} = -\frac{k_S k_P}{k_S + k_P} = (1+\varepsilon)k_N \tag{31}$$

Αντικαθιστώντας τις Εξισώσεις (10) και (20.α-γ) στην (31) οδηγούμαστε στην εκτίμηση του δείκτη στατικής ευστάθειας *ε*:

$$\varepsilon = \frac{1}{\kappa\left[1+(1+\kappa)^2 \mu\rho^2\right]} \tag{32}$$

Στο Σχήμα 5.γ παρουσιάζεται η επίδραση των *κ* και *μ* στο δείκτη στατικής ευστάθειας. Όπως παρατηρείται από την Εξίσωση (32) και το Σχήμα 5.γ, η αύξηση της αρνητικής στιβαρότητας είναι άνω φραγμένη από την στατική ευστάθεια, όπου ο *ε* τείνει στο μηδέν.

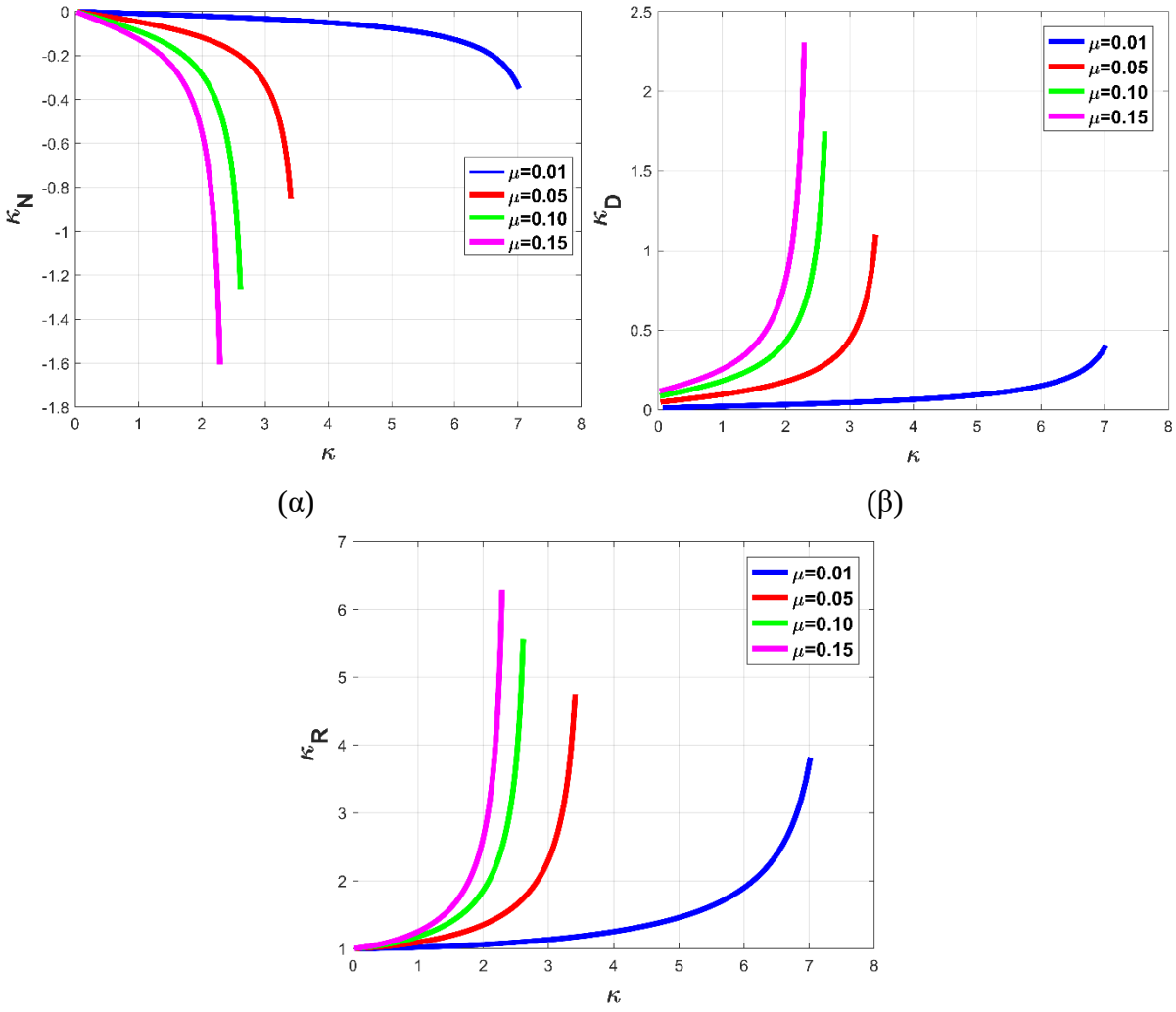

Σχήμα 6: *Επίδραση της αύξησης του κ στις τιμές των στοιχείων στιβαρότητας του KDamper. (α)* κ_N*, (β)* κ_P *και (γ)* κ_R*.*

Οι διευρυμένες εκδόσεις του KDamper στοχεύουν στην περεταίρω βελτίωση της δυναμικής συμπεριφοράς του υπό εξέταση συστήματος, και στην μείωση της σχετικής μετατόπισης των τερματικών του στοιχείου αρνητικής στιβαρότητας.

Η προαναφερθείσα διαδικασία για την βέλτιστη επιλογή των παραμέτρων του KDamper δεν λαμβάνει υπόψη τεχνικά κριτήρια, και δυσχεραίνει τον ρεαλιστικό σχεδιασμό των προτεινόμενων δυναμικών συστημάτων απορρόφησης ταλαντώσεων. Πιο συγκεκριμένα, δεν λαμβάνονται υπόψη κατασκευαστικοί και γεωμετρικοί περιορισμοί, δεν υπάρχει εποπτεία όσον αφορά τις μέγιστες τιμές των επιμέρους στοιχείων στιβαρότητας και απόσβεσης, και τέλος η επιλογή της διέγερσης δεν είναι ρεαλιστική.

Για αυτό τον λόγο, ο βέλτιστος σχεδιασμός των διευρυμένων εκδόσεων του KDamper ακολουθεί πρόβλημα βελτιστοποίησης, το οποίο βασίζεται σε τεχνικά κριτήρια, η επιλογή των

διεγέρσεων λαμβάνει υπόψη τους εκάστοτε κανονισμούς, και το στοιχείο αρνητικής στιβαρότητας υλοποιείται με ρεαλιστικές διατάξεις.

Ένα παράδειγμα για την υλοποίηση του στοιχείου αρνητικής στιβαρότητας του KDamper, σε μία διάσταση, απεικονίζεται στο Σχήμα 7. Αποτελείται από μια μάζα m (της κατασκευής) η οποία στηρίζεται σε δύο παράλληλα γραμμικά ελατήρια με στιβαρότητα k_R και k_D αντίστοιχα, ενώ υπάρχει και ένας αποσβεστήρας με σταθερά c_D. Ο αποσβεστήρας c_D και το ελατήριο k_D συνδέονται με την προστιθέμενη μάζα m_D. Το ελατήριο αρνητικής στιβαρότητας k_N προσομοιώνεται από ένα σετ δύο συμμετρικών γραμμικών οριζόντιων ελατηρίων με σταθερές k_H, τα οποία στηρίζουν τη μάζα m_D με έναν αρθρωτό μηχανισμό, όπως φαίνεται στο Σχήμα 7.β.

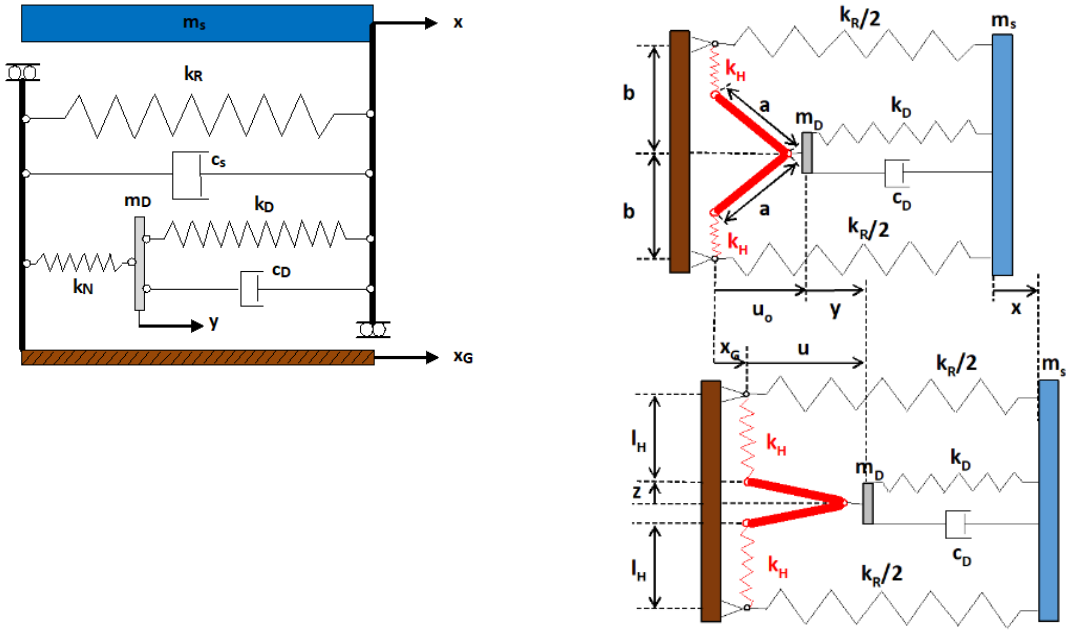

(α) (β)

Σχήμα 7: *Σχηματική παρουσίαση (α) του KDamper, και (β) της προτεινόμενης μονοδιάστατης διάταξης για την υλοποίηση του στοιχείου αρνητικής στιβαρότητας (κάτοψη).*

Η θέση στατικής ισορροπίας του συστήματος απεικονίζεται στο Σχήμα 7.β, μαζί με την μετατοπισμένη θέση μετά από μια εξωτερική διέγερση στη βάση $X_G(t)$. Οι εξισώσεις κίνησης του προτεινόμενου ταλαντωτή είναι:

$$m\ddot{u}_S + k_R u_S + c_S \dot{u}_S + k_P(u_S - u_D) + c_D(\dot{u}_S - \dot{u}_D) = -m\ddot{X}_G \qquad (33.\alpha)$$

$$m_D\ddot{u}_D - k_P(u_S - u_D) - c_D(\dot{u}_S - \dot{u}_D) + f_N(u) = -m_D\ddot{X}_G \qquad (33.\beta)$$

όπου, $u_S=X_S-X_G$ και $u_D=X_D-X_G$. Παρουσιάζονται οι ακόλουθες εξισώσεις για την δυναμική ενέργεια U_N, την μη γραμμική δύναμη f_N και την μη γραμμική στιβαρότητα k_N του σετ των δύο οριζόντιων ελατηρίων θετικής στιβαρότητας k_H:

$$U_N[u(y)] = 2\frac{1}{2}k_H(l_H - l_{HI})^2 \tag{34}$$

$$f_N(u) = \frac{\partial U_N}{\partial y} = \frac{\partial U_N}{\partial u} = -2k_H(1+\frac{l_{HI}-b}{\sqrt{a^2-u^2}})u = -2k_H\left[1+c_I\frac{1}{(1-u^2/a^2)^{1/2}}\right]u \tag{35}$$

$$k_N = \frac{\partial f_N}{\partial y} = \frac{\partial f_N}{\partial u} = -2k_H\left[1+\frac{l_{HI}-b}{a}\frac{1}{(1-u^2/a^2)^{3/2}}\right] = -2k_H\left[1+c_I\frac{1}{(1-u^2/a^2)^{3/2}}\right] \tag{36}$$

όπου l_{HI} είναι το αρχικό μήκος των μη-παραμορφωμένων ελατηρίων k_H, $l_H(t)$ είναι το μήκος των ελατηρίων k_H:

$$l_H(t) = b-(a^2-u^2)^{1/2} \tag{37}$$

και:

$$u = u_0 + u_D \tag{38}$$

$$c_I = (l_{HI}-b)/a \tag{39}$$

Στην περίπτωση όπου c_I=0 τα δύο οριζόντια ελατήρια είναι ισοδύναμα με ένα ελατήριο με σταθερή αρνητική στιβαρότητα ίση με k_N=-2k_H.

Ένα παράδειγμα για την υλοποίηση του στοιχείου αρνητικής στιβαρότητας του διευρυμένου KDamper, σε δύο διαστάσεις, απεικονίζεται στο Σχήμα 8. Αποτελείται από μια μάζα m η οποία στηρίζεται σε δύο παράλληλα γραμμικά ελατήρια με στιβαρότητα k_R και k_{NS} αντίστοιχα, ενώ υπάρχει και ένας αποσβεστήρας με σταθερά c_{NS}. Ο αποσβεστήρας c_{NS} και το ελατήριο k_{NS} συνδέονται με την προστιθέμενη μάζα m_D. Το ελατήριο θετικής στιβαρότητας k_{PS} και ο αποσβεστήρας c_{PS} συνδέουν την προστιθέμενη μάζα με την βάση. Το ελατήριο αρνητικής στιβαρότητας προσομοιώνεται από ένα γραμμικό κατακόρυφο ελατήριο με σταθερά k_H. Οι εξισώσεις κίνησης του συστήματος αυτού είναι:

$$(m+b)\ddot{u}_S + k_R u_S + f_{NS}(u_{NS}) + c_{NS}(\dot{u}_S - \dot{u}_D) = -m\ddot{X}_G \tag{40.α}$$

$$m_D\ddot{u}_D - f_{NS}(u_{NS}) - c_{NS}(\dot{u}_S - \dot{u}_D) + c_{PS}\dot{u}_D + k_{PS}u_D = -m_D\ddot{X}_G \quad (40.\beta)$$

και οι ακόλουθες εξισώσεις για την δυναμική ενέργεια U_N, την μη γραμμική δύναμη f_N και την μη γραμμική στιβαρότητα k_N του κατακόρυφου ελατηρίου k_H είναι:

$$U_{NS}[u_{NS}(u_D)] = \frac{1}{2}k_H(l_H - l_{HI})^2 \quad (41)$$

$$f_{NS}(u_{NS}) = \frac{\partial U_{NS}}{\partial u_D} = \frac{\partial U_{NS}}{\partial u_{NS}} = -k_H(1 + \frac{l_{HI} - b}{\sqrt{a^2 - u^2}})u = -k_H\left[1 + c_I\frac{1}{(1 - u_{NS}{}^2/a^2)^{1/2}}\right]u_{NS} \quad (42)$$

$$k_N = \frac{\partial f_{NS}}{\partial u_D} = \frac{\partial f_{NS}}{\partial u_{NS}} = -k_H\left[1 + \frac{l_{HI} - b}{a}\frac{1}{(1 - u_{NS}^2/a^2)^{3/2}}\right] = -k_H\left[1 + c_I\frac{1}{(1 - u_{NS}^2/a^2)^{3/2}}\right] \quad (43)$$

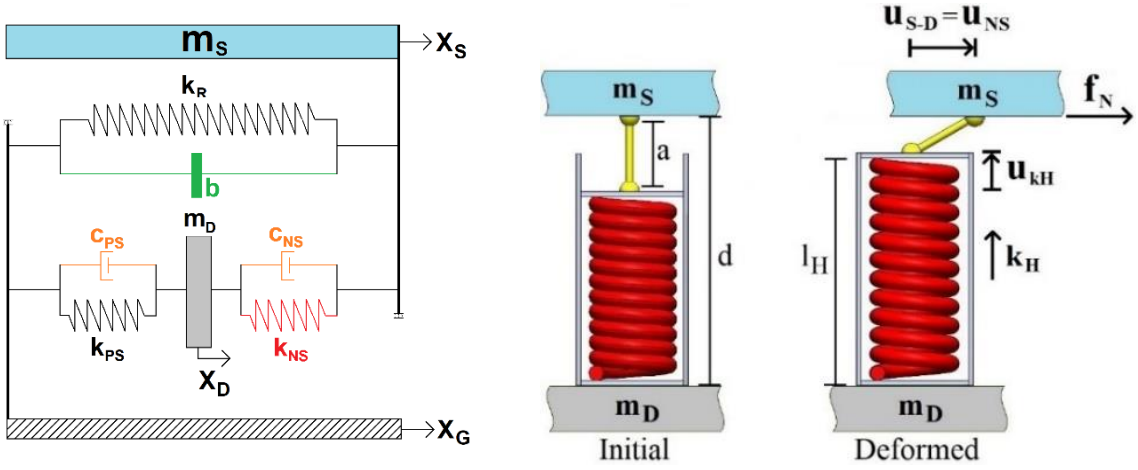

(α) (β)

Σχήμα 8: *Σχηματική παρουσίαση (α) του διευρυμένου KDamper, και (β) της προτεινόμενης δισδιάστατης διάταξης για την υλοποίηση του στοιχείου αρνητικής στιβαρότητας (όψη).*

Η άμεση εφαρμογή των φασμάτων απόκρισης των αντισεισμικών κανονισμών για την επιλογή των παραμέτρων του προτεινόμενων δυναμικών συστημάτων απορρόφησης ταλαντώσεων βασισμένα στον KDamper, δεν είναι εφικτή, καθώς η εφαρμογή αυτών των συστημάτων οδηγεί σε πολυβάθμια συστήματα πολλαπλών ιδιοσυχνοτήτων. Επομένως, ανάλυση στο πεδίο του χρόνου είναι απαραίτητη. Υπάρχουν αρκετοί τύποι επιταχυνσιογραφημάτων που μπορούν να χρησιμοποιηθούν, όπως α) συνθετικά επιταχυνσιογραφήματα, που παράγονται από σεισμολογικά μοντέλα, β) καταγραφές από πραγματικούς σεισμούς, και γ) τεχνητά επιταχυνσιογραφήματα σχεδιασμένα να είναι συμβατά

με κάποιο συγκεκριμένο φάσμα απόκρισης σχεδιασμού, με το τελευταίο να είναι το πιο κατάλληλο για σχεδιασμό με βάση τους κανονισμούς. Στην παρούσα διατριβή χρησιμοποιήθηκε το λογισμικό SeismoArtif (Seismosoft [2018], 2018). Στο Σχήμα 9.α, παρουσιάζεται το μέσο φάσμα απόκρισης 30 τεχνητών επιταχυνσιογραφημάτων, σχεδιασμένα με βάση τον EC8, για κατηγορία εδάφους C, κατηγορία σπουδαιότητας II, τύπο φάσματος I, και φασματική επιτάχυνση 0.36 g. Παρατηρείται πολύ καλή ταύτιση με το αντίστοιχο φάσμα απόκρισης του EC8 (λιγότερο από 10% απόκλιση) στο εύρος ιδιοπεριόδων από 0.2 μέχρι 2 δευτερόλεπτα. Το μέσο PGA των επιλεχθέντων 30 επιταχυνσιογραφημάτων είναι 5.19 m/sec^2. Στο Σχήμα 9.β, παρουσιάζεται το μέσο φάσμα διέγερσης των παραχθέντων τεχνητών επιταχυνσιογραφημάτων, και συγκρίνεται με εκείνο των (Cacciola and D'Amico, 2015), προσαρμοσμένο στο να έχουν την ίδια μέγιστη τιμή. Παρατηρείται πολύ καλή ταύτιση. Αντίστοιχα, για την κατακόρυφη σεισμική συνιστώσα, παράχθηκαν 50 τεχνητά επιταχυνσιογραφήματα, σχεδιασμένα με βάση τον EC8, για τύπο φάσματος I, και φασματική επιτάχυνση 0.36 g. Το μέσο φάσμα διέγερσης των 50 τεχνητών κατακόρυφων επιταχυνσιογραφημάτων παρουσιάζεται στο Σχήμα 10. Το μέσο PGA των επιλεχθέντων 50 επιταχυνσιογραφημάτων είναι 4.09 m/sec^2.

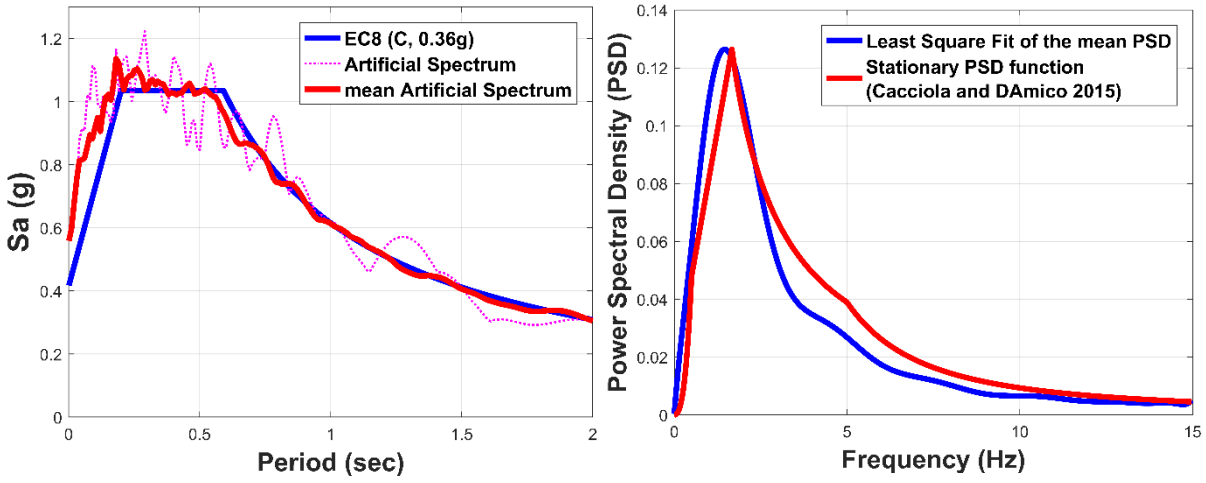

(α) (β)

Σχήμα 9: *(α) Μέσο φάσμα απόκρισης των 30 τεχνητών (οριζόντιων) επιταχυνσιογραφημάτων, και σύγκριση με το αντίστοιχο του EC8, και (β) μέσο φάσμα διέγερσης των τεχνητών επιταχυνσιογραφημάτων σε σύγκριση με εκείνο των (Cacciola and D'Amico, 2015).*

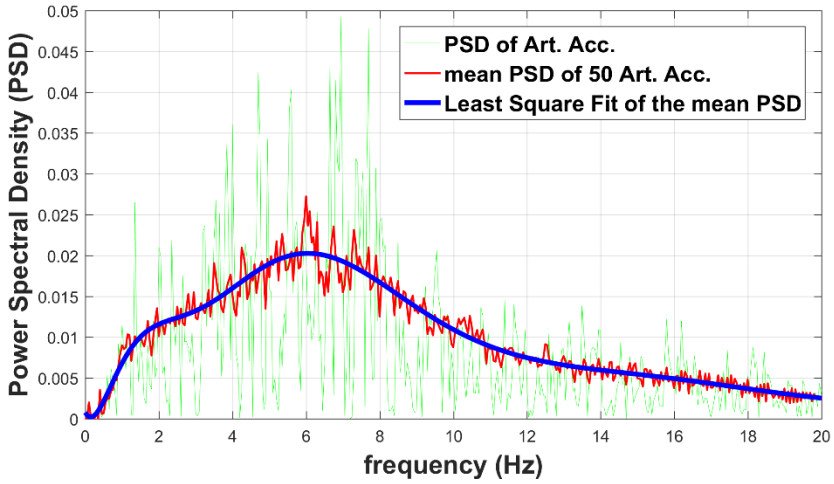

Σχήμα 10: *Μέσο φάσμα διέγερσης των 50 τεχνητών (κατακόρυφων) επιταχυνσιογραφημάτων.*

Για το πρόβλημα βελτιστοποίησης χρησιμοποιείται ο Harmony Search (HS) αλγόριθμος βελτιστοποίησης. Ο HS είναι ένας καινοτόμος μεταευριστικός αλγόριθμος που προτάθηκε από (Zong Woo Geem et al., 2001a). Οι τιμές των κύριων παραμέτρων του HS όπως οι HMS, HMCR, και PAR επιλέγονται να είναι ίσες με 75, 0.5, και 0.1, αντίστοιχα.

IV. Οριζόντια Σεισμική Προστασία με KDamper

Στη συνέχεια διερευνάται η εφαρμογή του KDamper ως σεισμική βάση απορρόφησης κραδασμών σε ένα πολυώροφο κτίριο, για οριζόντια σεισμική προστασία. Ο KDamper σχεδιάζεται με βάση την διαδικασία που περιεγράφηκε στην προηγούμενη ενότητα, για βέλτιστη απόκριση με βάση την επιτάχυνση (H_{AS} optimization). Το υπό εξέταση πολυώροφο κτίριο *n*-ορόφων απεικονίζεται στο Σχήμα 11. Οι παραδοχές που έγιναν για την μοντελοποίηση του είναι οι ακόλουθες:

i. Η συνολική μάζα του κτιρίου συγκεντρώνεται στο επίπεδο των ορόφων;
ii. Οι πλάκες και οι δοκοί των ορόφων θεωρούνται άκαμπτες σε σύγκριση με τις κολώνες;
iii. Οι κολώνες θεωρούνται αξονικά απαραμόρφωτες, αβαρείς, και προσφέρουν την συνολική οριζόντια στιβαρότητα;
iv. Η επιρροή της αλληλεπίδρασης εδάφους κατασκευής δεν λαμβάνεται υπόψη;
v. Η ανωδομή θεωρείται πως παραμένει στα ελαστικά όρια κατά τη διάρκεια της σεισμικής διέγερσης;

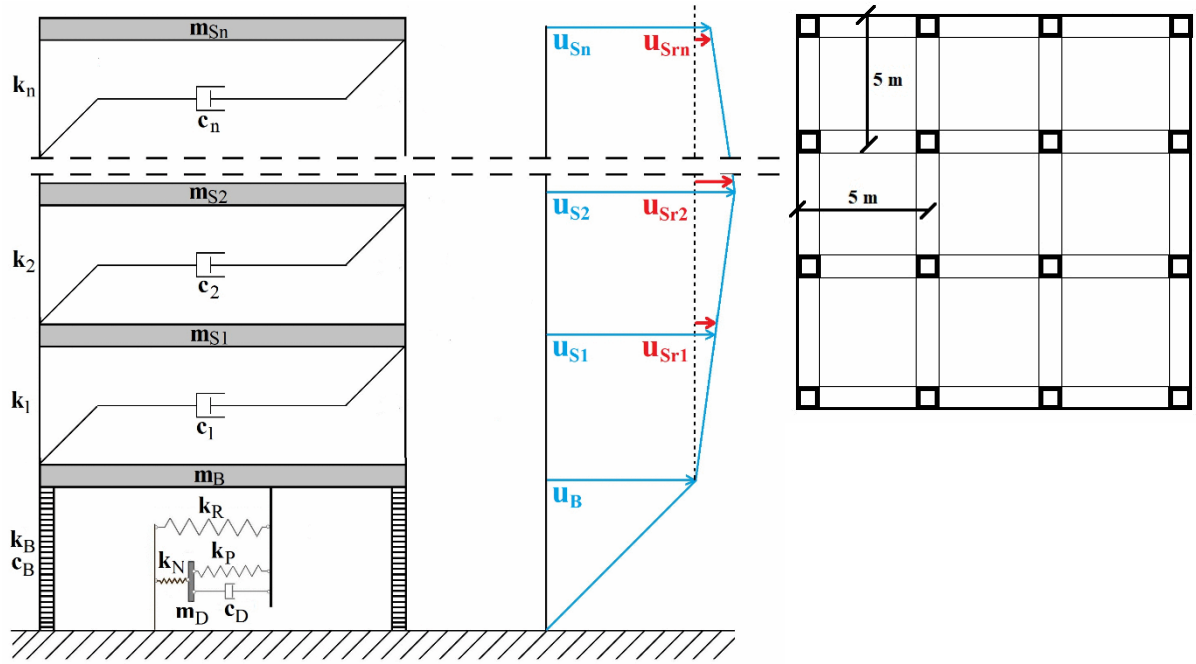

(α) (β)

Σχήμα 11: *Υπό εξέταση πολυώροφο κτίριο με το KDamper σας σεισμική βάση απορρόφησης κραδασμών, (α) σκίτσο του μοντέλου, και (β) κάτοψη ενός τυπικού ορόφου του κτιρίου.*

Ως αποτέλεσμα, η κατασκευή έχει *n* δυναμικούς βαθμούς ελευθερίας, οι οποίοι εκφράζονται από τις σχετικές μετατοπίσεις των *n* ορόφων ως προς την βάση της κατασκευής $[u_{Sr}](t)=[u_{Sr1}(t), u_{Sr2}(t), \ldots, u_{Srn}(t)]^T$. Οι εξισώσεις κίνησης του συστήματος με τον KDamper, εκφράζονται σε μητρωϊκή μορφή, και περιλαμβάνουν μητρώα διαστάσεων $r \times r$ με $r=n+2$:

$$[M][\ddot{u}(t)]+[C][\dot{u}(t)]+[K][u(t)]=-[\tau]a_G(t) \tag{44}$$

Τα μητρώα που υπεισέρχονται στην Εξίσωση (44) ορίζονται ως:

$$[M]_{(n+2)\times(n+2)}=\begin{bmatrix}[M_S]_{n\times n} & [0]_{n\times 1} & [0]_{n\times 1}\\ [0]_{1\times n} & m_B & 0\\ [0]_{1\times n} & 0 & m_D\end{bmatrix} \tag{45.α}$$

$$[K]_{(n+2)\times(n+2)}=\begin{bmatrix}[K_S]_{n\times n} & [0]_{n\times 1} & [0]_{n\times 1}\\ [0]_{1\times n} & k_P+k_R & -k_P\\ [0]_{1\times n} & -k_P & k_P+k_N\end{bmatrix} \tag{45.β}$$

$$[C]_{(n+2)\times(n+2)}=\begin{bmatrix}[C_S]_{n\times n} & [0]_{n\times 1} & [0]_{n\times 1}\\ [0]_{1\times n} & c_D & -c_D\\ [0]_{1\times n} & -c_D & c_D\end{bmatrix} \tag{45.γ}$$

$$[u_{(t)}]_{(n+2)\times 1}=\begin{bmatrix}[u_{S(t)}]\\ u_{B(t)}\\ u_{D(t)}\end{bmatrix};[\tau]_{(n+2)\times 1}=\begin{bmatrix}[M][1]_{n\times 1}\\ m_B\\ m_D\end{bmatrix};m_D=\mu_D m_{S,tot}=\mu_D\left(m_B+\sum_{i=1}^{n}m_i\right) \tag{45.δ}$$

όπου $[M_S]_{nxn}$, $[K_S]_{nxn}$, και $[C_S]_{nxn}$ είναι τα μητρώα μάζας, στιβαρότητας και απόσβεσης της αρχικής κατασκευής. Ως ενδεικτικό παράδειγμα, ο KDamper εφαρμόζεται ως σεισμική βάση απορρόφησης κραδασμών σε ένα 3-όροφο κτίριο από σκυρόδεμα με μέτρο ελαστικότητας ίσο με E=26000 MN/m^2. Οι μάζες των τριών ορόφων είναι ίσες με m_i=80000 kg ($i=1, 2, 3$). Οι ιδιοπερίοδοι του 3-όροφου κτιρίου είναι T_{Si} $[sec] = [0.495, 0.177, 0.122]$. Η μάζα της βάσης είναι ίση με $m_B=50000$ kg. Το μητρώο απόσβεσης της αρχικής κατασκευής είναι ανάλογο μάζας και στιβαρότητας (Rayleigh damping) με $\zeta_{Si}=0.02$ ($i=1, 2, 3$).

Η προστιθέμενη μάζα του KDamper επιλέγεται μ=5%, ο λόγος στιβαρότητας κ=3.41, και ο δείκτης στατικής ευστάθειας ε=5%. Επομένως, η ονομαστική συχνότητα του KDamper f_0 είναι η μόνη ελεύθερη παράμετρος σχεδιασμού. Για να παρατηρήσουμε την επιρροή της f_0 στις: 1) συναρτήσεις μεταφοράς, 2) φασματικές πυκνότητες ισχύος (PSD) των αποκρίσεων,

και 3) προβλεπόμενες (μέγιστες) τιμές (RMS) των αποκρίσεων, δύο χαρακτηριστικές περιπτώσεις εξετάστηκαν. Στην πρώτη περίπτωση, η ονομαστική συχνότητα του KDamper είναι ίση με εκείνη των συμβατικών συστημάτων σεισμικής μόνωσης f_0=0.4 *Hz* (KDAB-0.4). Στην δεύτερη περίπτωση, διερευνάται μια πιο 'στιβαρή' βάση με f_0=1.0 *Hz* (KDAB-1.0), ώστε να εξετάσουμε εάν μπορούν να αποφευχθούν οι μεγάλες σχετικές μετατοπίσεις που απαιτούνται για να επιτευχθεί βελτίωση της δυναμικής συμπεριφοράς της ανωδομής.

Στο Σχήμα 12 παρουσιάζονται οι συναρτήσεις μεταφοράς των κύριων αποκρίσεων του συστήματος. Το KDAB-0.4 σύστημα, βελτιώνει δραματικά την δυναμική συμπεριφορά της ανωδομής. Το KDAB-1.0 βελτιώνει την δυναμική συμπεριφορά της ανωδομής και ταυτόχρονα μειώνει δραματικά την μετακίνηση βάσης και της προστιθέμενης μάζας του KDamper.

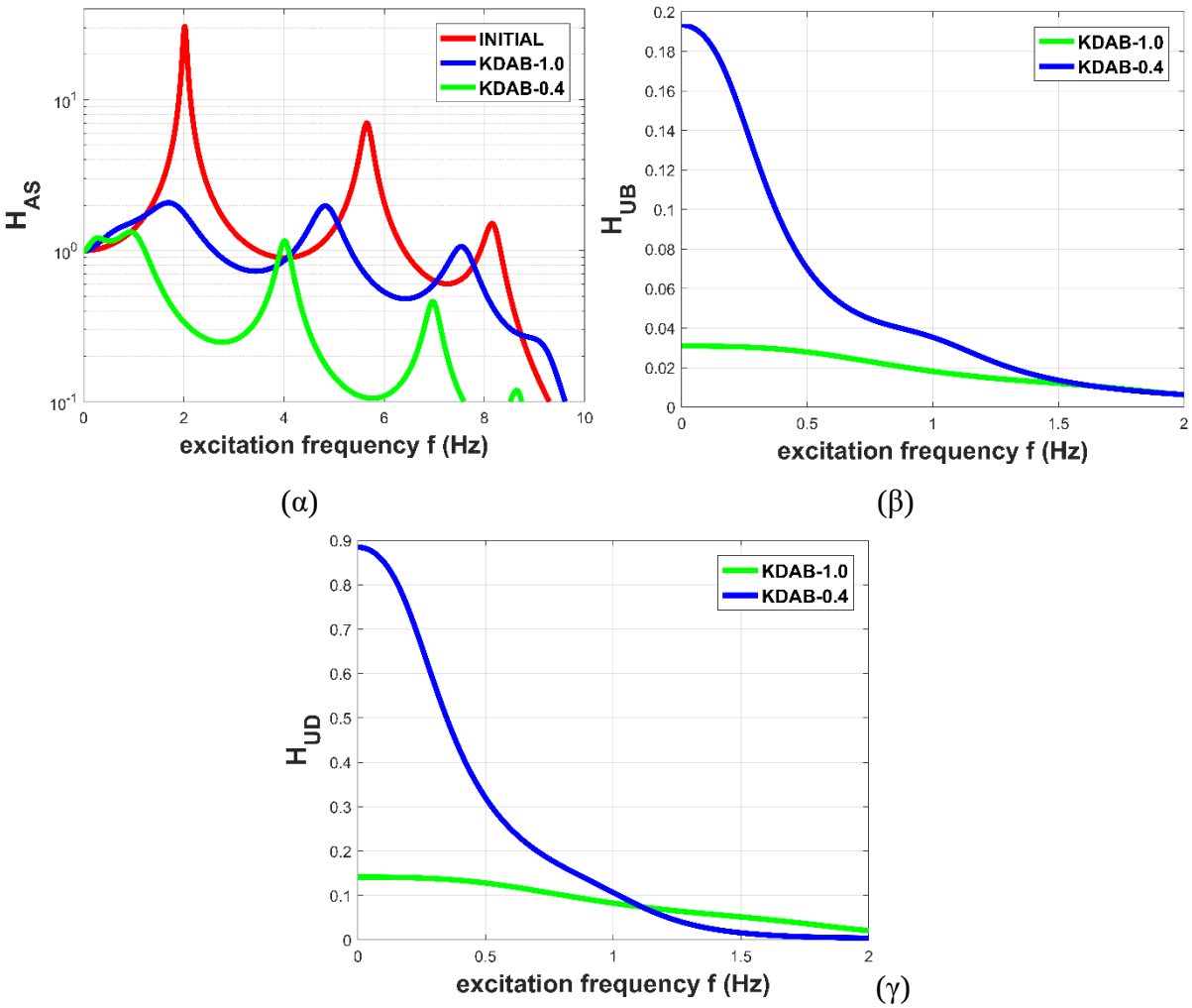

Σχήμα 12: *Συναρτήσεις μεταφοράς των κύριων αποκρίσεων του συστήματος: (α) επιτάχυνση κορυφαίου ορόφου H_{AS}, (β) σχετική μετακίνηση της βάσης H_{UB}, και (γ) σχετική μετακίνηση της προστιθέμενης μάζας του KDamper H_{UD}, για όλα τα εξεταζόμενα συστήματα: INITIAL, KDAB-0.4 and KDAB-1.0.*

Με βάση το μέσο φάσμα διέγερσης των 30 τεχνητών επιταχυνσιογραφημάτων της βάσης δεδομένων, για οριζόντια σεισμική κίνηση του Σχήματος 9.β, λαμβάνονται οι PSDs των κύριων αποκρίσεων του αρχικού αλλά και του συστήματος με τον KDamper, και παρουσιάζονται στο Σχήμα 13.

$$S_{USri}(\omega) = H_{USri}(\omega)^2 S_A(\omega) \quad (46.\alpha)$$

$$S_{UB}(\omega) = H_{UB}(\omega)^2 S_A(\omega) \quad (46.\beta)$$

$$S_{UD}(\omega) = H_{UD}(\omega)^2 S_A(\omega) \quad (46.\gamma)$$

$$S_{ASri}(\omega) = H_{ASri}(\omega)^2 S_A(\omega) \quad (46.\delta)$$

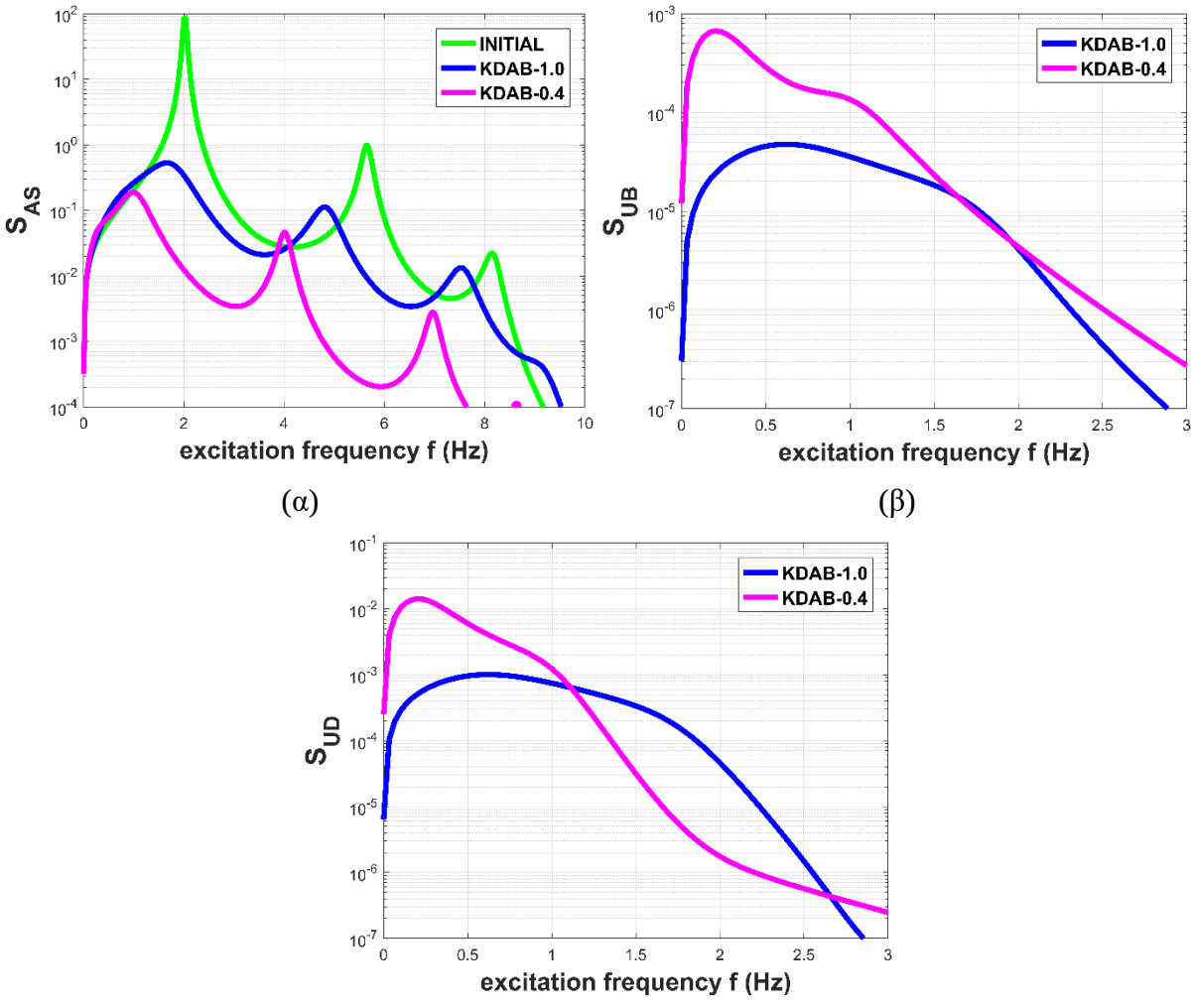

(α) (β)

(γ)

Σχήμα 13: *PSDs των κύριων αποκρίσεων του συστήματος: (α) επιτάχυνση κορυφής S_{AS}, (β) σχετική μετακίνηση βάσης S_{UB}, και (γ) σχετική μετακίνηση του KDamper S_{UD}, για όλα τα εξεταζόμενα συστήματα: INITIAL, KDAB-0.4 και KDAB-1.0.*

Παρατηρούμε πως και τα δύο συστήματα, KDAB-0.4 και KDAB-1.0 μειώνουν την μέγιστη τιμή της S_{AS} περισσότερο από δύο τάξεις μεγέθους, με το KDAB-0.4 να βελτιώνει την S_{AS} σε όλο το πεδίο συχνοτήτων, σε σύγκριση με το KDAB-1.0. Επιπλέον, με το να επιλέξουμε μια πιο στιβαρή βάση (KDAB-1.0 σύστημα) πετυχαίνουμε μείωση στη σχετική μετακίνηση βάσης, S_{UB}, αλλά και της μάζας του KDamper, S_{UD}, περισσότερο από μια τάξη μεγέθους, σε σύγκριση με το KDAB-0.4 σύστημα.

Οι RMS τιμές των αποκρίσεων ορίζονται ως το εμβαδό των PSD καμπύλων, σαν μια ένδειξη του πραγματικού ενεργειακού περιεχομένου των αποκρίσεων:

$$R_{USri} = \left[\int_{-\infty}^{+\infty} S_{USri}(\omega) \, \mathrm{d}\omega \right]^{0.5} \tag{47.α}$$

$$R_{UB} = \left[\int_{-\infty}^{+\infty} S_{UB}(\omega) \, \mathrm{d}\omega \right]^{0.5} \tag{47.β}$$

$$R_{UD} = \left[\int_{-\infty}^{+\infty} S_{UD}(\omega) \, \mathrm{d}\omega \right]^{0.5} \tag{47.γ}$$

$$R_{ASri} = \left[\int_{-\infty}^{+\infty} S_{ASri}(\omega) \, \mathrm{d}\omega \right]^{0.5} \tag{47.δ}$$

Στο Σχήμα 14 παρουσιάζονται οι RMS τιμές της επιτάχυνσης του κορυφαίου ορόφου, της σχετικής μετακίνησης της βάσης, και της σχετικής μετακίνησης του KDamper, κανονικοποιημένες ως προς τις αντίστοιχες RMS τιμές των αποκρίσεων της αρχικής κατασκευής.

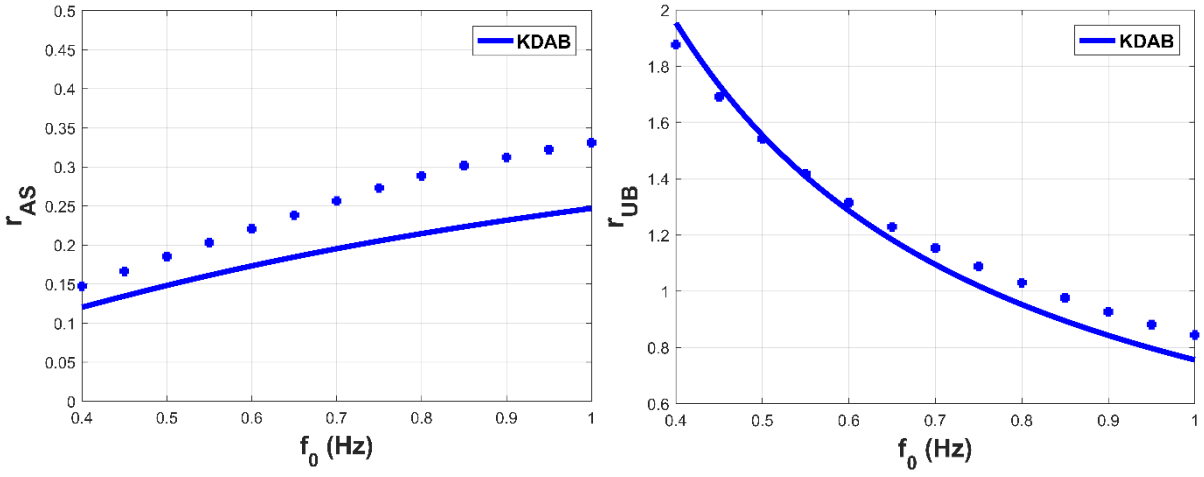

(α) (β)

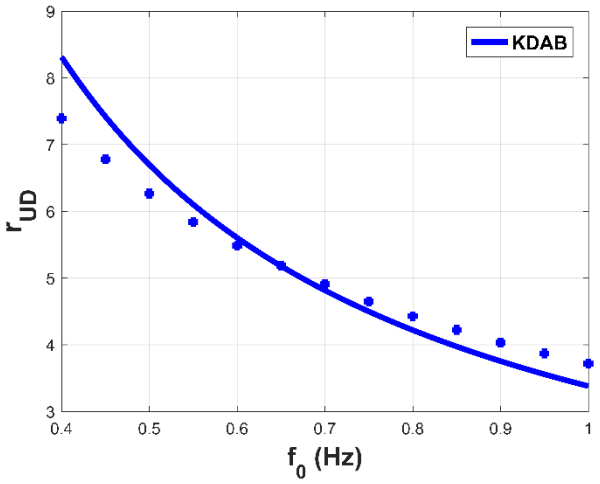

(γ)

Σχήμα 14: *Κανονικοποιημένες RMS τιμές των αποκρίσεων (συνεχείς καμπύλες) και επαλήθευσή τους στο πεδίο του χρόνου με τις κανονικοποιημένες μέγιστες μέσες τιμές των δυναμικών αποκρίσεων, για όλα τα 30 τεχνητά επιταχυνσιογραφήματα (διακεκομμένες καμπύλες), του KDAB συστήματος: (α) επιτάχυνση κορυφαίου ορόφου, (β) σχετική μετακίνηση βάσης, και (γ) σχετική μετακίνηση KDamper, για μεταβολή της ονομαστικής συχνότητας f_0 στο εύρος [0.4 1.0] Hz.*

Παρατηρούμε πως όσο αυξάνει η ονομαστική συχνότητα του KDamper (πιο στιβαρό σύστημα), μειώνονται οι σχετικές μετατοπίσεις, βάσης και KDamper, και αντίστοιχα η μέγιστη επιτάχυνση της κατασκευής αυξάνει. Οι μέγιστες κανονικοποιημένες μέσες τιμές των δυναμικών αποκρίσεων, για όλα τα 30 τεχνητά επιταχυνσιογραφήματα, παρουσιάζονται επίσης στο Σχήμα 14, και επιβεβαιώνουν πως η επιλογή της ονομαστικής συχνότητας του KDamper είναι εφικτή και ακριβής στο πεδίο της συχνότητας.

Ο KDamper μπορεί να εφαρμοσθεί σαν μία ‘στιβαρή’ βάση απορρόφησης κραδασμών ενός 3-όροφου κτιρίου από σκυρόδεμα, επιτυγχάνοντας βελτίωση της δυναμικής του συμπεριφοράς, και ταυτόχρονα διατηρώντας τις μετακινήσεις της βάσης σε πολύ χαμηλά επίπεδα. Οι παράμετροι του KDAB-1.0 συστήματος παρουσιάζονται στον Πίνακα 1.

Πίνακας 1: *Παράμετροι του KDAB-1.0 συστήματος εφαρμοσμένο στο 3-όροφο κτίριο.*

Σύστημα	m_D (tn)	k_R (kN/m)	k_D (kN/m)	k_N (kN/m)	c_D (kNs/m)
KDAB-1.0	14.5	54288	12563	-9714.3	252.82

Οι συσκευές KDamper μπορούν να λειτουργήσουν παράλληλα, και επομένως πολλαπλές συσκευές μπορούν τα τοποθετηθούν ταυτόχρονα για να αποκτήσουν τις επιθυμητές τιμές των

στοιχείων μάζας, στιβαρότητας και απόσβεσης του KDAB-1.0 που παρουσιάστηκαν στον Πίνακα 1. Μια λύση είναι η τοποθέτηση μίας συσκευής KDamper κάτω από κάθε μια κολώνα του ισογείου, όπως στην περίπτωση χρήσης συμβατικών εφεδράνων για σεισμική μόνωση. Επομένως, 16 συσκευές KDamper χρησιμοποιούνται συνολικά. Στον Πίνακα 2, παρουσιάζεται το πλήρες σετ παραμέτρων για την κάθε μια συσκευή KDamper.

Πίνακας 2: *Πλήρες σετ παραμέτρων για κάθε μία από τις 16 συσκευές KDamper.*

μ_i	κ_i	ζ_{Di}	m_D (tn)	k_R (kN/m)	k_P (kN/m)	k_N (kN/m)	c_D (kNs/m)
0.05	3.41	0.622	0.90625	3393	785.1875	-607.143	15.80125

Για τον ρεαλιστικό σχεδιασμό των επιμέρους στοιχείων κάθε μίας από τις συσκευές KDamper, πρέπει να επιλυθεί αρχικά ένα γραμμικό πρόβλημα για να έχουμε μια εκτίμηση των μέγιστων μετακινήσεων και ταχυτήτων που αφορούν τα στοιχεία στιβαρότητας και απόσβεσης, αντίστοιχα. Πιο συγκεκριμένα, η σχετική με το έδαφος μετακίνηση της πρόσθετης μάζας του KDamper αφορά τον σχεδιασμό του στοιχείου αρνητικής στιβαρότητας k_N, η σχετική με το έδαφος μετακίνηση της βάσης αφορά το στοιχείο θετικής στιβαρότητας k_R, και τέλος η σχετική μετακίνηση και ταχύτητα μεταξύ της βάσης και της πρόσθετης μάζας αφορούν το στοιχείο θετικής στιβαρότητας k_P και του τεχνητού αποσβεστήρα c_D, αντίστοιχα. Όλες οι προαναφερθείσες δυναμικές αποκρίσεις του KDAB-1.0 συστήματος, καθώς επίσης και ενός αντίστοιχου σεισμικά μονωμένου συστήματος με απλά συμβατικά εφέδρανα (BI, 5%) αλλά και με εφέδρανα υψηλής απόσβεσης (BI-HD, 15%) παρουσιάζονται στον Πίνακα 3.

Πίνακας 3: *Δυναμικές αποκρίσεις του γραμμικού προβλήματος..*

Δυναμική απόκριση		Initial	BI (5%)	BI-HD (15%)	KDAB-1.0
Drift 1^{ου} ορόφου (m)	Max	0.0628	0.0056	0.0051	0.0165
	Mean	0.0468	0.005	0.0043	0.014
Επιτάχυνση 3^{ου} ορόφου (m/sec^2)	Max	22.6782	1.7936	1.8674	6.92
	Mean	17.2292	1.5804	1.5794	5.7031
Μετακίνηση βάσης (m)	Max	-	0.234	0.1967	0.0512
	Mean	-	0.206	0.1616	0.0395
Μετακίνηση KDamper (m)	Max	-	-	-	0.2344
	Mean	-	-	-	0.174
Σχετική μετακίνηση βάσης - KDamper (m)	Max	-	-	-	0.1877
	mean	-	-	-	0.1409

Τα αποτελέσματα αφορούν τις μέσες τιμές από τα μέγιστα των δυναμικών αποκρίσεων για τα 30 τεχνητά επιταχυνσιογραφήματα της βάσης δεδομένων. Αναφορικά με την υλοποίηση του σεισμικά μονωμένου συστήματος με απλά συμβατικά εφέδρανα, επιλέγονται απλά ελαστικά εφέδρανα χαμηλής απόσβεσης. Για το σεισμικά μονωμένο σύστημα με εφέδρανα υψηλής απόσβεσης, επιλέγονται 8 *SI-S 300/128* εφέδρανα από τον κατάλογο της FIP Industriale (Elastomeric isolators - Fip Industriale). Τα συγκεκριμένα εφέδρανα έχουν ισοδύναμη ιξώδη απόσβεση μεταξύ 10-15%, και επομένως επιλέχθηκε 15% λόγος απόσβεσης για το BI-HD σύστημα. Η μέγιστη μετακίνηση σχεδιασμού και για τα συγκεκριμένα εφέδρανα είναι 25 *cm*, αρκετά μεγαλύτερη από την αντίστοιχη μέγιστη τιμή του Πίνακα 3 (19.67 *cm*). Και τα δύο σεισμικά μονωμένα συστήματα έχουν σχεδιαστεί να έχουν συχνότητα βάσης ίση με 0.4 *Hz*, σημαντικά μικρότερη από την θεμελιώδη ιδιοσυχνότητα του μη-μονωμένου συστήματος ($1/T_1=1/0.495=2.02$ *Hz*).

Το στοιχείο αρνητικής στιβαρότητας υλοποιείται με βάση την προτεινόμενη διάταξη με προ-συμπιεσμένα ελατήρια που παρουσιάστηκε στην προηγούμενη ενότητα, για μονοδιάστατη αρνητική στιβαρότητα. Το πλήρες σετ παραμέτρων για την υλοποίηση του στοιχείου αρνητικής στιβαρότητας κάθε μίας από τις 16 συσκευές KDamper παρουσιάζεται στον Πίνακα 4, με k_{NC}=-607.1437 *kN/m*.

Πίνακας 4: *Πλήρες σετ παραμέτρων του μηχανισμού αρνητικής στιβαρότητας για κάθε μία από τις 16 συσκευές KDamper.*

k_H (*kN/m*)	l_{HI} (*m*)	*a* (*m*)	*b* (*m*)	c_I
322.743	0.504	0.324	0.520	-0.05

Στο Σχήμα 15 παρουσιάζεται η μεταβολή της παραγόμενης μονοδιάστατης αρνητικής στιβαρότητας, του KDAB-1.0 συστήματος, λόγω της σχετικής μετακίνησης της βάσης και της πρόσθετης μάζας του KDamper. Παρατηρούμε πως στο εύρος -0.2344 *m* μέχρι +0.2344 *m*, που είναι η μέγιστη σχετική μετακίνηση βάσης-KDamper του γραμμικού συστήματος, όπως παρουσιάστηκε στον Πίνακα 3, η παραγόμενη μονοδιάστατη αρνητική στιβαρότητα είναι λίγο πολύ σταθερή.

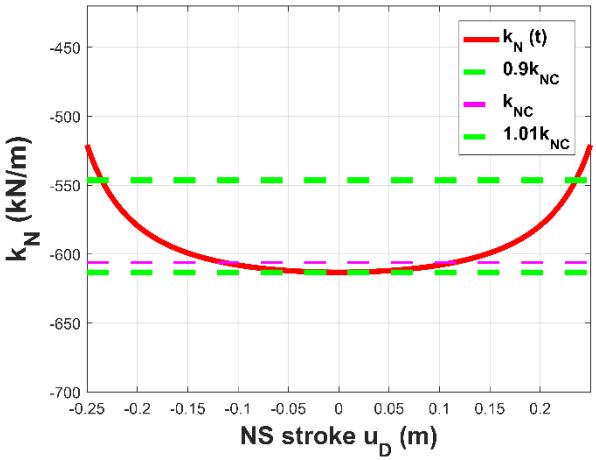

Σχήμα 15: *Μεταβολή της παραγόμενης αρνητικής στιβαρότητας, του KDAB-1.0 συστήματος, λόγω της σχετικής μετακίνησης μεταξύ της βάσης και της πρόσθετης μάζας του KDamper.*

Το υλικό που χρησιμοποιείται για την υλοποίηση της πρόσθετης μάζας για κάθε μία από τις 16 συσκευές KDamper είναι χάλυβας, με πυκνότητα ίση με ρ_{mat}=7850 kg/m^3. Υποθέτοντας κυβικό σχήμα για την πρόσθετη μάζα, η διάστασή της είναι:

$$x_{add,mass} = \sqrt[3]{(m_D / No.Columns) / \rho_{mat}} = \sqrt[3]{(14.5/16)/7.85} = 0.487m \quad (48)$$

Η μέγιστη σχετική μετακίνηση μεταξύ της βάσης και του KDamper είναι 18.77 cm. Επομένως, κοινά μεταλλικά σπειροειδή ελατήρια μπορούν να χρησιμοποιηθούν για την υλοποίηση του στοιχείου θετικής στιβαρότητας k_P. Κάθε ένας από τους αποσβεστήρες των 16 συσκευών KDamper έχει μικρή σταθερά απόσβεσης (15.8 *kNs/m*), και άρα κοινοί γραμμικοί αποσβεστήρες του εμπορίου μπορούν να τοποθετηθούν, όπως για παράδειγμα οι No./Model LD720 από τον κατάλογο της ITT Infrastructure viscous dampers catalog (Fluid Viscous Dampers, ITT Infrastructure), που έχουν μέγιστη μετακίνηση σχεδιασμού 20.0 *cm* και συνολικό αρχικό μήκος 52.2 *cm*. το στοιχείο θετικής στιβαρότητας k_R λειτουργεί τελείως ανεξάρτητα από τα υπόλοιπα στοιχεία στιβαρότητας και απόσβεσης των συσκευών KDamper, όπως φαίνεται στο Σχήμα (11.α). Επομένως, υπάρχουν ποικίλοι τρόποι υλοποίησής του, κάτι που είναι εκτός του πεδίου της παρούσας εφαρμογής. Κάποια ρεαλιστικά παραδείγματα υλοποίησης είναι απλά ελαστικά εφέδρανα, μονόπακτα μεταλλικά υποστυλώματα, κ.ά.

Η σχηματική αναπαράσταση μιας εκ των συσκευών KDamper απεικονίζεται στο Σχήμα 16, με όλες τις διαστάσεις των επιμέρους στοιχείων. Το σύστημα των μη-γραμμικών εξισώσεων κίνησης με μη-γραμμική αρνητική στιβαρότητα k_N επιλύθηκε για τα 30 τεχνητά

επιταχυνσιογραφήματα της βάσης δεδομένων με τη μέθοδο Newmark-β για γραμμικές επιταχύνσεις.

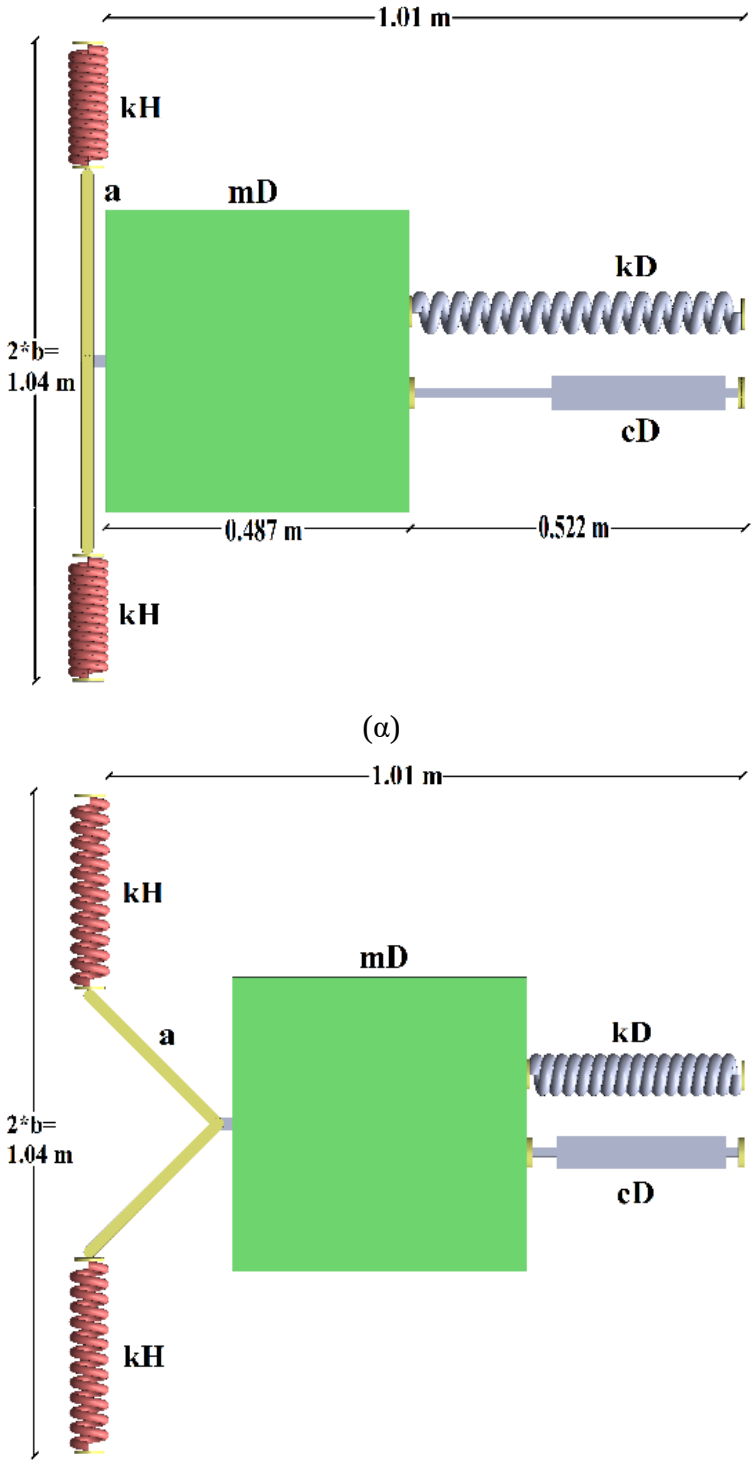

Σχήμα 16: *Σχηματική αναπαράσταση (κάτοψη) μιας εκ των 16 συσκευών KDamper του συστήματος KDAB-1.0: (α) αρχική θέση ισορροπίας, και (β) ακραία θέση.*

Στο Σχήμα 17 παρουσιάζονται συγκριτικά αποτελέσματα μεταξύ του γραμμικού και μη-γραμμικού προβλήματος θεωρώντας γραμμική και μη-γραμμική αρνητική στιβαρότητα, αντίστοιχα, μέσω της προτεινόμενης διάταξης για μονοδιάστατη αρνητική στιβαρότητα. Τα αποτελέσματα αφορούν την σχετική μετακίνηση βάσης-KDamper, την μετακίνηση βάσης, και το drift του 1^{ου} ορόφου, για ένα τεχνητό επιταχυνσιογράφημα και το KDAB-1.0 σύστημα. Παρατηρούμε ότι υπάρχει καλή ταύτιση ως προς τις κυματομορφές των αποκρίσεων, αλλά και ως προς τις μέγιστες τιμές τους.

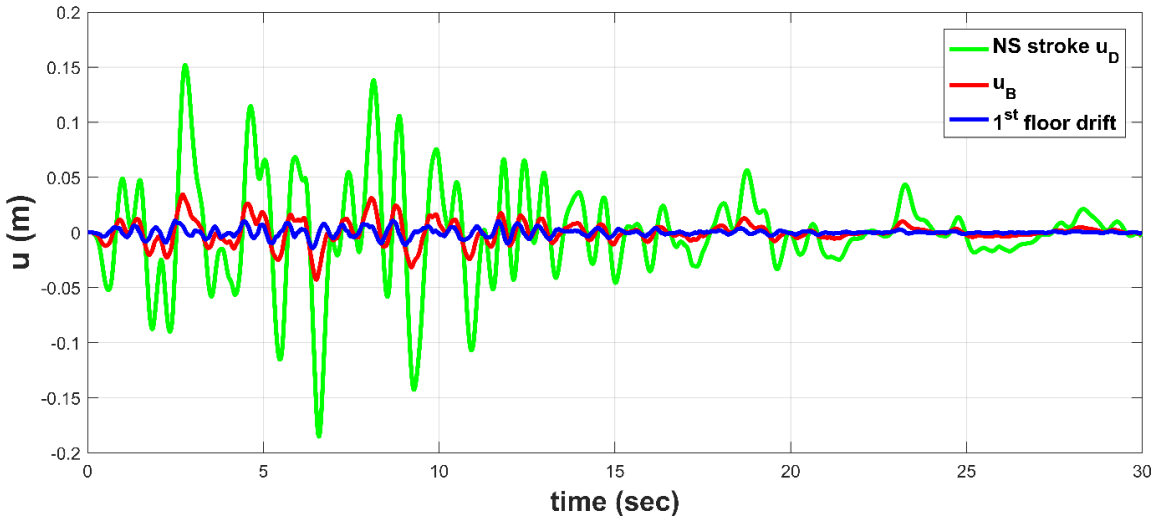

(α)

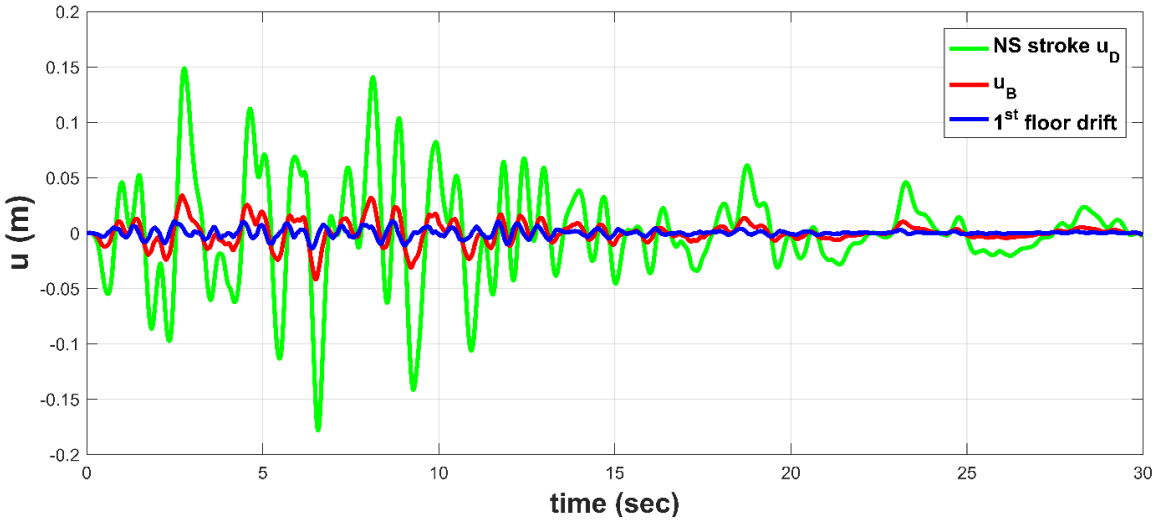

(β)

Σχήμα 17: *Δυναμικές αποκρίσεις του KDAB-1.0 συστήματος, σχετική μετακίνηση βάσης-KDamper, μετακίνηση βάσης, και drift 1^{ου} ορόφου: α) του γραμμικού προβλήματος max$|u_{KD}|$=0.1853 m, max$|u_B|$=0.0427 m, και max$|u_{drift}|$=0.0141 m, και β) του μη-γραμμικού προβλήματος max$|u_{KD}|$=0.1783 m, max$|u_B|$=0.0421 m, και max$|u_{drift}|$=0.014 m.*

Με βάση τα αποτελέσματα από τις αριθμητικές αναλύσεις, όπου ο KDamper εφαρμόστηκε ως σεισμική βάση απορρόφησης κραδασμών ενός 3-όροφου κτιρίου από σκυρόδεμα, τα ακόλουθα συγκεντρωτικά αποτελέσματα μπορούν να εξαχθούν:

i. Η επιλογή της ονομαστικής συχνότητας του KDamper στο πεδίο της συχνότητας είναι εφικτή και ακριβής, όπως επιβεβαιώθηκε από τις αναλύσεις στο πεδίο του χρόνου.
ii. Ακολουθώντας την προτεινόμενη διάταξη για την υλοποίηση του στοιχείου αρνητικής στιβαρότητας με προ-συμπιεσμένα ελατήρια, παρατηρούμε πως τα αποτελέσματα του γραμμικού και μη-γραμμικού προβλήματος είναι σε συμφωνία.
iii. Ο KDamper μπορεί να εφαρμοσθεί επιτυχώς σαν συμπλήρωμα των συμβατικών συστημάτων σεισμικής μόνωσης, μειώνοντας σημαντικά τις σχετικές μετακινήσεις μεταξύ της βάσης της κατασκευής με το έδαφος.
iv. Εναλλακτικά, ο KDamper μπορεί να εφαρμοσθεί σαν μια ‘στιβαρή’ βάση απορρόφησης κραδασμών, βελτιώνοντας την δυναμική συμπεριφορά της ανωδομής τουλάχιστον 50%, και ταυτόχρονα διατηρώντας την μετακίνηση της βάσης στην τάξη μεγέθους μερικών εκατοστών, 70% μικρότερη συγκριτικά με το υψηλής απόσβεσης σεισμικά μονωμένο σύστημα.
v. Η υλοποίηση των συσκευών KDamper είναι εφικτή με συμβατικά δομικά στοιχεία, χωρίς την ανάγκη ειδικών τύπων εφεδράνων ή πολύπλοκων διατάξεων.

V. Οριζόντια Σεισμική Προστασία με Διευρυμένα KDamper

Στη συνέχεια, παρουσιάζεται η διευρυμένη έκδοση του KDamper (EKD) και εφαρμόζεται ως σεισμική βάση απορρόφησης κραδασμών σε πολυώροφα κτίρια. Η προτεινόμενη αυτή διάταξη έχει ως στόχο την περαιτέρω μείωση των αναπτυσσόμενων μετακινήσεων της βάσης, και τη μείωση της σχετικής μετακίνησης των δύο τερματικών του στοιχείου αρνητικής στιβαρότητας, για έναν πιο ρεαλιστικό σχεδιασμό.

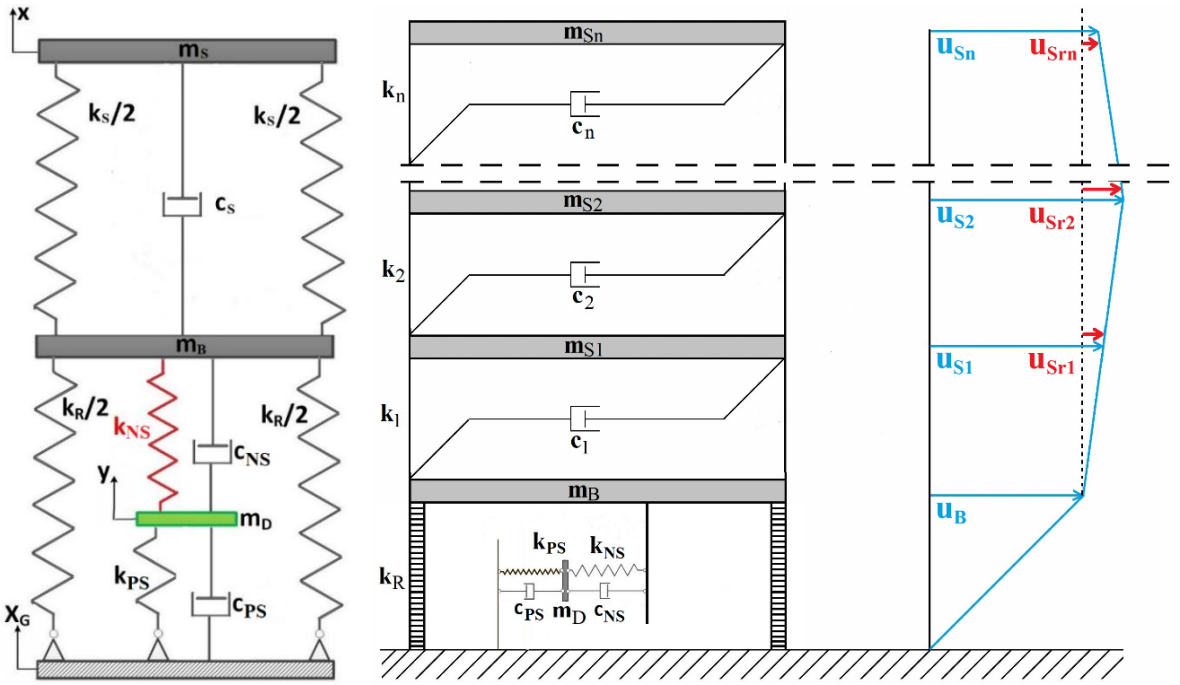

(α) (β)

Σχήμα 18: *Πιθανή εφαρμογή του EKD ως σεισμική βάση απορρόφησης κραδασμών σε: (α) ένα μονοβάθμιο ταλαντωτή, και (β) σε ένα πολυώροφο κτίριο.*

Αρχικά η βέλτιστη επιλογή των παραμέτρων του EKD γίνεται στο πεδίο της συχνότητας με την εφαρμογή του στη βάση ενός μονοβάθμιου συστήματος, αντιπροσωπευτικό μιας πολυβάθμιας κατασκευής, όπως παρουσιάζεται στο Σχήμα 18.α. Οι εξισώσεις κίνησης του συστήματος αυτού είναι:

$$m_S(\ddot{u}_S+\ddot{u}_B)+c_S\dot{u}_S+k_Su_S=-m_Sa_G \tag{49.α}$$

$$m_B\ddot{u}_B+m_S(\ddot{u}_S+\ddot{u}_B)+c_{NS}(\dot{u}_B-\dot{u}_D)+k_{NS}(u_B-u_D)+k_Ru_B=-(m_S+m_B)a_G \tag{49.β}$$

$$m_D\ddot{u}_D-c_{NS}(\dot{u}_B-\dot{u}_D)+c_{PS}\dot{u}_D-k_{NS}(u_B-u_D)+k_{PS}u_D=-m_Da_G \tag{49.γ}$$

όπου, $u_S = x_S - x_B$, $u_B = x_B - x_G$, και $u_D = x_D - x_G$. Υποθέτοντας αρμονική διέγερση στη βάση της κατασκευής της μορφής της Εξίσωσης (12), και αποκρίσεις σταθερής κατάστασης της μορφής:

$$u_S(t) = \tilde{U}_S \exp(j\omega t) \tag{50.α}$$

$$u_B(t) = \tilde{U}_B \exp(j\omega t) \tag{50.β}$$

$$u_D(t) = \tilde{U}_D \exp(j\omega t) \tag{50.γ}$$

Οι συναρτήσεις μεταφοράς των κύριων αποκρίσεων του συστήματος είναι:

$$\begin{bmatrix} \tilde{H}_{US} \\ \tilde{H}_{UB} \\ \tilde{H}_{UD} \end{bmatrix} = \begin{bmatrix} \tilde{U}_S / A_G \\ \tilde{U}_B / A_G \\ \tilde{U}_D / A_G \end{bmatrix} = -\tilde{H}^{-1} \begin{bmatrix} m_S \\ m_S + m_B \\ m_D \end{bmatrix} \tag{51.α}$$

$$\tilde{H}_{AS} = \tilde{A}_S / A_G = 1 - \omega^2 (\tilde{H}_{US} + \tilde{H}_{UB}) \tag{51.β}$$

$$\tilde{H}_{AB} = \tilde{A}_B / A_G = 1 - \omega^2 \tilde{H}_{UB} \tag{51.γ}$$

$$\tilde{H}_{AD} = \tilde{A}_D / A_G = 1 - \omega^2 \tilde{H}_{UD} \tag{51.δ}$$

$$\tilde{H} = \begin{bmatrix} -\omega^2 m_S + j\omega c_S + k_S & -\omega^2 m_S & 0 \\ -\omega^2 m_S & -\omega^2 (m_S + m_B) + j\omega c_{NS} + (k_{NS} + k_R) & -(j\omega c_{NS} + k_{NS}) \\ 0 & -(j\omega c_{NS} + k_{NS}) & -\omega^2 m_D + j\omega (c_{NS} + c_{PS}) + (k_{NS} + k_{PS}) \end{bmatrix} \tag{51.ε}$$

Η ονομαστική συχνότητα, ο λόγος απόσβεσης και οι υπόλοιποι παράμετροι του EKD συστήματος ορίζονται ως:

$$\omega_0 = 2\pi f_0 = \sqrt{k_0 / (m_S + m_B)} \tag{52.α}$$

$$\omega_D = \sqrt{(k_{PS} + k_{NS}) / \mathrm{m}_D} \tag{52.β}$$

$$\zeta_{PS} = c_{PS} / (2\omega_D m_D) = c_{PS} / \left(2\sqrt{(k_{PS} + k_{NS}) m_D}\right) \tag{52.γ}$$

$$\zeta_{NS} = c_{NS} / (2\omega_D m_D) = c_{NS} / \left(2\sqrt{(k_{PS} + k_{NS}) m_D}\right) \tag{52.δ}$$

$$k_0 = k_R + \frac{k_{PS} k_{NS}}{k_{PS} + k_{NS}} \tag{52.ε}$$

$$m_B = \mu_B m_S \tag{52.ζ}$$

$$m_D = \mu_D (m_S + m_B) \tag{52.η}$$

όπου k_0 είναι η ισοδύναμη στιβαρότητα του EKD, και μ_B, μ_D είναι ο λόγος μαζών της βάσης και του EKD, αντίστοιχα. Με βάση το φάσμα διέγερσης για οριζόντια σεισμική κίνηση του Σχήματος 9.β, λαμβάνονται οι PSDs των κύριων αποκρίσεων του EKD συστήματος:

$$S_{US} = H_{US}^2 S_A \tag{53.α}$$

$$S_{UB} = H_{UB}^2 S_A \tag{53.β}$$

$$S_{UD} = H_{UD}^2 S_A \tag{53.γ}$$

$$S_{AS} = H_{AS}^2 S_A \tag{53.δ}$$

Οι RMS τιμές των αποκρίσεων ορίζονται ως το εμβαδό των PSD καμπύλων, σαν μια ένδειξη του πραγματικού ενεργειακού περιεχομένου των αποκρίσεων:

$$R_{US} = \sqrt{\int_{-\infty}^{+\infty} S_{US}(\omega)\,\mathrm{d}\,\omega} \tag{54.α}$$

$$R_{UB} = \sqrt{\int_{-\infty}^{+\infty} S_{UB}(\omega)\,\mathrm{d}\,\omega} \tag{54.β}$$

$$R_{UD} = \sqrt{\int_{-\infty}^{+\infty} S_{UD}(\omega)\,\mathrm{d}\,\omega} \tag{54.γ}$$

$$R_{AS} = \sqrt{\int_{-\infty}^{+\infty} S_{AS}(\omega)\,\mathrm{d}\,\omega} \tag{54.δ}$$

Δεδομένου ότι είναι γνωστή η τιμή της προστιθέμενης μάζας m_D, και η τιμή του δείκτη στατικής ευστάθειας για το στοιχείο αρνητικής στιβαρότητας ε_{NS}, οι ελεύθερες παράμετροι σχεδιασμού του EKD που θα επιλεχθούν μέσα από το πρόβλημα βελτιστοποίησης είναι:

1. η ονομαστική συχνότητα του EKD, f_0;
2. η τιμή του στοιχείου αρνητικής στιβαρότητας k_{NS};
3. οι τιμές των τεχνητών αποσβεστήρων c_{NS} και c_{PS};

Τα χαρακτηριστικά του μονοβάθμιου αρχικού συστήματος (FBS) στο οποίο θα εφαρμοσθεί το EKD ως σεισμική βάση απορρόφησης κραδασμών είναι: μάζα κατασκευής m_S=300 *tn*, ιδιοσυχνότητα f_S=2 *Hz*, και λόγος απόσβεσης ζ_S=5%, ρεαλιστικές τιμές για μια κατασκευή από σκυρόδεμα. Η αντικειμενική συνάρτηση του προβλήματος βελτιστοποίησης είναι η RMS τιμή της σχετικής μετακίνησης της βάσης. Τα όρια των ελεύθερων παραμέτρων σχεδιασμού, καθώς και οι περιορισμοί που επιβάλλονται στις δυναμικές αποκρίσεις, πρέπει να είναι τέτοιοι ώστε ο σχεδιασμός του EKD συστήματος να είναι ρεαλιστικός και ταυτόχρονα αποτελεσματικός. Πιο συγκεκριμένα:

i. Ο δείκτης στατικής ευστάθειας επιλέγεται ως 10%, σε σχέση με τον KDamper που προέβλεπε 5% μεταβολή στο στοιχείο αρνητικής στιβαρότητας;
ii. Η προστιθέμενη μάζα του EKD επιλέγεται ως 5% της συνολικής μάζας του συστήματος;
iii. Με βάση την δημοσίευση (Kapasakalis at el., 2019), μια ρεαλιστική (απόλυτη μέγιστη) τιμή του στοιχείου αρνητικής στιβαρότητας είναι *-34171 kN/m*, για μια μάζα κατασκευής ίση με *300 tn*, χρησιμοποιώντας την προτεινόμενη διάταξη με προ-συμπιεσμένα ελατήρια για μονοδιάστατη αρνητική στιβαρότητα.
iv. Η μέγιστη τιμή των τεχνητών αποσβεστήρων c_{NS} και c_{PS} επιλέγεται ως *600 kNs/m*.
v. Το άνω όριο της RMS απόλυτης επιτάχυνσης της κατασκευής επιβάλλεται να είναι το πολύ 50% της αρχικής απόλυτης επιτάχυνσης του μονοβάθμιου συστήματος.

Οι συναρτήσεις μεταφοράς και οι PSD αποκρίσεις των κύριων αποκρίσεων του συστήματος παρουσιάζονται στα Σχήματα 19 και 20, όπως συγκρίνονται με το αρχικά πακτωμένο μονοβάθμιο σύστημα (FBS), και με ένα σεισμικά μονωμένο σύστημα με μια υψηλής απόσβεσης σεισμική βάση μόνωσης (BI-HD), σχεδιασμένη να έχει ονομαστική συχνότητα βάσης ίση με 0.4 *Hz* και λόγο απόσβεσης 20%. Η μέγιστη τιμή της συνάρτησης μεταφοράς της απόλυτης επιτάχυνσης της κατασκευής μειώνεται σε σχέση με το αρχικό σύστημα, σε παρόμοια επίπεδα με το BI-HD, διατηρώντας όμως σημαντικό συχνοτικό περιεχόμενο, όπως φαίνεται στο Σχήμα 19.α. Η Συνάρτηση Μεταφοράς της μετακίνησης της βάσης μειώνεται δραματικά σε όλο το εύρος συχνοτήτων με την εφαρμογή του EKD, σε σύγκριση με το υψηλής απόσβεσης σεισμικά μονωμένο σύστημα.

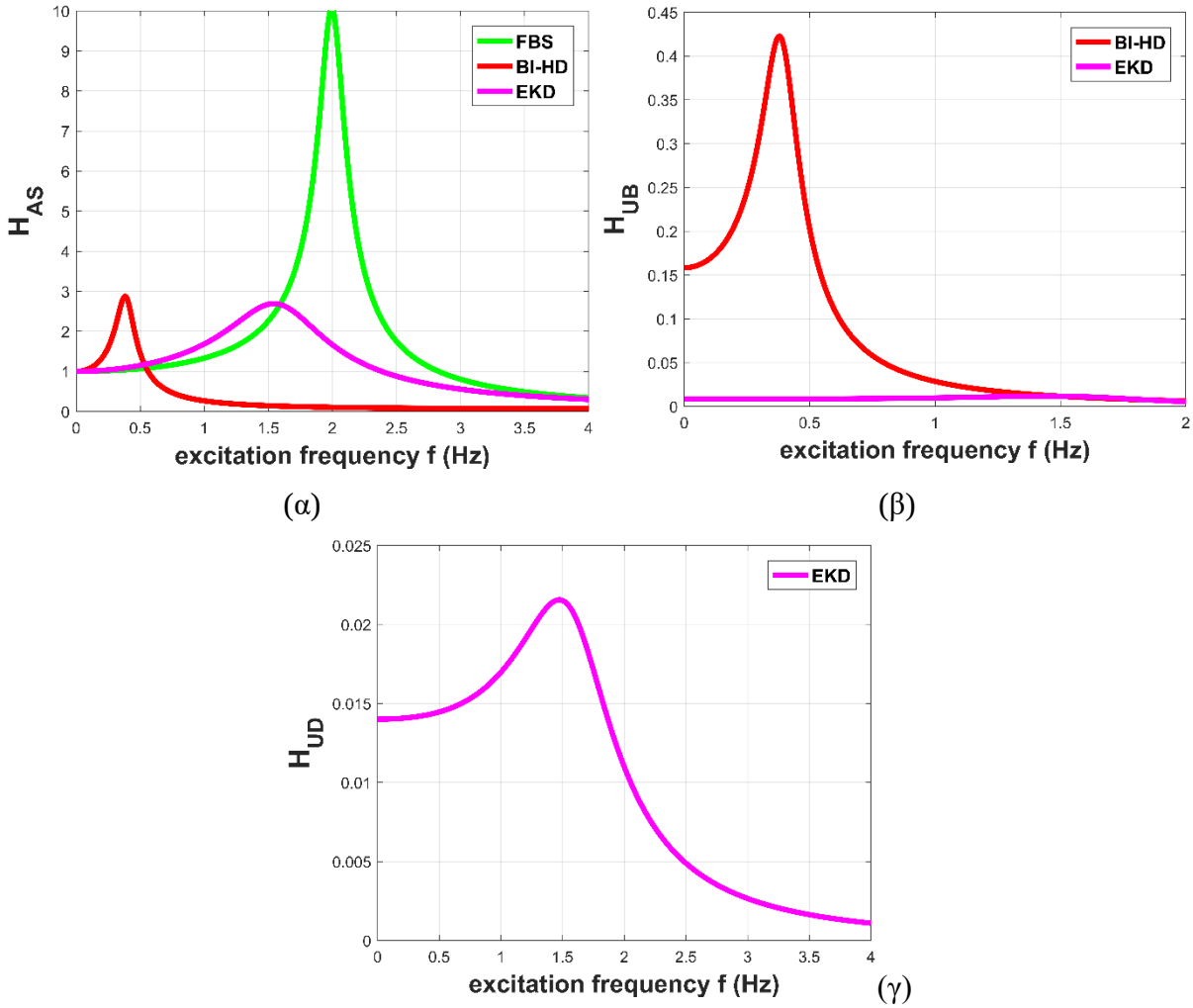

Σχήμα 19: *Συναρτήσεις Μεταφοράς των κύριων αποκρίσεων του συστήματος: (α) απόλυτη επιτάχυνση της κατασκευής* H_{AS}*, (β) σχετική μετακίνηση της βάσης* H_{UB}*, και (γ) σχετική μετακίνηση της πρόσθετης μάζας του EKD* H_{UD}*, για όλα τα εξεταζόμενα συστήματα: FBS, BI-HD, EKD.*

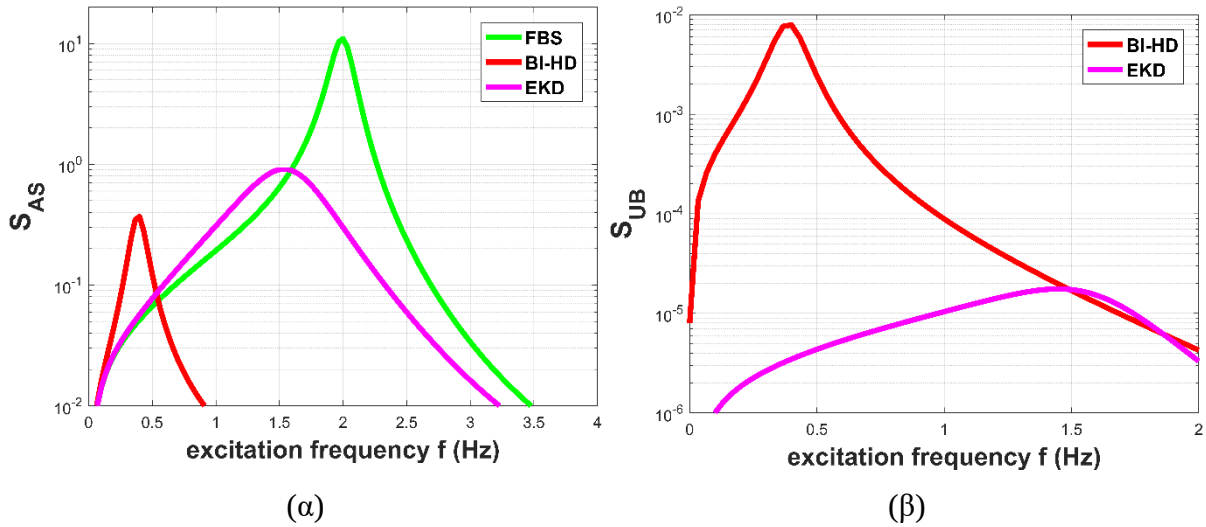

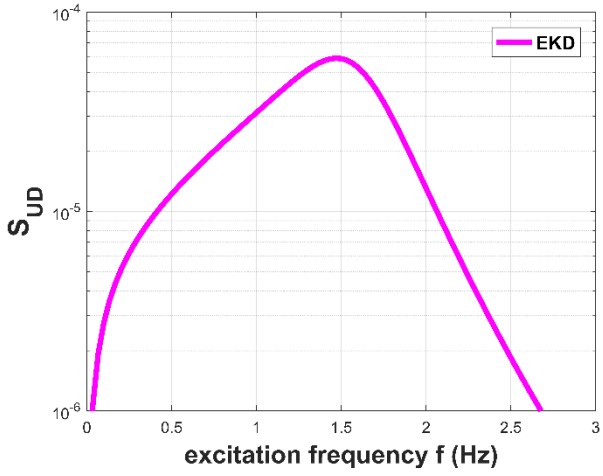

(γ)

Σχήμα 20: *PSD αποκρίσεις των κύριων αποκρίσεων του συστήματος: (α) απόλυτη επιτάχυνση της κατασκευής S_{AS}, (β) σχετική μετακίνηση της βάσης S_{UB}, και (γ) σχετική μετακίνηση της πρόσθετης μάζας του EKD S_{UD}, για όλα τα εξεταζόμενα συστήματα: FBS, BI-HD, EKD.*

Η μέγιστη τιμή της PSD επιτάχυνσης της κατασκευής με το EKD σύστημα, είναι μία τάξη μεγέθους μικρότερη σε σχέση με το αρχικό σύστημα, διατηρώντας όμως σημαντικό συχνοτικό περιεχόμενο. Η μέγιστη τιμή της PSD μετακίνησης της βάσης είναι πάνω από δύο τάξεις μεγέθους μικρότερη από εκείνη του υψηλής απόσβεσης σεισμικά μονωμένου συστήματος, με ταυτόχρονα μικρότερο συχνοτικό περιεχόμενο.

Στο Σχήμα 21 παρουσιάζονται οι RMS λόγοι των αποκρίσεων των EKD και BI-HD συστημάτων, ως προς το αρχικό πακτωμένο σύστημα (FBS) στο εύρος των ονομαστικών συχνοτήτων βάσης από 0.4 έως 2 *Hz*, και ορίζονται ως:

$$r_{AS} = \frac{R_{AS}}{R_{AS}(FBS)} \tag{55.α}$$

$$r_{UB} = \frac{R_{UB}}{R_{US}(FBS)} \tag{55.β}$$

$$r_{UD} = \frac{R_{UD}}{R_{US}(FBS)} \tag{55.γ}$$

όπου, οι τιμές $R_{US}(FBS)$ και $R_{AS}(FBS)$ αναφέρονται στο αρχικό FBS σύστημα με ιδιοσυχνότητα 2 *Hz* και λόγο απόσβεσης 5%. Όπως αναμενόταν, η r_{AS} του EKD δεν ξεπερνά το 50%, καθώς είχε τεθεί ως περιορισμός στο πρόβλημα βελτιστοποίησης. Η r_{UB} του EKD είναι πάντοτε τουλάχιστον 50% μικρότερη από εκείνη του BI-HD σε όλο το εύρος των εξεταζόμενων συχνοτήτων βάσης. Η r_{UD} του EKD μικραίνει καθώς η ονομαστική συχνότητα του EKD

μεγαλώνει. Τέλος, στο Σχήμα 21, παρουσιάζονται τα αντίστοιχα αποτελέσματα από τις δυναμικές αναλύσεις στο πεδίο του χρόνου, και παρατηρούμε πως η βέλτιστη επιλογή των παραμέτρων στο πεδίο της συχνότητας είναι ακριβής.

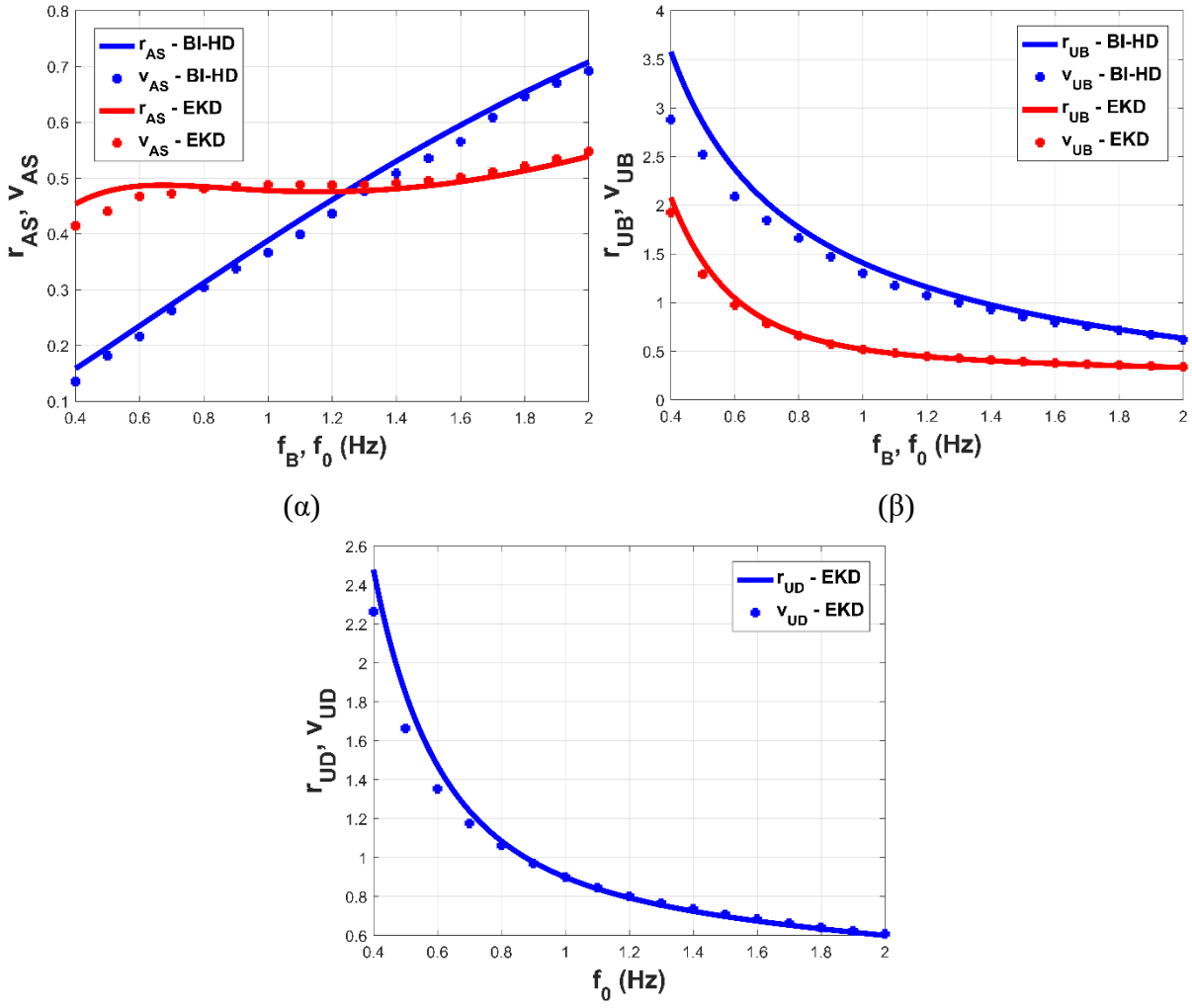

Σχήμα 21: *RMS λόγοι των αποκρίσεων (συνεχείς καμπύλες) και επαλήθευσή τους με τις δυναμικές αποκρίσεις από τις χρονοϊστορίες (διακεκομμένες καμπύλες), των BI-HD και EKD συστημάτων: (α) απόλυτη επιτάχυνση της κατασκευής, (β) σχετική μετακίνηση βάσης, και (γ) σχετική μετακίνηση της πρόσθετης μάζας του EKD, για μεταβολή της ονομαστικής συχνότητας βάσης f_B, f_0.*

Στη συνέχεια το EKD εφαρμόζεται ως σεισμική βάση απορρόφησης κραδασμών στο 3-όροφο κτίριο από σκυρόδεμα, που παρουσιάστηκε στην ενότητα 4. Οι εξισώσεις κίνησης του συστήματος με το EKD, εκφράζονται σε μητρωϊκή μορφή, και περιλαμβάνουν μητρώα διαστάσεων $r \times r$ με $r=n+2$:

$$[M][\ddot{u}(t)]+[C][\dot{u}(t)]+[K][u(t)]=-[\tau]a_G(t) \tag{56}$$

όπου τα μητρώα που υπεισέρχονται στην Εξίσωση (56) ορίζονται ως:

$$[M]_{(n+2)\times(n+2)}=\begin{bmatrix}[M_S]_{n\times n} & [0]_{n\times 1} & [0]_{n\times 1}\\ [0]_{1\times n} & m_B & 0\\ [0]_{1\times n} & 0 & m_D\end{bmatrix} \tag{57.α}$$

$$[K]_{(n+2)\times(n+2)}=\begin{bmatrix}[K_S]_{n\times n} & [0]_{n\times 1} & [0]_{n\times 1}\\ [0]_{1\times n} & k_{NS}+k_R & -k_{NS}\\ [0]_{1\times n} & -k_{NS} & k_{PS}+k_{NS}\end{bmatrix} \tag{57.β}$$

$$[C]_{(n+2)\times(n+2)}=\begin{bmatrix}[C_S]_{n\times n} & [0]_{n\times 1} & [0]_{n\times 1}\\ [0]_{1\times n} & c_{NS} & -c_{NS}\\ [0]_{1\times n} & -c_{NS} & c_{PS}+c_{NS}\end{bmatrix} \tag{57.γ}$$

$$[u_{(t)}]_{(n+2)\times 1}=\begin{bmatrix}[u_{S(t)}]\\ u_{B(t)}\\ u_{D(t)}\end{bmatrix};\quad [\tau]_{(n+2)\times 1}=\begin{bmatrix}[M][1]_{n\times 1}\\ m_B\\ m_D\end{bmatrix};\quad m_D=\mu_D m_{S,tot}=\mu_D\left(m_B+\sum_{i=1}^{n}m_i\right) \tag{57.δ}$$

Οι παράμετροι του EKD επιλέγονται από το πρόβλημα βελτιστοποίησης που διατυπώθηκε προηγουμένως, για την γενική περίπτωση που το EKD εφαρμόζεται ως σεισμική βάση απορρόφησης κραδασμών ενός μονοβάθμιου συστήματος, και αντιπροσωπεύει την ανωδομή της κατασκευής, που στην προκειμένη περίπτωση είναι το υπό εξέταση 3-όροφο κτίριο. Οι παράμετροι του συστήματος παρουσιάζονται στον Πίνακα 5.

Πίνακας 5: *Παράμετροι του EKD συστήματος.*

μ (%)	$kn=k_{NS}/ki$	$kp=k_{PS}/ki$	$kr=k_R/ki$	c_{NS} (*kNs/m*)	f_0 (Hz)
5	-0.53	0.83	1.93	588	1.65

όπου *ki* είναι η συνολική στιβαρότητα του *i*-ορόφου και είναι ίση με 65000 *kN/m*. Οι συναρτήσεις μεταφοράς των κύριων αποκρίσεων του συστήματος παρουσιάζονται στο Σχήμα 22. Το EKD μειώνει την μέγιστη τιμή της συνάρτησης μεταφοράς της απόλυτης επιτάχυνσης H_{AS}, σε σύγκριση με το αρχικό σύστημα, διατηρώντας ωστόσο σημαντικό συχνοτικό περιεχόμενο, όπως φαίνεται στο Σχήμα 22.α. Η συνάρτηση μεταφοράς της μετακίνησης της βάσης H_{UB} μειώνεται δραματικά σε όλο το φάσμα συχνοτήτων, σε σύγκριση με το BI-HD.

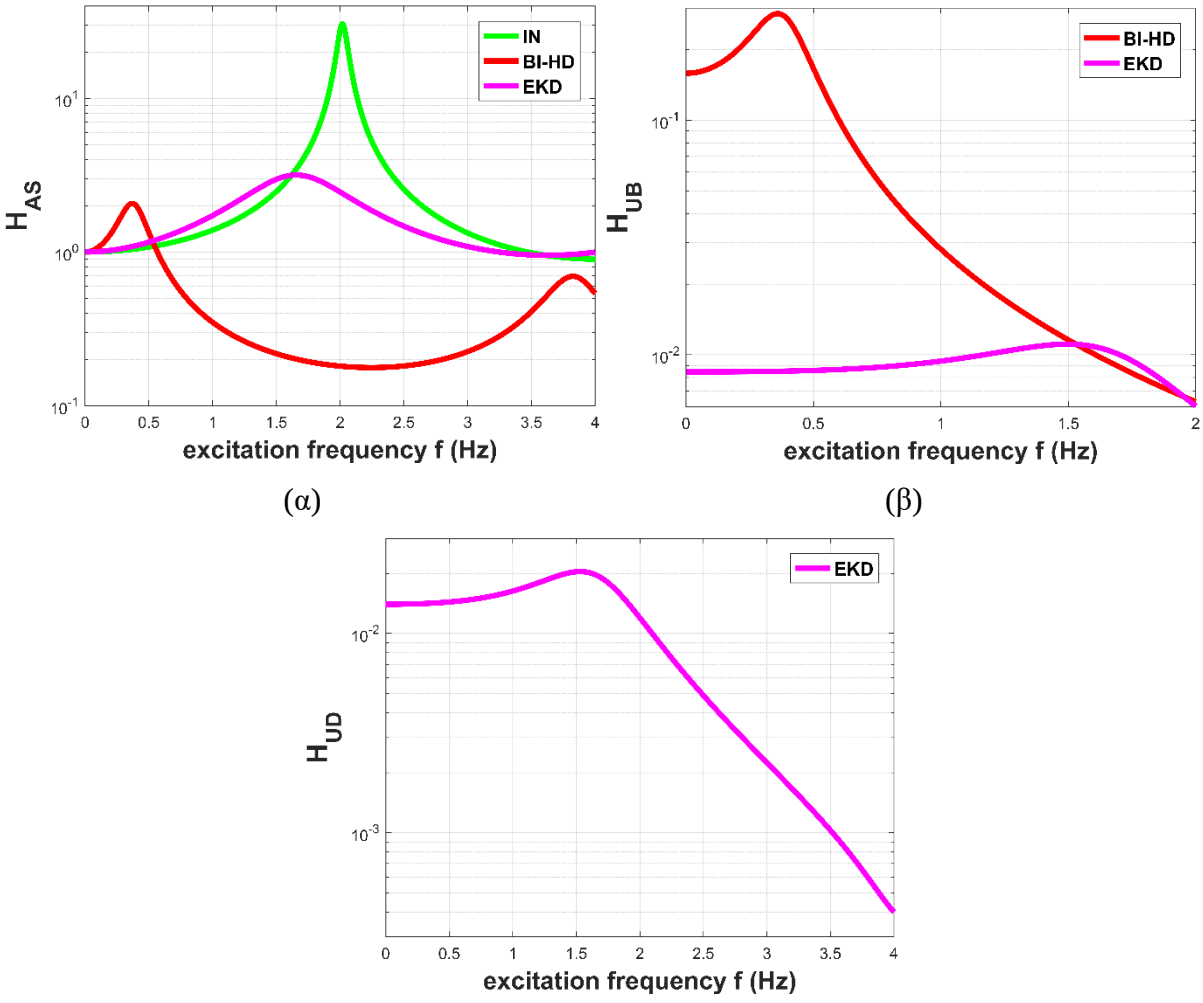

(α) (β)

(γ)

Σχήμα 22: *Συναρτήσεις Μεταφοράς των κύριων αποκρίσεων του συστήματος: (α) απόλυτη επιτάχυνση του ανώτερου ορόφου H_{AS}, (β) μετακίνηση της βάσης H_{UB}, και (γ) μετακίνηση της πρόσθετης μάζας του EKD H_{UD}, για όλα τα εξεταζόμενα συστήματα: IN, BI-HD, and EKD.*

Στη συνέχεια, διερευνάται η υλοποίηση των επιμέρους στοιχείων του EKD εφαρμοσμένο στο υπό εξέταση 3-όροφο κτίριο από σκυρόδεμα. Οι συνολικές παράμετροι παρουσιάζονται στον Πίνακα 5. Οι συσκευές EKD μπορούν να λειτουργήσουν παράλληλα, και επομένως πολλαπλές συσκευές EKD μπορούν να τοποθετηθούν, και στην προκειμένη περίπτωση τοποθετούνται τέσσερις στο σύνολο συσκευές. Αναφορικά με την υλοποίηση των επιμέρους στοιχείων της κάθε μιας παρουσιάζονται τα παρακάτω:

1. Το υλικό που χρησιμοποιείται για την υλοποίηση της πρόσθετης μάζας είναι άοπλο σκυρόδεμα με πυκνότητα ίση με ρ_{mat}=2400 kg/m^3. Οι διαστάσεις που προκύπτουν υποθέτοντας τετραγωνική κάτοψη είναι $2\times2\times0.4$ m.

2. Τέσσερις τεχνητοί αποσβεστήρες τοποθετούνται σε κάθε μια από τις τέσσερις συσκευές EKD, και επομένως η σταθερά του κάθε αποσβεστήρα είναι μικρή (36.75 *kNs/m*), οπότε κοινοί γραμμικοί αποσβεστήρες χρησιμοποιούνται, όπως για παράδειγμα το μοντέλο Catalog No./Model LD1160 από τον κατάλογο της ITT Infrastructure (Fluid Viscous Dampers | ITT Infrastructure, n.d.).
3. Τα στοιχεία θετικής στιβαρότητας k_R και k_{PS} υλοποιούνται με απλά ελαστικά εφέδρανα.
4. Το στοιχείο αρνητικής στιβαρότητας υλοποιείται με την δεύτερη προτεινόμενη διάταξη που παράγει δισδιάστατη αρνητική στιβαρότητα, που παρουσιάστηκε στην τρίτη ενότητα.

Για την υλοποίηση του κατακόρυφου στοιχείου θετικής στιβαρότητας k_H που χρησιμοποιείται στην προτεινόμενη διάταξη για δισδιάστατη αρνητική στιβαρότητα, χρησιμοποιούνται απλά μεταλλικά σπειροειδή ελατήρια. Για να αποφύγουμε πλευρικό λυγισμό και υπέρβαση της μέγιστης διατμητικής αντοχής τους, χρησιμοποιούνται τέσσερα τεμάχια που περιέχουν εννέα σπειροειδή ελατήρια το κάθε ένα. Στο Σχήμα 23 παρουσιάζεται το προαναφερθέντα τεμάχιο στην θέση ισορροπίας, καθώς και στην ακραία θέση με όλες τις διαστάσεις του. Τέλος, στο Σχήμα 24, παρουσιάζεται η συνολική διάταξη του EKD στην θέση ισορροπίας και στην ακραία θέση.

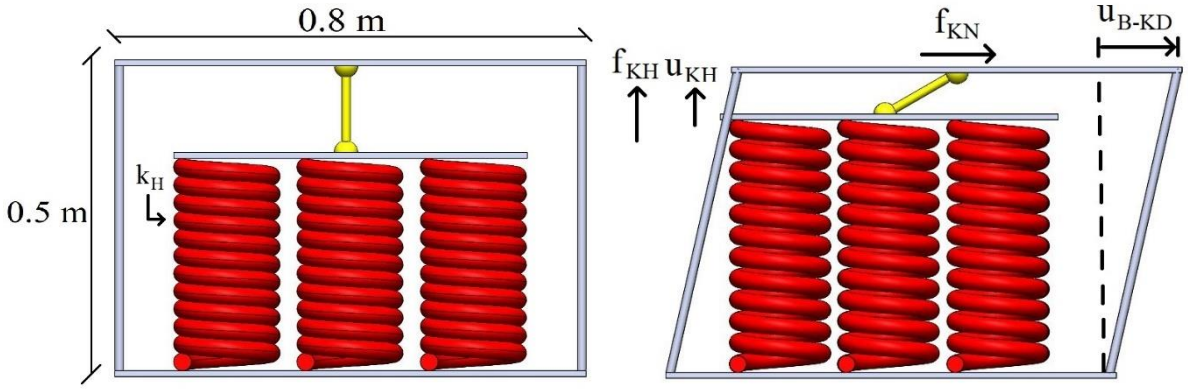

Σχήμα 23: *Προτεινόμενη διάταξη για την υλοποίηση δισδιάστατης αρνητικής στιβαρότητας. (α) Αρχική κατάσταση, και (β) ακραία θέση.*

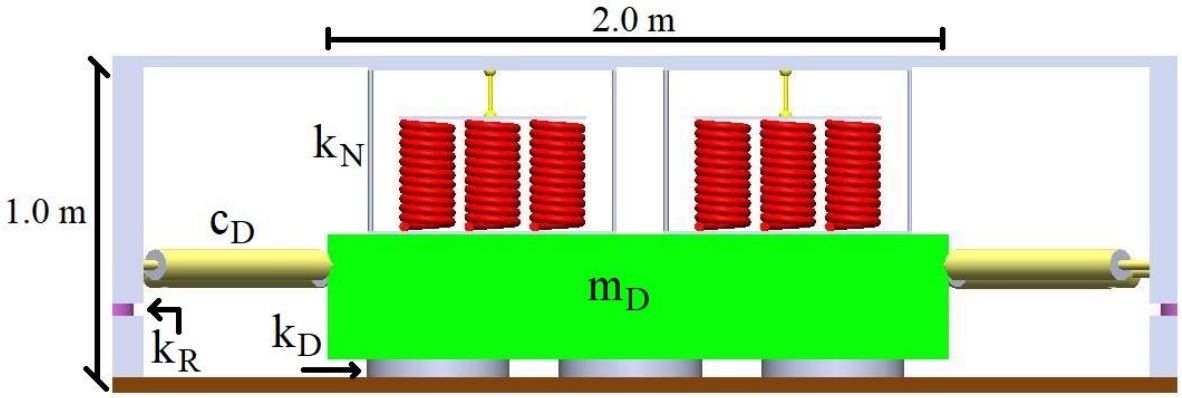

(α)

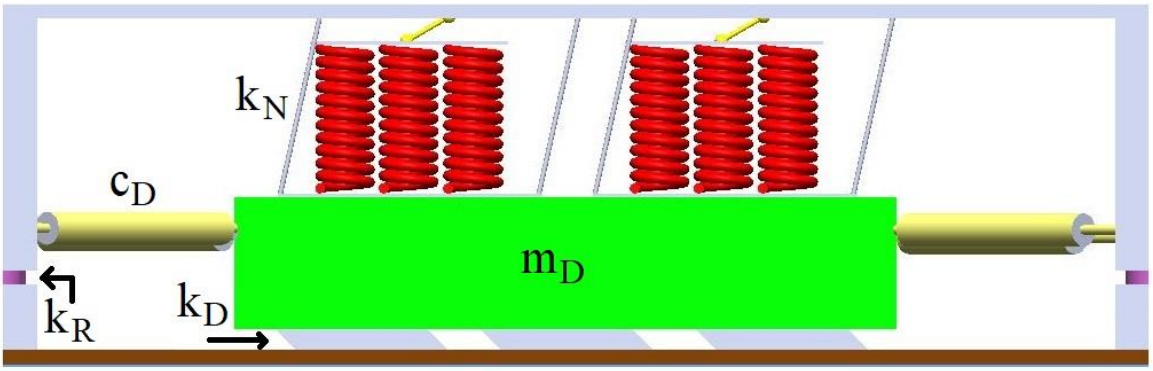

(β)

Σχήμα 24: *Σχηματική αναπαράσταση (όψη) της προτεινόμενης διάταξης του EKD στην (α) αρχική θέση ισορροπίας, και (β) στην ακραία θέση.*

Η εφαρμογή του EKD στο υπό εξέταση 3-όροφο κτίριο από σκυρόδεμα παρουσιάζεται λεπτομερώς στο Σχήμα 25.

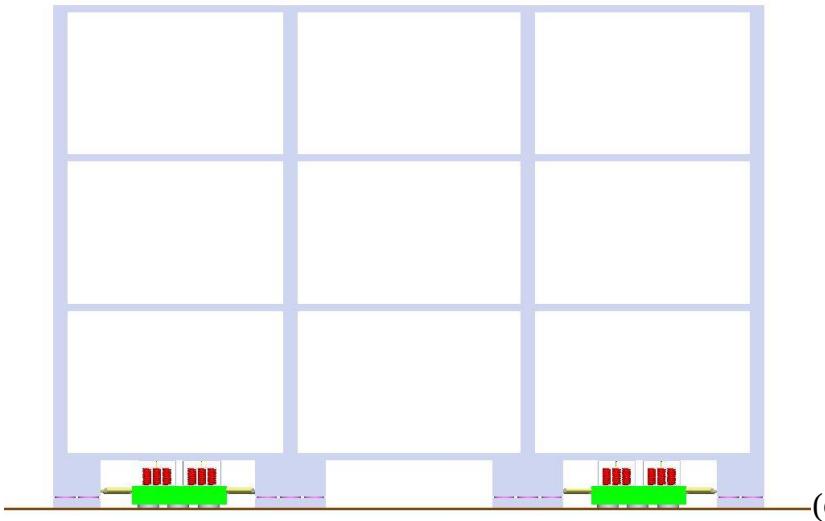

(α)

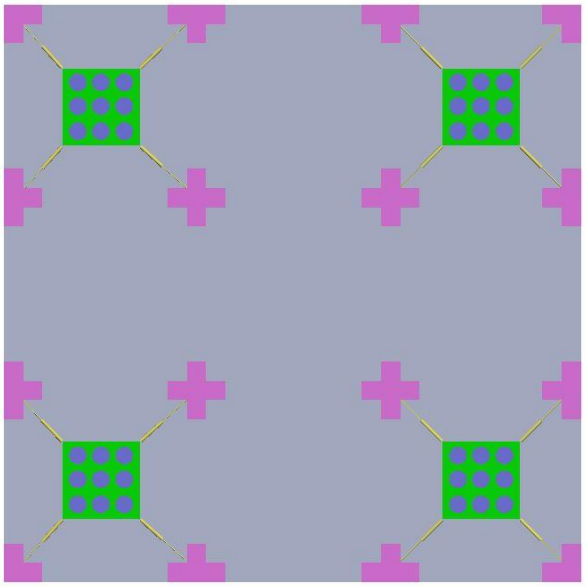

(β)

Σχήμα 25: *3-όροφο κτίριο από σκυρόδεμα με 4 συσκευές EKD στο σύνολο. (α) Όψη, και (β) άνοψη του κτιρίου.*

Η απόδοση του EKD αξιολογείται με πραγματικούς σεισμούς, που παρουσιάζονται στον Πίνακα 6. Ενδεικτικά αποτελέσματα παρουσιάζονται στις χρονοϊστορίες του Σχήματος 26. Τα αποτελέσματα αφορούν την απόλυτη επιτάχυνση του ανώτερου ορόφου και την μετακίνηση της βάσης, για τους σεισμούς του Izmit, L'Aquila, και ενός τεχνητού επιταχυνσιογραφήματος.

Πίνακας 6: *PGA των πραγματικών σεισμών που εξετάστηκαν.*

	Northridge	El Centro	Kobe	L'Aquila	Tabas	Izmit	Aigio
PGA (*g*)	0.43	0.35	0.28	0.34	0.85	0.23	0.54

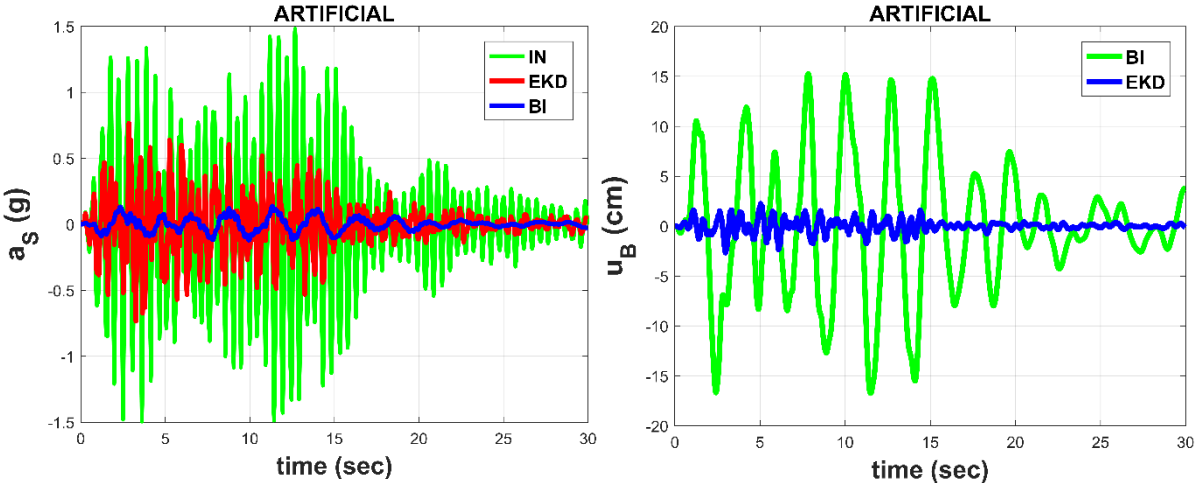

(α) (β)

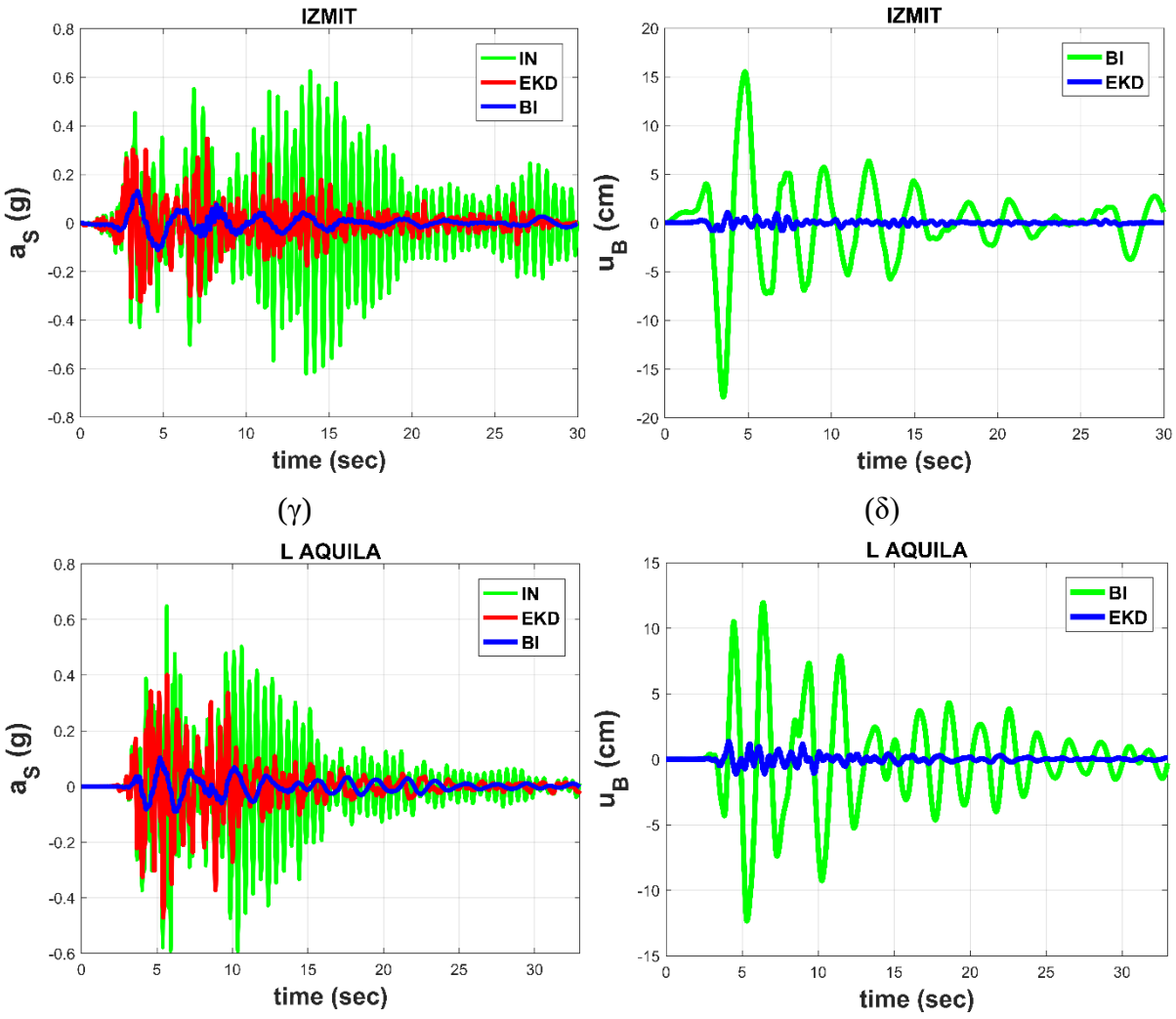

Σχήμα 26: *Συγκριτικά αποτελέσματα, σε όρους απόλυτης επιτάχυνσης του ανώτερου ορόφου και μετακίνησης βάσης, μεταξύ των IN, BI, και του EKD συστήματος, για (α, β) ένα τεχνητό επιταχυνσιογράφημα, (γ, δ) τον Izmit, και (ε, ζ) τον L' Aquila σεισμό.*

Στον Πίνακα 7 παρουσιάζονται οι μέγιστες τιμές και τα ποσοστά μείωσης σε σχέση με το αρχικά πακτωμένο 3-όροφο κτίριο από σκυρόδεμα της απόλυτης επιτάχυνσης του ανώτερου ορόφου, το drift του 1^{ου} ορόφου, η σχετική μετακίνηση της βάσης, η σχετική μετακίνηση της πρόσθετης μάζας του EKD, και η σχετική μετακίνηση των τερματικών του στοιχείου αρνητικής στιβαρότητας, k_{NS}, για τους πραγματικούς σεισμούς που εξετάστηκαν (Πίνακας 6), και τα 30 τεχνητά επιταχυνσιογραφήματα της βάσης δεδομένων (μέση τιμή των 30 μεγίστων) για οριζόντια σεισμική κίνηση.

Πίνακας 7: *Κύριες δυναμικές αποκρίσεις λαμβάνοντας υπόψη τις μέγιστες τιμές από τις δυναμικές αποκρίσεις, και τα ποσοστά μείωσης σε σχέση με το αρχικό 3-όροφο κτίριο.*

		Northridge	El Centro	Kobe	L'Aquila	Tabas	Izmit	Aigio	Artificial
a_S (m/sec^2) 3ου ορόφου	Initial	13,07	13,67	6,66	6,36	30,16	6,14	23,93	17.23
	KDamper	8,18	6,98	5,10	4,62	18,65	3,41	11,51	7.86
	(%)	**37,39**	**48,98**	**23,34**	**27,35**	**38,14**	**44,39**	**51,92**	**54,38**
Drift (m) 1ου ορόφου	Initial	0,033	0,033	0,021	0,017	0,071	0,016	0,061	0.047
	KDamper	0,022	0,021	0,016	0,010	0,038	0,008	0,030	0.02
	(%)	**33,17**	**34,84**	**23,44**	**39,05**	**46,47**	**49,77**	**51,02**	**57,45**
u_B (m)	KDamper	0,029	0,022	0,025	0,014	0,044	0,011	0,031	0.024
u_D (m)	KDamper	0,052	0,040	0,043	0,024	0,072	0,019	0,057	0.043
u_{B-D} (m)	KDamper	0,079	0,060	0,066	0,037	0,107	0,028	0,084	0.064

Με βάση τα αποτελέσματα από τις αριθμητικές αναλύσεις, όπου το EKD εφαρμόστηκε ως σεισμική βάση απορρόφησης κραδασμών ενός 3-όροφου κτιρίου από σκυρόδεμα, τα ακόλουθα συγκεντρωτικά αποτελέσματα μπορούν να εξαχθούν:

1. Τα drift των ορόφων είναι μικρά (2-3 *cm*), 30-60% χαμηλότερα σε σύγκριση με το αρχικό 3-όροφο κτίριο από σκυρόδεμα.
2. Οι επιταχύνσεις του ανώτερου ορόφου μειώνονται κατά 30-50%.
3. Η σχετική μετακίνηση των τερματικών του στοιχείου αρνητικής στιβαρότητας είναι σε αποδεκτά όρια (5-10 *cm*).
4. Η μετακίνηση της βάσης είναι πολύ μικρή (2-4 *cm*), και επομένως η υλοποίηση του στοιχείου θετικής στιβαρότητας k_R είναι εφικτή με συμβατικά δομικά στοιχεία, χωρίς την ανάγκη εξελιγμένων εφεδράνων ή πολύπλοκων διατάξεων.

Σύμφωνα με τα παραπάνω, το EKD είναι μια ρεαλιστική εναλλακτική των υπαρχόντων συστημάτων σεισμικής μόνωσης/προστασίας για πολυώροφα κτίρια.

Στη συνέχεια προστίθεται ένα στοιχείο αδράνειας (inerter) παράλληλα στο στοιχείο θετικής στιβαρότητας k_R. Η προτεινόμενη αυτή διάταξη (SBA) έχει ως στόχο την μείωση της θεμελιώδους ιδιοσυχνότητας της κατασκευής χωρίς την προσθήκη επιπλέον μαζών ή μείωση της συνολικής στιβαρότητας, με αποτέλεσμα την μείωση των επιταχύνσεων. Στην συνέχεια, οι μεγάλες σχετικές μετατοπίσεις που θα αναπτυσσόντουσαν, περιορίζονται σημαντικά με τις εξαιρετικές ιδιότητες απόσβεσης του προσφέρει ο EKD, όταν σχεδιαστεί κατάλληλα. Ο

βέλτιστος σχεδιασμός του SBA ακολουθεί αντίστοιχο πρόβλημα βελτιστοποίησης με το EKD, έχοντας μια επιπλέον ελεύθερη παράμετρο σχεδιασμού, τον inerter. Η σταθερά του inerter εκφράζεται ως ποσοστό της συνολικής μάζας της κατασκευής.

Ο σχεδιασμός του SBA συστήματος προβλέπει μεταβολή σε όλα τα στοιχεία στιβαρότητας, σε αντίθεση με το EKD, που προβλέπει μόνο στο στοιχείο αρνητικής στιβαρότητας. Επιπλέον, η προστιθέμενη μάζα του SBA επιλέγεται 0.1% της συνολικής μάζας της κατασκευής, σε σχέση με το 5% που θεωρήθηκε για τον σχεδιασμό του EKD. Δεδομένου ότι είναι γνωστές οι τιμές των δεικτών στατικής ευστάθειας (10%) και ο λόγος της πρόσθετης μάζας (0.1%), οι ελεύθερες παράμετροι σχεδιασμού του SBA είναι: 1) η ονομαστική συχνότητα του SBA f_0, 2) το στοιχείο αρνητικής στιβαρότητας k_{NS}, 3, 4) οι τεχνητοί αποσβεστήρες c_{NS} και c_{PS}, και 5) ο inerter, b. Επιπλέον, επιβάλλεται ένα φίλτρο επιτάχυνσης (AF), ώστε να παρατηρούμε πιο εύκολα την αποτελεσματικότητα του συστήματος. Κάθε σετ παραμέτρων του SBA-*AF* θα εκφράζει πως η μέγιστη επιτάχυνση του συστήματος θα είναι *AF*% του μέσου PGA. Στο Σχήμα 27, παρουσιάζονται τα αποτελέσματα της βελτιστοποίησης για μέγιστη τιμή της σταθεράς αδράνειας του inerter ίση με 0 (EKD σύστημα), 1 και 2.

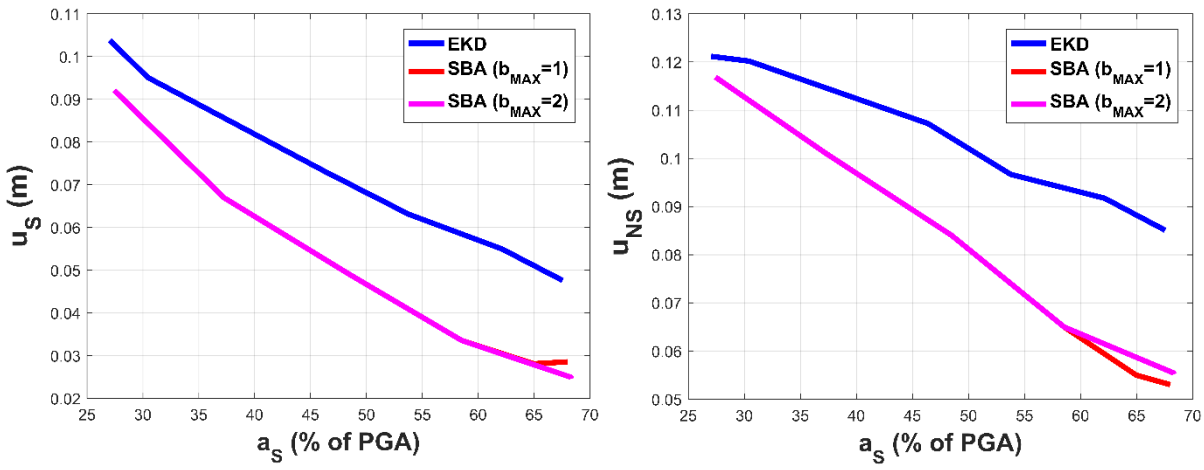

(α) (β)

Σχήμα 27: *(α) Σχετική μετατόπιση κατασκευής, και (β) σχετική μετατόπιση των τερματικών του στοιχείου αρνητικής στιβαρότητας, στο εύρος του επιβαλλόμενου φίλτρου επιταχύνσεων [25 70]%PGA, για διάφορα άνω όρια της σταθεράς του inerter.*

Παρατηρούμε ότι σε όλο το εύρος του επιβαλλόμενου φίλτρου επιτάχυνσης, η προσθήκη του inerter (SBA σύστημα) βελτιώνει τη δυναμική συμπεριφορά του συστήματος και μειώνει σημαντικά τη σχετική μετατόπιση των τερματικών του στοιχείου αρνητικής στιβαρότητας. Ωστόσο, αύξηση της σταθεράς του inerter άνω της μονάδας (100%) δεν έχει καμία επίδραση στην απόδοση του συστήματος.

Στη συνέχεια το SBA εφαρμόζεται ως σεισμική βάση απορρόφησης κραδασμών στο 3-όροφο κτίριο από σκυρόδεμα, που παρουσιάστηκε προηγουμένως. Οι εξισώσεις κίνησης του συστήματος με το SBA, εκφράζονται σε μητρωϊκή μορφή, και περιλαμβάνουν μητρώα διαστάσεων $r \times r$ με $r=n+2$:

$$[M][\ddot{u}(t)]+[C][\dot{u}(t)]+[K][u(t)]=-[\tau]a_G(t) \tag{58}$$

όπου τα μητρώα που υπεισέρχονται στην Εξίσωση (58) ορίζονται ως:

$$[M]_{(n+2)\times(n+2)}=\begin{bmatrix}[M_S]_{n\times n} & [0]_{n\times 1} & [0]_{n\times 1}\\ [0]_{1\times n} & m_B+m_b & 0\\ [0]_{1\times n} & 0 & m_D\end{bmatrix} \tag{59.α}$$

$$[K]_{(n+2)\times(n+2)}=\begin{bmatrix}[K_S]_{n\times n} & [0]_{n\times 1} & [0]_{n\times 1}\\ [0]_{1\times n} & k_{NS}+k_R & -k_{NS}\\ [0]_{1\times n} & -k_{NS} & k_{PS}+k_{NS}\end{bmatrix} \tag{59.β}$$

$$[C]_{(n+2)\times(n+2)}=\begin{bmatrix}[C_S]_{n\times n} & [0]_{n\times 1} & [0]_{n\times 1}\\ [0]_{1\times n} & c_{NS} & -c_{NS}\\ [0]_{1\times n} & -c_{NS} & c_{PS}+c_{NS}\end{bmatrix} \tag{59.γ}$$

$$[u_{(t)}]_{(n+2)\times 1}=\begin{bmatrix}[u_{S(t)}]\\ u_{B(t)}\\ u_{D(t)}\end{bmatrix};\quad [\tau]_{(n+2)\times 1}=\begin{bmatrix}[M][1]_{n\times 1}\\ m_B\\ m_D\end{bmatrix};\quad m_D=\mu_D m_{S,tot}=\mu_D\left(m_B+\sum_{i=1}^{n}m_i\right) \tag{59.δ}$$

Οι παράμετροι του SBA επιλέγονται από το πρόβλημα βελτιστοποίησης που διατυπώθηκε προηγουμένως, για την γενική περίπτωση που το SBA εφαρμόζεται ως σεισμική βάση απορρόφησης κραδασμών ενός μονοβάθμιου συστήματος, που αντιπροσωπεύει την ανωδομή της κατασκευής, που στην προκειμένη περίπτωση είναι το υπό εξέταση 3-όροφο κτίριο. Οι παράμετροι του SBA-*70* συστήματος παρουσιάζονται στον Πίνακα 8.

Πίνακας 8: *Παράμετροι του SBA συστήματος.*

	f_0 (Hz) without b	f_0 (Hz) with b	k_{NS} (kN/m)	k_{PS} (kN/m)	k_R (kN/m)	c_{NS} (kNs/m)	c_{PS} (kNs/m)	b (%m_{tot})	m_D (%m_{tot})
SBA-*70*	1.5	1.07	-14287	24467	60996	564.2	394.1	97	0.1

Για να αξιολογηθεί η αποδοτικότητα του SBA, συγκρίνεται με άλλα σεισμικά μονωμένα συστήματα. Πιο συγκεκριμένα, με ένα συμβατικά μονωμένο σύστημα με απλά ελαστικά εφέδρανα (BI, 5%), με ένα υψηλής απόσβεσης μονωμένο σύστημα με εφέδρανα υψηλής απόσβεσης ή με πυρήνα μολύβδου (BI-HD, 20%), με ένα συμβατικά σεισμικά μονωμένο σύστημα με inerter (BI-I), και με ένα σύστημα με EKD. Τα συστήματα αυτά υποβάλλονται στα 30 τεχνητά επιταχυνσιογραφήματα της βάσης δεδομένων, καθώς και σε 12 πραγματικούς σεισμούς κοντινού και μακρινού πεδίου, που παρουσιάζονται στον Πίνακα 9.

Πίνακας 9: *Λίστα και πληροφορίες των υπό εξέταση πραγματικών σεισμικών διεγέρσεων.*

No	Earthquake	Year	Station	Motion	Mw	PGA (g)	R_{jb} (km)	$Dur_{5\text{-}75\%}$ (sec)
1	Northridge-N	1994	N Hollywood	Near fault	6.69	0.309	7.89	7.0
2	Northridge-F	1994	Montebello	Far fault	6.69	0.176	43.2	7.8
3	Loma Prieta-N	1989	Corralitos	Near fault	6.93	0.645	0.16	4.6
4	Loma Prieta-F	1989	Apeel 10-Skyline	Far fault	6.93	0.103	41.9	8.3
5	L'Aquila-N	2009	V. Aterno	Near fault	6.3	0.402	0.0	4.7
6	L'Aquila-F	2009	Ortucchio	Far fault	6.3	0.066	35.1	6.2
7	Chi-Chi-N	1999	CHY006	Near fault	7.62	0.359	9.76	5.6
8	Chi-Chi-F	1999	CHY012	Far fault	7.62	0.063	59.0	42.8
9	Kocaeli-N	1999	Izmit	Near fault	7.51	0.165	3.62	8.2
10	Kocaeli-F	1999	Fatih	Far fault	7.51	0.162	53.3	27.8
11	Tabas-N	1978	Tabas	Near fault	7.35	0.854	1.79	8.3
12	Tabas-F	1978	Ferdows	Far fault	7.35	0.093	89.8	20.5
13	Kobe-N	1995	Amagasaki	Near fault	6.9	0.276	11.3	6.9
14	Kobe-F	1995	HIK	Far fault	6.9	0.139	95.7	6.1
15	Kozani-N	1995	Kozani	Near fault	6.4	0.207	14.1	3.3
16	Kozani-F	1995	Larisa	Far fault	6.4	0.031	74.1	21.7
17	Niigata-N	2004	NIG017	Near fault	6.63	0.378	4.22	6.1
18	Niigata-F	2004	FKS020	Far fault	6.63	0.043	101	22.5
19	Landers-N	1992	Joshua tree	Near fault	7.28	0.274	11.0	21.7
20	Landers-F	1992	Boron fire station	Far fault	7.28	0.119	89.7	9.6
21	Duzce-N	1999	Lamont 1059	Near fault	7.14	0.1524	4.17	10.4
22	Duzce-F	1999	Mudurnu	Far fault	7.14	0.1203	34.3	9.6
23	Friuli-N	1976	Tolmezzo	Near fault	6.5	0.3571	14.97	2.5
24	Friuli-F	1976	Barcis	Far fault	6.5	0.0292	49.13	4.3

Στο Σχήμα 28 παρουσιάζονται οι κύριες αποκρίσεις των προαναφερθέντων συστημάτων (μέσες μέγιστες τιμές) για όλες τις επιλεγμένες σεισμικές διεγέρσεις.

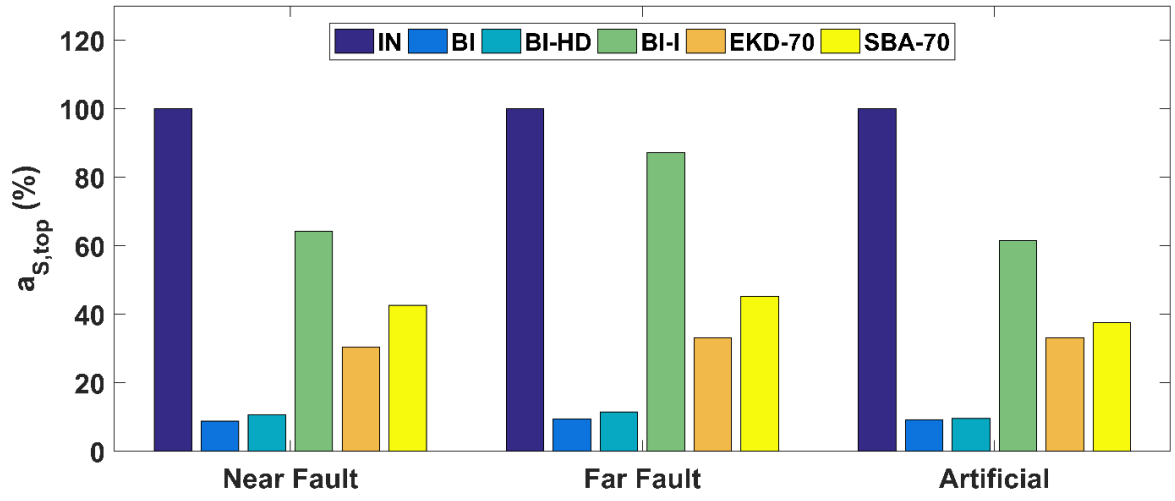

(α)

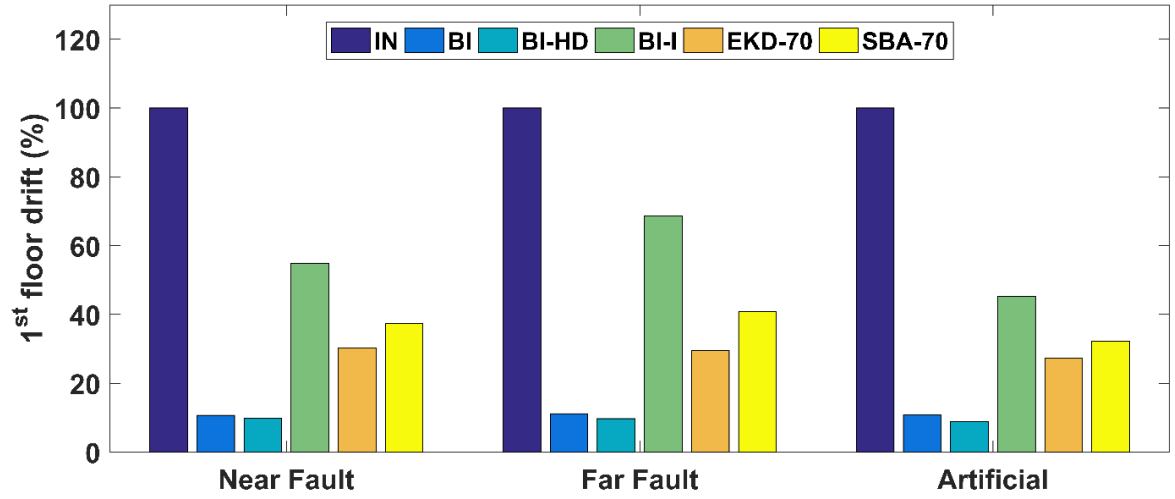

(β)

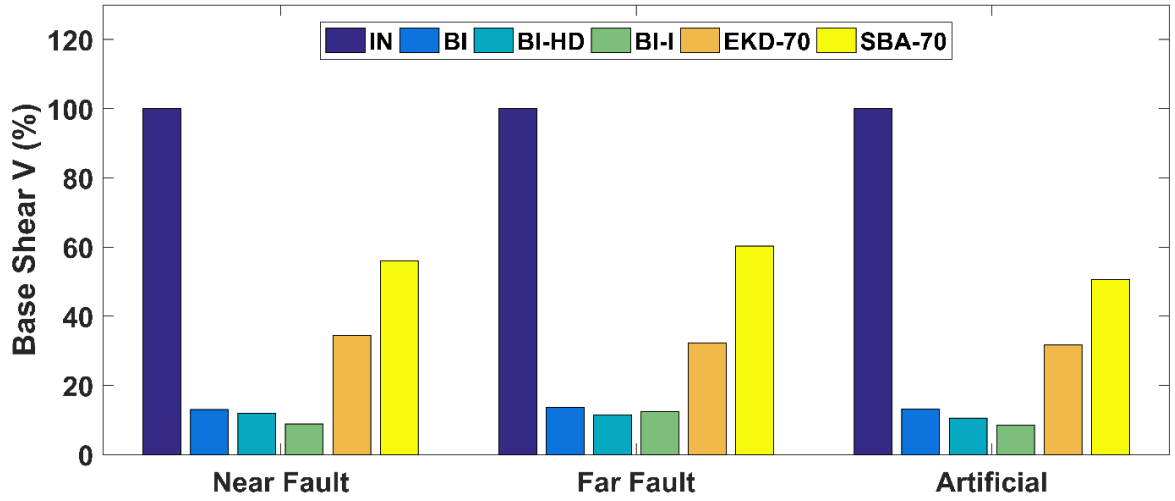

(γ)

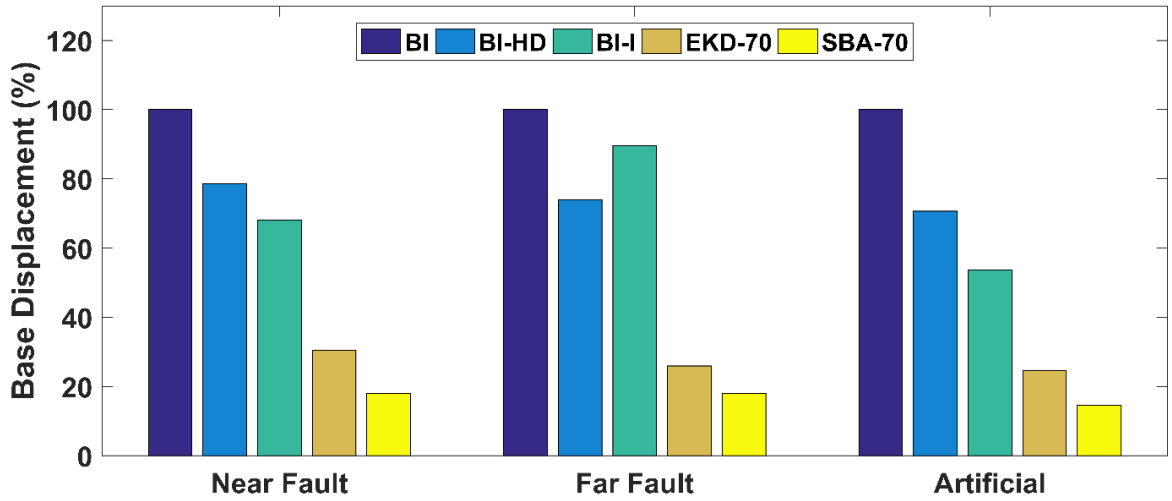

(δ)

Σχήμα 28: *Μέγιστες τιμές των κύριων δυναμικών αποκρίσεων για όλα τα εξεταζόμενα συστήματα (IN, BI, BI-HD, EKD-70, SBA-70) και όλες τις επιλεγμένες σεισμικές διεγέρσεις (30 τεχνητά επιταχυνσιογραφήματα, 12 πραγματικοί σεισμοί κοντινού και μακρινού πεδίου): (α) απόλυτη επιτάχυνση ανώτερου ορόφου, (β) drift 1^{ου} ορόφου, (γ) συνολική τέμνουσα βάσης, και (δ) σχετική μετακίνηση βάσης.*

Συγκριτικά αποτελέσματα για την απόλυτη επιτάχυνση του ανώτερου ορόφου, την συνολική τέμνουσα βάσης, και την σχετική μετακίνηση της βάσης, μεταξύ του αρχικού (IN), του συμβατικά μονωμένου (BI), και του SBA-*70* συστήματος παρουσιάζονται στο Σχήμα 29 για τον πραγματικό σεισμό του Chi-Chi (1999).

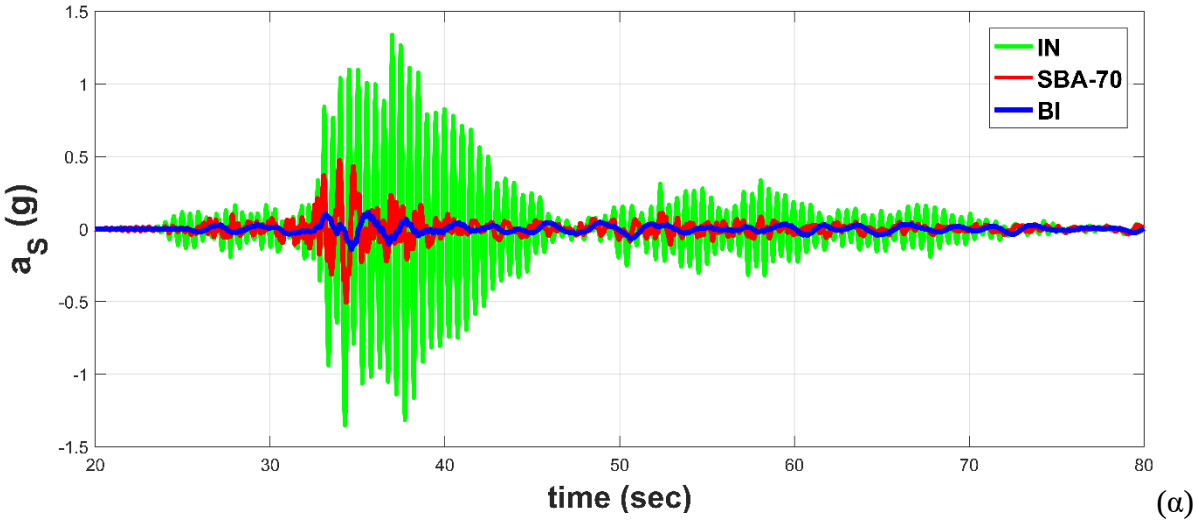

(α)

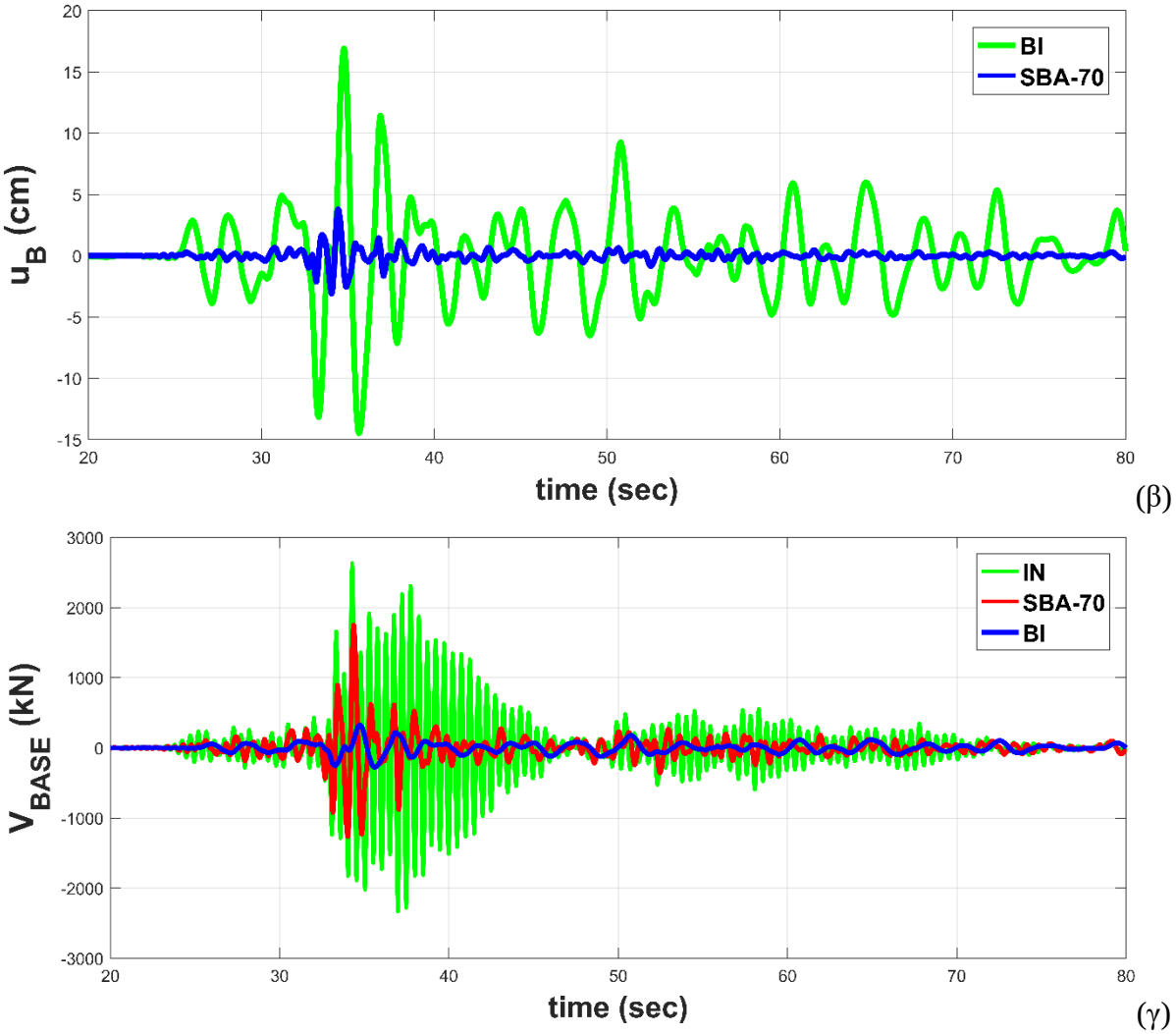

Σχήμα 29: *Συγκριτικά αποτελέσματα σε όρους: (α) απόλυτης επιτάχυνσης ανώτερου ορόφου (g), (β)σχετική μετακίνηση βάσης (cm), και (γ) συνολική τέμνουσα βάσης, μεταξύ των IN, BI, και του SBA-70, για τον Chi-Chi σεισμό (1999).*

Παρατηρούμε πως το SBA-*70* σύστημα βελτιώνει σημαντικά την δυναμική συμπεριφορά της ανωδομής, διατηρώντας την σχετική μετακίνηση της βάσης σε πολύ μικρά επίπεδα, της τάξης μερικών εκατοστών.

Στη συνέχεια, ελέγχεται η εγκυρότητα των βέλτιστων παραμέτρων του SBA, επιλεγμένων αρχικά για μονοβάθμιο σύστημα, και στη συνέχεια εφαρμοσμένο σε πολυώροφες κατασκευές. Για το σκοπό αυτό, πραγματοποιείται ανάλυση ευαισθησίας, όπου οι παράμετροι του SBA αποκλίνουν από την βέλτιστη τιμή τους, για να δούμε σε τι βαθμό μεταβάλλονται οι δυναμικές αποκρίσεις του συστήματος. Πραγματοποιούνται δυναμικές αναλύσεις για τα 30 τεχνητά επιταχυνσιογραφήματα της βάσης δεδομένων, όπου θεωρούμε μεταβολή των παραμέτρων f_0, k_N, c_{NS}, c_{PS}, b και m_D στο εύρος [50 150]% της αρχικής βέλτιστης τιμής τους. Στο Σχήμα 30 παρατηρούμε τη μεταβολή της απόλυτης επιτάχυνσης του ανώτερου ορόφου,

drift του 1ου ορόφου, και μετακίνησης της βάσης για ταυτόχρονη μεταβολή του στοιχείου αρνητικής στιβαρότητας και της ονομαστικής συχνότητας του SBA. Παρατηρούμε πως η επιλογή των βέλτιστων παραμέτρων του SBA για μονοβάθμιο σύστημα είναι αρκετά ακριβής θεώρηση, καθώς τα βέλτιστα αποτελέσματα των δυναμικών αναλύσεων για εφαρμογή στο υπό εξέταση πολυώροφο κτίριο, λαμβάνονται κοντά στις αρχικά επιλεγμένες βέλτιστες τιμές του SBA. Στο Σχήμα 31, οι κύριες αποκρίσεις του σεισμικά προστατευμένου κτιρίου εξετάζονται για μεταβολή των παραμέτρων c_{NS}, c_{PS}, b, και m_D, μία κάθε φορά, στο εύρος [50 150]% της αρχικής βέλτιστης τιμής τους. Παρατηρούμε πως δεν υπάρχει καμία ουσιαστική επιρροή στις δυναμικές αποκρίσεις, όσον αφορά τις παραμέτρους c_{PS} και m_D. Από την άλλη, μεταβάλλοντας την τιμή του c_{NS} επηρεάζεται η μετακίνηση της βάσης αλλά και των τερματικών του στοιχείου αρνητικής στιβαρότητας. Μεταβολή του b επηρεάζει την μέγιστη απόλυτη επιτάχυνση και μετακίνηση του ανώτερου ορόφου. Ωστόσο, μεταβολή 50% των προαναφερθέντων παραμέτρων επηρεάζει τις αποκρίσεις του συστήματος λιγότερο από 30%.

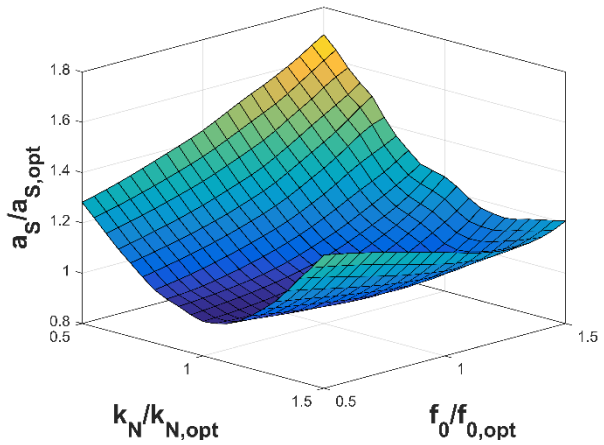

(α)

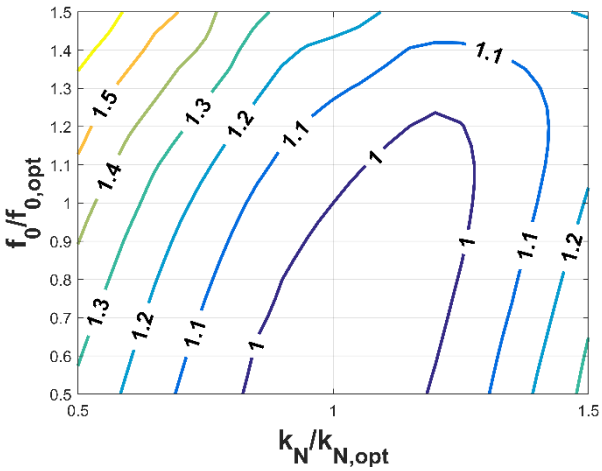

(β)

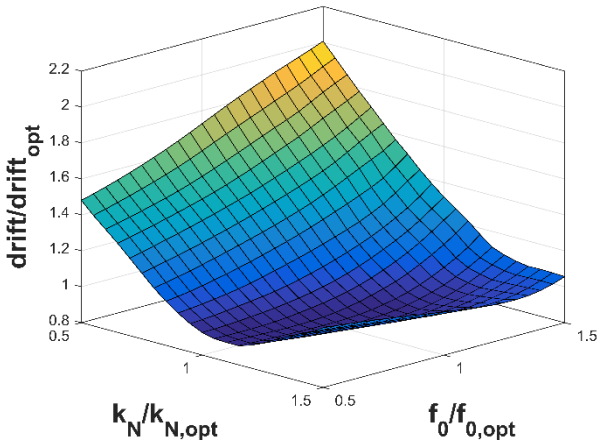

(γ)

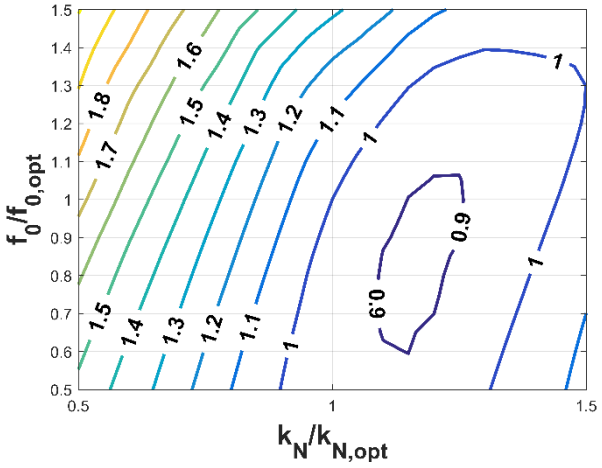

(δ)

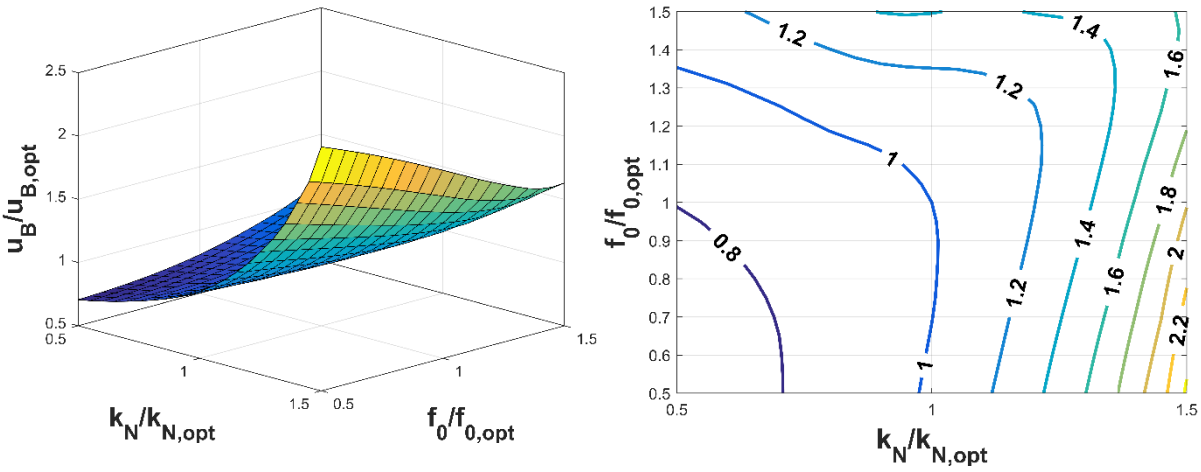

(ε) (ζ)

Σχήμα 30: *Ανάλυση ευαισθησίας και φαινόμενα αποσυντονισμού για την απόλυτη επιτάχυνση του ανώτερου ορόφου (α-β), drift του 1ου ορόφου (γ-δ), και μετακίνησης της βάσης (ε-ζ) για μεταβολή 50% των ελεύθερων παραμέτρων του SBA-70 σετ παραμέτρων, f_0 και k_N, από τις βέλτιστες τιμές τους.*

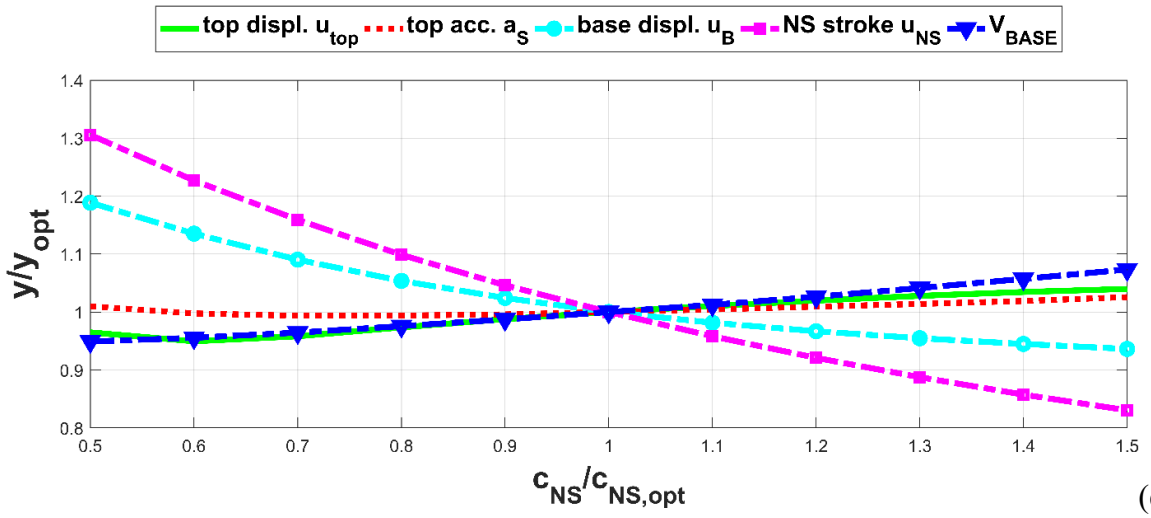

(α)

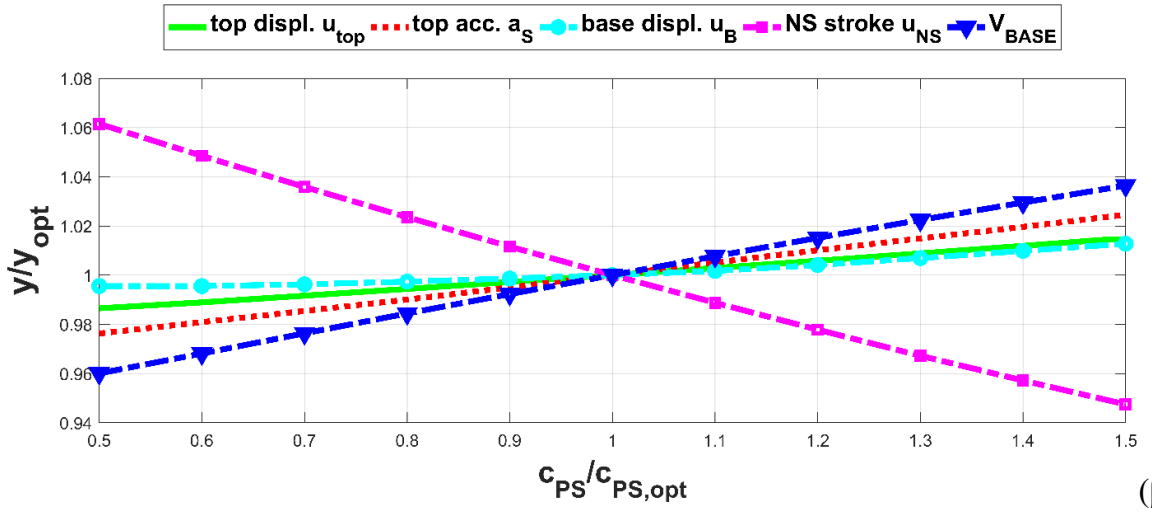

(β)

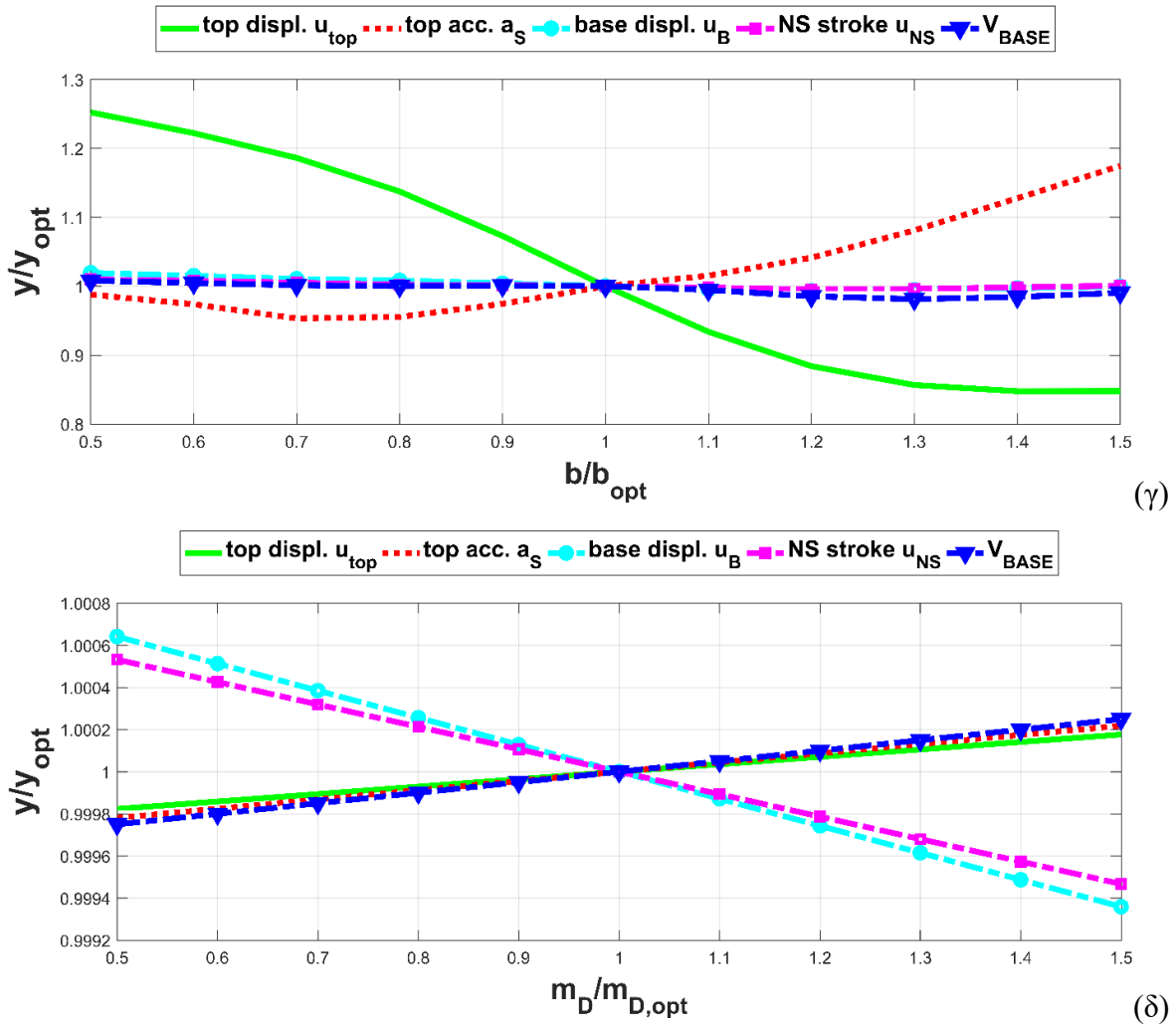

Σχήμα 31: *Ανάλυση ευαισθησίας και φαινόμενα αποσυντονισμού για τις αποκρίσεις u_{top}, a_S, u_B, u_{NS} και V_{BASE} μεταβάλλοντας 50% τις παραμέτρους του SBA-70 συστήματος: (α) c_{NS}, (β) c_{PS}, (γ) b και (δ) m_D.*

Με βάση τα αριθμητικά αποτελέσματα από την εφαρμογή του SBA ως σεισμικά βάση απορρόφησης κραδασμών μιας 3-όροφης κατασκευής από σκυρόδεμα, παρουσιάζονται τα παρακάτω συγκεντρωτικά αποτελέσματα:

i. Το SBA σύστημα είναι ρεαλιστικά σχεδιασμένο, καθώς προβλέπει μεταβολή όλων των στοιχείων στιβαρότητας (10%) και θεωρεί πολύ μικρή πρόσθετη μάζα (0.1%).
ii. Το SBA σύστημα δεν είναι ευαίσθητο σε φαινόμενα αποσυντονισμού.
iii. Η δυναμική συμπεριφορά της ανωδομής του υπό εξέταση πολυώροφου κτιρίου είναι σημαντικά βελτιωμένη με το SBA σύστημα. Πιο συγκεκριμένα, οι απόλυτες επιταχύνσεις και τα drift των ορόφων είναι αρκετά μειωμένα, και ταυτόχρονα η σχετική

μετακίνηση της βάσης είναι δραματικά μικρότερη, συγκριτικά με όλα τα εξεταζόμενα συστήματα σεισμικής προστασίας/μόνωσης.

iv. Η πολύ μικρές μετακινήσεις της βάσης με το SBA σύστημα, καθιστούν την εφαρμογή του εφικτή χωρίς τη θεώρηση ειδικών τύπων εδράνων ή πολύπλοκών διατάξεων, χρησιμοποιώντας συμβατικά δομικά στοιχεία. Σαν συνέπεια, η εφαρμογή του SBA είναι πιθανή για ενίσχυση υφιστάμενων κατασκευών.

VI. Κατακόρυφη Σεισμική Προστασία με Διευρυμένα KDamper

Στη συνέχεια εφαρμόζεται η διευρυμένη έκδοση του KDamper με inerter για σεισμική προστασία των κατασκευών από την κατακόρυφη σεισμική συνιστώσα. Ο κύριος λόγος για την δυσκολία υλοποίησης συστημάτων κατακόρυφης μόνωσης είναι η απαίτηση του συστήματος σε στιβαρότητα μόνωσης. Πιο συγκεκριμένα, ένα κατακόρυφα σεισμικά μονωμένο σύστημα πρέπει να έχει επαρκή κατακόρυφη ακαμψία για να μπορεί να παραλάβει επαρκώς τα κατακόρυφα φορτία λόγω βάρους, διατηρώντας παράλληλα τις στατικές κατακόρυφες παραμορφώσεις του σε αποδεκτά επίπεδα, όπως φαίνεται στη Εξίσωση (60):

$$X_{SVD} = \frac{mg}{k} = \frac{g}{(2\pi f)^2} \tag{60}$$

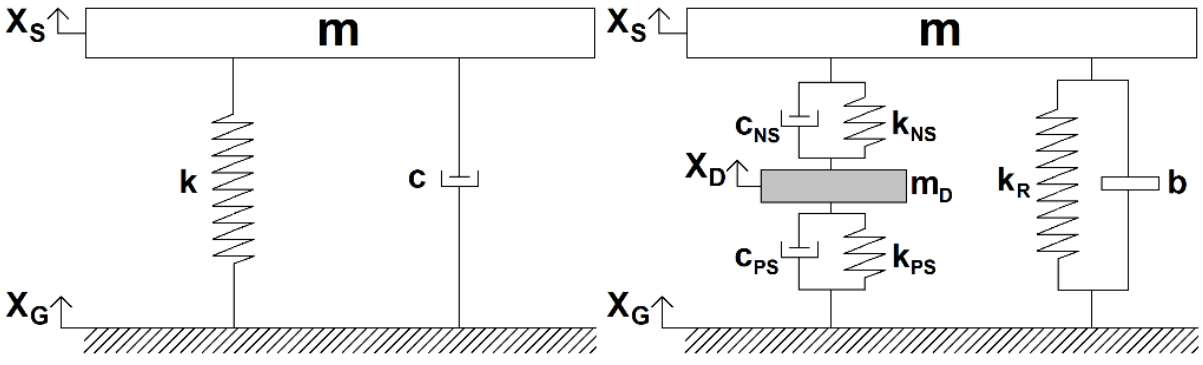

(α) (β)

Σχήμα 32: *(α) Συμβατικά σεισμικά μονωμένο σύστημα στην κατακόρυφη διεύθυνση, και (β) προτεινόμενη διάταξη με διευρυμένο KDamper με inerter για κατακόρυφη σεισμική προστασία (VSA).*

Από την άλλη, ένα σεισμικά μονωμένο σύστημα πρέπει να έχει αρκετή ευκαμψία ώστε να μπορεί να μονώσει τις επιταχύνσεις που ‘φτάνουν’ στην κατασκευή. Ένα συμβατικά μονωμένο σύστημα στην κατακόρυφη διεύθυνση παρουσιάζεται στο Σχήμα 32.α. Η εξίσωση κίνησης για το σύστημα αυτό είναι:

$$m\ddot{u}_S + c\dot{u}_S + ku_S = -m\ddot{X}_G \tag{61}$$

όπου $u_S=X_S-X_G$. Για να μορφώσουμε τις συναρτήσεις μεταφοράς θεωρούμε αρμονική διέγερση στη βάση του συστήματος της μορφής:

$$\ddot{X}_G(t) = A_G \exp(j\omega t) \tag{62}$$

και αποκρίσεις σταθερής κατάστασης της μορφής:

$$u_S(t) = \tilde{U}_S \exp(j\omega t) \tag{63}$$

Η εξίσωση κίνησης, Εξίσωση (61), γίνεται:

$$-\omega^2 m\tilde{U}_S + j\omega c\tilde{U}_S + k\tilde{U}_S = -mA_G \tag{64}$$

και οι συναρτήσεις μεταφοράς για την συγκεκριμένη αρμονική διέγερση είναι:

$$\tilde{H}_{US} = \tilde{U}_S / A_G = -\tilde{H}^{-1} m_S \tag{65.α}$$

$$\tilde{H}_{AS} = \tilde{A}_S / A_G = (-\omega^2 \tilde{X}_S) / A_G = 1 - \omega^2 \tilde{H}_{US} \tag{65.β}$$

$$\tilde{H} = [-\omega^2 m + j\omega c + k] \tag{65.γ}$$

Η ιδιοσυχνότητα και ο λόγος απόσβεσης του συμβατικά σεισμικά μονωμένου συστήματος ορίζονται ως:

$$f = \sqrt{k/m}/(2\pi) \tag{66.α}$$

$$\zeta = c/(2\sqrt{mk}) \tag{66.β}$$

Το διευρυμένο KDamper με inerter εφαρμοσμένο για σεισμική προστασία στην κατακόρυφη διεύθυνση (VSA) παρουσιάζεται στο Σχήμα 32.β. Οι εξισώσεις κίνησης του συστήματος αυτού είναι:

$$(m+b)\ddot{u}_S + c_{NS}(\dot{u}_S - \dot{u}_D) + k_R u_S + k_{NS}(u_S - u_D) = -m\ddot{X}_G \tag{67.α}$$

$$m_D\ddot{u}_D - c_{NS}(\dot{u}_S - \dot{u}_D) + c_{PS}\dot{u}_D - k_{NS}(u_S - u_D) + k_{PS}u_D = -m_D\ddot{X}_G \tag{67.β}$$

όπου u_D=X_D-X_G. Για να μορφώσουμε τις συναρτήσεις μεταφοράς του VSA συστήματος θεωρούμε αρμονική διέγερση στη βάση της μορφής της Εξίσωσης (62). Οι αποκρίσεις σταθερής κατάστασης του VSA είναι:

$$u_S(t) = \tilde{U}_S \exp(j\omega t) \tag{68.α}$$

$$u_D(t) = \tilde{U}_D \exp(j\omega t) \tag{68.β}$$

Οι εξισώσεις κίνησης, Εξισώσεις (67), του VSA συστήματος γίνονται:

$$-\omega^2(m+b)\tilde{U}_S + j\omega c_{NS}(\tilde{U}_S - \tilde{U}_D) + k_R\tilde{U}_S + k_{NS}(\tilde{U}_S - \tilde{U}_D) = -mA_G \tag{69.α}$$

$$-\omega^2 m_D\tilde{U}_D - j\omega c_{NS}(\tilde{U}_S - \tilde{U}_D) + j\omega c_{PS}\tilde{U}_D - k_{NS}(\tilde{U}_S - \tilde{U}_D) + k_{PS}\tilde{U}_D = -m_D A_G \tag{69.β}$$

και οι συναρτήσεις μεταφοράς:

$$\begin{bmatrix} \tilde{H}_{US} \\ \tilde{H}_{UD} \end{bmatrix} = \begin{bmatrix} \tilde{U}_S / A_G \\ \tilde{U}_D / A_G \end{bmatrix} = -\tilde{H}^{-1}\begin{bmatrix} m_S \\ m_D \end{bmatrix} \tag{70.α}$$

$$\tilde{H}_{AS} = \tilde{A}_S / A_G = 1 - \omega^2\tilde{H}_{US} \tag{70.β}$$

$$\tilde{H}_{AD} = \tilde{A}_D / A_G = 1 - \omega^2\tilde{H}_{UD} \tag{70.γ}$$

$$\tilde{H} = \begin{bmatrix} -\omega^2(m+b) + j\omega c_{NS} + k_R + k_{NS} & -j\omega c_{NS} - k_{NS} \\ -j\omega c_{NS} - k_{NS} & -\omega^2 m_D + j\omega(c_{NS} + c_{PS}) + k_{NS} + k_{PS} \end{bmatrix} \tag{70.δ}$$

Οι PSD των κύριων αποκρίσεων του συστήματος αποκρίσεων ορίζονται ως:

$$S_{US} = H_{US}^2 S_A \tag{71.α}$$

$$S_{UD} = H_{UD}^2 S_A \tag{71.β}$$

$$S_{AS} = H_{AS}^2 S_A \tag{71.γ}$$

$$S_{AD} = H_{AD}^2 S_A \tag{71.δ}$$

όπου S_A είναι το μέσο φάσμα διέγερσης των 50 τεχνητών επιταχυνσιογραφημάτων της βάσης δεδομένων για κατακόρυφη κίνηση εδάφους, όπως παρουσιάστηκε στο Σχήμα 10. Οι RMS τιμές των αποκρίσεων ορίζονται στη συνέχεια ως το εμβαδόν κάτω από τις καμπύλες PSD, σαν μια ένδειξη της πραγματικού ενεργειακού περιεχομένου των αποκρίσεων:

$$R_{US} = \sqrt{\int_{-\infty}^{+\infty} S_{US}(\omega)\,\mathrm{d}\,\omega} \tag{72.α}$$

$$R_{UD} = \sqrt{\int_{-\infty}^{+\infty} S_{UD}(\omega)\,\mathrm{d}\,\omega} \tag{72.β}$$

$$R_{AS} = \sqrt{\int_{-\infty}^{+\infty} S_{AS}(\omega)\,\mathrm{d}\,\omega} \tag{72.γ}$$

$$R_{AD} = \sqrt{\int_{-\infty}^{+\infty} S_{AD}(\omega)\,\mathrm{d}\,\omega} \tag{72.δ}$$

Τέλος, οι παράμετροι του VSA συστήματος ορίζονται ως:

$$m_D = \mu_D m \tag{73.α}$$

$$b = \mu_b m \tag{73.β}$$

$$\zeta_{NS} = c_{NS} / (2m_D\omega_D) = c_{NS} / (2\sqrt{(k_{NS} + k_{PS})m_D}) \tag{73.γ}$$

$$\zeta_{PS} = c_{PS} / (2m_D\omega_D) = c_{PS} / (2\sqrt{(k_{NS} + k_{PS})m_D}) \tag{73.δ}$$

$$\omega_D = \sqrt{\frac{k_{NS} + k_{PS}}{m_D}} \tag{73.ε}$$

όπου μ_D, μ_b είναι ο αδρανειακός λόγος της πρόσθετης μάζας m_D και του inerter b προς την μάζα της κατασκευής m, και ζ_{NS}, ζ_{PS} είναι οι λόγοι απόσβεσης των τεχνητών αποσβεστήρων c_{NS} και c_{PS}, αντίστοιχα.

Όπως αναφέρθηκε προηγουμένως, ένα άλυτο πρόβλημα όταν θεωρούμε σεισμική μόνωση στην κατακόρυφη διεύθυνση, είναι οι μεγάλες στατικές παραμορφώσεις. Στην περίπτωση που μια μάζα εδράζεται στο VSA σύστημα, η στατική παραμόρφωση της μάζας υπό το ίδιο βάρος της εκφράζεται ως:

$$\left[F_g\right]_{(2\times1)} = \left[K\right]_{(2\times2)} \begin{bmatrix} X_{SVD} \\ X_{SVD,VSA} \end{bmatrix} \Rightarrow X_{SVD} = \left[\begin{bmatrix} k_R + k_{NS} & -k_{NS} \\ -k_{NS} & k_{NS} + k_{PS} \end{bmatrix}^{-1} \begin{bmatrix} mg \\ m_D g \end{bmatrix} \right](1,1) \tag{74}$$

Κατ' αυτόν τον τρόπο, οι στατικές παραμορφώσεις στην κατακόρυφη διεύθυνση διατηρούνται σε οποιοδήποτε επιθυμητό επίπεδο, και επομένως η στατική κατακόρυφη παραμόρφωση του συστήματος, X_{SVD} θεωρείται ως ελεύθερη παράμετρος σχεδιασμού. Όπως και στην περίπτωση της οριζόντιας σεισμικής προστασίας με διευρυμένο KDamper με inerter, προβλέπεται μεταβολή σε όλα τα στοιχεία στιβαρότητας με την βοήθεια των δεικτών στατικής

ευστάθειας ε_{NS}, $\varepsilon_{PS,}$ και ε_R. Στην οριακή περίπτωση που η ορίζουσα του μητρώου στιβαρότητας του VSA συστήματος μηδενιστεί, το σύστημα γίνεται ασταθές:

$$\det[K]=0 \Rightarrow (1-\varepsilon_R)k_R+\frac{(1-\varepsilon_{PS})k_{PS}(1+\varepsilon_{NS})k_{NS}}{(1-\varepsilon_{PS})k_{PS}+(1+\varepsilon_{NS})k_{NS}}=0 \tag{75}$$

Με δεδομένη την τιμή του στοιχείου αρνητικής στιβαρότητας k_{NS}, τα υπόλοιπα στοιχεία στιβαρότητας λαμβάνονται με την βοήθεια των Εξισώσεων (74) και (75). Συγκεντρωτικά, οι ελεύθερες παράμετροι σχεδιασμού του VSA συστήματος είναι:

1. Η στατική κατακόρυφη παραμόρφωση X_{SVD};
2. Η τιμή του στοιχείου αρνητικής στιβαρότητας k_{NS};
3. Οι λόγοι απόσβεσης ζ_{NS} και ζ_{PS};
4. Ο λόγος αδράνειας του inerter μ_b;

Ο σκοπός του συστήματος VSA είναι η σεισμική προστασία από την κατακόρυφη συνιστώσα των σεισμικών διεγέρσεων. Ο βέλτιστος σχεδιασμός του VSA πρέπει να είναι ταυτόχρονα ρεαλιστικός και αποτελεσματικός. Για αυτόν τον λόγο διατυπώνεται πρόβλημα βελτιστοποίησης στο πεδίο της συχνότητας, βασισμένο σε τεχνικά κριτήρια, όπου επιβάλλονται όρια και περιορισμοί στις ελεύθερες παραμέτρους σχεδιασμού και δυναμικές αποκρίσεις, αντίστοιχα. Πιο συγκεκριμένα:

i. Η RMS τιμή της απόλυτης επιτάχυνσης της κατασκευής, R_{AS}, επιλέγεται ως αντικειμενική συνάρτηση;
ii. Ο λόγος της πρόσθετης μάζας του VSA συστήματος μ_D επιλέγεται ίσος με 5%;
iii. Οι δείκτες στατική ευστάθειας των στοιχείων στιβαρότητας, ε_{NS}, $\varepsilon_{PS,}$ και ε_R, επιλέγονται ίσοι με *10%*;
iv. Το άνω όριο των λόγων απόσβεσης ζ_{NS} και ζ_{PS} είναι 0.4 και 0.2, αντίστοιχα;
v. Το άνω όριο του λόγου αδράνειας του inerter μ_b είναι 2;
vi. Η μέγιστη (απόλυτη) τιμή του στοιχείου αρνητικής στιβαρότητας είναι ίση με *-100 N/m* ανά *kg* της μάζας κατασκευής, όπως παρουσιάστηκε στην δημοσίευση (Antoniadis et al., 2018);
vii. Η RMS τιμή της σχετικής μετατόπισης των τερματικών του στοιχείου αρνητικής στιβαρότητας $R_{US\text{-}D}$ τίθεται ως περιορισμός με άνω όριο το *50%* της ελεύθερης παραμέτρου σχεδιασμού X_{SVD};

Για μία μάζα αναφοράς m=1000 kg, οι βέλτιστες παράμετροι του VSA συστήματος, στο εύρος των στατικών κατακόρυφων παραμορφώσεων X_{SVD} = [1 5] (cm), παρουσιάζονται στον Πίνακα 10. Στα Σχήματα 33 και 34 παρουσιάζονται οι συναρτήσεις μεταφοράς και οι PSDs, αντίστοιχα, των κύριων αποκρίσεων του VSA για διάφορες τιμές του X_{SVD}, για να εξετάσουμε την ευαισθησία των συναρτήσεων μεταφοράς και των PSD λόγω μεταβολής της παραμέτρου X_{SVD}. Αναφορικά με την απόλυτη επιτάχυνση του συστήματος, παρατηρούμε πως δεν υπάρχει σημαντική επιρροή της X_{SVD}, λόγω της ύπαρξης του στοιχείου αδράνειας (inerter, b). Οι σχετικές μετατοπίσεις του συστήματος, αλλά και της πρόσθετης μάζας του VSA, επηρεάζονται από την X_{SVD}, ιδιαίτερα στο εύρος των χαμηλών συχνοτήτων.

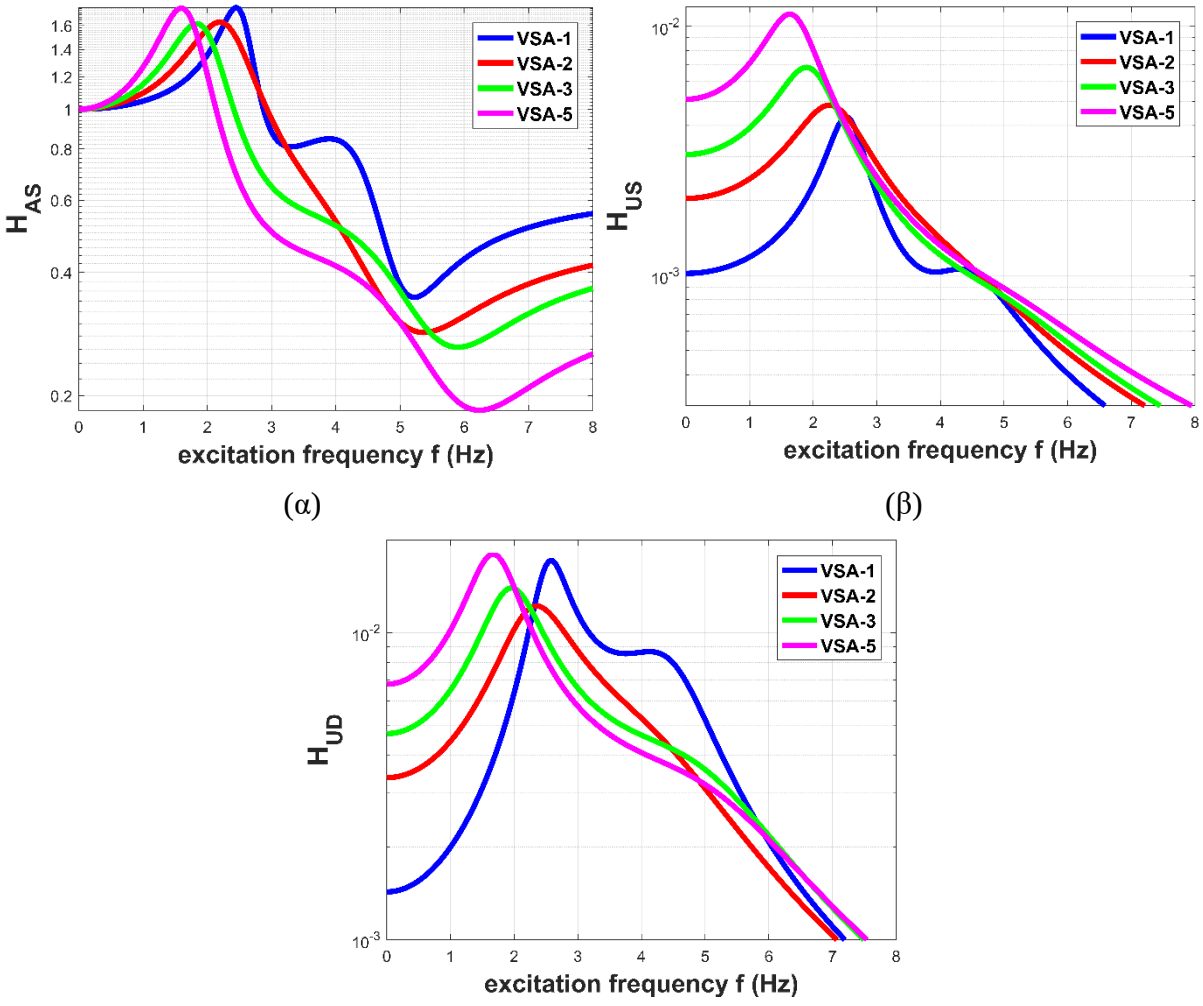

Σχήμα 33: *Συναρτήσεις μεταφοράς των κύριων αποκρίσεων του VSA για μεταβολή του X_{SVD} στο εύρος [1 5] (cm): (α) απόλυτη επιτάχυνση του συστήματος H_{AS}, (β) σχετική μετατόπιση H_{US}, και (γ) σχετική μετατόπιση της πρόσθετης μάζας του VSA H_{UD}.*

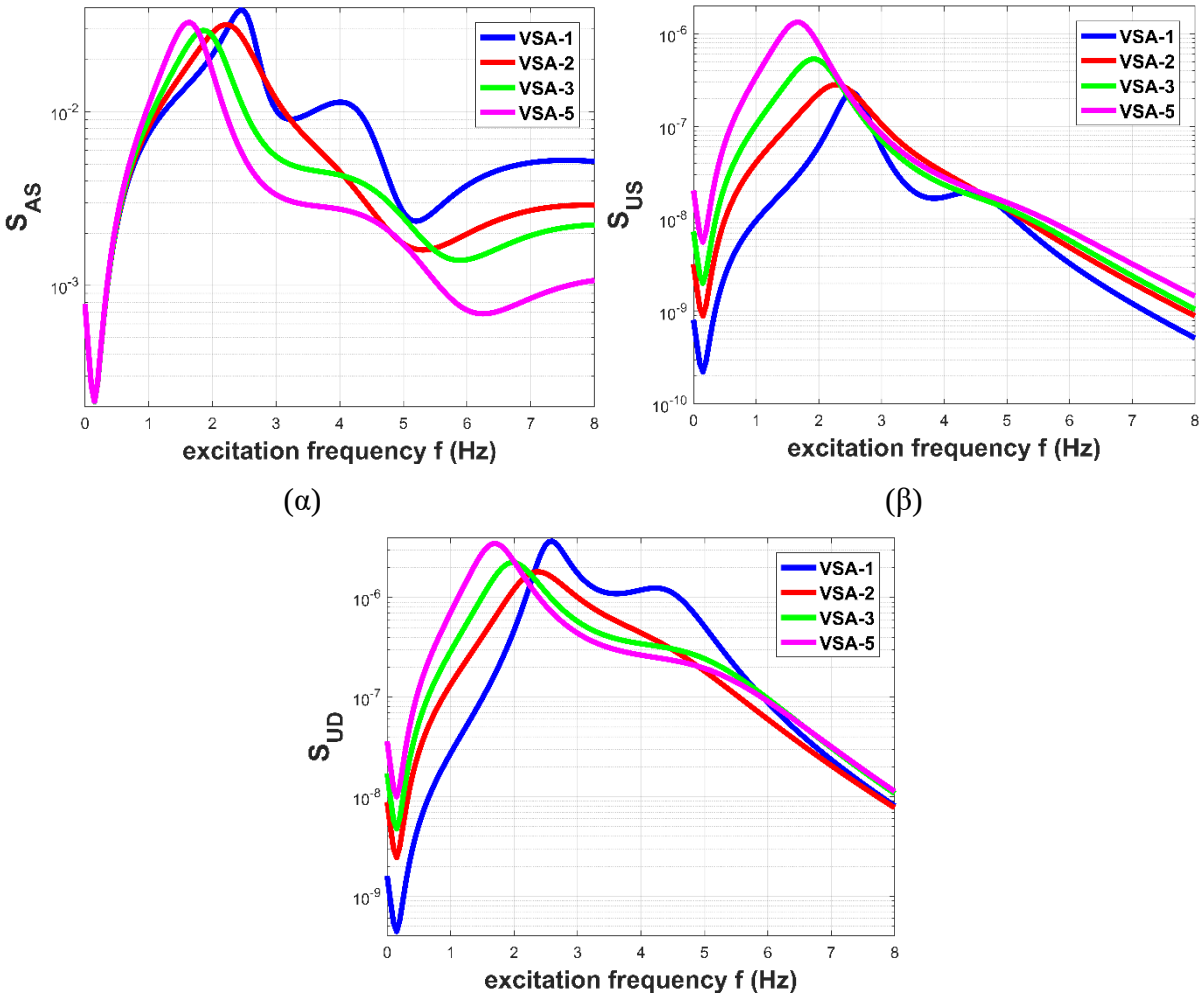

Σχήμα 34: *PSDs των κύριων αποκρίσεων του VSA για μεταβολή του X_{SVD} στο εύρος [1 5] (cm): (α) απόλυτη επιτάχυνση του συστήματος S_{AS}, (β) σχετική μετατόπιση S_{US}, και (γ) σχετική μετατόπιση της πρόσθετης μάζας του VSA S_{UD}.*

Πίνακας 10: *Πλήρες σετ παραμέτρων του VSA συστήματος , στο εύρος των στατικών κατακόρυφων παραμορφώσεων X_{SVD} = [1 5] (cm).*

VSA set	μ_D	μ_b	k_{NS} (kN/m)	k_{PS} (kN/m)	k_R (kN/m)	ζ_{NS} (%)	c_{NS} (kNs/m)	ζ_{PS} (%)	c_{PS} (kNs/m)
X_{SVD}=1 *cm*	0.05	1.85	-97.97	132.82	1216.5	6.9	0.182	16.5	0.436
X_{SVD}=2 *cm*	0.05	1.09	-95.15	137.88	742.94	27.6	0.806	17.7	0.518
X_{SVD}=3 *cm*	0.05	0.91	-97.93	151.15	575.02	36.7	1.197	0.3	0.01
X_{SVD}=4 *cm*	0.05	0.65	-85.95	136.44	456.65	37.85	1.203	7.3	0.233
X_{SVD}=5 *cm*	0.05	0.57	-86.96	144.88	399.00	32.14	1.094	5.9	0.200

Για να εξετάσουμε καλύτερα την αποτελεσματικότητα του VSA, το συγκρίνουμε με ένα υψηλής απόσβεσης (15%) σεισμικά μονωμένο σύστημα (BI) με μεταβλητή ιδιοσυχνότητα, ανάλογη της επιθυμητής στατικής κατακόρυφης παραμόρφωσης X_{SVD}. Τέλος, ορίζονται οι αδιάστατοι δείκτες των δυναμικών αποκρίσεων στις Εξισώσεις (76), και παρουσιάζονται στο Σχήμα 35, για μεταβολή του X_{SVD}.

$$r_{AS,BI,X_{SVD}} = \frac{R_{AS,BI,X_{SVD}}}{\sqrt{\int S_A(\omega)\,\mathrm{d}\,\omega}\ (=PGA)} \tag{76.α}$$

$$r_{AS,VSA,X_{SVD}} = \frac{R_{AS,VSA,X_{SVD}}}{\sqrt{\int S_A(\omega)\,\mathrm{d}\,\omega}\ (=PGA)} \tag{76.β}$$

$$r_{US,BI,X_{SVD}} = \frac{R_{US,BI,X_{SVD}}}{R_{US,BI,X_{SVD}}(ref)} \tag{76.γ}$$

$$r_{US,VSA,X_{SVD}} = \frac{R_{US,VSA,X_{SVD}}}{R_{US,VSA,X_{SVD}}(ref)} \tag{76.δ}$$

$$r_{UD,VSA,X_{SVD}} = \frac{R_{UD,VSA,X_{SVD}}}{R_{UD,VSA,X_{SVD}}(ref)} \tag{76.ε}$$

Για να επιβεβαιώσουμε την αποτελεσματικότητα του προβλήματος βελτιστοποίησης στο πεδίο της συχνότητας, στα αποτελέσματα του Σχήματος 35, παρουσιάζονται και οι αντίστοιχες τιμές (διακεκομμένες καμπύλες) που λαμβάνονται από τις δυναμικές αναλύσεις στο πεδίο του χρόνου, χρησιμοποιώντας την μέθοδο Newmark-β. Οι αντίστοιχοι δείκτες για τις δυναμικές αποκρίσεις στο πεδίο του χρόνου ορίζονται ως:

$$v_{AS,BI,X_{SVD}} = \frac{V_{AS,BI,X_{SVD}}}{meanPGA(=0.417g)} \tag{77.α}$$

$$v_{US,BI,X_{SVD}} = \frac{V_{US,BI,X_{SVD}}}{V_{US,BI,X_{SVD}}(ref)} \tag{77.β}$$

$$v_{AS,VSA,X_{SVD}} = \frac{V_{AS,VSA,X_{SVD}}}{meanPGA(=0.417g)} \tag{77.γ}$$

$$v_{US,VSA,X_{SVD}} = \frac{V_{US,VSA,X_{SVD}}}{V_{US,VSA,X_{SVD}}(ref)} \tag{77.δ}$$

$$v_{UD,VSA,X_{SVD}} = \frac{V_{UD,VSA,X_{SVD}}}{V_{UD,VSA,X_{SVD}}(ref)} \tag{77.ε}$$

όπου $V_{US,BI,Xsvd}$, $V_{AS,BI,Xsvd}$, $V_{US,VSA,Xsvd}$, $V_{AS,VSA,Xsvd}$, και $V_{UD,VSA,Xsvd}$ είναι οι μέσες τιμές των μεγίστων των δυναμικών αποκρίσεων ανάλογα με την ελεύθερη παράμετρο σχεδιασμού X_{SVD}, και $V_{US,BI,Xsvd}$ *(ref)*, $V_{US,VSA,Xsvd}$ *(ref)*, και $V_{UD,VSA,Xsvd}$*(ref)* αντιστοιχούν στις μέσες τιμές των μεγίστων των αποκρίσεων για X_{SVD}=3 *cm*. Παρατηρούμε την αποτελεσματικότητα του VSA συστήματος, συγκρινόμενο με το BI, καθώς και την ακρίβεια της μεθόδου βελτιστοποίησης στο πεδίο της συχνότητας.

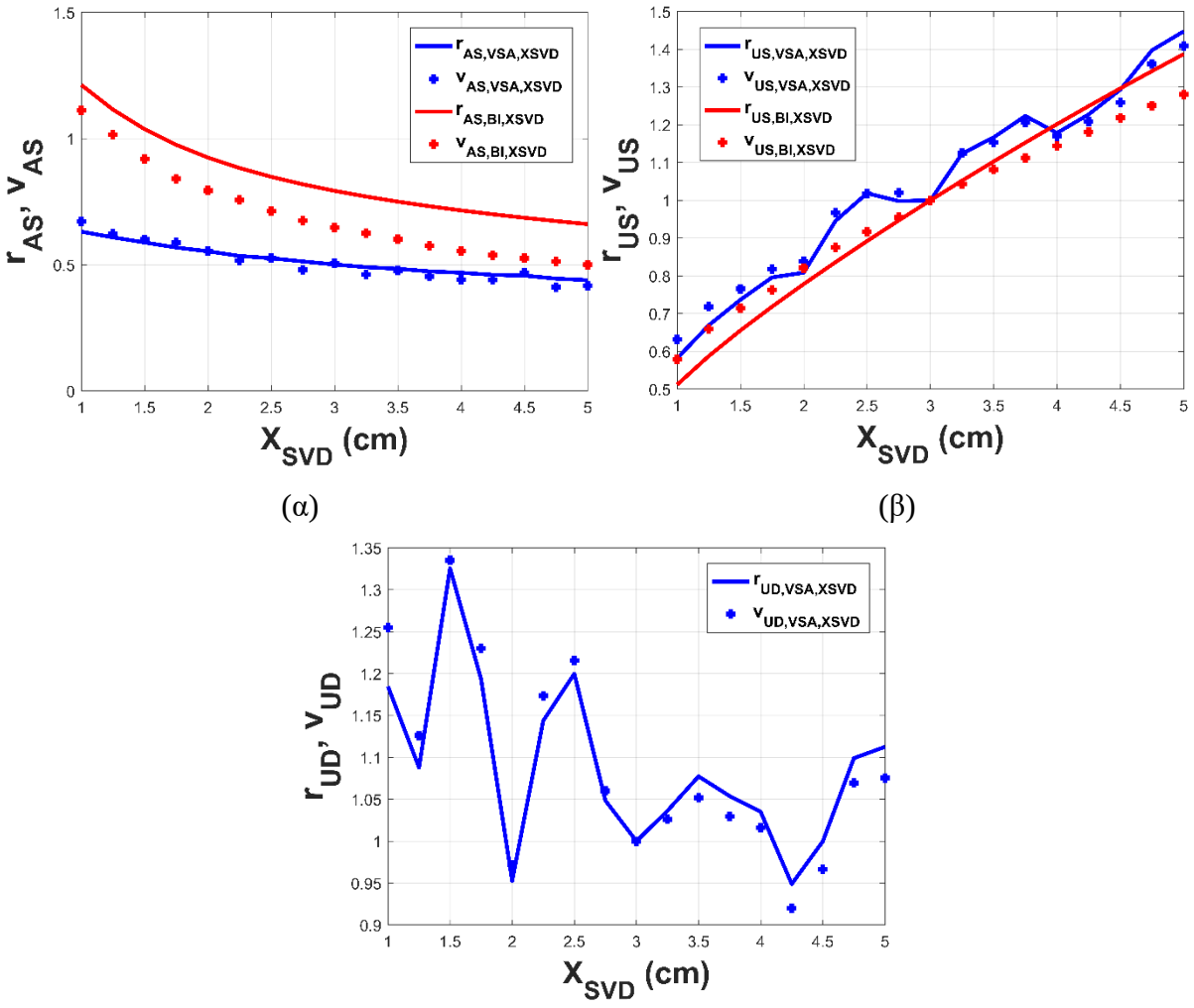

Σχήμα 35: *Μεταβολή των αδιάστατων δεικτών απόκρισης: (α) της απόλυτης επιτάχυνσης του συστήματος r_{AS}, (β) της σχετικής μετατόπισης του συστήματος r_{US}, και (γ) της σχετικής μετατόπισης της πρόσθετης μάζας του VSA r_{UD} για μεταβολή του X_{SVD}, των VSA και BI συστημάτων, και επαλήθευσή τους στο πεδίο του χρόνου με τους αντίστοιχους δείκτες v_{AS}, v_{US}, και v_{UD}.*

Η αποτελεσματικότητα του VSA συστήματος εξετάζεται και με πραγματικούς σεισμούς που παρουσιάζονται στον Πίνακα 11, των οποίων η κατακόρυφη συνιστώσα έχει εξαιρετικά

μεγάλη τιμή. Στα Σχήματα 36 και 37 παρουσιάζονται τα αποτελέσματα των δυναμικών αναλύσεων για τους εξεταζόμενους πραγματικούς σεισμούς των VSA και BI συστημάτων, για κατακόρυφη στατική παραμόρφωση 1 και 2 εκατοστά, αντίστοιχα.

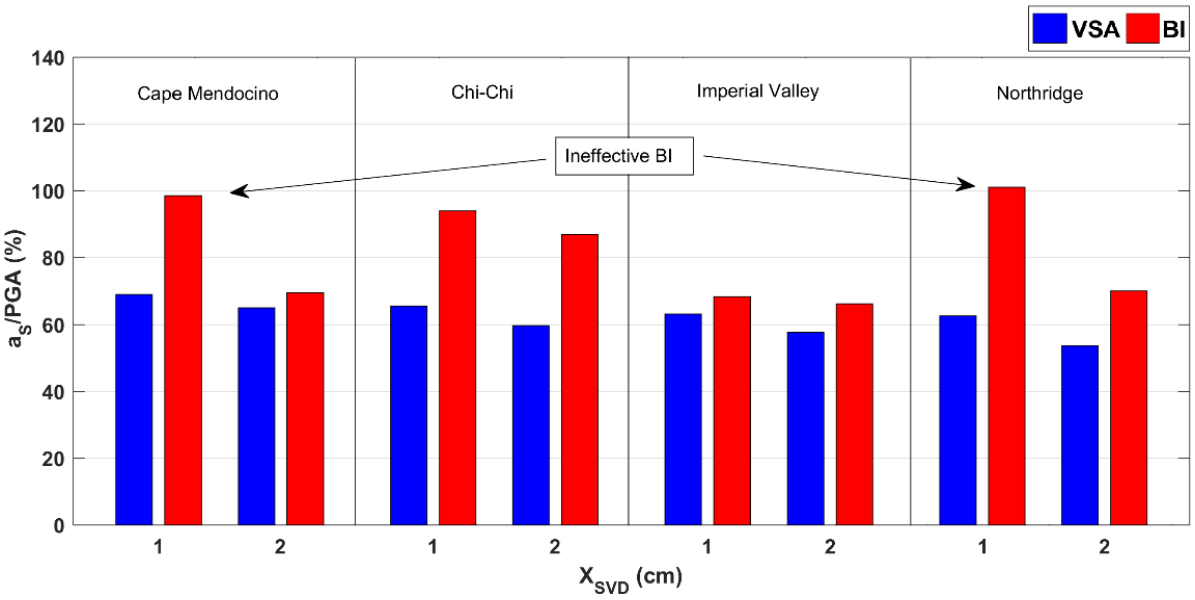

(α)

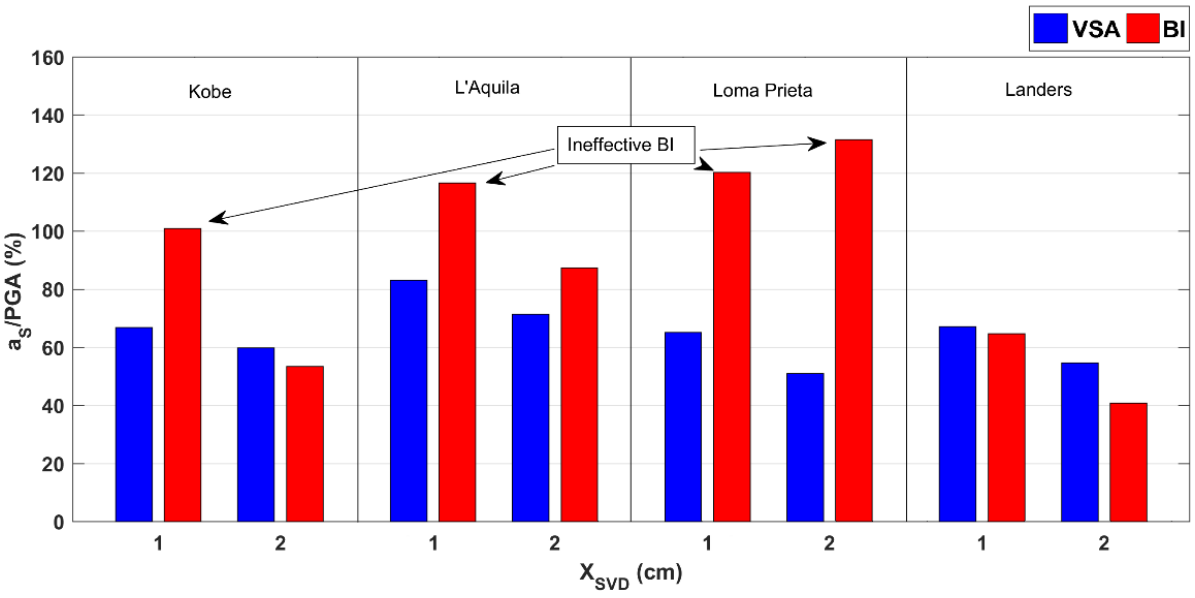

(β)

Σχήμα 36: *Μέγιστη απόλυτη επιτάχυνση των VSA και BI συστημάτων για όλες τις εξεταζόμενες πραγματικές σεισμικές διεγέρσεις.*

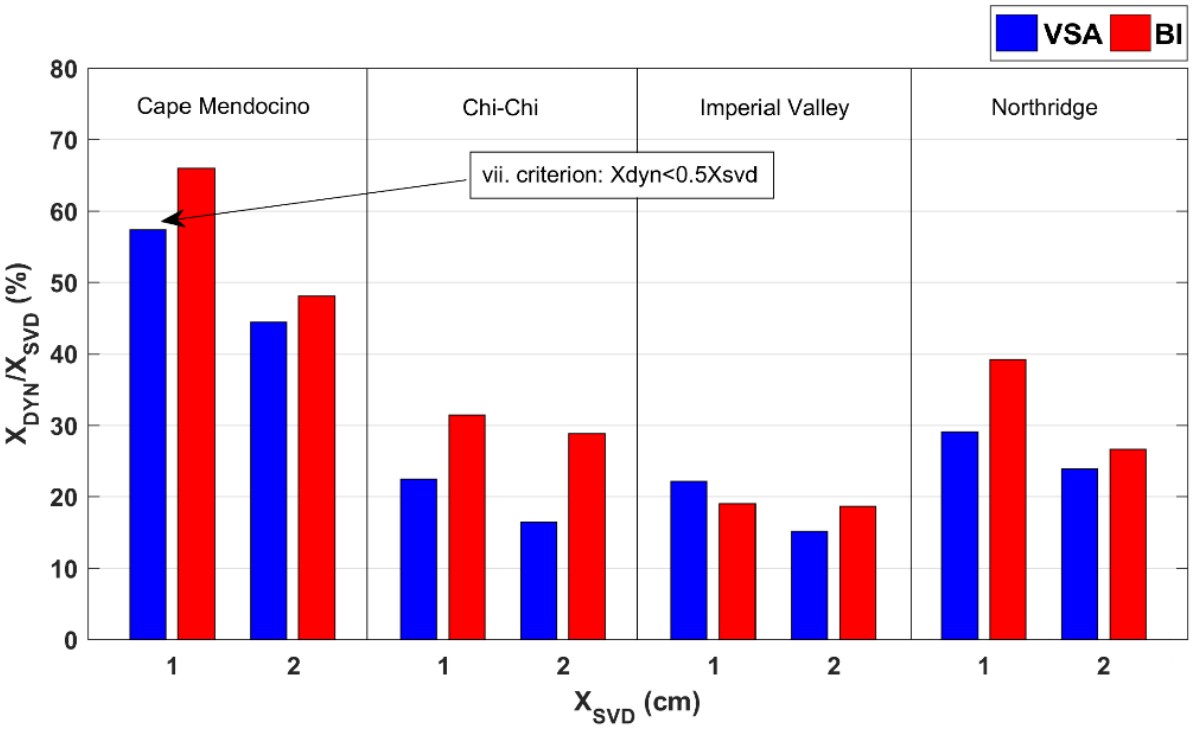

(α)

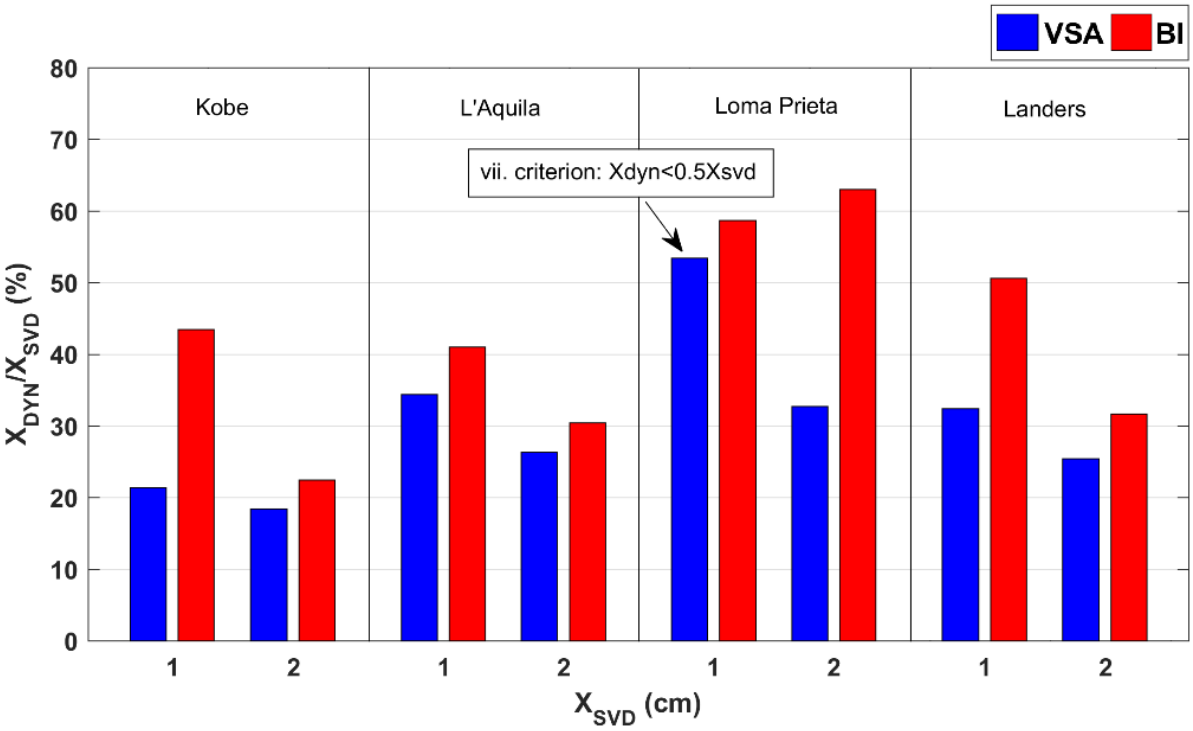

(β)

Σχήμα 37: *Μέγιστες δυναμικές κατακόρυφες παραμορφώσεις των VSA και BI συστημάτων για όλες τις εξεταζόμενες πραγματικές σεισμικές διεγέρσεις.*

Πίνακας 11: *Πραγματικές σεισμικές διεγέρσεις με μεγάλη κατακόρυφη συνιστώσα.*

Σεισμός	Ημερομηνία	Σταθμός	*Mw*	PGA (*g*)	R_{jb} (*km*)	dt (*sec*)	$Dur._{5\text{-}95}$ (*sec*)
Cape Mendocino	4/25/1992	Cape Mendocino	7.01	0.74	0.0	0.02	9.7
Chi-Chi	9/20/1999	CHY028	7.62	0.34	3.12	0.005	8.7
Imperial Valley	10/15/1979	El Centro Array #4	6.53	0.29	4.9	0.005	10.3
Northridge	1/17/1994	Simi Valley – Katherine Rd	6.69	0.40	0.0	0.01	6.7
Kobe	1/16/1995	Kobe University	6.9	0.45	0.9	0.01	7.0
L'Aquila	4/6/2009	L'Aquila -Parking	6.3	0.37	0.0	0.005	11.6
Loma Prieta	10/18/1989	BRAN	6.93	0.51	3.85	0.005	9.8
Landers	6/28/1992	Lucerne	7.28	0.82	2.19	0.005	13.8

Τέλος πραγματοποιείται ανάλυση ευαισθησίας για να εξετάσουμε αν το VSA είναι ευαίσθητο σε φαινόμενα αποσυντονισμού. Αρχικά, μεταβάλουμε τις τιμές των βέλτιστων παραμέτρων του VSA, k_{NS} και *b* στο εύρος 80-120% της βέλτιστης τιμής τους, και παρατηρούμε στο Σχήμα 38 τι επίπτωση έχει αυτό στην αποτελεσματικότητα του συστήματος, δηλαδή στην απόλυτη επιτάχυνση. Στο Σχήμα 39, μεταβάλλουμε τις τιμές όλων των στοιχείων στιβαρότητας μία κάθε φορά στο εύρος 80-120% της βέλτιστης τιμής τους, και παρατηρούμε την μεταβολή της ελεύθερης παραμέτρου σχεδιασμού X_{SVD}. Σημειώνεται πως το σετ παραμέτρων του VSA που εξετάστηκε είναι εκείνο σχεδιασμένο για X_{SVD}=1 *cm*.

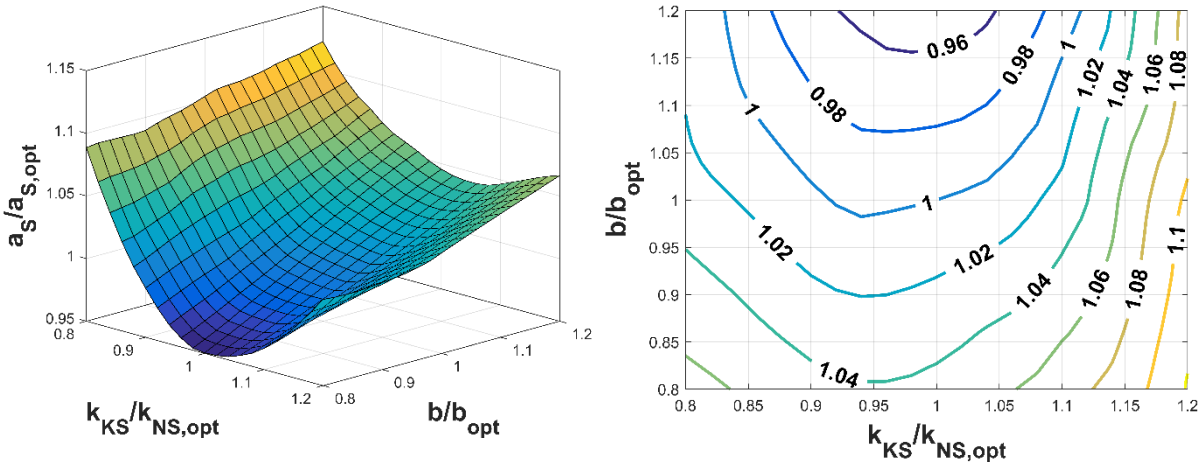

(α) (β)

Σχήμα 38: *Ανάλυση ευαισθησίας και φαινόμενα αποσυντονισμού για την απόλυτη επιτάχυνση του συστήματος μεταβάλλοντας (20%) τις ελεύθερες παραμέτρους σχεδιασμού k_{NS} και b του VSA-1 σετ παραμέτρων από τις βέλτιστες τιμές τους.*

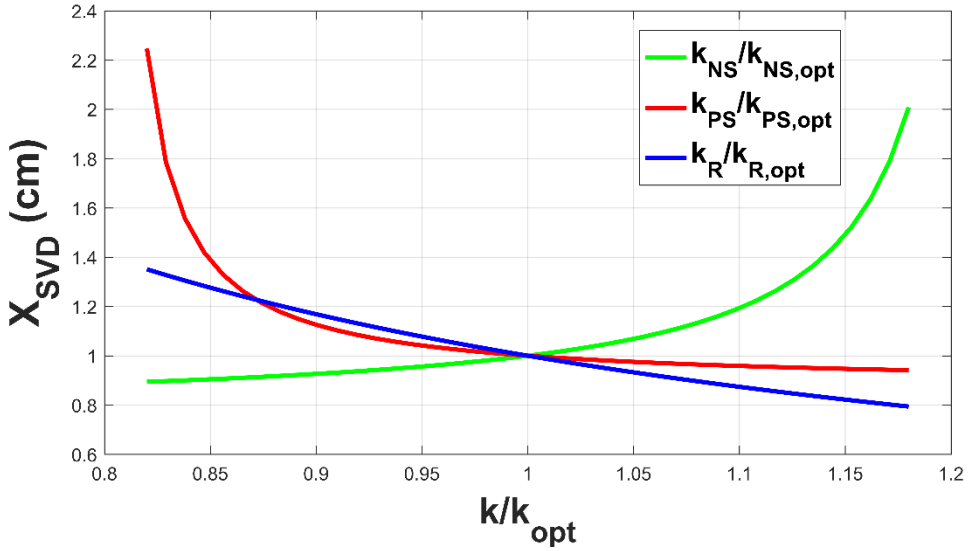

Σχήμα 39: *Ανάλυση ευαισθησίας και φαινόμενα αποσυντονισμού για την στατική κατακόρυφη παραμόρφωση X_{SVD} μεταβάλλοντας (20%) τα στοιχεία στιβαρότητας k_{NS}, k_{PS}, και k_R του VSA-1 σετ παραμέτρων από τις βέλτιστες τιμές τους..*

Με βάση τα αποτελέσματα των αριθμητικών αναλύσεων, τα ακόλουθα συγκεντρωτικά συμπεράσματα μπορούν να εξαχθούν για το προτεινόμενο δυναμικό σύστημα απορρόφησης ταλαντώσεων στην κατακόρυφο διεύθυνση:

1. Ο σχεδιασμός του VSA είναι ρεαλιστικός, καθώς εισάγει μικρές πρόσθετες μάζες, προβλέπει ταυτόχρονη μεταβολή σε όλα τα στοιχεία στιβαρότητας, και σχεδιάζεται μέσω προβλήματος βελτιστοποίησης βασισμένο σε τεχνικά κριτήρια;
2. Η επιλογή των βέλτιστων παραμέτρων στο πεδίο της συχνότητας είναι ακριβής, όπως επιβεβαιώθηκε από τις δυναμικές αναλύσεις στο πεδίο του χρόνου;
3. Η αποτελεσματικότητα του VSA εξετάστηκε και με πραγματικές σεισμικές διεγέρσεις με μεγάλη κατακόρυφη συνιστώσα;
4. Οι μέγιστες κατακόρυφες απόλυτες επιταχύνσεις μειώνονται κατά 30-40%, και ταυτόχρονα οι κατακόρυφες στατικές παραμορφώσεις διατηρούνται σε πολύ μικρά επίπεδα (1-2 *cm*), σημαντικά μικρότερες σε σύγκριση με ένα υψηλής απόσβεσης σεισμικά μονωμένο σύστημα;
5. Εξετάστηκαν τα φαινόμενα αποσυντονισμού μέσω ανάλυσης ευαισθησίας, και επιβεβαιώθηκε πως το VSA σύστημα δεν είναι ευαίσθητο σε αποσυντονισμό;

VII. Βελτίωση Δυναμικής Συμπεριφοράς Πυλώνων Ανεμογεννητριών Μέσω Αύξησης της Ισοδύναμης Απόσβεσής τους με Διευρυμένα KDamper

Στη συνέχεια εφαρμόζονται τα προτεινόμενα δυναμικά συστήματα απορρόφησης ταλαντώσεων, με βάση τον KDamper, σε πυλώνες ανεμογεννητριών με στόχο την βελτίωση της δυναμικής συμπεριφοράς τους, μέσω της αύξησης της ισοδύναμης απόσβεσης των πυλώνων τους.

Στο Σχήμα 40 παρουσιάζονται όλα τα εξεταζόμενα συστήματα ελέγχου. Η χρήση Αποσβεστήρων Συντονισμένης Μάζας (TMD) είναι πιθανότατα η πιο ευρέως χρησιμοποιούμενη τακτική για προστασία πυλώνων ανεμογεννητριών, όπως παρουσιάζεται στο Σχήμα 40.β, όπου η προστιθέμενη μάζα τοποθετείται στην κορυφή του πυλώνα ή μέσα κέλυφος της ανεμογεννήτριας, χρησιμοποιώντας ένα στοιχείο θετικής στιβαρότητας και ένα γραμμικό αποσβεστήρα. Στο Σχήμα 40.γ παρουσιάζεται μια εναλλακτική διάταξη εμπνευσμένη από τη χρήση των TMD και τις αρχές στης σεισμικής μόνωσης (nacelle-isolation σύστημα), στην οποία γίνεται αποσύζευξη του πυλώνα της ανεμογεννήτριας από τη μάζα που αντιστοιχεί στα μηχανικά μέρη (κέλυφος, ρότορας, πτερύγια), η οποία χρησιμοποιείται πλέον ως η πρόσθετη μάζα του TMD. Σε μια προσπάθεια να συνδυάσουμε τα προαναφερθέντα συστήματα, τα προτεινόμενα δυναμικά συστήματα απορρόφησης ταλαντώσεων, με βάση τον KDamper, εφαρμόζονται όπως παρουσιάζονται στα Σχήματα 40.δ-ε. Στις συγκεκριμένες διατάξεις, όπως στην περίπτωση του nacelle-isolation συστήματος, ο πυλώνας δεν είναι πλέον άκαμπτα συνδεδεμένος με τη μάζα που αντιστοιχεί στα μηχανικά μέρη (κέλυφος, ρότορας, πτερύγια), αλλά παρεμβάλλεται ένα σύστημα ελέγχου με βάση τον KDamper (κλασικό, διευρυμένο EKD, και διευρυμένο με inerter EKDI).

Για να μπορέσουμε να εισάγουμε αλλά και να βελτιστοποιήσουμε τα προαναφερθέντα συστήματα, κρίνεται απαραίτητη η ανάπτυξη ενός δυναμικού μοντέλου του πυλώνα της ανεμογεννήτριας που να διευκολύνει την εισαγωγή των συστημάτων αυτών. Στην παρούσα ενότητα, ο πυλώνας της ανεμογεννήτριας είναι κυκλικής κοίλης διατομής και υποστηρίζει την 5-MW γεννήτρια (Quilligan et al., 2012). Για να ληφθούν υπόψη οι αδρανειακές δυνάμεις από τα μηχανικά μέρη (κέλυφος, ρότορας, πτερύγια) τοποθετείται μια συγκεντρωμένη μάζα στην κορυφή του πυλώνα $m_{top} = 403.22\ tn$ (Quilligan et al., 2012). Ο πυλώνας μοντελοποιείται από πρισματικά στοιχεία δοκού, με τους μετατοπισιακούς βαθμούς ελευθερίας να θεωρούνται οι δυναμικοί βαθμοί ελευθερίας. Οι επιπλέον θεωρήσεις που λαμβάνονται υπόψη για την μοντελοποίηση του πυλώνα είναι : (i) ο πυλώνας της ανεμογεννήτριας παραμένει στα ελαστικά όρια καθόλη τη διάρκεια της διέγερσης, (ii) η επιρροή της αλληλεπίδρασης εδάφους-κατασκευής δεν λαμβάνεται υπόψη, και (iii) οι αξονικοί βαθμοί ελευθερίας δεν λαμβάνονται

υπόψη στην ανάπτυξη του μοντέλου, καθώς μας ενδιαφέρει η βελτίωση της δυναμικής συμπεριφοράς λόγω οριζόντιων δυναμικών φορτίων (ανέμου). Στο Σχήμα 41 παρουσιάζεται το δυναμικό μοντέλο του πυλώνα με πρισματικά στοιχεία δοκού.

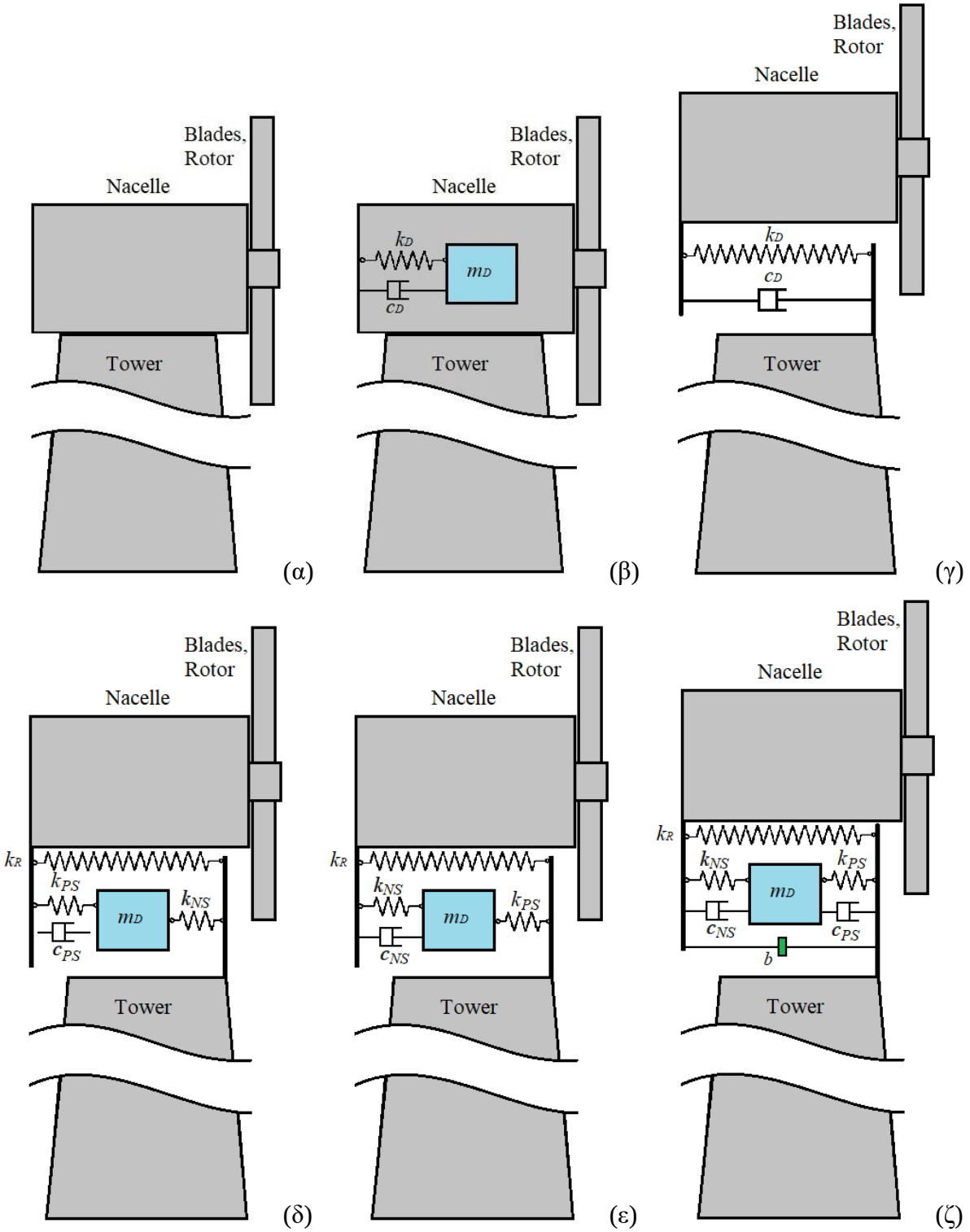

Σχήμα 40: *Παρουσίαση των εξεταζόμενων συστημάτων: (α) αρχική ανεμογεννήτρια, (β) TMD, (γ) nacelle-isolation, (δ) KDamper, (ε) EKD, και (ζ) EKDI.*

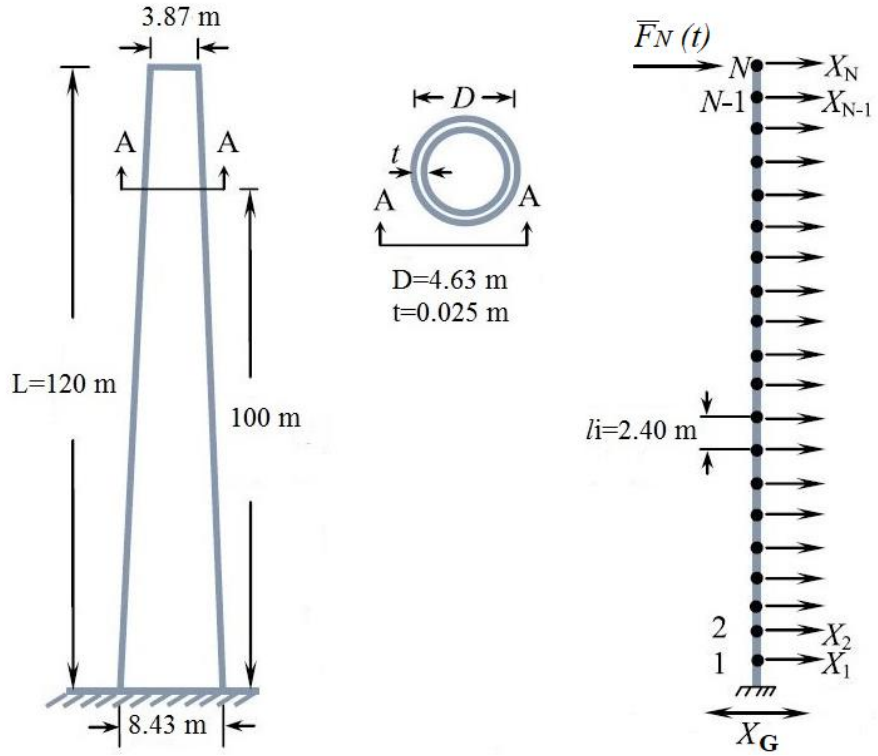

Σχήμα 41: *Δυναμικό μοντέλο της ανεμογεννήτριας με πρισματικά στοιχεία δοκού, με τους μετατοπισιακούς βαθμούς ελευθερίας να θεωρούνται οι δυναμικοί βαθμοί ελευθερίας.*

Οι εξισώσεις κίνησης της αρχικής ανεμογεννήτριας θεωρώντας ισορροπία δυνάμεων στη θέση κάθε ενός βαθμού ελευθερίας είναι:

$$[M_S]\{\ddot{X}_S\}+[C_S]\{\dot{X}_S\}+[K_S]\{X_S\}=[P_S]\pm[M_S]\ddot{X}_G \tag{78}$$

όπου $[M_S]$, $[C_S]$ και $[K_S]$ είναι τα μητρώα μάζας, απόσβεσης και στιβαρότητας της αρχικής ανεμογεννήτριας, αντίστοιχα, τάξης μεγέθους ($N \times N$), N υποδεικνύοντας τον αριθμό των πρισματικών στοιχείων δοκού που επιλέχθηκαν για την μοντελοποίηση του πυλώνα. Το μητρώο απόσβεσης μορφώνεται με την Rayleigh προσέγγιση χρησιμοποιώντας λόγο απόσβεσης για όλες τις ιδιομορφές *1*% (Quilligan et al., 2012). Στην παρούσα εργασία χρησιμοποιήθηκαν $N = 24$ πρισματικά στοιχεία δοκού.

Για να επιβεβαιώσουμε την αποτελεσματικότητα και την εγκυρότητα του προτεινόμενου μοντέλου, πραγματοποιήθηκαν απλοποιημένες αναλύσεις και συγκρίσεις με το SOFiSTiK πακέτο λογισμικού, βασισμένο σε FEM (FEM Software for Structural Engineers | SOFiSTiK AG, n.d.). Πιο συγκεκριμένα, στον Πίνακα 12 παρουσιάζονται οι πρώτες 5 ιδιομορφές του πυλώνα της ανεμογεννήτριας χρησιμοποιώντας το SOFiSTiK και το προτεινόμενο μοντέλο

που παρουσιάστηκε προηγουμένως για N=24 πρισματικά στοιχεία δοκού, ενώ στο Σχήμα 42 παρουσιάζονται οι πρώτες 5 κανονικές μορφές ταλάντωσης. Επιπρόσθετα, οι στατικές αποκρίσεις, και πιο συγκεκριμένα η μετατόπιση της κορυφής του πυλώνα παρουσιάζονται και συγκρίνονται επίσης στον Πίνακα 12, για μια συγκεντρωμένη δύναμη στην κορυφή του πυλώνα $\bar{F}_N = 1353.258\ kN$ (αρχική τιμή του αεροδυναμικού φορτίου που θα χρησιμοποιηθεί παρακάτω). Παρατηρούμε πως το προτεινόμενο δυναμικό μοντέλου είναι αρκετά ακριβές, όπως επιβεβαιώθηκε από τις προαναφερθέντες συγκρίσεις.

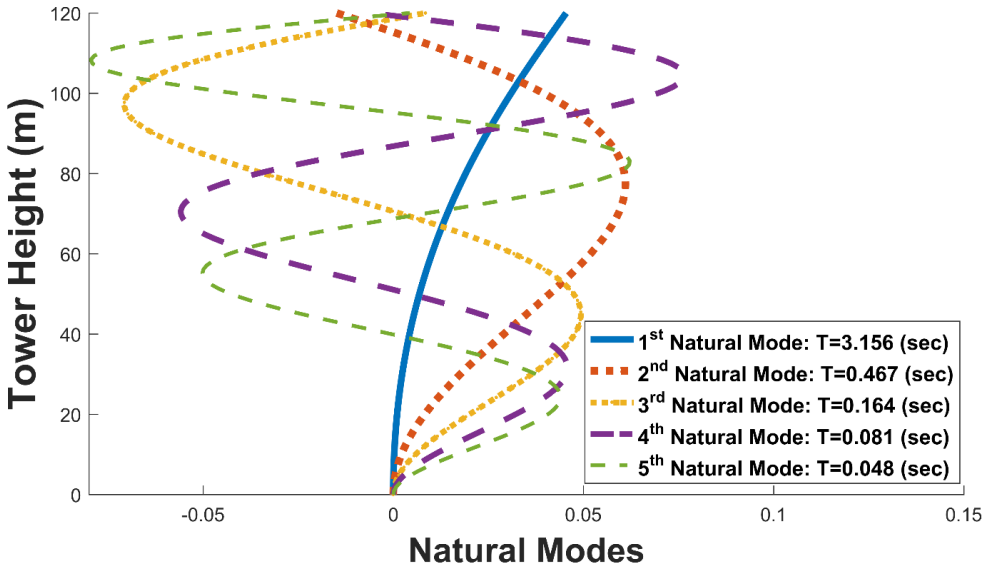

Σχήμα 42: *Πρώτες 5 κανονικές μορφές ταλάντωσης και τιμές των ιδιοπεριόδων της αρχικής ανεμογεννήτριας από το προτεινόμενο δυναμικό μοντέλο του πυλώνα.*

Πίνακας 12: *Ιδιομορφές της αρχικής ανεμογεννήτριας και οι στατικές παραμορφώσεις της κορυφής του πυλώνα της ανεμογεννήτριας.*

	Eigenperiods (*sec*)					Στατική παραμόρφωση κορυφής πυλώνα X_{top} (m)
	T1	T2	T3	T4	T5	
Προτεινόμενο μοντέλο	3.156	0.467	0.164	0.081	0.048	0.7063
SOFiSTiK	3.164	0.474	0.172	0.089	0.056	0.711

Οι εξισώσεις κίνησης της ανεμογεννήτριας με το αντίστοιχο σύστημα ελέγχου λαμβάνονται από την ισορροπία δυνάμεων σε κάθε βαθμό ελευθερίας, και εκφράζονται σε μητρωϊκή μορφή:

$$[M]\{\ddot{X}\}+[C]\{\dot{X}\}+[K]\{X\}=[P]\pm[M]\ddot{X}_G \tag{79}$$

όπου τα μητρώα μάζας [M], απόσβεσης [C], και στιβαρότητας [K] είναι τάξης μεγέθους $(N+n)$ x $(N+n)$. Όπως ειπώθηκε προηγουμένως, N εκφράζει τον αριθμό των πρισματικών στοιχείων δοκού που χρησιμοποιήθηκαν για την μοντελοποίηση του πυλώνα της ανεμογεννήτριας, και n είναι οι επιπλέον βαθμοί ελευθερίας από το αντίστοιχο σύστημα ελέγχου. Επιπλέον, $\{X\} = \{\{X_N\}, \{X_n\}\}^T$ είναι το μητρώο των άγνωστων μετατοπίσεων όλων των βαθμών ελευθερίας σε σχέση με την βάση του πυλώνα. Τα μητρώα μάζας [M], απόσβεσης [C], και στιβαρότητας [K] εκφράζονται ως:

$$[M]=\left[\begin{bmatrix}[M_S]_{N\times N} & [0]_{N\times n}\\ [0]_{n\times N} & [0]_{n\times n}\end{bmatrix}+\begin{bmatrix}[M_{n,a}]_{N\times N} & [0]_{N\times n}\\ [0]_{n\times N} & [M_{n,d}]_{n\times n}\end{bmatrix}\right]_{(N+n)\times(N+n)} \tag{80.α}$$

$$[K]=\left[\begin{bmatrix}[K_S]_{N\times N} & [0]_{N\times n}\\ [0]_{n\times N} & [0]_{n\times n}\end{bmatrix}+\begin{bmatrix}[K_{n,a}]_{N\times N} & -[K_{n,b}]_{N\times n}\\ -[K_{n,c}]_{n\times N} & [K_{n,d}]_{n\times n}\end{bmatrix}\right]_{(N+n)\times(N+n)} \tag{80.β}$$

$$[C]=\left[\begin{bmatrix}[C_S]_{N\times N} & [0]_{N\times n}\\ [0]_{n\times N} & [0]_{n\times n}\end{bmatrix}+\begin{bmatrix}[C_{n,a}]_{N\times N} & -[C_{n,b}]_{N\times n}\\ -[C_{n,c}]_{n\times N} & [C_{n,d}]_{n\times n}\end{bmatrix}\right]_{(N+n)\times(N+n)} \tag{80.γ}$$

όπου τα υπομητρώα $[M_{n,i}]$, $[C_{n.i}]$, and $[K_{n,i}]$ μορφώνονται ανάλογα με το αντίστοιχο σύστημα ελέγχου που εφαρμόζεται. Ο πυλώνας της ανεμογεννήτριας υποβάλλεται στο αεροδυναμικό φορτίο $\overline{F}_N(t)$ όπως φαίνεται στο Σχήμα 43.

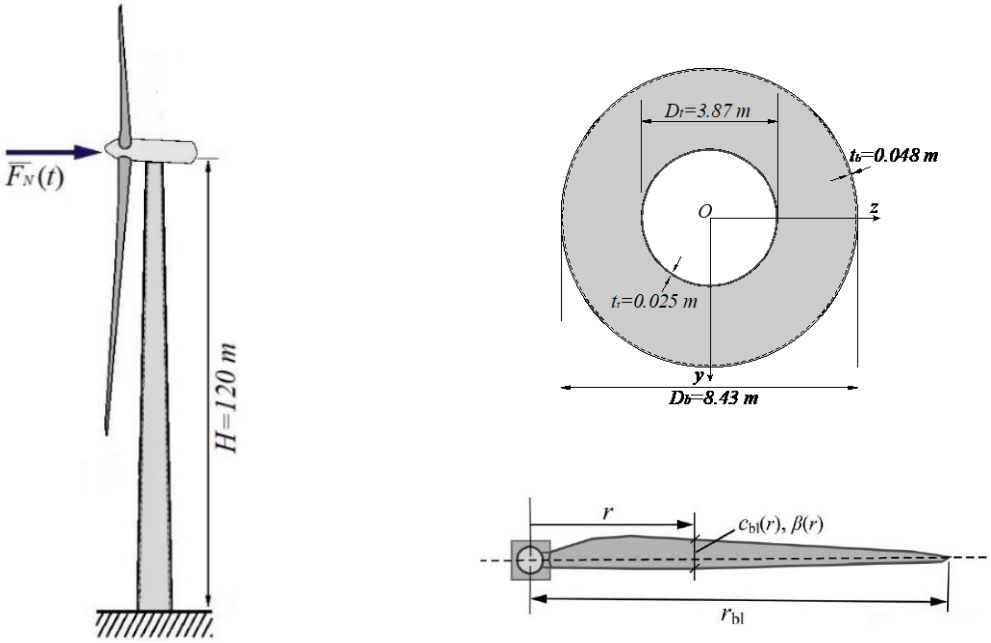

Σχήμα 43: *Πυλώνας ανεμογεννήτριας μεταβλητής κοίλης κυκλικής διατομής, και πτερύγια.*

Περισσότερες πληροφορίες αναφορικά με την έκφραση του αεροδυναμικού φορτίου με βάση την βασική ταχύτητα ανέμου στα 10 *m* βρίσκονται στο (Hansen, 2008). Στην παρούσα εργασία η βασική ταχύτητα ανέμου στα 10 *m* λαμβάνεται υπόψη με βάση τις διατάξεις του EC1, Part1,4 (*EN 1991 - Wind actions*, 2010), και έχει τιμή V_b = 27.0 m/s με τυπική απόκλιση σ = 3.30 m/s ($V_m(120m)$ = 39.93 *m/s*). Η μέση ταχύτητα ανέμου και η παραγόμενη συγκεντρωμένη δύναμη λόγω του αεροδυναμικού φορτίου παρουσιάζονται στο Σχήμα 44.

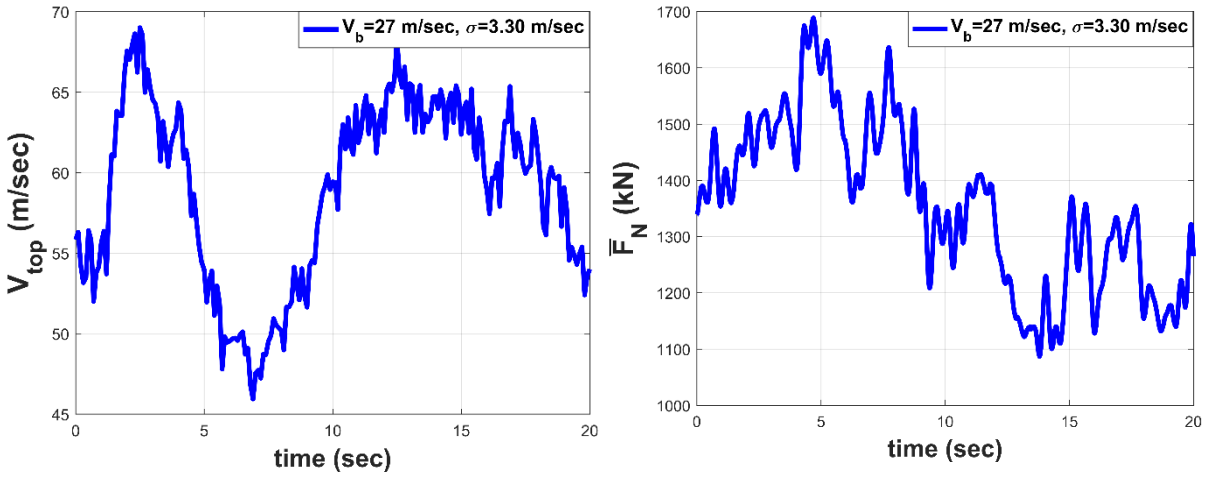

(α) (β)

Σχήμα 44: *Βασική ταχύτητα ανέμου V_b ασε ύψος 10 m (α) και (β) χρονοϊστορία της επιβαλλόμενης δύναμης $\overline{F}_N(t)$ εφαρμοσμένη στην κορυφή του πυλώνα της ανεμογεννήτριας.*

Οι βασικές παράμετροι του KDamper εφαρμοσμένου σε πυλώνες ανεμογεννητριών, όπως παρουσιάστηκε στο Σχήμα 40.δ παρουσιάζονται παρακάτω:

$$\mu_D = m_D / m_{top} \tag{81.α}$$

$$k_D = k_{NS} + k_{PS} \tag{81.β}$$

$$\omega_D = 2\pi f_D = \sqrt{k_D / m_D} = \sqrt{\frac{k_{NS} + k_{PS}}{m_D}} \tag{81.γ}$$

$$k_0 = k_R + \frac{k_{NS} k_{PS}}{k_{NS} + k_{PS}} \tag{81.δ}$$

$$\omega_0 = 2\pi f_0 = \sqrt{k_0 / \left(m_D + m_{top}\right)} = \sqrt{\left(k_R + \frac{k_{NS} k_{PS}}{k_{NS} + k_{PS}}\right) / \left(m_D + m_{top}\right)} \tag{81.ε}$$

$$\zeta_{PS} = c_{PS} / (2 m_D \omega_D) = c_{PS} / (2\sqrt{k_D m_D}) \quad (81.\zeta)$$

όπου μ_D είναι η πρόσθετη μάζα του KDamper. Με βάση την αναλύσεις ευαισθησίας που πραγματοποιήθηκαν στις προηγούμενες ενότητες, ο τεχνητός αποσβεστήρας c_{PS} που τοποθετείται παράλληλα στο στοιχείο θετικής στιβαρότητας k_{PS}, δεν επηρεάζει ιδιαίτερα την δυναμική συμπεριφορά των διευρυμένων KDamper, και επομένως δεν λαμβάνεται υπόψη στην παρούσα ενότητα. Οι βασικές παράμετροι που αφορούν τις διευρυμένες εκδόσεις του KDamper είναι οι παρακάτω:

$$\mu_D = m_D / m_{top} \quad (82.\alpha)$$

$$k_D = k_{NS} + k_{PS} \quad (82.\beta)$$

$$\omega_D = 2\pi f_D = \sqrt{k_D / m_D} = \sqrt{\frac{k_{NS} + k_{PS}}{m_D}} \quad (82.\gamma)$$

$$k_0 = k_R + \frac{k_{NS} k_{PS}}{k_{NS} + k_{PS}} \quad (82.\delta)$$

$$\omega_0 = 2\pi f_0 = \sqrt{k_0 / \left(m_D + m_{top}\right)} = \sqrt{\left(k_R + \frac{k_{NS} k_{PS}}{k_{NS} + k_{PS}}\right) / \left(m_D + m_{top}\right)} \quad (82.\varepsilon)$$

$$\zeta_{NS} = c_{NS} / (2 m_D \omega_D) = c_{NS} / (2\sqrt{k_D m_D}) \quad (82.\zeta)$$

$$\mu_b = m_b / m_{top} \quad (82.\eta)$$

Δεδομένου ότι προβλέπεται ταυτόχρονη μεταβολή στην τιμή των στοιχείων στιβαρότητας, και για συγκεκριμένη τιμή της πρόσθετης μάζας, οι ελεύθερες παράμετροι σχεδιασμού είναι:

1. Η ονομαστική συχνότητα f_0;
2. Η τιμή του στοιχείου αρνητικής στιβαρότητας k_{NS};
3. Η τιμή του τεχνητού αποσβεστήρα c_{NS};
4. Η τιμή του στοιχείου αδράνειας b;

Ο σκοπός των προτεινόμενων δυναμικών συστημάτων απορρόφησης ταλαντώσεων, βασισμένα στον KDamper είναι η βελτίωση της δυναμικής συμπεριφοράς των πυλώνων ανεμογεννητριών, μέσω της αύξησης της ισοδύναμης απόσβεσης των πυλώνων. Για να είναι

ο σχεδιασμός των συστημάτων ελέγχου ρεαλιστικός και ταυτόχρονα αποτελεσματικός, πρέπει να επιβάλλονται περιορισμοί με βάση τεχνικά κριτήρια στα όρια των ελεύθερων παραμέτρων σχεδιασμού και στις δυναμικές αποκρίσεις του συστήματος. Πιο συγκεκριμένα:

i. Η μετατόπιση της κορυφής του πυλώνα της ανεμογεννήτριας τίθεται ως αντικειμενική συνάρτηση του προβλήματος βελτιστοποίησης.
ii. Επιβάλλεται ένας γεωμετρικός περιορισμός που αφορά την σχετική μετατόπιση της πρόσθετης μάζας (m_D) με την κορυφή του πυλώνα της ανεμογεννήτριας, $u_{D,REL}=u_D - u_{TOP}$. Το άνω όριο της σχετικής μετατόπισης $u_{D,REL}$ είναι 1.5 *m*, μικρότερο από την μισή διάμετρο της κορυφής του πυλώνα (3.84/2=1.92 *m*).
iii. Ένας ακόμα γεωμετρικός περιορισμός που επιβάλλεται είναι η σχετική μετατόπιση μεταξύ του κελύφους (nacelle) και της κορυφής του πύργου της ανεμογεννήτριας, $u_{NAC,REL}=u_{NAC} - u_{TOP}$, να είναι μικρότερη από 0.5 *m*.
iv. Η πρόσθετη μάζα των KDamper-βασισμένων συστημάτων ελέγχου πρέπει να είναι σε ρεαλιστικά όρια, καθώς είναι εξαιρετικά ανεπιθύμητες μεγάλες τιμές πρόσθετης μάζας στην κορυφή του πυλώνα. Για αυτόν τον λόγο, διάφορες τιμές της πρόσθετης μάζας στο εύρος [0.1 0.5] % επιλέγονται για να ληφθούν τα αντίστοιχα σετ παραμέτρων.
v. Η ονομαστική συχνότητα f_0 επιλέγεται στο εύρος *[0.1 2.0]* (*Hz*).
vi. Το άνω όριο του λόγου μάζας του inerter μ_b τίθεται ίσο με 0.5.
vii. Το άνω όριο των τεχνητών αποσβεστήρων είναι *1000 kNs/m*.
viii. Το στοιχείο αρνητικής στιβαρότητας υλοποιείται με βάση την 2^{η} προτεινόμενη διάταξη για δισδιάστατη αρνητική στιβαρότητα. Το άνω όριο της τιμής του στοιχείου αρνητικής στιβαρότητας τίθεται ίσο με *-50 kN/m* ανά *tn* μάζας της κατασκευής, 50% μικρότερο συγκριτικά με την δημοσίευση (Antoniadis et al., 2018);

Αναφορικά με τον βέλτιστο σχεδιασμό του TMD, αρχικά παρουσιάζονται οι παράμετροι του συστήματος:

$$\mu_D = m_D / m_{top} \tag{83.α}$$

$$\omega_D = 2\pi f_D = \sqrt{k_D / m_D} \tag{83.β}$$

$$\zeta_D = c_D / \left(2\omega_D m_D\right) = c_D / \left(2\sqrt{k_D m_D}\right) \tag{83.γ}$$

όπου μ_D είναι ο λόγος μάζας της πρόσθετης μάζας του TMD. Μια συνήθης τακτική για τον βέλτιστο σχεδιασμό του TMD είναι ο συντονισμός των παραμέτρων του, Εξίσωση (83.β), με την ιδιοσυχνότητα του αρχικού συστήματος. Ο πυλώνας ανεμογεννήτριας είναι πολυβάθμιο σύστημα, και κατ' επέκταση πρέπει να επιβεβαιώσουμε αν η προσέγγιση αυτή είναι όντως βέλτιστη στην περίπτωση που το TMD εφαρμόζεται σε πυλώνες ανεμογεννητριών. Στο Σχήμα 45 παρουσιάζεται η μέγιστη τιμή της απόκρισης της κορυφής του πυλώνα σε σχέση με την συχνότητα συντονισμού του TMD, για διάφορες τιμές του λόγου απόσβεσης. Η πρόσθετη μάζα του TMD επιλέγεται ίση με 5%.

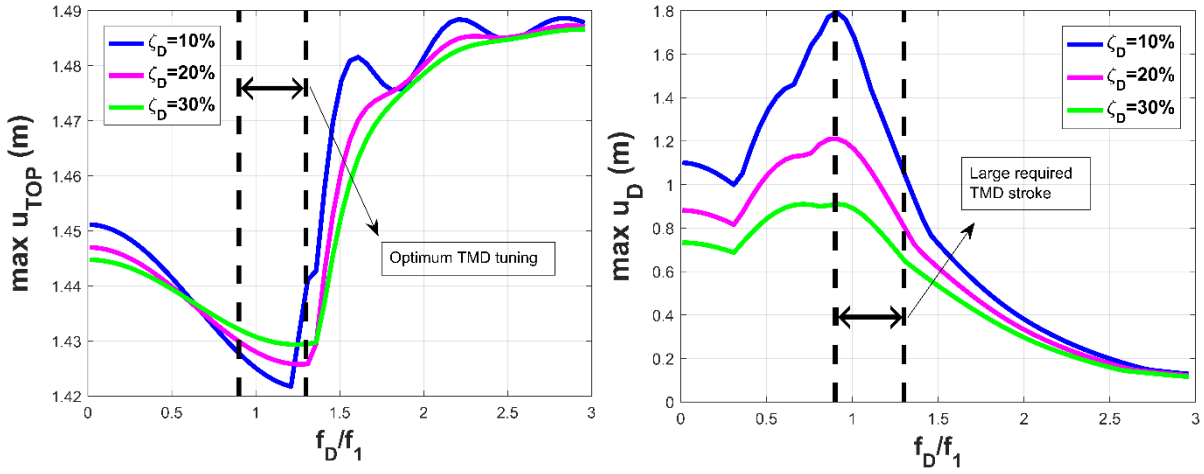

(α) (β)

Σχήμα 45: *Βέλτιστος σχεδιασμός του TMD. (α) Μέγιστη μετατόπιση του πυλώνα της ανεμογεννήτριας, και (β) μέγιστη σχετική μετατόπιση μεταξύ της πρόσθετης μάζας του TMD και του πυλώνα, σε σχέση με την συχνότητα του TMD f_D/f_1, για διάφορες τιμές του λόγου απόσβεσης ζ_D.*

Η βέλτιστη τιμή της συχνότητας του TMD παρατηρείται στο εύρος [0.9 1.3]f_1 της πρώτης ιδιοσυχνότητας του πυλώνα της ανεμογεννήτριας, και επιλέγεται ως $1.25f_1$=0.396 *Hz*. Ο λόγος απόσβεσης, όπως παρατηρείται από το Σχήμα 45, επηρεάζει σημαντικά της μέγιστες δυναμικές αποκρίσεις, και επομένως επιλέγεται ως 30%, τιμή που στη βιβλιογραφία θεωρείται ως ακραία, αλλά για τον σκοπό της σύγκρισης επιλέγεται.

Στο Σχήμα 46 παρουσιάζεται η επιρροή της πρόσθετης μάζας του TMD στην μέγιστη τιμή της μετατόπισης της κορυφής του πυλώνα (Σχήμα 46.α) και της σχετικής μετατόπισης μεταξύ της πρόσθετης μάζας και της κορυφής του πυλώνα (Σχήμα 46.β). Επιπλέον, η επιρροή της εφαρμογής του TMD στην ισοδύναμη απόσβεση του πυλώνα της ανεμογεννήτριας παρουσιάζεται στο Σχήμα 46.γ. Για να υπολογίζουμε την ισοδύναμη απόσβεση του συστήματος, επιβάλλεται σε ελεύθερη ταλάντωση με αρχικές συνθήκες, εκείνες της πρώτης

ιδιομορφής του αρχικού συστήματος. Η τιμή του ισοδύναμου λόγου απόσβεσης υπολογίζεται από την ακόλουθη σχέση:

$$\ln\left[\frac{X_N(t)}{X_N(t+T)}\right]=\frac{2\pi\zeta_{eff}}{\sqrt{1-\zeta_{eff}^2}} \tag{84}$$

όπου T είναι ο χρόνος μεταξύ δύο διαδοχικών μεγίστων της δυναμικής απόκρισης, και X_N είναι η μετατόπιση της κορυφής του πυλώνα.

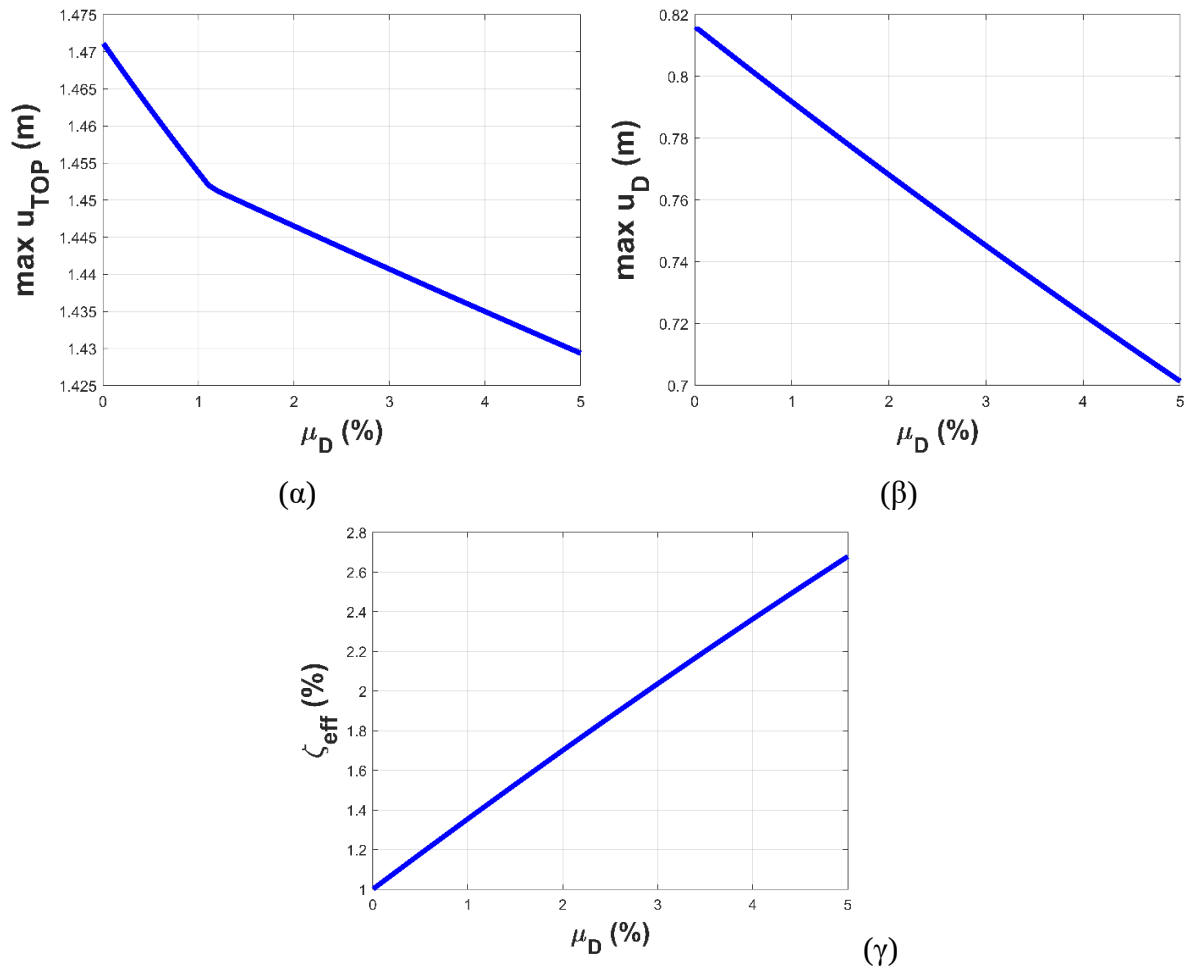

Σχήμα 46: *Επίδραση του λόγου μάζας μ_D του TMD στην: (α) μέγιστη μετατόπιση του πυλώνα της ανεμογεννήτριας, (β) σχετική μετατόπιση μεταξύ του TMD και του πυλώνα, και (γ) ισοδύναμη απόσβεση του πυλώνα της ανεμογεννήτριας.*

Αναφορικά με το nacelle-isolation σύστημα ελέγχου, οι ελεύθερες παράμετροι σχεδιασμού είναι το στοιχείο θετικής στιβαρότητας k_D, και ο τεχνητός αποσβεστήρας c_D. Οι αντίστοιχοι περιορισμοί με τα KDamper-βασισμένα συστήματα επιβάλλονται, δηλαδή της

μέγιστης σχετικής μετατόπισης μεταξύ nacelle-πυλώνα να είναι μικρότερη από 0.50 m, και η μέγιστη τιμή του τεχνητού αποσβεστήρα είναι 1000 *kNs/m*. Πραγματοποιήθηκαν παραμετρικές αναλύσεις και παρουσιάστηκαν στο Σχήμα 47, για να επιλέξουμε τις βέλτιστες παραμέτρους του συστήματος, που αναφέρονται παρακάτω:

$$\omega_D = 2\pi f_D = \sqrt{k_D / m_{tot}} \tag{85.α}$$

$$\zeta_D = c_D / \left(2\omega_D m_D\right) = c_D / \left(2\sqrt{k_D m_{tot}}\right) \tag{85.β}$$

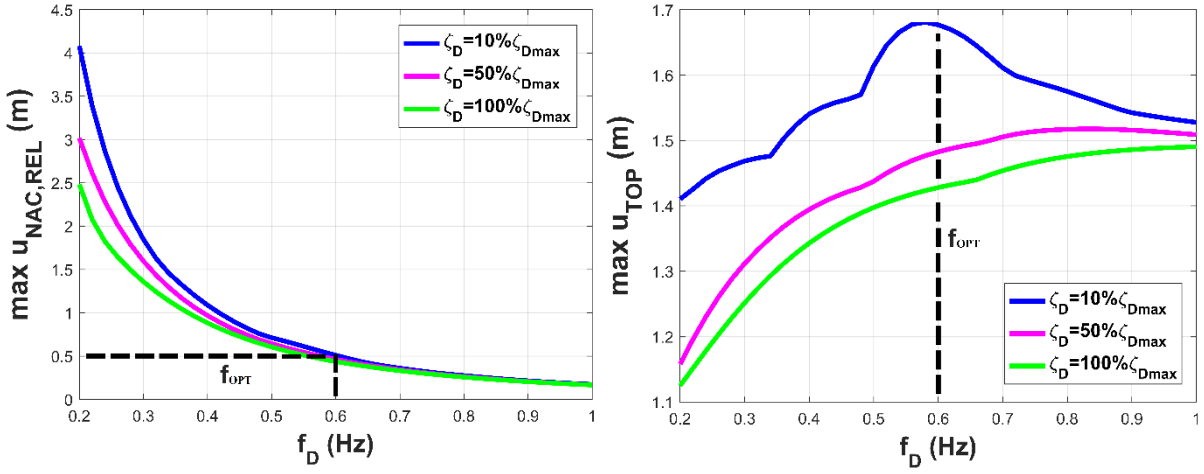

(α) (β)

Σχήμα 47: *Βέλτιστος σχεδιασμός του nacelle-isolation συστήματος ελέγχου. (α) Επιλογή της συχνότητας συντονισμού, και (β) επιλογή του λόγου απόσβεσης του συστήματος.*

Οι παράμετροι σχεδιασμού για να πληρούνται οι περιορισμοί που αναφέρθηκαν παραπάνω, είναι f_D=0.556 *Hz* (οριακή περίπτωση όπου $u_{NAC,\,REL}$=0.5 *m*), και ζ_D=35.5 %.

Οι βέλτιστες παράμετροι των προτεινόμενων δυναμικών συστημάτων απορρόφησης ταλαντώσεων βασισμένα στον KDamper, παρουσιάζονται στους Πίνακες 13-15. Οι δυναμικές αποκρίσεις του πυλώνα της ανεμογεννήτριας και η ισοδύναμη απόσβεσή του παρουσιάζονται στο Σχήμα 48 για κάθε τιμή της επιλεγμένης πρόσθετης μάζας m_D στο εύρος [0.1 0.5]%. Η δυναμική συμπεριφορά της nacelle είναι εξαιρετικής σημασίας για την απόδοση της ανεμογεννήτριας, και επομένως η επίδραση της πρόσθετης μάζας των προτεινόμενων συστημάτων με βάση τον KDamper, παρουσιάζεται στο Σχήμα 49. Τέλος, οι μέγιστες τιμές της σχετικής μετατόπισης μεταξύ της πρόσθετης μάζας και του πυλώνα, καθώς και η σχετική μετατόπιση των τερματικών του στοιχείου αρνητικής στιβαρότητας παρουσιάζονται στο Σχήμα 50.

Πίνακας 13: *Παράμετροι του KDamper.*

μ_D (%)	f_0 (Hz)	k_{NS} (kN/m)	c_{PS} (kNs/m)	k_{PS} (kN/m)	k_R (kN/m)
0.1	0.547	-3558.16	993.13	6714.58	12343.34
0.2	0.557	-3492.81	966.73	6472.92	12538.02
0.3	0.547	-3674.95	931.00	7006.28	12514.36
0.4	0.550	-3371.66	831.60	6227.71	12181.48
0.5	0.548	-3504.47	989.40	6564.08	12326.82

Πίνακας 14: *Παράμετροι του διευρυμένου KDamper (EKD).*

μ_D (%)	f_0 (Hz)	k_{NS} (kN/m)	c_{NS} (kNs/m)	k_{PS} (kN/m)	k_R (kN/m)
0.1	0.541	-9501.00	986.08	32385.78	18103.61
0.2	0.532	-9335.64	968.12	32313.48	17638.61
0.3	0.532	-8822.59	996.64	28789.43	17240.72
0.4	0.532	-8758.40	963.99	28341.94	17201.80
0.5	0.523	-8668.35	993.72	28732.58	16783.15

Πίνακας 15: *Παράμετροι του διευρυμένου KDamper με inerter (EKDI).*

μ_D (%)	f_0 (Hz)	k_{NS} (kN/m)	c_{NS} (kNs/m)	μ_b (%)	k_{PS} (kN/m)	k_R (kN/m)
0.1	0.551	-12543.61	997.34	0.498	58079.07	20829.40
0.2	0.545	-10395.09	986.69	0.496	38285.04	19015.52
0.3	0.544	-10380.34	960.28	0.497	38435.78	18938.34
0.4	0.538	-8995.40	939.73	0.493	29242.48	17618.43
0.5	0.540	-9086.47	996.11	0.497	29604.58	17772.91

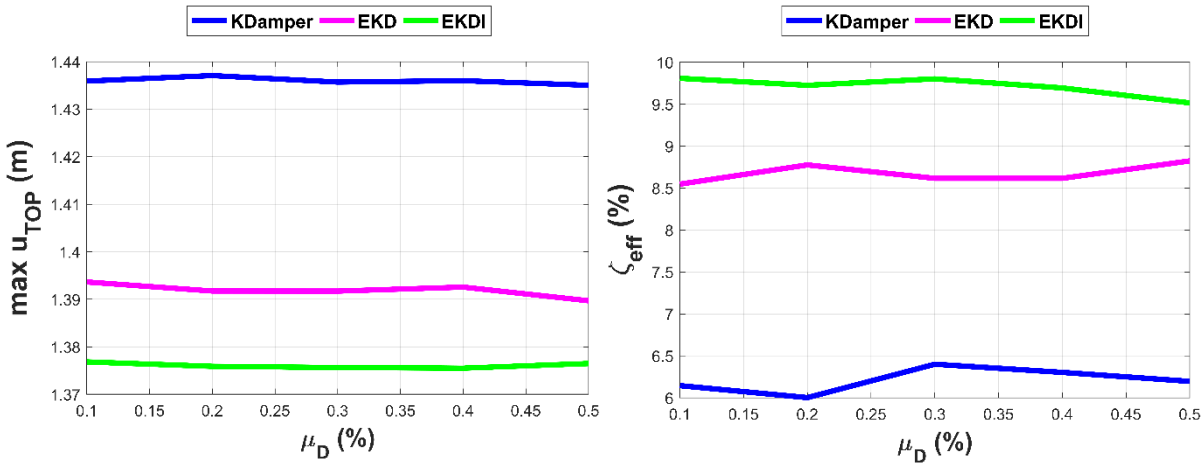

(α) (β)

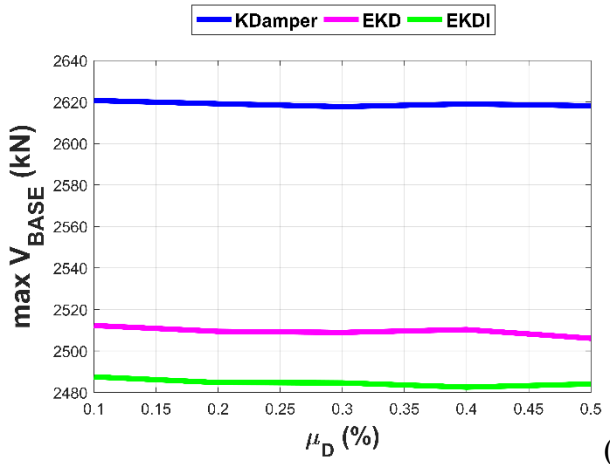

(γ)

Σχήμα 48: *Αποτελέσματα της βελτιστοποίησης των προτεινόμενων συστημάτων ελέγχου με βάση τον KDamper, KDamper, EKD, και EKDI. (α) Μετατόπιση του πυλώνα, (β) ισοδύναμος λόγος απόσβεσης του πυλώνα, και (γ) συνολική τέμνουσα βάσης.*

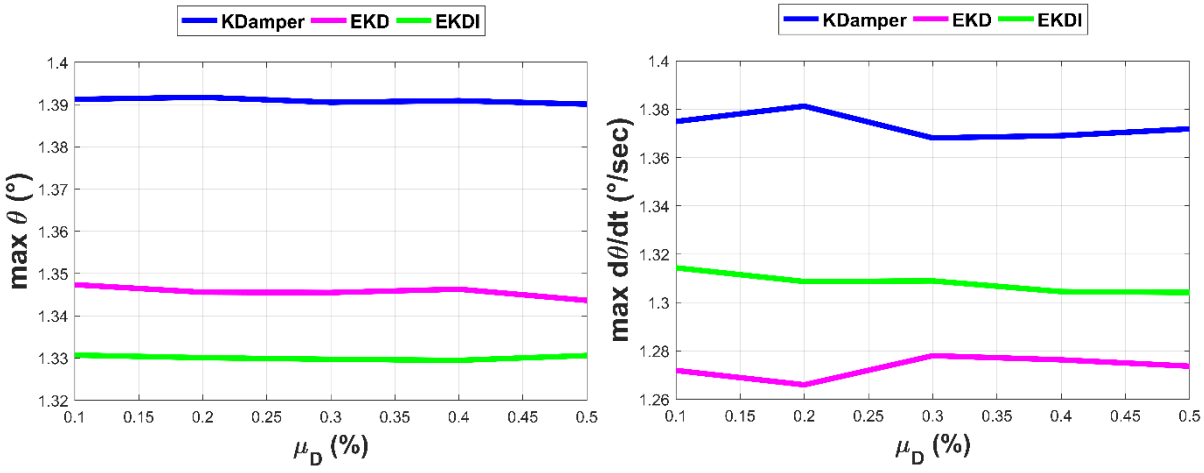

(α) (β)

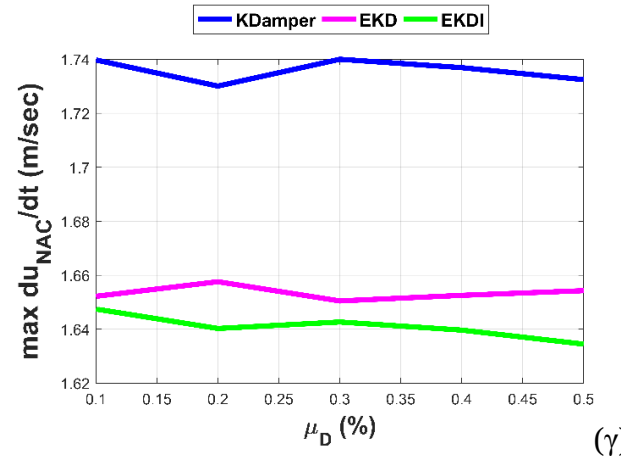

(γ)

Σχήμα 49: *Αποτελέσματα της βελτιστοποίησης των προτεινόμενων συστημάτων ελέγχου με βάση τον KDamper, KDamper, EKD, και EKDI. (α) Γωνία εκτροπής, (β) γωνιακή ταχύτητα, και (γ) σχετική (με τη βάση) ταχύτητα της nacelle.*

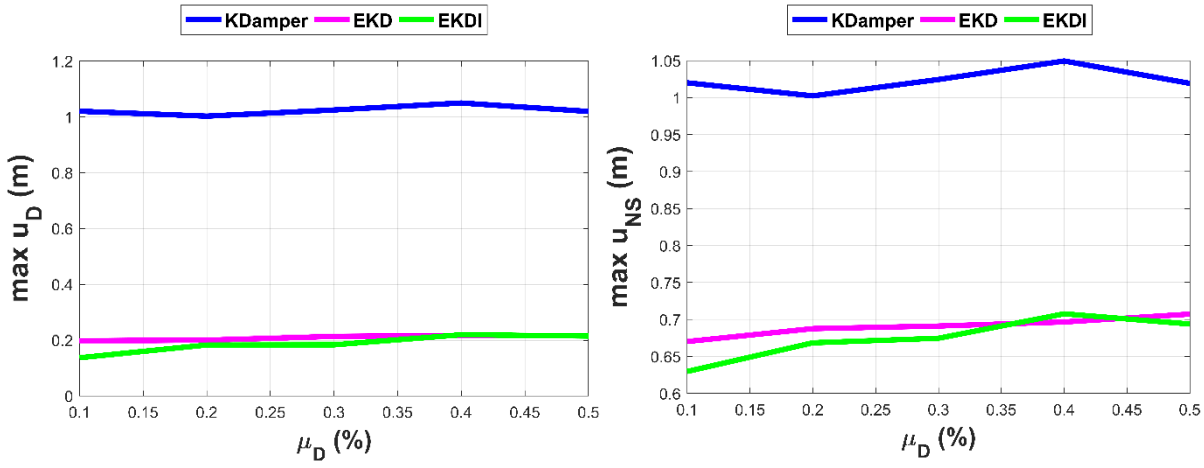

(α) (β)

Σχήμα 50: *Αποτελέσματα της βελτιστοποίησης των προτεινόμενων συστημάτων ελέγχου με βάση τον KDamper, KDamper, EKD, και EKDI. Σχετικές μετατοπίσεις μεταξύ(α) πρόσθετης μάζας-πυλώνα, (β) τερματικών του στοιχείου αρνητικής στιβαρότητας.*

Για να αξιολογήσουμε την αποτελεσματικότητα των προτεινόμενων συστημάτων ελέγχου, η απόδοσή τους συγκρίνεται με εκείνη των TMD και nacelle-isolation συστημάτων. Οι μέγιστες τιμές των δυναμικών αποκρίσεων του πυλώνα της ανεμογεννήτριας, της nacelle, αλλά και οι καινούριες τιμές του ισοδύναμου λόγου απόσβεσης του πυλώνα παρουσιάζονται στον Πίνακα 16. Αναφορικά με τα συστήματα βασισμένα στον KDamper, παρουσιάζονται τα αποτελέσματα που αφορούν τα σετ παραμέτρων για πρόσθετη μάζα ίση με 0.1%.

Πίνακας 16: *Μέγιστες τιμές των δυναμικών αποκρίσεων του πυλώνα της ανεμογεννήτριας, της nacelle, αλλά και οι καινούριες τιμές του ισοδύναμου λόγου απόσβεσης του πυλώνα.*

	Συστήματα Ελέγχου					
	Αρχική ανεμογεννήτρια	TMD (5%)	Nacelle-isolation	KDamper (0.1%)	EKD (0.1 %)	EKDI (0.1%)
u_{TOP} (m)	1.471	1.429	1.4167	1.436	1.394	1.377
ζ_{eff} $(\%)$	1	2.68	7.82	6.14	8.55	9.81
V_{BASE} (kN)	2677.6	2308.6	2547.1	2620.7	2512.3	2487.5
θ $(^\circ)$	1.424	1.391	1.368	1.391	1.347	1.331
$d\theta/dt$ $(^\circ/sec)$	1.484	1.451	1.238	1.375	1.272	1.314
du_{NAC}/dt (m/sec)	1.448	1.406	1.703	1.740	1.652	1.647
u_D (m)	-	0.701	0.500	1.020	0.198	0.136
u_{NS} (m)	-	-	-	1.020	0.670	0.629

Στο Σχήμα 51 παρουσιάζονται οι δυναμικές αποκρίσεις της κορυφής του πυλώνα της ανεμογεννήτριας και της τέμνουσας βάσης υποβαλλόμενου στο αεροδυναμικό φορτίο, και σε ελεύθερη ταλάντωση, για τα συστήματα ελέγχου TMD, nacelle-isolation, και EKDI.

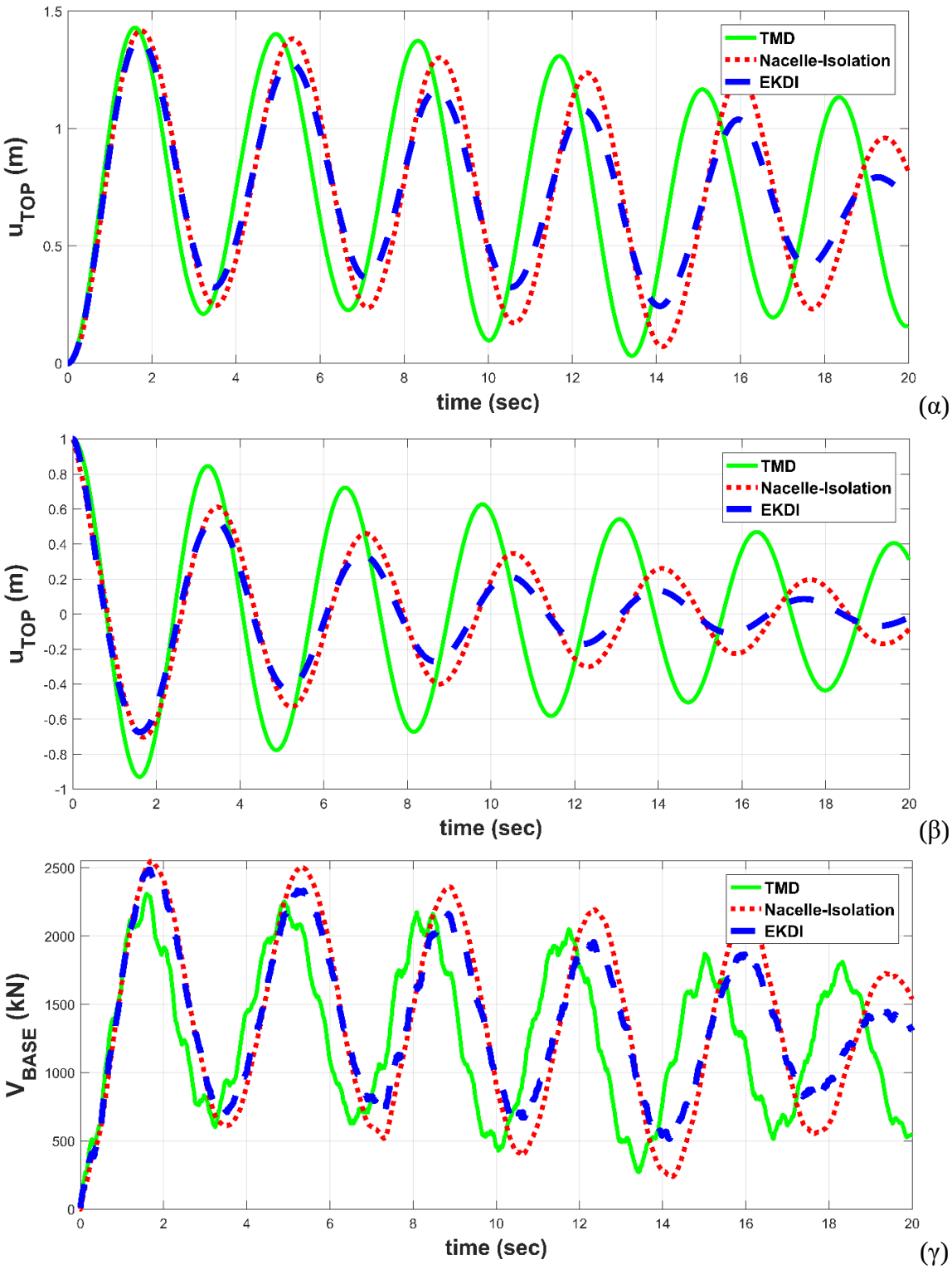

Σχήμα 51: *Δυναμικές αποκρίσεις της κορυφής του πυλώνα για: (α) το αεροδυναμικό φορτίο, (β) ελεύθερη ταλάντωση. (γ) Τέμνουσα βάσης λόγω του αεροδυναμικού φορτίου.*

Τέλος, στο Σχήμα 52 παρουσιάζονται οι δυναμικές αποκρίσεις που αφορούν την πρόσθετη μάζα των συστημάτων ελέγχου βασισμένα στον KDamper.

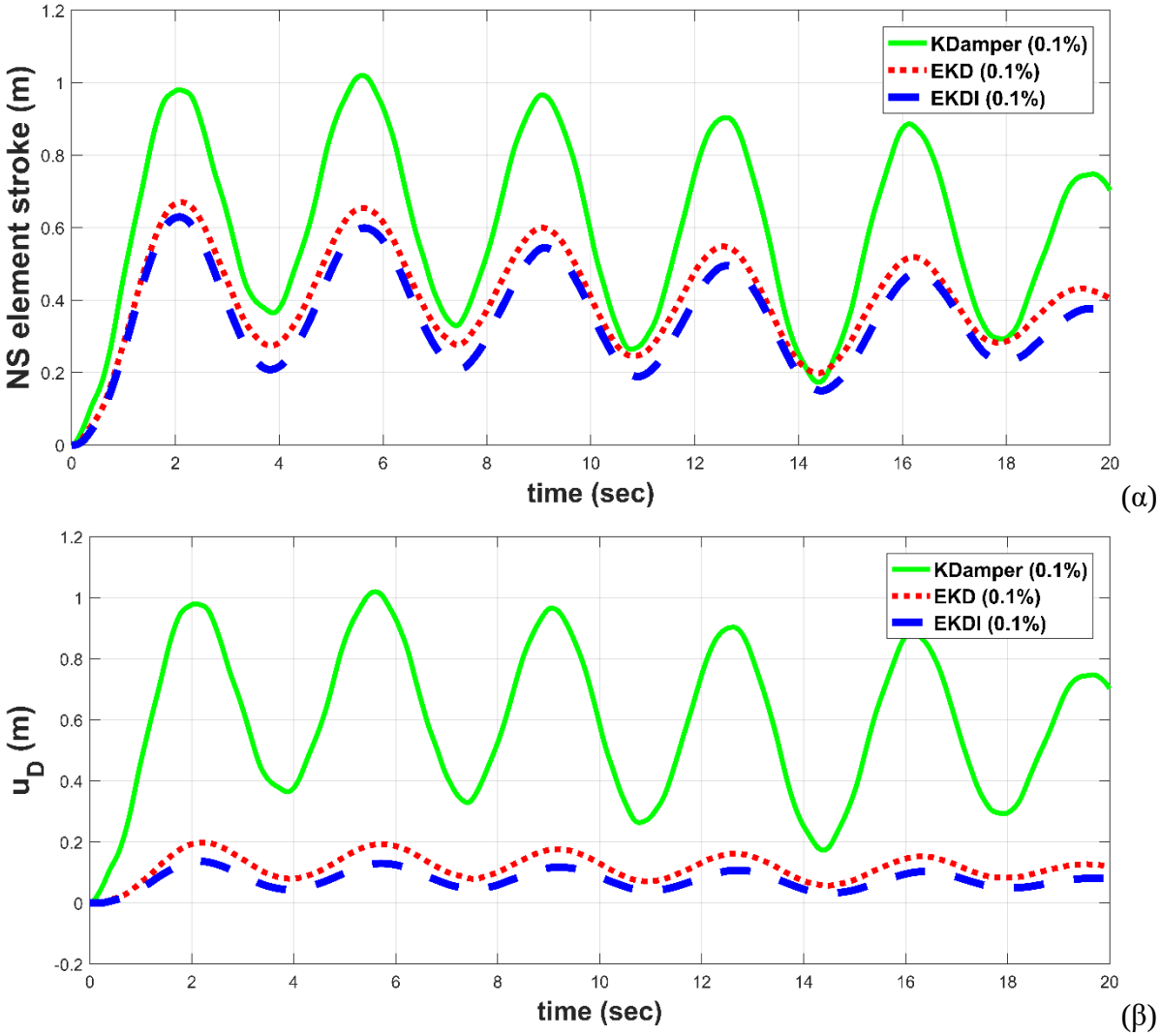

Σχήμα 52: *Δυναμικές αποκρίσεις της πρόσθετης μάζας των συστημάτων ελέγχου με βάση τον KDamper: (α) σχετική μετατόπιση μεταξύ των τερματικών του στοιχείου αρνητικής στιβαρότητας και (β) σχετική μετατόπιση μεταξύ πρόσθετης μάζας και κορυφής του πυλώνα, λόγω του αεροδυναμικού φορτίου*

Με βάση τα αριθμητικά αποτελέσματα από την εφαρμογή των συστημάτων ελέγχου βασισμένα στον KDamper στον πυλώνα που υποστηρίζει την 5MW NREL ανεμογεννήτρια, παρουσιάζονται τα παρακάτω συγκεντρωτικά αποτελέσματα:

i. Το δυναμικό μοντέλο του πυλώνα της ανεμογεννήτριας που αναπτύχθηκε στην παρούσα διδακτορική διατριβή είναι εύχρηστο για την εισαγωγή και βελτιστοποίηση

των προτεινόμενων συστημάτων ελέγχου, η εγκυρότητα του οποίου επιβεβαιώθηκε μέσα από σύγκριση με λογισμικό πακέτο με βασισμένο σε FEM.

ii. Η ισοδύναμη απόσβεση του πυλώνα της ανεμογεννήτριας αυξήθηκε σημαντικά με τα προτεινόμενα συστήματα ελέγχου (6.14%, 8.55%, 9.81%), όπως συγκρίθηκε με εκείνη του TMD (2.68%) με πρόσθετη μάζα 5%, και με του nacelle-isolation συστήματος (7.82%).

iii. Τα προτεινόμενα δυναμικά συστήματα απορρόφησης ταλαντώσεων με βάση τον KDamper είναι πολύ πιο αποτελεσματικά σε σύγκριση με τον TMD, χρησιμοποιώντας μικρή πρόσθετη μάζα 0.1%, 50 φορές μικρότερη σε σύγκριση με του TMD.

iv. Η δυναμική συμπεριφορά του πύργου της ανεμογεννήτριας παρουσίασε την μεγαλύτερη βελτίωση με τα προτεινόμενα συστήματα ελέγχου, ενώ η δυναμική συμπεριφορά της nacelle δεν επηρεάστηκε σημαντικά.

v. Οι προτεινόμενες διευρυμένες εκδόσεις του KDamper μειώνουν σημαντικά την σχετική μετατόπιση των τερματικών του στοιχείου αρνητικής στιβαρότητας, και διευκολύνουν άρα τον ρεαλιστικό σχεδιασμό του.

vi. Η προσθήκη του στοιχείου αδράνειας inerter στην διευρυμένη έκδοση του KDamper έχει ευεργετικό ρόλο στη συνολική δυναμική συμπεριφορά της ανεμογεννήτριας.

VIII. Συμπεράσματα

Στην παρούσα διδακτορική διατριβή, εξετάστηκε η απορρόφηση των ταλαντώσεων που οφείλονται σε περιβαλλοντικές διεγέρσεις σε κατασκευές Πολιτικού Μηχανικού με την εφαρμογή προηγμένων δυναμικών συστημάτων απορρόφησης ταλαντώσεων, βασισμένων σε στοιχεία αρνητικής στιβαρότητας. Τα κύρια σημεία που διερευνήθηκαν είναι τα ακόλουθα:

- Ο βέλτιστος σχεδιασμός των προτεινόμενων διατάξεων, λαμβάνοντας υπόψη τους περιορισμούς που επιβάλλει η εκάστοτε εξεταζόμενη εφαρμογή.
- Η οριζόντια σεισμική προστασία των πολυώροφων κατασκευών.
- Η κατακόρυφη σεισμική προστασία δομικών συστημάτων.
- Η αύξηση του κύκλου ζωής ανεμογεννητριών μέσω της αύξησης της ισοδύναμης απόσβεσης των πυλώνων τους.

Για την αποτελεσματική εφαρμογή των προτεινόμενων δυναμικών συστημάτων απορρόφησης ταλαντώσεων, σχεδιάστηκαν ρεαλιστικές διατάξεις και ελήφθησαν υπόψη οι αντίστοιχοι κανονισμοί του εκάστοτε κώδικα. Εξετάστηκαν διαφορετικά σενάρια εφαρμογής, στα οποία αφενός αξιολογήθηκε η απόδοση των προτεινόμενων συστημάτων προστασίας και αφετέρου έγινε σύγκριση με αντίστοιχες συσκευές απορρόφησης ταλαντώσεων ευρέως γνωστές στη βιβλιογραφία. Τα κύρια συμπεράσματα, στα οποία καταλήγει η παρούσα διδακτορική διατριβή είναι:

i. Η συστηματική προσέγγιση για τον βέλτιστο σχεδιασμό του KDamper οδηγεί στην βελτίωση των χαρακτηριστικών απόσβεσης του ταλαντωτή χωρίς παράλληλα να είναι απαραίτητη η αύξηση της πρόσθετης μάζας.
ii. Οι ιδιότητες μόνωσης ταλαντώσεων και απόσβεσης του KDamper προκύπτουν ουσιαστικά από τις ιδιότητες στιβαρότητας του συστήματος και γι’ αυτό μελλοντικές τεχνολογικές εξελίξεις μπορεί να ανακύψουν έναντι του TMD, αναφορικά με τη μάζα, την πολυπλοκότητα και την αξιοπιστία του συστήματος, χωρίς περιορισμούς στη συνολική του στιβαρότητα, όπως συμβαίνει στις διατάξεις QZS.
iii. Οι επιβαλλόμενες διεγέρσεις ακολουθούν τις διατάξεις των κανονισμών που αφορούν στο υπό εξέταση δομικό σύστημα.

iv. Η προτεινόμενη προσέγγιση για την επιλογή της ονομαστικής συχνότητας του KDamper στο πεδίο της συχνότητας είναι ακριβής, όπως επαληθεύτηκε από τις δυναμικές αναλύσεις στο πεδίο του χρόνου.

v. Κατά τον ενδεικτικό σχεδιασμό του KDamper αποδείχθηκε ότι η προστιθέμενη μάζα, ο τεχνητός αποσβεστήρας και τα στοιχεία στιβαρότητας κυμαίνονται σε λογικά και τεχνολογικά υλοποιήσιμα εύρη.

vi. Τα αποτελέσματα του μη-γραμμικού προβλήματος βρίσκονται σε πολύ καλή συμφωνία με τα αντίστοιχα του αρχικού, γραμμικού προβλήματος, όσον αφορά την προτεινόμενη διάταξη για την υλοποίηση του μονοδιάστατου στοιχείου αρνητικής στιβαρότητας.

vii. Το σύστημα KDamper μπορεί να εφαρμοστεί επιτυχώς στη βάση κατασκευών, ως προσθήκη στα συμβατικά συστήματα μόνωσης βάσης, και να μειώσει σε μεγάλο βαθμό τις απαιτήσεις για μετακίνηση στη βάση.

viii. Μία εναλλακτική εφαρμογή του KDamper ως στιβαρή βάση απορρόφησης κραδασμών μπορεί να βελτιώσει σημαντικά τη δυναμική συμπεριφορά της ανωδομής, διατηρώντας παράλληλα τις μετακινήσεις της βάσης στην τάξη των μερικών εκατοστών.

ix. Η αποδοτικότητα του KDamper αξιολογήθηκε με βάση πραγματικές σεισμικές καταγραφές, αποδεικνύοντας την αποτελεσματική του εφαρμογή τόσο σε μονοβάθμια συστήματα όσο και σε πολυώροφες κατασκευές.

x. Προτάθηκε μία διευρυμένη εκδοχή του KDamper (EKD), η οποία προβλέπει ταυτόχρονη μεταβολή στην τιμή των στοιχείων στιβαρότητας και εισάγει μικρότερες προστιθέμενες μάζες, συγκριτικά με το KDamper.

xi. Ο σχεδιασμός του EKD βασίζεται σε τεχνικά κριτήρια. Σε σύγκριση με τον KDamper, η αποδοτικότητα του συστήματος βελτιώθηκε, ενώ παράλληλα οι τιμές των στοιχείων στιβαρότητας μειώθηκαν κατά 50%.

xii. Βάσει των αναλύσεων ευαισθησίας που πραγματοποιήθηκαν, κατά τις οποίες τα στοιχεία του EKD μεταβάλλονταν από τις βέλτιστες τιμές τους, το σύστημα EKD δεν είναι ευάλωτο σε φαινόμενα αποσυντονισμού.

xiii. Το EKD μπορεί να εφαρμοστεί επιτυχώς ως βάση απορρόφησης ταλαντώσεων σε πολυώροφες κατασκευές, βελτιώνοντας σημαντικά τη δυναμική τους συμπεριφορά. Η δυναμική απόκριση της ανωδομής βελτιώνεται σε επίπεδα συγκρίσιμα με ένα συμβατικά σεισμικά μονωμένο σύστημα, παράλληλα μειώνοντας δραστικά τις μετακινήσεις της βάσης.

xiv. Η μικρή μετατόπιση βάσης του EKD καθιστά δυνατή την εφαρμογή της προτεινόμενης συσκευής με χρήση συμβατικών δομικών στοιχείων, χωρίς την ανάγκη ειδικού τύπου εφεδράνων ή πολύπλοκων διατάξεων.

xv. Η εφαρμογή του EKD είναι δυνατή σε υφιστάμενες πολυώροφες κατασκευές. Οι επιταχύνσεις στην ανωδομή και οι σχετικές μετατοπίσεις των ορόφων μειώνονται, χωρίς όμως να μειώνεται η στιβαρότητα του αρχικού συστήματος ή να εισάγονται μεγάλες προστιθέμενες μάζες.

xvi. Η προτεινόμενη διάταξη για την υλοποίηση του στοιχείου αρνητικής στιβαρότητας του EKD συστήματος δημιουργεί «γραμμική» δισδιάστατη αρνητική στιβαρότητα.

xvii. Η επέκταση του KDamper με την προσθήκη inerter παρουσιάστηκε ως μια στιβαρή βάση απορρόφησης ταλαντώσεων (SBA), σχεδιασμένη βάσει τεχνικών κριτηρίων.

xviii. Το SBA εφαρμόζεται σε πολυώροφες κατασκευές, βελτιώνοντας σε μεγάλο βαθμό τη δυναμική τους συμπεριφορά. Οι επιταχύνσεις και οι σχετικές μετατοπίσεις των ορόφων είναι σημαντικά μειωμένες, αλλά και οι μετατοπίσεις στη βάση είναι δραστικά μικρότερες, σε σύγκριση με άλλες προσεγγίσεις σεισμικής μόνωσης στη βάση, αλλά και σε σύγκριση με τα συστήματα KDamper και EKD όταν αυτά εφαρμόζονται στη βάση κατασκευών.

xix. Βάσει των αναλύσεων ευαισθησίας που πραγματοποιήθηκαν, το SBA δεν είναι ευάλωτο σε φαινόμενα αποσυντονισμού.

xx. Οι μικρές μετατοπίσεις βάσης του συστήματος SBA, καθιστούν δυνατή την εφαρμογή της προτεινόμενης συσκευής με χρήση συμβατικών δομικών στοιχείων, χωρίς την ανάγκη για ειδικού τύπου εφέδρανα. Επομένως, είναι εφικτή η εφαρμογή σε υφιστάμενες κατασκευές.

xxi. Το προτεινόμενο δυναμικό σύστημα απορρόφησης κατακόρυφων ταλαντώσεων (VSA), βασισμένο στις διευρυμένες εκδοχές του KDamper, είναι ρεαλιστικά σχεδιασμένο στο πεδίο συχνοτήτων βάσει τεχνικών κριτηρίων.

xxii. Το VSA επιτυγχάνει σημαντική μείωση στις μέγιστες κατακόρυφες επιταχύνσεις και παράλληλα διατηρεί τις στατικές κατακόρυφες μετατοπίσεις σε αποδεκτά επίπεδα, ξεπερνώντας το μειονέκτημα των υφιστάμενων προσεγγίσεων κατακόρυφης μόνωσης.

xxiii. Η απόδοση του VSA αξιολογήθηκε με πραγματικές σεισμικές καταγραφές και χρησιμοποιήθηκαν ρεαλιστικές διατάξεις για την υλοποίηση του στοιχείου αρνητικής στιβαρότητας.

xxiv. Τα φαινόμενα αποσυντονισμού εξετάσθηκαν μέσω αναλύσεων ευαισθησίας και επιβεβαιώθηκε ότι το VSA δεν είναι ευάλωτο σε φαινόμενα αποσυντονισμού.

xxv. Τα προτεινόμενα συστήματα απορρόφησης δυναμικών ταλαντώσεων βασισμένα στον KDamper είναι ρεαλιστικά σχεδιασμένα για εφαρμογή σε ανεμογεννήτριες (WT), χρησιμοποιώντας μικρές προστιθέμενες μάζες.

xxvi. Το δυναμικό μοντέλο του πύργου της ανεμογεννήτριας που αναπτύχθηκε στην παρούσα διδακτορική διατριβή είναι λειτουργικό, διότι μπορεί εύκολα να ενσωματώσει τα προτεινόμενα συστήματα. Η αξιοπιστία του μοντέλου επαληθεύτηκε μέσω συγκρίσεων με εμπορικό πακέτο λογισμικού Πεπερασμένων Στοιχείων.

xxvii. Η απόσβεση του πύργου της ανεμογεννήτριας αυξήθηκε σημαντικά και βελτιώθηκε η δυναμική του συμπεριφορά, σε σύγκριση με άλλα συστήματα απορρόφησης ταλαντώσεων για ανεμογεννήτριες, τα οποία είναι ευρέως γνωστά στη βιβλιογραφία.

IX. Προτάσεις για Μελλοντική Έρευνα

Η παρούσα διδακτορική διατριβή συνεισφέρει στην απορρόφηση ταλαντώσεων σε κατασκευές Πολιτικού Μηχανικού. Οι παρακάτω ερευνητικές κατευθύνσεις θα βελτιώσουν περαιτέρω την παρούσα εργασία και θα προσφέρουν ακόμα πιο ρεαλιστικές διατάξεις για την προστασία κατασκευών Πολιτικού Μηχανικού έναντι περιβαλλοντικών διεγέρσεων.

i. Η έμφυτη μη-γραμμική φύση της αρνητικής στιβαρότητας μπορεί να χρησιμοποιηθεί ώστε να προσφέρει περαιτέρω πλεονεκτήματα στα συστήματα ελέγχου με βάση τον KDamper.
ii. Η διερεύνηση εναλλακτικών και ρεαλιστικών διατάξεων για την υλοποίηση του στοιχείου αρνητικής στιβαρότητας, χρησιμοποιώντας συμβατικά δομικά στοιχεία ικανά να προσφέρουν τις απαιτούμενες ελαστικές δυνάμεις όταν εφαρμόζονται σε κατασκευές Πολιτικού Μηχανικού.
iii. Η προσομοίωση των εξεταζόμενων εφαρμογών σε εμπορικό πακέτο λογισμικού Πεπερασμένων Στοιχείων με χρήση ρεαλιστικών καταστατικών μοντέλων για την ανωδομή και τα στοιχεία στιβαρότητας του προτεινόμενου συστήματος απορρόφησης δυναμικών ταλαντώσεων. Επισημαίνεται ότι στην παρούσα διδακτορική διατριβή θεωρήθηκαν γραμμικά μοντέλα για την προσομοίωση όλων των εφαρμογών που εξετάσθηκαν, με εξαίρεση την γεωμετρική μη-γραμμικότητα του στοιχείου αρνητικής στιβαρότητας.
iv. Η εκτέλεση πειραμάτων σε ρεαλιστικά και υπό κλίμακα δομικά συστήματα με την εφαρμογή των προτεινόμενων συστημάτων απορρόφησης ταλαντώσεων, χρησιμοποιώντας απλές διατάξεις με προ-συμπιεσμένα ελατήρια για την υλοποίηση του στοιχείου αρνητικής στιβαρότητας.
v. Η εφαρμογή των προτεινόμενων συσκευών απορρόφησης δυναμικών ταλαντώσεων ως ρεαλιστικές επιλογές ενίσχυσης/προσθήκης σε υφιστάμενες κατασκευές, λαμβάνοντας παράλληλα υπόψη τον ευεργετικό ρόλο της αλληλεπίδρασης εδάφους-κατασκευής.
vi. Ο ρεαλιστικός σχεδιασμός μιας συσκευής για τρισδιάστατη απορρόφηση δυναμικών ταλαντώσεων ως ένα σύστημα σεισμικής προστασίας σε υφιστάμενες, αλλά και νέες κατασκευές.
vii. Η αύξηση του κύκλου ζωής των υφιστάμενων αλλά και των καινούργιων ανεμογεννητριών για την αποφυγή του κόστους αντικατάστασης σε περίπτωση

αστοχίας, καθώς και τη μείωση των διαστάσεων του πύργου και άρα του κόστους κατασκευής.

viii. Η διερεύνηση συστημάτων παραγωγής ενέργειας σε συνδυασμό με τον έλεγχο των ταλαντώσεων σε ανεμογεννήτριες, λόγω των φορτίων ανέμου και κυματισμών.

Abstract

Ph.D. Dissertation by Kapasakalis A. Konstantinos

Dynamic Vibration Absorbers in Civil Engineering Structures

The scope of this dissertation concerns the mitigation of ambient vibrations, such as earthquakes and wind loads, in civil engineering structures. Specifically, three individual aspects are examined. The first deals with horizontal seismic protection of multi-story building structures, the second with vertical seismic protection, while the third deals with vibration absorption in wind turbine towers.

The proposed dynamic vibration absorbers are based on the KDamper oscillator. The KDamper is a novel passive vibration isolation and damping concept, based essentially on the optimal combination of appropriate stiffness elements, including a negative stiffness element. The design of the KDamper-based absorbers follows an engineering-criteria driven optimization procedure, with proper constraints and limitations depending on the structure to be employed. The excitation input is selected according to the provisions of the codes with respect to the considered application. Finally, two alternative displacement-dependent configurations are proposed for the realization of the negative stiffness element, generating one and two-dimensional negative stiffness, respectively.

The performance of KDamper is assessed with representative case studies, and its effectiveness is verified by comparisons with existing vibration absorption approaches found in the literature. On the basis of the obtained results, the KDamper-based dynamic vibration absorbers can provide a realistic alternative to the existing horizontal and vertical seismic isolation approaches, as well as provide viable retrofitting options for seismic protection. In addition, the feasibility of wind turbines is extended, as their dynamic performance is enhanced by increasing the effective damping of the wind turbine tower.

Table of Contents

List of Figures

List of Tables

Chapter 1

Introduction

1.1 Introduction and Motivation

The foundation of this work consists in the mitigation of ambient vibrations in Civil Engineering structures. The common goal of each application is the energy absorption due to environmental excitations, wind and seismic, for the purpose of enhancing the dynamic performance of the respective structural system, and thus preventing it from collapsing, due to extreme stress loading exciding structural strength (earthquakes), or structural fatigue (aerodynamic loads).

In response to the damage generated by earthquakes occurring in densely populated areas, seismic design codes for buildings, bridges and infrastructure changed towards the design of structures with better seismic performance. Regarding the horizontal component of earthquake ground motions, seismic isolation appears to be the most promising alternative to conventional antiseismic techniques, as it is based on the concept of reducing the seismic demand rather than increasing the earthquake resistance capacity of the structure. The concept of seismic isolation relies on a laterally flexible layer between the structure and its base. This way, the fundamental period of the system (base isolated) is significantly longer, and thus, the structural peak accelerations are reduced. A number of isolation devices from simple elastomeric bearings to more sophisticated ones have been developed and advanced within the years. However, in order to isolate the building from its base, large displacements are required that are not always acceptable for numerous reasons, such as structural pounding, sensitivity in horizontal loads, proper connection for utilities, and more, that render this system inadequate for retrofitting.

During the latest years, many earthquake excitations whose vertical component of accelerations is almost 1g or more have been recorded. To protect building structures, as well as nonstructural components, such as fragile objects, precision equipment, and fine arts, from these strong ground motions, needs for not only horizontal vibration isolators but also vertical ones. Horizontal seismic isolators have been employed effectively, while vertical ones have

not reached yet such a maturity level. The main reason is due to the conflict concerning the demand for isolation stiffness. More specifically, a vertical isolated system must have sufficient vertical rigidity to sustain the weight of the isolated object/system and retain the static vertical deflections in reasonable limits. On the other hand, the isolated system must also have enough flexibility to isolate the accelerations.

Another type of dynamic load that causes structural failure due to excessive and fatigue stresses is the aerodynamic one. As wind power continues its rapid growth worldwide, wind farms are likely to comprise a significant portion of the total production of wind energy, and may even become a sizable contributor to the total electricity production in some countries. However, the annual rate of Wind Turbine (WT) installation decreases in the latest years, compared to the start of their industrial growth. In addition, several failures have been recorded in existing WT due to structural failure. Thus, it emerges as top priority to extend the feasibility of WT towers by mean of structural control.

The above comments have motivated the development of alternative vibration control strategies, which among others, include: (i) Tuned Mass Dampers (TMDs), (ii) Inerters, (iii) Negative Stiffness Devices (NSD) and "Quazi Zero Stiffness" (QZS) oscillators, and (iv) Negative Stiffness driven Absorbers/KDampers.

Having all this in mind, the development of dynamic vibration absorbers, that can combine the beneficial characteristics of the aforementioned control systems, without their respective drawbacks is considered essential.

1.2 Brief Literature Review and Originalities of the Dissertation

The Tuned Mass Damper (TMD) has a long history, already more than 100 years. The first application of the TMD concept was made by Frahm (Frahm, 1911). Since Den Hartog, (Den Hartog, 1956), first proposition of optimal design theory for the TMD for an undamped SDoF structure, the TMD has been employed on a vast array of systems with the most interesting case being skyscrapers (Haskett et al., 2004; Luft, 1979; McNamara, 1977; Qin et al., 2009; Ramezani et al., 2018). Recent studies also include the use of TMDs for vibration absorption in seismic or other forms of excitation of structures (Debnath et al., 2016), wind and wave excitation in wind turbines (Chen and Georgakis, 2015) and torsional vibrations in rotating and reciprocating machines (Mayet and Ulbrich, 2015). In addition, the TMD can be used as a possible supplement to the conventional base isolation approaches, implemented in the bases of structures, aiming to reduce the displacement demand (Hashimoto et al., 2015; Taniguchi et

al., 2008; Xiang and Nishitani, 2014). Semi-active, active and non-linear configurations are found in (Ankireddi and Yang, 1996; Chung et al., 2009; Han and Li, 2006; Rafieipour et al., 2014; Ricciardelli et al., 2003; Wang et al., 2012; Yang et al., 2002). The downside of such designs is that their performance is directly depended by the accuracy of the actuators output, which over time can have an alternation in its performance. Alternative forms of the conventional TMD have been applied in wind turbines, such as Tuned Liquid Column Damper (TCLD) or even multiple TMDs (Colwell and Basu, 2009; Lackner and Rotea, 2011). The main disadvantages of the TMD related vibration absorption approaches is that large additional masses are required in order for the TMD to be effective, and that a slight alteration in its parameters can alter the TMD tuning and consequently the system's performance is significantly reduced (Weber and Feltrin, 2010).

In an attempt to reduce the requirements for heavy oscillating masses in the TMD concept, the inerter has been introduced in the early 2000s in (Smith, 2002). The inerter is a two-terminal element which has the property that the force generated at its ends is proportional to the relative acceleration of its terminals. The main advantage of the inerter is that the inerter need not have large mass in order to achieve the same inertia effect as the additional mass of the TMD. However, according to (Chen and Smith, 2009), since inerters, dampers and springs can be connected in multiple configurations, the comparison of the structure of the Frequency Response functions of the inerter and of the TMD becomes very complicated. In 2005 the inerter was profitably used as a part of suspension in Formula 1 racing car under the name of ''J-damper'' (Chen et al., 2009). Since then, other applications emerged, such as in suspensions of railway vehicles (Wang et al., 2012) or in seismic protection of structures (Takewaki et al., 2012). Recently, an alternative passive vibration control technique combining the conventional base isolation (BI) with a Tuned Inerter Damper (TID) (De Angelis et al., 2019; Peng et al., 2012; Radu et al., 2019; Sun et al., 2019) or a Tuned Mass Damper Inerter (TMDI) (De Domenico and Ricciardi, 2018b; Lazar et al., 2014; Pietrosanti et al., 2017). In the concept of TMDI, the secondary mass of the TMD is supported to the ground by an ideal inerter (Smith, 2002). Although the initial inerter configuration is for linear accelerations, rotary versions, or even active configurations (Wang and Wu, 2016) have been proposed. Still, to work efficiently, all considered devices have to be precisely tuned which can be hard to achieve or even impossible in some cases. Moreover, proposed TMDs with inerters suffer from susceptibility to detuning. Although variable inertance mechanical configurations have been proposed for this purpose (Brzeski et al., 2015), the essential limitation of the inerter is the complex and elaborate mechanical design configurations needed for its implementation.

A parallel direction to the various TMD approaches is the concept of introducing negative stiffness (NS) elements for vibration absorption. The use of negative stiffness elements (or "anti-springs) for vibration isolation was first introduced in the pioneering publication of Molyneaux (Molyneaux, 1957), as well as in the milestone developments of Platus (Platus 1992). The central concept of these approaches is the significant reduction of the isolator's stiffness, which, consequently, leads to the decrease of the natural frequency of the system (the system's natural period is increased) even at almost zero levels, as in (Carrella et al., 2007), being, thus, called "Quasi-Zero Stiffness" (QZS) oscillators. An initial comprehensive review of such designs can be found in (Ibrahim, 2008). Nagarajaiah (Nagarajaiah et al., 2013) introduced a new structural modification approach for the seismic protection of structures using an adaptive negative stiffness device that resulted in the decrease of the dynamic forces imposed on the structure. The simultaneous growth of structural displacements, was prohibited by a damper, placed in parallel with the negative stiffness device. The negative stiffness behavior is primarily achieved by special mechanical designs, some of which can be found in (Winterflood et al., 2002) and (Virgin et al., 2008). However, alternatively to elastic forces, other forms of physical forces can be used to produce an equivalent negative stiffness effect, such as gravitational (Dyskin and Pasternak, 2012), magnetic (Robertson et al., 2009) or electromagnetic (Zhou and Liu, 2010). However, when dealing with seismic effects mitigation on buildings or bridge structures, where the values of negative stiffness required are quite high, elastic forces seem to be the only feasible choice. The significant advance of mechanical expertise has facilitated the implementation of more complex devices, such as newly-fabricated hardware incorporating negative stiffness elements (Quazi Zero Stiffness oscillators), finding numerous applications in seismic isolation (Attary et al., 2017; Carrella et al., 2007; DeSalvo, 2007; Iemura and Pradono, 2009; Pasala et al., 2013; Shen et al., 2017; Sun et al., 2017; Wang, Sun, et al., 2019; Wang, et al., 2019), in all types of automotive suspensions (Le and Ahn, 2011; Lee et al., 2007; Lee and Goverdovskiy, 2012) or in torsional vibrations (Zhou et al., 2015). Quite recently, periodic cellular structures with advanced dynamic behavior have been also proposed (Baravelli and Ruzzene, 2013; Correa et al., 2015; Michelis and Spitas, 2010; Virk et al., 2013), combining high positive and negative stiffness. Although the physical mechanisms that generate increased damping in cellular structures are not well understood, micro-buckling or slip-stick phenomena (Lakes et al., 1993; Saravanos et al., 2013; Spitas et al., 2013), could be among the possible explanations. Parallel, quite interesting possibilities towards achieving significant damping have been demonstrated to exist also in materials comprising a negative stiffness phase (Lakes, 2001), not only at a material level (Jaglinski et al., 2007), but also at macroscopic devices (Dong and Lakes, 2013). Moreover, such a behavior

can be combined with high stiffness properties (Wojnar and Kochmann, 2014). However, QZS oscillators suffer from their fundamental requirement for a drastic reduction of the stiffness of the structure almost to negligible levels, which limits the static load capacity of such structures.

A promising class of absorbers is based on increasing the damping by the appropriate introduction of negative stiffness elements. Increased damping has been first demonstrated to exist in materials that include a negative stiffness phase (Lakes, 2001). Recently, a stiff and stable linear oscillator that incorporates a negative stiffness element is proposed by Antoniadis (Antoniadis et al., 2015). This novel type of oscillator can exhibit extraordinary damping properties. Moreover, the damping ratio of flexural waves propagating within layered periodic structures that incorporate such NS oscillators is increased by several orders of magnitude (Chronopoulos et al., 2015). A similar concept, that introduces a negative stiffness amplifying damper, is proposed in (Wang, et al., 2019) and (Wang, F Sun, et al., 2019), and is proven to achieve significant damping magnification effects.

Exploiting the advantages of the traditional Tuned Mass Dampers and the 'Quazi Zero Stiffness' designs, a novel passive vibration absorption and damping concept, the KDamper is introduced, which is a product of the research activity of Dynamics & Structures Laboratory of the School of Mechanical Engineering. NTUA (Antoniadis et al., 2018). The KDamper incorporates a negative stiffness element, and can exhibit extraordinary damping properties, without presenting the drawbacks of the traditional linear oscillator, or of the "zero-stiffness" designs. This oscillator is designed to present the same overall (static) stiffness as a traditional reference original oscillator. However, it differs both from the original SDoF oscillator, as well as from the known negative stiffness oscillators, by appropriately redistributing the individual stiffness elements, and by reallocating the damping. Although the proposed oscillator incorporates a negative stiffness element, it is designed to be both statically and dynamically stable. The presence of an additional mass also serves in mitigating the effects of a vibrating load, operating as an energy dissipation mechanism (energy is transferred from the structure to the additional mass). The device overcomes the sensitivity problems of TMDs as the tuning is mainly controlled by the negative stiffness element's parameters.

The prime objective of this dissertation is to investigate KDamper-based configurations for vibration mitigation in Civil Engineering structural systems, due to external dynamic excitations. The motivation towards that scope is justified from the intention of combining the advantages of the previously mentioned vibration absorption approaches, while at the same time, retaining the effect of their respective drawbacks in reasonable ranges. In addition, the proposed dynamic vibration absorbers are designed following an engineering-criteria

optimization procedure, in order for the realization to be as simple as possible, and within reasonable technological capabilities.

The research work presented herein is considered original and its essential features and novel aspects are summarized as follows:

i. The KDamper concept is explored as a dynamic vibration absorber in Civil Engineering structures, exploiting the advantages of the existing vibration absorption approaches, without their respective drawbacks.

ii. Alternative extended versions of KDamper are presented, in order to optimize the effectiveness of the proposed control systems, with respect to the considered structural problem.

iii. A constrained dedicated engineering-criteria optimization procedure is followed for the selection of the KDamper-based configuration parameters, that accounts for the geometrical and constructional limitations of the employed system.

iv. Two realistic displacement-dependent configurations, regarding the negative stiffness (NS) element are proposed, that generate 'linear' one and two-dimensional NS, respectively.

v. The KDamper-based designs are effectively implemented in the bases of structures, for horizontal seismic protection, as a possible supplement to the conventional base isolation approaches.

vi. An alternative option that foresees the implementation of the KDamper designs as a stiff seismic base absorber is presented.

vii. Various retrofitting options are investigated for the extended versions of KDamper in existing structures, that do not affect the structural stiffness, either introduce large additional masses.

viii. The proposed vibration absorbers are effectively implemented for vertical seismic protection, without the drawbacks of the existing vertical seismic isolation approaches, such as large static settlements.

ix. The KDamper-based configurations are implemented in wind turbine (WT) towers for vibration mitigation due to aerodynamic loading, by increasing the effective damping of the WT tower.

1.3 Outline of the Dissertation and Publications

This doctoral dissertation is organized in eight chapters and three appendices. The structure of each chapter comprises the literature review of the corresponding section *"State of the Art"*, the statement of the problem, the proposed configurations, the representative numerical examples, and finally the obtained concluding remarks. In the final chapter, the main conclusions drawn in this dissertation are summarized while directions for further research are proposed. The appendices include information necessary to understand the content of the main chapters of the dissertation.

In this research work the KDamper concept, and two extended versions of it are employed as dynamic vibration absorbers in Civil Engineering structures. The proposed configurations are optimally designed following two alternative approaches: i) the minmax approach ($H\infty$), first proposed by (Den Hartog, 1956), and ii) an engineering-criteria optimization procedure, that follows the provisions of the seismic design codes. The negative stiffness element is realistically designed with two proposed configurations, that can generate one and two-dimensional 'linear' negative stiffness. Several applications are performed, where the KDamper-based approaches are implemented for horizontal, as well as vertical seismic protection. The performance of these vibration control systems is assessed with real earthquake excitations, as well as artificial ones, designed according to the provisions of the seismic design codes. In addition, the proposed control systems are implemented for vibration mitigation of wind turbine towers, due to aerodynamic loads. The effectiveness of the employed systems is verified by comparison with isolated systems, widely used in the literature.

In ***Chapter 2***, an overview of the conventional vibration absorption systems is presented, and the KDamper-based designs are introduced. The KDamper concept is briefly described, along with the extended versions of it, that alternate the initial configuration of KDamper and introduce an inerter coefficient. The general idea of these approaches is based on introducing an unstable negative stiffness element inside a stable environment. This way, the static stiffness of the controlled system in maintained at any desired level, enhancing the inertia effect of the additional oscillating mass, via the elastic force of the negative stiffness element. As a result, the system exhibits extraordinary damping properties, without the need for large additional masses. The equations of motion of the aforementioned vibration control system are presented, and the transfer functions are formed.

In ***Chapter 3***, the optimal design of the KDamper-based designs is presented. The optimal approach for the selection of the KDamper parameters follows exactly the corresponding steps of the classical minmax ($H\infty$) procedure, first proposed by Den Hartog (1956), and is presented

in section 3.2. A base acceleration excitation is assumed, since this dissertation encounters problems from earthquake excitations. The Transfer Functions (TF) of the system main dynamic responses are selected for minimization, i.e. the relative displacement, and the absolute acceleration TFs, in order to evaluate which one performs more effectively. Section 3.3, presents the optimization procedure from which the parameters of the extended versions of KDamper are obtained. The complexity of these configurations renders the conventional minmax ($H\infty$) approaches ineffective. In addition, the properties of the KDamper and the physical and manufacturing limitations that might occur during its implementation (e.g., the negative stiffness (NS) element stroke), lead to the conclusion that a constrained optimal design based on engineering criteria should be followed. The optimization problem is solved using the Harmony Search metaheuristic algorithm, presented in (Geem et al., 2001), and the excitation input is selected according to the provisions of the seismic design codes. Finally, the NS element is realized with two simple displacement-dependent configurations, generating as far as possible 'linear' negative stiffness, in one and two-dimensions, respectively.

In ***Chapter 4***, the KDamper concept is implemented for horizontal seismic protection. Section 4.2 presents thoroughly the inherent conflict between the absolute acceleration and relative displacement minimization, when considering conventional horizontal seismic isolation approaches. In section 4.3, the proposed seismic protection configurations, based on KDamper are presented, that aim to reduce the structural accelerations, and at the same time retain the large required relative displacements at acceptable levels. The KDamper is designed for optimal acceleration response, as the Numerical Example 1, of Chapter 3 indicated that the H_{AS}-set presented an overall improved dynamic behavior, compared to the H_{US}-set (displacement response), and the optimized KDamper using the Harmony Search (HS) optimization algorithm, HS-set. The nominal KDamper frequency is selected with three alternative spectra driven approaches, with respect to the considered system in which the KDamper is implemented. A preliminary assessment of the KDamper implemented in the base of a multi-story building structure, where the NS element is realistically designed and the rest of the KDamper components are realized with conventional structural elements is presented. Finally, the performance of KDamper is assessed with real earthquake records in three numerical examples, and its effectiveness is evaluated by comparison with other seismic isolation approaches.

In ***Chapter 5***, alternative designs of KDamper are investigated, that aim to further reduce the structural relative displacements required (base displacement, and NS element stroke) to acquire the desired improvement in the superstructure dynamic behavior. In section 5.2, the extension of KDamper (EKD) is presented, that based on its alternative configuration aims to

reduce the NS element stroke. The optimization of the proposed extension in presented, and the EKD is implemented for horizontal seismic protection of SDoF, as well as multi-story structural systems. Based on the numerical results, the performance of the EKD manages to greatly improve the structural dynamic hehavior, and simultaneously significantly reduces the NS element stroke and base displacements, compared to KDamper, rendering its realization more realistic. In section 5.3, two retrofitting options of the EKD for seismic protection of multi-story structures are examined. In the first one, multiple EKD are placed in between each floor, and in the second one, only one EKD is placed in the first floor, exploiting the soil structure interaction (SSI) effects. Section 5.4 introduces a stiff base absorber (SBA) which is a combination of the EKD with an inerter. This idea is based on decreasing the nominal system frequency with the inerter, and subsequently control the structural relative displacements with the extraordinary damping properties that the EKD offers. The optimization problem for the design of the SBA is presented, and is subsequently the EKD is implemented in SDoF and MDoF structural systems. Based on the numerical results, the superstructure dynamic behavior is greatly improved, and at the same time, the small base displacements and NS element stroke, render the implementation of the proposed control system, SBA, feasible using conventional structural elements, making it the more effiecient retrofitting option for horizontal seismic protection.

In ***Chapter 6***, a stiff vertical seismic absorber (VSA) is proposed. The main drawback of conventional seismic isolation approaches, regarding the vertical direction, is that in order to isolate the accelerations, large static settlements are required, due to the demand for isolation stiffness. The VSA is a combination of an Extension of KDamper (EKD) with an inerter, and aims to control the vertical accelerations, while at the same time retain the static vertical deformations at acceptable levels. This idea is based on reducing the natural frequency of the system with the inerter and then control the structure accelerations with the extraordinary damping properties that the EKD offers. In section 6.2, the VSA is presented, along with the Transfer Functions, response power spectral densities and root mean square response, when considering vertical acceleration excitation. In section 6.3, the free design variables of the system are presented, along with the optimization procedure from which the optimal VSA parameters are selected. Proper engineering-criteria constraints and limitations are imposed in the system dynamic responses and free design variables, respectively. The optimized parameters of the VSA are presented and based on a comparison with a highly damped base isolated system, it is observed that the VSA significantly reduces the vertical accelerations as compared to the BI, especially at the high-frequency range, where small static settlements are

allowed. Finally, in section 6.4, the SDoF nonlinear dynamic performance is evaluated with real earthquake records and the detuning phenomena are observed via sensitivity analysis.

In ***Chapter 7***, the KDamper-based designs are implemented for vibration control of wind turbine (WT) towers, due to aerodynamic loads. A KDamper (or an extension of it) is intervened between the nacelle and the WT tower. Thus, the nacelle is no longer rigidly connected to the WT tower, but is mounted on a KDamper device. An alternative vibration absorption approach is also introduced, where the nacelle is released from the WT tower (nacelle-isolation concept), using a low stiffness connection. Section 7.2 presents the vibration mitigation approaches considered, along with the dynamic model of the WT tower. The developed model is an assemblage of prismatic beam elements with sway degrees of freedom considered to be the dynamic ones. The validity and the efficiency of the developed formulation is verified by a comparison with a commercial software package based on FEM. The aerodynamic load is taken into account by generating artificial basic wind velocities applying the corresponding regulations of EC1, Part1, 4. Section 7.3, presents the optimization procedure from which the optimal KDamper, and the extended versions of it, are designed. The free design variables are presented, and proper limitations and constraints are imposed on the free design variables and the system main dynamic responses, respectively, based on the proposed engineering-criteria driven optimization procedure. The NS element is realistically designed according to the Proposed Configuration II of Chapter 3. Finally, in section 7.4 a numerical example is presented, where the effectiveness of the proposed KDamper-based vibration mitigation approaches is verified. Based on a comparison with a conventional TMD, and the proposed nacelle-isolation concept, the KDamper designs manage to significantly increase the effective damping of the WT tower, and thus mitigate the WT dynamic responses, with small additional masses and a realistically designed configuration.

In ***Chapter 8***, the main conclusions drawn in this dissertation are summarized and the key advantages and novelties of the proposed dynamic vibration absorbers are highlighted. Moreover, directions for further research are suggested.

This doctoral dissertation contains also three appendices. In the first ***Appendix A1***, a concise derivation of the KDamper stiffness elements is presented, and the coefficients of the optimization process are obtained. In the second ***Appendix A2***, the extension of the optimal design of the KDamper-based configuration to multi-story building structures is presented. The proposed vibrations absorbers are implemented in the bases of multi-story structures, and two retrofitting options are presented. In addition, the matrices entering the equations of motion of the controlled system are presented in detail. In the last ***Appendix A3***, the formation of all the

employed vibration mitigation approaches to WT towers is presented, and the submatrices entering the controlled system's equations of motion are presented.

Finally, it is worth mentioning that the outcome of the conducted research activity presented in this doctoral dissertation has been published in international journals, in national and international conferences, in workshops and seminars.

International Scientific Journals

1. **Kapasakalis, K.A.**, Antoniadis, I.A. and Sapountzakis, E.J., "Performance Assessment of the KDamper as a Seismic Absorption Base", *Structural Control and Health Monitoring*, DOI: 10.1002/stc.2482, 2019. https://onlinelibrary.wiley.com/doi/10.1002/stc.2482
2. **Kapasakalis, K.A.**, Antoniadis, I.A. and Sapountzakis, E.J., "Implementation of the KDamper as a Stiff Seismic Absorption Base: A Preliminary Assessment", *Vibration and Acoustics Research Journal*, Vol. 1, No. 1, pp. 1-26, 2019. http://www.cansrg.com/journals/varj/2019/Kapasakalis-et-al/index.html

International Scientific Conferences

1. **Kapasakalis, K.A.,** Sapountzakis, E.J. and Antoniadis, I.A. (2017) "Implementation of the KDamper Concept to Wind Turbine Towers", *Proceedings of the 6th International Conference on Computational Methods in Structural Dynamics and Earthquake Engineering (COMPDYN 2017)*, Rhodes Island, Greece, 15-17 June.
2. **Kapasakalis, K.A.,** Sapountzakis, E.J. and Antoniadis, I.A. (2018) "KDamper Concept in Seismic Isolation of Multi Storey Building Structures", *Proceedings of the 9th GRACM International Congress on Computational Mechanics (9GRACM 2018)*, Chania, Greece, 4-6 June.
3. **Kapasakalis, K.A.,** Sapountzakis, E.J. and Antoniadis, I.A. (2018) "Optimal Design of the KDamper Concept for Structures on Compliant Supports", *Proceedings of the 16th European Conference on Earthquake Engineering (16ECEE 2018)*, Thessaloniki, Greece, 18-21 June.

4. **Kapasakalis, K.A.,** Sapountzakis, E.J. and Antoniadis, I.A. (2018) "Kdamper concept in seismic isolation of building structures with soil structure interaction", *Proceedings of the 13th International Conference on Computational Structures Technology (CST2018),* Sitges, Barcelona, Spain, 4-6 September.

5. **Kapasakalis, K.A.,** Antoniadis, I.A. and Sapountzakis, E.J. (2019) "Control of Multi Storey Building Structures with a New Passive Vibration Control System Combining Base Isolation with KDamper", *Proceedings of the 7th International Conference on Computational Methods in Structural Dynamics and Earthquake Engineering (COMPDYN 2019),* Crete, Greece, 24-26 June.

6. Antoniadis I.A., **Kapasakalis, K.A.** and Sapountzakis, E.J. (2019) "Isolation or Damping? A Soil-dependent approach based on the KDamper concept", *Proceedings of the 2nd International Conference on Natural Hazards & Infrastructure (ICONHIC 2019),* Crete, Greece, 23-26 June. **Invited for Theme Lecture**

7. Sapountzakis, E.J., **Kapasakalis, K.A.** and Antoniadis I.A. (2019) "Negative Stiffness Elements in Seismic Isolation of Bridges", *Proceedings of the 2nd International Conference on Natural Hazards & Infrastructure (ICONHIC 2019),* Crete, Greece, 23-26 June. **Invited for Theme Lecture**

8. **Kapasakalis, K.A.,** Antoniadis, I.A. and Sapountzakis, E.J. (2019) "Implementation of the KDamper Concept for Base Isolation to a Typical Concrete Building Structure", *Proceedings of the 12th International Congress on Mechanics (12HSTAM2019),* Thessaloniki, Greece, 22-25 September.

9. **Kapasakalis, K.A.,** Antoniadis I.A. and Sapountzakis E.J (2019) "KDamper Concept for Base Isolation and Damping of High-Rise Building Structures", *Proceedings of the 14th International Conference on Vibration Problems (ICOVP 2019),* Crete, Greece, 1-4 September.

10. **Kapasakalis, K.A.,** Alamir, C.H.T., Antoniadis I.A. and Sapountzakis E.J (2019) "Frequency Base Design of the KDamper Concept for Seismic Isolation of Bridges", *Proceedings of the 14th International Conference on Vibration Problems (ICOVP 2019),* Crete, Greece, 1-4 September. **Invited for Keynote Lecture**

11. Bollano, P-O.N, **Kapasakalis, K.A.,** Sapountzakis, E.J. and Antoniadis I.A. (2019) "Design and Optimization of the KDamper Concept for Seismic Protection of Bridges", *Proceedings of the 14th International Conference on Vibration Problems (ICOVP 2019),* Crete, Greece, 1-4 September.

12. **Kapasakalis, K.A.,** Antoniadis I.A. and Sapountzaki A.E (2019) "Implementation of the KDamper Concept for Seismic Protection of Bridges", *Proceedings of the 14th International Conference on Vibration Problems (ICOVP 2019)*, Crete, Greece, 1-4 September.

13. Antoniadis, I.A., **Kapasakalis, K.A.** and Sapountzakis, E.J. (2019) "Advanced Negative Stiffness Absorbers for the Seismic Protection of Structures", *Proceedings of the International Conference on Key Enabling Technologies 2019 (KEYTECH2019)*, Istanbul, Turkey, 24-26 April 2019. https://doi.org/10.1063/1.5123704

14. **Kapasakalis, K.A.**, Antoniadis, I.A. and Sapountzakis, E.J. (2020) "Optimal Design of Advanced Negative Stiffness Absorbers", *Proceedings of the XI International Conference on Structural Dynamics (EURODYN 2020)*, Athens, Greece, 22-24 June, 2020.

15. **Kapasakalis, K.A.**, Bollano, P-O.N., Antoniadis, I.A. and Sapountzakis, E.J. (2020) "Comparison of Alternative Dynamic Vibration Mitigation Approaches for Wind Turbine Towers", *Proceedings of the XI International Conference on Structural Dynamics (EURODYN 2020)*, Athens, Greece, 22-24 June, 2020.

16. **Kapasakalis, K.A.**, Florakis, G.I., Antoniadis, I.A. and Sapountzakis, E.J. (2020) "Seismic Protection of Multi Story Building Structures with Distributed KDamper Devices", *Proceedings of the 27th International Congress on Sound and Vibration, Prague (ICSV27 2020)*, Czech Republic, 12-16 July, 2020.

17. **Kapasakalis, K.A.**, Antoniadis, I.A. and Sapountzakis, E.J. (2020) "Novel Negative Stiffness Devices Based on KDamper for Vertical Vibration Absorption of Structures", *Proceedings of the 27th International Congress on Sound and Vibration (ICSV27 2020)*, Prague, Czech Republic, 12-16 July, 2020.

18. **Kapasakalis, K.A.**, Alvertos, A.E., Mantakas, A.G., Antoniadis, I.A. and Sapountzakis, E.J. (2020) "Advanced Negative Stiffness Vibration Absorber Coupled with Soil-Structure Interaction for Seismic Protection of Buildings", *Proceedings of the XI International Conference on Structural Dynamics (EURODYN 2020)*, Athens, Greece, 22-24 June, 2020.

National Scientific Conferences, Workshops, and Seminars

1. Antoniadis, I., Sapountzakis, I., Syrimi, P., **Kapasakalis, K.** and Sapountzakis, E.J. (2017) "New concepts for the seismic protection of structures based on negative stiffness damping and seismic metamaterials", *SAFE Athens 2017*, Athens, Greece, 28-30 June.
2. **Κ. Καπασακάλης,** Ε. Σαπουντζάκης, Ι. Αντωνιάδης (2017) "Συστήματα Μόνωσης Ταλαντώσεων σε Ανεμογεννήτριες", *2η Ημερίδα Νέων Ερευνητών και Μηχανικών στην Αντισεισμική Μηχανική (ΕΤΑΜ)*, Αίθουσα Τελετών ΕΜΠ, Αθήνα, Ελλάδα, 3 Νοεμβρίου 2017.
3. Ε. Σαπουντζάκης, **Κ. Καπασακάλης,** Π. Συρίμη (2018) "Συστήματα με Στοιχεία Αρνητικής Στιβαρότητας για τη Σεισμική Μόνωση Κατασκευών", *2ο Πανελλήνιο Συνέδριο Φοιτητών Πολιτικών Μηχανικών*, Θεσσαλονίκη, 23-25 Μαρτίου 2018.
4. **Κ. Καπασακάλης,** Ι. Αντωνιάδης, Ε. Σαπουντζάκης (2019) "Καινοτόμα Συστήματα Μόνωσης με Στοιχεία Αρνητικής Στιβαρότητας για τη Σεισμική Προστασία των Κατασκευών", *4ο Πανελλήνιο Συνέδριο Αντισεισμικής Μηχανικής και Τεχνικής Σεισμολογίας (ΕΤΑΜ)*, Αθήνα, Ελλάδα, 5-7 Σεπτεμβρίου 2019.
5. Antoniadis, I.A., **Kapasakalis, K.A.** and Sapountzakis, E.J. (2019) "Seismic Metabases: Implementation of the KDamper as a Seismic Absorption Base: A Spectra Driven Feasibility Assessment", *4th Workshop on Seismic Metamaterials: from Optics to Geophysics*, Marseille, France, 15-17 April 2019.

Chapter 2

Proposed Negative Stiffness Based Dynamic Vibration Absorbers – KDampers

2.1 Introduction

Seismic isolation is considered perhaps the best-established design approach of antiseismic protection (Naeim and Kelly, 1999) because it relies on reducing the seismic demand (usually by increasing the natural period of the structure) rather than increasing the earthquake resistance capacity of the structure. Isolation systems implemented in the bases of the structures, provide horizontal isolation from the effects of earthquakes, by decoupling the superstructure from the base-foundation during earthquakes. Therefore, a number of isolation devices, such as the elastomeric bearings, frictional/sliding bearings, roller bearings have been developed (Farag et al., 2015; Gang et al., 2018; Peng et al., 2012; Wang et al., 2016).

The increased flexibility, provided by the decoupling of the structure from the ground, for base isolated structures (BIS) significantly reduces the earthquake-induced forces in the superstructure, which essentially behaves as a rigid body. On the other hand, the earthquake-induced displacement of the ground is essentially decoupled from the structure, which undergoes large relative displacements. Apart from the significant technological demands and implications imposed on the base isolators, this fact can affect the overall performance of the structure. Proper connections for utilities (e.g., waterworks, gas fittings and electrical conduits) are needed. An adequate separation distance between adjacent buildings is necessary in order to prevent mutual collisions or structural pounding (Anagnostopoulos and Spiliopoulos, 1992). The structural sensitivity in horizontal loads is increased. The most important drawback is that BIS is essentially prohibitive for retrofitting. Increasing the BIS damping ζ_B or, alternatively, providing supplementary dampers inside the structure to reduce the excessively large displacements does not consist a mainstream alternative (Symans et al., 2007). Apart from the severe technological requirements imposed on the devices, the direct increase of the damping results to the increase of interstory drifts and floor accelerations (Kelly, 1999).

2.2 Overview of Conventional Vibration Absorbers

These drawbacks have motivated the development of alternative vibration control strategies for seismic protection of building structures which, among others, include: (a) Negative Stiffness Devices (NSD) and "Quazi Zero Stiffness" (QZS) oscillators, Tuned Mass Dampers (TMDs), Inerters, and (d) Tuned Mass Damper Inerters (TMDIs). The schematic representation of the aforementioned concepts is illustrated in Figure 2.1.

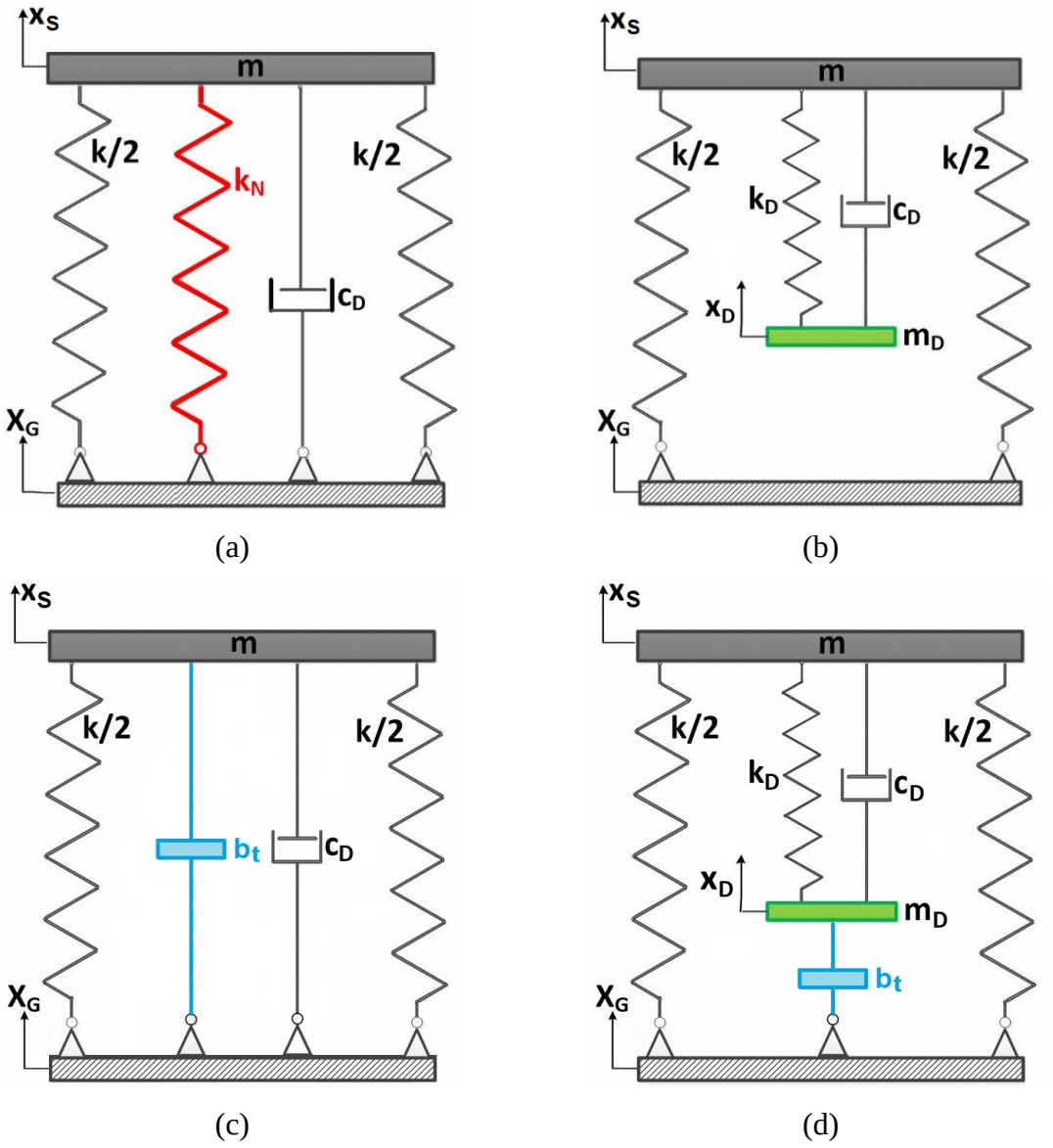

Figure 2.1: *Schematic presentation of the considered vibration absorption concepts (a) Quasi-Zero Stiffness (QZS) oscillator, (b) Tuned Mass Damper (TMD), (c) Inerter (JDamper) and Tuned Mass Damper Inerter (TMDI).*

2.2.1 Quazi Zero Stiffness Oscillators (QZS)

True negative stiffness is defined as a force that assists motion instead of resisting it, like a positive stiffness spring (Figure 2.2).

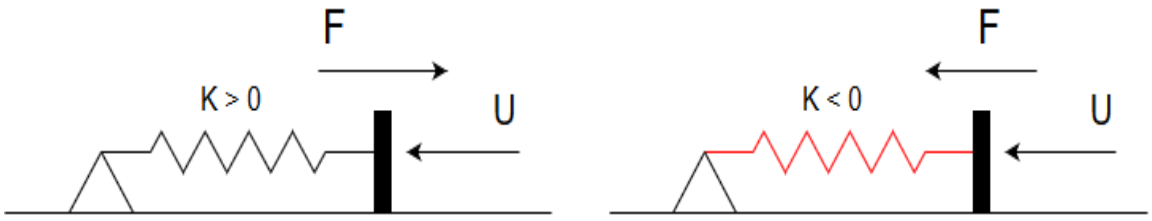

(a) (b)

Figure 2.2: *Schematic representation of (a) a positive stiffness element and (b) a negative stiffness element.*

The use of negative stiffness elements (or "anti-springs) for vibration isolation was first introduced in the pioneering publication of Molyneaux (Molyneaux, 1957), as well as in the milestone developments of Platus (Platus 1992). The central concept of these approaches is the significant reduction of the isolator's stiffness, which, consequently, leads to the decrease of the natural frequency of the system (the system's natural period is increased) even at almost zero levels, as in (Carrella et al., 2007), being, thus, called "Quasi-Zero Stiffness" (QZS) oscillators. This way, enhanced vibration absorption is achieved, since the system exhibits reduced transmissibility for all operating frequencies above the natural one. Through numerical simulations and experimental testing, numerous researchers have demonstrated the effectiveness of this kind of devices. An initial comprehensive review of such designs can be found in (Ibrahim, 2008). Nagarajaiah (Nagarajaiah et al., 2013) introduced a new structural modification approach for the seismic protection of structures using an adaptive negative stiffness device that resulted in the decrease of the dynamic forces imposed on the structure. The simultaneous growth of structural displacements, is prohibited by a damper, placed in parallel with the negative stiffness device.

The negative stiffness behavior is primarily achieved by special mechanical designs involving conventional positive stiffness pre-stressed elastic mechanical elements, such as post-buckled beams, plates, shells and pre-compressed springs, arranged in appropriate geometrical configurations. Some interesting designs are described in (Winterflood et al., 2002) and (Virgin et al., 2008). However, alternatively to elastic forces, other forms of physical forces can be used to produce an equivalent negative stiffness effect, such as gravitational

(Dyskin and Pasternak, 2012), magnetic (Robertson et al., 2009) or electromagnetic (Zhou and Liu, 2010). However, when dealing with seismic effects mitigation on buildings or bridge structures, where the values of negative stiffness required are quite high, elastic forces seem to be the only feasible choice.

Among others, Quazi Zero Stiffness (QZS) oscillators are finding numerous applications in seismic isolation (Attary et al., 2017; DeSalvo, 2007; Iemura and Pradono, 2009; Sarlis et al., 2012), in all types of automotive suspensions (Le and Ahn, 2011; Lee et al., 2007; Lee and Goverdovskiy, 2012) or in torsional vibrations (Zhou et al., 2015). Quite recently, periodic cellular structures with advanced dynamic behavior have been also proposed (Baravelli and Ruzzene, 2013; Correa et al., 2015; Michelis and Spitas, 2010; Virk et al., 2013), combining high positive and negative stiffness. Although the physical mechanisms that generate increased damping in cellular structures are not well understood, micro-buckling or slip-stick phenomena (Lakes et al., 1993; Saravanos et al., 2013; Spitas et al., 2013), could be among the possible explanations.

Parallel, quite interesting possibilities towards achieving significant damping have been demonstrated to exist also in materials comprising a negative stiffness phase (Lakes, 2001), not only at a material level (Jaglinski et al., 2007), but also at macroscopic devices (Dong and Lakes, 2013). Moreover, such a behavior can be combined with high stiffness properties. A theoretical approach has been performed for the analysis of the static and dynamic stability of composite materials, incorporating negative stiffness elements (Wojnar and Kochmann, 2014). However, Quazi Zero Stiffness (QZS) oscillators suffer from their fundamental requirement for a drastic reduction of the stiffness of the structure almost to negligible levels, which limits the static load capacity of such structures.

In Figure 2.3.a, one of the simplest configurations exhibiting quasi-zero stiffness behavior is depicted, proposed by (Carrella et al., 2007), comprising of a combination of positive and negative stiffness elements. While the force, f is augmenting, for instance, due to loading with a suitably sized mass, the springs compress such that the oblique springs, k_0 become horizontal and the static load is undertaken by the vertical spring, k_v. This state is the static equilibrium position of the system. Considering any movement about this equilibrium position, the positive stiffness of the vertical spring is counteracted by the oblique springs, which act as a negative stiffness element in the vertical direction. A typical force-displacement curve for this system is given in Figure 2.3.b. In this diagram, x_e denotes the static equilibrium position and for this case, the system is designed such that the dynamic stiffness at this point is equal to zero. However, the penalty for this choice is that for large excursions from the equilibrium position, the system becomes stiffer than the vertical spring alone.

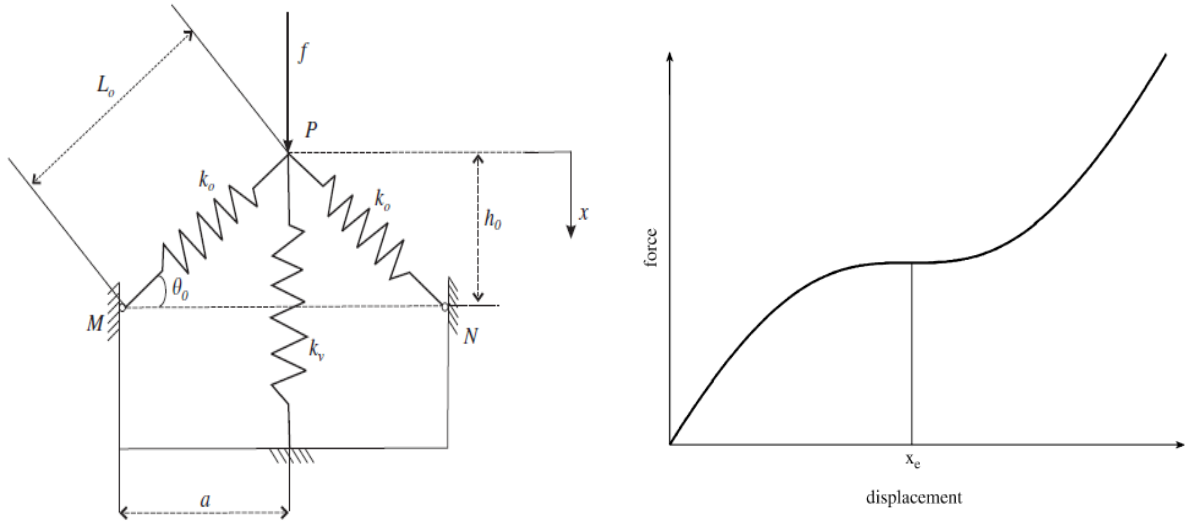

(a) (b)

Figure 2.3: *(a) Schematic representation of the simplest system which can exhibit quasi-zero stiffness. (b) Typical force-displacement characteristic of the system (Carrella et al., 2007).*

For the configuration of Figure 2.3.a, the non-dimensional stiffness, $\hat{K}_{QZS}$ along with the geometric dimension, *a*, aiming to achieve the desired QZS effect are calculated according to Equations (2.1):

$$\hat{K}_{QZS} = 1 + \frac{\gamma_{QZS}}{1-\gamma_{QZS}}\left[1 - \frac{\gamma_{QZS}^2}{(\hat{x}^2 - 2\sqrt{1-\gamma_{QZS}^2}\,\hat{x} + 1)^{3/2}}\right] \tag{2.1.a}$$

$$a = \frac{\gamma_{QZS}}{2(1-\gamma_{QZS})} \tag{2.1.b}$$

where $\hat{x}$ is the non-dimensional displacement of the system from its equilibrium position, and γ_{QZS} is a geometrical parameter. After the solution of a suitable optimization problem regarding the range of displacements for which the system's non-dimensional stiffness, $\hat{K}_{QZS}$ remains lower than a prescribed value $\hat{K}_0$, namely, $\hat{K}_0 < \hat{K}_{QZS}$, the optimal value of $\gamma_{QZS} = \gamma_{opt}$ is given from Equation (2.2).

$$\gamma_{opt} \approx \left(\frac{2}{3}\right)^{\left(\hat{K}_0/2\right)+1} \tag{2.2}$$

It should be noted here that, since all aforementioned parameters are non-dimensional with regard to the vertical spring's stiffness, k_v and the oblique springs' length, Lo , $\hat{K}_0 = 1$ means that the system's stiffness is equal to that of the vertical spring. For a thorough description of the mechanism's function and properties and an analytical presentation of its optimal design readers are referenced to (Carrella et al., 2007).

The concept of a simple QZS oscillator, presented in Figure 2.1.a, is to add a negative stiffness (NS) element k_N in parallel to the conventional positive stiffness element k. The equation of motion of the Quazi Zero Stiffness (QZS) oscillator becomes:

$$m\ddot{u}_S + c_D\dot{u}_S + (k + k_N)u_S = m\ddot{u}_S + c_D\dot{u}_S + k_{QZS}u_S = -m\ddot{X}_G \tag{2.3}$$

where, $u_S=X_S-X_G$. Assuming a harmonic base acceleration excitation in the form of:

$$\ddot{X}_G(t) = A_G \exp(j\omega t) \tag{2.4}$$

and a steady-state response of:

$$u_S(t) = \tilde{U}_S \exp(j\omega t) \tag{2.5}$$

where $\tilde{U}_S$ denotes the response complex amplitude, the equation of motion (2.3) of the QZS system becomes:

$$-\omega^2 m\tilde{U}_S + j\omega c_D\tilde{U}_S + k_{QZS}\tilde{U}_S = -mA_G \tag{2.6}$$

The Transfer Functions of the QZS system considering a harmonic base acceleration excitation are:

$$\tilde{H}_{US} = \tilde{U}_S / A_G = -\tilde{H}^{-1}m \tag{2.7.a}$$

$$\tilde{H}_{AS} = \tilde{A}_S / A_G = 1 - \omega^2 \tilde{H}_{US} \quad (2.7.b)$$

$$\tilde{H} = -\omega^2 m + j\omega c_D + k_{QZS} \quad (2.7.c)$$

The following position that concern the design of the QZS are introduced:

$$\omega_{QZS} = 2\pi f_0 = \sqrt{k_{QZS} / m} \quad (2.8.a)$$

$$\zeta_{QZS} = c_D / \left(2\sqrt{k_{QZS} / m}\right) \quad (2.8.b)$$

Since k_N is negative, the overall static stiffness of the system is reduced, $k_{QZS}=k+k_{NS}$, as illustrated in Equation (2.3). This limits the static loading capacity and correspondingly decreases the natural frequency of the system (Equation (2.8.a)). Accordingly, the system attracts lower lateral seismic forces and develops reduced peak accelerations, as in the case of a seismically isolated system.

However, reducing the static loading capacity of the structure, may result to unsolvable problems, especially for vertical vibration isolation. For example, if X_{SVD} denotes the static deflection of such an isolation system under its own weight in the vertical direction:

$$X_{SVD} = \frac{mg}{k} = \frac{g}{\left(2\pi f_0\right)^2} \quad (2.9)$$

2.2.2 Tuned Mass Dampers (TMDs)

Among the numerous passive and active control techniques, the implementation of an additional mass (Tuned Mass Dampers, TMD), is probably the most popular and mature theory. A TMD, also known as a dynamic vibration absorber, is a classical engineering device that consists of a mass, a spring, and a viscous damper. Usually, it is attached to a vibrating primary system, to suppress any unwanted vibrations induced by wind and earthquake loads. The first application of the TMD concept was made by Frahm (Frahm, 1911). Since Den Hartog, (Den Hartog, 1956), first proposition of optimal design theory for the TMD for an undamped SDoF structure, the TMD has been employed on a vast array of systems with the most interesting case being skyscrapers (Luft, 1979; McNamara, 1977; Qin et al., 2009; Ramezani et al., 2018). A characteristic example of its implementation on skyscrapers can be found in one of the tallest

buildings in the world, Taipei 101 Tower (101 stories, 504 m) in Taiwan (Haskett et al., 2004). Recent studies also include the use of TMDs for vibration absorption in seismic or other forms of excitation of structures (Debnath et al., 2016), wind and wave excitation in wind turbines by (Chen and Georgakis, 2015) and torsional vibrations in rotating and reciprocating machines by (Mayet and Ulbrich, 2015). Semi-active, active and non-linear configurations are found in (Chung et al., 2009; Han and Li, 2006; Rafieipour et al., 2014; Z Wang et al., 2012; Yang et al., 2002). The Active TMD (ATMD) is a hybrid devise consisting of a passive TMD supplemented by an actuator parallel to the spring and damper. It is a well-known concept in structural control and has been proved to yield enhanced damping performance compared to the passive TMD (Ankireddi and Yang, 1996; Ricciardelli et al., 2003). The downside of such designs is that their performance is directly depended by the accuracy of the actuators output, which over time can have an alternation in its performance by false estimation of the desirable function of the vibration absorption concept and eventually burden the structure. Various forms of Dynamic Vibration Absorbers (DVA) have been used, such as Tuned Liquid Column Damper (TCLD) or a TMD. Some of the pioneering work concerning applications in wind turbines include the work by (Colwell and Basu, 2009) in which the damping effect of a TLCD installed in an offshore wind turbine has been investigated by assuming correlated wind and wave load conditions, whereas the potential of using a pair of TMDs simultaneously targeting the dominant fore-aft ad side-side modes has been demonstrated by (Lackner and Rotea, 2011).

The natural frequency of the TMD is tuned in resonance with the fundamental mode of the primary structure. Thus, a large amount of the structural vibrating energy is transferred to the TMD and then dissipated by damping. Even though TMDs are known for their effectiveness and their reliability, their usage encounters significant disadvantages. Environmental influences and other external parameters may alter the TMD properties, disturbing its tuning. Consequently, the device's performance can be significantly reduced (Weber and Feltrin, 2010). In addition, the large required displacements of the additional oscillating mass, impose manufacturing limitations during its implementation. Another essential limitation of the TMD is that a large oscillating mass is required in order to achieve significant vibration reduction rendering its construction and placement procedure rather difficult.

The concept of the Tuned Mass Damper is presented in Figure 2.1.b. The resulting equations of motion are:

$$m\ddot{u}_S + c_D(\dot{u}_S - \dot{u}_D) + k_D(u_S - u_D) + ku_S = -m\ddot{X}_G \tag{2.10.a}$$

$$m_D\ddot{u}_D - c_D(\dot{u}_S - \dot{u}_D) - k_D(u_S - u_D) = -m_D\ddot{X}_G \tag{2.10.b}$$

where, $u_D=X_D-X_G$. Assuming a harmonic base acceleration excitation in the form of Equation (2.4), and steady-state responses of:

$$u_S(t)=\tilde{U}_S \exp(j\omega t) \tag{2.11.a}$$

$$u_D(t)=\tilde{U}_D \exp(j\omega t) \tag{2.11.b}$$

where $\tilde{U}_S$ and $\tilde{U}_D$ denote the response complex amplitudes. The Equations of motion (2.10) of the TMD become:

$$-\omega^2 m\tilde{U}_S + j\omega c_D(\tilde{U}_S-\tilde{U}_D)+k_D(\tilde{U}_S-\tilde{U}_D)+k\tilde{U}_S=-mA_G \tag{2.12.a}$$

$$-\omega^2 m_D\tilde{U}_D - j\omega c_D(\tilde{U}_S-\tilde{U}_D)-k_D(\tilde{U}_S-\tilde{U}_D)=-m_D A_G \tag{2.12.b}$$

The Transfer Functions of the TMD system considering a harmonic base acceleration excitation are:

$$\begin{bmatrix}\tilde{H}_{US}\\ \tilde{H}_{UD}\end{bmatrix}=\begin{bmatrix}\tilde{U}_S/A_G\\ \tilde{U}_D/A_G\end{bmatrix}=-\tilde{H}^{-1}\begin{bmatrix}m\\ m_D\end{bmatrix} \tag{2.13.a}$$

$$\tilde{H}_{AS}=\tilde{A}_S/A_G=1-\omega^2\tilde{H}_{US} \tag{2.13.b}$$

$$\tilde{H}_{AD}=\tilde{A}_D/A_G=1-\omega^2\tilde{H}_{UD} \tag{2.13.c}$$

$$\tilde{H}=\begin{bmatrix}-\omega^2 m+j\omega c_D+k_D+k & -j\omega c_D-k_D\\ -j\omega c_D-k_D & -\omega^2 m_D+j\omega c_D+k_D\end{bmatrix} \tag{2.13.d}$$

And the following position that concern the design of the TMD are introduced:

$$\rho=\omega_D/\omega_0 \tag{2.14.a}$$

$$\omega_0=\sqrt{k/m} \tag{2.14.b}$$

$$\omega_D=\sqrt{k_D/m_D} \tag{2.14.c}$$

$$\zeta_D=c_D/\left(2\sqrt{k_D/m_D}\right) \tag{2.14.d}$$

$$\mu=m_D/m \tag{2.14.e}$$

where the parameter ρ controls the tuning of the TMD, ζ_D is the damping ratio of the TMD, and the parameter μ refers to the additional oscillating mass of the TMD, and is the free design variable of the system.

Considering the optimal approach for the selection of the TMD parameters ρ and ζ_D numerous approaches can be found in the literature with respect to the selected Transfer Function to be optimized for a specific harmonic excitation. A common practice is to tune the TMD with the fundamental frequency of the primary system (parameter ρ), and then calculate the damping ratio ζ_D numerically.

2.2.3 Inerters and Tuned Mass Damper Inerters (TMDI)

In an attempt to reduce the requirement for heavy oscillating masses, the inerter concept has been introduced in early 2000s by (Malcolm C. Smith, 2002). The inerter is a two-terminal element which has the property that the force generated at its ends is proportional to the relative acceleration of its terminals. This constant of proportionality is called ‘‘inertance’’ and is measured in kilograms. The main advantage of the inerter is that the inerter need not have large mass in order to achieve the same inertia effect as the additional mass of the TMD. However, according to (Chen and Smith, 2009) since inerters, dampers and springs can be connected in multiple configurations, the comparison of the structure of the Frequency Response functions of the inerter and of the TMD becomes very complicated. In 2005 the inerter was profitably used as a part of suspension in Formula 1 racing car under the name of ‘‘J-damper’’ (Chen et al., 2009). Since then, other applications emerged, such as in suspensions of railway vehicles (FC Wang et al., 2012) or in seismic protection of structures (Takewaki et al., 2012). Although the initial inerter configuration is for linear accelerations, rotary versions, or even active configurations (Wang and Wu, 2016) have been proposed. Still, to work efficiently, all considered devices have to be precisely tuned which can be hard to achieve or even impossible in some cases. Moreover, proposed TMDs with inerters suffer from susceptibility to detuning. Although variable inertance mechanical configurations have been proposed for this purpose (Brzeski et al., 2015), the essential limitation of the inerter is the complex and elaborate mechanical design configurations needed for its implementation.

An indicative form of the implementation of the inerter is presented in Figure 2.1.c. It connects the structure mass directly with the ground/base, and thus manages to decrease the natural frequency of the system, and as a consequence reduce the seismic load, as in the seismic

isolation concept, without having to reduce the static stiffness of the structure or increase its actual mass. The equation of motion of this system is:

$$(m+b_t)\ddot{u}_S + c_D\dot{u}_S + ku_S = -m\ddot{X}_G \tag{2.15}$$

Assuming a harmonic base acceleration excitation in the form of Equation (2.4) and a steady-state response in the form of Equation (2.5), the equation of motion (2.15) of the system becomes:

$$-\omega^2(m+b_t)\tilde{U}_S + j\omega c_D\tilde{U}_S + k\tilde{U}_S = -mA_G \tag{2.16}$$

The Transfer Functions of the inerter system considering a harmonic base acceleration excitation are:

$$\tilde{H}_{US} = \tilde{U}_S / A_G = -\tilde{H}^{-1}m \tag{2.17.a}$$

$$\tilde{H}_{AS} = \tilde{A}_S / A_G = 1-\omega^2\tilde{H}_{US} \tag{2.17.b}$$

$$\tilde{H} = -\omega^2(m+b_t) + j\omega c_D + k \tag{2.17.c}$$

And the following position that concern the design of the inerter are introduced:

$$\omega_t = 2\pi f_t = \sqrt{k/(m+b_t)} \tag{2.18.a}$$

$$\zeta_t = c_D / \left(2\sqrt{k/(m+b_t)}\right) \tag{2.18.b}$$

$$\mu_t = b_t / m \tag{2.18.c}$$

where μ_t is the inertance ratio with respect to the structure mass m. As a result, the inerter manages to reduce the natural frequency of the system, as observed from Equation (2.18.a), without having to reduce the stiffness or increase the actual mass, and therefore seismic load.

As a more effective alternative, the combination of a traditional Tuned Mass Damper system with an inerter (TMDI) has been recently proposed (De Domenico and Ricciardi, 2018a; De Domenico et al., 2018; Giaralis and Taflanidis, 2018; Lazar et al., 2014). In this concept, the secondary mass of the TMD is supported to the ground by an ideal inerter. This way, the additional mass of the TMD does not necessarily have to be extremely high as the

inertance coefficient increased the effective inertia of the TMD without increasing its actual additional mass. The configuration of the TMDI is illustrated in Figure 2.1.d, and the equations of motion of this system are:

$$m\ddot{u}_S + c_D(\dot{u}_S - \dot{u}_D) + k_D(u_S - u_D) + ku_S = -m\ddot{X}_G \tag{2.19.a}$$

$$(m_D + b_t)\ddot{u}_D - c_D(\dot{u}_S - \dot{u}_D) - k_D(u_S - u_D) = -m_D\ddot{X}_G \tag{2.19.b}$$

Assuming a harmonic base acceleration excitation in the form of Equation (2.4) and steady-state responses in the form of Equation (2.11), the equation of motion (2.19) become:

$$-\omega^2 m\tilde{U}_S + j\omega c_D(\tilde{U}_S - \tilde{U}_D) + k_D(\tilde{U}_S - \tilde{U}_D) + k\tilde{U}_S = -mA_G \tag{2.20.a}$$

$$-\omega^2(m_D + b_t)\tilde{U}_D - j\omega c_D(\tilde{U}_S - \tilde{U}_D) - k_D(\tilde{U}_S - \tilde{U}_D) = -m_D A_G \tag{2.20.b}$$

The Transfer Functions of the TMD system considering a harmonic base acceleration excitation are:

$$\begin{bmatrix}\tilde{H}_{US}\\ \tilde{H}_{UD}\end{bmatrix} = \begin{bmatrix}\tilde{U}_S / A_G\\ \tilde{U}_D / A_G\end{bmatrix} = -\tilde{H}^{-1}\begin{bmatrix}m\\ m_D\end{bmatrix} \tag{2.21.a}$$

$$\tilde{H}_{AS} = \tilde{A}_S / A_G = 1 - \omega^2\tilde{H}_{US} \tag{2.21.b}$$

$$\tilde{H}_{AD} = \tilde{A}_D / A_G = 1 - \omega^2\tilde{H}_{UD} \tag{2.21.c}$$

$$\tilde{H} = \begin{bmatrix}-\omega^2 m + j\omega c_D + k_D + k & -j\omega c_D - k_D\\ -j\omega c_D - k_D & -\omega^2(m_D + b_t) + j\omega c_D + k_D\end{bmatrix} \tag{2.21.d}$$

And the following position that concern the TMDI design are introduced:

$$\rho = \omega_D / \omega_0 \tag{2.22.a}$$

$$\omega_D = \sqrt{k_D / (m_D + b_t)} \tag{2.22.b}$$

$$\zeta_D = c_D / \left(2\sqrt{k_D / (m_D + b_t)}\right) \tag{2.22.c}$$

$$\mu = m_D / m \tag{2.22.d}$$

$$\mu_t = b_t / m \tag{2.22.e}$$

$$\mu_{eff} = \mu + \mu_t = \frac{m_D + b_t}{m} = \frac{m_{eff}}{m} \tag{2.22.f}$$

where the parameter ρ control the tuning of the TMDI, ζ_D is the damping ratio of the TMDI, μ refers to the actual additional oscillating mass of the TMDI, μ_t is the inertance ratio, and finally μ_{eff} is the effective inertia ratio of the TMDI.

The free design variable of the TMDI is the additional mass m_D. Considering the optimal approach for the selection of the TMDI parameters ω_D, ζ_D and μ_t numerous approaches can be followed, as for example for implementation of the TMDI as a seismic isolation supplement (De Domenico and Ricciardi, 2018a; De Domenico et al., 2018).

Although an improvement in the overall behavior of the structure is observed, the dynamic behavior of the inerter is marginally superior to that of a high mass TMD. Due to the saturation effects observed, its effectiveness is limited and comparable to a highly damped base isolation system.

2.3 Proposed Negative Stiffness – Based Dynamic Vibration Absorbers

A promising class of absorbers is based on increasing the damping by the appropriate introduction of negative stiffness elements. Increased damping has been first demonstrated to exist in materials that include a negative stiffness phase (Lakes, 2001). Recently, Antoniadis (Antoniadis et al., 2015) proposed a stiff and stable linear oscillator that incorporates a negative stiffness element. This novel type of oscillator can exhibit extraordinary damping properties. Moreover, the damping ratio of flexural waves propagating within layered periodic structures that incorporate such NS oscillators is increased by several orders of magnitude (Chronopoulos et al., 2015). A similar concept, that introduces a negative stiffness amplifying damper, is proposed in (Wang, F fei Sun, et al., 2019) and (Wang, F Sun, et al., 2019), and is proven to achieve significant damping magnification effects.

Exploiting the advantages of the traditional Tuned Mass Dampers and the ‘Quazi Zero Stiffness’ design, a novel passive vibration absorption and damping concept, the KDamper concept, has been proposed in (Antoniadis et al., 2018), and is presented in Figure (2.4.a). The KDamper incorporates a negative stiffness element, which can exhibit extraordinary damping properties, without presenting the drawbacks of the traditional linear oscillator, or of the “zero-stiffness” designs. This oscillator is designed to present the same overall (static) stiffness as a traditional reference original oscillator. However, it differs both from the original SDoF

oscillator, as well as from the known negative stiffness oscillators, by appropriately redistributing the individual stiffness elements and by reallocating the damping. Although the proposed oscillator incorporates a negative stiffness element, it is designed to be both statically and dynamically stable. The presence of an additional mass also serves in mitigating the effects of a vibrating load, operating as an energy dissipation mechanism (energy is transferred from the structure to the additional mass). The device overcomes the sensitivity problems of TMDs as the tuning is mainly controlled by the negative stiffness element's parameters.

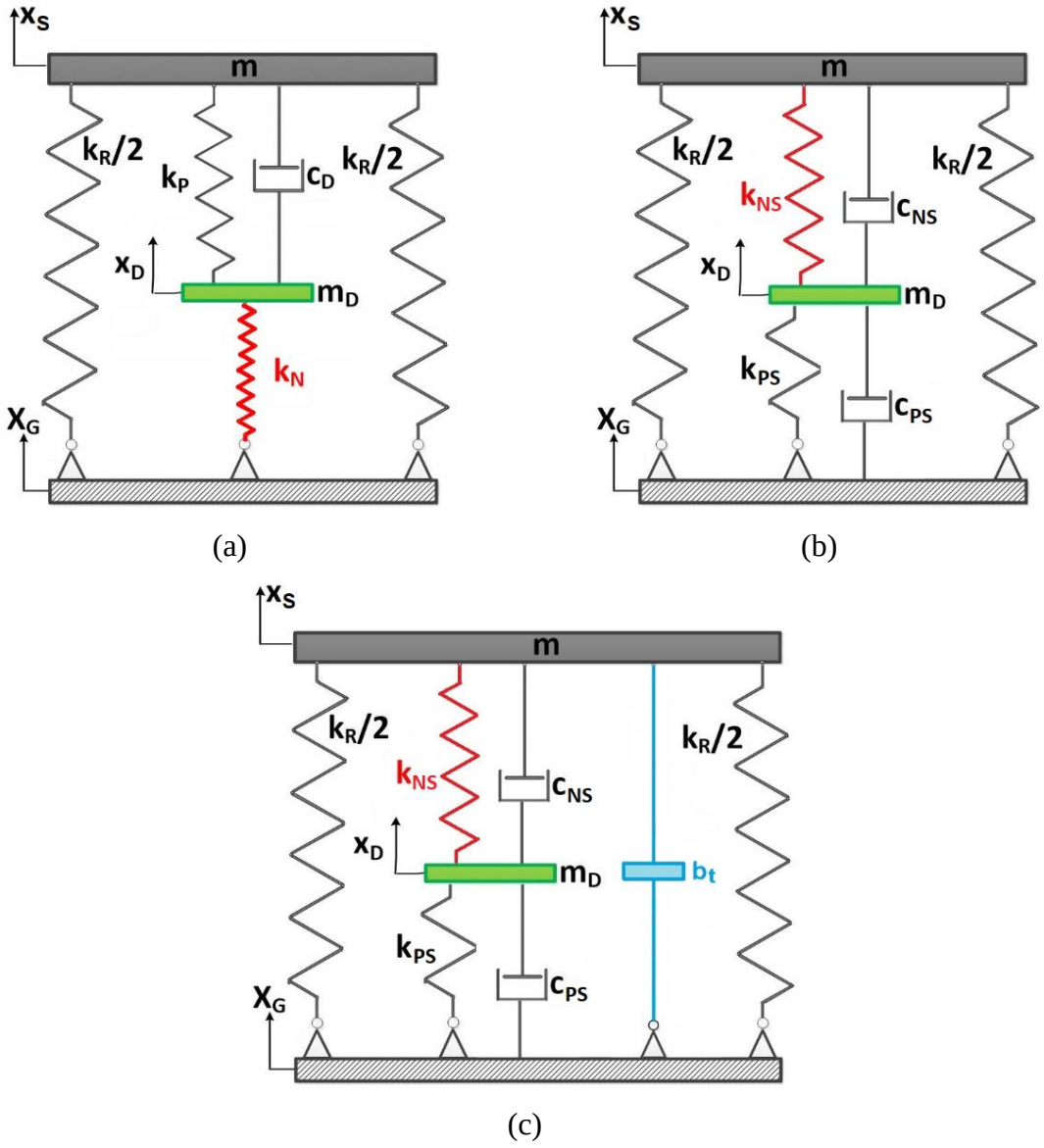

Figure 2.4: *Schematic presentation of the KDamper-based vibration absorption concepts (a) KDamper concept, (b) extended version of KDamper, and (c) extended KDamper equipped with inerter.*

The KDamper has been effectively implemented in a variety of structural systems for vibration absorption, such as bridge structures (I Antoniadis et al., 2019; Bollano et al., 2019; Kapasakalis, Alamir, et al., 2019; Kapasakalis, Antoniadis and Sapountzaki, 2019; Sapountzakis et al., 2019), wind turbine towers (Kapasakalis et al., 2017, 2018c), structural systems (Kapasakalis et al., 2018a, 2018b), and recently in the bases of multi-story building structures (I Antoniadis et al., 2019; Kapasakalis, Antoniadis and Sapountzakis, 2019a, 2019b, 2019c, 2019d, 2019e).

2.3.1 The KDamper Concept

Figure 2.4.a presents the fundamental concept of KDamper. Similarly to the 'Quazi Zero Stiffness' oscillators, it uses a negative stiffness element k_N. However, contrary to the QZS isolator, the first basic requirement of the KDamper is that the overall static stiffness of the system is maintained:

$$k_R + \frac{k_P k_N}{k_P + k_N} = k = (2\pi f_0)^2 (m + m_D) \tag{2.23}$$

In this way, the KDamper can overcome the fundamental disadvantage of negative stiffness (NS) isolators. Compared to the TMD damper or the TMDI (Figure 2.1.b, d), the KDamper uses an additional negative stiffness element k_N, which connects the additional mass to the base. Thus, the equations of motion of the KDamper become:

$$m\ddot{u}_S + c_D(\dot{u}_S - \dot{u}_D) + k_P(u_S - u_D) + k_R u_S = -m\ddot{X}_G \tag{2.24.a}$$

$$m_D\ddot{u}_D - c_D(\dot{u}_S - \dot{u}_D) - k_P(u_S - u_D) + k_N u_D = -m_D\ddot{X}_G \tag{2.24.b}$$

Assuming a harmonic excitation in the form of Equation (2.4) and steady-state responses in the form of Equation (2.11), the equations of motion (2.24) of the KDamper become:

$$-\omega^2 m\tilde{U}_S + j\omega c_D(\tilde{U}_S - \tilde{U}_D) + k_P(\tilde{U}_S - \tilde{U}_D) + k_R\tilde{U}_S = -mA_G \tag{2.25.a}$$

$$-\omega^2 m_D\tilde{U}_D - j\omega c_D(\tilde{U}_S - \tilde{U}_D) - k_P(\tilde{U}_S - \tilde{U}_D) + k_N\tilde{U}_D = -m_D A_G \tag{2.25.b}$$

And the Transfer Functions of the KDamper system finally result:

$$\begin{bmatrix} \tilde{H}_{US} \\ \tilde{H}_{UD} \end{bmatrix} = \begin{bmatrix} \tilde{U}_S / A_G \\ \tilde{U}_D / A_G \end{bmatrix} = -\tilde{H}^{-1} \begin{bmatrix} m \\ m_D \end{bmatrix} \tag{2.26.a}$$

$$\tilde{H}_{AS} = \tilde{A}_S / A_G = 1 - \omega^2 \tilde{H}_{US} \tag{2.26.b}$$

$$\tilde{H}_{AD} = \tilde{A}_D / A_G = 1 - \omega^2 \tilde{H}_{UD} \tag{2.26.c}$$

$$\tilde{H} = \begin{bmatrix} -\omega^2 m + j\omega c_D + k_P + k_R & -j\omega c_D - k_P \\ -j\omega c_D - k_P & -\omega^2 m_D + j\omega c_D + k_P + k_N \end{bmatrix} \tag{2.26.d}$$

A careful examination of Equations (2.25) reveals that the amplitude F_{MD} of the inertia force of the additional mass and the amplitude F_N of the negative stiffness force:

$$F_{MD} = -\omega^2 m_D \left| \tilde{U}_D \right| \tag{2.27.a}$$

$$F_N = k_N \left| \tilde{U}_D \right| \leq 0 \tag{2.27.b}$$

are exactly in phase, due to the negative value of k_N. Thus, similarly to the TMDI, the KDamper can be considered as an indirect approach to increase the inertia effect of the additional mass m_D without however increasing directly the mass m_D itself. Moreover, it should be noted that the value of F_{MD} depends on the frequency, while the value of F_N is constant in the entire frequency range, a fact which is of importance for low-frequency vibration isolation and consists an essential dynamic advantage over the inerter. Finally, the following positions that concern the KDamper are introduced:

$$\mu = m_D / m \tag{2.28.a}$$

$$k_D = k_N + k_P \tag{2.28.b}$$

$$\omega_D = \sqrt{k_D / m_D} = \sqrt{(k_N + k_P) / m_D} \tag{2.28.c}$$

$$\zeta_D = c_D / 2\omega_D m_D = c_D / 2\sqrt{(k_N + k_P) m_D} \tag{2.28.d}$$

$$m_{tot} = m + m_D \tag{2.28.e}$$

$$f_0 = \sqrt{k / m_{tot}} / 2\pi = \sqrt{\left(k_R + k_P k_N / k_P + k_N\right) / \left(m + m_D\right)} / 2\pi \tag{2.28.f}$$

where μ is the mass ratio of the additional mass of the KDamper, ζ_D is the damping ratio of the artificial damper c_D, and f_0 is the KDamper nominal frequency. Further information regarding

the optimal selection of the KDamper parameters are presented thoroughly in section 3.2 of Chapter 3.

2.3.2 Extension of KDamper

The proposed vibration absorption concept is an extension of the KDamper referred to herein as the EKD system, and is illustrated in Figure 2.4.b. In a similar way to the KDamper, the EKD incorporates a system of masses, negative stiffness and positive stiffness elements as well as artificial dampers. The main variation would be the change of the system configuration where the positive stiffness spring (k_{PS}) connects the damper mass (m_D) to the base of the system while the negative stiffness element (k_{NS}), is attached between the damper mass (m_D) and the mass of the oscillator (m). Also, an additional artificial damper is adopted and placed in parallel with the negative stiffness element so that we end up having two dampers, namely C_{NS} and C_{PS}. Based on the original formulation of the KDamper expressions (Equations (2.24)), the following equations of motion for the EKD are derived:

$$m\ddot{u}_S + c_{NS}(\dot{u}_S - \dot{u}_D) + k_{NS}(u_S - u_D) + k_R u_S = -m\ddot{X}_G \tag{2.29.a}$$

$$m_D\ddot{u}_D - c_{NS}(\dot{u}_S - \dot{u}_D) - k_{NS}(u_S - u_D) + c_{PS}\dot{u}_D + k_{PS}u_D = -m_D\ddot{X}_G \tag{2.29.b}$$

Assuming a harmonic excitation in the form of Equation (2.4) and steady-state responses in the form of Equation (2.11), the equation of motions (2.29) of the EKD become:

$$-\omega^2 m\tilde{U}_S + j\omega c_{NS}(\tilde{U}_S - \tilde{U}_D) + k_{NS}(\tilde{U}_S - \tilde{U}_D) + k_R\tilde{U}_S = -mA_G \tag{2.30.a}$$

$$-\omega^2 m_D\tilde{U}_D - j\omega c_{NS}(\tilde{U}_S - \tilde{U}_D) - k_{NS}(\tilde{U}_S - \tilde{U}_D) + j\omega c_{PS}\tilde{U}_D + k_{PS}\tilde{U}_D = -m_D A_G \tag{2.30.b}$$

And the Transfer Functions of the EKD system finally result:

$$\begin{bmatrix}\tilde{H}_{US}\\ \tilde{H}_{UD}\end{bmatrix} = \begin{bmatrix}\tilde{U}_S / A_G\\ \tilde{U}_D / A_G\end{bmatrix} = -\tilde{H}^{-1}\begin{bmatrix}m\\ m_D\end{bmatrix} \tag{2.31.a}$$

$$\tilde{H}_{AS} = \tilde{A}_S / A_G = 1 - \omega^2\tilde{H}_{US} \tag{2.31.b}$$

$$\tilde{H}_{AD} = \tilde{A}_D / A_G = 1 - \omega^2\tilde{H}_{UD} \tag{2.31.c}$$

$$\tilde{H}=\begin{bmatrix} -\omega^2 m + j\omega c_{NS} + k_{NS} + k_R & -j\omega c_{NS} - k_{NS} \\ -j\omega c_{NS} - k_{NS} & -\omega^2 m_D + j\omega(c_{NS} + c_{PS}) + k_{NS} + k_{PS} \end{bmatrix} \tag{2.31.d}$$

As this is an extended version of the classical KDamper concept, it is expected that the effect of this vibration control strategy with the EKD to be similar with the KDamper with respect to the controlled system dynamic behaviour. The purpose of this configuration is to retain the internals' DoF displacements and velocities within reasonable limits as for the design to realistic and efficient at the same time. Finally, the following positions that concern the EKD are introduced:

$$\mu = m_D / m \tag{2.32.a}$$

$$k_D = k_{NS} + k_{PS} \tag{2.32.b}$$

$$\omega_D = \sqrt{k_D / m_D} = \sqrt{(k_{NS} + k_{PS}) / m_D} \tag{2.32.c}$$

$$\zeta_{NS} = c_{NS} / 2\omega_D m_D = c_{NS} / 2\sqrt{(k_{NS} + k_{PS}) m_D} \tag{2.32.d}$$

$$\zeta_{PS} = c_{PS} / 2\omega_D m_D = c_{PS} / 2\sqrt{(k_{NS} + k_{PS}) m_D} \tag{2.32.e}$$

$$m_{tot} = m + m_D \tag{2.32.f}$$

$$f_0 = \sqrt{k / m_{tot}} / 2\pi = \sqrt{\left(k_R + k_{PS} k_{NS} / k_{PS} + k_{NS}\right) / \left(m + m_D\right)} / 2\pi \tag{2.32.g}$$

where μ is the mass ratio of the additional mass of the EKD, ζ_{NS} and ζ_{PS} are the damping ratios of the artificial dampers c_{NS} and c_{PS}, respectively, and f_0 is the EKD nominal frequency. Further information regarding the optimal selection of the EKD parameters are presented thoroughly in section 3.3 of Chapter 3.

2.3.3 Extension of KDamper Equipped with Inerter

The proposed configurations that combines the extension of KDamper (EKD) with an inerter is illustrated in Figure 2.4.c. An inerter is first implemented, connecting directly the structure to the ground. This results to the decrease of the natural frequency f_0 of the system, and therefore the reduction of the seismic load of the structure, without decreasing the structural stiffness or increasing its actual mass. At the same time, the EKD is implemented to control the large required structure relative displacements by the increase of the effective damping of

the system. Thus, the equations of motion of the proposed system combining EKD with an inerter are:

$$(m+b_t)\ddot{u}_S + c_{NS}(\dot{u}_S - \dot{u}_D) + k_{NS}(u_S - u_D) + k_R u_S = -m\ddot{X}_G \tag{2.33.a}$$

$$m_D\ddot{u}_D - c_{NS}(\dot{u}_S - \dot{u}_D) - k_{NS}(u_S - u_D) + c_{PS}\dot{u}_D + k_{PS}u_D = -m_D\ddot{X}_G \tag{2.33.b}$$

Assuming a harmonic excitation in the form of Equation (2.4) and steady-state responses in the form of Equation (2.11), the equations of motions (2.33) of the EKD equipped with inerter become:

$$-\omega^2(m+b_t)\tilde{U}_S + j\omega c_{NS}(\tilde{U}_S - \tilde{U}_D) + k_{NS}(\tilde{U}_S - \tilde{U}_D) + k_R\tilde{U}_S = -mA_G \tag{2.34.a}$$

$$-\omega^2 m_D\tilde{U}_D - j\omega c_{NS}(\tilde{U}_S - \tilde{U}_D) - k_{NS}(\tilde{U}_S - \tilde{U}_D) + j\omega c_{PS}\tilde{U}_D + k_{PS}\tilde{U}_D = -m_D A_G \tag{2.34.b}$$

And the Transfer Functions of the KDamper system finally result:

$$\begin{bmatrix}\tilde{H}_{US}\\ \tilde{H}_{UD}\end{bmatrix} = \begin{bmatrix}\tilde{U}_S / A_G\\ \tilde{U}_D / A_G\end{bmatrix} = -\tilde{H}^{-1}\begin{bmatrix}m\\ m_D\end{bmatrix} \tag{2.35.a}$$

$$\tilde{H}_{AS} = \tilde{A}_S / A_G = 1 - \omega^2\tilde{H}_{US} \tag{2.35.b}$$

$$\tilde{H}_{AD} = \tilde{A}_D / A_G = 1 - \omega^2\tilde{H}_{UD} \tag{2.35.c}$$

$$\tilde{H} = \begin{bmatrix}-\omega^2(m+b_t) + j\omega c_{NS} + k_{NS} + k_R & -j\omega c_{NS} - k_{NS}\\ -j\omega c_{NS} - k_{NS} & -\omega^2 m_D + j\omega(c_{NS} + c_{PS}) + k_{NS} + k_{PS}\end{bmatrix} \tag{2.35.d}$$

Finally, the positions that concern the EKD equipped with an inerter are presented in Equations (2.32) with the addition of the inertance coefficient:

$$\mu_t = b_t / m \tag{2.36.a}$$

where μ_t is the inertance ratio with respect to the structure mass m. Further information regarding the optimal selection of the EKD equipped with inerter parameters are presented thoroughly in section 3.3 of Chapter 3.

Chapter 3

Optimal Design of Advanced Negative Stiffness Dynamic Vibration Absorbers

3.1 Introduction

The proposed advanced negative stiffness-based dynamic vibration absorbers were presented in Chapter 2, along with their equations of motion, transfer functions and their basic design parameters. In the present Chapter, the optimization procedure regarding the design of the aforementioned configurations is presented, in order to improve the dynamic performance of the controlled system, with a realistic and robust design.

The KDamper is a relatively new passive vibration absorption and damping concept. Regarding the optimal design of KDamper, numerous approaches could be followed, as found in the literature for the optimal design of other passive vibration absorption concepts (TMDs, QZS, NS designs, TMDIs, etc.). In this Chapter, the optimal design approach for the selection of the KDamper parameters follows exactly the corresponding steps of the classical minmax ($H\infty$) procedure, proposed by Den Hartog (1956). A base acceleration excitation is assumed, since this dissertation encounters problem from earthquakes. Further information regarding the Transfer Function selected for optimization are found in section 3.2 of this Chapter.

Extended KDamper designs, are configurations based on the classical KDamper, first proposed by (Antoniadis et al., 2018), that aim to further improve its dynamic behaviour. The complexity of these configurations renders the conventional minmax ($H\infty$) approaches ineffective. In addition, the properties of the KDamper and the physical and manufacturing limitations that might occur during its implementation (negative stiffness (NS) element stroke), lead to the conclusion that a constrained optimal design based on engineering criteria should be followed. Section 3.3, presents thoroughly the optimization procedure of extended KDamper configurations. The excitation input is selected according to the provisions of the seismic design codes, and the realization of the NS elements are realized with simple displacement-dependent configurations, generating as far as possible ‘linear’ negative stiffness.

3.2 Conventional minmax ($H\infty$) approaches for the KDamper Design

The optimal design approach for the selection of the KDamper parameters follows exactly the corresponding steps of the classical minmax ($H\infty$) procedure. The Transfer Functions of the KDamper concept, are expressed analytically with respect to the KDamper parameters:

$$\tilde{H}_{US} = \frac{\tilde{U}_S}{A_G} = -\frac{\tilde{N}_{US}}{\tilde{D}} \tag{3.1.a}$$

$$\tilde{H}_{UD} = \frac{\tilde{U}_D}{A_G} = \frac{(j\omega c_D + k_P)H_{US} - m_D}{(-\omega^2 m_D + j\omega c_D + k_p + k_N)} = \frac{\tilde{N}_{UD}}{\tilde{D}} \tag{3.1.b}$$

$$\tilde{H}_{AS} = \frac{\tilde{A}_S}{A_G} = 1 - \omega^2 \tilde{H}_{US} = \frac{\tilde{N}_{AS}}{\tilde{D}} \tag{3.1.c}$$

where:

$$\tilde{N}_{US} = -\omega^2 m m_D + j\omega c_D(m + m_D) + m(k_P + k_N) + m_D k_P \tag{3.2.a}$$

$$\tilde{N}_{UD} = -\omega^2 m m_D + j\omega c_D(m + m_D) + m k_P + m_D(k_R + k_P) \tag{3.2.b}$$

$$\tilde{N}_{AS} = -\omega^2 m_D k_R + j\omega c_D(k_R + k_N) + k(k_P + k_N) \tag{3.2.c}$$

$$\begin{aligned}\tilde{D} = {} & \omega^4 m m_D - \omega^2[m(k_P + k_R) + m_D(k_P + k_R)] \\ & - j\omega^3(m + m_D)c_D + j\omega c_D(k_R + k_N) + k(k_P + k_N)\end{aligned} \tag{3.2.d}$$

Furthermore, the following parameters of the KDamper configuration are introduced:

$$\kappa = -k_N / (k_P + k_N) \tag{3.3.a}$$

$$\mu = m_D / m \tag{3.3.b}$$

$$\rho = \omega_D / \omega_0 \tag{3.3.c}$$

$$q = \omega / \omega_0 \tag{3.3.d}$$

$$\omega_0 = \sqrt{k / m} \tag{3.3.e}$$

$$\omega_D = \sqrt{k_D / m_D} \tag{3.3.f}$$

$$\zeta_D = c_D / 2\sqrt{k_D m_D} \tag{3.3.g}$$

The minmax approach ($H\infty$) minimizes a specific Transfer Function for a harmonic excitation, which in this case is a base acceleration excitation. The free design variables of the system are the additional mass ratio μ and the stiffness ratio κ, introduced in Equations (3.3.a) and (3.3.b). Considering the selection of ζ_D, numerous approaches are possible, the detailed treatment of which is beyond the scope of the dissertation. A straightforward approach is to calculate ζ_D numerically, so that it minimizes the peak of the selected Transfer Function (q,ζ_D). The parameter ρ is calculated with respect to the Transfer Function selected for optimization. Once the values of the four parameters μ, κ, ζ_D and ρ are determined and after some algebraic manipulations presented thoroughly in section A.1.1 of Appendix A.1, the values of the KDamper's elements, can be finally obtained from the following relations:

$$k_N / k = \kappa_N = -\kappa\mu\rho^2 \tag{3.4.a}$$

$$k_P / k = \kappa_P = (1+\kappa)\mu\rho^2 \tag{3.4.b}$$

$$k_R / k = \kappa_S = 1+\kappa(1+\kappa)\mu\rho^2 \tag{3.4.c}$$

$$m_D = \mu m \tag{3.4.d}$$

$$c_D = 2\zeta_D\sqrt{(k_P + k_N)m_D} \tag{3.4.e}$$

3.2.1 Base Acceleration Excitation – Minimization of the Structure Relative Displacement Transfer Function

In this section the structure relative displacement Transfer Function H_{US}, Equation (3.1.a) is selected for minimization, considering base acceleration excitation, and is expressed:

$$\tilde{H}_{US} = \frac{\tilde{U}_S}{A_G} = -\frac{1}{\omega_0^2}\frac{A+(j2\zeta_D)B}{C+(j2\zeta_D)D} \tag{3.5}$$

and consequently:

$$H_{US} = \frac{\left|\tilde{U}_S\right|}{A_G} = \frac{U_S}{A_G} = \frac{1}{\omega_0^2}\sqrt{\frac{A^2+(2\zeta_D)^2B^2}{C^2+(2\zeta_D)^2D^2}} \tag{3.6}$$

where:

$$A = \rho^2[1+(1+\kappa)\mu]-q^2 \tag{3.7.a}$$

$$B = \rho q(1+\mu) \tag{3.7.b}$$

$$C = q^4 - q^2[1+\rho^2+(1+\kappa)^2\mu\rho^2]+\rho^2 \tag{3.7.c}$$

$$D = \rho q[(1+\kappa^2\mu\rho^2)-q^2(1+\mu)] \tag{3.7.d}$$

In the limit cases of $\zeta_D = 0$ or $\zeta_D \to \infty$, Equation (3.6) becomes:

$$H_{US}(0) = \frac{1}{\omega_0^2}\left|\frac{A}{C}\right| \tag{3.8.a}$$

$$H_{US}(\infty) = \frac{1}{\omega_0^2}\left|\frac{B}{D}\right| \tag{3.8.b}$$

In view of Equations (3.8.a, 3.8.b), the Transfer Function $H_{US}(q,\zeta_D)$ of Equation (3.6) has two poles for two different values of q and therefore presents two different maximal values (peaks) at these points. The optimal selection of the KDamper parameters requires that both these peaks are minimized and become equal to each other. This is ensured by the optimal design approach followed in (Den Hartog, 1956), which will be also used in the current section. The approach is based on the identification of a pair of frequencies q_L <1 and q_R>1, where the values $H_{US}(q_L)$ and $H_{US}(q_R)$ become independent of ζ_D. The first step for the optimization procedure is the requirement that the values of the Transfer Functions $H_{US}(q)$ at these points are equal:

$$H_{US}(q_L) = H_{US}(q_R) = H_{USI} = H_{US}(\infty) \tag{3.9}$$

In order that a solution for such a pair of frequencies exists, two alternative conditions must be fulfilled as in (Den Hartog, 1956):

Case I: $AD = BC$ (3.10.a)

Case II: $AD = -BC$ (3.10.b)

As it can be verified, no solution of Equation (3.10.a) exists for a positive q^2, when the values κ, μ, and ρ are positive. Elaboration of Equation (3.10.b) results to:

$$(A_2D_2+B_0)q^4+(A_0D_2+A_2D_0+B_0C_2)q^2+(A_0D_0+B_0C_0)=0 \tag{3.11}$$

where the coefficients A_i, B_i, C_i, D_i are given in section A.1.2 of Appendix A.1. As a result of Equation (3.11), the pair of roots of Equation (3.11) must satisfy:

$$q_L^2+q_R^2=-\frac{(A_0D_2+A_2D_0+B_0C_2)}{(A_2D_2+B_0)} \tag{3.12}$$

Additionally, both roots q_L and q_R must fulfill Equation (3.9), which results to:

$$\frac{B_0}{D_0+D_2q_L^2}=-\frac{B_0}{D_0+D_2q_R^2}\Rightarrow q_L^2+q_R^2=-\frac{2D_0}{D_2} \tag{3.13}$$

The combination of Equations (3.12, 3.13) leads to the optimal value of the parameter ρ:

$$A_\rho\rho^4+B_\rho\rho^2+C_\rho=0 \tag{3.14}$$

Since A_ρ=0, the optimum value of ρ for a set of parameters κ and μ results as:

$$\rho(\kappa,\mu)=\sqrt{-C_\rho/B_\rho} \tag{3.15}$$

After substitution of the coefficients of Equations (A.11-13) and the coefficients in Table A.1 into Equation (3.15) the following expression for the optimal value of ρ is obtained:

$$\rho(\kappa,\mu)=\sqrt{\frac{2-\mu}{\kappa^2\mu(\mu-2)+(2+2\mu+3\kappa\mu)(1+\mu)}} \tag{3.16}$$

The ζ_D is calculated numerically, so that it minimizes the peak of the Transfer Function $H_{US}(q,\zeta_D)$. Figure 3.1 presents the variation of $H_{US}(q,\zeta_D)$ due to variation of ζ_D. As it can be observed, for the optimum value of $\zeta_{Dopt}=\zeta_{min}$, both peaks of $H_{US}(q,\zeta_D)$ are equal and minimum.

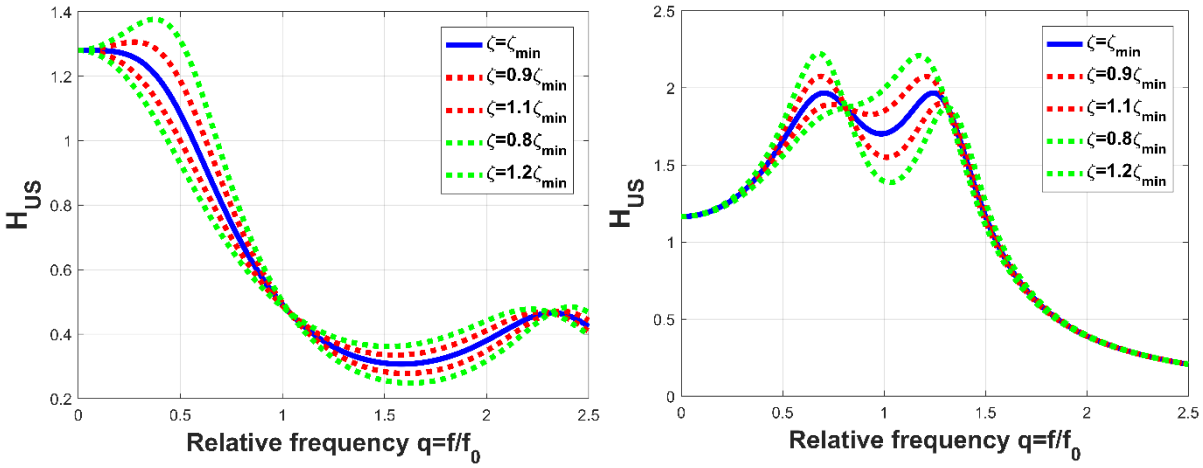

(a) (b)

Figure 3.1: *Dependence of Transfer Function H_{US} on the damping ratio ζ_D (a) μ=0.05, κ=4.6 and (b) μ=0.05, κ=2.3.*

3.2.1.1 Basic Properties

A first fundamental property of KDamper is that the addition of a negative stiffness spring reduces the magnitude of the Transfer Function, as compared to that of the TMD, as observed in Figure 3.2. Moreover, increasing the value of κ, reduces the maximum part of the Transfer Function H_{US}, which becomes flatter. As a consequence, the KDamper is more robust to detuning, than the TMD.

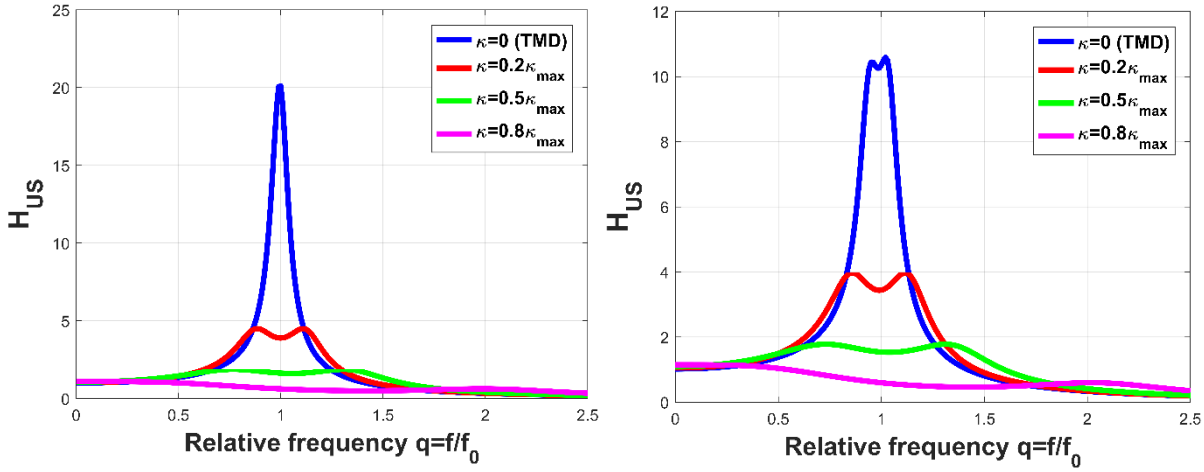

(a) (b)

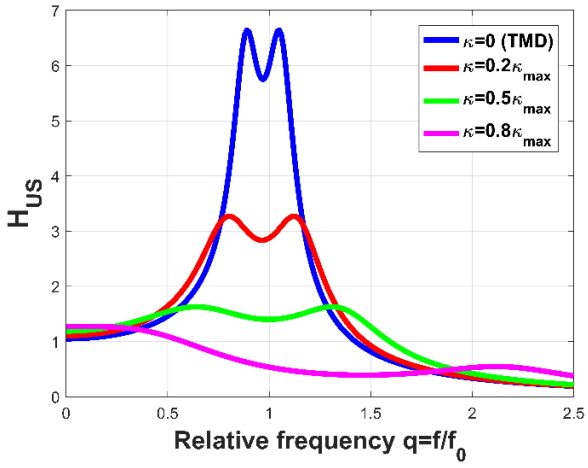

(c)

Figure 3.2: *Effect of the stiffness ratio κ on the Transfer Function H_{US} of the KDamper for (a) μ=0.01, (b) μ=0.05 and (c) μ=0.1.*

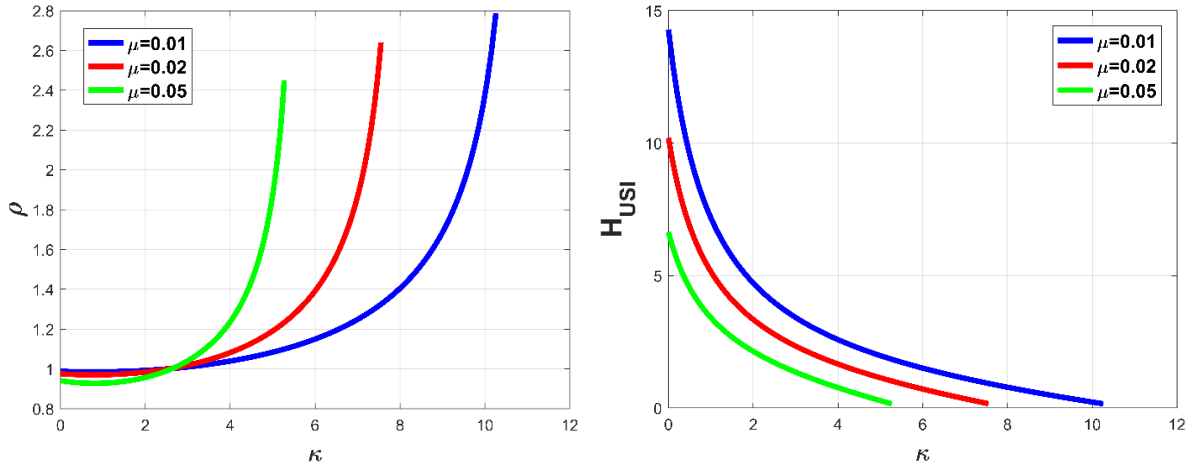

(a) (b)

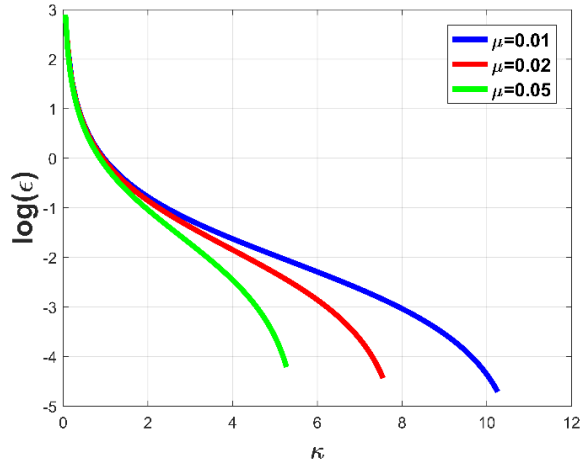

(c)

Figure 3.3: *Variation of the κ and μ KDamper parameters on a) the value of $\rho=\omega_D/\omega_0$, b) the value H_{USI} at the invariant points q_L, q_R and c) the static stability margin ε.*

However, increasing κ has a number of implications in the design of the KDamper. First, high stiffness values result, as presented in Figure 3.4. Moreover, increasing the stiffness and especially k_N may endanger the static stability of the structure. Although theoretically the value of k_N is selected according to Equation (2.23) to ensure the static stability, variations of k_N result in practice due to various reasons, such as temperature variations, manufacturing tolerances, or non-linear behavior, since almost all negative stiffness designs result from unstable non-linear systems. Consequently, an increase of the absolute value of k_N by a factor ε may lead to a new value of k_{NL} where the system becomes unstable:

$$k_S + \frac{k_P k_{NL}}{k_P + k_{NL}} = 0 \Leftrightarrow k_{NL} = -\frac{k_S k_P}{k_S + k_P} = (1+\varepsilon)k_N \tag{3.17}$$

Substitution of Equations (3.4.a) to (3.4.c) into (3.17) leads to the following estimate for the static stability margin ε:

$$\varepsilon = \frac{1}{\kappa\left[1+(1+\kappa)^2 \mu\rho^2\right]} \tag{3.18}$$

Figure 3.3.c presents the variation of ε over κ and μ. As it can be observed from Equation (3.18) and Figure 3.3.c, the increase of the negative stiffness of the system is upper bounded by the static stability limit of the structure, where ε tends to zero.

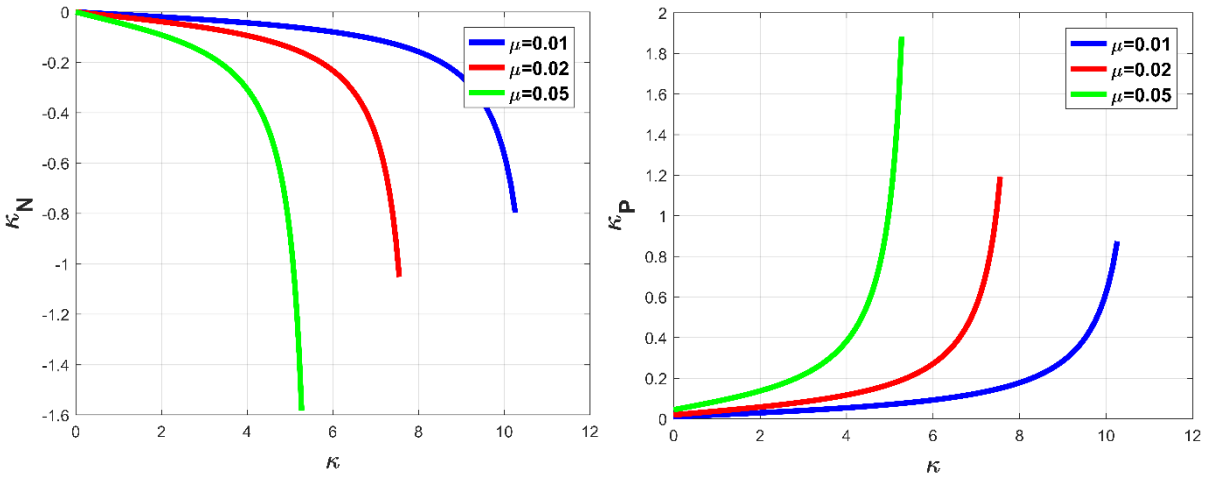

(a) (b)

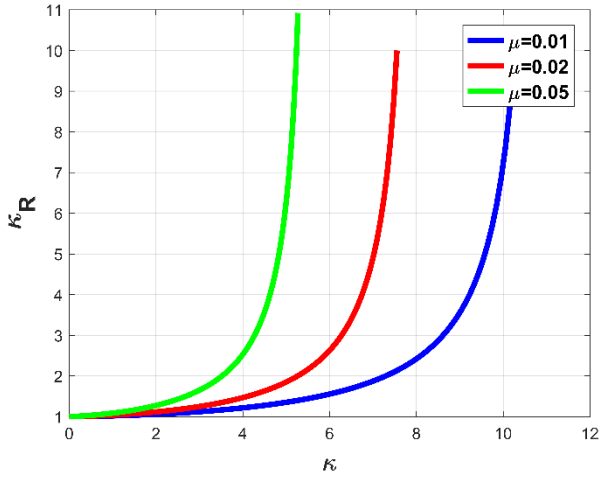

(c)

Figure 3.4: *Increase of values of stiffness elements of the KDamper by increasing κ, (a) κ_N (b) κ_P and (c) κ_R.*

3.2.2 Base Acceleration Excitation – Minimization of the Structure Absolute Acceleration Transfer Function

In this section the structure absolute acceleration Transfer Function H_{AS}, Equation (3.1.c) is selected for minimization, considering base acceleration excitation. Equation (3.1.c) can be written in the following form:

$$\tilde{H}_{AS} = -\frac{A+(j2\zeta_D)B}{C+(j2\zeta_D)D} \tag{3.19}$$

and consequently:

$$H_{AS} = \frac{\left|\tilde{A}_S\right|}{A_G} = \frac{A_S}{A_G} = \sqrt{\frac{A^2+(2\zeta_D)^2B^2}{C^2+(2\zeta_D)^2D^2}} \tag{3.20}$$

where:

$$A = -q^2[1+\kappa(1+\kappa)\mu\rho^2]+\rho^2 \tag{3.21.a}$$

$$B = \rho q(1+\kappa^2\mu\rho^2) \tag{3.21.b}$$

$$C = q^4 - q^2[1+\rho^2+(1+\kappa^2)\mu\rho^2]+\rho^2 \tag{3.21.c}$$

$$D = \rho q[(1+\kappa^2\mu\rho^2)-q^2(1+\mu)] \tag{3.21.d}$$

In the limit cases of $\zeta_D = 0$ or $\zeta_D \to \infty$, H_{AS} of Equation (3.20) becomes:

$$H_{AS}(0) = \left|\frac{A}{C}\right| \tag{3.22.a}$$

$$H_{AS}(\infty) = \left|\frac{B}{D}\right| \tag{3.22.b}$$

The Transfer Function $H_{AS}(q,\zeta_D)$ of Equation (3.20) has two poles for two different values of q and therefore, it presents two different maximal values (peaks) at these points. The optimal selection of the parameters of the KDamper requires that both these peaks are minimized and become equal to each other. This is ensured, similarly to section 3.2.1, by the optimal design approach followed in (Den Hartog, 1956). The approach is based on the identification of a pair of frequencies q_L <1 and q_R>1, where the values $H_{AS}(q_L)$ and $H_{AS}(q_R)$ become independent of ζ_D. The first step for the optimization procedure is the requirement that the values of the transfer functions at these points are equal:

$$H_{AS}(q_L) = H_{AS}(q_R) = H_{ASI} = H_{AS}(\infty) \tag{3.23}$$

In order that a solution for such a pair of frequencies exists, two alternative conditions must be fulfilled as in (Den Hartog, 1956):

Case I: $AD = BC$ (3.24.a)

Case II: $AD = -BC$ (3.24.b)

As it can be verified, no solution of Equation (3.24.a) exists for a positive q^2, when the values κ, μ, and ρ are positive. Elaboration of Equation (3.24.b) results to:

$$(A_2D_2 + B_0)q^4 + (A_0D_2 + A_2D_0 + B_0C_2)q^2 + (A_0D_0 + B_0C_0) = 0 \tag{3.25}$$

where the coefficients A_i, B_i, C_i, D_i are given in section A.1.3 of Appendix A.1. As a result of Equation (3.25), the pair of roots of Equation (3.25) must satisfy:

$$q_L^2 + q_R^2 = -\frac{(A_0 D_2 + A_2 D_0 + B_0 C_2)}{(A_2 D_2 + B_0)} \tag{3.26}$$

Additionally, both roots q_L and q_R must fulfill Equation (3.23), which results in:

$$\frac{B_0}{D_0 + D_2 q_L^2} = -\frac{B_0}{D_0 + D_2 q_R^2} \Rightarrow q_L^2 + q_R^2 = -\frac{2D_0}{D_2} \tag{3.27}$$

The combination of Equations (3.26) and (3.27) leads to an equation for the optimal value of the parameter ρ:

$$A_\rho \rho^4 + B_\rho \rho^2 + C_\rho = 0 \tag{3.28}$$

The optimal value of ρ is selected as the minimum positive value of the two roots of Equation (3.28). The damping ratio ζ_D is calculated numerically so that it minimizes the peak of the Transfer Function $H_{AS}(q,\zeta_D)$. Figure 3.5 presents the variation of $H_{AS}(q,\zeta_D)$ due to variation of ζ_D. As it can be observed, for the optimum value of $\zeta_{Dopt}=\zeta_{min}$, both peaks of the Transfer Function $H_{AS}(q,\zeta_D)$ are equal and minimum.

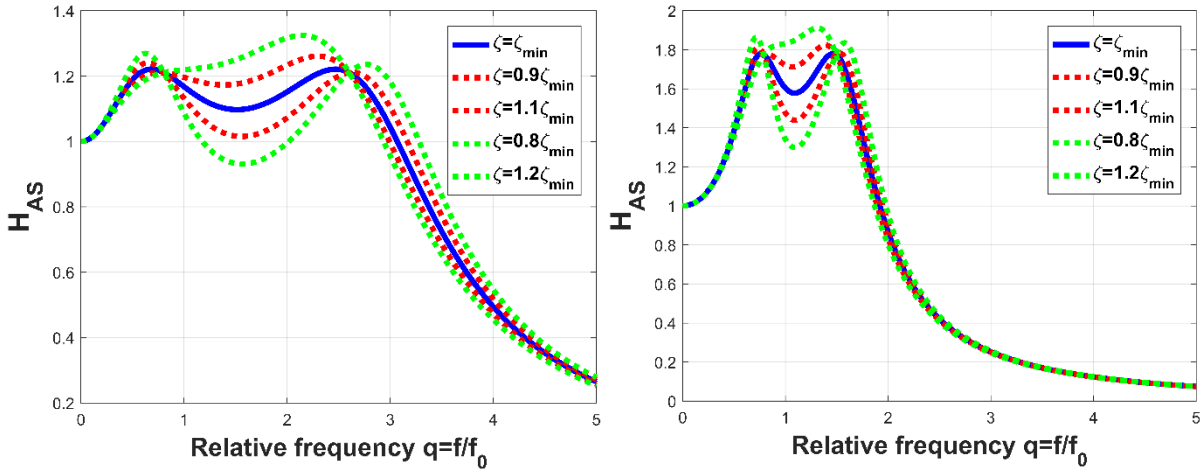

(a) (b)

Figure 3.5: *Dependence of Transfer Function H_{AS} on the damping ratio ζ_D (A) μ=0.05, κ=3.41 (B) μ=0.05, κ=2.56.*

3.2.2.1 Basic Properties

Again, as stated in section 3.2.2, the first fundamental property of KDamper is that the addition of a negative stiffness spring reduces the magnitude of the Transfer Function, as compared to that of a TMD with the same value of μ, as observed in Figure 3.6. Moreover, increasing the value of κ, reduces the maximum part of the transfer function H_{AS}, which becomes more flat. As a consequence, the KDamper is more robust to detuning, than the TMD. The increase in the value of κ is upper limited by a value of κ_{max}. As observed in Figure 3.7.a, when κ reaches κ_{max} the frequency ratio ρ tends to infinity. At the same time, the transfer function H_{ASI} (Equation (3.23), Figure 3.7.b) of the KDamper at the points q_L and q_R tends to one.

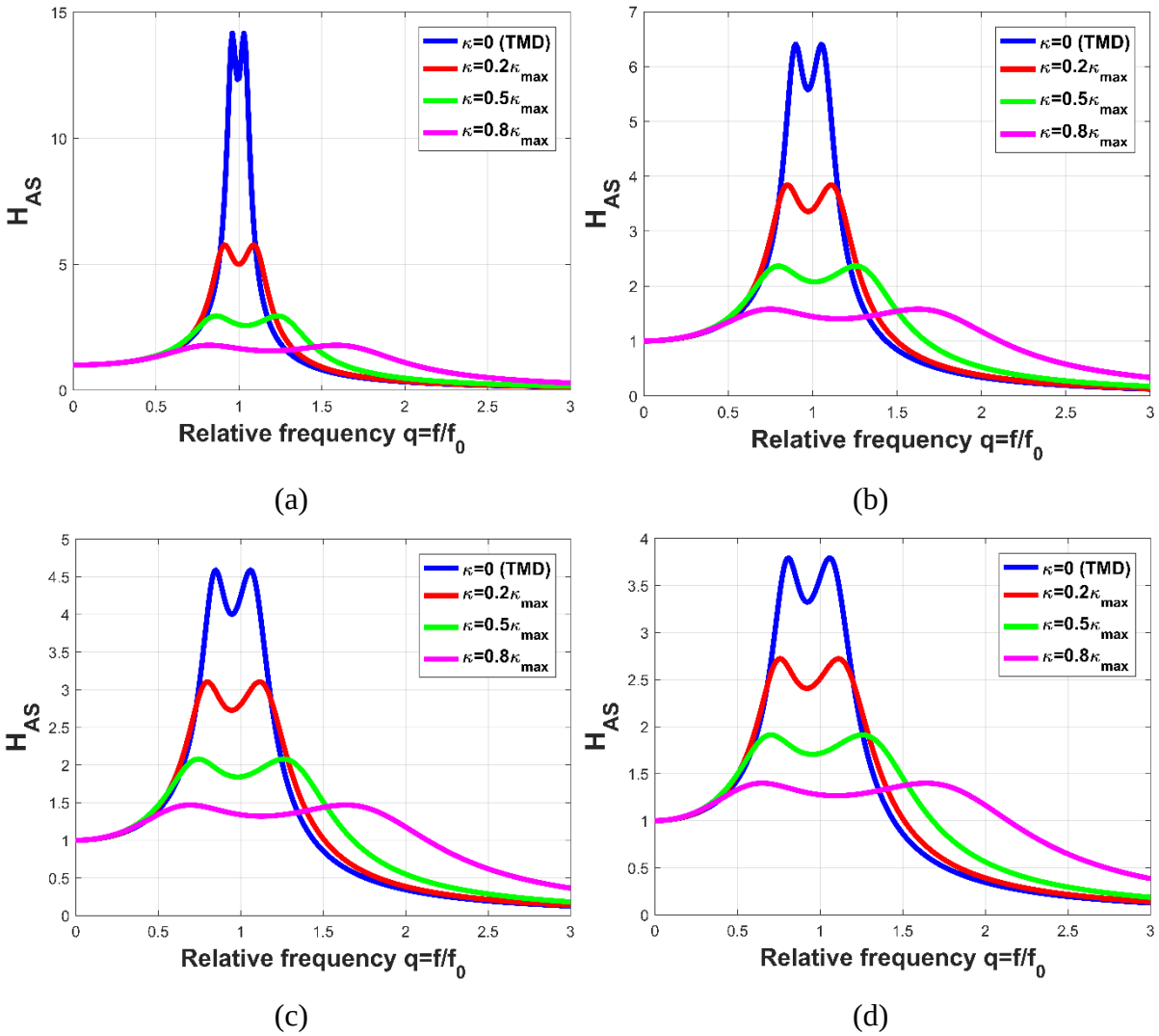

Figure 3.6: *Effect of the stiffness ratio κ on the Transfer Function H_{AS} of the KDamper for (a) μ=0.01, (b) μ=0.05, (c) μ=0.10 and (d) μ=0.15.*

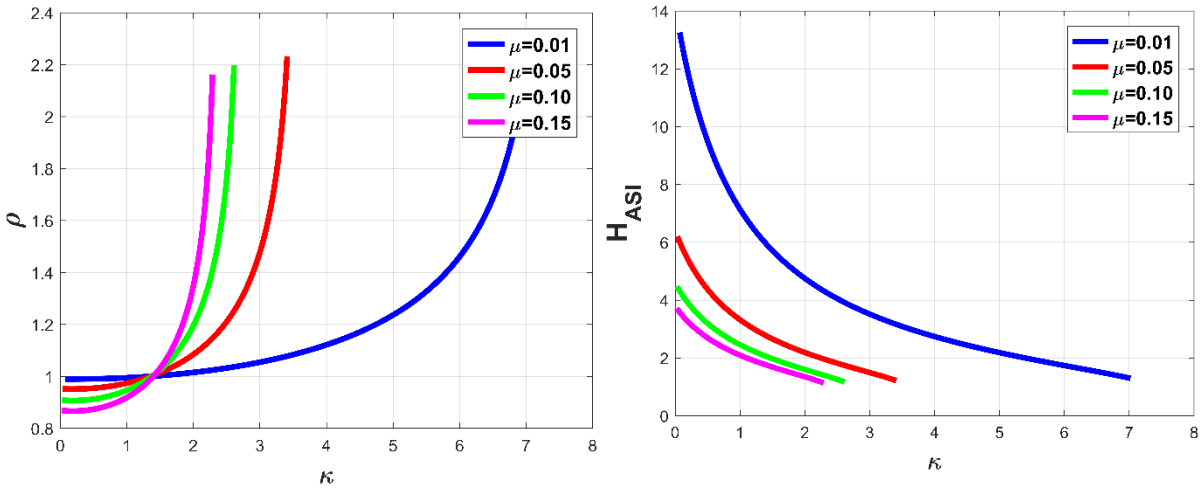

(a) (b)

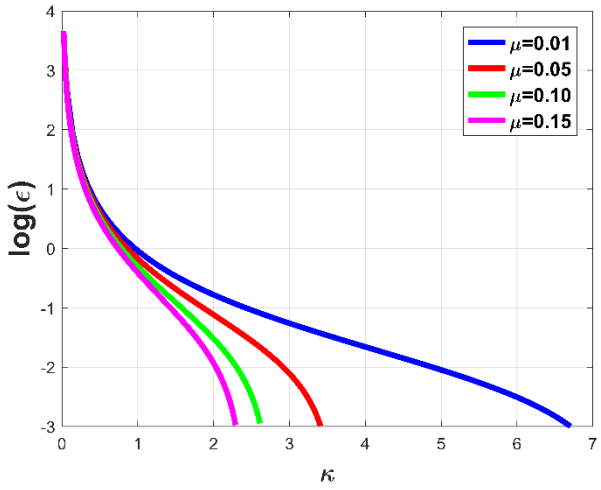

(c)

Figure 3.7: *Variation of the κ and μ KDamper parameters on: a) the value of $\rho=\omega_D/\omega_0$. b) the value H_{ASI} of the Transfer Function at the invariant points q_L, q_R. c) the static stability margin ε.*

However, increasing κ has a number of implications in the design of the KDamper. From a dynamics point of view, the Transfer Function tends to present a more broadband behavior, as for example observed in Figures 3.5 and 3.6. Moreover, the displacement of the "internal" degree of freedom u_D tends to increase. In view of Equations (3.1):

$$\frac{H_{UD}}{H_{US}} = \frac{-\omega^2 m m_D + j\omega c_D(m+m_D) + mk_P + m_D(k_R+k_P)}{-\omega^2 m m_D + j\omega c_D(m+m_D) + m(k_P+k_N) + m_D k_P} \tag{3.29}$$

or in a non-dimensional form:

$$\frac{H_{UD}}{H_{US}} = \frac{-q^2 + 2j\rho q\zeta_D(1+\mu) + 1 + (1+\kappa)(1+(1+\mu+\kappa\mu)\rho^2}{-q^2 + 2j\rho q\zeta_D(1+\mu) + (1+\mu+\kappa\mu)\rho^2} \tag{3.30}$$

In the specific case of ω=0, m_D=0 Equation (3.30) becomes:

$$\frac{H_{UD}}{H_{US}} = 1+\kappa \tag{3.31}$$

Figure 3.8 presents the effect of the stiffness ratio κ on the ratio of the Transfer Functions H_{UD}/H_{US} of the KDamper. As a qualitative remark from Figure 3.8, increasing κ tends to increase u_D while increasing μ tends to decrease u_D.

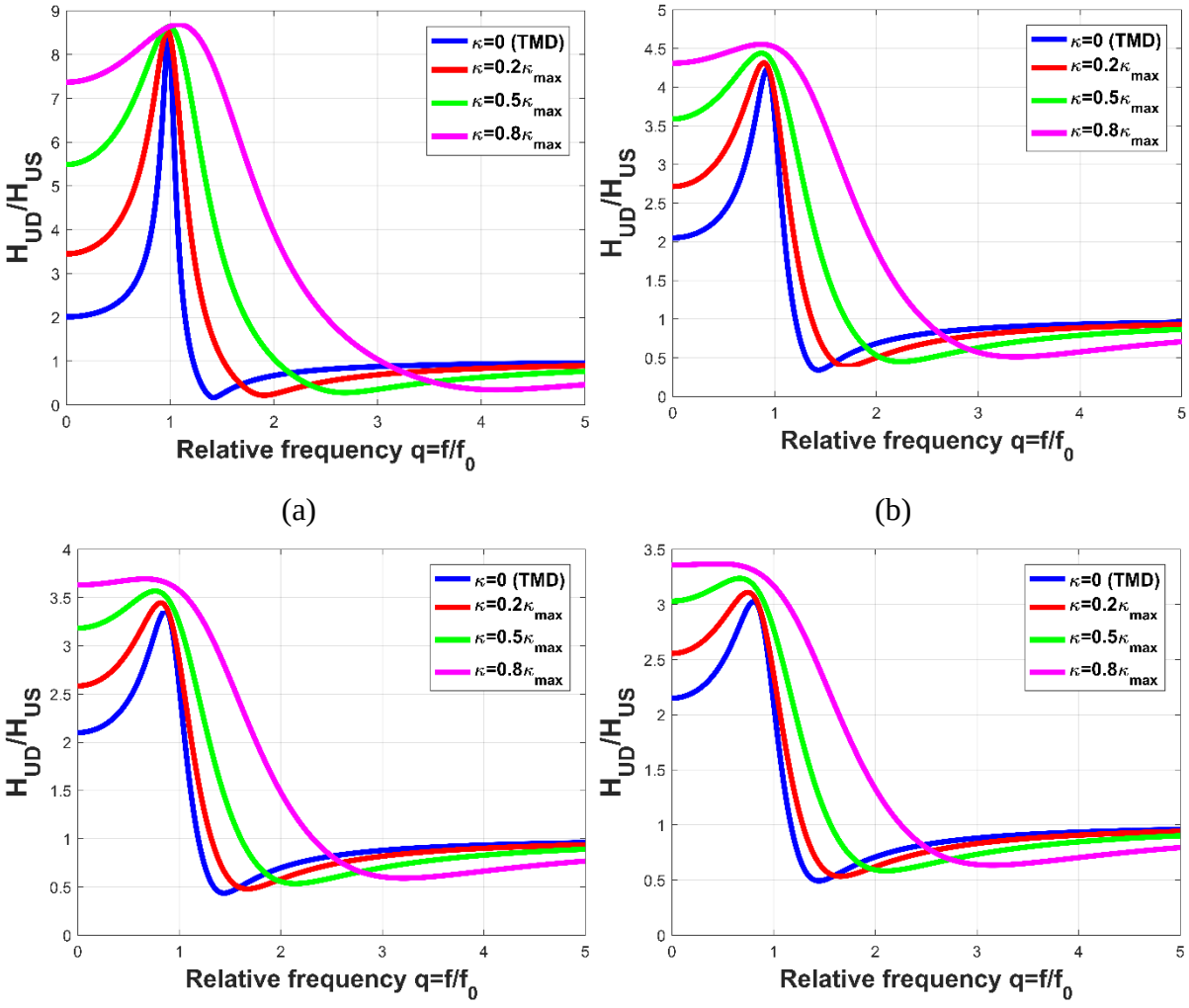

Figure 3.8: *Effect of the stiffness ratio κ on the ratio of Transfer Functions H_{UD}/H_{US} of the KDamper for (a) μ=0.01, (b) μ=0.05, (c) μ=0.10 and (d) μ=0.15.*

Figure 3.7.c presents the variation of ε over κ and μ. As it can be observed from the aforementioned expression of the static stability margin ε, Equation (3.18) and Figure 3.7.c, the increase of the negative stiffness of the system is upper bounded by the static stability limit of the structure, where ε tends to zero. Finally, high values of the stiffness ratio κ result to high stiffness values, as presented in Figure 3.9.

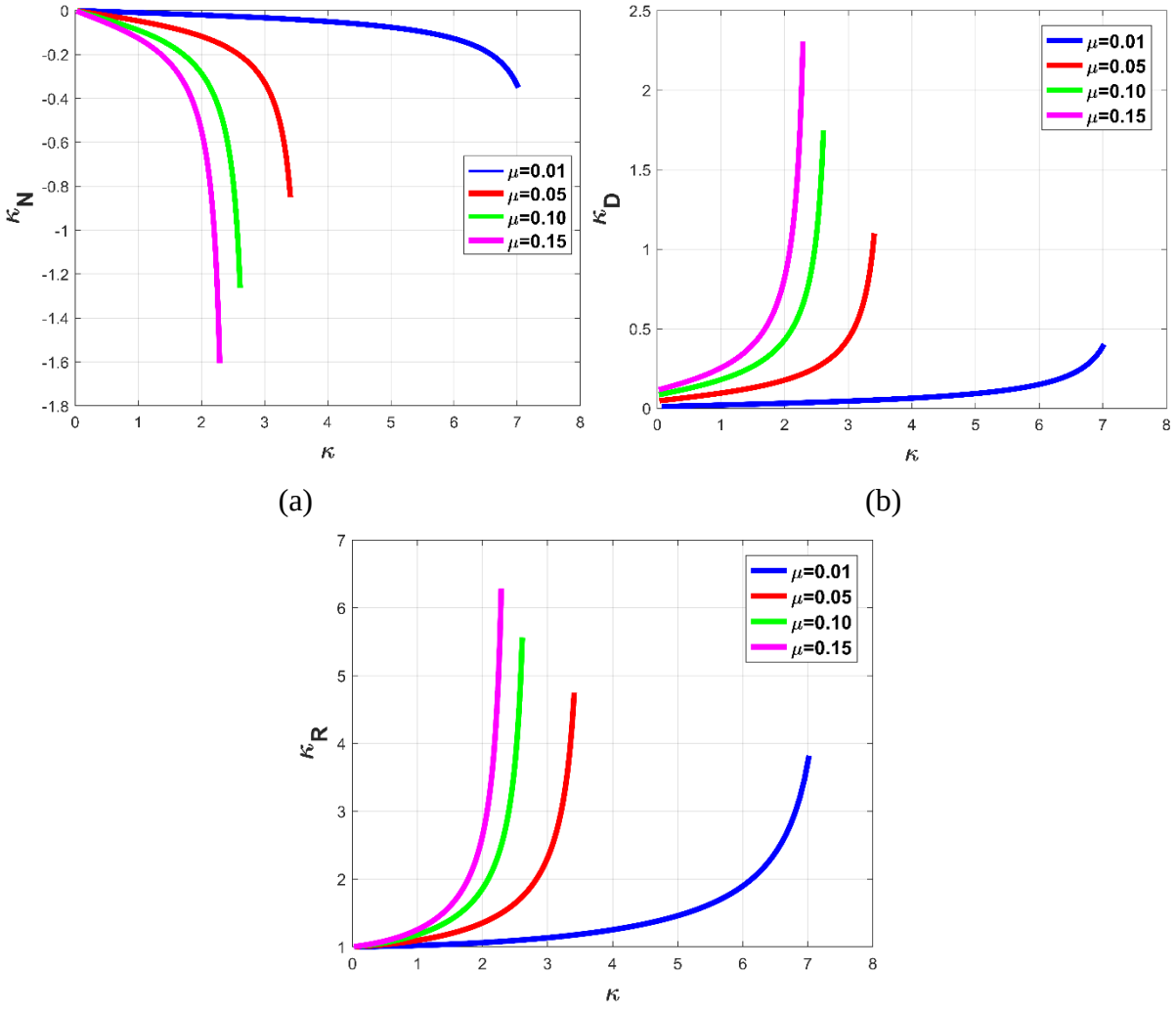

Figure 3.9: *Effect of increasing κ on the values of stiffness elements of the KDamper. (a) κ_N, (b) κ_P and (c) κ_R.*

3.3 Engineering – Criteria Driven Optimization of the Extended KDamper Designs

Extended KDamper designs, are configurations based on the classical KDamper, first proposed by (Antoniadis et al., 2018), that aim to further improve its dynamic behaviour. In the Extended

KDamper, the negative and positive stiffness elements are swapped, and furthermore a damping coefficient is placed in parallel to each stiffness element. Depending on the system to be controlled an inerter coefficient may be implemented, connecting directly the structure and the base. The complexity of these configurations renders the conventional minmax ($H\infty$) approaches ineffective. In addition, the properties of the KDamper and the physical and manufacturing limitations that might occur during its implementation (e.g. upper limit of internal DoF displacement, negative stiffness element stroke), lead to the conclusion that a constrained optimal design based on engineering criteria should be followed.

3.3.1 Realization of the Negative Stiffness Element with Pre – Compressed Springs

Negative stiffness is primarily achieved by special mechanical designs involving conventional positive stiffness pre-stressed elastic mechanical elements, such as post-buckled beams, plates, shells and pre-compressed springs, arranged in appropriate geometrical configurations. Some interesting designs are described in (Virgin et al., 2008; Winterflood et al., 2002). However, alternatively to elastic forces, other forms of physical forces can be used to produce an equivalent negative stiffness effect, such as gravitational (Dyskin and Pasternak, 2012), magnetic (Robertson et al., 2009) or electromagnetic (Zhou and Liu, 2010).

In this section, the proposed configurations for the realization of the negative stiffness element involve mechanisms with pre-compressed springs. That is due to the simple design they offer, and that the negative stiffness is easily controlled. Such configurations can support/achieve the needed negative stiffness for implementations in structural systems, such as seismic protection of structures etc.

3.3.1.1 Proposed Configuration I: *One – Dimensional Negative Stiffness*

Regarding the properties and features of the simple QZS configuration proposed by Carrella (Carrella et al., 2007), an alternative mechanism is hereby described, as depicted in Figure 3.10. The static equilibrium position and the perturbed position due to an external base dynamic excitation, $x_G(t)$ are both presented in Figure 3.10.b. The necessary notation concerning the various displacements of the system is also presented.

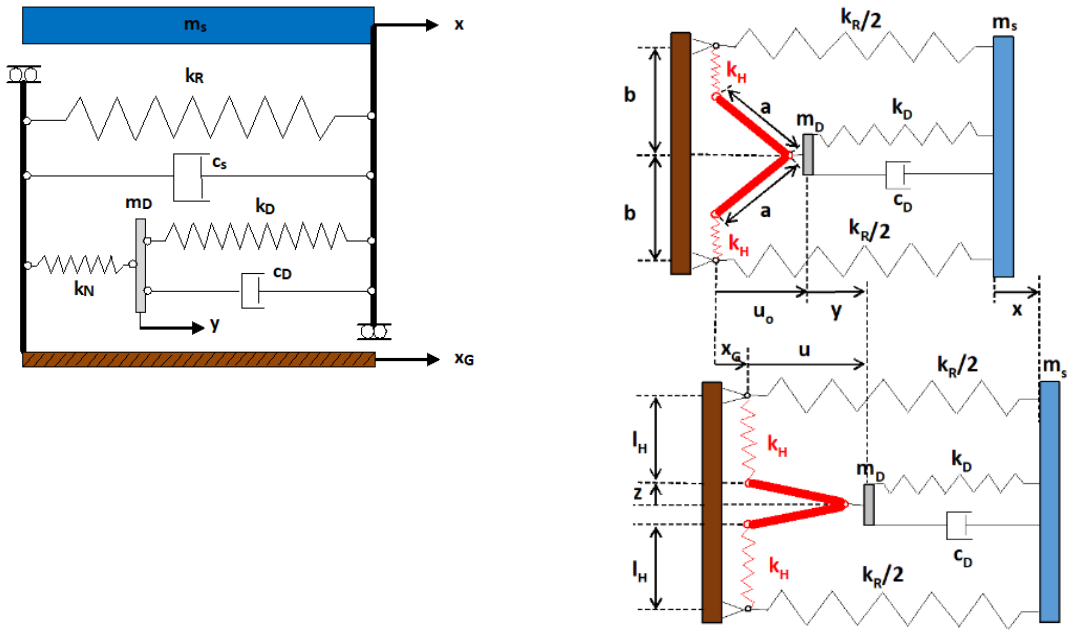

(a) (b)

Figure 3.10: *Schematic representation (a) of the KDamper concept and (b) of the Proposed Configuration I (plan view).*

The negative stiffness spring k_N (Figure 3.10.a) is realized by a set of two symmetric linear horizontal springs with constants k_H, which support the mass m_D by an articulated mechanism. In order to calculate the value of the negative stiffness produced by this pair of positive stiffness springs, the ensuing procedure is followed. The equations of motions of the proposed oscillator are:

$$m\ddot{u}_S + k_R u_S + c_S \dot{u}_S + k_P(u_S - u_D) + c_D(\dot{u}_S - \dot{u}_D) = -m\ddot{X}_G \tag{3.32.a}$$

$$m_D \ddot{u}_D - k_P(u_S - u_D) - c_D(\dot{u}_S - \dot{u}_D) + f_N(u) = -m_D \ddot{X}_G \tag{3.32.b}$$

where u_S=X-X_G and u_D=Y-X_G. The following expressions can be derived for the potential energy U_N, the nonlinear force f_N and the equivalent nonlinear stiffness k_N of the set of horizontal springs k_H:

$$U_N[u(y)] = 2\frac{1}{2}k_H(l_H - l_{HI})^2 \tag{3.33}$$

$$f_N(u) = \frac{\partial U_N}{\partial y} = \frac{\partial U_N}{\partial u} = -2k_H\left(1 + \frac{l_{HI} - b}{\sqrt{a^2 - u^2}}\right)u = -2k_H\left[1 + c_I \frac{1}{(1 - u^2/a^2)^{1/2}}\right]u \tag{3.34}$$

$$k_N = \frac{\partial f_N}{\partial y} = \frac{\partial f_N}{\partial u} = -2k_H \left[1 + \frac{l_{HI} - b}{a} \frac{1}{(1-u^2/a^2)^{3/2}} \right] = -2k_H \left[1 + c_I \frac{1}{(1-u^2/a^2)^{3/2}} \right] \quad (3.35)$$

where l_{HI} is the initial length of the un-deformed springs k_H, $l_H(t)$ is the length of the springs k_H:

$$l_H = b - (a^2 - u^2)^{1/2} \quad (3.36)$$

and:

$$u = u_0 + u_D \quad (3.37)$$

$$c_I = (l_{HI} - b)/a \quad (3.38)$$

In the case of c_I=0 the two horizontal springs are equivalent to a spring with a constant negative stiffness of k_N=-2k_H. Next, the parameters of the negative stiffness element and the corresponding mechanism are selected. The parameter u_0 is selected equal to 0.1 *cm*. This value is close to zero so that an almost symmetric response around u=0 is obtained. The rest of the parameters are selected so that $k_N(0)$=1.01k_{NC} and $k_N(umax)$=0.90k_{NC}, where k_{NC} is the constant negative stiffness of the KDamper device. Since $k_N(u=0)$ is the minimum value of the negative stiffness element, the system remains statically and dynamically stable, as stated in Equation (2.23), for the entire operating range. The value of c_I is selected -0.05, in order to achieve as far as possible a linear behavior.

3.3.1.2 Proposed Configuration II: *Two – Dimensional Negative Stiffness*

Proposed configuration I generates negative stiffness in only one dimension. This configuration is effective when is applied in automotive suspensions, torsional vibrations, vertical vibration absorption, and generally in structural systems that are subjected to dynamic loads in one direction. In this section, a configuration that generates two-dimensional negative stiffness is proposed, as presented in Figure 3.11, in order to be effective as a horizontal seismic protection mechanism. This configuration is selected for the realization of the negative stiffness elements in the Extended KDamper designs.

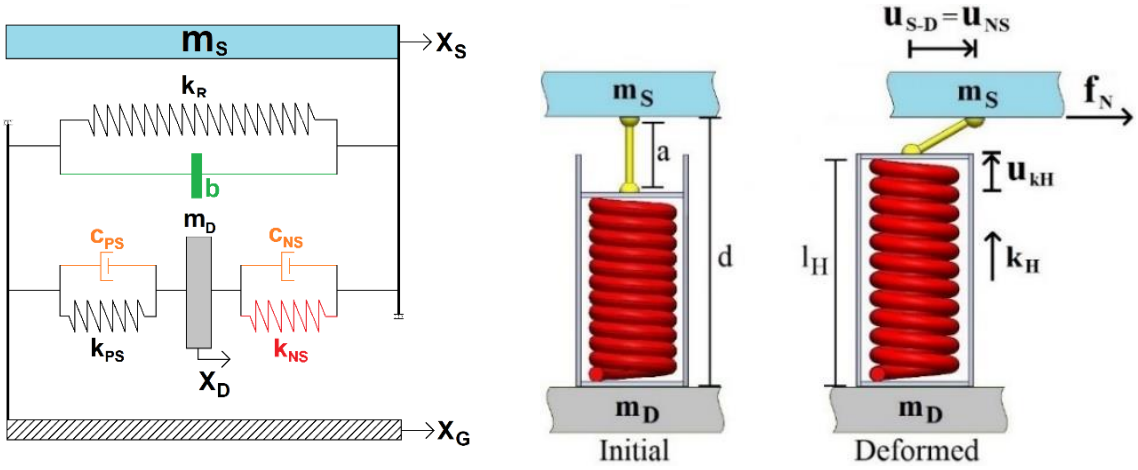

(a) (b)

Figure 3.11: *Schematic representation (a) of the KDamper concept and (b) of the Proposed Configuration II (front view).*

The equations of motions of the proposed system are:

$$(m+b)\ddot{u}_S + k_R u_S + f_{NS}(u_{NS}) + c_{NS}(\dot{u}_S - \dot{u}_D) = -m\ddot{X}_G \tag{3.39.a}$$

$$m_D\ddot{u}_D - f_{NS}(u_{NS}) - c_{NS}(\dot{u}_S - \dot{u}_D) + c_{PS}\dot{u}_D + k_{PS}u_D = -m_D\ddot{X}_G \tag{3.39.b}$$

where u_S=X_S-X_G and u_D=X_D-X_G. The potential energy U_N, the nonlinear force f_N and the equivalent nonlinear stiffness k_N are expressed with the following relations:

$$U_{NS}[u_{NS}(u_D)] = \frac{1}{2}k_H(l_H - l_{HI})^2 \tag{3.40}$$

$$f_{NS}(u_{NS}) = \frac{\partial U_{NS}}{\partial u_D} = \frac{\partial U_{NS}}{\partial u_{NS}} = -k_H(1+\frac{l_{HI}-b}{\sqrt{a^2-u^2}})u = -2k_H\left[1+c_I\frac{1}{(1-{u_{NS}}^2/a^2)^{1/2}}\right]u_{NS} \tag{3.41}$$

$$k_N = \frac{\partial f_{NS}}{\partial u_D} = \frac{\partial f_{NS}}{\partial u_{NS}} = -k_H\left[1+\frac{l_{HI}-b}{a}\frac{1}{(1-u_{NS}^2/a^2)^{3/2}}\right] = -k_H\left[1+c_I\frac{1}{(1-u_{NS}^2/a^2)^{3/2}}\right] \tag{3.42}$$

where l_{HI} is the initial length of the undeformed springs k_H, $l_H(t)$ is the length of the springs k_H:

$$l_H = b-(a^2-u_{NS}^2)^{1/2} \tag{3.43}$$

and:

$$u_{NS} = u_0 + u_D \tag{3.44}$$

$$c_I = (l_{HI} - b)/a \tag{3.45}$$

The parameter u_0 is selected equal to 0.1 *cm*, the value of c_I is selected -0.05 and the rest of the parameters are selected so that $k_N(0)=1.01k_{NC}$ and $k_N(umax)=0.90k_{NC}$, where k_{NC} is the constant negative stiffness of the KDamper device.

3.3.2 Spectrum – Compatible Earthquake Excitation Input Based on the Provisions of the Seismic Design Codes

According to seismic design codes, the structure's relative displacement and absolute acceleration, are within specified limits for a system with given characteristics (fundamental structure period and damping ratio). The parameters that mainly control these limits are the ground conditions, the expected seismic intensity, the damping ratio of the system as well as the fundamental period of the structure. A typical form of the so-called "Design Response Spectra" is depicted in Figure 3.12.

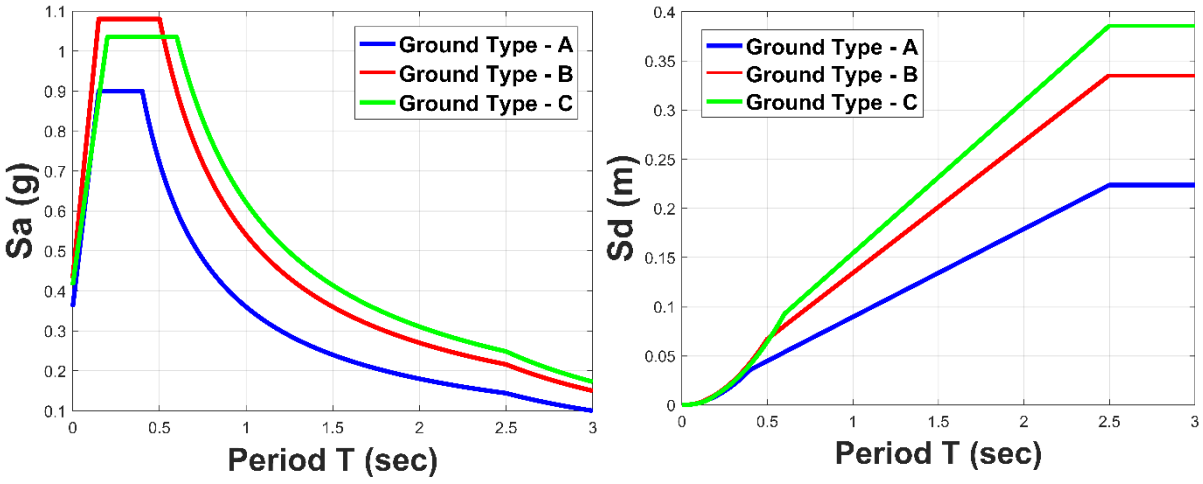

(a) (b)

Figure 3.12: *EC8 Design response spectra: (a) Spectral acceleration and (b) Spectral displacement.*

The direct application of such approached however for the selection of the KDamper-based design parameters, is not possible, since the application of the KDamper as a seismic absorption base leads to MDoF systems with multiple frequencies. Therefore, analysis in the

time-domain is required for the optimal design of the proposed dynamic vibration absorbers. Strong earthquake records can be generated from various types of accelerograms, the fundamental of which being: synthetic records obtained from seismological models, real earthquakes excitations (not all soil types, not smoothed spectra) and artificial accelerogram, compatible with a specific design response spectrum, with the latter being the most suitable.

Towards this direction, the generation of design response spectrum compatible ground acceleration excitations is necessary. This is far from being a trivial task, with rich background research, overviews of which can be found among others in (Cacciola and D'Amico, 2015; Giaralis and Spanos, 2012). For this reason, the approach followed in this Chapter is based on generating a database of artificial accelerograms, with response spectra closely compatible with the EC8 design response spectra (*EN 1998-1: Eurocode 8 – Part 1*, 2004). Artificial spectrum-compatible accelerograms are generated using the SeismoArtif Software (Seismosoft [2018], 2018). SeismoArtif computes a power spectral density function from a specified smooth response spectrum, in this case, EC8, and uses this function to derive the amplitudes of sinusoidal signals with random phase angles. The signals are then summed and an iterative procedure can be invoked to improve the match with the target response spectra. The power spectral density function is then adjusted by the square of the ordinate ratio and a new motion is generated.

3.3.2.1 Horizontal Ground Motions

In this study, the artificial accelerograms are designed to match the EC8 elastic horizontal acceleration response spectrum incorporating the following seismic properties: ground type C, spectral acceleration 0.36 *g*, spectrum type I and importance class II. A sample of 30 artificial accelerograms, with a mean PGA of 5.19 m/sec^2 is generated and plotted in Figure 3.13.b, along with the EC8 response spectrum for comparison with the design guidelines. An accurate match is observed (percentage deviation less than *10%*) in the range of periods from *0.2* to *2* sec, which are considered relevant for the structural performance.

Next, the mean power spectral density S_{AM} of the accelerograms is calculated as:

$$S_{AM} = \frac{1}{N_a} \sum S_{ai} \tag{3.46}$$

where S_{ai} is the PSD of an acceleration record and N_a is the number of accelerograms.

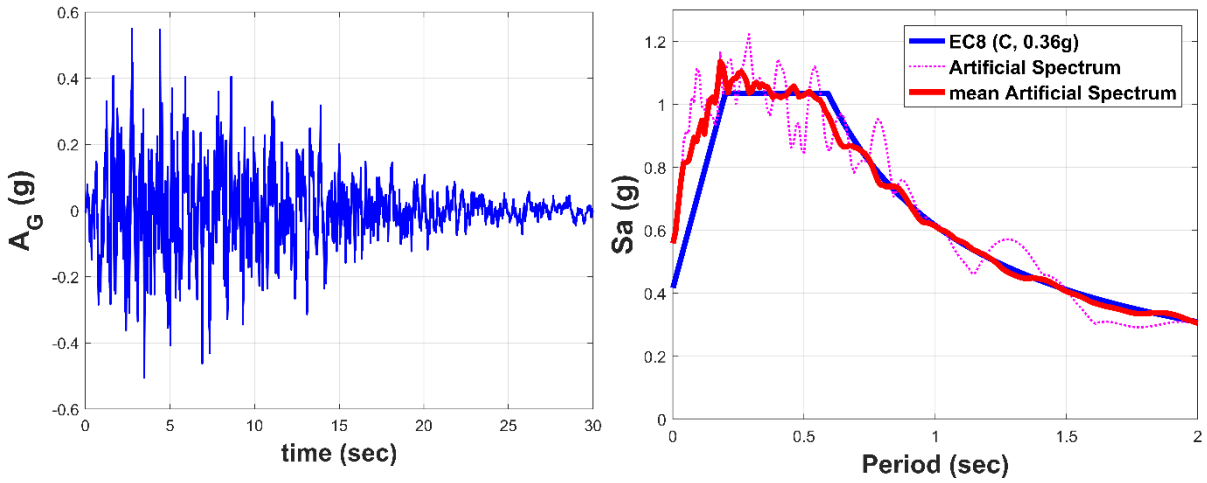

(a) (b)

Figure 3.13: *(a) Random artificial accelerogram and (b) mean artificial acceleration response spectrum, of the 30 generated artificial accelerograms in the database compared to the EC8 horizontal acceleration response spectrum.*

The mean power spectral density S_{AM} of the Na=30 accelerations in the selected database is presented in Figure 3.14.a, along with the least square fitting which will be subsequently used as the ground motion excitation acceleration PSD S_A. Parallel, in Figure 3.14.b a stationary power-spectral density function generated from (Cacciola and D'Amico, 2015) is presented, and adapted to the same peak value of the considered PSD, S_A. A very good fit can be observed.

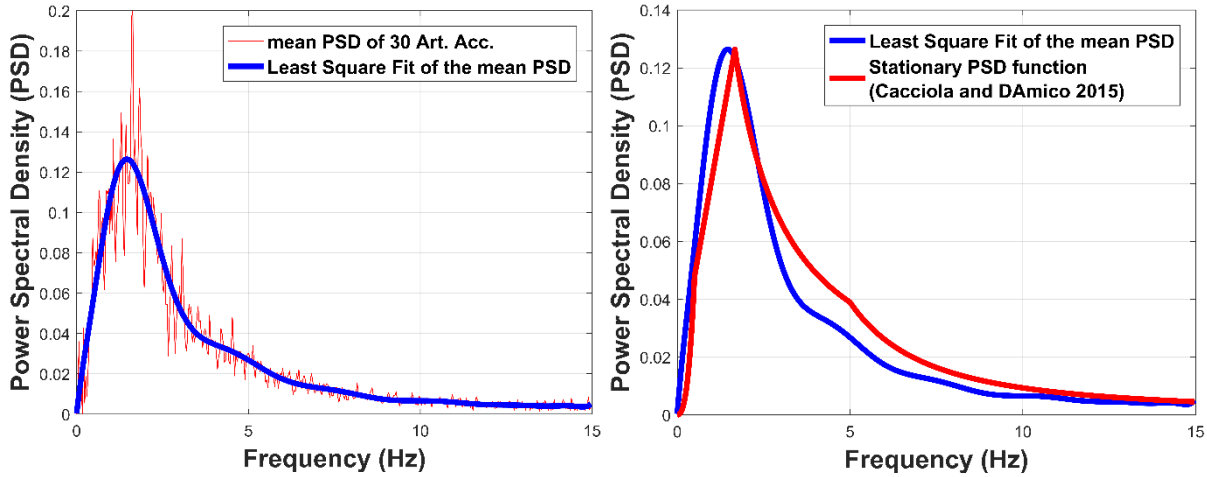

(a) (b)

Figure 3.14: *(A) Mean Power Spectral Density of the 30 Artificial Accelerograms S_{AM} in the selected database with the least square fitting S_A and (B) least square fitting S_A compared with stationary power-spectral density function, as described in (Cacciola and D'Amico, 2015).*

3.3.2.2 Vertical Ground Motions

The vertical component of the ground motion is described in (*EN 1998-1: Eurocode 8 – Part 1*, 2004) by an elastic ground acceleration response spectrum. For each seismic zone the vertical acceleration is given by the ratio a_{vg}/a_g, the recommended values of which are 0.9 for seismic action Type 1 (Mw>5.5) and 0.45 for Type 2. The basic shape of the spectrum is similar to the recommended horizontal. However, the spectral amplification in the vertical case is 3.0 instead of 2.5. Furthermore, it should be mentioned that, contrary to what is indicated for the horizontal components, it is considered that the vertical ground motion is not very much affected by the underlying ground conditions and so no use of the soil factor S is made. The vertical acceleration spectrum with a_g=0.36 g and Type 1 is presented in Figure 3.15.b.

In this dissertation, a database of 50 artificial accelerograms is generated designed to match the EC8 spectrum with characteristics: Type 1 with a_{vg} (g)=0.9*0.36. In Figure 3.15.a, an artificial accelerogram is presented, using the calculation method "Artificial Accelerogram Generation and Adjustment". In Figure 3.15.b, the mean acceleration spectrum of the 50 artificial accelerograms is compared with the EC8 vertical acceleration spectrum. An accurate match is observed with a percentage deviation under 10% in all the range of the natural periods.

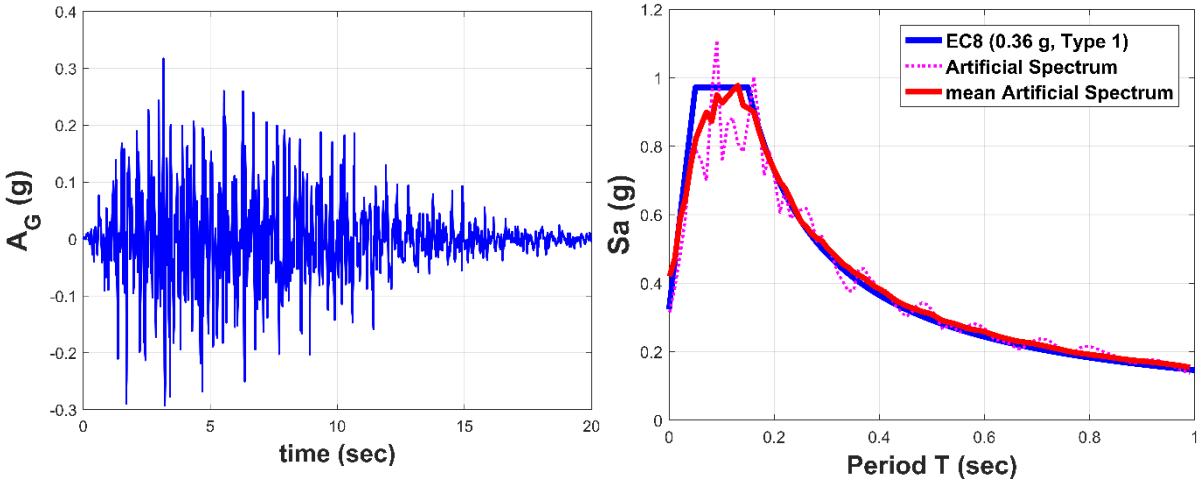

(a) (b)

Figure 3.15: *(a) Artificial accelerogram, (b) mean artificial acceleration spectrum compared to the EC8 design spectrum.*

Next, the mean power spectral density S_{AM} of the 50 accelerograms is calculated and presented in Figure 3.16, along with its least-square fitting which will be subsequently used as the ground motion acceleration excitation PDS, S_A.

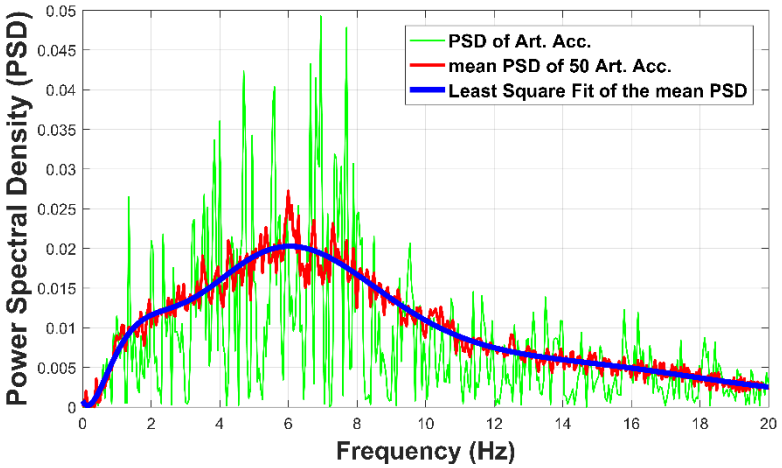

Figure 3.16: *Power Spectral Density (PSD) of a random Artificial Accelerogram, mean PSD of the 50 Artificial Accelerograms, S_{AM}, in the database and Least Square Fitting (LSF), S_A, of the mean PSD.*

3.3.3 Harmony Search Optimization Algorithm

Harmony search algorithm (HS) is a novel metaheuristic algorithm proposed in 2001 (Geem et al., 2001). Similarly to the genetic algorithms (GA) (Goldberg and Holland, 1988; Holland, 1975), HS exhibits numerous positive characteristics that render it suitable for various optimization problems including the traveling salesman problem (Geem et al., 2001), optimization of data classification systems (Wang et al., 2009) and pipe network design (Geem et al., 2002). Considering the solution of structural problems, HS has been successfully applied to the optimum design of truss structures (Lee and Geem, 2004), steel sway frames (Saka, 2009) and grillage systems (Saka and Erdal, 2009). Recently, HS has been employed for the optimum design of the implementation of TMDs to multistory buildings (Nigdeli et al., 2014; Nigdeli and Bekdaş, 2017). A detailed description of HS algorithm, along with its special features and unique properties is given in the following sections of the current chapter.

In the following, the positive properties of HS algorithm are described. First of all, HS can handle problems with both discrete and continuous variables (Lee et al., 2005; Lee and Geem, 2005) and is characterized by the distinguishing features of algorithm simplicity and search efficiency. Since it is not a hill-climbing algorithm, the probability of becoming entrapped to a local optimum is significantly reduced. Moreover, it uses a stochastic random search instead of a gradient search, as other metaheuristic algorithms do, gaining in simplicity. Stochastic derivatives are useful for a number of scientific and engineering problems where mathematical derivatives cannot be calculated or easily treated (Geem, 2008) and also serve to

the reduction of the required number of iterations. A summary of the aforementioned HS distinguishing features and advantages is presented in the flowchart of Figure 3.17.

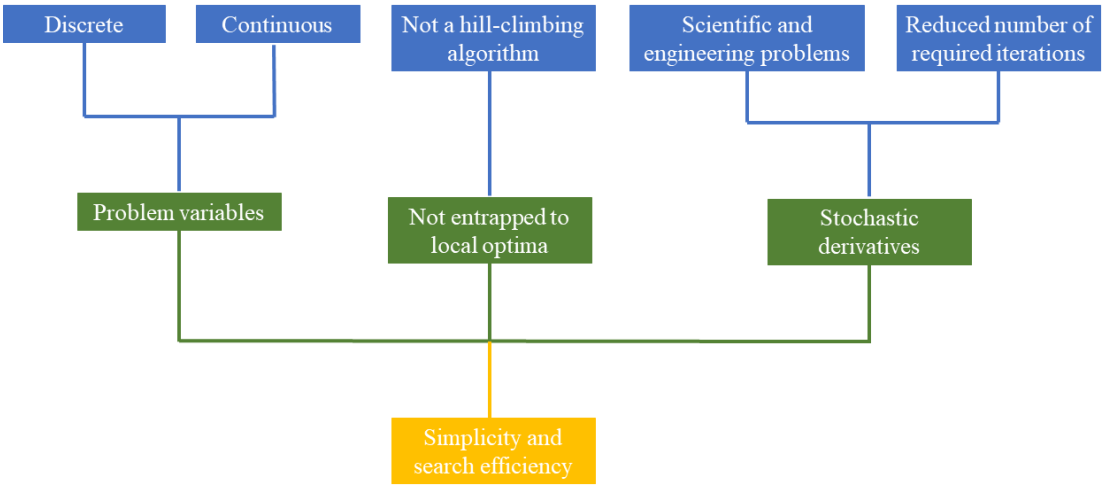

Figure 3.17: *Distinguishing features and advantages of the HS algorithm.*

As it has already been mentioned in the previous, HS algorithm exhibits certain useful characteristics and properties that render it a suitable and powerful tool for the solution of complex mathematical and engineering problems. At the same time, HS appears to be a promising alternative to conventional optimization techniques, especially considering problems where the latter cannot be applied. As a result, the HS algorithm is used for the optimal design of the extended KDamper configurations. Further information regarding the constraints and limitations imposed can be found in Chapter 5.

A detailed description of the HS algorithm can be found in (Nigdeli et al., 2014; Nigdeli and Bekdaş, 2017; Geem et al., 2001). However, the four basic steps of the algorithm are, also, cited in the following:

Step 1: Initialization of the HS Memory matrix (HM). HM matrix contains vectors representing possible solutions to the examined optimization problem. The initial HM matrix is created using randomly generated solutions. For an n-dimension problem, HM has the form:

$$HM = \begin{bmatrix} x_1^1, x_2^1, \ldots, x_n^1 \\ x_1^2, x_2^2, \ldots, x_n^2 \\ . \\ . \\ . \\ x_1^{HMS}, x_2^{HMS}, \ldots, x_n^{HMS} \end{bmatrix} \tag{3.47}$$

where $[x_1^1, x_2^1, \ldots, x_n^1]$ $(i=1, 2, \ldots, HMS)$ is a solution candidate. HMS is typically set to values between 50 and 100. The value of the objective function is calculated for every solution vector of the HM matrix.

Step 2: Improvisation of a $[x_1', x_2', \ldots, x_n']$ new solution from the HM. Each one of the components of this new solution, x_j', is obtained based on the Harmony Memory Considering Rate (HMCR), which is defined as the probability of selecting a component from the HM members. 1 – HMCR is, therefore, the probability of generating a new component randomly. If x_j' is chosen from the HM matrix, it is further mutated according to the Pitching Adjusting Rate (PAR), which determines the probability of a candidate from the HM to be mutated.

Step 3: Update of the HM matrix. The value of the objective function of the new solution, obtained in Step 2, is calculated and compared to the ones that correspond to the original HM matrix vectors. If it results in better fitness than that of the worst member in the HM, it will replace that one. In the typical case of a minimization optimization process, the new solution replaces a member of the HM matrix, only if that member has a bigger value of objective function than the new one. If there is more than one member in the HM with larger values of the objective function that the new solution, the one with the higher value is replaced. Otherwise, the new solution is eliminated and the HM matrix remains intact.

Step 4: Repetition of Steps 2 and 3 until a preset termination criterion is met. A commonly used termination criterion is the maximum number of total iterations.

The flowchart of the proposed HS algorithm is presented in Figure 3.18.

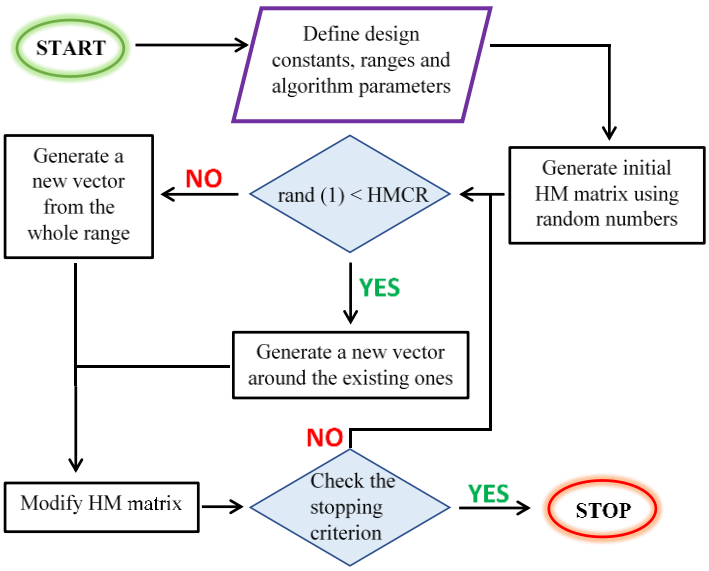

Figure 3.18: *Flowchart of the proposed HS algorithm.*

As far as the parameters inherently involved in the HS algorithm are concerned, a common practice is to adopt commonly found values found in relative literature (Table 3.1). The same is true for the termination criterion, as the maximum number of repetitions is pre-determined.

Table 3.1. *Values of the HS algorithm parameters.*

HMS	HMCR	PAR
75	0.5	0.1

3.4 Numerical Example 1 – *Comparison of Optimization Approaches of the KDamper Concept for Horizontal Seismic Protection*

The vibrations of a SDoF system of mass m=1 *tn*, which has a natural frequency of 0.4 *Hz* and a damping ratio of 5%, are to be controlled with the KDamper. Three cases are considered regarding the optimal design of the KDamper. In the first case, the procedure described in section 2.2.1 of this Chapter is followed for optimal displacement control, and this set of parameters will be referred to hereafter as H_{US}-set. In the second case, the procedure described in section 2.2.3 of this Chapter is followed for optimal acceleration control, and this set of parameters will be referred to hereafter as H_{AS}-set, and finally, in the third case the parameters of KDamper are selected according to the optimization procedure described in section 3.3 of this Chapter, and this set of parameters will be referred to hereafter as HS-set. The system is subjected to the 30 Artificial Accelerograms in the database, generated according to section 3.3.2.1 of this Chapter. In order to have an equal comparison basis, the additional mass ratio and the stiffness ratio of KDamper are selected equal to 5% and 2.56, respectively.

The limits of the HS-set in the optimization procedure are [0 1.5] and [0 0.5] for the parameters ρ and ζ_D, respectively. The mean of the maximum structural relative displacements, u_S, is set as the objective function, and proper constraints regarding the structural absolute acceleration and NS element stroke are selected. In Table 3.2, are the non-dimensional KDamper parameters of all the aforementioned cases.

In Figure 3.19, the Transfer Functions of the aforementioned systems with KDamper, optimized according to the procedures mentioned previously, H_{US}-set, H_{AS}-set, and HS-set are presented. Figure 3.20, presents comparative results between the three test cases, for a random Artificial Accelerogram of the database.

Table 3.2: *Non-dimensional KDamper parameters of the three considered test cases.*

	μ	κ	ρ	κ_N	κ_P	κ_R	ζ_D	ε
H_{US}-set	0.05	2.56	0.9955	-0.1268	0.1763	1.4512	0.494	0.24
H_{AS}-set	0.05	2.56	1.2319	-0.1943	0.2701	1.6915	0.473	0.20
HS-set	0.05	2.56	1.4785	-0.2798	0.3891	1.9961	0.4430	0.1638

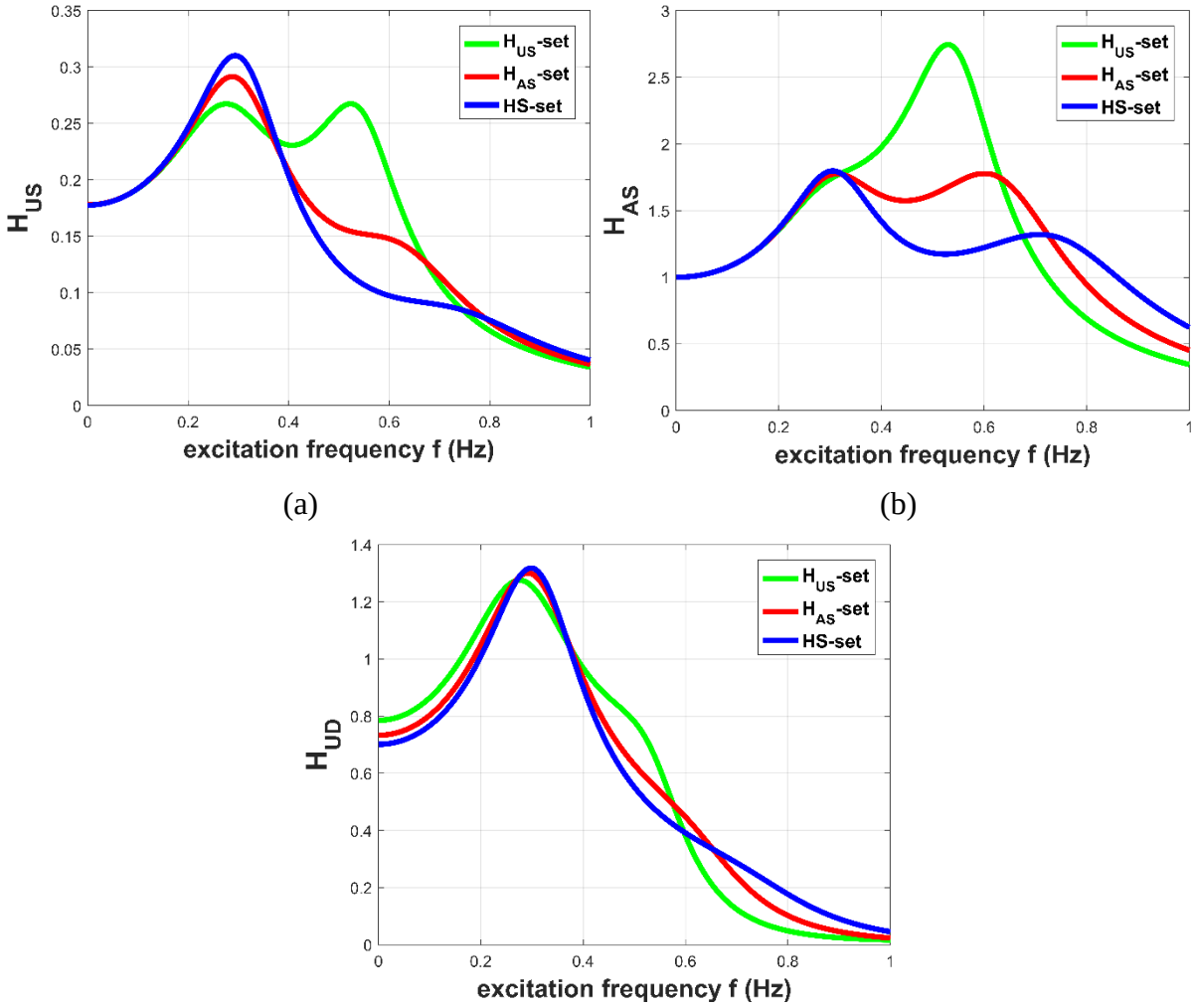

Figure 3.19: *Transfer Functions of three different optimized KDamper cases, namely H_{US}-set, H_{AS}-set, and HS-set. (a) relative displacement, (b) absolute acceleration, and (c) NS element stroke.*

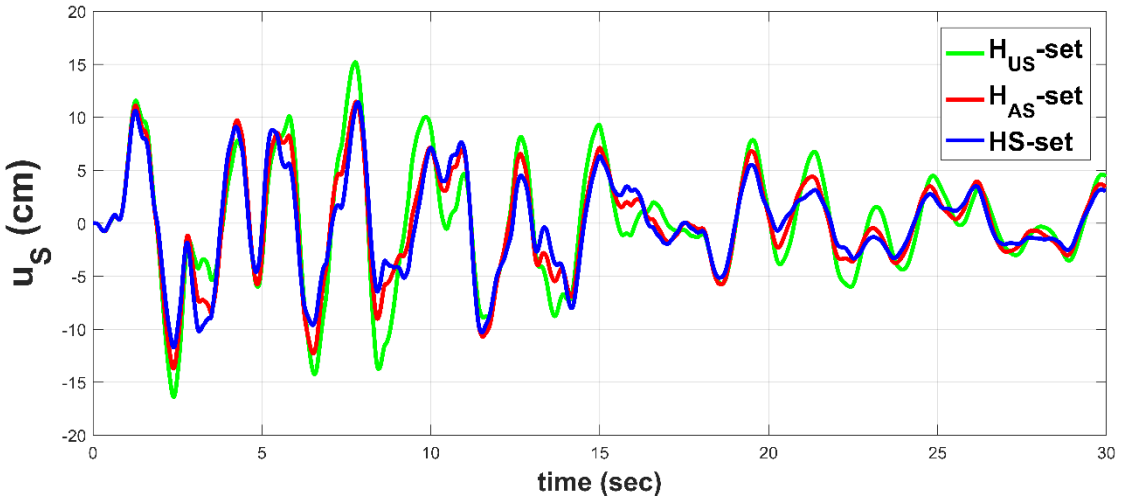

(a)

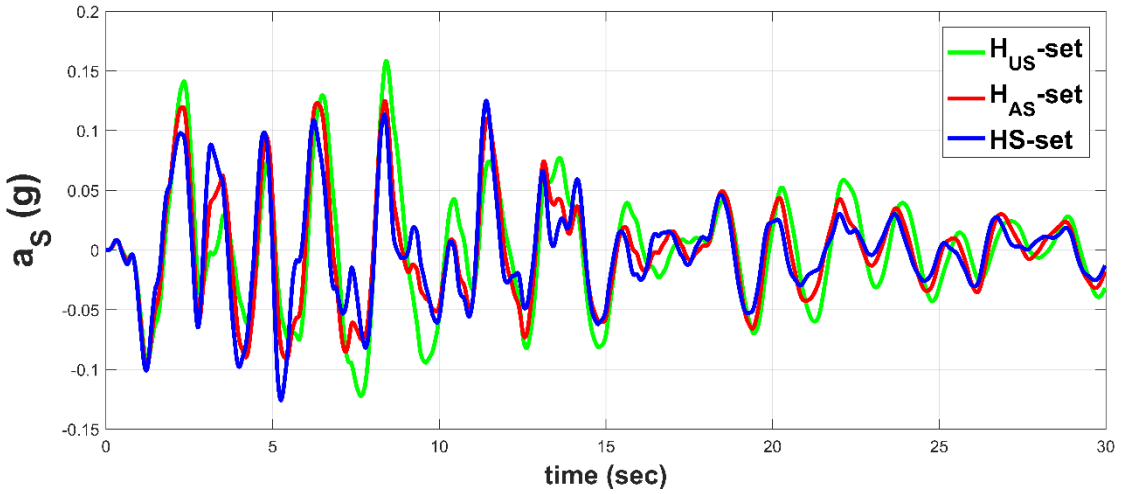

(b)

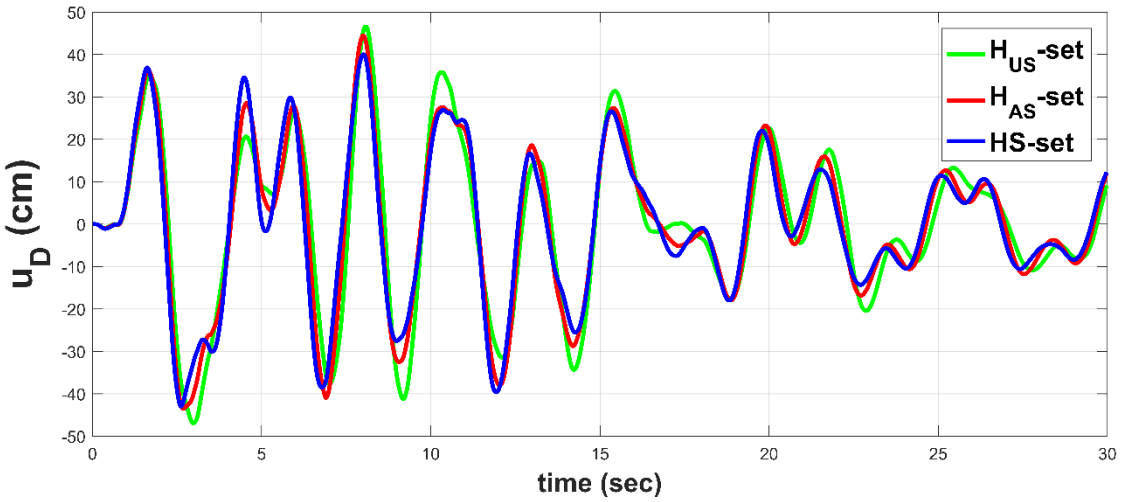

(c)

Figure 3.20: *Time histories of three different optimized KDamper cases, namely H_{US}-set, H_{AS}-set, and HS-set. (a) relative displacement u_S (cm), (b) absolute acceleration a_S (g), and (c) NS element stroke u_D (cm), for a random Artificial Accelerogram.*

The systems main dynamic responses, considering the max values of the dynamic responses for all the Artificial Accelerograms in the database (mean of 30 max), of the controlled SDoF system with KDamper, considering all the examined optimization procedures for the optimal selection of the KDamper parameters, namely H_{US}-set, H_{AS}-set, and HS-set, are presented in Table 3.3.

Table 3.3: *Peak values (mean of max) of the dynamic responses of controlled SDoF system with KDamper for the three considered test cases.*

	H_{US}-set	H_{AS}-set	HS-set
u_S (cm)	19.23	15.91	14.48
a_S (g)	0.175	0.153	0.146
u_D (cm)	59.83	57.45	54.93

Overall, the HS-set of optimized parameters presents an improved dynamic performance, of both the structural dynamic responses and the additional oscillating mass relative displacement, in comparison with the other two test cases however, marginally superior to that of the H_{AS}-set. The H_{US}-set presented the worst results in terms of both the structural responses, i.e. structure relative displacement u_S, and absolute acceleration a_S, and the internal DoF's relative displacement u_D, which is related to the NS element stroke, and therefore the NS design.

3.5 Concluding Remarks

In this Chapter, the optimization procedure regarding the proposed passive dynamic vibration absorbers, based on the KDamper concept is presented. The optimal design approach for the selection of the KDamper parameters follows exactly the corresponding steps of the classical minmax ($H\infty$) procedure, proposed by Den Hartog (1956). Two alternative cases for the Transfer Function selected for minimization are presented. Subsequently, the optimal design for the extended versions of KDamper is presented. In an effort to account the manufacturing limitations that might occur during the implementation of such configurations, and taking into consideration their complexity, as compared to the KDamper, a constrained optimal design based on engineering-criteria is followed. The excitation input is selected according to the provisions of the seismic design codes, and the NS elements are realized with two alternative simple displacement-dependent configurations. For the optimization procedure, the

metaheuristic optimization algorithm Harmony Search (HS) is used. Based on the described procedures regarding the design of the proposed KDamper-based designs, the following conclusive remarks can be made:

i. The systematic design procedure of the KDamper concept leads to a performance that can inherently offer far better isolation and damping properties than the Tuned Mass Damper (TMD).
ii. Since the isolation and damping properties of the KDamper essentially result from the stiffness properties of the system, further technological advantages can emerge over the variants of TMD like the inerter, in terms of weight, complexity and reliability, without the need for compromises in the overall stiffness of the primary structure as in the case of the QZS configurations.
iii. The KDamper design for optimal acceleration response presented an overall improved dynamic behavior, comparable with the optimized KDamper using the Harmony Search (HS) optimization algorithm.
iv. The proposed displacement-dependent configurations for the realization of the NS element generate as far as possible ‘linear’ negative stiffness.
v. The selected artificial accelerograms match accurately the design response spectra of the seismic design codes regarding the horizontal and the vertical component.

Chapter 4

Horizontal Seismic Protection with KDamper

4.1 Introduction

In response to the damage generated by earthquakes occurring in densely populated areas, seismic design codes for buildings, bridges, and infrastructure changed towards the design of structures with better seismic performance. Seismic isolation appears to be the most promising alternative to conventional antiseismic techniques, as it is based on the concept of reducing the seismic demand rather than increasing the earthquake resistance capacity of the structure (Naeim and Kelly, 1999). Isolation systems in the bases of the structures essentially provide horizontal isolation from the effects of earthquake shaking, by decoupling the superstructure from base-foundation during earthquakes. As a result, the fundamental structural period is increased, leading to the descending branch of the response spectrum of accelerations, and thus reduce the acceleration peak responses. However, excessively high values of the natural period, result in an undesirable increase of the structure's base relative displacements. Although the use of dampers, in order to increase the equivalent damping ratio of the system, manage to mitigate the dynamic response of the system both in terms of absolute acceleration and relative displacement, the inherent conflict between the absolute acceleration and relative displacement in seismic isolation of structures cannot be avoided. This conflict is presented thoroughly is section 4.2.

In the context of reducing the displacement demand, a variety of isolation devises has been developed, such as implementations of TMDs in the bases of structures (Hashimoto et al., 2015; Taniguchi et al., 2008; Xiang and Nishitani, 2014). A more effective alternative is a new passive vibration control technique combining the conventional base isolation (BI) with a Tuned Inerter Damper (TID) (De Angelis et al., 2019; Peng et al., 2012; Radu et al., 2019; Sun et al., 2019) or a Tuned Mass Damper Inerter (TMDI) (De Domenico and Ricciardi, 2018b; Lazar et al., 2014; Pietrosanti et al., 2017). In the concept of TMDI, the secondary mass of the TMD is supported to the ground by an ideal inerter (Malcolm C Smith, 2002). Furthermore,

the significant advance of mechanical expertise has facilitated the implementation of more complex devices, such as newly-fabricated hardware incorporating negative stiffness elements (Quazi Zero Stiffness oscillators), finding numerous applications in seismic isolation (Carrella et al., 2007; DeSalvo, 2007; Iemura and Pradono, 2009; Pasala et al., 2013; Shen et al., 2017; Sun et al., 2017; Wang, F fei Sun, et al., 2019; Wang, F Sun, et al., 2019).

In this Chapter, the KDamper is implemented for horizontal seismic protection, exploiting the advantages of the aforementioned vibrations absorption concepts, aiming to reduce the structural accelerations, and at the same time retain the large required displacements at acceptable levels. The selection of the KDamper parameters follows the procedure described in section 3.2.2, for optimal acceleration response, as the results of the Numerical Example 1 of Chapter 3 indicated that the H_{AS}-set presented an overall improved dynamic behavior, comparable with the optimized KDamper using the Harmony Search (HS) optimization algorithm. The selection of the KDamper nominal frequency is selected with spectra driven approaches, described in section 4.3 of this Chapter. Finally, the performance of the KDamper implemented in SDoF, as well as MDoF structural systems (multi-story building structures) is assessed with real earthquake records in section 4.3.2.

4.2 Inherent Conflict Between Structure Absolute Acceleration and Relative Displacement Minimization

Seismic isolation of structures is based on the following principle: decreasing the fundamental structure's frequency (or increasing the natural period) leads to the descending branch of the response spectrum of accelerations, as presented in Figure 3.12.a. This principle applies both to the horizontal spectra and the vertical ones. Excessively low values of the natural frequency, result in an undesirable increase of the structure's relative displacements, as presented in Figure 3.12.b. Although the use of dampers, in order to increase the equivalent damping ratio of the system, manage to mitigate the dynamic response of the system both in terms of absolute acceleration and relative displacement, the inherent conflict between the absolute acceleration and relative displacement minimization in seismic isolation of structures cannot be avoided.

In order to get a deeper insight into this inherent conflict, the equations of motion, and assuming a harmonic base acceleration excitation in the form of Equation (2.4) and a steady state response in the form of Equation (2.5), the Transfer Function of an initial SDoF fixed base structure (FBS) are presented:

$$m_S\ddot{u}_S + c_D\dot{u}_S + ku_S = -m_S\ddot{X}_G \quad (4.1)$$

$$\tilde{H}_{US} = \tilde{U}_S / A_G = -\tilde{H}^{-1}m \quad (4.2.a)$$

$$\tilde{H}_{AS} = \tilde{A}_S / A_G = 1-\omega^2\tilde{H}_{US} \quad (4.2.b)$$

$$\tilde{H} = -\omega^2 m + j\omega c_D + k_{QZS} \quad (4.2.c)$$

The magnitudes of the relative displacement and absolute acceleration Transfer Functions (Equations 4.2) of the SDoF system are considered:

$$H_{US} = 1/\sqrt{(\omega_S^2-\omega^2)+(2\zeta_S\omega\omega_S)^2} \quad (4.3.a)$$

$$H_{AS} = \sqrt{(\omega_S^2)^2+(2\zeta_S\omega\omega_S)^2} / \sqrt{(\omega_S^2-\omega^2)+(2\zeta_S\omega\omega_S)^2} \quad (4.3.b)$$

The characteristic values of these Transfer Functions are presented below:

$$H_{US}(\omega=0) = 1/\omega_S^2 \quad (4.4.a)$$

$$H_{US}(\omega=\omega_S) = 1/(2\zeta_S\omega_S^2) \quad (4.4.b)$$

$$H_{US}(\omega\to\infty) = 0 \quad (4.4.c)$$

$$H_{AS}(\omega=0) = 1 \quad (4.5.a)$$

$$H_{AS}(\omega=\omega_S) = \sqrt{1+(2\zeta_S)^2} / 2\zeta_S \quad (4.5.b)$$

$$H_{AS}(\omega\to\infty) = 0 \quad (4.5.c)$$

A traditional isolation approach typically requires to reduce the natural frequency f_S of the SDoF system. In view of Equation (4.3.b), the effect of reducing ωs ($\omega_S=2\pi f_S$), improves the acceleration Transfer Function H_{AS}. However, it results in an increase of the displacement transfer function H_{US} in the low-frequency range, which is of major significance in seismic isolation. In order to better understand this effect, the initial FBS system has a natural frequency of $fs=2$ *Hz* ($T_S=0.5$ *sec*) and a constant damping ratio of $\zeta s=5$ %. Next, in order to evaluate the effect of the seismic isolation concept, the natural frequency of the system is reduced to *1 Hz (1 sec)* and *0.5 Hz (2 sec)* respectively. The resulting Transfer Functions are presented in Figure 4.1 and clearly verify the above remark. An attempt to increase the damping ratio of the isolated system from 5% to 20% does not result in a major improvement regarding the relative displacement Transfer Function, as presented in Figure 4.2.

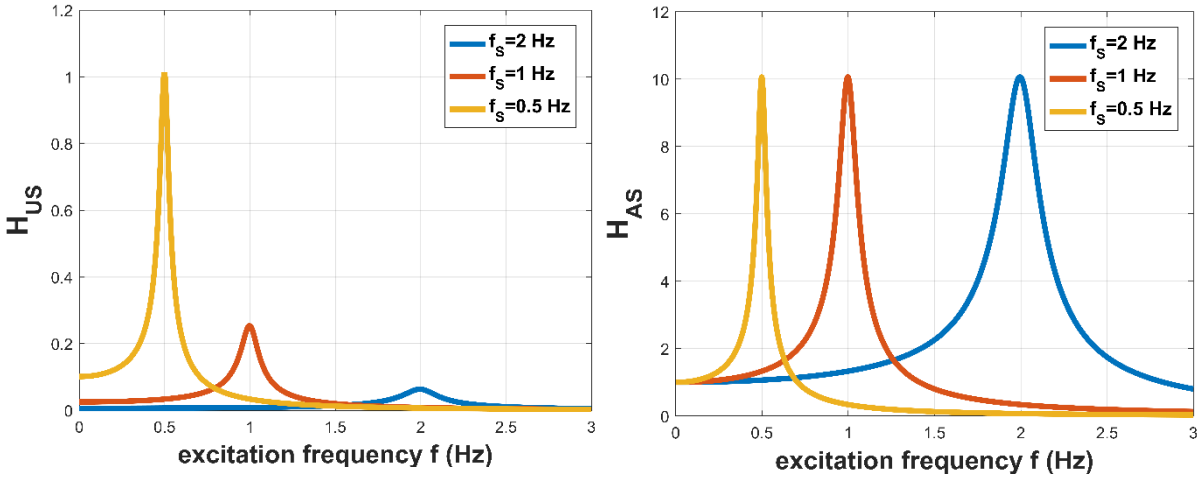

(a) (b)

Figure 4.1: *Transfer Functions: (a) structure's relative displacement H_{US} and (b) structure's absolute acceleration H_{AS} of a SDoF system with a constant ζs=5 %, for 3 different values of its natural frequency, 2 Hz, 1Hz and 0.5 Hz.*

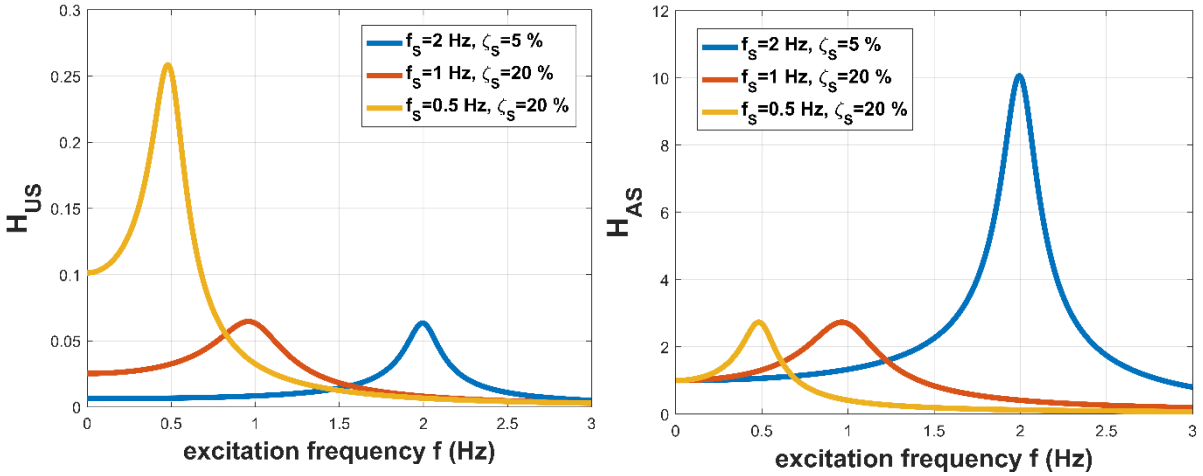

(a) (b)

Figure 4.2: *Transfer Functions: (a) structure's relative displacement H_{US} and (b) structure's absolute acceleration H_{AS} of the initial SDoF system (f_S=2 Hz, ζs=5 %), and an isolated system of 1 Hz and 0.5 Hz, respectively, with ζs=20%.*

Based on the design spectrum compatible horizontal excitation acceleration power spectral densities (PSD) S_A (Figure 3.14), presented in section 3.3.2.1 of Chapter 3, the response power spectral densities S_{US}, S_{AS} of the system main responses of the three considered systems of Figure 4.2 are obtained from Equations (4.6) and depicted in Figure 4.3.

$$S_{US}(\omega) = H_{US}(\omega)^2 S_A(\omega) \qquad (4.6.a)$$

$$S_{AS}(\omega) = H_{AS}(\omega)^2 S_A(\omega) \tag{4.6.b}$$

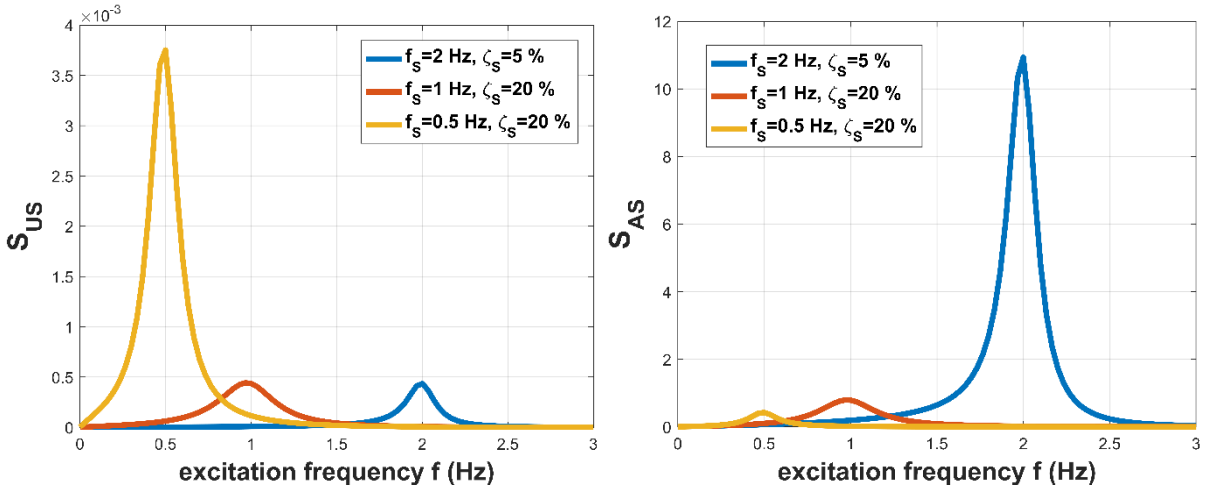

(a) (b)

Figure 4.3: *Response PSD: (a) structure's relative displacement S_{US}, and (b) structure's absolute acceleration S_{AS} of the initial SDoF system (f_S=2 Hz, ζs=5 %), and an isolated system of 1 Hz and 0.5 Hz, respectively, with ζs=20%.*

It should be emphasized that the design response spectra of the seismic design codes (e.g. those in Figure 3.12), are entirely different than the response PSD of Equations (4.6) and Figure 4.3. The root mean square (RMS) value of the responses is defined as the root of the area under the PSD curve, as an indication of the actual energy content of the response:

$$R_{US} = \left[\int_{-\infty}^{+\infty} S_{US}(\omega)\, \mathrm{d}\omega \right]^{0.5} \tag{4.7.a}$$

$$R_{AS} = \left[\int_{-\infty}^{+\infty} S_{AS}(\omega)\, \mathrm{d}\omega \right]^{0.5} \tag{4.7.b}$$

Figure 4.4, presents the relative displacement and absolute acceleration RMS responses ratio, over the natural frequency f_S:

$$r_{US} = \frac{R_{US}}{R_{US}(ref)} \tag{4.8.a}$$

$$r_{AS} = \frac{R_{AS}}{R_{AS}(ref)} \tag{4.8.b}$$

where $R_{US}(ref)$ and $R_{AS}(ref)$ pertain to the initial FBS system with a natural frequency of *2 Hz* and a damping ratio of *5%*. The results presented in Figure 4.4, r_{US}, r_{AS} concern the FBS system with a damping ratio of ζ_S*=5%* and *20%*, respectively, and a variation of the natural frequency in the range of *fs=[0.5-2] Hz*. An inherent conflict between the requirement for the simultaneous minimization of the absolute acceleration and relative displacement is observed.

Next, the equation of motion, Equation (4.1), of the FBS is solved for all the 30 Artificial Accelerograms of the database, in the time domain using the Newmark-β method with linear acceleration. The mean of the maximum responses ratio of the dynamic responses are defined:

$$v_{US} = \frac{V_{US}}{V_{US}(ref)} \tag{4.9.a}$$

$$v_{AS} = \frac{V_{AS}}{V_{AS}(ref)} \tag{4.9.b}$$

where V_{US}, V_{AS} are the mean of the maximum systems dynamic responses and $V_{US}(ref)$, $V_{AS}(ref)$ pertain to the initial FBS system with a natural frequency of *2 Hz* and a damping ratio of *5%*. The results are also presented in Figure 4.4 and clearly confirm the ability of the RMS responses to represent the effect of the variation of the natural frequency to the system responses.

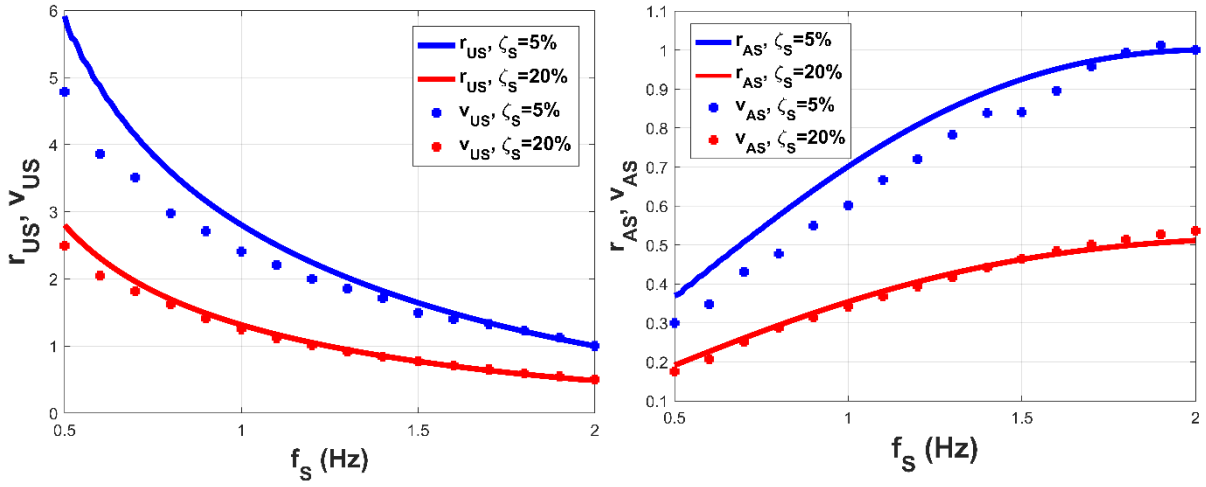

(a) (b)

Figure 4.4: *RMS responses ratio (solid lines) and verification with the mean of the maximum dynamic responses ratio (dotted lines), of the FBS system with a damping ratio 5% and 20%, respectively: (a) structure's relative displacements and (b) structure's absolute accelerations, over the structure's natural frequency f_S.*

It should be noted that for the FBS, the RMS responses of the relative displacement and absolute acceleration are functions of the natural frequency fs and of the damping ratio ζs: $R_{US}(f_S, \zeta_S)$, $R_{AS}(f_S, \zeta_S)$, and can be thus used as an alternative to the design response spectra of the seismic codes. However, it should be noted that R_{AS} is not equal to $(2\pi fs)^2 R_{US}$.

4.3 Seismic Protection Configurations Based on KDamper

In this section, the KDamper is implemented in structural systems for seismic protection from horizontal ground motions. As observed from Numerical Example 1, of Chapter 3, the KDamper presented an improved overall dynamic behaviour, considering optimal acceleration response, compared with other optimization designs. For this reason, in the current Chapter, the KDamper parameters are selected according to the procedure described in section 3.2.2 of Chapter 3, for optimal acceleration response.

4.3.1 Spectra Driven Approaches for the Selection of the KDamper Nominal Frequency

The KDamper nominal frequency is a free design variable, as the purpose of KDamper is not to isolate the vibrations of a structural system, retaining its original stiffness intact, but to overall improve its dynamic behaviour, reducing the displacements and accelerations at the same time, complying with the constraints and limitations imposed by the respective desired design. The application of KDamper for seismic protection of structural systems leads to MDoF systems with multiple frequencies, and therefore the selection of the KDamper nominal frequency is not possible with the design response spectrum approaches of the seismic codes. For this reason, the generation of design response spectrum compatible ground acceleration excitations is necessary. A detailed description for the selection of the ground motion excitation acceleration input according to the EC8 design codes is presented in section 3.3.2.

4.3.1.1 Approach I: *SDoF System with KDamper*

The KDamper parameters are selected according to section 3.2.2 of Chapter 3, for optimal acceleration response. The parameters μ, κ are selected as $\mu=0.05$, $\kappa=3.41$, ζ_D is calculated numerically so that it minimizes the peak of H_{AS} and is equal to $\zeta_D=0.622$, and the frequency

ratio ρ results as a function of κ, μ, following the minmax approach described in section 3.2.2. The performance of the KDamper system strongly depends on the selection of the nominal frequency f_0. In order to observe the effect of the nominal frequency of KDAB system to: 1) the Transfer Functions, 2) the response PSD, 3) the RMS responses and 4) the mean peak amplitude responses, of the main system parameters, two characteristic cases are considered. The first case is to match the nominal frequency of the KDamper with the frequency of the conventional seismic isolation designs (low frequency of *0.4 Hz*). This case will be referred to hereafter as KDamper-0.4. In the second case, a stiffer system is considered, with a natural frequency of *1 Hz*, in order to examine if the large structural displacements, that are required in the classical seismic isolation concept, can be avoided. This case will be referred to hereafter as KDamper-1.0. Figure 4.5 presents the Transfer Functions of the main system responses.

In order to assess the performance of KDamper, it is compared to a highly damped base isolated system, with a natural frequency of f_B*=0.4 Hz* and a damping ratio of *20%*, and will be referred to hereafter as BI-HD. The KDamper systems have a nominal frequency of *0.4 Hz* (KDamper-0.4) and *1.0 Hz* (KDamper-1.0), respectively. The implementation of KDamper leads to a significant reduction to the BI-HD maximum value of the transfer function H_{AS} (absolute acceleration), which becomes now a low pass filter (Figure 4.5.a), while at the same time retains a significant frequency content. The structure relative displacement Transfer Function H_{US} is dramatically improved in all frequency range with the implementation of the KDamper system. Increasing the natural frequency of the KDamper from 0.4 *Hz* (KDamper-0.4) to 1.0 *Hz* (KDamper-1.0), the structure's relative displacement H_{US}, as well as the KDamper's relative displacement H_{UD} (negative stiffness stroke), are dramatically improved, as observed from Figures 4.5.b, c.

Having defined the Transfer Functions of the KDamper, the response PSD of the main system responses can be derived with respect to the selected ground motion excitation acceleration PSD, S_A (Figure 3.14):

$$S_{US}(\omega) = H_{US}(\omega)^2 S_A(\omega) \tag{4.10.a}$$

$$S_{UD}(\omega) = H_{UD}(\omega)^2 S_A(\omega) \tag{4.10.b}$$

$$S_{AS}(\omega) = H_{AS}(\omega)^2 S_A(\omega) \tag{4.10.c}$$

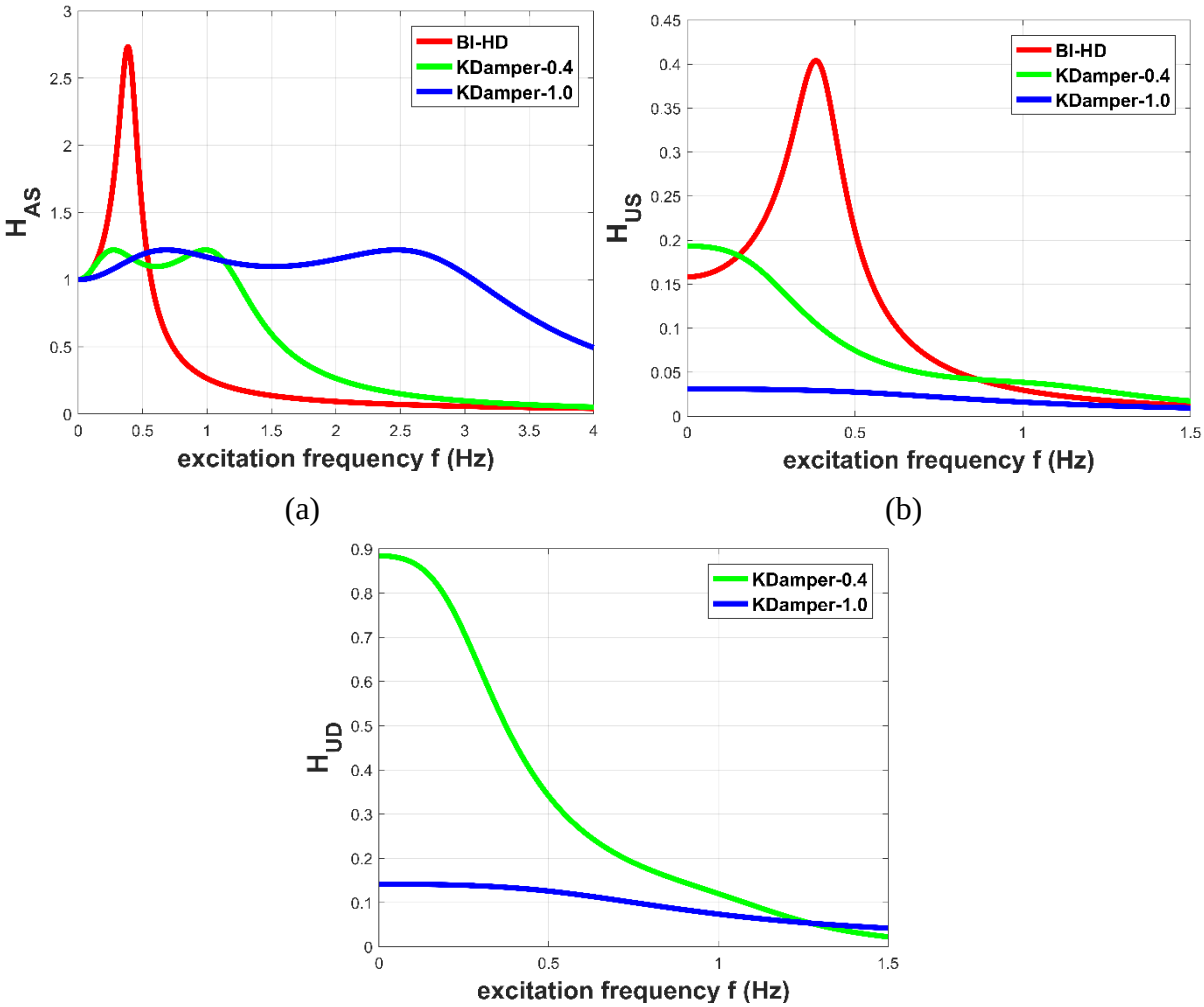

Figure 4.5: *Transfer Functions of the main system responses: (a)structure's absolute acceleration H_{AS}, (b) structure's relative displacement H_{US}, and (c) KDamper relative displacement H_{UD}, for all the considered systems: BI-HD, KDamper-0.4, and KDamper-1.0.*

The PSDs of all three alternative systems presented in Figure 4.5, are obtained and depicted in Figure 4.6. Figure 4.6.a presents the response PSD S_{AS}. It is observed that the KDamper control systems (KDamper-0.4 and KDamper-1.0) manage to reduce the BI-HD's maximum value of the S_{AS}. The frequency content of these response power spectral densities is increasing in the following order: BI-HD, KDamper-0.4, and KDamper-1.0. The KDamper concept presents a dramatic improvement in the response PSD S_{US}, compared with the BI-HD system. More specifically, although the KDamper-0.4 system has the same natural frequency (*0.4 Hz*), it manages to reduce the maximum value of the S_{US} over one order of magnitude, and KDamper-1.0, which represents the same concept with the KDamper-0.4 but with a stiffer base (higher nominal frequency), reduces the maximum value of S_{US} more than two orders of

magnitude. Finally, by making a stiffer base (KDamper-1.0), the KDamper's relative displacement (NS stoke) PSD is reduced more than one order of magnitude (Figure 4.6.c).

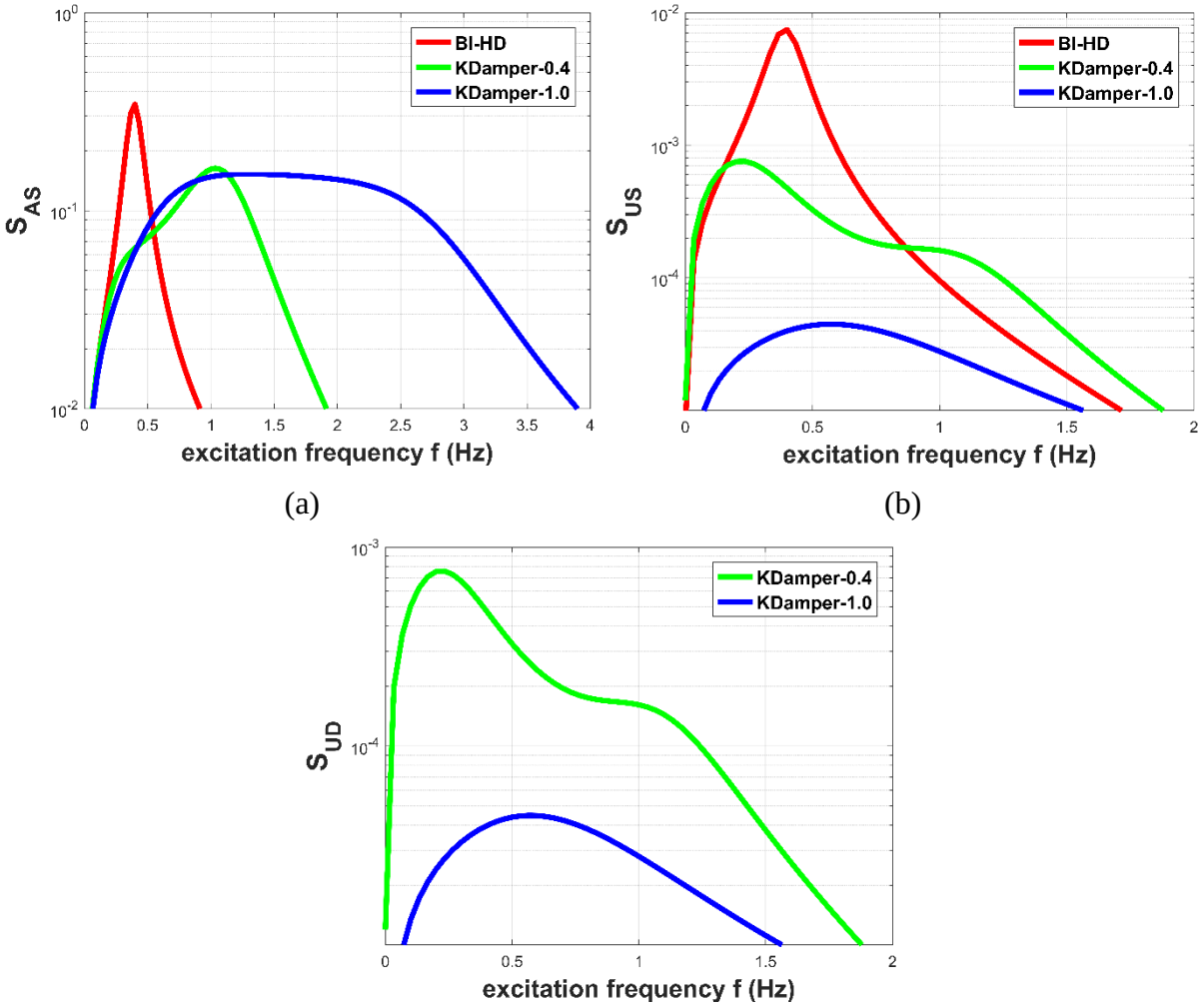

Figure 4.6: *Response PSD of the main system responses: (a)structure's absolute acceleration S_{AS}, (b) relative displacement S_{US} and (c) KDamper relative displacement S_{UD}, for all the considered systems: BI-HD, KDamper-0.4, and KDamper-1.0.*

The root mean square (RMS) value of the responses is defined as the root of the area under the PSD curves, as an indication of the actual energy content of the response:

$$R_{US} = \left[\int_{-\infty}^{+\infty} S_{US}(\omega)\, \mathrm{d}\,\omega \right]^{0.5} \tag{4.11.a}$$

$$R_{UD} = \left[\int_{-\infty}^{+\infty} S_{UD}(\omega)\, \mathrm{d}\,\omega \right]^{0.5} \tag{4.11.b}$$

$$R_{AS} = \left[\int_{-\infty}^{+\infty} S_{AS}(\omega)\, \mathrm{d}\omega \right]^{0.5} \tag{4.11.c}$$

Figure 4.7, presents the structure's absolute acceleration, relative displacement, and the KDamper's relative displacement (NS stroke) mean square responses ratio:

$$r_{US} = \frac{R_{US}}{R_{US}(ref)} \tag{4.12.a}$$

$$r_{UD} = \frac{R_{UD}}{R_{US}(ref)} \tag{4.12.b}$$

$$r_{AS} = \frac{R_{AS}}{R_{AS}(ref)} \tag{4.12.c}$$

where $R_{US}(ref)$ and $R_{AS}(ref)$ pertain to the BI-HD system with a natural frequency of *0.4 Hz* and a damping ratio of *20%*, in order to better observe the effectiveness of the KDamper. The results concern the BI-HD system with a damping ratio of *20%* and a continuous variation of its natural frequency in the range f_B*= [0, 4 - 2.0] Hz,* and the KDamper system with parameters μ*=5%*, κ*=3.41*, ζ_D*=0.622* and a continuous variation of its nominal frequency in the range f_0*= [0,4 - 2.0] Hz*. The inherent conflict between the requirement for the simultaneous minimization of the structure's absolute acceleration and relative displacement is again observed. Figure 4.7.b shows that the structural absolute acceleration reduction of the BI-HD and KDamper systems, are at similar levels, while the base becomes less stiff (decreasing the base's natural frequency).

The implementation of the KDamper reduces the structure's relative displacement more than 50% in all the considered nominal frequency range (f_B, f_0), as presented in Figure 4.7.a. Next, the equations of motion of the BI-HD and KDamper, respectively, are solved for all the 30 accelerograms of the database in the time domain, using the Newmark-β method with linear acceleration. The mean of the maximum of the dynamic response's ratio is defined as:

$$v_{US} = \frac{V_{US}}{V_{US}(ref)} \tag{4.13.a}$$

$$v_{UD} = \frac{V_{UD}}{V_{US}(ref)} \tag{4.13.b}$$

$$v_{AS} = \frac{V_{AS}}{V_{AS}(ref)} \tag{4.13.c}$$

where V_{US}, V_{AS}, V_{UD} are the mean of the maximum systems dynamic responses and $V_{US}(ref)$, $V_{AS}(ref)$ pertain to the initial BI-HD system with a natural frequency of *0.4 Hz* and a damping ratio of *20%*. The results are also presented in Figure 4.7 (dotted lines), and clearly confirm that a spectral driven approach for the design of a control system is accurate, with respect to the shape of the curves, and more specifically a spectral driven optimization of the KDamper nominal frequency is possible.

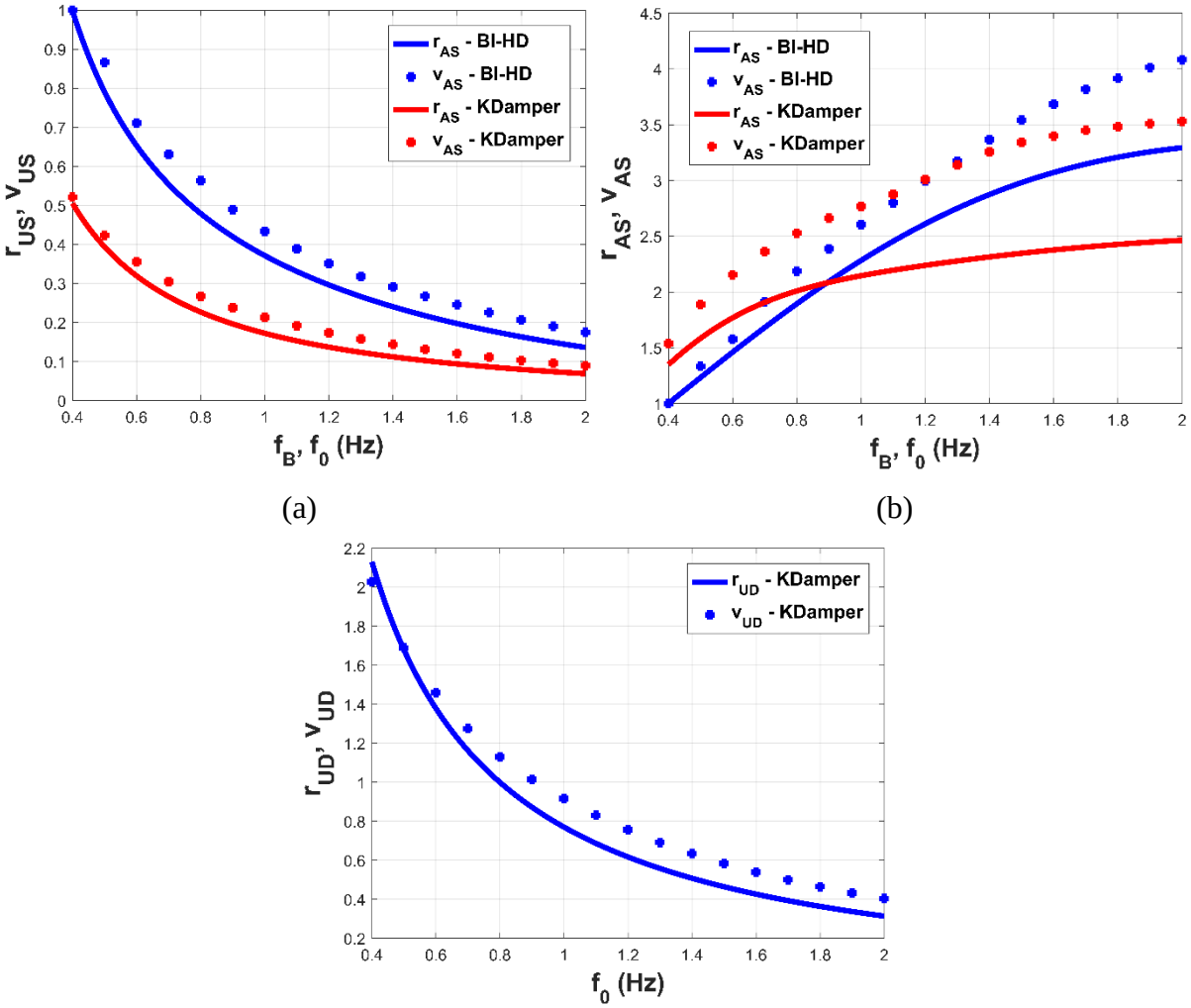

Figure 4.7: *RMS responses ratio (solid lines) and verification with mean of the maximum dynamic responses ratio (dotted lines), of the BI-HD and the KDamper system: (a) structure relative displacement, (b) structure absolute acceleration, and (c) KDamper's relative displacement, over the natural frequency f_B, f_0.*

4.3.1.2 Approach II: *KDamper as an Absorption Base (KDAB) of SDoF Systems*

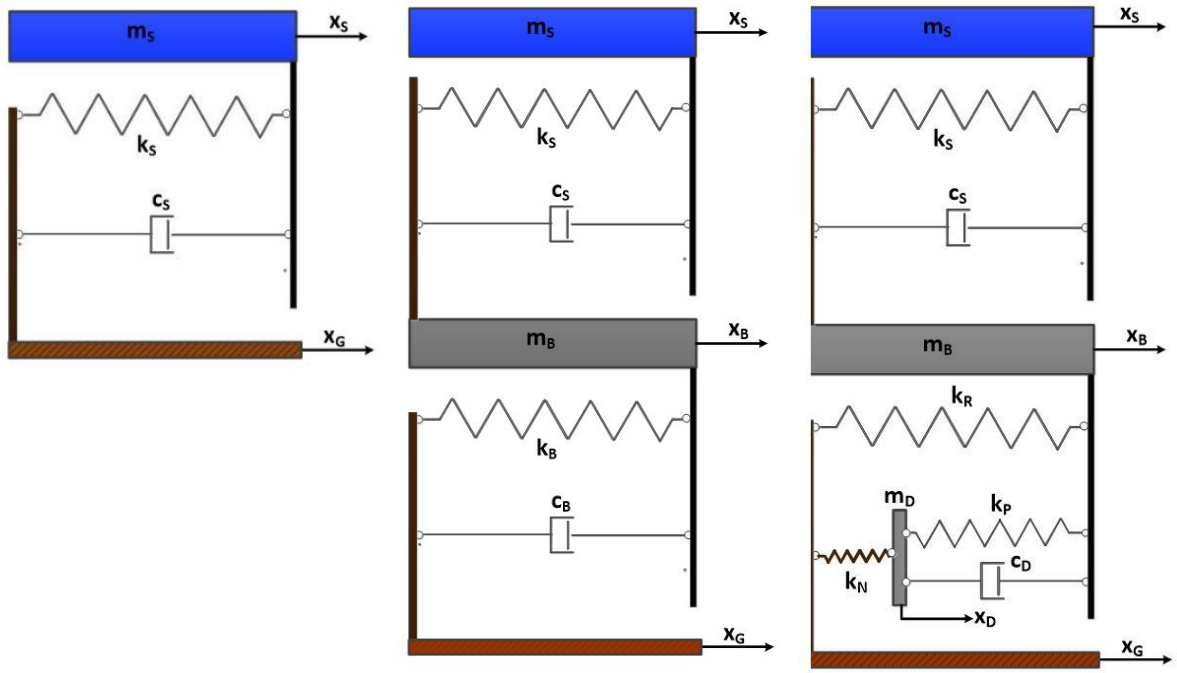

(a) (b) (c)

Figure 4.8: *A possible implementation of the KDamper for seismic isolation/absorption. (a) Flexible structure on a fixed base, (b) flexible structure on a conventional or highly damped seismic isolation base, and (c) possible implementation of KDamper as a seismic absorption/damping base (KDAB).*

The SDoF system's equation of motion and Transfer Functions are described in section 4.2 of the current Chapter. The initial SDoF mounted on a seismic isolating base (Figure 4.8.b) assimilates to another SDoF system. The flexible structure on a conventional or highly damped seismic isolation base will be referred hereafter as BI (conventional Base Isolation), or BI-HD if it is highly damped. The equations of motion of the coupled structure and base isolation system (Figure 4.8.b) are:

$$m_S(\ddot{u}_S+\ddot{u}_B)+c_S\dot{u}_S+k_S u_S=-m_S a_G \tag{4.14.a}$$

$$m_B\ddot{u}_B+m_S(\ddot{u}_S+\ddot{u}_B)+c_B\dot{u}_B+k_B u_B=-(m_S+m_B)a_G \tag{4.14.b}$$

where $u_S = x_S - x_B$, $u_B = x_B - x_G$. Assuming a harmonic base acceleration excitation in the form of Equation (2.4), the steady-state responses of:

$$u_S(t) = \tilde{U}_S \exp(j\omega t) \tag{4.15.a}$$

$$u_B(t) = \tilde{U}_B \exp(j\omega t) \tag{4.15.b}$$

the Transfer Functions of this system result as:

$$\begin{bmatrix} \tilde{H}_{US} \\ \tilde{H}_{UB} \end{bmatrix} = \begin{bmatrix} \tilde{U}_S / A_G \\ \tilde{U}_B / A_G \end{bmatrix} = -\tilde{H}^{-1} \begin{bmatrix} m_S \\ m_S + m_B \end{bmatrix} \tag{4.16.a}$$

$$\tilde{H}_{AS} = \tilde{A}_S / A_G = 1 - \omega^2 (\tilde{H}_{US} + \tilde{H}_{UB}) \tag{4.16.b}$$

$$\tilde{H}_{AB} = \tilde{A}_B / A_G = 1 - \omega^2 \tilde{H}_{UB} \tag{4.16.c}$$

$$\tilde{H} = \begin{bmatrix} -\omega^2 m_S + j\omega c_S + k_S & -\omega^2 m_S \\ -\omega^2 m_S & -\omega^2 (m_B + m_S) + j\omega c_B + k_B \end{bmatrix} \tag{4.16.d}$$

The natural frequency and the damping ratio of the base isolated system are defined as:

$$\omega_B = 2\pi f_B = \sqrt{k_B / M_{tot}} \tag{4.17.a}$$

$$\zeta_B = c_B / (2\omega_B M_{tot}) \tag{4.17.b}$$

where $M_{tot} = (1+\mu_B)m_S$, $\mu_B = m_B/m_S$. The performance of the base isolated system strongly depends on the selection of the natural base frequency f_B. The base isolated system is designed to have a natural base frequency of *0.4 Hz*. The damping ratio of the conventional base isolated (BI) and the highly damped (BI-HD) base isolated system, is *5%* and *20%* respectively.

Among the large variety of possibilities, a possible implementation of the KDamper for seismic protection is as an alternative, or supplement, of a conventional seismic isolation base. The possible implementation of KDamper as a seismic absorption/damping base, is presented in Figure 4.8.c, and will be referred to hereafter as KDAB (KDamper Absorption Base). The equations of motion of this system are:

$$m_S(\ddot{u}_S + \ddot{u}_B) + c_S\dot{u}_S + k_S u_S = -m_S a_G \tag{4.18.a}$$

$$m_B\ddot{u}_B + m_S(\ddot{u}_S + \ddot{u}_B) + c_D(\dot{u}_B - \dot{u}_D) + k_P(u_B - u_D) + k_R u_B = -(m_S + m_B)a_G \tag{4.18.b}$$

$$m_D\ddot{u}_D - c_D(\dot{u}_B - \dot{u}_D) - k_P(u_B - u_D) + k_N u_D = -m_D a_G \tag{4.18.c}$$

where $u_S = x_S - x_B$, $u_B = x_B - x_G$, $u_D = x_D - x_G$. Assuming a harmonic base acceleration excitation in the form of Equation (2.4), the steady-state responses of:

$$u_S(t) = \tilde{U}_S \exp(j\omega t) \tag{4.19.a}$$

$$u_B(t) = \tilde{U}_B \exp(j\omega t) \tag{4.19.b}$$

$$u_D(t) = \tilde{U}_D \exp(j\omega t) \tag{4.19.c}$$

The Transfer Functions of this system result as:

$$\begin{bmatrix} \tilde{H}_{US} \\ \tilde{H}_{UB} \\ \tilde{H}_{UD} \end{bmatrix} = \begin{bmatrix} \tilde{U}_S / A_G \\ \tilde{U}_B / A_G \\ \tilde{U}_D / A_G \end{bmatrix} = -\tilde{H}^{-1} \begin{bmatrix} m_S \\ m_S + m_B \\ m_D \end{bmatrix} \tag{4.20.a}$$

$$\tilde{H}_{AS} = \tilde{A}_S / A_G = 1 - \omega^2 (\tilde{H}_{US} + \tilde{H}_{UB}) \tag{4.20.b}$$

$$\tilde{H}_{AB} = \tilde{A}_B / A_G = 1 - \omega^2 \tilde{H}_{UB} \tag{4.20.c}$$

$$\tilde{H}_{AD} = \tilde{A}_D / A_G = 1 - \omega^2 \tilde{H}_{UD} \tag{4.20.d}$$

$$\tilde{H} = \begin{bmatrix} -\omega^2 m_S + j\omega c_S + k_S & -\omega^2 m_S & 0 \\ -\omega^2 m_S & -\omega^2 (m_S + m_B) + j\omega c_D + (k_P + k_R) & -(j\omega c_D + k_P) \\ 0 & -(j\omega c_D + k_P) & -\omega^2 m_D + j\omega c_D + (k_P + k_N) \end{bmatrix} \tag{4.20.e}$$

The natural frequencies of the subsystems, the damping ratio of the KDAB and the rest of the parameters are defined as:

$$\omega_0 = 2\pi f_0 = \sqrt{k_0 / (m_S + m_B)} \tag{4.21.a}$$

$$\omega_D = \sqrt{(k_P + k_N) / \mathrm{m}_D} \tag{4.21.b}$$

$$\zeta_D = c_D / (2\omega_D m_D) \tag{4.21.c}$$

$$k_0 = k_R + \frac{k_P k_N}{k_P + k_N} \tag{4.21.d}$$

$$m_B = \mu_B m_S \tag{4.21.e}$$

$$m_D = \mu_D (m_S + m_B) \tag{4.21.f}$$

where k_0 is the equivalent static stiffness of the KDAB and μ_B and μ_D are the base's and KDamper's mass ratios, respectively. The KDamper parameters are selected according to section 3.2.2 of Chapter 3. The parameters μ, κ are selected as $\mu=0.05$, $\kappa=3.41$, ζ_D is calculated numerically so that it minimizes the peak of H_{AS} and is equal to $\zeta_D=0.622$, and the frequency ratio ρ results as a function of κ, μ, following the minmax approach described in section 3.2.2. The performance of the KDAB system strongly depends on the selection of the nominal frequency f_0.

In order to observe the effect of the natural frequency of the KDAB system to: 1) the Transfer Functions, 2) the response PSDs, 3) the RMS responses and 4) the mean peak amplitude responses, of the main system parameters, two characteristic cases are considered. The first case is to match the natural frequency of the KDAB with the BI system's frequency (low frequency of *0.4 Hz*). This case will be referred to hereafter as KDAB-0.4. In the second case, a stiffer base is considered, with a natural frequency of *1 Hz*, in order to examine if the large base's displacements, that are required in the classical seismic isolation concept, can be avoided. This case will be referred to hereafter as KDAB-1.0.

Figure 4.9 presents the Transfer Functions of the main system responses. A Fixed Base System (FBS) with a natural frequency of *2 Hz* and a damping ratio of *5%* is first assumed for a comparison basis. The base isolated system of Figure 4.8.b has a $f_B=0.4$ *Hz* and a damping ratio of *20%* (BI-HD system), and the KDamper Absorption Base systems have a natural base frequency of *0.4 Hz* (KDAB-0.4) and *1.0 Hz* (KDAB-1.0), respectively As it can be observed from Figure 4.9.a, b, the effect of the initial seismic isolation base is to shift the natural frequency of the structure from *2 Hz* to *0.4 Hz*, well below the main frequency content of the earthquakes. The effect of the KDamper, implemented to the base isolation system, leads to a significant reduction of the FBS Transfer Function H_{US} and H_{AS} of the relative displacement and absolute acceleration, respectively, which becomes now a low pass filter (Figures 4.9.a, b).

However, compared with the Transfer Functions H_{US} and H_{AS} of the BI-HD, the KDAB-0.4 and KDAB-1.0 systems significantly reduce the maximum values of these Transfer Functions, while at the same time retain a significant frequency content. Although the KDAB-0.4 system has the same natural frequency with the BI-HD system, it significantly enhances the base relative displacement, while retaining the structures absolute acceleration and relative displacement to acceptable levels. Increasing the natural frequency of the KDAB from *0.4 Hz* (KDAB-0.4) to *1.0 Hz* (KDAB-1.0), the base's relative displacement, as well as the KDamper's relative displacement (NS stroke), are dramatically reduced.

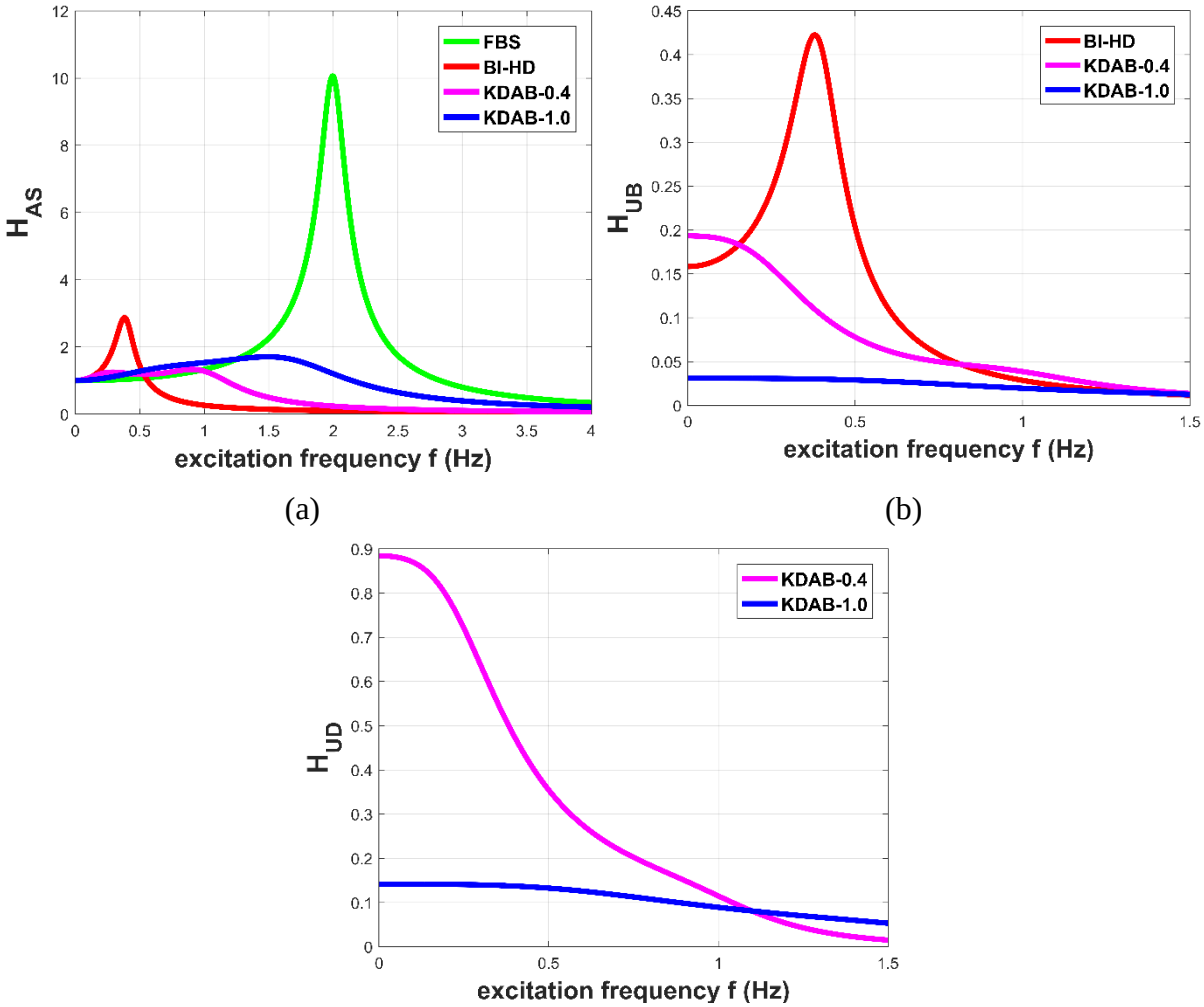

Figure 4.9: *Transfer Functions of the main system responses: (a) structure's relative displacement H_{US}, (b) structure's absolute acceleration H_{AS}, (c) base's relative displacement H_{UB}, and (d) KDamper relative displacement H_{UD}, for all the considered systems: FBS, BI-HD, KDAB-0.4 and KDAB-1.0.*

Having defined the Transfer Functions of the KDAB, the response PSD of the main system responses can be derived with respect to the selected ground motion excitation acceleration PSD, S_A (Figure 3.14):

$$S_{US}(\omega) = H_{US}(\omega)^2 S_A(\omega) \tag{4.22.a}$$

$$S_{UB}(\omega) = H_{UB}(\omega)^2 S_A(\omega) \tag{4.22.b}$$

$$S_{UD}(\omega) = H_{UD}(\omega)^2 S_A(\omega) \tag{4.22.c}$$

$$S_{AS}(\omega) = H_{AS}(\omega)^2 S_A(\omega) \tag{4.22.d}$$

Figures 4.10.a and b present the response PSDs S_{US} and S_{AS}. It is observed that all the considered control systems (BI-HD, KDAB-0.4, and KDAB-1.0) manage to reduce the FBS's maximum values of the S_{US} and S_{AS} over one order of magnitude. The frequency content of these response power spectral densities is increasing in the following order: BI-HD, KDAB-0.4, and KDAB-1.0.

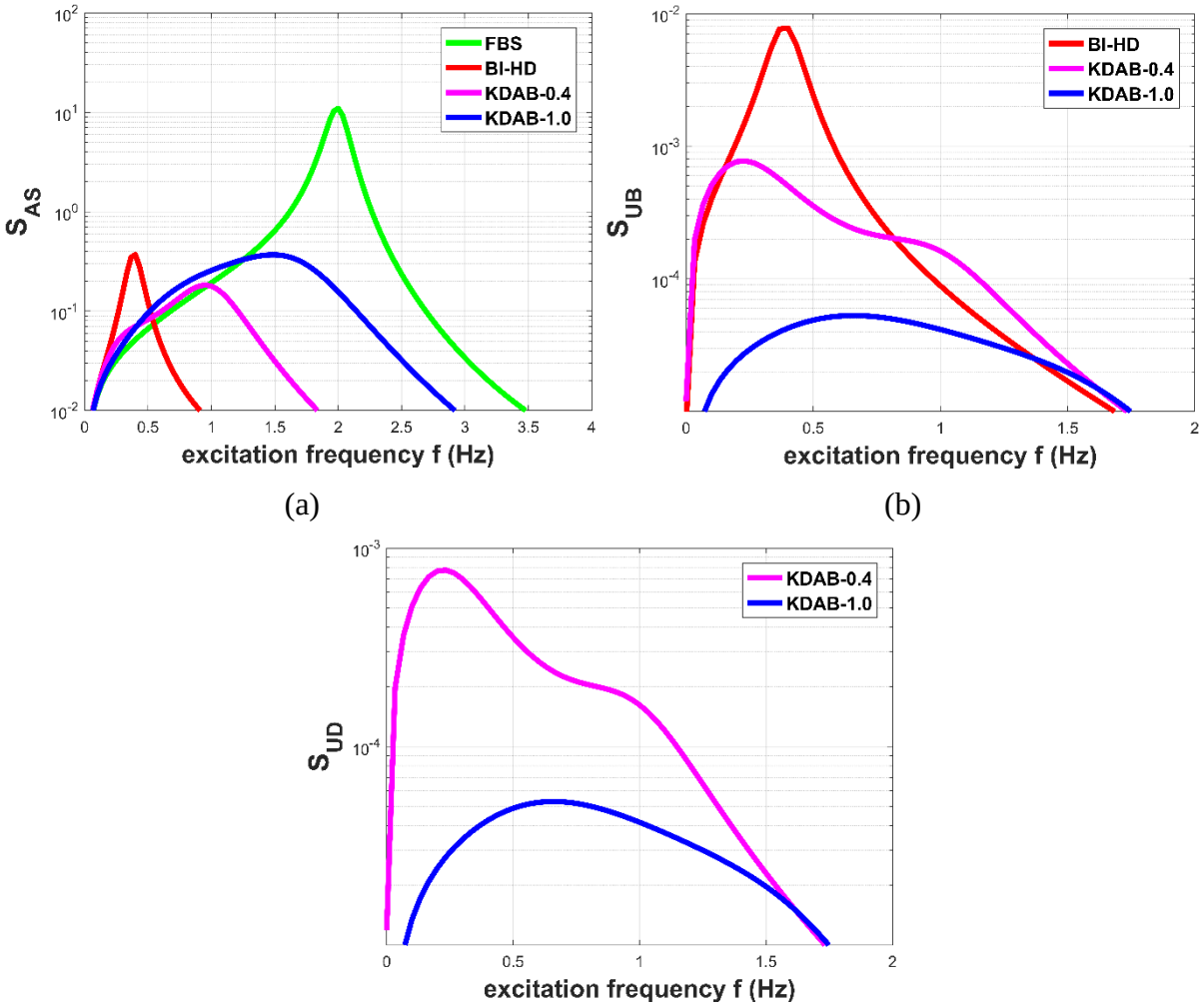

Figure 4.10: *Response Spectrum Power Densities of the main system responses: (a) structure's relative displacement S_{US}, (b) structure's absolute acceleration S_{AS}, (c) base's relative displacement S_{UB}, and (d) KDamper relative displacement S_{UD} for all the considered systems: FBS, BI-HD, KDAB-0.4, and KDAB-1.0.*

KDamper absorption base (KDAB) concepts present a dramatic improvement in the response PSD S_{UB}, compared with the BI-HD system (Figure 4.10.b). More specifically, although the KDAB-0.4 system has the same base natural frequency (*0.4 Hz*), it manages to reduce the maximum value of the S_{UB} over one order of magnitude, and KDAB-1.0 which

represents the same concept with the KDAB-0.4, but with a stiffer base (higher nominal frequency), reduces the maximum value of S_{UB} more than two orders of magnitude. Finally, by making a stiffer base (KDAB-1.0), the KDamper's relative displacement PSD is reduced more than one order of magnitude.

The RMS value of the responses is defined as the root of the area under the PSD curves, as an indication of the actual energy content of the response:

$$R_{US} = \left[\int_{-\infty}^{+\infty} S_{US}(\omega) \, \mathrm{d}\omega \right]^{0.5} \tag{4.23.a}$$

$$R_{UB} = \left[\int_{-\infty}^{+\infty} S_{UB}(\omega) \, \mathrm{d}\omega \right]^{0.5} \tag{4.23.b}$$

$$R_{UD} = \left[\int_{-\infty}^{+\infty} S_{UD}(\omega) \, \mathrm{d}\omega \right]^{0.5} \tag{4.23.c}$$

$$R_{AS} = \left[\int_{-\infty}^{+\infty} S_{AS}(\omega) \, \mathrm{d}\omega \right]^{0.5} \tag{4.23.d}$$

Figure 4.11, presents the structure's absolute acceleration, the base's relative displacement, and the KDamper's relative displacement mean square responses ratio:

$$r_{US} = \frac{R_{US}}{R_{US}(ref)} \tag{4.24.a}$$

$$r_{AS} = \frac{R_{AS}}{R_{AS}(ref)} \tag{4.24.b}$$

$$r_{UB} = \frac{R_{UB}}{R_{US}(ref)} \tag{4.24.c}$$

$$r_{UD} = \frac{R_{UD}}{R_{US}(ref)} \tag{4.24.d}$$

where $R_{US}(ref)$ and $R_{AS}(ref)$ pertain to the initial FBS system with a natural frequency of *2 Hz* and a damping ratio of *5%*. The results concern the BI-HD system with a damping ratio of $\zeta_B = 20\%$ and a continuous variation of the its natural frequency in the range $f_B = [0,4 - 2.0]$ *Hz*, and the KDAB system with parameters $\mu = 5\%$, $\kappa = 3.41$, $\zeta_D = 0.622$ and a continuous variation of the base's natural frequency in the range $f_0 = [0,4 - 2.0]$ *Hz*. Again, the inherent conflict

between the requirement for the simultaneous minimization of the structure's absolute acceleration and base's relative displacement is observed. Figure 4.11.a shows that the structure's absolute acceleration reduction of the BI-HD and KDAB systems, are at similar levels, while the base becomes less stiff (decreasing the base's natural frequency).

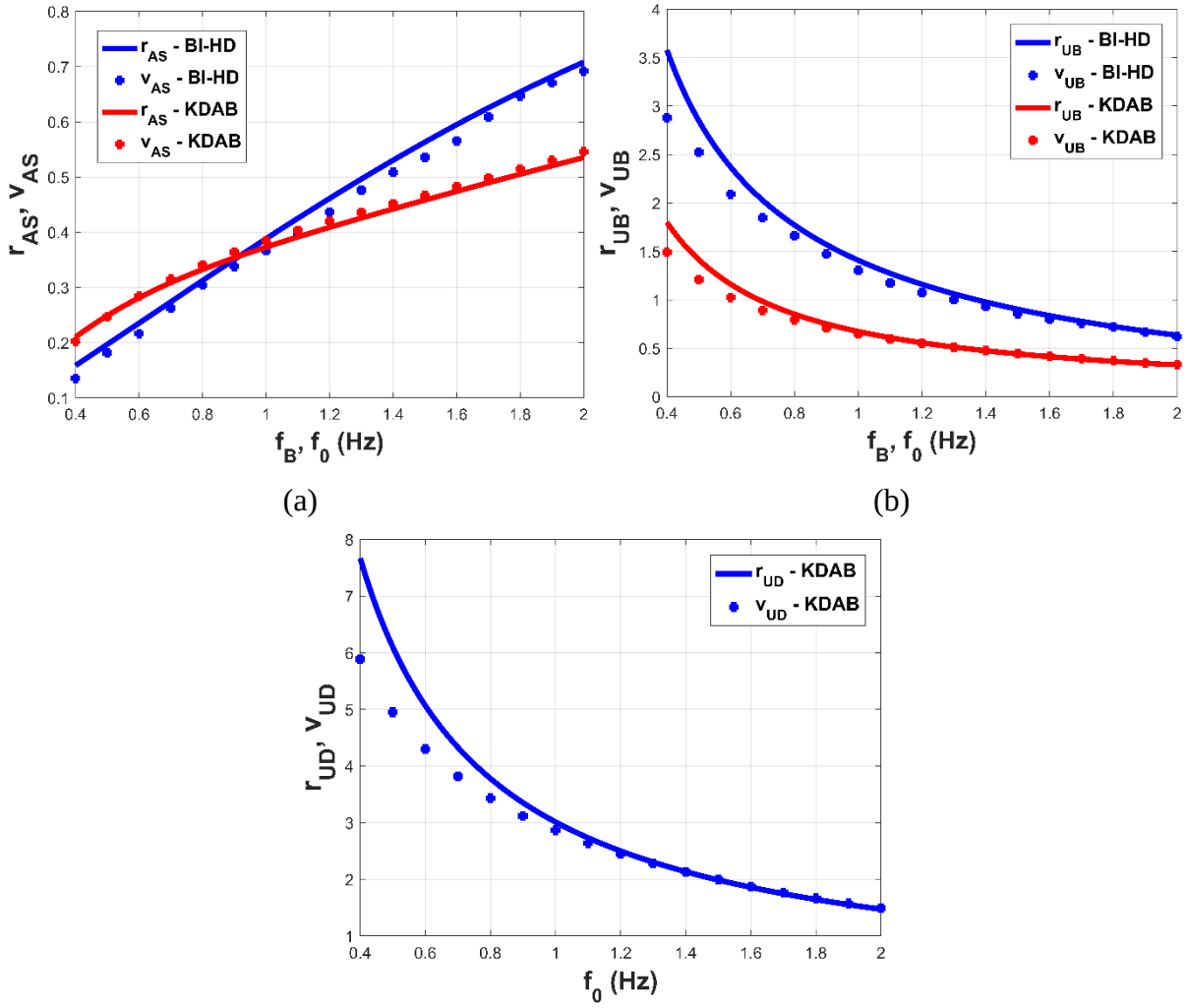

Figure 4.11: *RMS responses ratio (solid lines) and verification with mean of the maximum dynamic responses ratio (dotted lines), of the BI-HD and the KDAB systems: (a) structure's absolute acceleration, (b) base's relative displacement, and (c) KDAB's relative displacement, over the base's natural frequency f_B, f_0.*

The implementation of a KDamper as an absorption base reduces the base's relative displacement more than 50% in all the considered base's frequency range (f_B, f_0). Next, the equations of motion, Equations (4.14) and (4.18), of the BI-HD and KDAB, respectively, are solved for all the 30 accelerograms of the database in the time domain, using the Newmark-β

method with linear acceleration. The mean of the maximum responses ratio of the dynamic response is defined as:

$$v_{US} = \frac{V_{US}}{V_{US}(ref)} \tag{4.25.a}$$

$$v_{AS} = \frac{V_{AS}}{V_{AS}(ref)} \tag{4.25.b}$$

$$v_{UB} = \frac{V_{UB}}{V_{US}(ref)} \tag{4.25.c}$$

$$v_{UD} = \frac{V_{UD}}{V_{US}(ref)} \tag{4.25.d}$$

where V_{US}, V_{AS}, V_{UB}, V_{UD} are the mean of the maximum systems dynamic responses and $V_{US}(ref)$, $V_{AS}(ref)$ pertain to the initial FBS system with a natural frequency of *2 Hz* and a damping ratio of *5%*. The results are also presented in Figure 4.11 (dotted lines) and clearly confirm that a spectral driven design of a control system is very accurate, and more specifically a spectral driven optimization of the KDAB base's natural frequency is possible.

4.3.1.3 Approach III: *KDamper as an Absorption Base (KDAB) of Multi-Story Building Structures*

In this section, the proposed vibration absorption concept, KDAB, is implemented in the bases of multi-story building structures, as an alternative or supplement of the conventional base isolation approaches. A planar *n*-story structure is depicted in Figure 4.12.a, along with a typical ground floor plan of the structure (Figure (4.12.b)). The assumptions made for the modeling of this structure are:

i. the total structure mass is concentrated at the floor levels;
ii. the slabs and grinders on the floors are rigid as compared to the columns;
iii. the columns are considered inextensible and weightless providing the lateral stiffness;
iv. the effect of soil-structure-interaction (SSI) is not taken into consideration;
v. the superstructure is considered to remain within the elastic limit during the analysis;

As a result, the superstructure has *n* dynamic DOFs, represented by the relative to the base displacements of the *n*-story masses m_{Sj} ($j=1,\ldots, n$), as presented in Figure 4.12.a, which are collected in the array $[u_{Sr}](t)=[u_{Sr1}(t), u_{Sr2}(t), \ldots, u_{Srn}(t)]^T$.

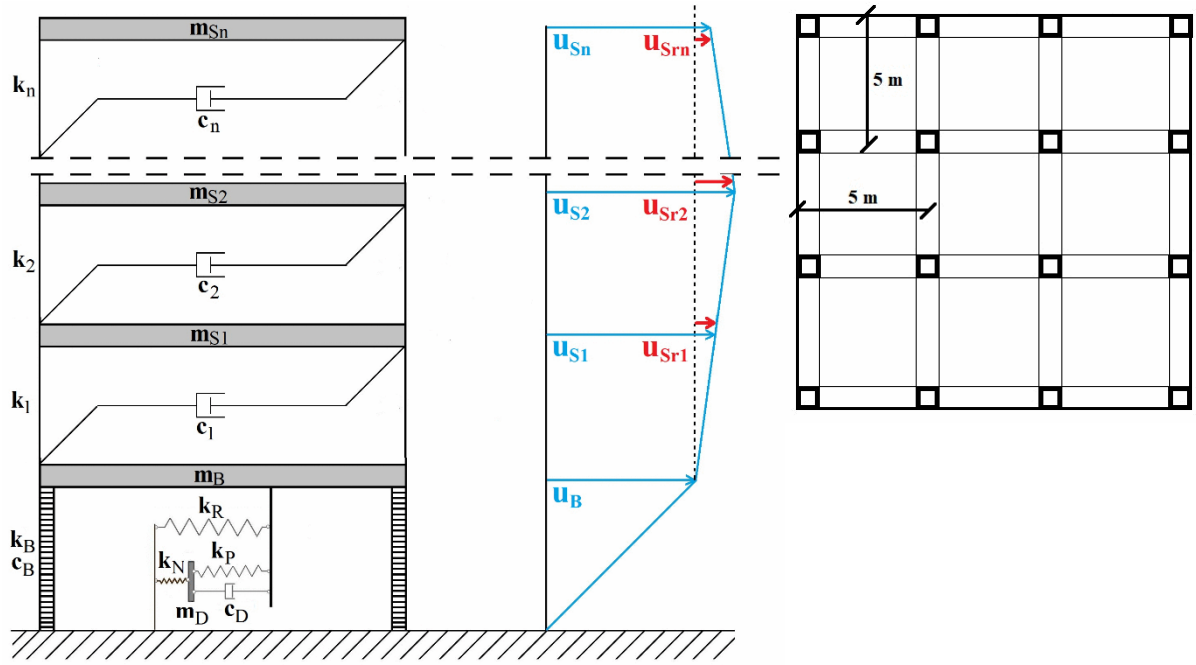

(a) (b)

Figure 4.12: *Examined n-story concrete building structure with the proposed absorption base system (KDAB), (a) sketch of the model and (b) typical ground floor plan of the structure.*

The equations of motion Equations (4.18) still hold, but now expressed in a matrix form, involving matrices with dimensions $r\times r$ with $r=n+2$:

$$[M][\ddot{u}(t)]+[C][\dot{u}(t)]+[K][u(t)]=-[\tau]a_G(t) \tag{4.26}$$

As an indicative example of the Approach III for the selection of the KDAB implemented in the bases of multi-story buildings, a 3-story building structure is considered, with elastic modulus equal to $E=26000\ MN/m^2$ (typical of a reinforced concrete frame). The mass of the 3 floors is $m_i=80000\ kg$ ($i=1, 2, 3$). Applying the classical modal analysis to the superstructure leads to the following natural periods $T_{Si}\ [sec] = [0.495, 0.177, 0.122]$. The basement mass is assumed to be $m_B=50000\ kg$, resulting in a base mass ratio $\mu_B=0.2083$. The damping coefficients of the superstructure are assumed to be mass and stiffness proportional (Rayleigh damping) with $\zeta_{Si}=0.02$ ($i=1, 2, 3$).

The calculation of the matrices of mass [M], stiffness [K], and damping [C] of the initial 3-story structure, the procedure from which the KDAB design is extended for implementation in MDoF structural systems, as well as the Transfer Functions of the controlled system with the KDAB are presented in Appendix A2.

In order to observe the effect of the nominal KDAB frequency to: 1) the Transfer Functions, 2) the response PSDs, and 3) the RMS responses, of the main system parameters, two cases are considered. In the first one, the nominal frequency of the KDAB is equal to the low frequency (0.4 *Hz*) of the BI system. This case will be referred to hereafter as KDAB-0.4. In the second one, a stiffer base is considered, with a nominal KDAB frequency of 1 *Hz*, in order to examine if the large base displacements, that are required in the classical base isolation concepts, can be avoided. This case will be referred to hereafter as KDAB-1.0.

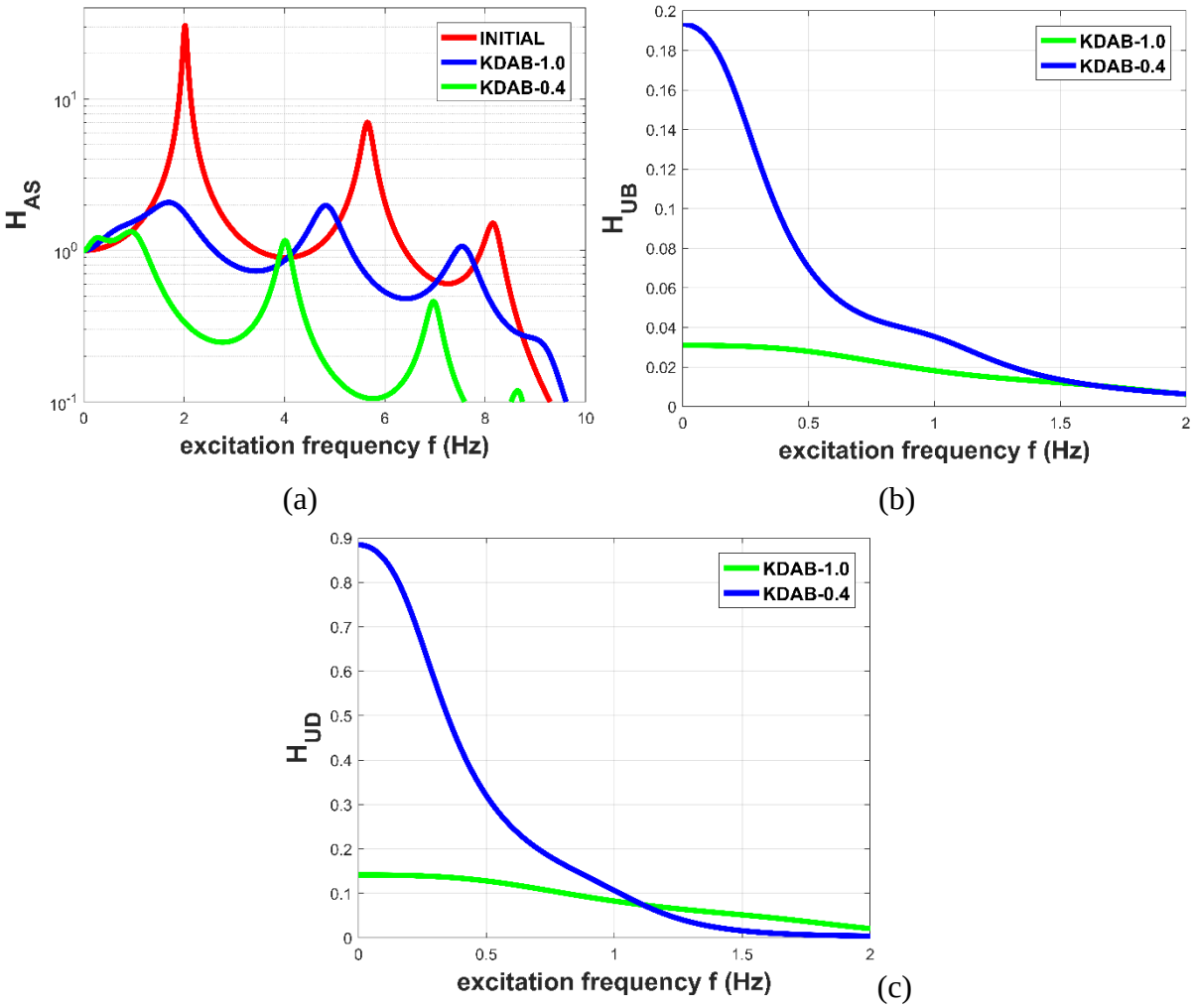

Figure 4.13: *Transfer Functions of the main system responses: (a) top floor acceleration H_{AS}, (b) base's relative displacement H_{UB}, and (c) KDAB relative displacement H_{UD} for all the considered systems: INITIAL, KDAB-0.4 and KDAB-1.0.*

Figure 4.13 presents the Transfer Functions of the controlled structure. The top floor absolute acceleration presented the worst dynamic behavior before and after the implementation of KDAB, and therefore, in the following, only the results concerning the top floor absolute acceleration will be presented. The KDAB-1.0 system, with a nominal frequency of 1 *Hz*, significantly enhances the superstructure's dynamic behavior both in terms of floor drifts and absolute accelerations. The KDAB-0.4 system, with a natural frequency equal to the low frequency of conventional base isolation systems (0.4 *Hz*), dramatically improves the floor drifts and absolute accelerations, as in the case of conventionally base isolated structures. Finally, it is observed from Figures 4.13.b and c, that the increase of the nominal KDAB frequency improves the dynamic behavior of the base and the additional mass of KDAB in all frequency range.

Based on the design spectrum compatible ground motion acceleration excitation PSD S_A of Figure 3.14, the response PSDs of the initial system as well as the controlled structure with KDAB, are obtained and depicted in Figure 4.14.

$$S_{USri}(\omega) = H_{USri}(\omega)^2 S_A(\omega) \tag{4.27.a}$$

$$S_{UB}(\omega) = H_{UB}(\omega)^2 S_A(\omega) \tag{4.27.b}$$

$$S_{UD}(\omega) = H_{UD}(\omega)^2 S_A(\omega) \tag{4.27.c}$$

$$S_{ASri}(\omega) = H_{ASri}(\omega)^2 S_A(\omega) \tag{4.27.d}$$

Figure 4.14 presents the response PSDs of: a) the top floor absolute acceleration $S_{AS,top}$, b) the base displacement S_{UB}, and c) the KDAB relative displacement S_{UD}. It is observed that the considered control systems (KDAB-0.4, and KDAB-1.0) manage to reduce the initial system's maximum value of the S_{AS} over two orders of magnitude. More specifically, the KDAB-0.4 system always displays an improved behavior in all frequency range as compared with the KDAB-1.0 system.

However, although the KDAB-1.0 (f_0=1 *Hz*) represents the same concept with the KDAB-0.4 (f_0=0.4 *Hz*) system, with a stiffer base (higher nominal frequency), it manages to reduce the maximum value of S_{UB} more than one order of magnitude, as compared with the KDAB-0.4 system (Figure 4.14.b). Finally, by making a stiffer base (KDAB-1.0), the KDAB's maximum value of the relative displacement PSD is reduced more than one order of magnitude (Figure 4.14.c).

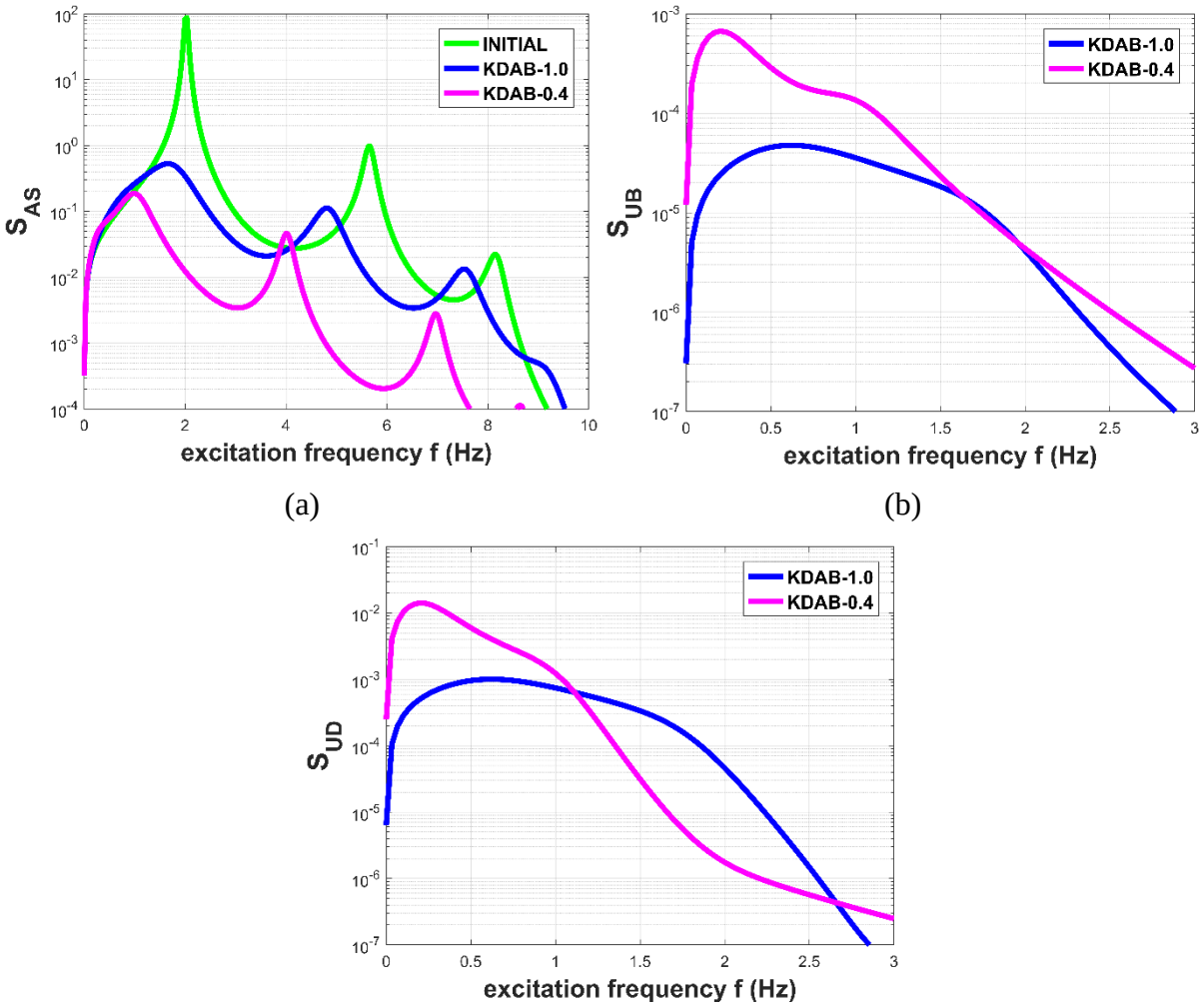

Figure 4.14: *PSDs of the main system responses: (a) top floor absolute acceleration HAS, (b) base's relative displacement HUB, and (c) KDAB relative displacement HUD for all the considered systems: INITIAL, KDAB-0.4 and KDAB-1.0.*

The RMS value of the responses is defined as the root of the area under the PSD curves, as an indication of the actual energy content of the response:

$$R_{USri} = \left[\int_{-\infty}^{+\infty} S_{USri}(\omega) \, \mathrm{d}\omega \right]^{0.5} \tag{4.28.a}$$

$$R_{UB} = \left[\int_{-\infty}^{+\infty} S_{UB}(\omega) \, \mathrm{d}\omega \right]^{0.5} \tag{4.28.b}$$

$$R_{UD} = \left[\int_{-\infty}^{+\infty} S_{UD}(\omega) \, \mathrm{d}\omega \right]^{0.5} \tag{4.28.c}$$

$$R_{ASri} = \left[\int_{-\infty}^{+\infty} S_{ASri}(\omega)\, \mathrm{d}\omega \right]^{0.5} \tag{4.28.d}$$

Figure 4.15 presents top floor absolute acceleration, base relative displacement, and the KDamper's relative displacement RMS ratios, which are defined as:

$$r_{USri} = \frac{R_{USri}}{R_{USri}(ref)} \tag{4.29.a}$$

$$r_{ASri} = \frac{R_{ASri}}{R_{ASri}(ref)} \tag{4.29.b}$$

$$r_{UB} = \frac{R_{UB}}{R_{US}(ref)} \tag{4.29.c}$$

$$r_{UD} = \frac{R_{UD}}{R_{US}(ref)} \tag{4.29.d}$$

where $R_{USri}(ref)$ and $R_{ASri}(ref)$ pertain to the initial 3-story uncontrolled building structure. $R_{USri}(ref)$ is the first floor's maximum relative displacement and $R_{ASri}(ref)$ the top (3^{rd}) floor's maximum absolute acceleration. The results concern the KDAB system with parameters $\mu=5\%$, $\kappa=3.41$, $\zeta_D=0.622$ and a continuous variation of the KDamper's nominal frequency in the range $f_0= [0{,}4 - 1.0]$ *Hz*. The inherent conflict between the requirement for simultaneous minimization of the structure's absolute acceleration/floor drift and the base's relative displacement is observed. The KDAB system with a nominal frequency of 0.4 *Hz* (KDAB-0.4) can be used as a possible supplement to the conventional seismic isolation approaches, significantly improving the superstructure's dynamic performance while retaining the base displacement at acceptable levels, as compared with the conventional base isolation concepts. As an alternative, the KDAB can be implemented as a "stiff absorption base" with a much higher nominal frequency (1 *Hz*, KDAB-0.1 system). This way the superstructure's dynamic performance is greatly improved while at the same time the base's relative displacement is in the order of a few centimeters (comparable displacement to a floor drift), as it can be observed in Figure 4.15. Finally, the KDAB's relative displacement is greatly reduced as the nominal KDamper frequency increases, as observed in Figure 4.15.c. Next, the equations of motion, Equations (4.26) of the controlled system with KDAB are solved for all the 30 accelerograms of the database in the time domain, using the Newmark-β method with linear acceleration.

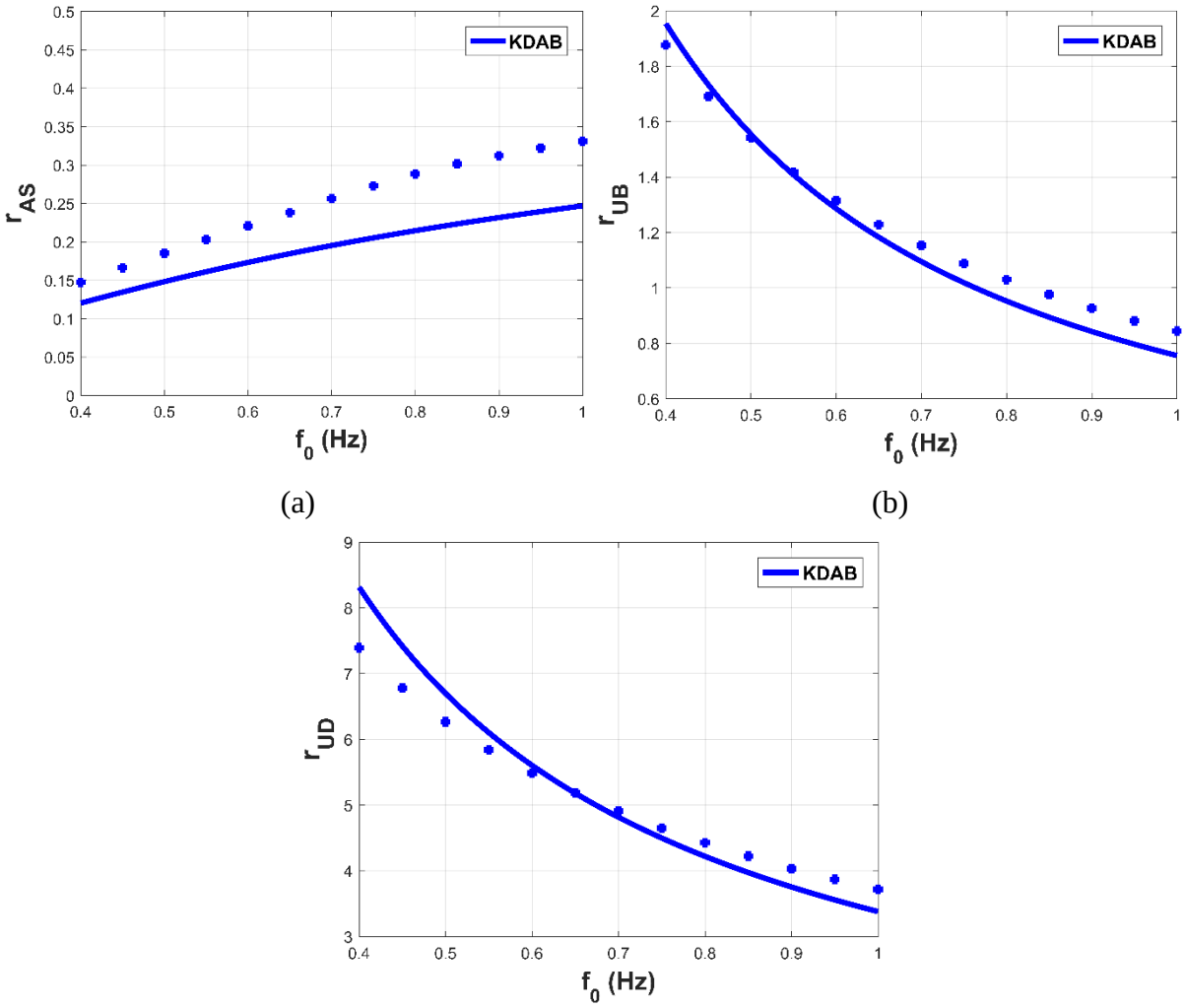

Figure 4.15: *RMS responses ratio (solid lines) and verification with mean of the maximum dynamic responses ratio (dotted lines), of the KDAB system: (a) structure's to floor (3^{rd}) absolute acceleration, (b) base's relative displacement, and (c) KDAB's relative displacement, over the nominal KDAB frequency f0.*

The mean of the maximum responses ratio of the dynamic response is defined as:

$$v_{USri} = \frac{V_{USri}}{V_{USri}(ref)} \tag{4.30.a}$$

$$v_{ASri} = \frac{V_{ASri}}{V_{ASri}(ref)} \tag{4.30.b}$$

$$v_{UB} = \frac{V_{UB}}{V_{US}(ref)} \tag{4.30.c}$$

$$v_{UD} = \frac{V_{UD}}{V_{US}(ref)} \tag{4.30.d}$$

where $V_{USri}(ref)$ and $V_{ASri}(ref)$ pertain to the initial 3-story uncontrolled building structure. $V_{USri}(ref)$ is the first floor's maximum relative displacement and $V_{ASri}(ref)$ the top (3rd) floor's maximum absolute acceleration. The results are also presented in Figure 4.15 (dotted lines) and clearly confirm that a spectral driven design of a controlled multi-story structure with KDAB is very accurate, and more specifically a spectral driven optimization of the KDAB base's nominal frequency is possible.

4.3.2 Numerical Example 1 – *Preliminary Assessment of the KDamper Implemented in the Base of a 3-Story Building Structure*

The KDamper implemented as a "stiff seismic absorption base", mentioned in the previous as KDAB-1.0 system, combines a drastic reduction in the base's relative displacement with an acceptable superstructure dynamic behavior, in terms of floor drifts and absolute accelerations, and therefore will be examined as an alternative to the conventional seismic isolation approaches. The parameters for this proposed configuration are presented in Table 4.1 (KDAB-1.0 system). Considering the test case presented in Section 4.1, the resulting stiffness values, as well as the additional mass and the damping coefficient of the KDAB-H system, are presented in Table 4.2.

Table 4.1: *Parameters of the proposed configuration (KDAB-1.0).*

System	m_D (*tn*)	k_R (*kN/m*)	k_D (*kN/m*)	k_N (*kN/m*)	C_D (*kNs/m*)
KDAB-1.0	14.5	54288	12563	-9714.3	252.82

KDAB devices can operate in parallel, and therefore multiple KDAB devices can be placed under each of the structure's columns, as in the case of seismic isolation bearings. For the considered 3-story concrete building structure, one KDAB device is designed to be placed under each of the structure's columns.

Thus, 16 KDAB devices provide the necessary values presented in Table 4.1. In Table 4.2 is the full set of parameters for each of the 16 KDAB devices, the realization of each will be discussed below.

Table 4.2: *Full set of parameters for each one of the 16 KDAB devices.*

μ_i	κ_i	ζ_{Di}	m_D (*tn*)	k_R (*kN/m*)	k_P (*kN/m*)	k_N (*kN/m*)	C_D (*kNs/m*)
0.05	3.41	0.622	0.90625	3393	785.1875	-607.143	15.80125

The selection of the NS element's set-up as well as the design of the positive stiffness elements and the artificial damper, require the solution of a linear problem first in order to estimate the maximum absolute displacement and velocity values that are necessary for the design. More specifically, the internal DoF's (KDAB's) displacement is required for the design of the NS element, the base's displacement for the positive stiffness element k_R and the relative displacement and velocity between the base and the KDAB for the positive stiffness element k_P as well as for the artificial damper c_D. All the aforementioned maximum dynamic response together with the main dynamic responses of a conventional (BI, 5%) and a highly (BI-HD, 15%) damped base isolated system are presented in Table 4.3. The results concern the mean and maximum values of all the 30 Artificial Accelerograms in the database.

Table 4.3: *Dynamic responses of the linear problem.*

Dynamic Responses		Initial	BI (5%)	BI-HD (15%)	KDAB-1.0
1st floor drift (*m*)	Max	0.0628	0.0056	0.0051	0.0165
	Mean	0.0468	0.005	0.0043	0.014
3rd floor abs. acc (m/sec^2)	Max	22.6782	1.7936	1.8674	6.92
	Mean	17.2292	1.5804	1.5794	5.7031
Base displ. (*m*)	Max	-	0.234	0.1967	0.0512
	Mean	-	0.206	0.1616	0.0395
KDamper displ. (*m*)	Max	-	-	-	0.2344
	Mean	-	-	-	0.174
Base-KDamper displ. (*m*)	Max	-	-	-	0.1877
	mean	-	-	-	0.1409

Considering the conventional base isolated system (BI, 5%) simple seismic isolation bearing are selected. In the case of the highly damped (BI-HD, 15%) base isolated system, 8 *SI-S 300/128* elastomeric isolators from the FIP Industriale catalog (Elastomeric isolators - Fip Industriale) are selected. The equivalent viscous damping coefficient is 10-15 *%*, thus a 15*%* damping ratio is selected for the analysis. Their maximum designed displacement is 25 *cm*, sufficiently greater than the maximum value presented in Table 4.3 (19.67 *cm*). In both cases

(conventional and highly damped base isolated system), the base's frequency (0.4 *Hz*) is designed to be significantly lower than that of the fundamental frequency of the structure (1/*T1* =1/0.495=2.02 *Hz*).

The negative stiffness element is realized according to the Proposed Configuration I, presented in Section 3.3.1. Table 4.4 presents the entire set of parameters of the proposed configuration concerning the negative stiffness element for each one of the sixteen KDamper devices, with k_{NC}=-607.1437 *kN/m*.

Table 4.4: Negative stiffness spring and mechanism parameters for each one of the sixteen KDAB devices.

k_H (*kN/m*)	l_{HI} (*m*)	a (*m*)	b (*m*)	c_I
322.743	0.504	0.324	0.520	-0.05

Figure 4.16 presents the variation of the negative stiffness, of the proposed configuration, over the KDAB's relative displacement. It is observed, that in the range of -0.2344 *m* to +0.2344 *m*, which is the maximum range of the KDAB's relative displacement of all the artificial accelerograms in the database, the generated negative stiffness is pretty much constant.

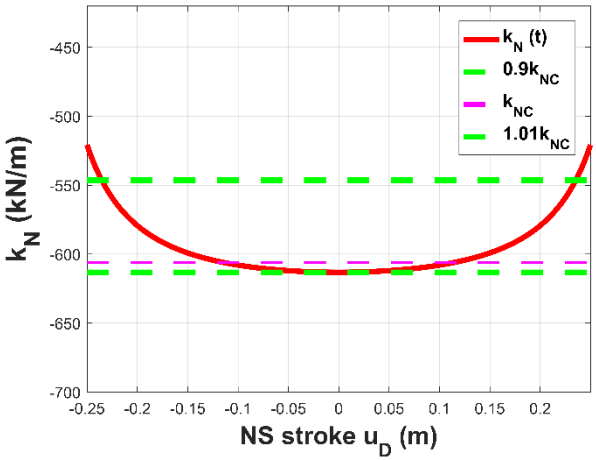

Figure 4.16: *Variation of the generated negative stiffness, of the proposed configuration, over the KDAB's relative displacement.*

The material used to realize the additional mass of each of the 16 KDAB devices is steel, with a value of density equal to ρ_{mat}=7850 kg/m^3. Assuming cubic shape for the additional mass, the resulting dimension of the additional mass of each device is:

$$x_{add,mass} = \sqrt[3]{(m_D / No.Columns) / \rho_{mat}} = \sqrt[3]{(14.5/16)/7.85} = 0.487m \quad (4.31)$$

The maximum relative displacement between the base and the additional mass of the device is 0.1877 *m*. Therefore, conventional spiral springs can be used in the making of the positive stiffness element k_D. Each one of the sixteen KDAB's artificial damper coefficient is low (15.8 *kNs/m*), so common linear damping devices can be used, as for example Catalog No./Model LD720 from ITT Infrastructure viscous dampers catalog (Fluid Viscous Dampers, ITT Infrastructure), with a designed maximum stroke of 20 *cm* and a total initial length of 52.2 *cm*. The positive stiffness element k_R works totally independent from the other stiffness elements, the additional mass, and the artificial damper, as shown in Figure 4.12.a. Thus, there are numerous alternatives for the realization of k_R, the design of which is beyond the scope of the current section. Some realistic examples are for instance simple elastomeric bearings or steel simply supported cantilever beams.

Finally, a schematic representation of the proposed configuration with all the resulting dimensions of the KDAB parameters is given in Figure 4.17. The system of non-linear equations, of the KDAB-1.0 system with non-linear negative stiffness, k_N, is solved using the Newmark-β method with linear accelerations.

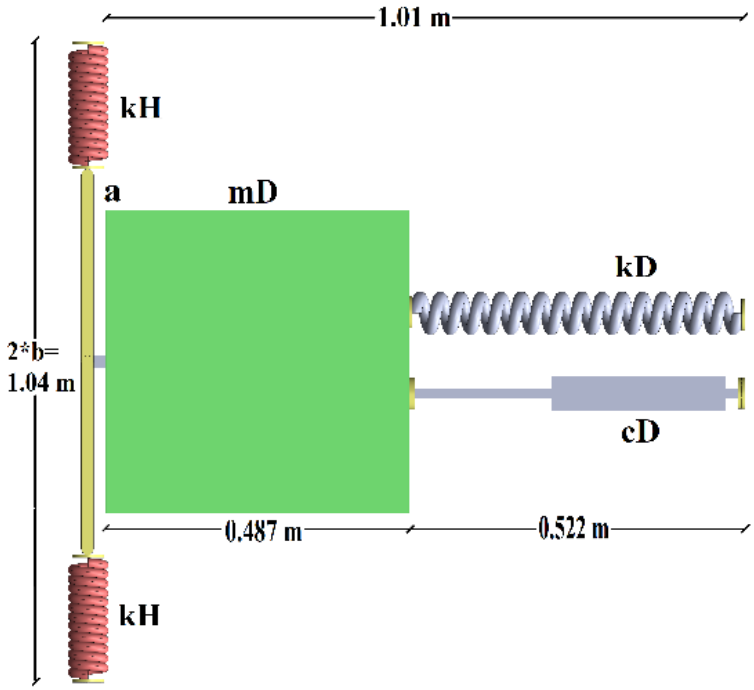

(a)

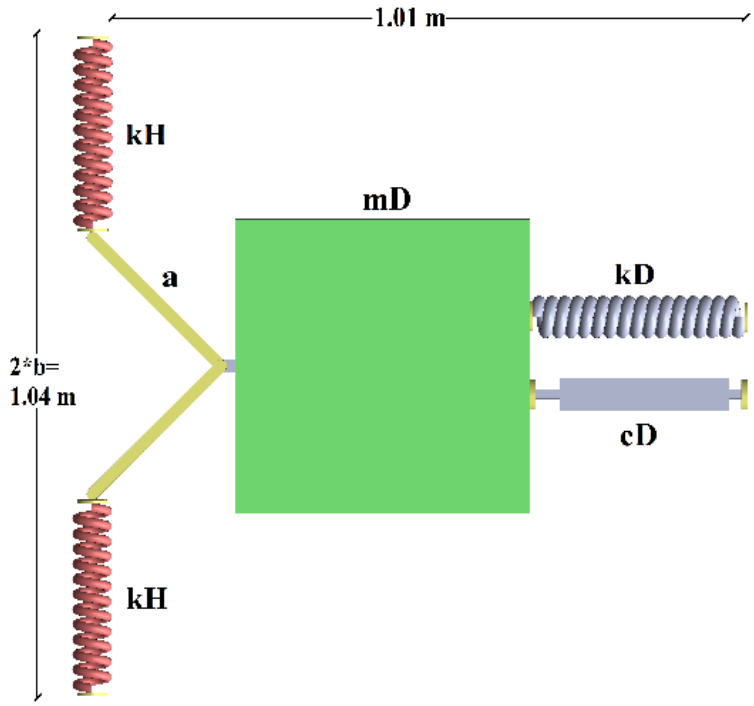

(b)

Figure 4.17: *Schematic representation (plan view) of the proposed configuration of the KDAB concept: (a) undeformed state, and (b) deformed state.*

Figure 4.18 presents comparative results between the linear problem and the proposed non-linear configuration (Proposed Configuration I). The results refer to the internal KDAB displacement (relative to the ground), the base displacement and the 1st-floor drift, for a random artificial accelerogram of the database. It is proven that the results of the proposed non-linear system are in a very good agreement to that of the linear one previously solved.

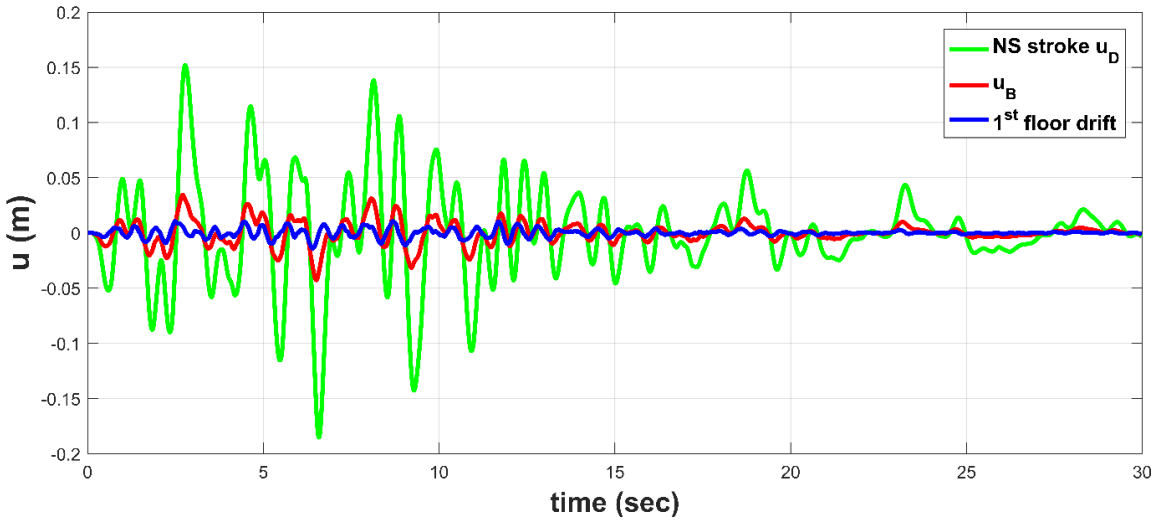

(a)

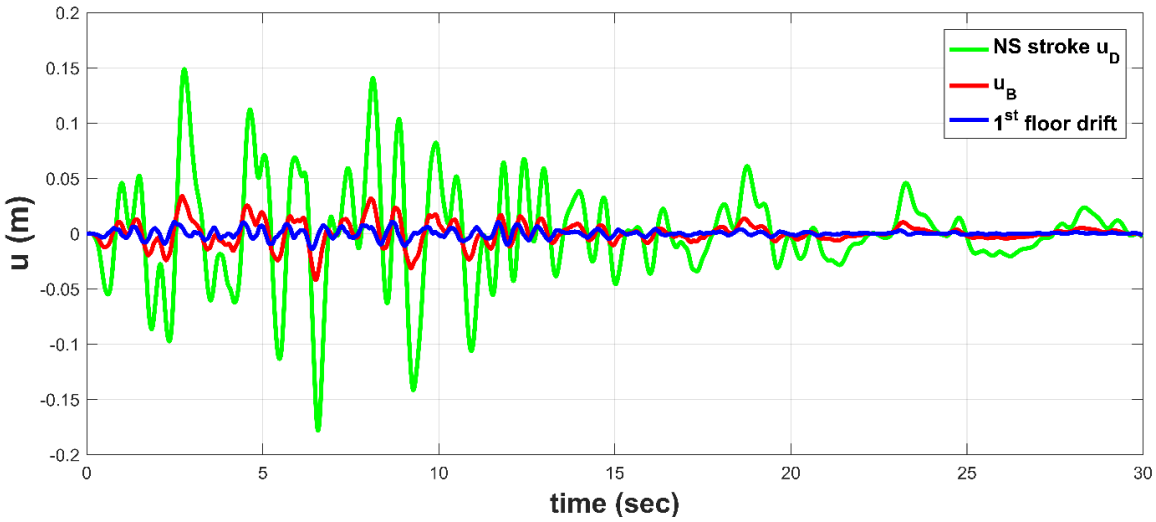

(b)

Figure 4.18: *Dynamic responses of the controlled system with KDAB, internal KDAB, base and 1st floor drift displacements: of a) the linear problem max|u_{KD}|=0.1853 m, max|u_B|=0.0427 m, and max|u_{drift}|=0.0141 m, and b) the non-linear configuration max|u_{KD}|=0.1783 m, max|u_B|=0.0421 m, and max|u_{drift}|=0.014 m.*

4.3.3 Performance Assessment of KDamper with Real Earthquake Records

Real earthquakes are neither stationary nor have a fixed duration. Therefore, it is of utmost importance to scrutinize the effectiveness of the proposed vibration control strategy also with real earthquake records. In this section, 20 real earthquake records are selected. They are widely used in the literature and are known to have had a devastating impact on structural systems. The information about each ground motion is presented in Table 4.5. In this study, earthquakes with an epicentral distance R_{jb} of fewer than *25 km*, were classified as near-fault.

Table 4.5: *List and information of the considered real earthquake records.*

No	Earthquake	Year	Station	Ground Motion	Mw	PGA (g)	R_{jb} (km)	$DUR_{5\text{-}75\%}$ (sec)
1	Northridge-N	1994	N Hollywood	Near fault	6.69	0.309	7.89	7.0
2	Northridge-F	1994	Montebello	Far fault	6.69	0.176	43.2	7.8
3	Loma Prieta-N	1989	Corralitos	Near fault	6.93	0.645	0.16	4.6
4	Loma Prieta-F	1989	APEEL 10-Skyline	Far fault	6.93	0.103	41.9	8.3
5	L'Aquila-N	2009	V. Aterno	Near fault	6.3	0.402	0.0	4.7

6	L'Aquila-F	2009	Ortucchio	Far fault	6.3	0.066	35.1	6.2
7	Chi-Chi-N	1999	CHY006	Near fault	7.62	0.359	9.76	5.6
8	Chi-Chi-F	1999	CHY012	Far fault	7.62	0.063	59.0	42.8
9	Kocaeli-N	1999	Izmit	Near fault	7.51	0.165	3.62	8.2
10	Kocaeli-F	1999	Fatih	Far fault	7.51	0.162	53.3	27.8
11	Tabas-N	1978	Tabas	Near fault	7.35	0.854	1.79	8.3
12	Tabas-F	1978	Ferdows	Far fault	7.35	0.093	89.8	20.5
13	Kobe-N	1995	Amagasaki	Near fault	6.9	0.276	11.3	6.9
14	Kobe-F	1995	HIK	Far fault	6.9	0.139	95.7	6.1
15	Kozani-N	1995	Kozani	Near fault	6.4	0.207	14.1	3.3
16	Kozani-F	1995	Larisa	Far fault	6.4	0.031	74.1	21.7
17	Niigata-N	2004	NIG017	Near fault	6.63	0.378	4.22	6.1
18	Niigata-F	2004	FKS020	Far fault	6.63	0.043	101	22.5
19	Landers-N	1992	Joshua tree	Near fault	7.28	0.274	11.0	21.7
20	Landers-F	1992	Boron fire station	Far fault	7.28	0.119	89.7	9.6

In order to assess the performance of the KDamper, it is compared with a conventional (ζ=5%) and a highly damped (ζ=20%) base isolated systems, named BI and BI-HD respectively, and a TMDI. In order to provide an equal comparison basis to the KDamper, the selection of the TMDI parameters must follow the same procedure, described in section 3.2.2 of Chapter 3, for optimal absolute acceleration responses.

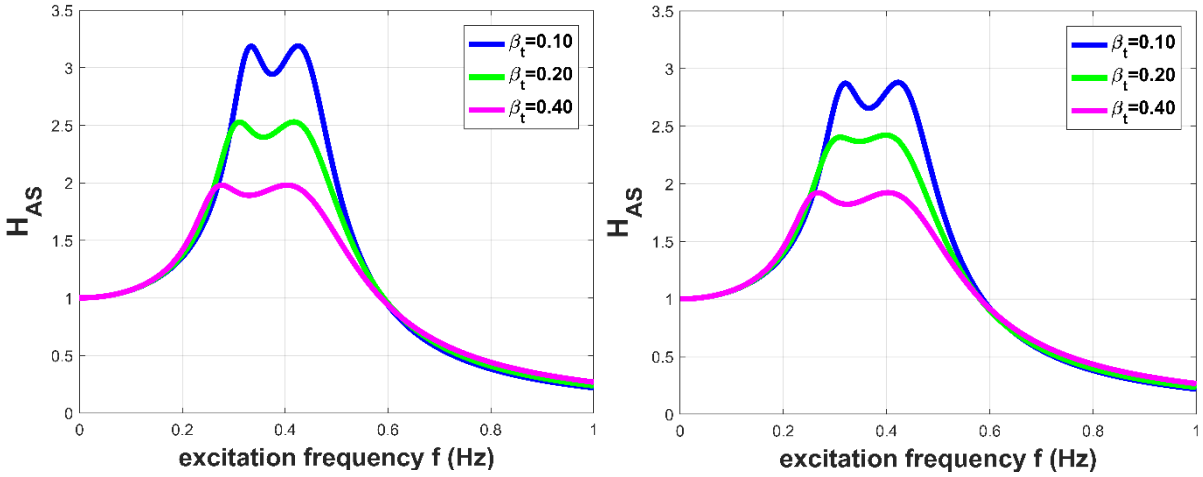

(a) (b)

Figure 4.19: *Dependence of Transfer Function H_{AS} of the TMDI on the inertance-related mass ratio μ_t, for additional mass of the TMDI (a) μ=0.01, and (b) μ=0.05.*

The absolute acceleration transfer function H_{AS} is optimized for a harmonic base acceleration excitation. However, in the literature, no closed-form exists for the optimal parameters of the TMDI for base acceleration excitation/absolute acceleration response Transfer Function minimization. Therefore, the system's parameters ζ_t and ω_t are calculated numerically so that the peak of the $H_{AS}(q,\zeta_t,\omega_t)$ is minimized in all frequency range, as presented in Figure 4.19. The base isolated systems and the TMDI system are all designed to have a base natural frequency equal to 0.4 *Hz*. By increasing the inertance-related mass ratio μ_t, the magnitude of the transfer function H_{AS} is reduced. Moreover, for high values of the parameter μ_t, the physical mass ratio μ doesn't affect the acceleration transfer function H_{AS}. Thus, the physical mass ratio μ and the apparent (inertance-related) mass ratio μ_t, are selected as in (De Domenico et al., 2018) and are: $\mu_t=0.01$ and $\beta_t=0.4$, ζ_t and ω_t are calculated numerically and are: $\zeta_t=0.3563$, $\omega_t=1.8874$. The lower limit of f_0 is selected to be equal to the low frequency of the conventional base isolated systems (*0.4 Hz*), making the KDAB a possible supplement to the classic base isolation approach. By setting the upper limit to *1 Hz*, a nominal frequency much higher than that of the base isolation system, another interesting option is revealed, which foresees the implementation of the KDAB as a "stiff absorption base".

4.3.3.1 Numerical Example 2 – *Rigid Structure Mounted on KDAB*

In order to assess the performance of the KDAB as a base isolation supplement, the KDAB with a nominal frequency of *0.4 Hz*, equal to the BI system's frequency, is compared to the base isolation-related systems: BI, BI-HD, and BI-TMDI. The transfer functions of these systems are formed and depicted in Figure 4.20. The addition of the TMDI, improves the dynamic behavior in terms of the absolute acceleration (H_{AS}), compared to the BI and BI-HD, while at the same time, the systems relative displacement H_{US}, compared to the BI-HD, is not improved. The KDAB-0.4 system dramatically reduces the H_{US} in all the frequency range. However, although the maximum value of H_{AS} is greatly reduced, more than all the aforementioned systems retains a large frequency range where the maximum values occur.
The effect of the natural frequency f_0, of the KDAB system, on the Transfer Functions of the system main responses, is presented in Figure 4.21. The maximum value of H_{AS} is exactly the same, but it is observed that as the nominal frequency f_0 increases, the frequency range where the maximum values are presented also increases. On the other hand, by increasing the natural frequency f_0, the Transfer Functions H_{US} and H_{UD}, that relate to the structure's and the damper's relative displacement respectively, are dramatically improved in all the frequency range.

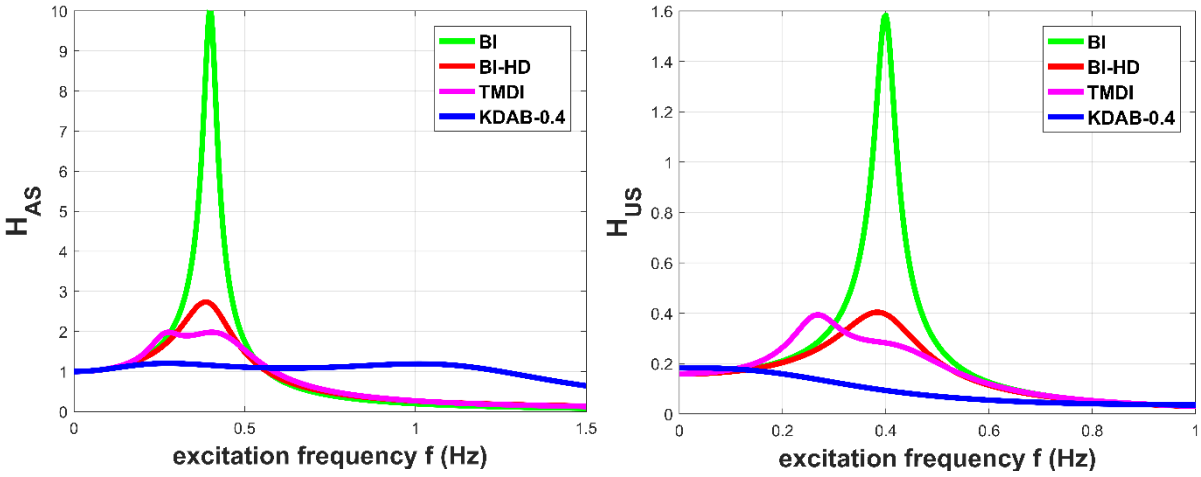

(a) (b)

Figure 4.20: *Transfer Functions of the main system responses: (a) structure's absolute acceleration H_{AS}, and (b) structure's relative displacement H_{US} of the controlled systems: BI, BI-HD, BI-TMDI, and KDAB-0.4.*

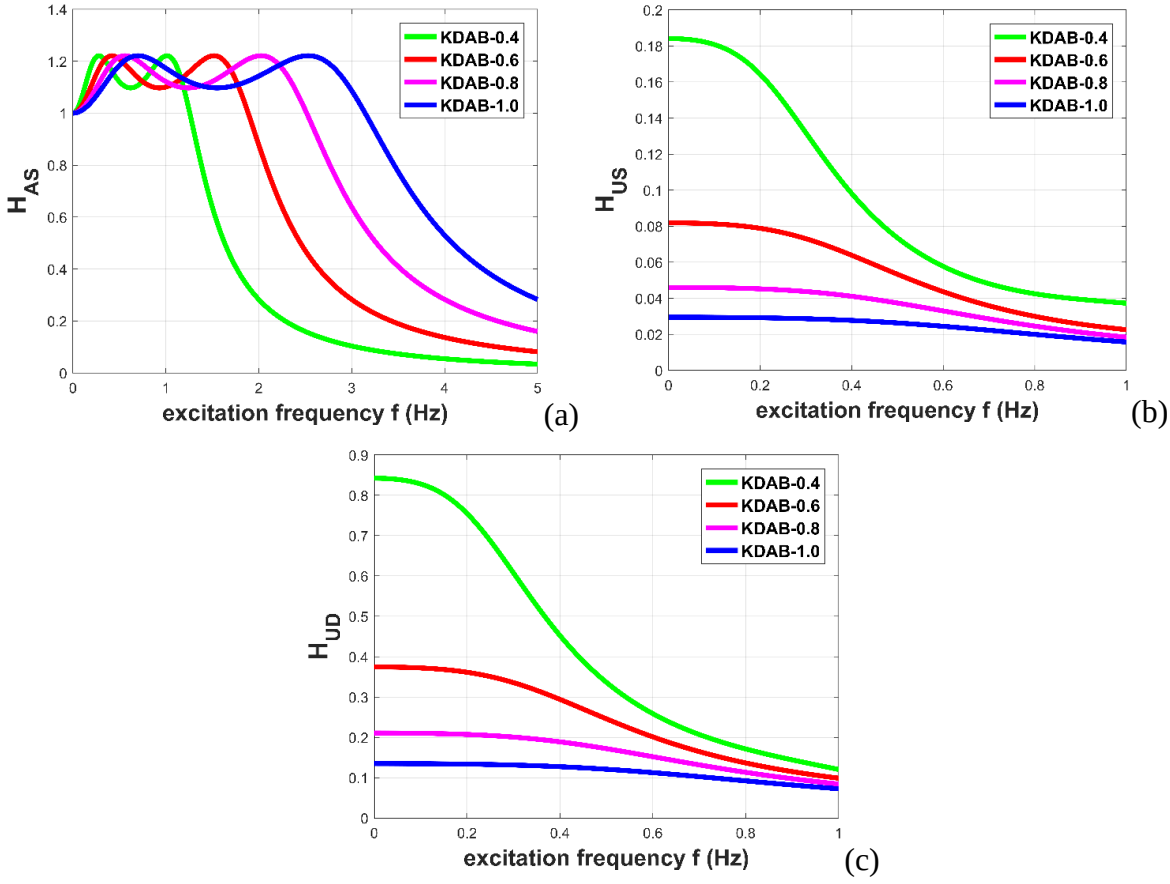

(a) (b) (c)

Figure 4.21: *Transfer Functions of the main system responses: (a) structure's absolute acceleration H_{AS}, (b) structure's relative displacement H_{US}, and (c) KDamper relative displacement H_{UD} for all the selected nominal frequencies of the KDAB: KDAB-0.44, KDAB-0.6, KDAB-0.8, and KDAB-1,0.*

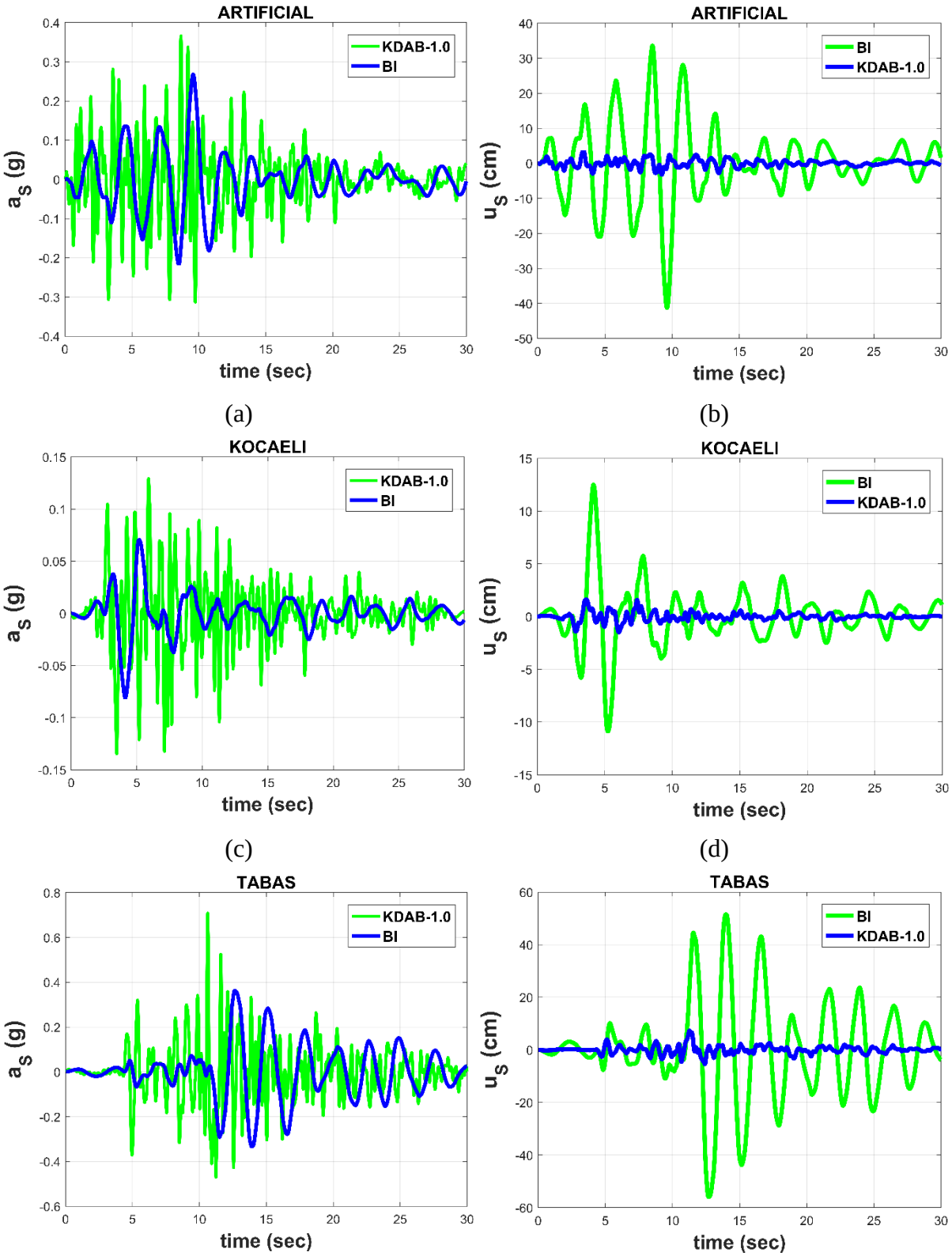

Figure 4.22: *Comparative results, in terms of structure's absolute acceleration (g) and structure's relative displacement (cm), between the conventional base isolated system (BI) and the KDAB-1.0 system, for (a, b) an artificial acceleration, (c, d) the Kocaeli earthquake record and (e, f) the Tabas earthquake record.*

Comparative results between the BI and the KDAB-1.0 system are presented in Figure 4.22. The presented time histories relate to: 1) an artificial accelerogram, 2) Kocaeli earthquake record, and 3) Tabas earthquake record. The systems main dynamic responses, considering the max values of the dynamic responses for all the Artificial Accelerograms in the database (mean of 30 maximum values), as well as the selected real near and far fault earthquake records in this section (mean of 10 max each), of the rigid body, mounted directly on a compliant base, considering all the examined control systems (BI, BI-HD, BI-TMDI, KDAB-f_0), are presented in Figure 4.23.

In the first case, where the nominal KDAB frequency is selected equal to the low frequency of a conventional base isolation system, KDAB-0.4, a drastic improvement of the overall structural performance is observed. The second case foresees the implementation of the KDAB with a much higher nominal frequency, KDAB-1.0, leading to a drastic reduction of the relative base displacement, in the order of a few centimeters, retaining the absolute acceleration to acceptable levels.

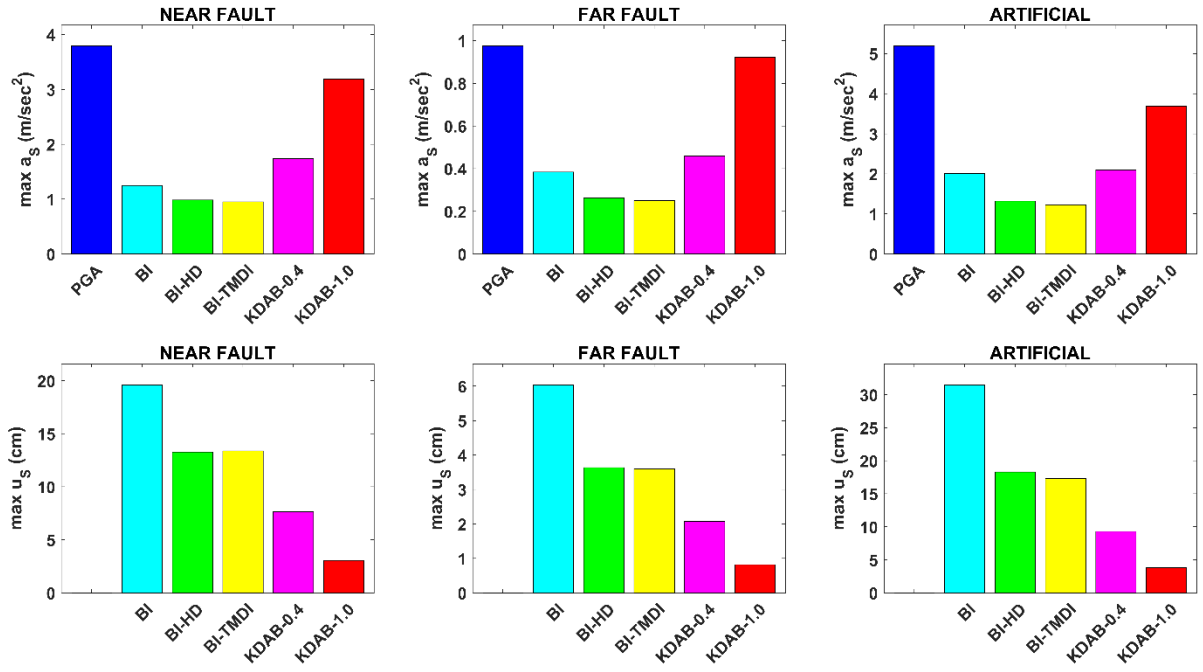

Figure 4.23: *Max values of the main dynamic responses of the examined control systems (BI, BI-HD, BI-TMDI, KDAB-f_0), for all the artificial accelerograms (mean of 30 max), real near-fault earthquake records (mean of 10 max) and real far-fault earthquake records (mean of 10 max).*

4.3.3.2 Numerical Example 3 – *5-Story Building Mounted on KDAB*

A 5-story symmetric-plan concrete building structure is considered. The system has 5 dynamic DoFs represented by the displacements of the 5 stories relative to the ground/base. The elastic modulus is $E=26000\ MN/m^2$ (typical of a reinforced concrete frame), the mass of the superstructure is lumped at the floor levels, with $m_i=60\ tn$ denoting the mass of the 5 floors ($i=1,\ldots,5$). Applying the classical modal analysis to the superstructure leads to the following natural periods $T_{Si}\ [sec] = [0.504, 0.173, 0.109, 0.085, 0.075]$. The basement mass is assumed to be $m_B=50\ tn$. The damping coefficients of the superstructure are assumed to be mass and stiffness proportional (Rayleigh damping) with $\zeta_{Si}=0.02$ ($i=1,\ldots,5$).

In order to assess the performance of the KDAB as a base isolation supplement, the KDAB-0.4 is compared with the base isolation-related systems: BI, BI-HD, and BI-TMDI. The Transfer Functions of these systems are formed according to Appendix A2, and are depicted in Figure 4.24. The increase of the damping ratio from *5%* (BI) to *20%* (BI-HD), reduces the maximum values of the transfer functions, retaining the same frequency range. The addition of the TMDI in the conventional base isolation concept (BI-TMDI), improves the dynamic behavior in terms of the H_{AS}, compared with the BI and BI-HD, while at the same time, the H_{UB}, compared with the BI-HD, is not improved. The KDAB-0.4 system dramatically reduces the H_{UB} in all the frequency range. However, although the maximum value of H_{AS} is greatly reduced, more than all the aforementioned systems, retains a large frequency range.

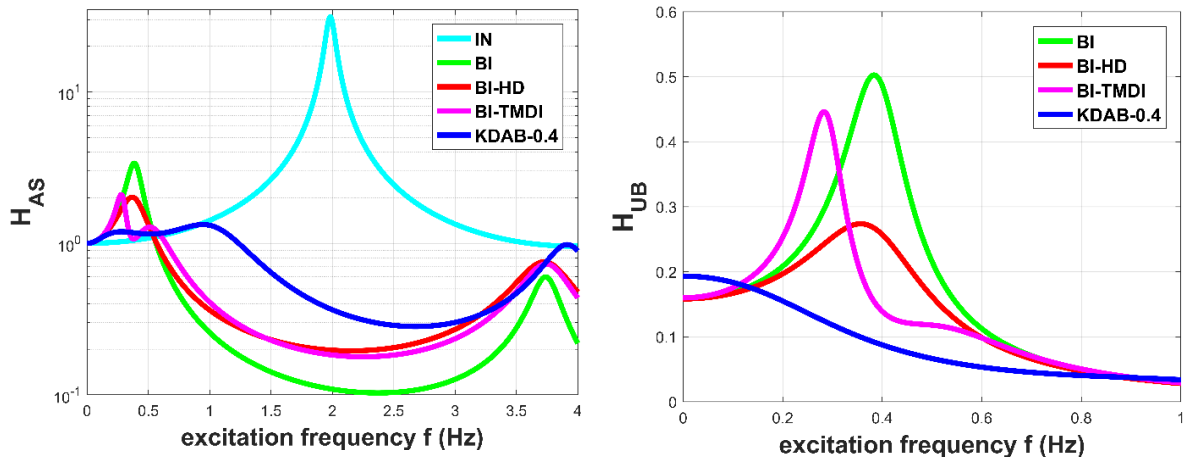

(a) (b)

Figure 4.24: *Transfer Functions of the main system responses: (a) structure's absolute acceleration H_{AS} for systems: IN, BI, BI-HD, BI-TMDI and KDAB-0.4, and (b) base's relative displacement H_{UB} for the control systems: BI, BI-HD, BI-TMDI, and KDAB-0.4.*

The effect of the natural frequency f_0, of the KDAB system, on the Transfer Functions of the system main responses, is presented in Figure 4.25. The absolute acceleration Transfer Function H_{AS} is improved in all the frequency range, as the natural frequency f_0 decreases. On the other hand, by increasing the natural frequency f_0, the transfer functions H_{UB} and H_{UD}, which relate to the base's and the damper's relative displacement respectively, are dramatically improved in all the frequency range.

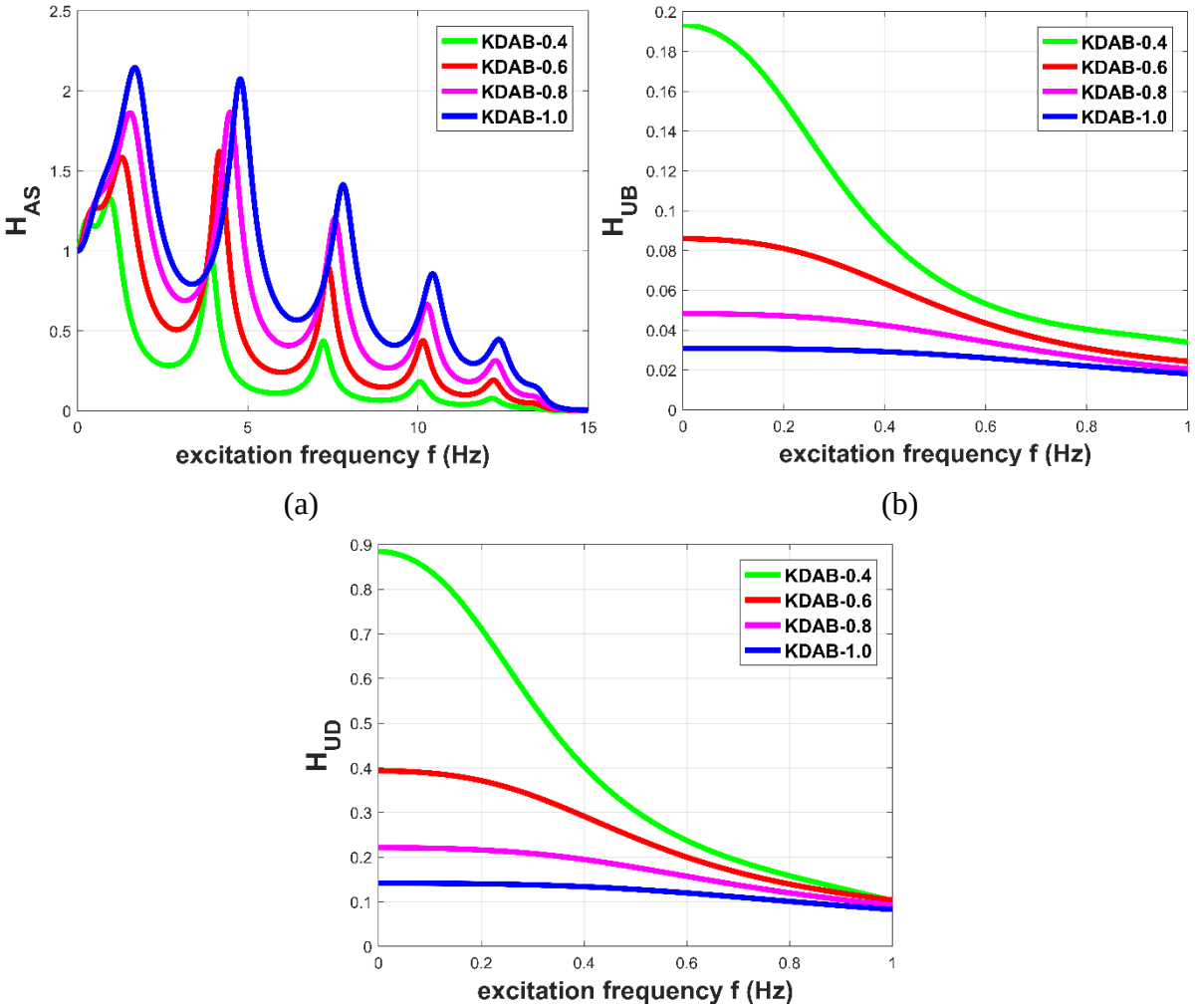

Figure 4.25: *Transfer Functions of the main system responses: (a) structure's absolute acceleration (top floor) H_{AS}, (b) structure's base relative displacement H_{UB} and (C) KDamper relative displacement H_{UD} for all the selected nominal frequencies of the KDamper: KDAB-0.4, KDAB-0.6, KDAB-0.8, and KDAB-1.0.*

Comparative results between the BI and the KDAB-1.0 system are presented in Figure 4.26. The presented time histories relate to: 1) an artificial accelerogram, 2) Kocaeli earthquake record and 3) Tabas earthquake record.

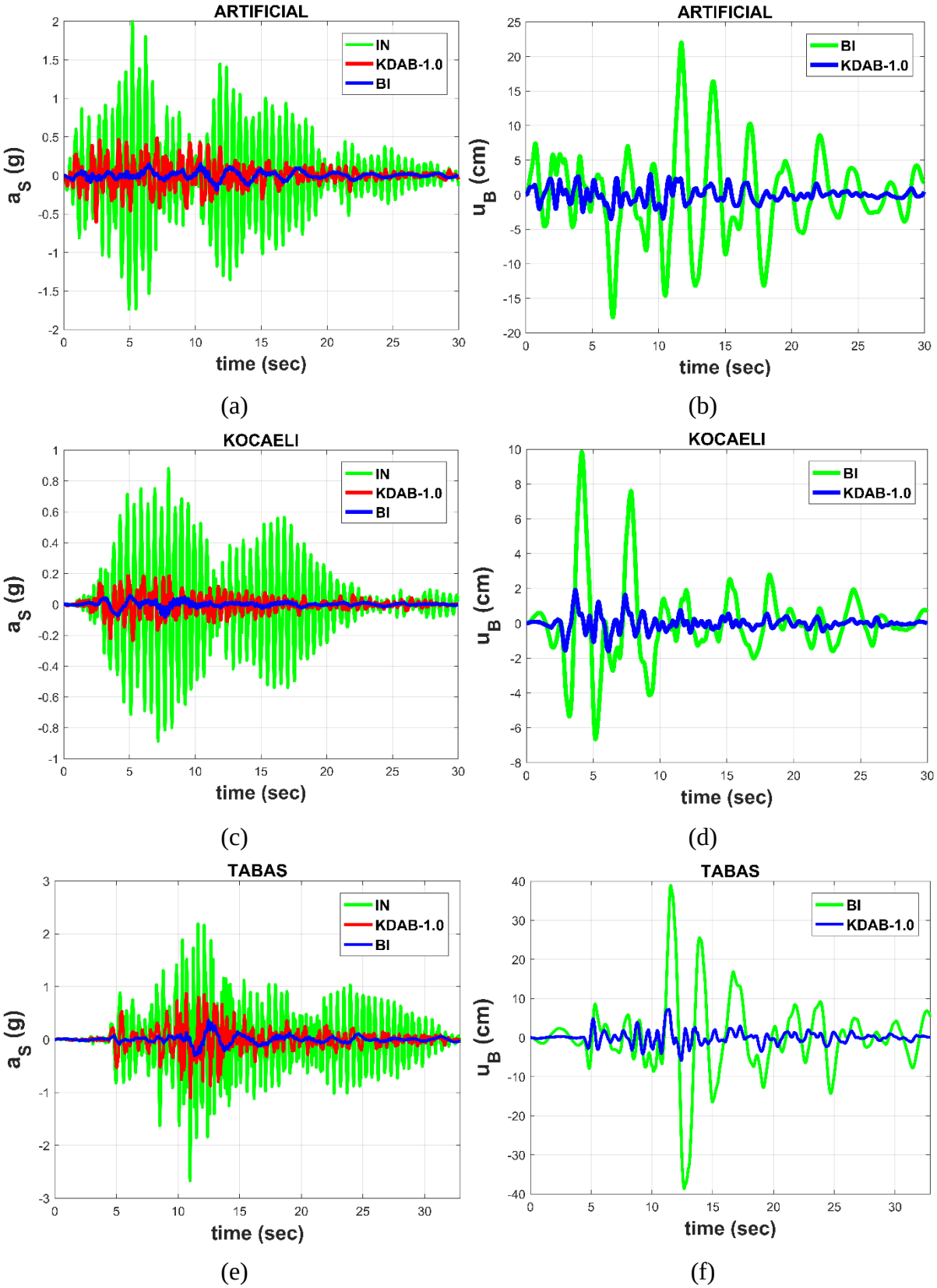

Figure 4.26: *Comparative results, in terms of structure's absolute acceleration (m/sec^2) and base's relative displacement (m), between the BI and the KDAB-1.0 system, for (a,b) an artificial accelerogram, (c,d) the Kocaeli, and (e,f) Tabas earthquake.*

The systems main dynamic responses, considering the max values of the dynamic responses for all the artificial accelerograms in the database (mean of 30 max), as well as the selected real near and far fault earthquake records in this paper (mean of 10 max each), of the initial (IN) 5-story concrete building structure, and the considered concepts for base isolation/absorption (BI, BI-HD, BI-TMDI, KDAB-f_0) are presented in Figure 4.27.

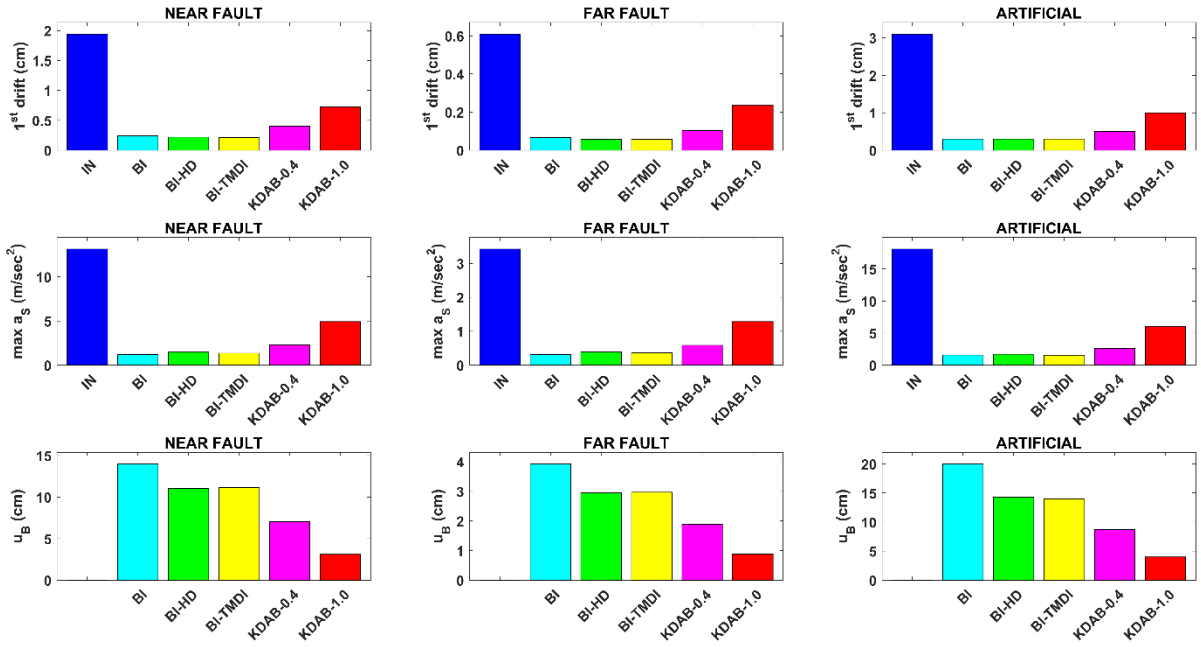

Figure 4.27: *Max values of the main dynamic responses of the examined control systems (BI, BI-HD, BI-TMDI, KDAB-f_0), for all the artificial accelerograms (mean of 30 max), real near-fault earthquake records (mean of 10 max) and real far fault earthquake records (mean of 10 max).*

4.3.3.3 Numerical Example 4 – *10-Story Building Mounted on KDAB*

A 10-story building is considered with 10 dynamic DoFs. The mass of each floor is m_i*=60 tn* and the natural periods are T_{Si}*[sec] = [0.961, 0.323, 0.196, 0.143, 0.115, 0.098, 0.087, 0.079, 0.075, 0.073]*. In order to assess the performance of the KDAB as a base isolation supplement, the KDAB-0.4 is compared with the base isolation-related systems: BI, BI-HD, and BI-TMDI. The Transfer Functions of these systems are formed according to Appendix A2, and are depicted in Figure 4.28.

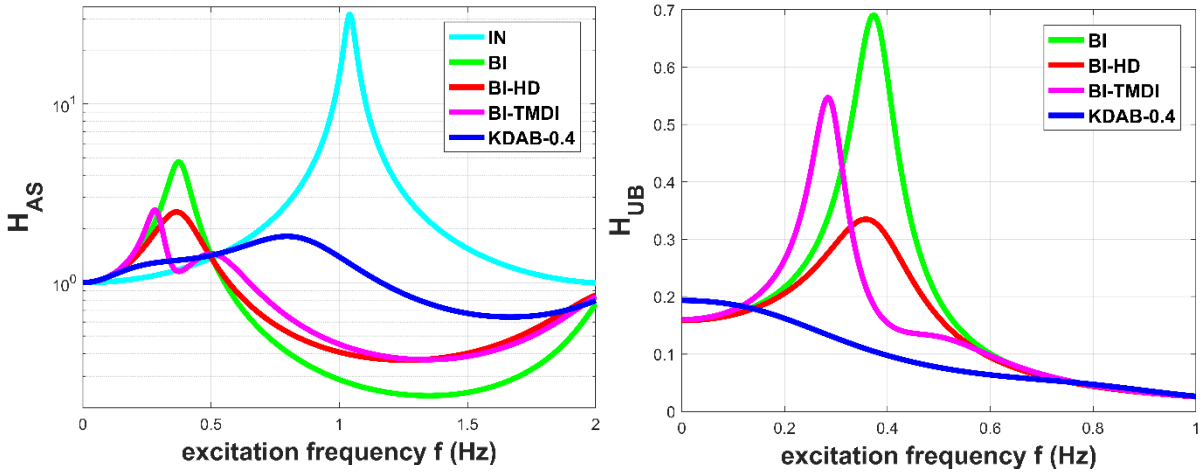

(a) (b)

Figure 4.28: *Transfer Functions of the main system responses: (a) structure's absolute acceleration H_{AS} for the initial (IN) and the control systems: BI, BI-HD, BI-TMDI and KDAB-0.4, and (b) base's relative displacement H_{UB} for the control systems: BI, BI-HD, BI-TMDI, and KDAB-0.4.*

The increase of the damping ratio from 5% (BI) to 20% (BI-HD), reduces the maximum values of the transfer functions, retaining the same frequency range. The BI-TMDI system improves the dynamic behavior in terms of the absolute acceleration H_{AS}, compared with the BI and BI-HD, while at the same time, the H_{UB}, compared with the BI-HD, is not improved. The KDAB-0.4 system dramatically reduces the H_{UB} in all the frequency range. However, although the maximum value of H_{AS} is greatly reduced, more than all the aforementioned systems, retains a large frequency range. The effect of the natural frequency f_0, of the KDAB system, on the Transfer Functions of the system main responses, is presented in Figure 4.29.

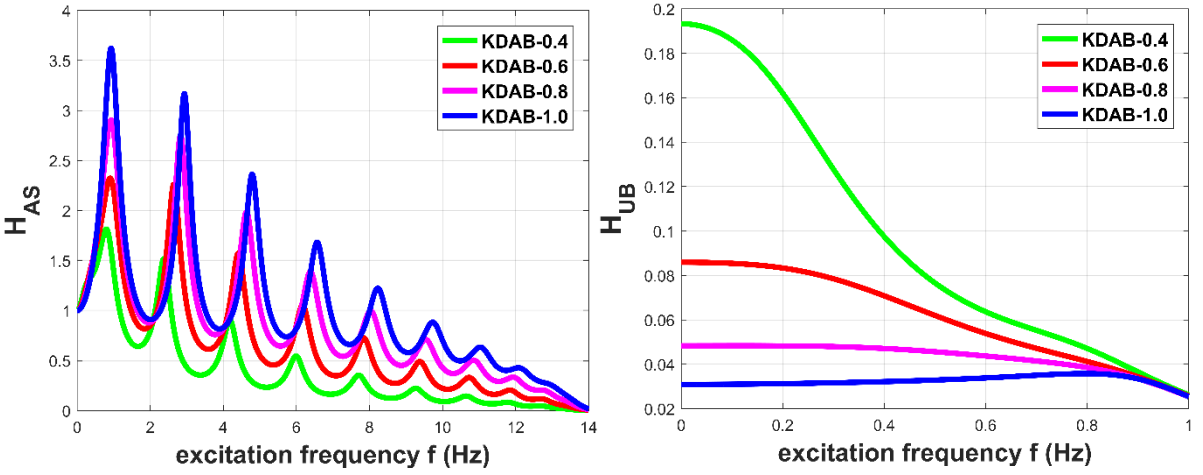

(a) (b)

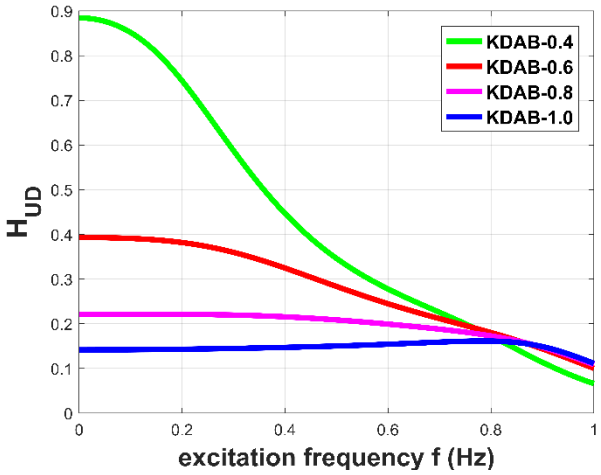

(c)

Figure 4.29: *Transfer Functions of the main system responses: (a) structure's absolute acceleration (top floor) H_{AS}, (b) structure's base relative displacement H_{UB} and (c) KDamper relative displacement H_{UD} for all the selected nominal frequencies of the KDamper: KDAB-0.4, KDAB-0.6, KDAB-0.8, and KDAB-1.0.*

The absolute acceleration transfer function H_{AS} is improved in all the frequency range, as the natural frequency f_0 decreases. On the other hand, by increasing the natural frequency f_0, the transfer functions H_{UB} and H_{UD}, which relate to the base's and the damper's relative displacement respectively, are dramatically improved in all the frequency range.

Comparative results between the BI and the KDAB-1.0 system are presented in Figure 4.30. The presented time histories relate to: 1) an artificial accelerogram, 2) Kocaeli earthquake record, and 3) Tabas earthquake record.

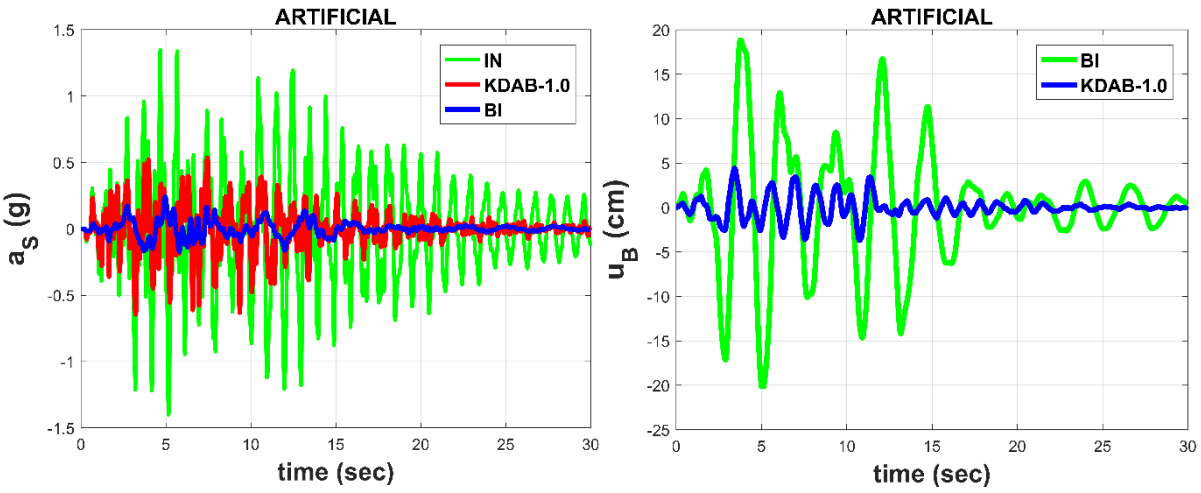

(a) (b)

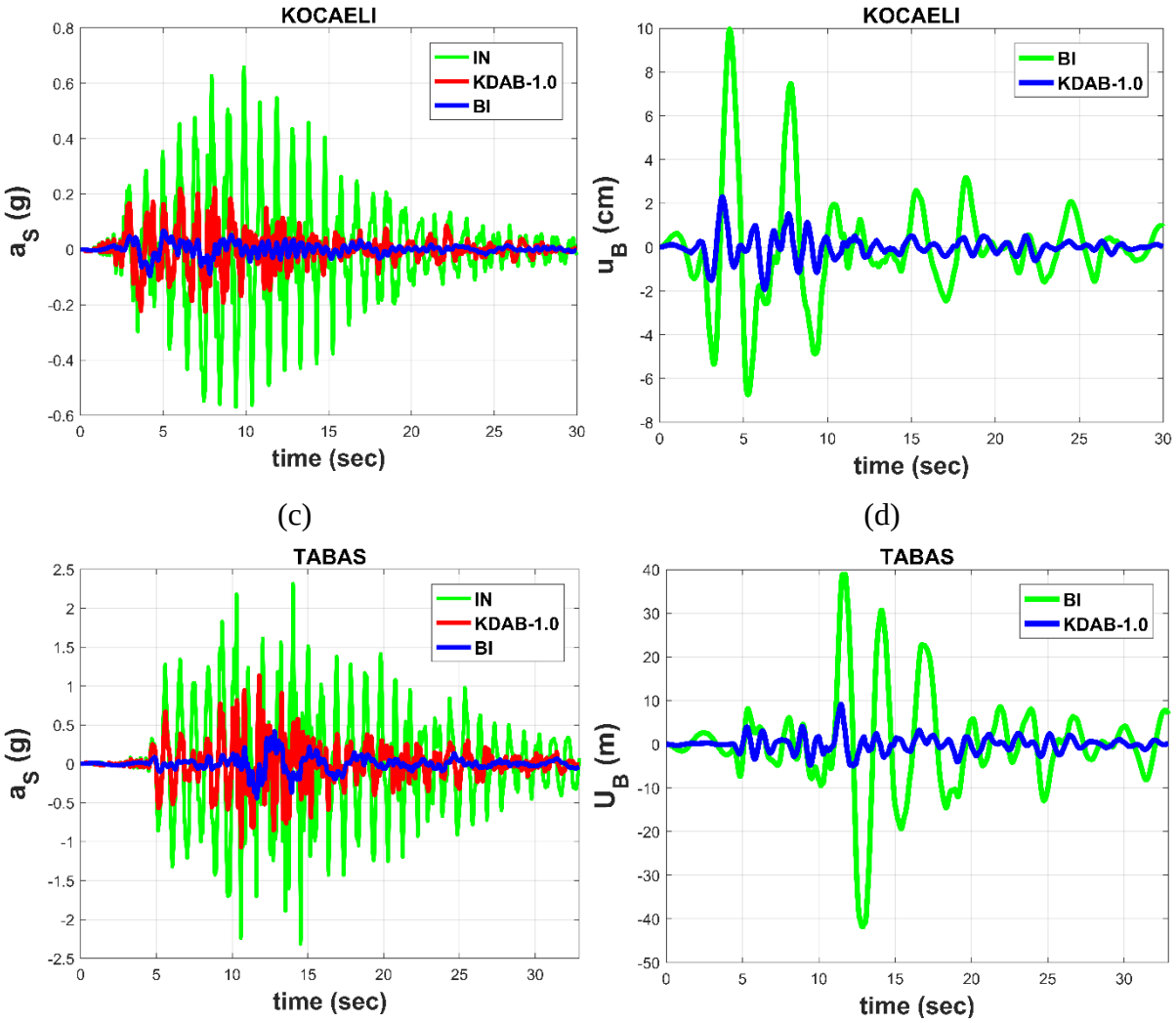

Figure 4.30: *Comparative results, in terms of structure's absolute acceleration (g) and base's relative displacement (cm), between the BI and the KDAB-1.0 system, for (a,b) an artificial accelerogram, (c,d) the Kocaeli, and (e,f) Tabas earthquake record.*

The system main dynamic responses, considering the max values of the dynamic responses for all the Artificial Accelerograms in the database (mean of 30 maximum values), as well as the selected real near fault and far fault earthquake records in this paper (mean of 10 max each) presented in Table 4.5, of the initial (IN) 10-story concrete building structure, and the considered concepts for base isolation/absorption (BI, BI-HD, BI-TMDI, KDAB-f_0) are presented in Figure 4.31.

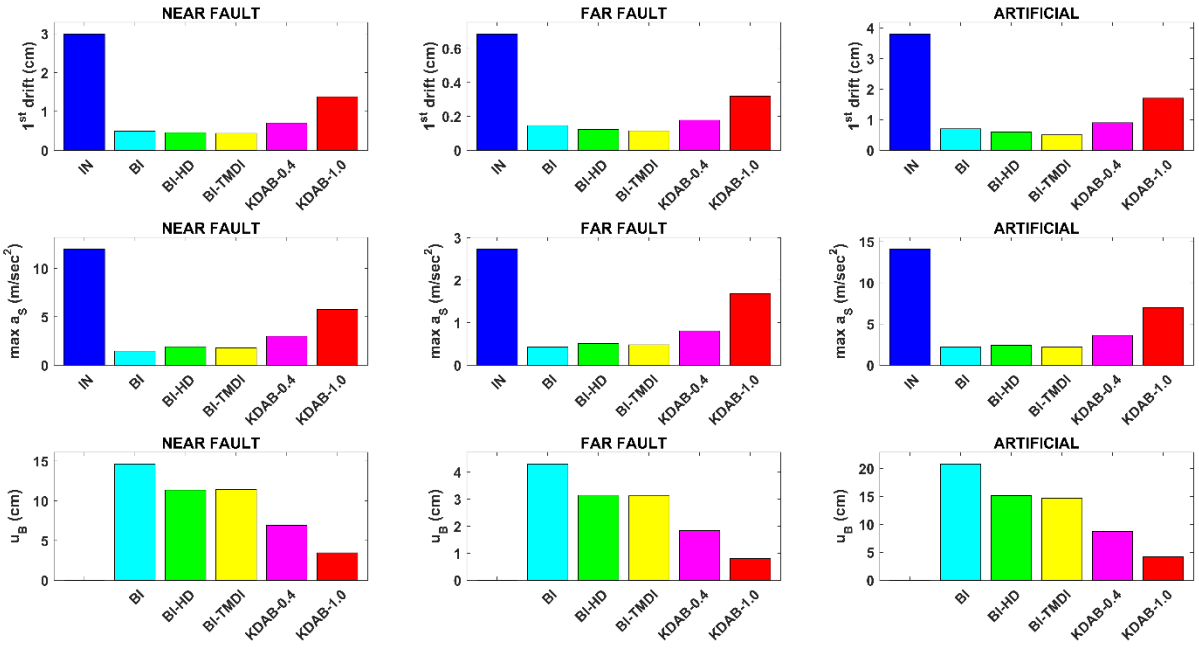

Figure 4.31: *Max values of the main dynamic responses of the examined control systems (BI, BI-HD, BI-TMDI, KDAB-f_0), for all the artificial accelerograms (mean of 30 max), real near-fault earthquake records (mean of 10 max) and real far fault earthquake records (mean of 10 max).*

4.4 Concluding Remarks

In this Chapter, the KDamper is implemented for horizontal seismic protection as an alternative or possible supplement of a conventional seismic isolation base. The KDamper parameters are selected according to the procedure described in section 3.2.2 of Chapter 3, for optimal acceleration response. For the selection of the KDamper nominal frequency, three spectra driven approaches are considered. The ground acceleration excitation PSD is calculated according to section 3.3.2.1 of Chapter 3, according to the provisions of the EC8 seismic design codes. In the first approach, a SDoF system controlled with KDamper is considered, in the second approach the KDamper is implemented as an Absorption Base (KDAB) of a SDoF system, and finally, in the third approach the KDAB is examined in multi-story structures. Subsequently, where the devices are realistically designed. More specifically, the NS element is realized according to the Proposed Configuration I of Chapter 3, and the rest of the KDamper components are realized with conventional structural elements. Finally, the performance of KDamper is assessed with real earthquake records. Based on the dynamic analysis and the results obtained, the following concluding remarks can be made:

i. The spectra driven approaches (Approach I-III) for the selection of the KDamper nominal frequency are very accurate, as confirmed in the time domain.

ii. The indicative design of the KDamper devices proves that the additional mass, the artificial damper, and the stiffness elements, of each implemented device, are within reasonable technological capabilities.

iii. Following the proposed procedure for the realization of the negative stiffness element, the results of the non-linear problem are in a very good agreement to that of the initial linear problem.

iv. The KDamper can be implemented effectively as an alternative to the conventional seismic isolation approaches, achieving reductions of more than 50% to the superstructure's dynamic responses, as compared to the initial system, while retaining the base displacement in the order of a few centimeters, 70% lower as compared to the highly damped base isolated system.

v. The performance of KDamper assessed with real earthquake records, confirms the effectiveness of KDamper implemented in SDoF, as well as, multi-story building structures.

vi. The KDamper with a nominal frequency equal to the low frequency of a conventional base isolation system (*0.4 Hz*), mentioned in this Chapter as KDAB-0.4, presents similar reductions to the structure's maximum absolute accelerations with the BI, BI-HD and BI-TMDI systems. At the same time, the base's relative displacement is greatly reduced compared with all the base-related isolation concepts. More specifically, a reduction of more than *50%* to the base's relative displacement, is observed, compared with the BI system, thus making the KDamper concept a possible supplement to the classical base isolation system.

vii. The KDamper implemented with a nominal frequency much higher (*1 Hz*) than that of the BI system (*0.4 Hz*), mentioned in the paper as KDAB-1.0, leads to a drastic reduction of the base's relative displacement ($u_{B,\ KDAB\text{-}1}$*=4-5 cm*). Compared with all the base-related isolation concepts, the base's relative displacement is reduced more than two times, combined with acceptable structural performance with respect to the structure's relative displacement and absolute acceleration, with reductions more than *50%*, compared to the initial structure (IN). As a consequence, the KDamper can be implemented as α "stiff seismic absorption base", overcoming the disadvantages of the conventional base isolation systems, and thus leading towards alternative seismic protection technologies.

Chapter 5

Horizontal Seismic Protection with Extended KDamper Designs

5.1 Introduction

As presented in Chapter 4, the KDamper is effectively implemented for horizontal seismic protection of SDoF, as well as MDoF (multi-story buildings) structural systems. Based on comparison with various base isolated (BI) structures, conventional, highly damped, and combination of BI with Tuned Mass Damper Inerters (TMDI), the KDamper manages to greatly improve the system dynamic behavior, in terms of structural absolute accelerations, and at the same time retains the structural relative (base) displacements in the order of a few centimetres, 50-70% lower than the aforementioned BI systems. However, the negative stiffness element stroke's relative displacement value is usually high, and renders the design of a realistic configuration regarding the NS element rather difficult. In addition, the base displacements required for the KDamper to be effective may be low, as compared with other BI system, but in most cases remain prohibitive for retrofitting in existing structures, or realization with conventional structural elements.

For this reason, this Chapter investigates alternative designs of KDamper that aim to further reduce the structural relative displacements required (base displacement and NS element stroke) to acquire the desired improvement in the superstructure dynamic behavior. Initially, an extension of KDamper (EKD) is introduced in section 5.2 of this Chapter, that aims to reduce the NS element stroke. The optimization of the proposed extension in presented, and the EKD is implemented for horizontal seismic protection of SDoF, as well as multi-story building structures. Based on the numerical results, the performance of the EKD indeed manages to greatly improve the structural dynamic hehavior, and simultaneously significantly reduces the NS element stroke and base displacements, rendering its realization realistic. Finally, section 5.3 examines retrofitting options of the EKD for seismic protection of multi-story building structures.

Section 5.4 introduces a stiff base absorber (SBA) which is a combination of the extend KDamper concept with an inerter. This idea is based on decreasing the nominal system frequency with the inerter, and thus attract lower seismic forces, without having to reduce the structural stiffness. Subsequently, the EKD controls the structural relative displacements with the extraordinary damping properties it offers. The optimization problem for the design of the SBA is presented, and is then implemented in SDoF and MDoF structural systems. Based on the numerical results, the superstructure dynamic behavior is greatly improved, and at the same time, the small base displacements and NS element stroke, render the implementation of the proposed control system, SBA, feasible using conventional structural elements, making it the most efficient and realistic retrofitting option for horizontal seismic protection.

5.2 Seismic Protection Configurations Based on Extended KDamper

In this section, the proposed extension of KDamper (EKD), presented thoroughly in section 2.3.2 is implemented in structural systems for seismic protection from horizontal ground motions. The parameters of the EKD are selected following a dedicated optimization procedure base on engineering criteria. The EKD dynamic performance is examined with real earthquake records and realistic configurations regarding the realization of the NS element. Finally, the design of EKD is extended for implementation in the bases of multi-story building structures.

5.2.1 Optimal Design of Extended KDamper (EKD)

The configuration of the extended KDamper (EKD) is presented in section 2.3.2 of Chapter 2, along with the equations of motions and the Transfer Function of the system main responses. Similarly to the KDamper, it incorporates a negative stiffness element. The difference between these two concepts is that in the proposed configuration the positive stiffness element k_{PS} connects the additional mass m_D to the base, instead of the negative stiffness element k_{NS}, which now connects m_D to the structure. Furthermore, an artificial damper is placed in parallel to the negative stiffness element. Equation (2.23) still stands, as the overall static stiffness is maintained. However, increasing the absolute value of k_{NS}, or decreasing the absolute values of k_{PS} or k_R, may endanger the static stability of the structure. Although theoretically the values of k_{NS}, $k_{PS,}$ and k_R are selected according to Equation (2.23) to ensure the static stability, due to various reasons, such as temperature variations, manufacturing tolerances, or non-linear

behavior, k_{NS}, k_{PS} and k_R may present significant variations in practice, since almost all negative stiffness designs result from unstable non-linear systems. Consequently, an increase of the absolute value of k_N and/or a decrease of the values of k_{PS} *and* k_{RS} by a factor ε_{NS}, ε_{PS} and ε_R, respectively, may result in the system being unstable:

$$(1-\varepsilon_R)k_R + \frac{(1-\varepsilon_{PS})k_{PS}(1+\varepsilon_{NS})k_{NS}}{(1-\varepsilon_{PS})k_{PS} + (1+\varepsilon_{NS})k_{NS}} = 0 \tag{5.1}$$

Contrary to the KDamper concept, which foresees variation only in the negative stiffness element k_{NS}, in the proposed extension of the KDamper concept, a variation in all stiffness elements are taken into account. Assuming the negative stiffness ratio $kn=k_{NS}/k_0$ or the absolute value of the negative stiffness element k_{NS} is known, using Equations (2.23) and (5.1), the rest of the stiffness elements result as:

$$kr = \frac{-b-\sqrt{b^2-4*a*c}}{2a} \Rightarrow k_R = kr*k_0 \tag{5.2.a}$$

$$kp = \frac{kn-kr*kn}{kr+kn-1} \Rightarrow k_{PS} = kp*k_0 \tag{5.2.b}$$

where parameters *a*, *b* and *c* are defined as:

$$a = R(P-N) \tag{5.3.a}$$

$$b = kn*N(P-R)+R(N-P) \tag{5.3.b}$$

$$c = -P*N*\mathrm{kn} \tag{5.3.c}$$

$$(1-\varepsilon_R) = R \tag{5.4.a}$$

$$(1+\varepsilon_{NS}) = N \tag{5.4.b}$$

$$(1-\varepsilon_{PS}) = P \tag{5.4.c}$$

5.2.1.1 Statement of the Optimization Problem

Assuming that the following parameters of the EKD system are known: a) the additional mass m_D, and b) the stability factors ε_{NS}, $\varepsilon_{PS,}$ and ε_R, the free design variables sought in the optimization problem are:

1. the nominal EKD frequency f_0;
2. the value of the negative stiffness (NS) element k_{NS};
3. the damping coefficients c_{NS} and c_{PS};

The design of the proposed control strategy must be efficient and realistic at the same time. For this reason, proper constraints that refer to the structural dynamic responses must be applied. More specifically, the system is subjected to 30 Artificial Accelerograms generated according to section 3.3.2.1 of Chapter 3. The relative to the base structure displacement is set as the objective function (mean of 30 maximum responses). In order to better observe the efficiency of the proposed configuration, an acceleration filter is placed. Therefore, each set of optimized parameters of the extended KDamper refers to the maximum structure acceleration, expressed as a percentage of mean PGA. The mean PGA of the 30 Artificial Accelerograms of the database is *0.519g*. Finally, the limits of the free design variables and the constraints imposed in the system dynamic responses must be within reasonable technological capabilities in order for design to be realistic. In particular:

i. In previous work of KDamper (I Antoniadis et al., 2019; I Antoniadis et al., 2019; Kapasakalis, Antoniadis and Sapountzakis, 2019a, 2019b, 2019c, 2019e), the stability factor ε_{NS} that relates to the variation of the negative stiffness element k_{NS}, is taken as *5%*. In this Chapter, a variation in all stiffness elements is taken into account, making the design of the proposed vibration absorption concept pretty conservative, since all the stability factors ε_{NS}, ε_{PS} and ε_R are selected equal to *10%*.
ii. The purpose of this design is to implement the proposed control strategy for seismic protection of building structures. Since KDamper can be implemented in the bases of structures, there are no strict limitations regarding the additional mass. According to the previous work of KDamper implemented as an Absorption Base (KDAB) of multi-story building structures in (I Antoniadis et al., 2019; Kapasakalis, Antoniadis and Sapountzakis, 2019a, 2019b, 2019c, 2019e), an *5%* additional mass is efficient and realistic.
iii. The stiffness elements must be within reasonable technological capabilities. The negative stiffness element k_{NS}, in the proposed configuration of EKD, is realized with the Proposed Configuration I presented in Chapter 3, with pre-compressed springs. Based on previous indicative designs of KDamper with pre-compressed springs in (Antoniadis et al., 2018) and in (Kapasakalis, Antoniadis and Sapountzakis, 2019d), for a total superstructure mass of *300 tn*, a realistic value of k_{NS} is *-34171 kN/m*. In this

section, the negative stiffness element is set at least *50%* lower. The same reduction applies to the rest of the stiffness elements, $k_{R,}$ and k_{PS}.

iv. The damping coefficients maximum value is set *600 kNs/m* for the whole configuration (multiple KDamper devices can be implemented), therefore, common linear damping devices can be used.

v. The negative stiffness element stroke ($X_{S\text{-}D}$) is set as a constraint, with an upper limit that of *15 cm*, which based on previous work of Kapasakalis (Kapasakalis, Antoniadis and Sapountzakis, 2019d) proves to be a realistic value for the design of the negative stiffness element with pre-compressed springs.

Finally, the limits of the free design variables are: a) the nominal KDamper frequency f_0 (*Hz*) [*0.15 1.5*], b) the negative stiffness element k_{NS} (*kN/m*) [*-15000 -1*] and c) the damping coefficients c_{PS} and c_{NS} (*kNs/m*) [*1 600*].

Based on the previous, each set of optimized parameters, for a reference structure mass of *300 tn* is presented in Table 5.1. Each set of optimized parameters refers to the maximum structure acceleration. The extended KDamper (EKD) with Acceleration Filter as a percentage of PGA will be referred hereafter as EKD-*AF (%)*. The system dynamic responses (mean of max values) of the proposed vibration absorption system (EKD) are presented in Figure 5.1.

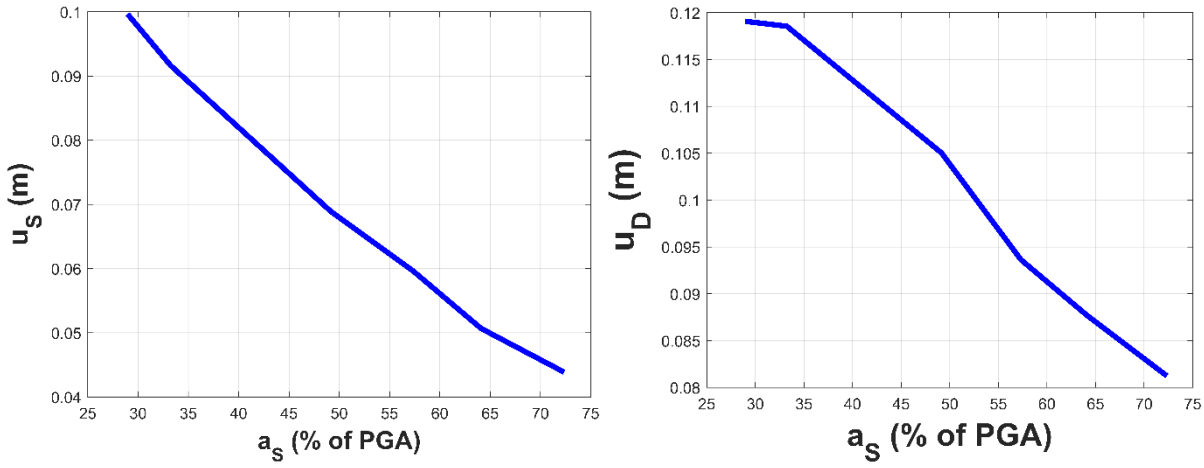

(a) (b)

Figure 5.1: *(a) Structure relative displacement and (b) negative stiffness element stroke displacement maximum values over the structure absolute acceleration expressed as a percentage of the mean PGA (Acceleration Filter).*

Furthermore, the EKD is compared with the previous optimal design of KDamper, designed for optimal acceleration response, as presented in section 3.2.2 of Chapter 3. For this

reason, two sets of parameters of each concept, that present similar results, in terms of the structure's main dynamic responses, are selected and compared in Table 5.2.

Table 5.1. *Set of optimized parameters with respect to the imposed acceleration filter (AF) following the procedure described in section 3.2.*

Acceleration Filter *AF* (%), (a_S=*AF* *PGA)	f_0 (*Hz*)	k_N (*kN/m*)	k_P (*kN/m*)	k_R (*kN/m*)	C_{UP} (*kNs/m*)	C_{DOWN} (*kNs/m*)
30	0.3965	-5815.3	34587	8946	581.3	473.8
40	0.377	-4145.4	16601	7292	590.8	224.4
50	0.664	-9246.7	26575	19664	541.3	91.1
60	0.7287	-8909.3	21968	21591	571.9	262.6
70	0.9857	-14857	34747	38038	517.8	115.6
80	1.02	-12440	25887	36844	577.8	21.5

Table 5.2. *Comparison of the SDOF system implemented with KDamper and EKD.*

Set of parameters	Examined system	A_S (*m/sec2*)	% (reduction)	U_S (*m*)	U_{NS} (*m*) NS Stroke	ε_i (%)
Set #1	EKD	1.725	66.76	0.092	0.118	$\varepsilon_{NS,PS,R}=10$
	KDamper in	2.085	59.83	0.093	0.363	$\varepsilon_{NS}=5$
Set #2	EKD	3.755	27.65	0.0439	0.0812	$\varepsilon_{NS,PS,R}=10$
	KDamper in	3.692	28.86	0.0379	0.163	$\varepsilon_{NS}=5$

The Transfer Functions of the EKD system main responses are plotted in Figure 5.2, for different values of the acceleration filter (*AF*). It is observed that as the acceleration filter increases, the peak of the absolute acceleration Transfer Function H_{AS} also increased along with its frequency content. That is to be expected due to the fact that as the acceleration filter increases, the permissible structural maximum acceleration also increases. On the other hand, by increasing the acceleration filter, the structural relative displacement Transfer Function H_{US} and EKD relative displacement Transfer Function H_{UD} are dramatically improved in all frequency range, as observed from Figures 5.12.a and b. This remark again is to be expected, because as the acceleration filter increases, the system becomes stiffer, and as a result the displacements (structural and EKD's) are reduced.

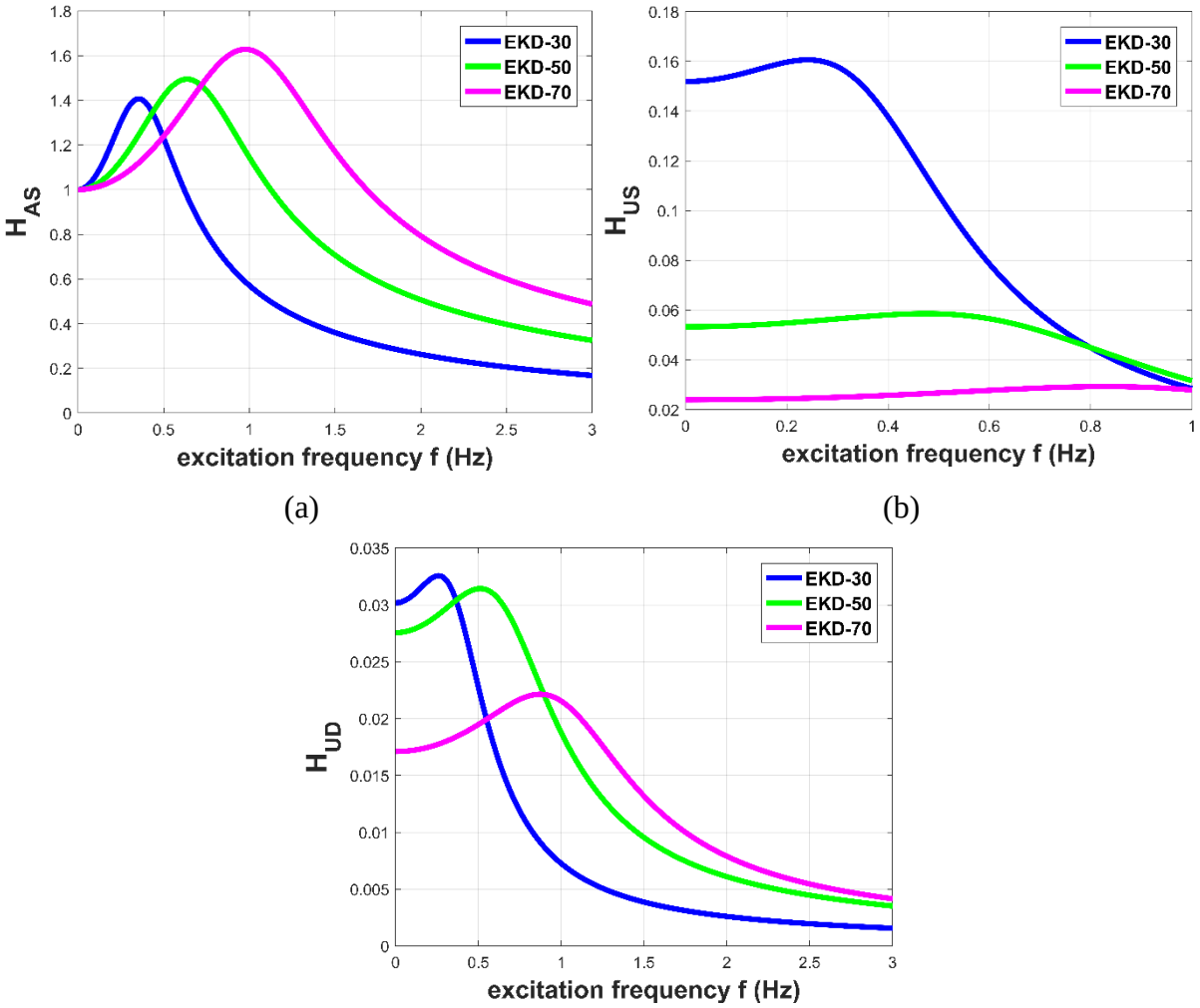

Figure 5.2: *Transfer Functions of the main system responses: (a) structure's absolute acceleration H_{AS}, (b) structure's relative displacement H_{US}, and (c) EKD relative displacement H_{UD} for different values of the acceleration filter AF.*

5.2.1.2 Numerical Example 1 – *SDoF Dynamic Performance and Detuning Phenomena*

Real earthquake ground excitations aren't stationary and do not have a fixed duration. For this reason, it is very important to examine the effectiveness of the proposed vibration absorption concept (EKD) also with real strong earthquake records. In this section, 24 real earthquake records are selected. They are widely used in the literature and are known to have had a devastating impact on structural systems. Table 5.3 presents the details of each ground motion. Earthquakes with an epicentral distance R_{jb} of fewer than *25 km*, are classified as near-fault earthquakes.

Table 5.3: *List and information of the considered real earthquake records.*

No	Earthquake	Year	Station	Ground Motion	Mw	PGA (g)	R_{jb} (km)	$DUR_{5\text{-}75\%}$ (sec)
1	Northridge-N	1994	N Hollywood	Near fault	6.69	0.309	7.89	7.0
2	Northridge-F	1994	Montebello	Far fault	6.69	0.176	43.2	7.8
3	Loma Prieta-N	1989	Corralitos	Near fault	6.93	0.645	0.16	4.6
4	Loma Prieta-F	1989	APEEL 10-Skyline	Far fault	6.93	0.103	41.9	8.3
5	L'Aquila-N	2009	V. Aterno	Near fault	6.3	0.402	0.0	4.7
6	L'Aquila-F	2009	Ortucchio	Far fault	6.3	0.066	35.1	6.2
7	Chi-Chi-N	1999	CHY006	Near fault	7.62	0.359	9.76	5.6
8	Chi-Chi-F	1999	CHY012	Far fault	7.62	0.063	59.0	42.8
9	Kocaeli-N	1999	Izmit	Near fault	7.51	0.165	3.62	8.2
10	Kocaeli-F	1999	Fatih	Far fault	7.51	0.162	53.3	27.8
11	Tabas-N	1978	Tabas	Near fault	7.35	0.854	1.79	8.3
12	Tabas-F	1978	Ferdows	Far fault	7.35	0.093	89.8	20.5
13	Kobe-N	1995	Amagasaki	Near fault	6.9	0.276	11.3	6.9
14	Kobe-F	1995	HIK	Far fault	6.9	0.139	95.7	6.1
15	Kozani-N	1995	Kozani	Near fault	6.4	0.207	14.1	3.3
16	Kozani-F	1995	Larisa	Far fault	6.4	0.031	74.1	21.7
17	Niigata-N	2004	NIG017	Near fault	6.63	0.378	4.22	6.1
18	Niigata-F	2004	FKS020	Far fault	6.63	0.043	101	22.5
19	Landers-N	1992	Joshua tree	Near fault	7.28	0.274	11.0	21.7
20	Landers-F	1992	Boron fire station	Far fault	7.28	0.119	89.7	9.6
21	Duzce-N	1999	Lamont 1059	Near fault	7.14	0.1524	4.17	10.4
22	Duzce-F	1999	Mudurnu	Far fault	7.14	0.1203	34.3	9.6
23	Friuli-N	1976	Tolmezzo	Near fault	6.5	0.3571	14.97	2.5
24	Friuli-F	1976	Barcis	Far fault	6.5	0.0292	49.13	4.3

In order to observe the efficiency of the EKD, it is compared with a conventional base isolated (BI) system and a highly damped base isolated system (BI-HD) with damping ratios of *5%* and *20%* respectively. Both base isolated systems are designed to have a base natural frequency of *0.4 Hz*. The system main dynamic responses, considering the max values of the dynamic responses for all the Artificial Accelerograms in the database (mean of 30 max), as well as the selected real near and far fault earthquake records in this paper (mean of 12 max

each), of the rigid body mounted directly on a compliant base, considering all the examined control systems, BI, BI-HD and EKD with Acceleration percentage Filter, EKD-*AF*, are presented in Figure 5.3.

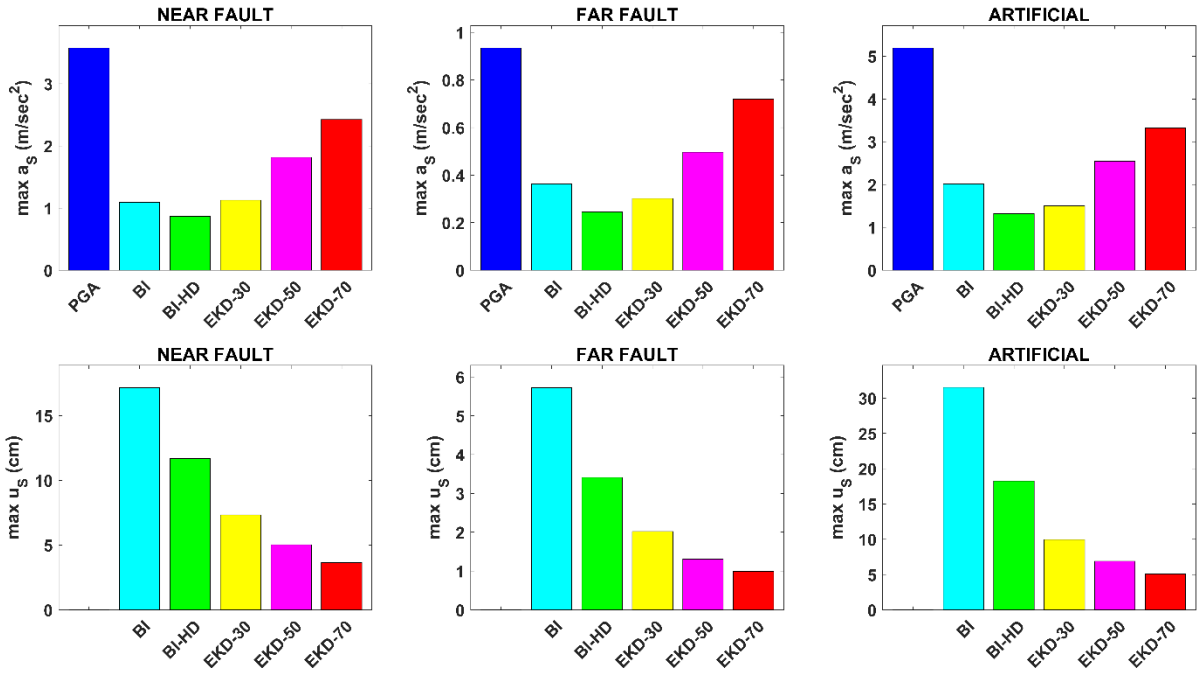

Figure 5.3: *Max values of the main dynamic responses of the examined control systems (BI, BI-HD, EKD-AF), for all the artificial accelerograms (mean of 30 max), real near-fault and far-fault earthquake records (mean of 12 max each).*

Comparative results between the conventional base isolated system (BI) and the EKD-*30* and EKD-70 systems are presented in Figures 5.4 and 5.5. The results concern the Kobe earthquake record and an Artificial Accelerogram.

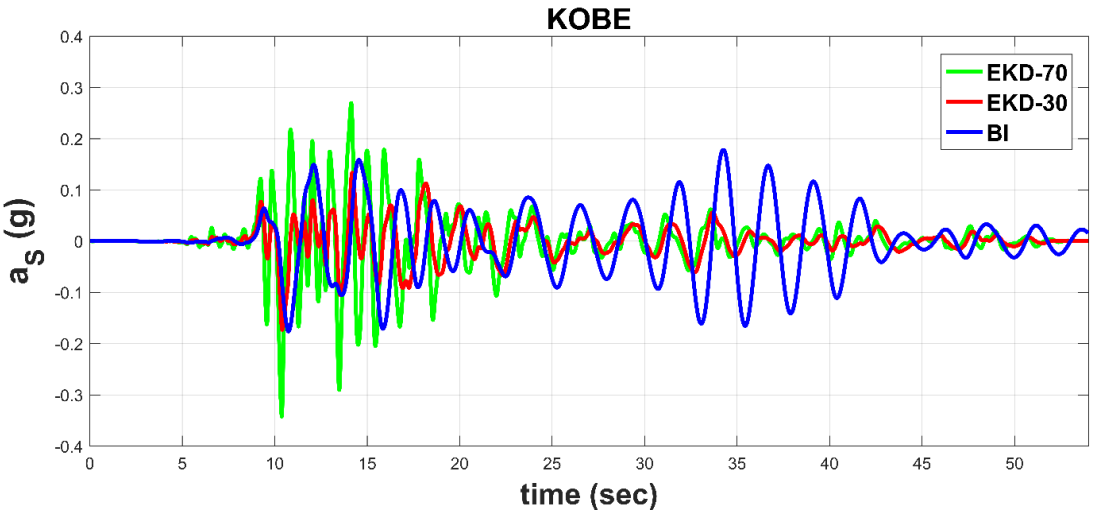

(a)

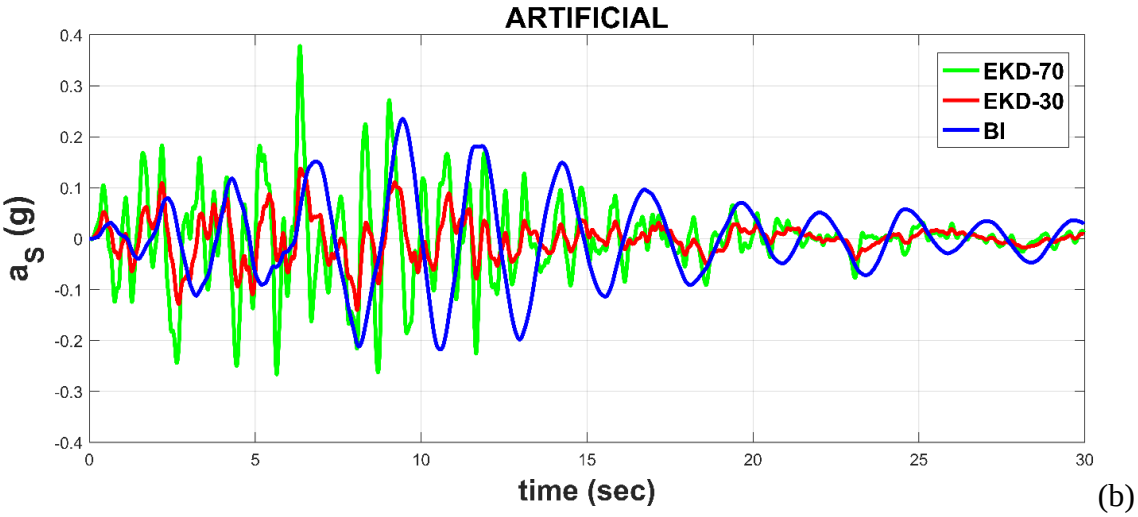

(b)

Figure 5.4: *Comparative results, in terms of structural absolute acceleration (g), between the BI, EKD-30, and EKD-70, for (a) Kobe, and (b) an artificial accelerogram.*

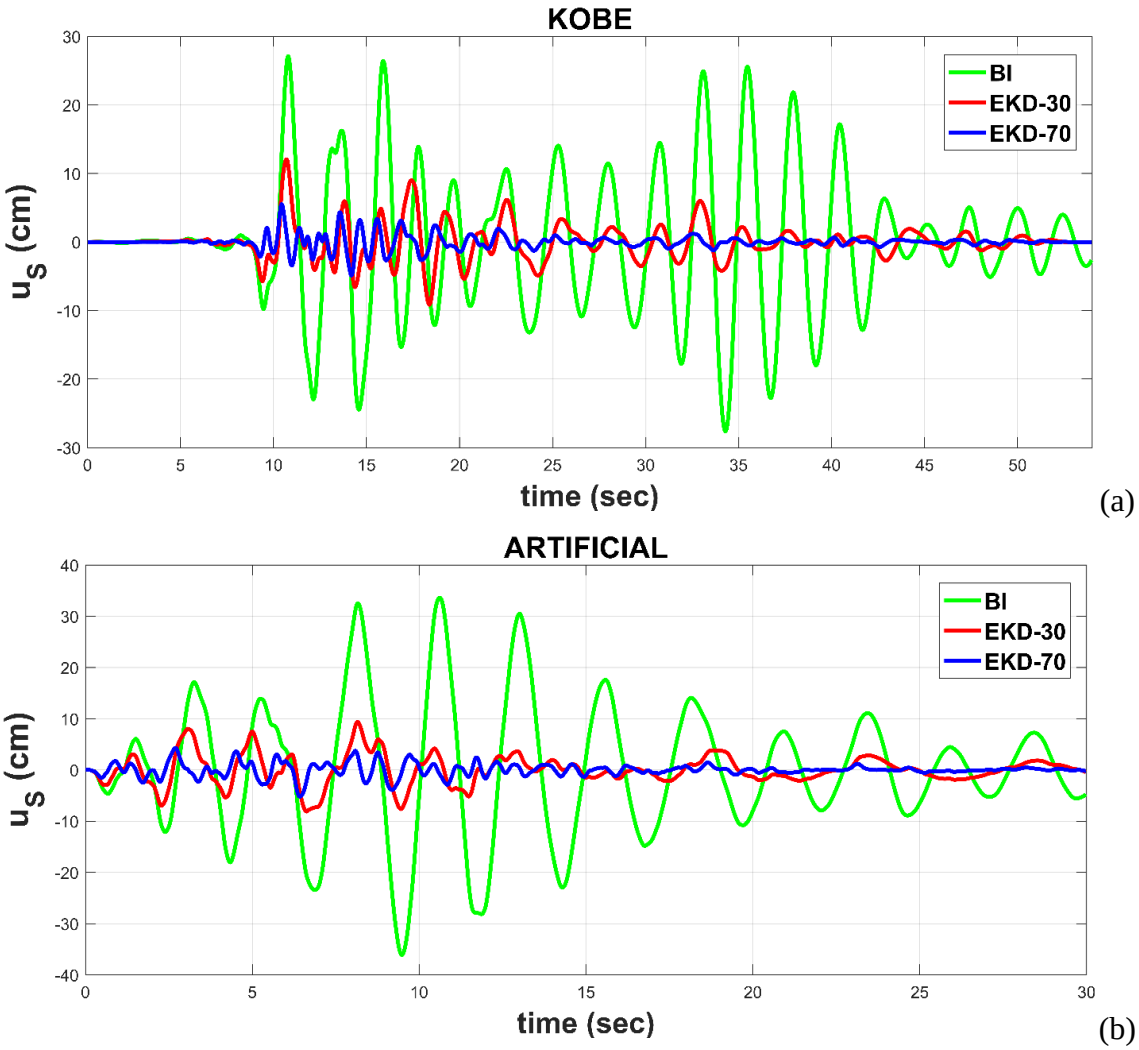

(a)

(b)

Figure 5.5: *Comparative results, in terms of structural relative displacement (m), between the BI, EKD-30, and EKD-70, for (a) Kobe, and (b) an artificial accelerogram.*

It is important to analyze how the main system responses vary by shifting the optimal EKD parameters from their respective values (effect of detuning). We expect that as the system parameters depart from their optimal values (Table 5.1), the effectiveness of the proposed passive vibration control strategy decreases. In Figure 5.6, we observe the effect of detuning of the EKD-*50* set of optimized parameters. The stiffness elements of the EKD are designed to have a *10%* variation as described in the statement of the optimization problem in section 5.2.1.1 of this Chapter. In Figures 6.a-c, the system main responses are depicted in a range of *20%* variation of the optimal stiffness elements. Sensitivity analysis reveals that the variation of the stiffness elements k_{NS} and k_R have a greater influence on the system responses, up to *30%*, compared to k_{PS} (up to *10%*). In Figures 6.d-e, we observe that the variation of the damping coefficient that is parallel to the negative stiffness element, k_{NS}, presents an increased influence, as compared with the camping coefficient parallel with k_{PS}. Finally, the effect of the variation of the additional mass m_D has no significant influence on the system responses.

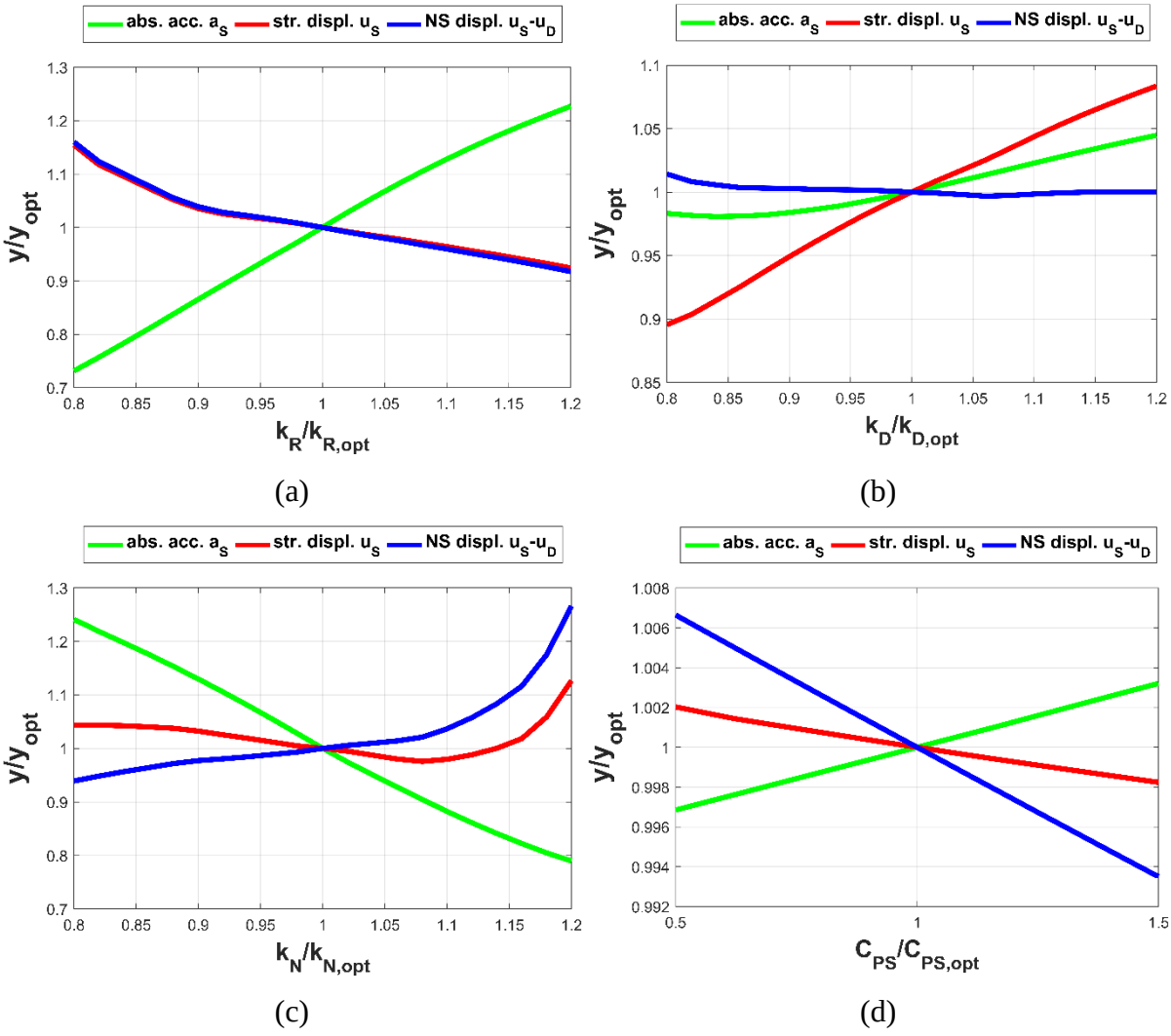

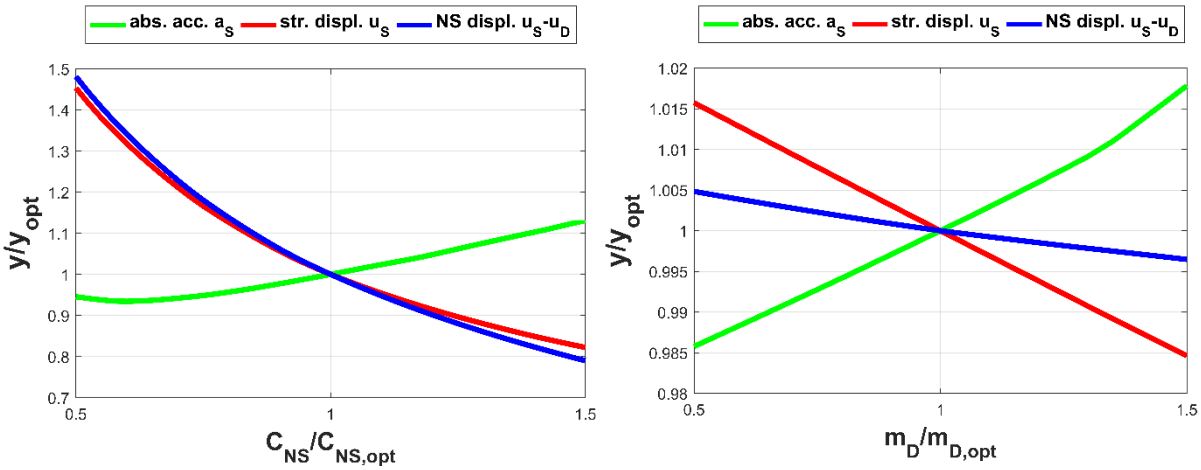

(e) (f)

Figure 5.6: *Sensitivity analysis. Main system responses (mean of 30 max values) by varying the system parameters. (a-c) 20% variation of the stiffness elements and (d-f) 50% variation of the damping coefficients and additional mass.*

Based on the optimization results obtained in section 5.2.1 of this Chapter, and the results from Numerical Example 1, the following remarks can be made:

i. EKD presents similar/marginally superior results as compared to the previously optimal KDamper concept (Kapasakalis et al., 2019c), while it foresees variation in all stiffness elements (ε_N, ε_P, ε_R*=10%*), while in the KDamper concept only the negative stiffness element (ε_N*=5%*) is examined. Furthermore, the negative stiffness element stroke is reduced by *50-67%*, which is critical for the whole configuration design.

ii. The evaluation of the optimization constraints is based on engineering criteria and render the implementation of the EKD feasible. As compared with previous indicative designs of KDamper, all the stiffness elements are at least *50%* lower. Thus, the realization of the additional mass, the damping coefficients, and the stiffness elements are within reasonable technological capabilities.

iii. Based on the performed sensitivity analysis, where the stiffness elements, the additional mass, and the artificial damper varied from their optimal values by 20, 50, and 50%, respectively, the EKD is not vulnerable to detuning.

iv. The EKD implemented in a SDOF system manages to retain the structure absolute acceleration at acceptable levels (based on the selected design Acceleration Filter) while at the same time the structural relative displacement is significantly low, in the order of a few centimeters, 50-80% lower as compared to conventional and highly damped base isolation systems.

5.2.1.3 Numerical Example 2 – *3-Story Building Mounted on EKD*

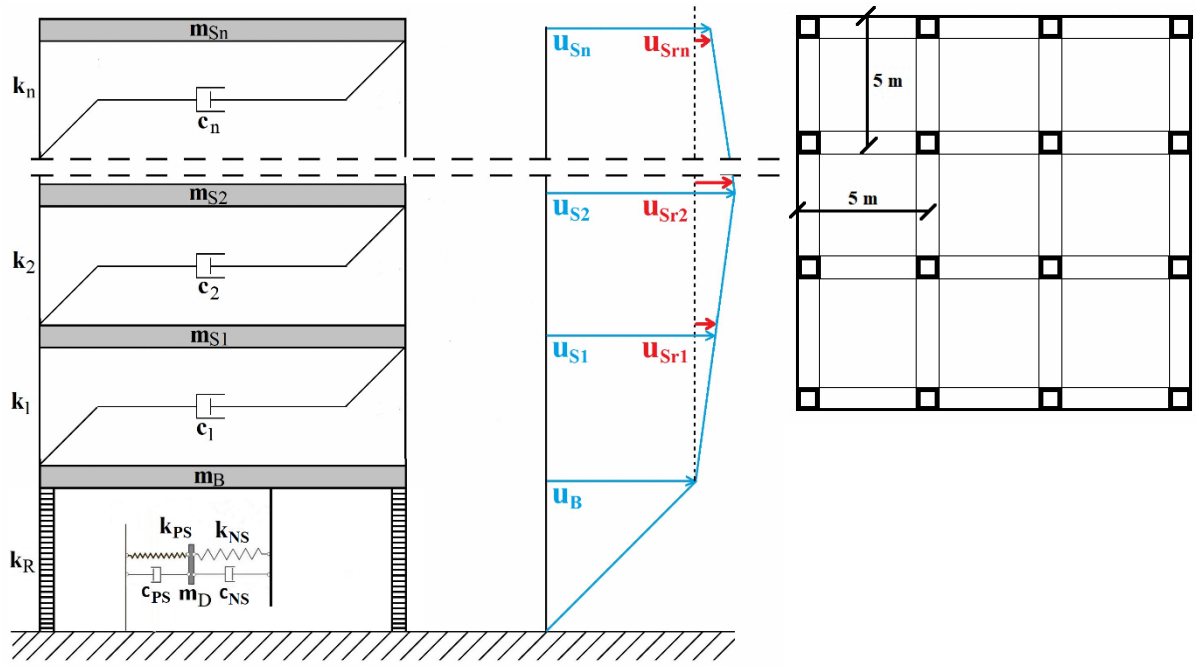

(a) (b)

Figure 5.7: *(a) Multi-story building with the proposed seismic base absorber system, EKD (sketch of the model), and (b) typical ground floor plan of the structure.*

In this numerical example, the proposed control strategy based on an extension of KDamper (EKD) is implemented in the basis of multi-story building structures. A planar *n*-story building is considered and sketched in Figure 5.7.a, in which the proposed absorption system, EKD is implemented for seismic protection. The assumptions made for the modeling of the initial building structure are:

i. the total structure mass is concentrated at the floor levels;
ii. the slabs and grinders on the floors are rigid as compared to the columns;
iii. the columns are considered inextensible and weightless providing the lateral stiffness;
iv. the effect of soil-structure-interaction (SSI) is not taken into consideration;
v. the superstructure is considered to remain within the elastic limit during the analysis;

As a result, the superstructure has *n* dynamic DOFs, represented by the relative to the base displacements of the *n*-story masses m_{Sj} ($j=1,\ldots, n$), as presented in Figure 5.7.a, which are collected in the array $[u_{Sr}](t)=[u_{Sr1}(t), u_{Sr2}(t), \ldots, u_{Srn}(t)]^T$. The equations of motion of the

controlled system with EKD are expressed in a matrix form, involving matrices with dimensions $n+2 \times n+2$.

$$[M][\ddot{u}(t)]+[C][\dot{u}(t)]+[K][u(t)]=-[\tau]a_G(t) \quad (5.5)$$

A 3-story symmetric-plan concrete building structure is considered, with a typical ground floor plan as sketched in Figure 5.7.b. The original structure has 3 dynamic DoFs represented by the relative to the ground/base displacements of the 3 stories. The elastic modulus is $E=26$ *GPa* (typical value for a reinforced concrete frame), the mass of the superstructure is concentrated at the floor levels, with $m_i=80$ *tn* denoting the mass of the 3 floors ($i=1$-3). Applying the classical modal analysis to the superstructure, the following natural periods results as: T_{Si} *[sec] = [0.4953, 0.1768, 0.1223]*. The basement mass is assumed to be $m_B=60$ *tn*, so resulting in a base mass ratio $\mu_B=0.25$. The damping coefficients of the original superstructure are assumed to be mass and stiffness proportional (Rayleigh damping) with $\zeta_{Si}=0.02$ ($i=1$-3).

The calculation of the matrices of mass [M], stiffness [K], and damping [C] of the initial 3-story structure, the procedure from which the KDAB design is extended for implementation in MDoF structural systems, as well as the Transfer Functions of the controlled system with the KDAB are presented in Appendix A2.

The systems main dynamic responses, considering the maximum values of the dynamic responses for all the Artificial Accelerograms in the database (mean of 30 maximum values), as well as the selected real near fault and far fault earthquake records in this paper (mean of 12 max each) presented in Table 5.3, of the initial (IN) 3-story concrete building structure, and the considered concepts for base isolation/absorption (BI, BI-HD, EKD-*AF*), are presented in Figures 5.8 and 5.9.

Comparative results: a) of the top floor absolute accelerations between the initial (IN), the conventional Base Isolated system (BI) and the EKD-*70*, are presented in Figure 5.10, b) of the base relative displacement between the BI, EKD-*30* and EKD-*70* are presented in Figure 5.11 and c) the total base shear of the IN and the EKD-70 systems as well as the base shear that relates only to the independent element k_R of the EKD-*70*, are presented in Figure 5.12. The presented time histories relate to: 1) the Loma Prieta earthquake record, and 2) an Artificial Accelerogram.

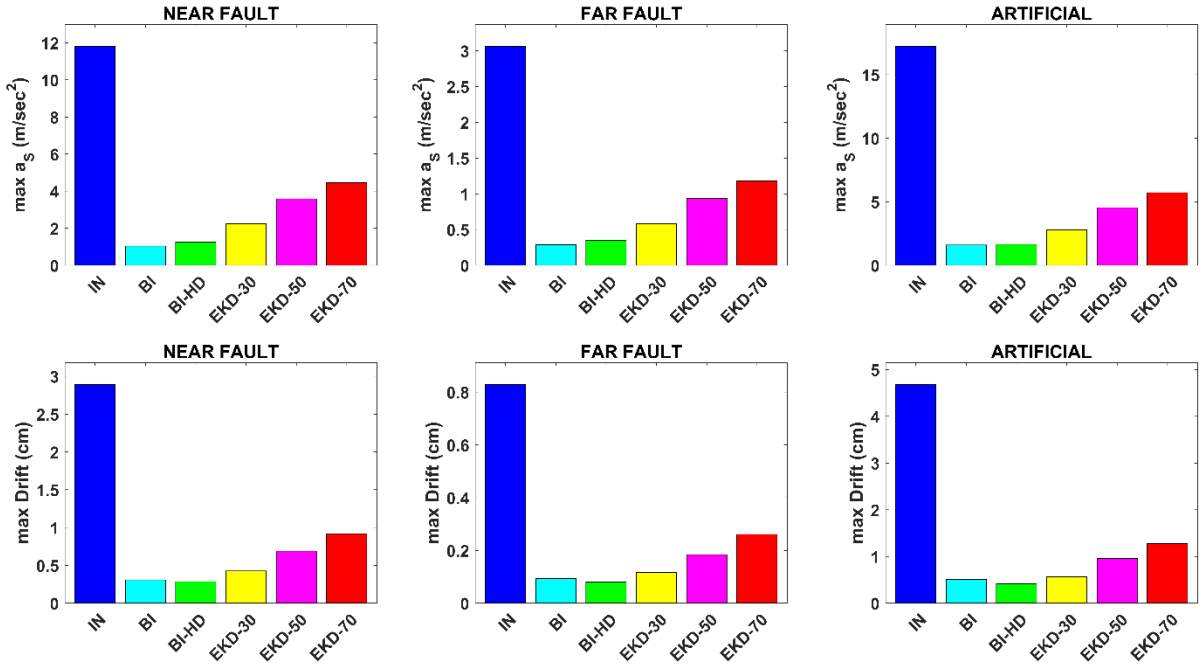

Figure 5.8: *Max values of the superstructure floor absolute accelerations and inter-story drifts of the examined control systems (BI, BI-HD, EKD-AF) for all the artificial accelerograms (mean of 30 max), real near-fault earthquake records (mean of 12 max) and real far-fault earthquake records (mean of 12 max).*

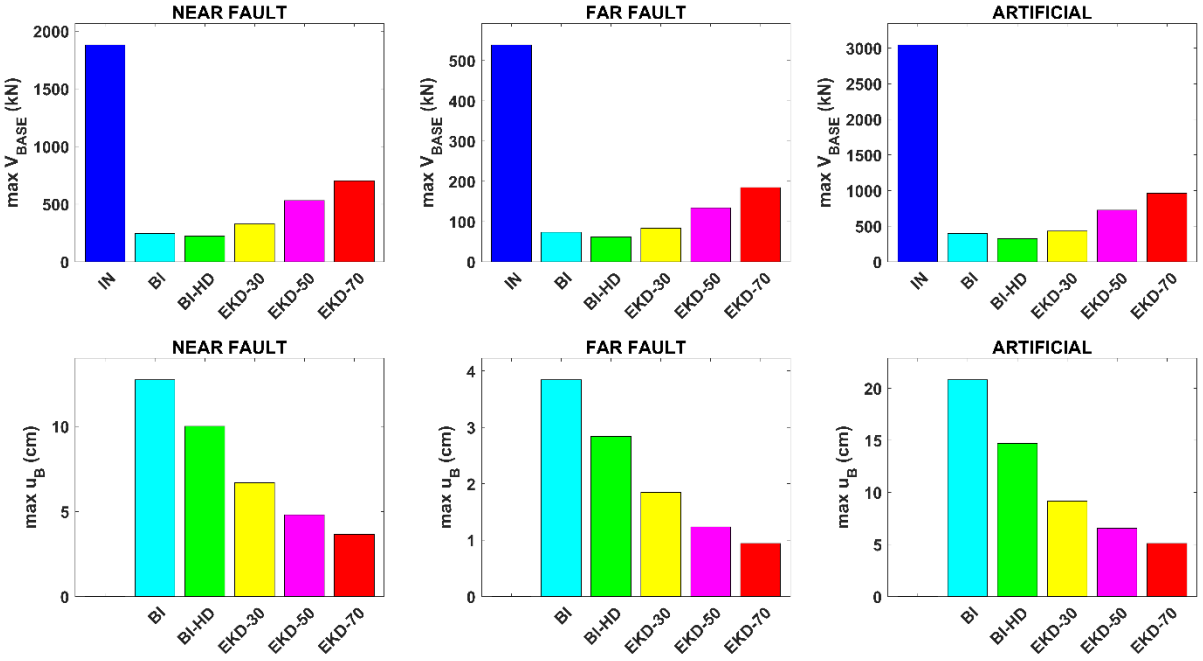

Figure 5.9: *Max values of the base shear and base relative displacement of the examined control systems (BI, BI-HD, EKD-AF) for all the artificial accelerograms (mean of 30 max), real near-fault earthquake records (mean of 12 max) and real far-fault earthquake records (mean of 12 max).*

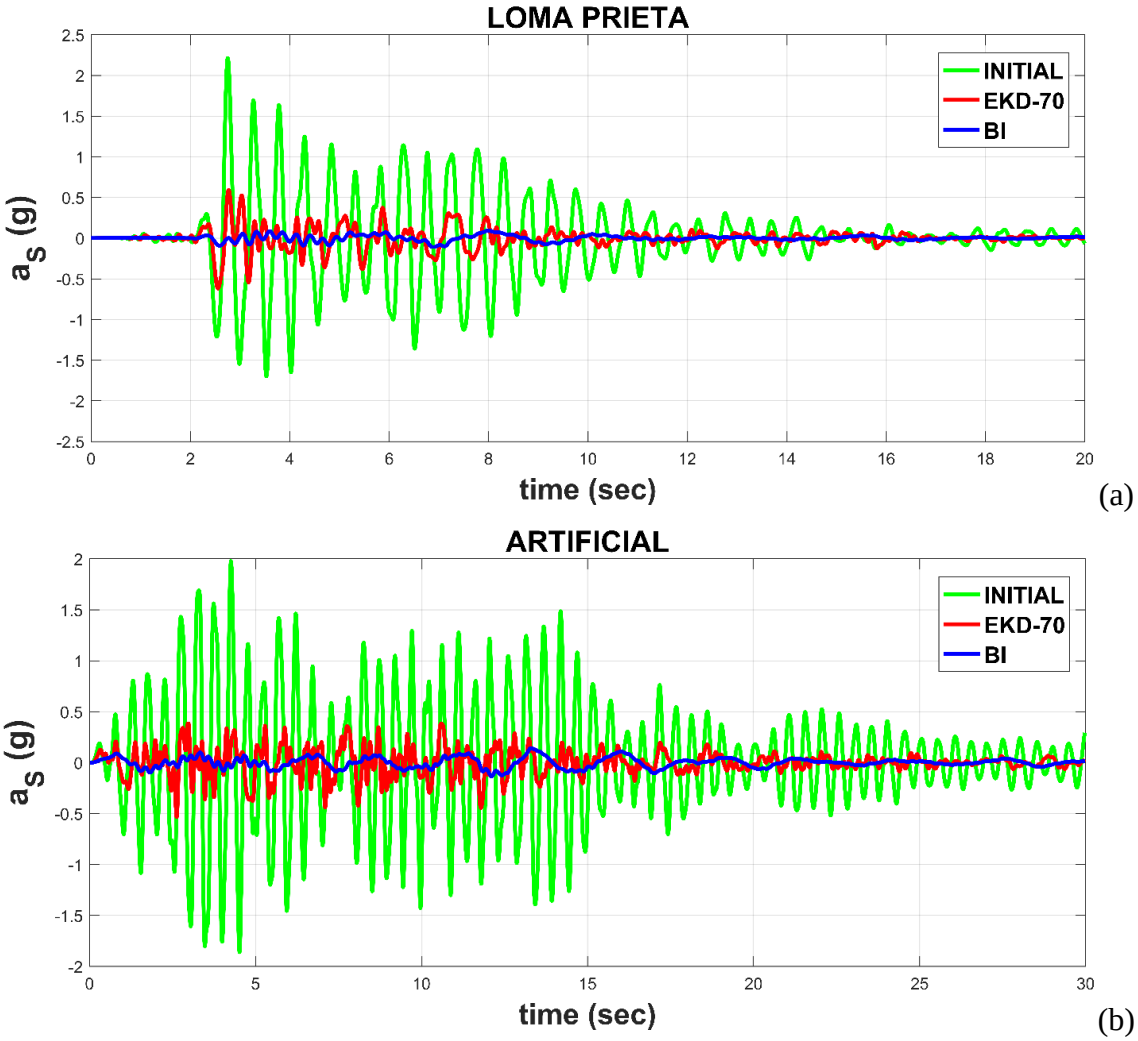

Figure 5.10: *Comparative results, in terms of top floor absolute acceleration (g), between the initial (IN), the conventional base isolated system (BI) and the EKD-70 system, for (A) Loma Prieta earthquake record and (B) an Artificial Accelerogram.*

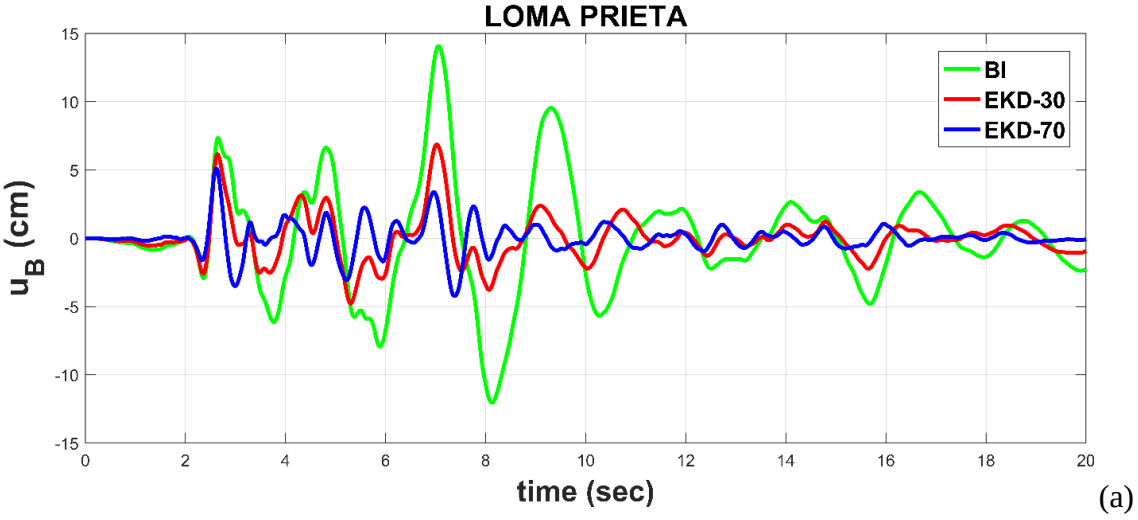

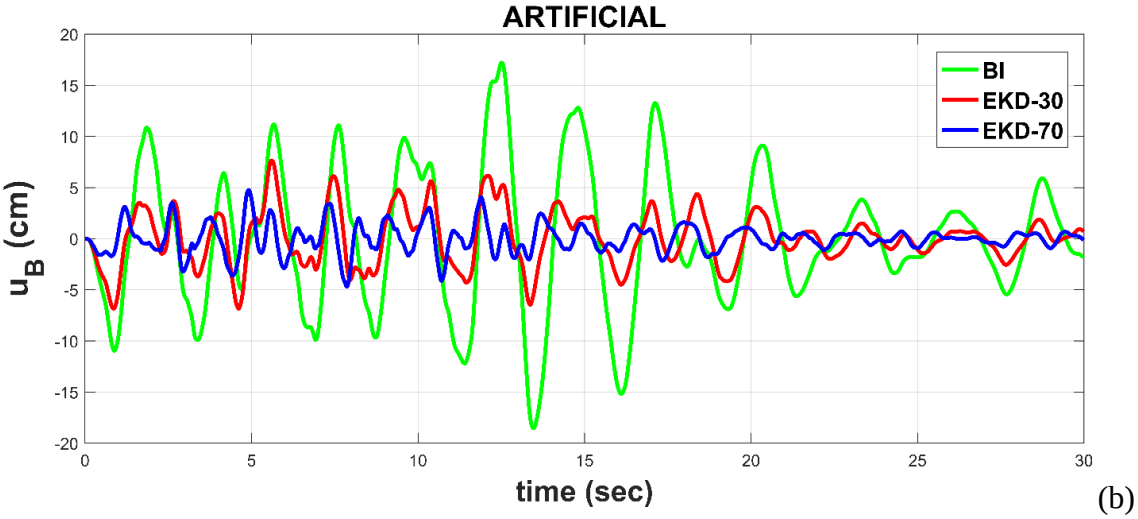

(b)

Figure 5.11: *Comparative results, in terms of base displacement (m), between the BI, EKD-30 and EKD-70 system, for (a) Loma Prieta, and (b) an Artificial Accelerogram.*

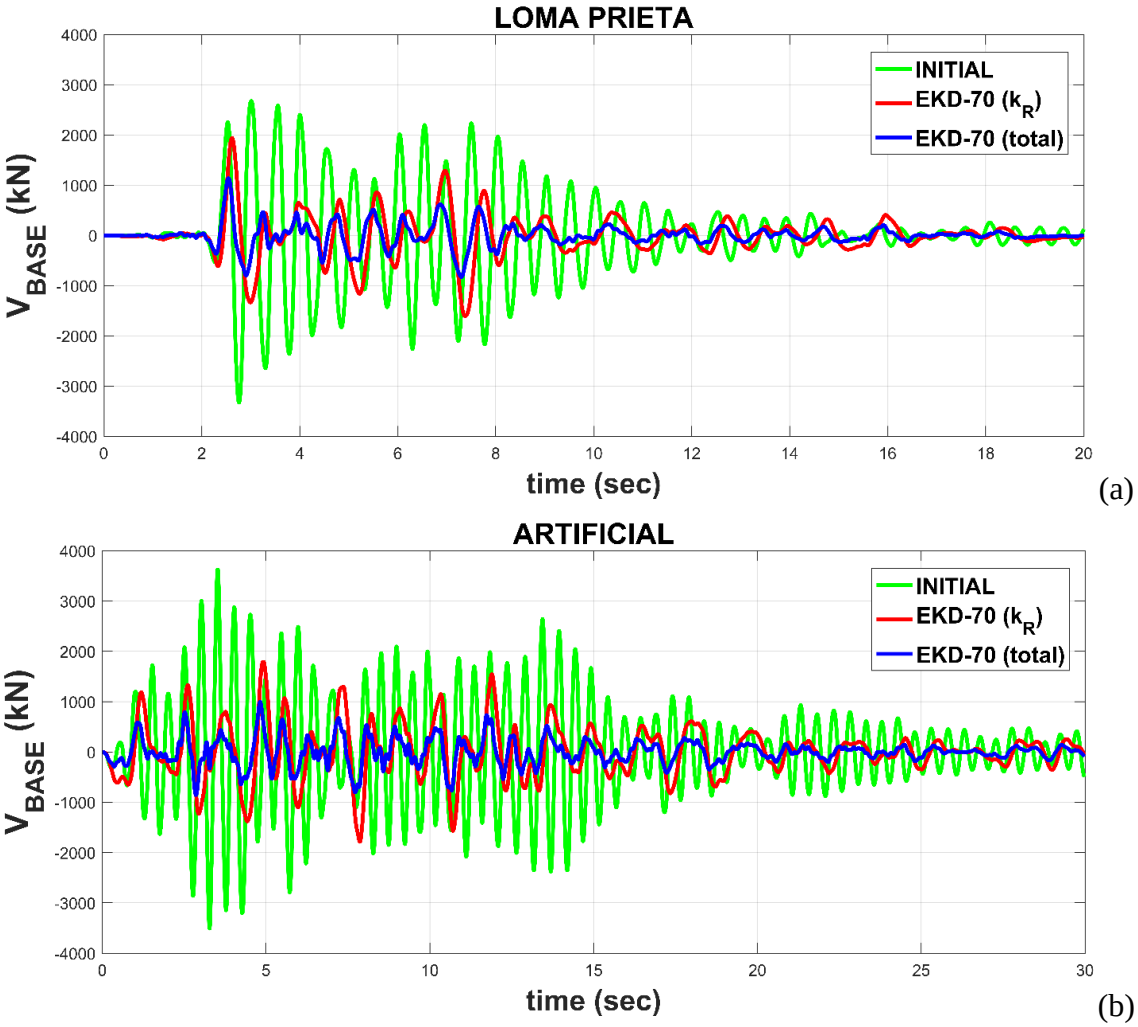

(a)

(b)

Figure 5.12: *Comparative results, in terms of base shear (kN), between the BI, EKD-30 and EKD-70 system, for (a) Loma Prieta, and (b) an Artificial Accelerogram.*

Based on the results of the Numerical Example 2, the following remarks can be made:

i. The 3-story building structure controlled with EKD, presents an improved dynamic behavior. More specifically, the floor accelerations and the inter-story drift are reduced *65-85%*, results comparable with the base isolated system (*90%* reductions). At the same time, the base displacement is greatly reduced (up to *75%*) as compared with the base isolated concepts, retained at very low levels (*5-9cm*).

ii. The small base displacement of the EKD with high Acceleration Filters (*70*, *80%*), render the implementation of the proposed device feasible using conventional structural elements, without the need of special type of bearings. Furthermore, the base shear of the whole proposed configuration as well as the base shear of the independent component k_R, is reduced, as compared with the initial system total base shear. As a consequence, retrofitting is possible.

5.2.2 Spectra Driven Approach for the Optimal Design of the EKD as an Absorption Base of SDoF Systems

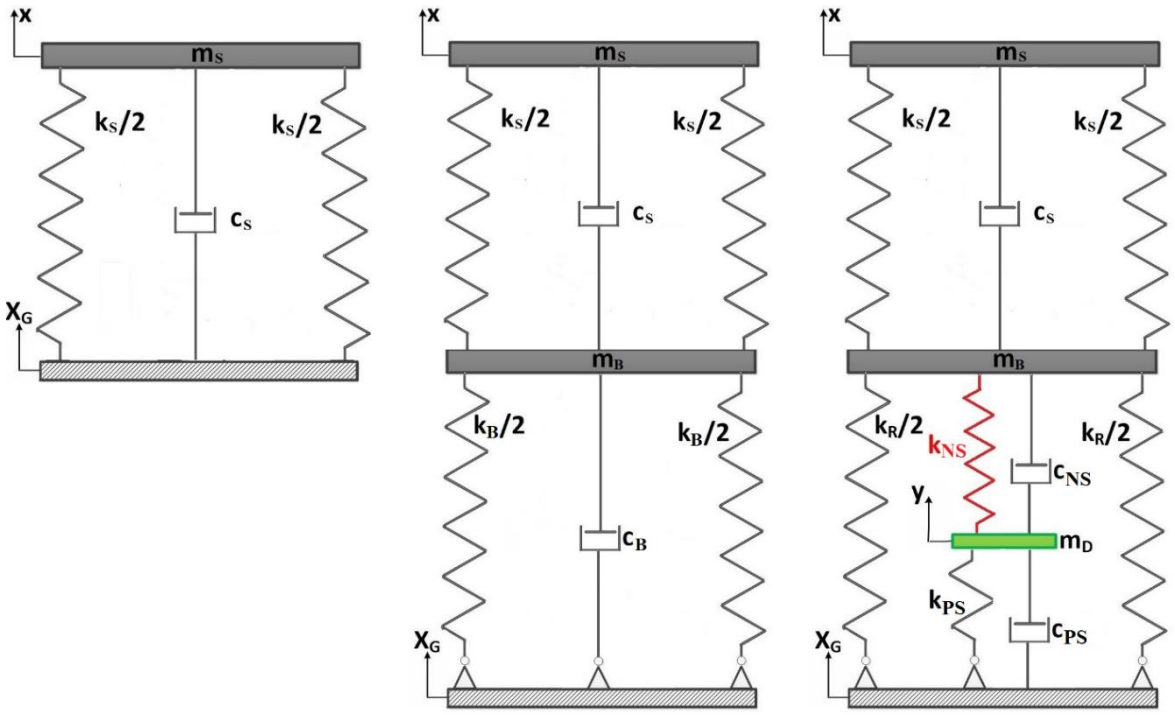

(a) (b) (c)

Figure 5.13: *A possible implementation of the EKD as a seismic absorption base. (a) Fixed base structure, (b) seismically isolated structure, and (c) EKD.*

The SDoF as well as the conventional base isolated (BI) systems, presented in Figure 5.13.a, b, equations of motion and Transfer Functions are presented thoroughly in Chapter 4. In this section of the current Chapter, the EKD is implemented as a base absorption layer of a SDoF system, as presented in Figure 5.13.c. The equations of motion of this system are:

$$m_S(\ddot{u}_S+\ddot{u}_B)+c_S\dot{u}_S+k_S u_S=-m_S a_G \tag{5.6.a}$$

$$m_B\ddot{u}_B+m_S(\ddot{u}_S+\ddot{u}_B)+c_{NS}(\dot{u}_B-\dot{u}_D)+k_{NS}(u_B-u_D)+k_R u_B=-(m_S+m_B)a_G \tag{5.6.b}$$

$$m_D\ddot{u}_D-c_{NS}(\dot{u}_B-\dot{u}_D)+c_{PS}\dot{u}_D-k_{NS}(u_B-u_D)+k_{PS}u_D=-m_D a_G \tag{5.6.c}$$

where $u_S = x_S - x_B$, $u_B = x_B - x_G$, $u_D = x_D - x_G$. Assuming a harmonic base acceleration excitation in the form of Equation (2.4), the steady-state responses of:

$$u_S(t)=\tilde{U}_S\exp(j\omega t) \tag{5.7.a}$$

$$u_B(t)=\tilde{U}_B\exp(j\omega t) \tag{5.7.b}$$

$$u_D(t)=\tilde{U}_D\exp(j\omega t) \tag{5.7.c}$$

The Transfer Functions of this system result as:

$$\begin{bmatrix}\tilde{H}_{US}\\ \tilde{H}_{UB}\\ \tilde{H}_{UD}\end{bmatrix}=\begin{bmatrix}\tilde{U}_S/A_G\\ \tilde{U}_B/A_G\\ \tilde{U}_D/A_G\end{bmatrix}=-\tilde{H}^{-1}\begin{bmatrix}m_S\\ m_S+m_B\\ m_D\end{bmatrix} \tag{5.8.a}$$

$$\tilde{H}_{AS}=\tilde{A}_S/A_G=1-\omega^2(\tilde{H}_{US}+\tilde{H}_{UB}) \tag{5.8.b}$$

$$\tilde{H}_{AB}=\tilde{A}_B/A_G=1-\omega^2\tilde{H}_{UB} \tag{5.8.c}$$

$$\tilde{H}_{AD}=\tilde{A}_D/A_G=1-\omega^2\tilde{H}_{UD} \tag{5.8.d}$$

$$\tilde{H}=\begin{bmatrix}-\omega^2m_S+j\omega c_S+k_S & -\omega^2m_S & 0\\ -\omega^2m_S & -\omega^2(m_S+m_B)+j\omega c_{NS}+(k_{NS}+k_R) & -(j\omega c_{NS}+k_{NS})\\ 0 & -(j\omega c_{NS}+k_{NS}) & -\omega^2m_D+j\omega(c_{NS}+c_{PS})+(k_{NS}+k_{PS})\end{bmatrix} \tag{5.8.e}$$

The natural frequencies of the subsystems, the damping ratio of the EKD and the rest of the parameters are defined as:

$$\omega_0 = 2\pi f_0 = \sqrt{k_0 / (m_S + m_B)} \tag{5.9.a}$$

$$\omega_D = \sqrt{(k_{PS} + k_{NS}) / \mathrm{m}_D} \tag{5.9.b}$$

$$\zeta_{PS} = c_{PS} / (2\omega_D m_D) = c_{PS} / \left(2\sqrt{(k_{PS} + k_{NS}) m_D}\right) \tag{5.9.c}$$

$$\zeta_{NS} = c_{NS} / (2\omega_D m_D) = c_{NS} / \left(2\sqrt{(k_{PS} + k_{NS}) m_D}\right) \tag{5.9.d}$$

$$k_0 = k_R + \frac{k_{PS} k_{NS}}{k_{PS} + k_{NS}} \tag{5.9.e}$$

$$m_B = \mu_B m_S \tag{5.9.f}$$

$$m_D = \mu_D (m_S + m_B) \tag{5.9.g}$$

where k_0 is the equivalent static stiffness of the EKD and μ_B and μ_D are the base's and EKD's mass ratios, respectively. Based on the horizontal ground acceleration excitation PSD described in section 3.3.2.1 of Chapter 3, the response power spectral densities (PSD) are derived:

$$S_{US} = H_{US}^2 S_A \tag{5.10.a}$$

$$S_{UB} = H_{UB}^2 S_A \tag{5.10.b}$$

$$S_{UD} = H_{UD}^2 S_A \tag{5.10.c}$$

$$S_{AS} = H_{AS}^2 S_A \tag{5.10.d}$$

where S_A is the ground motion excitation acceleration PSD. The root mean square (RMS) values of the responses are next defined as the root under the area of the PSD curve, as an indicator of the actual energy content of the response:

$$R_{US} = \sqrt{\int_{-\infty}^{+\infty} S_{US}(\omega)\,\mathrm{d}\,\omega} \tag{5.11.a}$$

$$R_{UB} = \sqrt{\int_{-\infty}^{+\infty} S_{UB}(\omega)\,\mathrm{d}\,\omega} \tag{5.11.b}$$

$$R_{UD} = \sqrt{\int_{-\infty}^{+\infty} S_{UD}(\omega)\,\mathrm{d}\,\omega} \tag{5.11.c}$$

$$R_{AS} = \sqrt{\int_{-\infty}^{+\infty} S_{AS}(\omega)\,\mathrm{d}\,\omega} \tag{5.11.d}$$

5.2.2.1 Statement of the Optimization Problem

In this section, a spectra driven approach is followed for the optimal selection of the EKD parameters, implemented as a base absorption layer. Based on section 5.2.1, the artificial damper placed in parallel to the positive stiffness element k_{PS}, i.e. c_{PS}, did not have a significant influence on the EKD performance, and thus is ignored in this section. Assuming that the following parameters of the EKD system are known: a) the additional mass m_D, and b) the stability factor ε_{NS}, the free design variables sought in the optimization problem are:

1. the nominal EKD frequency f_0;
2. the value of the negative stiffness (NS) element k_{NS};
3. the damping coefficient c_{NS};

The system is subjected to ground acceleration PSD generated according to section 3.3.2.1 of Chapter 3. The RMS response of the base relative displacement is set as the objective function. Finally, the limits of the free design variables and the constraints imposed in the system dynamic responses must be within reasonable technological capabilities in order for design to be realistic. In particular:

i. In the previous work of KDamper, the stability factor ε_{NS} that relates to the variation of the negative stiffness element k_{NS}, is taken as *5%*. In this section, the variation of the NS element ε_{NS} is selected equal to *10%*.
ii. Similarly to section 5.2.1.1, the additional mass of the EKD is selected to be equal to *5%* additional mass is efficient and realistic.
iii. The stiffness elements must be within reasonable technological capabilities. The negative stiffness element k_{NS}, in the proposed configuration of EKD, is realized with the Proposed Configuration I presented in Chapter 3, with pre-compressed springs. Based on the work of (Kapasakalis at el., 2019) (in Greek), a realistic value of k_{NS} for a total superstructure mass of *300 tn*, is *-34171 kN/m*.
iv. The damping coefficients maximum value cNS is set *600 kNs/m*.
v. The RMS response of the structure acceleration upper limit is set $0.5R_{AS}$(initial).

Finally, the limits of the free design variables are: a) the nominal KDamper frequency f_0 (*Hz*) [*0.2 2.0*], b) the negative stiffness element k_{NS} (*kN/m*) [*-35000 0*] and c) the damping coefficient c_{NS} (*kNs/m*) [*1 600*].

The Transfer Functions and response PSDs of the system main responses are presented in Figure 5.14 and 5.14, and are compared with a highly damped base isolated system (BI-HD) designed to have a base natural frequency and a damping ratio equal to 0.4 *Hz* and 20%, respectively, as well as a fixed base structure (FBS) having a natural frequency and a damping ratio equal to 2 *Hz* and 5%, respectively. The maximum value of the acceleration Transfer Function H_{AS} of the EKD is slightly lower compared to the maximum value of the BI-HD, however the frequency range where the maximum values occur is larger. On the other hand, the base relative displacement Transfer Function H_{UB} of the EKD is significantly lower than that of the BI-HD in all frequency range. Finally, the maximum value of the EKD displacement H_{UD} occurs in the nominal EKD frequency obtained from the optimization procedure.

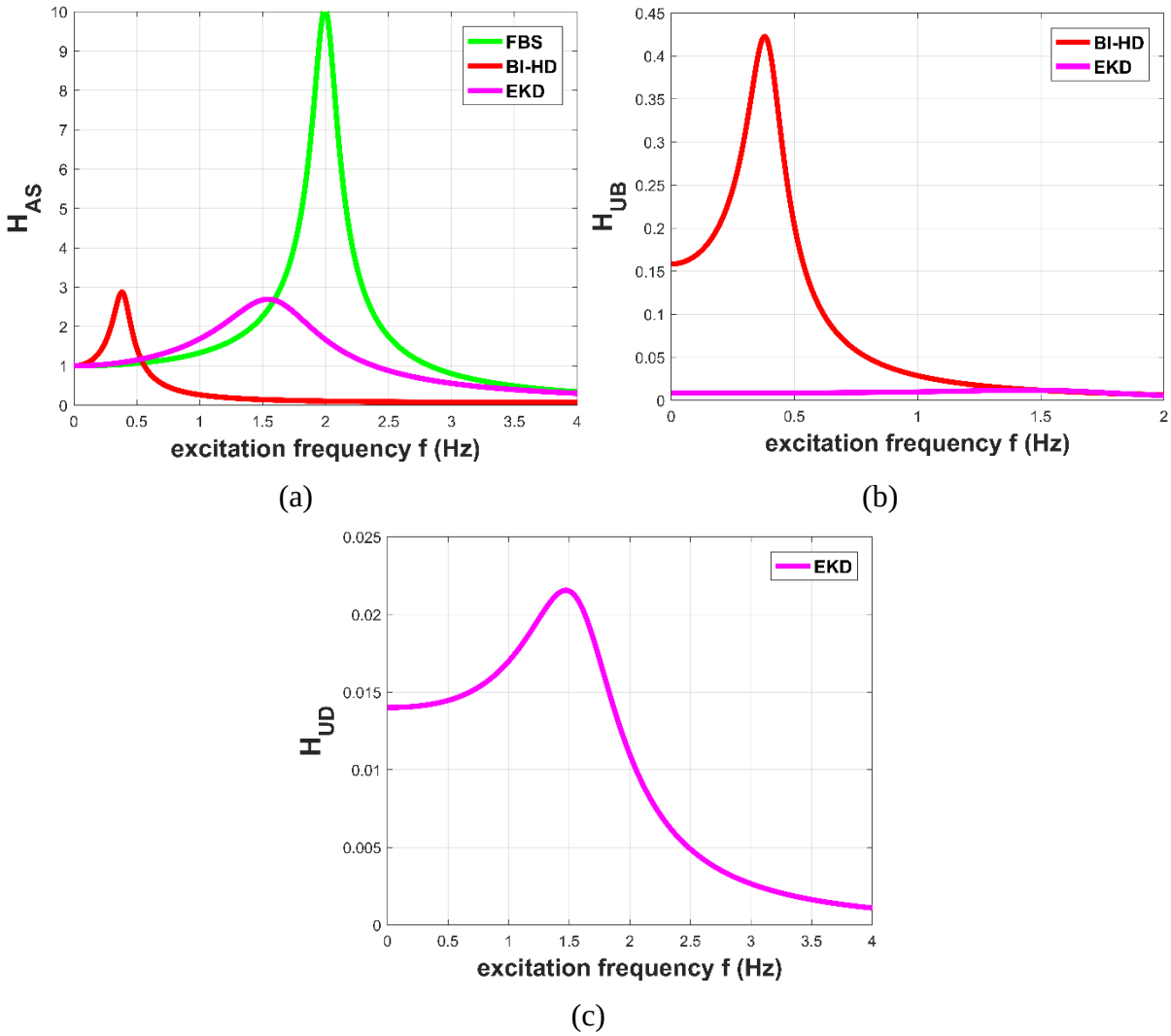

Figure 5.14: *Transfer Functions of the main system responses: (a) structure's absolute acceleration HA_S, (b) base's relative displacement H_{UB}, and (c) EKD relative displacement H_{UD}, for all the considered systems: FBS, BI-HD, EKD.*

The maximum value of the acceleration response PSD HAS of the EKD is one order of magnitude lower than the FBS system's, retaining a large frequency content. The base response PSD of the EKD is more than two orders of magnitude lower than that of the BI-HD and has a smaller frequency content.

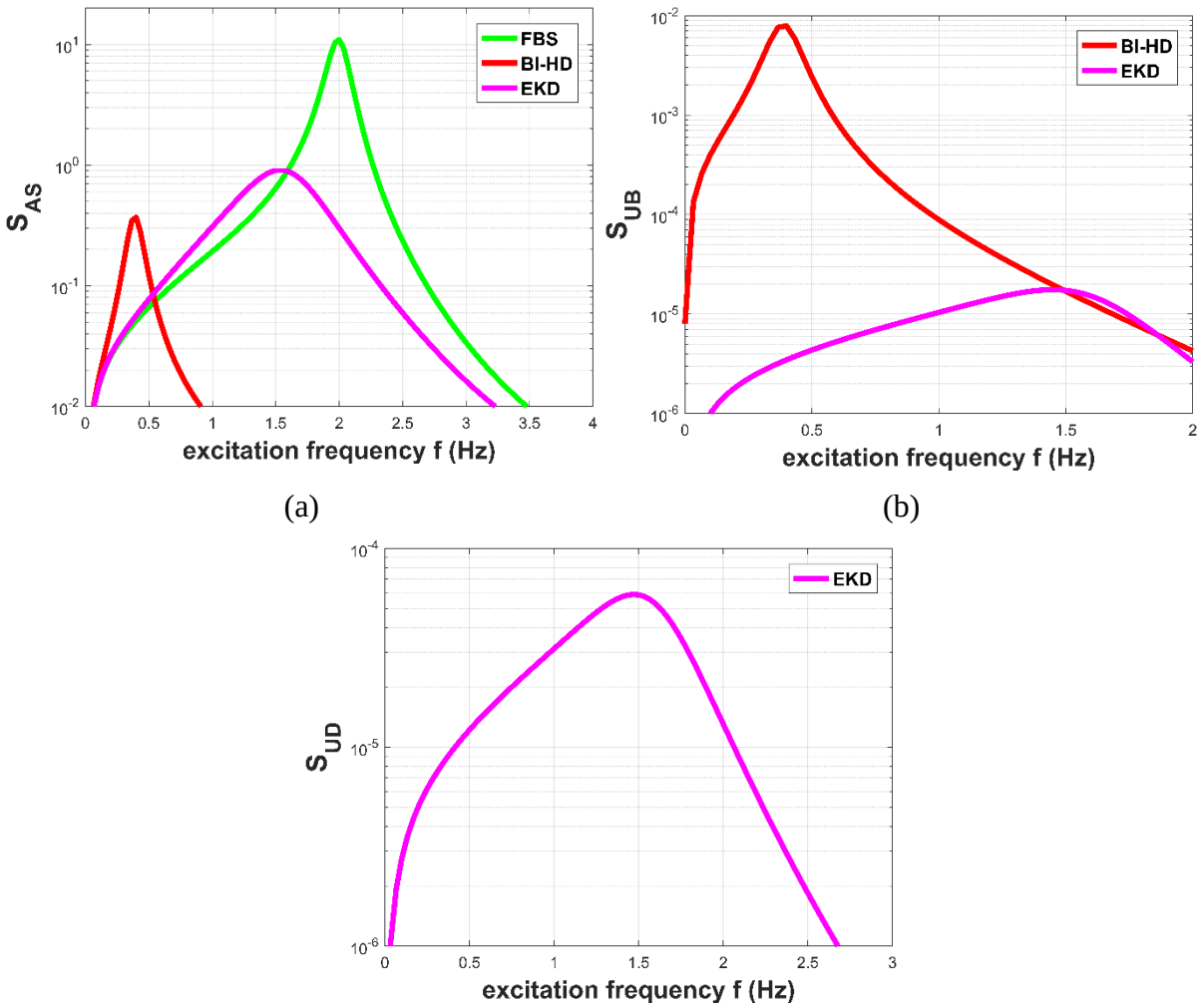

Figure 5.15: *Response PSDs of the main system responses: (a) structure's absolute acceleration HAS, (b) base's relative displacement HUB, and (c) EKD relative displacement HUD, for all the considered systems: FBS, BI-HD, EKD.*

Figure 5.16, presents the root mean square responses ratio of the highly damped BI system, as well as the EKD system, which are defined as:

$$r_{AS} = \frac{R_{AS}}{R_{AS}(FBS)} \tag{5.12.a}$$

$$r_{UB} = \frac{R_{UB}}{R_{US}(FBS)} \tag{5.12.b}$$

$$r_{UD} = \frac{R_{UD}}{R_{US}(FBS)} \tag{5.12.c}$$

where $R_{US}(FBS)$ and $R_{AS}(FBS)$ pertain to the FBS system with a natural frequency of *2 Hz* and a damping ratio of *5%*. The r_{AS} of the EKD as expected has the value 0.5 in all the range of f_0, as imposed in the optimization problem. The r_{UB} of the EKD is always at least 50% lower as compared with the BI in all frequency range. Finally, the r_{UD} decreases as the f_0 increases.

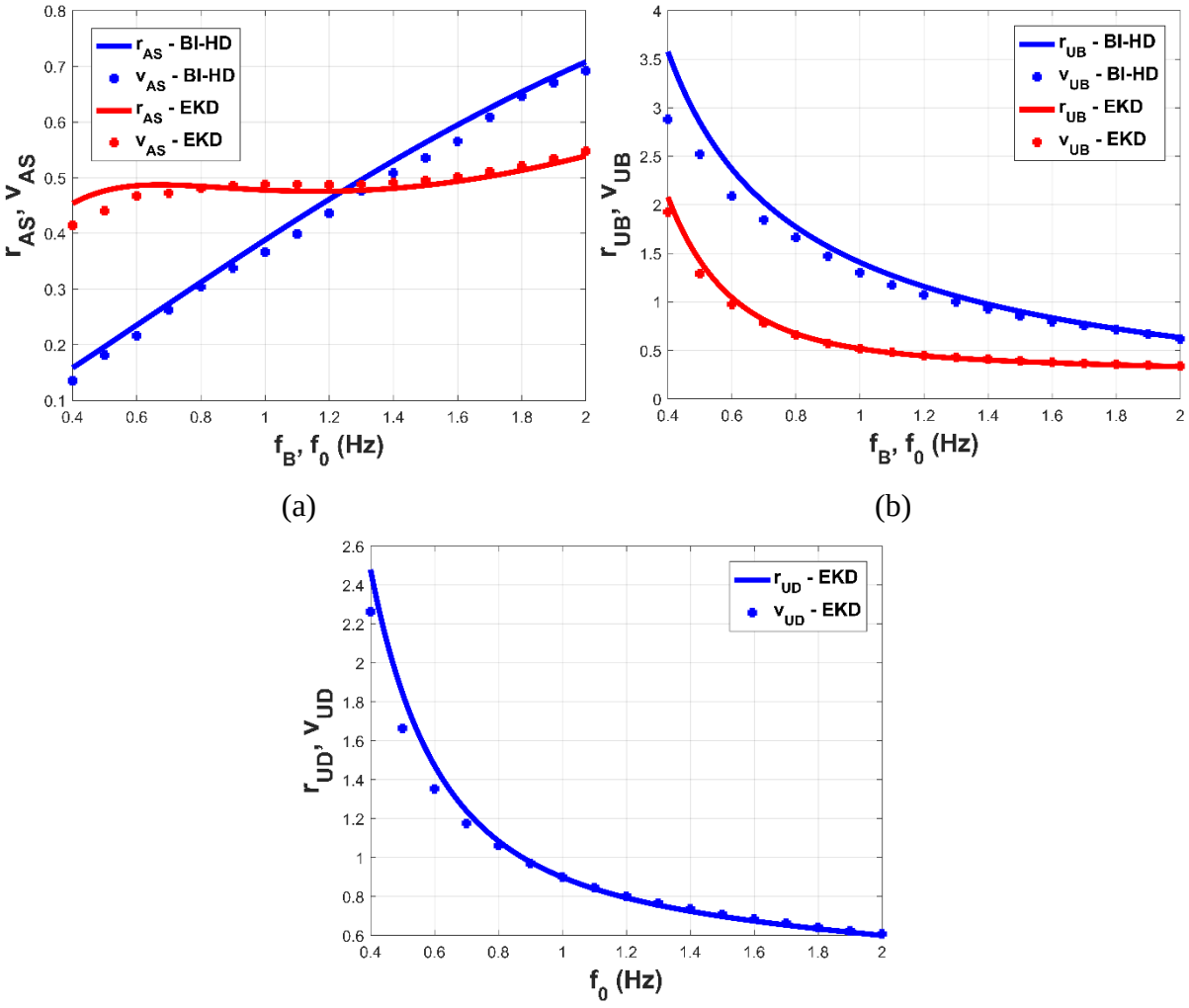

Figure 5.16: *RMS responses ratio (solid lines) and verification with mean of the maximum dynamic responses ratio (dotted lines), of the BI and the EKD systems: (a) structure's absolute acceleration, (b) base's relative displacement, and (c) EKD's relative displacement, over the base's natural frequency f_B, f_0.*

5.2.2.2 Numerical Example 3 – *Preliminary Assessment of the EKD Implemented in the Base of a 3-Story Building Structure*

In this numerical example, the EKD, optimized as a base absorption layer with the spectra driven approach described in section 5.2.2.1 is implemented in the base of a 3-story building structure. The extension of the EKD for implementation in the bases of multi-story building is previously presented in the Numerical Example 2 of this Chapter. The EKD parameters are presented in Table 5.4.

Table 5.4: *EKD parameters.*

μ (%)	$kn=k_{NS}/ki$	$kp=k_{PS}/ki$	$kr=k_R/ki$	c_{NS} (*kNs/m*)	f_0 (*Hz*)
5	-0.53	0.83	1.93	588	1.65

where *ki* is the stiffness of the i^{th} floor, and is equal to 65000 *kN/m*. The Transfer Functions of the system main responses are presented in Figure 5.17. It is observed from Figure 5.17.a that the EKD manages to reduce the peak of the acceleration Transfer Function H_{AS}, as compared to the initial uncontrolled structure, however retaining a significant frequency content. Figure 5.17.b illustrates the Transfer Function of the base relative displacement H_{UB} of the EKD system compared to the BI-HD system, design to have a base natural frequency equal to 0.4 *Hz* and a damping ratio of 20%. It is observed that the EKD greatly reduces the H_{UB} in all frequency range, as compared to the BI-HD. Finally, the maximum value of the EKD relative displacement Transfer Function H_{UD} occurs in the nominal EKD frequency obtained from the optimization procedure (f_0=1.65 *Hz*).

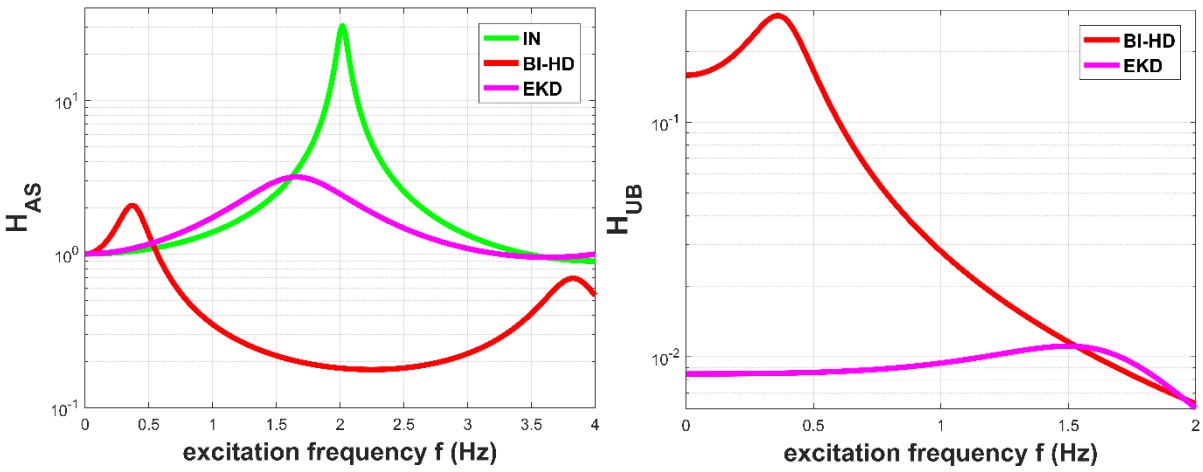

(a) (b)

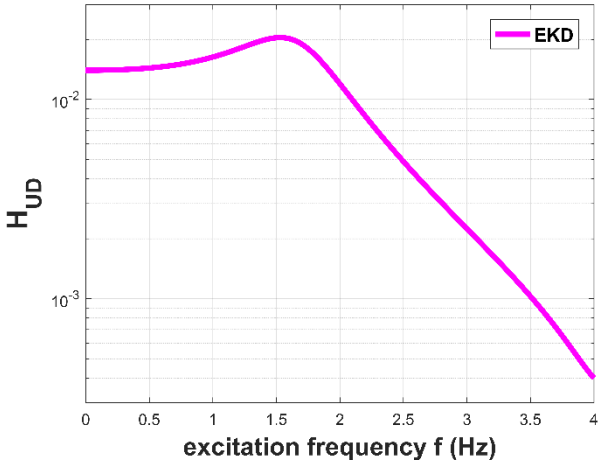

(c)

Figure 5.17: *Transfer Functions of the main system responses: (a) top floor absolute acceleration HA_S, (b) base relative displacement H_{UB}, and (c) EKD relative displacement H_{UD}, for all the considered systems: IN, BI-HD, and EKD.*

Subsequently, the realization of the EKD devices is investigated for the considered implementation in the base of the examined 3-story building structure. The total EKD parameters are presented in Table 5.4. EKD devices can operate in parallel, and therefore four EKD devices are placed in total. Regarding the realization of each one of their individual components, the following are presented:

1. The material used to realize the additional mass of each of the 4 EKD devices is concrete, with a value of density equal to ρ_{mat}=2400 kg/m^3. The resulting dimensions, assuming square floor plan is $2\times2\times0.4$ m.
2. Four artificial damper are placed in each EKD device, and therefore the damping coefficient of each damper is low (36.75 kNs/m), so common linear damping devices can be used, as for example Catalog No./Model LD1160 from ITT Infrastructure viscous dampers catalog (Fluid Viscous Dampers | ITT Infrastructure, n.d.).
3. The positive stiffness elements k_R and k_{PS} are realized with simple elastomeric bearings.
4. The negative stiffness elements are designed according to the procedure described in Proposed Configuration II of Chapter 3.

Simple metallic spiral springs are used for the realization of the positive stiffness elements (k_H) used in the Proposed Configuration II. To avoid lateral buckling and excess of shear strength, four compound pieces consisting of nine spiral springs are implemented in total. Figure 5.18 presents one compact piece in its initial and deformed state, to better understand

the generation of negative stiffness. Finally, a schematic representation of the proposed configuration with all the resulting dimensions of the EKD parameters is given in Figure 5.19.

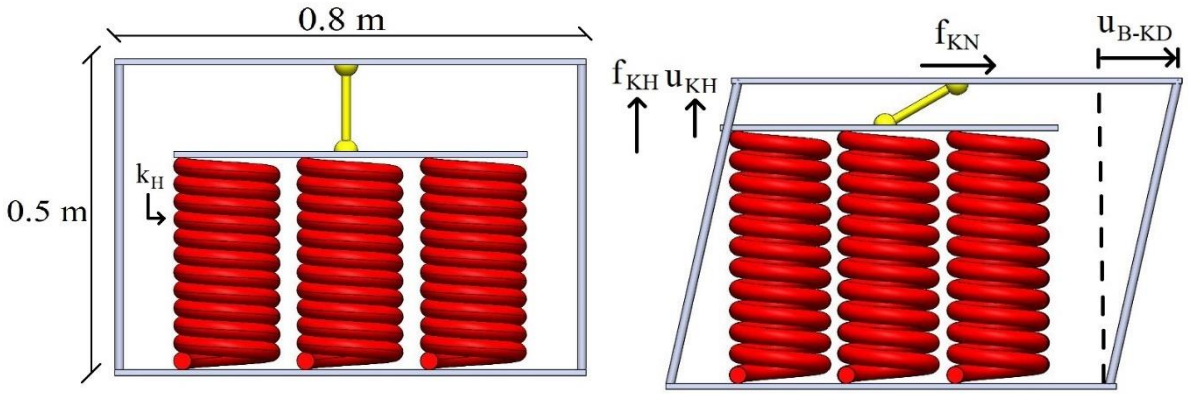

(a) (b)

Figure 5.18: *Proposed configuration for the realization of the negative stiffness element. Compound piece in its (a) initial, and (b) deformed state.*

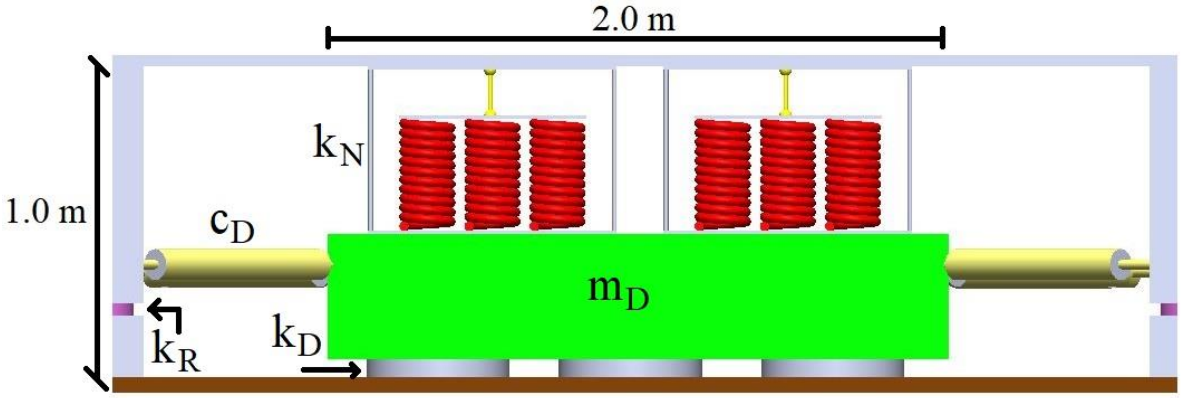

(a)

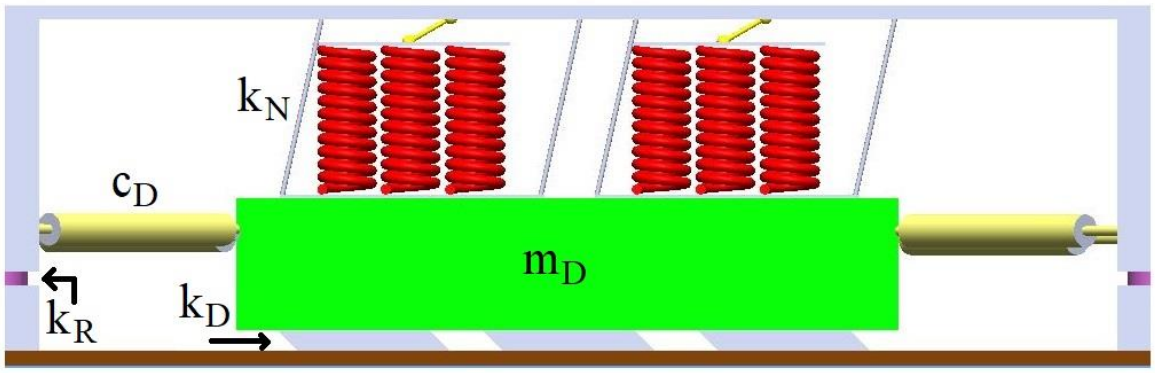

(b)

Figure 5.19: *Schematic representation (front view) of the proposed configuration of the EKD concept in its (a) initial undeformed, and (b) deformed state.*

The indicative implementation of the EKD in the considered 3-story building structure is presented in detail in Figure 5.20.

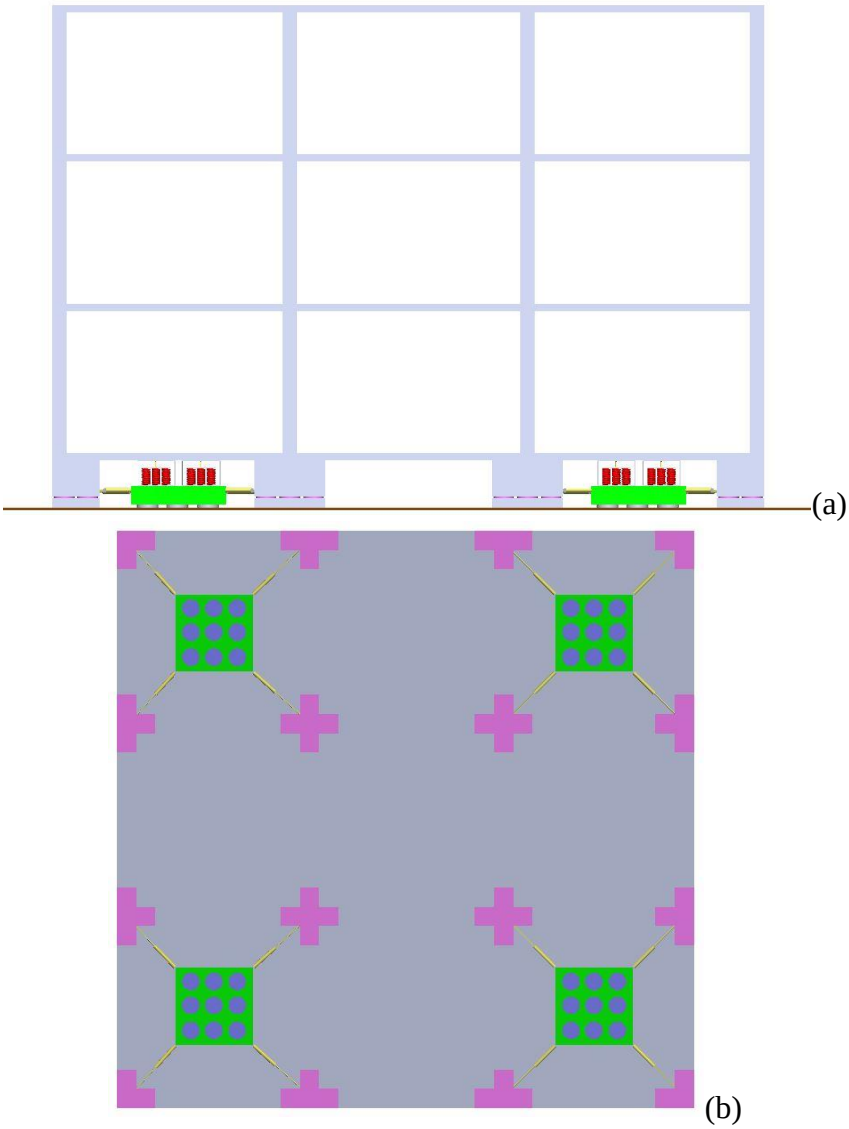

Figure 5.20: *Isolated 3-story building structure with 4 EKD devices in total. (a) Front view, and (b) underneath view of the controlled structure.*

The performance of the EKD is assessed with real earthquake record, presented in Table 5.5. Indicatively, the time histories of the top floor absolute acceleration and base displacement are presented in Figure 5.21, regarding the Izmit, L'Aquila and an artificial accelerogram.

Table 5.5: *PGA of the selected real earthquake motions.*

	Northridge	El Centro	Kobe	L'Aquila	Tabas	Izmit	Aigio
PGA (*g*)	0.43	0.35	0.28	0.34	0.85	0.23	0.54

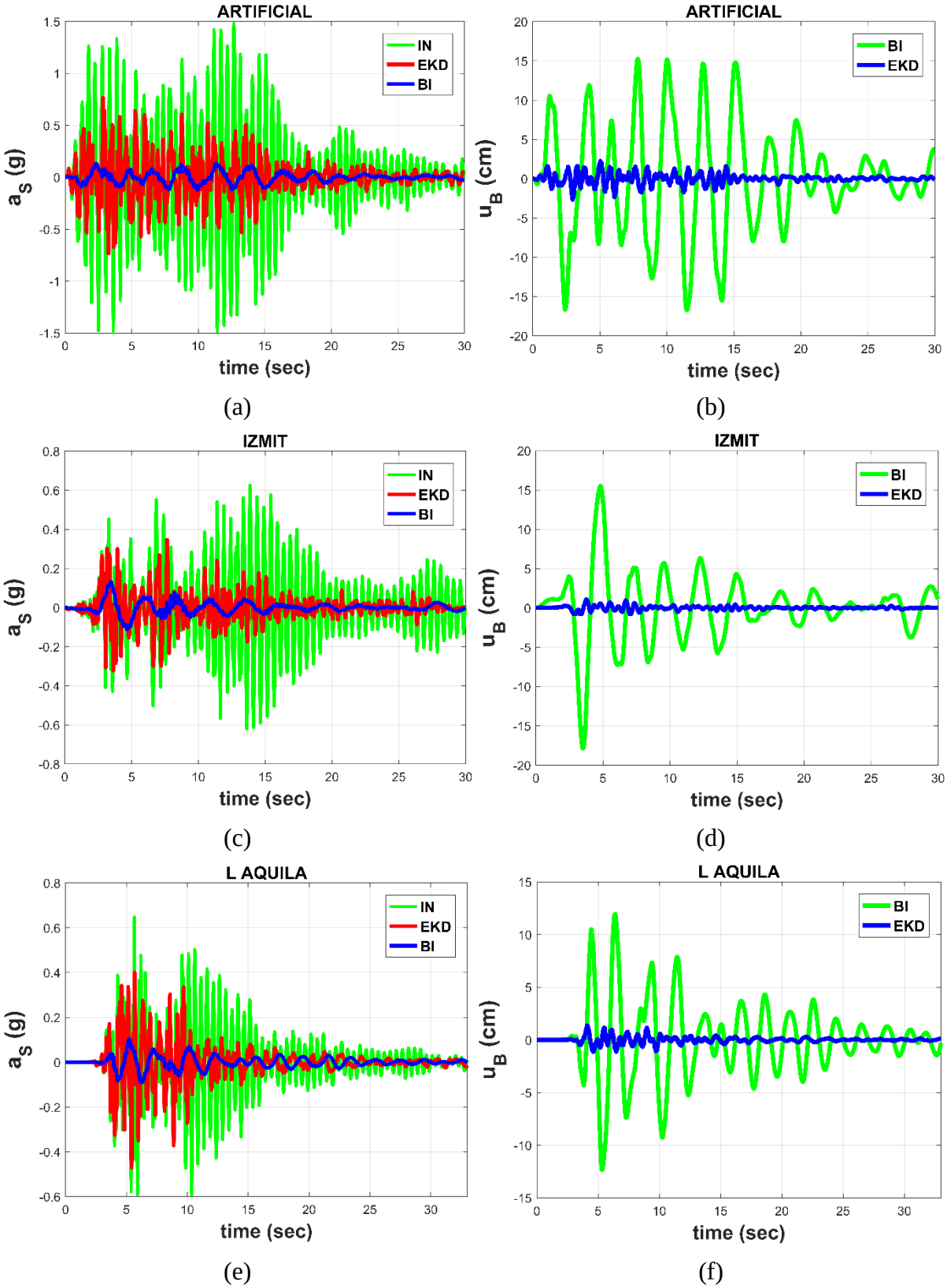

Figure 5.21: *Comparative results, in terms of top floor absolute acceleration (g) and base's relative displacement (cm), between the IN, BI, and the EKD, for (a, b) an artificial, (c, d) the Kocaeli, and (e, f) the Tabas earthquake record.*

Table 5.6 presents the maximum values of the top floor absolute acceleration, inter-story drift, base displacement, EKD relative displacement, and NS element stroke, regarding the selected real earthquake records presented in Table 5.5, and the database of horizontal artificial accelerograms (mean of 30 maximum values).

Table 5.6: *List of structure's main dynamic responses, considering max values of the dynamic responses, and the % reduction compared to the initial 3-story.*

		Northridge	El Centro	Kobe	L'Aquila	Tabas	Izmit	Aigio	Artificial
a_S (m/sec^2) top floor	Initial	13,07	13,67	6,66	6,36	30,16	6,14	23,93	17.23
	KDamper	8,18	6,98	5,10	4,62	18,65	3,41	11,51	7.86
	(%)	**37,39**	**48,98**	**23,34**	**27,35**	**38,14**	**44,39**	**51,92**	**54,38**
Drift (m) 1^{st} floor	Initial	0,033	0,033	0,021	0,017	0,071	0,016	0,061	0.047
	KDamper	0,022	0,021	0,016	0,010	0,038	0,008	0,030	0.02
	(%)	**33,17**	**34,84**	**23,44**	**39,05**	**46,47**	**49,77**	**51,02**	**57,45**
u_B (m)	KDamper	0,029	0,022	0,025	0,014	0,044	0,011	0,031	0.024
u_D (m)	KDamper	0,052	0,040	0,043	0,024	0,072	0,019	0,057	0.043
u_{B-D} (m)	KDamper	0,079	0,060	0,066	0,037	0,107	0,028	0,084	0.064

In this numerical example, the EKD is implemented as a base absorption layer. Based on results obtained, the following concluding remarks can be made:

1. The inter-story drifts are low (2-3 *cm*), 30-60% lower as compared to the initial 3-story building structure.
2. The top floor absolute accelerations are reduced by 30-50%.
3. The relative displacement between the base and the EKD, i.e. NS element stroke, are retained at acceptable levels (5-10 *cm*).
4. The base relative displacements are in the order of a few centimetres (2-4 *cm*). Therefore, the realization of the k_R element is possible with conventional structural elements, without the need of special type of bearing or complex configurations.

According to the above comments, the EKD concept is a realistic alternative to the existing seismic isolation approaches for building structures. The reliability and simplicity of the system are also advantages that render the device suitable for various technological implementations and competitive against conventionally used seismic isolation bearings.

5.3 Retrofitting Options of the EKD

Based on the performed Numerical Examples 2 and 3, the EKD is effectively employed for seismic protection of multi-story structures, as a base absorption layer. More specifically, the EKD manages to greatly improve the superstructure dynamic behavior, retaining the values of its individual components in reasonable ranges. Furthermore, the maximum values of the resulting relative displacements, regarding the EKD elements, are in the order of a few centimetres. As a result, the realization of the EKD is feasible with conventional structural elements, rendering the proposed control system with EKD a realistic alternative to the existing seismic isolation approaches for building structures, with possible retrofitting options.

In this section, two alternative approaches are examined for the implementation of the EKD as a retrofitting option of multi-story building structures. In the first one, multiple EKD devices are distributed in between each floor, in order to find the best possible floor-combination choice regarding its implementation. Specifically, a dynamic system consisting of a simplified flexible structure model and distributed EKD devices is considered, and in order to examine the seismic performance of the structure, four Test Cases with different distribution of EKDs are considered and compared with the performance of the original structure. In the second one, the EKD system is placed at the ground level of a multi-story structure and the soil-structure interaction (SSI) between the building foundations and superstructure is utilized as a means to effectively transfer the dynamic forces of the EKD to the building and to distribute the required displacements between the structural elements and foundation, thus leading to absorption of the vibration energy. The effectiveness of the EKD is subsequently investigated with artificial and real earthquake records. Results indicate the beneficial role of SSI on the reduction of the spectral acceleration and displacements.

5.3.1 Seismic Protection of Multi-Story Building Structure with Distributed EKD Devices

In this section, the performance of the EKD for the seismic protection of a 3-story building is examined, by distributing it between each floor. For this purpose, an optimization procedure is followed, in order to determine not only the optimal parameters of each device but also which floor-combination is the best possible choice regarding the implementation of the EKD. More specifically, a dynamic system consisting of a simplified flexible 3-story structure and the vertically distributed EKD devices is considered and is subjected to artificial accelerograms designed to match the EC8 acceleration response spectra.

5.3.1.1 Statement of the Optimization Problem

The given parameters of the EKD are the additional mass m_D and the stability factors ε_{NS}, $\varepsilon_{PS,}$ and ε_R. The free design variables sough in the optimization problem are: a, b) the damping coefficients c_{NS}, $c_{PS,}$ c) the NS element value k_N, and d) the stiffness k_R. The value of the nominal frequency f_0 and the positive stiffness element k_{PS} of the KDamper are derived from Equations (2.23) and (5.1), respectively.

In this section, the performance of the EKD is examined for the seismic protection of a 3-story building. Specifically, five Test Cases with different vertical distribution of EKDs are examined. In the 1st Test Case, the structure has no seismic isolation devices, Figure 5.22.a. In the 2nd Test Case, the EKD is placed only in the first floor, Figure 5.22.b, and in the 3rd Test Case, EKDs are placed in all three floors, Figure 5.22.c. In the 4th Test Case, the EKD is implemented as a seismic absorption base, Figure 5.22.d. Similarly, in the 5th Test Case, an extra EKD is placed in the first floor, Figure 5.22.e. In order for the proposed control strategy to be efficient and realistic, the constraints that refer to the structural dynamic responses and the limits of the free design variables must be engineering-criteria based. In particular:

i. The drift of the first floor is set as the objective function for Test Cases 2 and 3. For Test Cases 4 and 5, the objective function is the relative to the base displacement.
ii. The maximum acceleration of the floors and the NS element stroke are set as constraints. For Test Cases 2 and 3 the upper limit of the maximum acceleration is $14m/s^2$ and $8m/s^2$ respectively and for both Test Cases 3 and 4 is $4m/s^2$. For all Test Cases, the upper limit of the NS element stroke is $0.12m$, which is a realistic value for the design of the negative stiffness element with pre-compressed springs.
iii. The floor's mass is $80tn$ and the mass of the base is $50tn$. Therefore, the total mass of the structure for Test Cases 2 and 3 is $m_{tot23}=240tn$ and for Test Cases 4 and 5 is $m_{tot45}=290tn$. The additional mass of the EKD for Test Case 2 is $m_D=0.03\times m_{tot23}$, for Test Case 3 $m_{Di}=0.01\times m_{tot23}$ for each EKD, for Test Case 4 $m_D=0.03\times m_{tot45}$ and for Test Case 5 $m_{Di}=0.015\times m_{tot23}$ for each EKD.
iv. The stability factors ε_{NS}, $\varepsilon_{PS,}$ and ε_R are selected equal to 10%.
v. The damping coefficients c_{PS} and c_{NS} upper limit set to equal to $600\ kNs/m$.
vi. The absolute maximum value of the NS element k_N is set equal to $|-15000|\ kN/m$.
vii. The maximum value of the positive stiffness element k_R of the EKD is set as $60000\ kN/m$ when the EKD is placed in the base and as $32500\ kN/m$ when it is placed in the floor. The stiffness of each floor is selected as $65000kN/m$.

5.3.1.2 Numerical Example 4 – *Case Study on a 3-Story Building Structure*

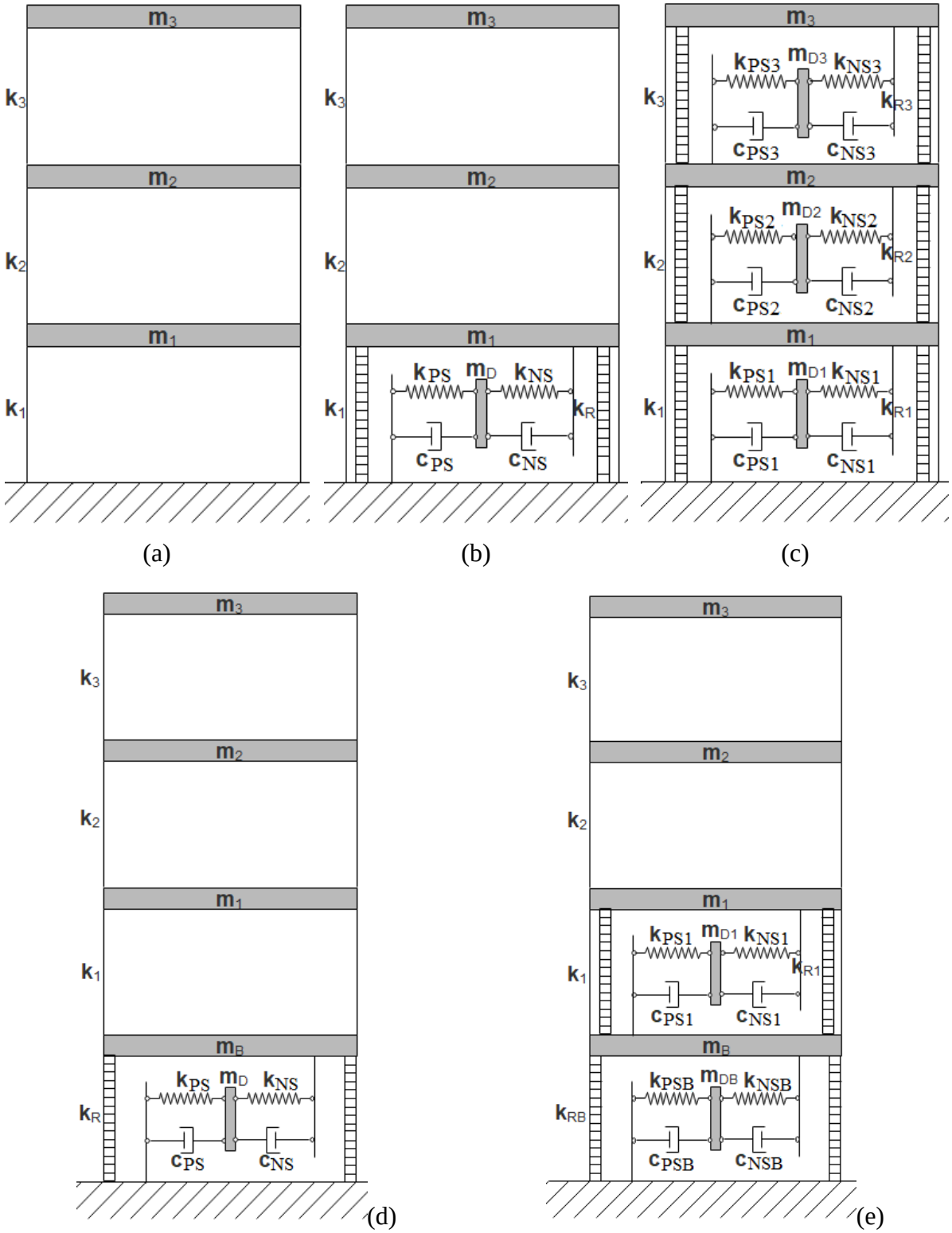

Figure 5.22: *(a) Initial 3-story building structure. Implementation cases of the extended KDamper (EKD) for the seismic isolation of the considered 3-story building: (b) Test Case 2, (c) Test Case 3, (d) Test Case 4, (e) Test Case 5*

A planar symmetric 3-story building is considered, for each Test Case, as sketched in Figure 5.22.a. The extension of the EKD for implementation in the bases of multi-story building is previously presented in the Numerical Example 2 of this Chapter. The system's main dynamic responses, considering the max values of the dynamic responses for all the Artificial Accelerograms in the database (mean of 30 max), generated according to section 3.3.2.1, are presented in Table 5.7. More specifically, $\alpha_{S,top}$ is the max acceleration of the third floor, u_{base} is the max relative displacement of the base, u_{NS} is the max relative displacement of the negative stiffness element and u_{top} is the max displacement of the third floor. Comparative results: 1) of the top floor acceleration for Test Cases 1, 2 and 3, are presented in Figure 5.23.a, 2) of the first floor's drift for Test Cases 1, 2 and 3, are presented in Figure 5.23.b, 3) of the top floor acceleration for Test Cases 1, 4 and 5, in Figure 5.23.c, and 4) of the relative displacement of the base for Test Cases 4,5, in Figure 5.23.d, for a random artificial accelerogram of the database.

Table 5.7: *Main dynamic responses of each Test Case.*

Test Case	$a_{S,top}$ (m/s^2)	1st floor Drift (m)	u_B (m)	u_{NS} (m)	u_{top} (m)
1	17.229	0.0468	-	-	0.1032
2	12.556	0.0212	-	0.0332	0.0593
3	8.792	0.0175	-	0.0278	0.0380
4	3.879	0.0104	0.0643	0.0907	0.0825
5	3.929	0.0079	0.0615	0.0966	0.0768

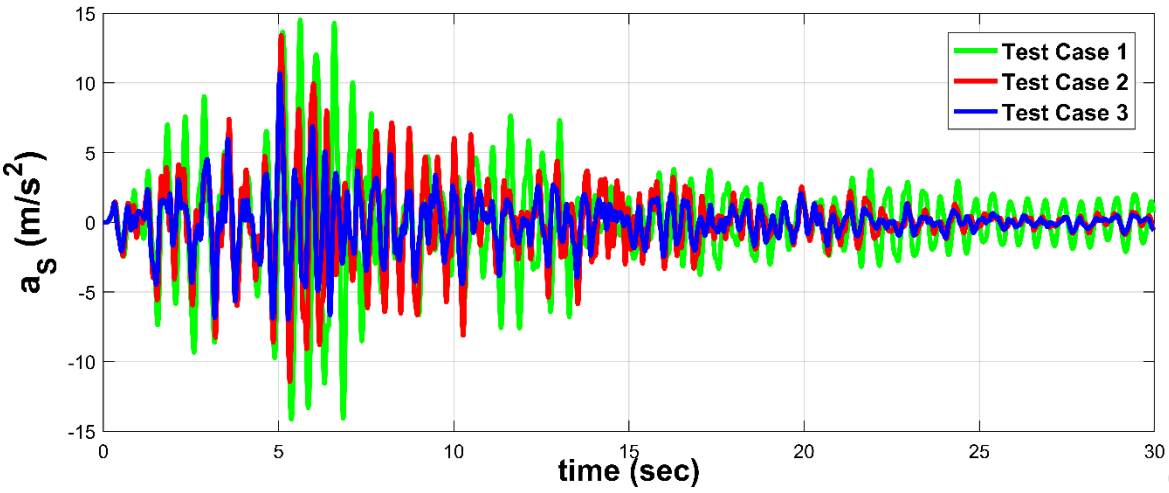

(a)

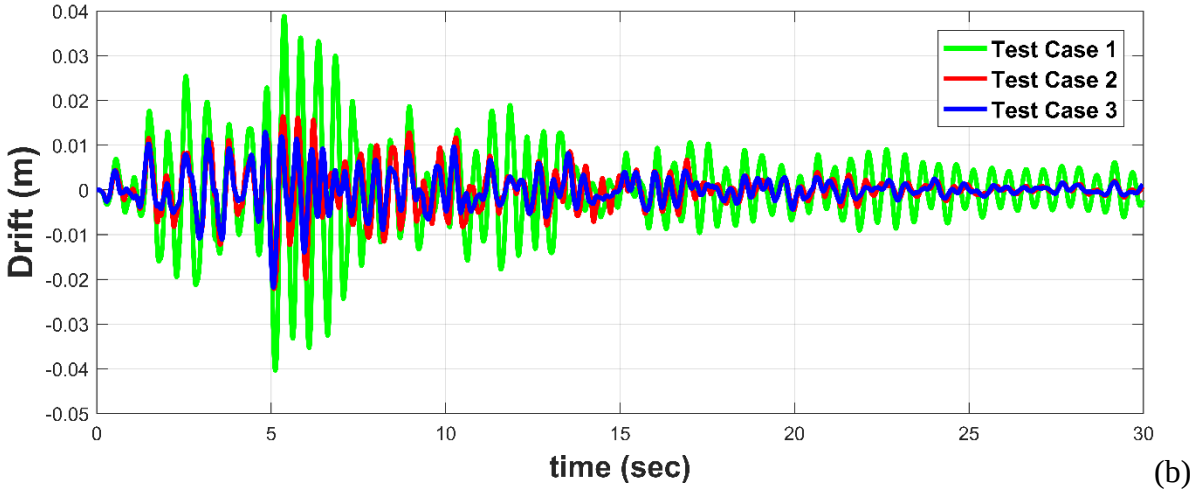

(b)

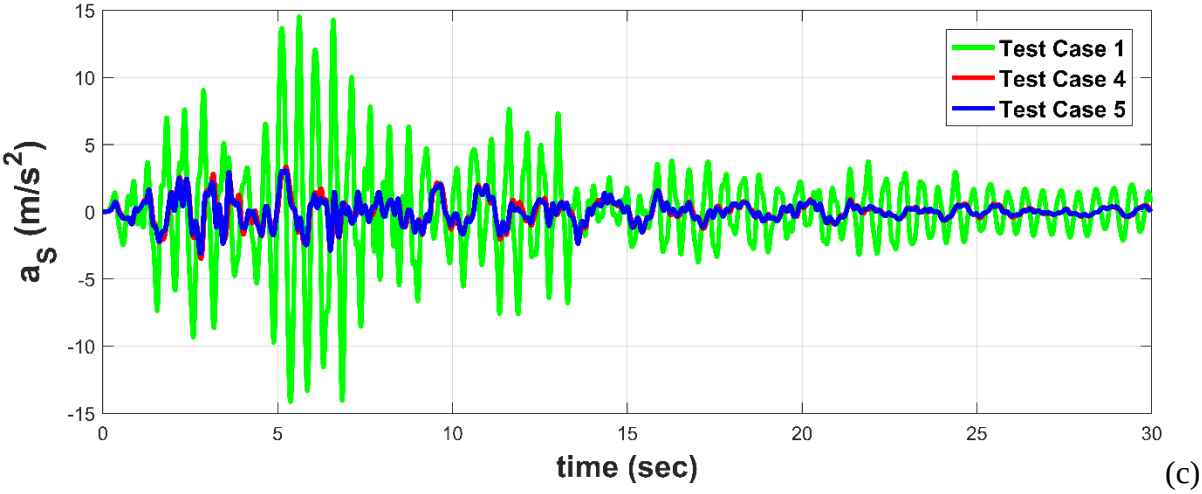

(c)

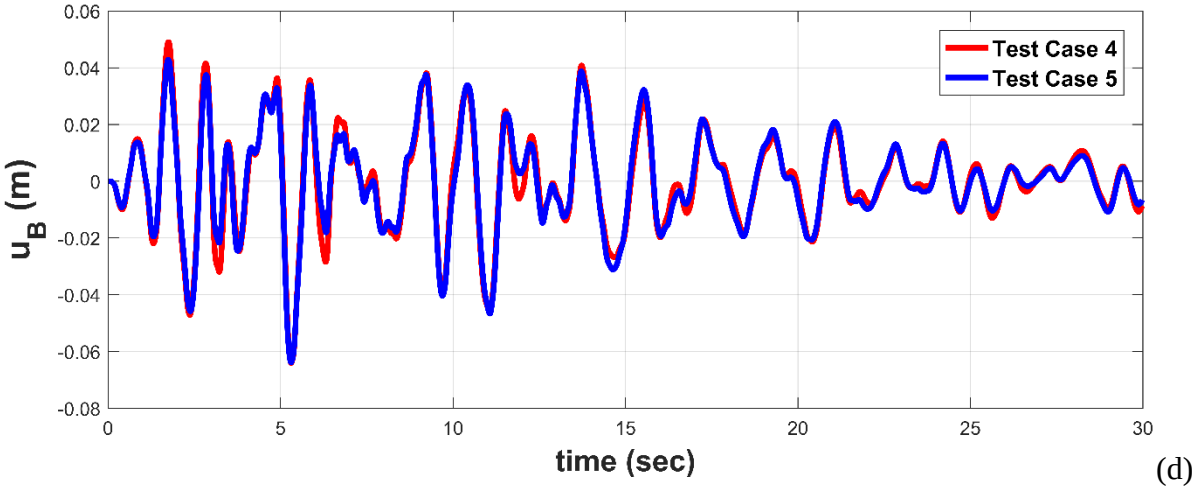

(d)

Figure 5.23: *Comparative results of: (a) Test Cases 1, 2 and 3, in terms of top floor acceleration, Test Cases 1,2 and 3, in terms of first floor's drift, (c) Test Cases 1, 4 and 5, in terms of top floor acceleration, and (d) Test Cases 4, 5, in terms of relative base displacement.*

In Test Case 2, the 3-story building structure presents an improved dynamic behaviour compared to the original structure (Test Case 1). Specifically, the maximum floor acceleration and the inter-story drift of the first floor are reduced by approximately *27%* and *55%* respectively, while the displacement of the top floor is reduced by *43%*. By placing two more EKDs in the second and third floor (Test Case 3) the aforementioned dynamic responses results, compared to the original structure are reduced by approximately *49%, 63%* and *63%* respectively. Therefore, the responses in Test Case 3 are reduced greatly compared to Test Case 2. However, in the case of one EKD only in the first floor, the dynamic performance of the structure is still significantly improved. Also, implementing the EKDs on the floors (Test Case 2 and 3) instead of the structure's base (Test Case 4 and 5) constitutes a retrofitting option.

Applying the EKD, only in the base of the 3-story building (Test Case 4), the maximum floor acceleration, the inter-story drift of the first floor and the displacement of the top floor are reduced by approximately *77%, 78%,* and *20%* respectively, compared to the Test Case 1. By placing one more EKD in the first floor except from the base (Test Case 5) the aforementioned dynamic responses results, compared to the original structure are reduced by approximately *77%, 83%* and *26%* respectively. The responses between Test Cases 4 and 5 do not differ significantly. Therefore, the implementation of the EKD as an absorption base improves greatly by itself the dynamic performance of the structure.

5.3.2 Seismic Protection of Multi-Story Building Structures with EKD Exploiting Soil Structure Interaction (SSI) Effects

In this section, the EKD is implemented as a seismic protection measure between the foundations and the first floor of a typical residential structure (Ground / 'Pilotis' level). The effects of the Soil-Structure interaction coupled with the EKD damping properties are investigated and results indicate the significant benefits of the methodology at the seismic response of the structure. As a consequence, the stiffness k_R, presented in Figure 5.24, is the resultant stiffness of both the columns and foundation. The beneficial effect of the Soil-Structure Interaction (SSI) is taken into consideration with the use of non-linear spring stiffnesses (k_{SSI}) coupled in series with the stiffness of the ground floor columns (k_{col}). As a result, the benefits of a softer foundation response can be compared with the conventional approach of a fully fixed model. The SSI effects are first introduced, then the optimization procedure is formed from which the EKD optimal parameters are selected, and finally, a numerical case study is conducted on a 4-story building structure.

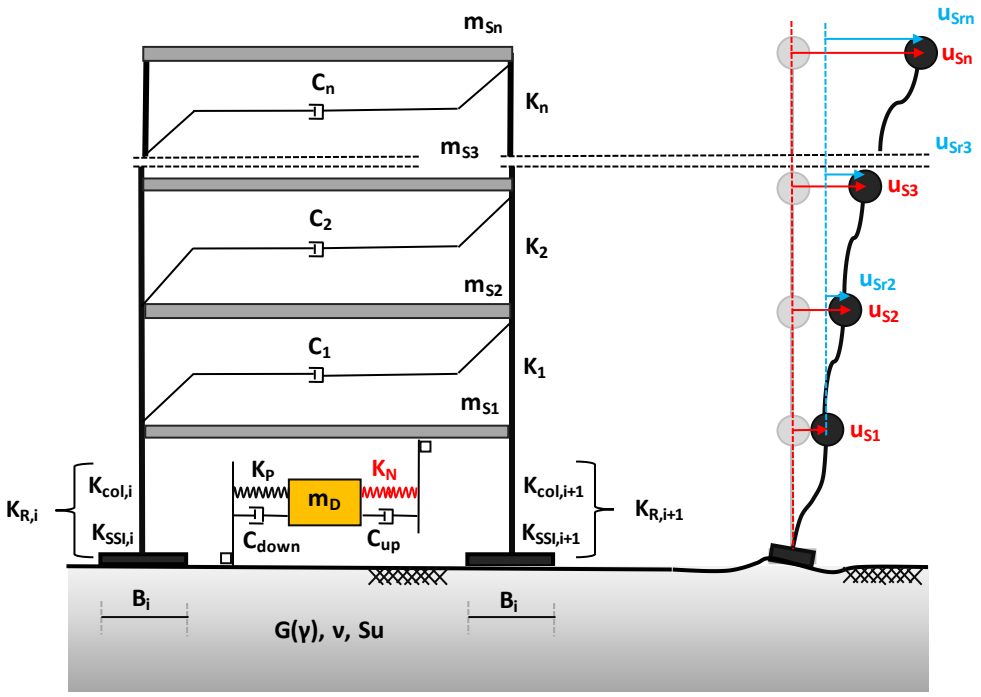

Figure 5.24: *Multi-storey building with the proposed seismic vibration absorber system, EKD (sketch of the model) together with SSI effects.*

A planar *n*-storey building is considered and presented in the sketch of Figure 5.24, in which the proposed base absorber system, EKD is implemented for seismic protection between the foundations and the first floor of a typical residential structure (Ground / 'Pilotis' level). The following assumptions are made for the modelling of this system:

1. the total structure mass is concentrated at floor levels;
2. the slabs and girders on the floors are rigid when compared to the columns;
3. the columns are considered inextensible and weightless, providing the lateral stiffness of the structure;
4. the effect of soil-structure-interaction (SSI) is taken into consideration with the use of non-linear elastic springs coupled in series with the column stiffnesses of the first floor;
5. the superstructure is considered to remain within the elastic limit during the analysis.

As a result, the superstructure has *n* dynamic DoFs, represented by the relative to the ground displacements of the *n*-story masses m_{Sj} ($j=1,\ldots, n$), as presented in Figure 5.24, which are collected in the array $[u_{Sr}](t)=[u_{Sr1}(t), u_{Sr2}(t), \ldots, u_{Srn}(t)]^T$.

The parameter k_R refers to the coupling of the stiffness of the columns (k_{col}) connecting the foundation of the structure with the first floor together with the stiffness of the foundation

system (k_{SSI}) that is derived due to the SSI effects. As a result, the total stiffness of the columns-foundations system is calculated in Equation (5.13) as the k_R of the structure. More details on the derivation of the k_R and incorporation of the SSI effects are provided in section 5.3.2.1 of this Chapter.

$$k_R = \frac{k_{SSI} k_{col}}{k_{SSI} + k_{col}} \tag{5.13}$$

The equations of motion of the controlled system with EKD are expressed in a matrix form, involving matrices with dimensions $r \times r$ with $r=n+1$:

$$[M][\ddot{u}(t)]+[C][\dot{u}(t)]+[K][u(t)] = -[\tau]a_G(t) \tag{5.14}$$

The calculation of the matrices of mass [M], stiffness [K], and damping [C] of the controlled structure with EKD taking into account the SSI effects with the use of non-linear elastic springs coupled in series with the column stiffnesses of the first floor are presented in Appendix A2.

5.3.2.1 Introduction of Soil Structure Interaction (SSI) Effects

For the purposes of this study, the EKD is implemented as a vibration absorption technology positioned between the foundations and the first floor of the structure (Ground / 'Pilotis' level). As a consequence, the stiffness k_R (Figure 5.24) is the resultant stiffness of both the columns and foundation system and can be expressed as in Equation (5.13). The beneficial effect of the Soil-Structure Interaction (SSI) is taken into consideration with the use of non-linear spring stiffnesses (k_{SSI}) coupled in series with the stiffness of the ground floor columns (k_{col}). As a result, the benefits of a softer foundation response can be compared with the conventional approach of a fully fixed model.

The problem is analysed by employing the FE code ABAQUS and a typical foundation and column are modelled in 3D as depicted in Figure 5.25.a. The soil stratum is considered to be isotropic/homogeneous and modelled using non-linear 8-noded hexahedral continuum elements. The same is applied for the footing which is, however, considered to be elastic (Reinforced Concrete). The column is modelled using linear beam elements and is considered

to be fixed on the top of the foundation. The interface between the foundation and the soil is considered to be 'fully bonded' with the foundation elements considered attached to the ground. The boundaries of the model have been strategically selected sufficiently far to avoid spurious boundary-effects on the system response. Static pushover analyses are subsequently undertaken in order to derive the non-linear soil-foundation stiffness relationships (k_{SSI}).

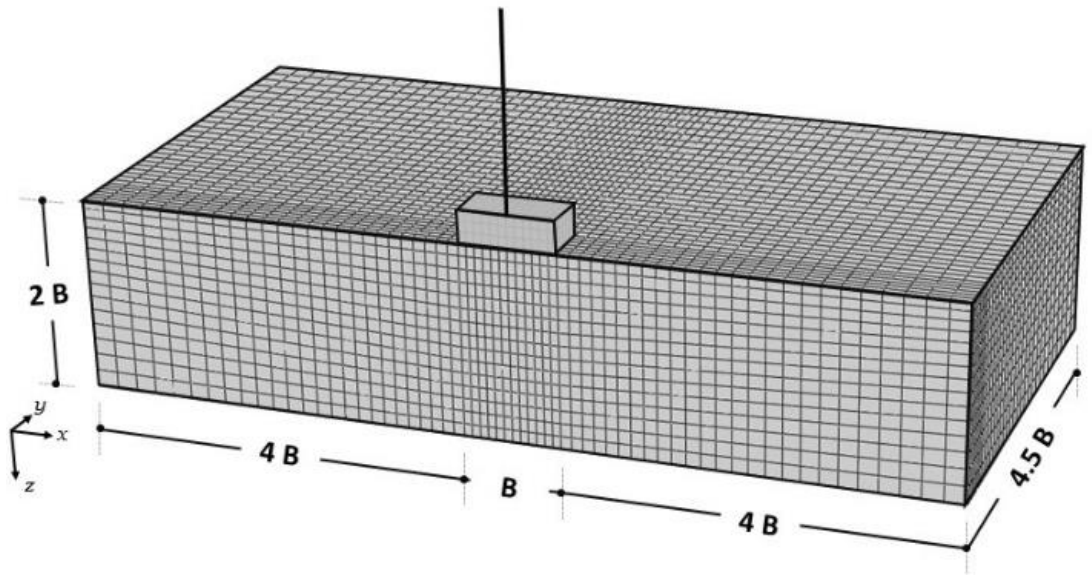

(a)

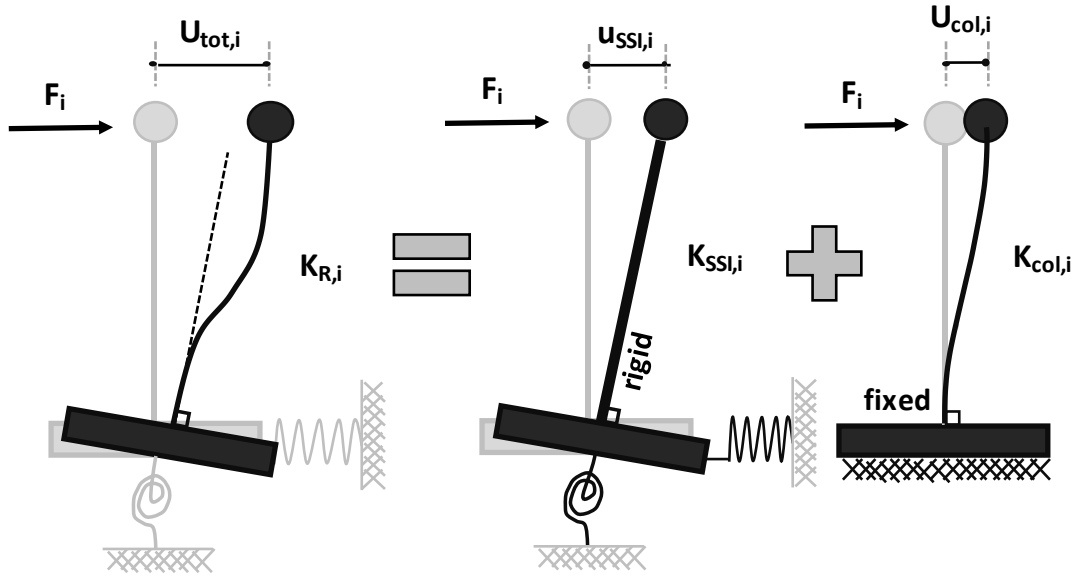

(c)

Figure 5.25: *(a) A view of the ABAQUS 3D FE model for a rigid footing with B=1.5m, and (b) a simplified approach to account for the SSI effects (horizontal and rotational stiffness of the soil) for horizontal displacement at the top of each column.*

Non-linear soil behaviour and stress-strain relationship is described by a simplified kinematic hardening model that follows a Von Mises failure criterion with associated flow rule. The formulation of this modified Von Mises model is adopted as a subroutine in ABAQUS code and has been parametrised by (Gerolymos and Gazetas, 2005) and (Anastasopoulos et al., 2012) in order to appropriately simulate the response of clayey materials. Despite its simplicity, this constitutive model has been validated against physical model testing hence ensuring its ability to capture realistically the foundation behaviour and the non-linearity of the soil stiffness.

The foundation system is designed based on the properties and approximate loading of a typical residential 4-storey building as described in the Numerical Example 5 of this Chapter. To this end, a series of parametric analyses have been conducted by adopting different foundation widths (B) and various material properties (S_u=70, 200 and 300 kPa) resulting in different FoS (Factor of Safety) against vertical loading. On the basis of empirical correlations, the initial, small strain, elastic modulus (E_0) of the soil was considered equal to $1800S_u$ and its non-linear behaviour is simulated realistically by the constitutive relations of the model.

As indicated in Figure 5.25.b, the equivalent soil-foundation stiffness (k_{SSI}) is calculated assuming a rigid column subjected to horizontal displacement at the top. The height of the column is equal to 3.5m, aligned with the height of the column considered in our case study (section 5.3.3). As a consequence, the calculated stiffness (k_{SSI}), is a result of both the rotational and horizontal displacement of the soil footing and is expressed at the top of the rigid column. The total stiffness (k_R) of the system can be then calculated as the resultant of the structural column stiffness (k_{col}) and the equivalent stiffness at the top of the beam due to the rotational and horizontal displacement of the footing (k_{SSI}). Results for a few foundation widths (B) and soil profiles that have been considered relevant for the study are presented in Figure 5.26 below. The horizontal displacement at the top of the column is plotted against the reaction force (RF) and soil-foundation stiffness (k_{SSI}) respectively. All foundations considered below have a total FoS against vertical loading between 3.5 and 4 thus ensuring the stability of the structure under static loading. For the purposes of the study, the footing geometry selected represents a relatively soft foundation that allows deformation of the soil-foundation system during earthquake excitation as a means to reduce the forces transmitted to the structural members. This design is based on the idea of "rocking" foundations which has been investigated using numerical and physical models by several researchers (Anastasopoulos et al., 2010; Gajan et al., 2005; Loli et al., 2014; Paolucci et al., 2008).

After the equations of motion of the EKD and structural system are derived, the aim is to determine efficient parameters for the proposed configuration in order to achieve an optimized

vibration control strategy. As stated in the previous sections, the parameters f_0, k_{NS}, c_{PS} and c_{NS} are the free design variables taken into consideration in the optimization problem, while parameters such as the additional damper mass m_D and the stability factors ε_{NS}, ε_{PS}, and ε_R are considered known.

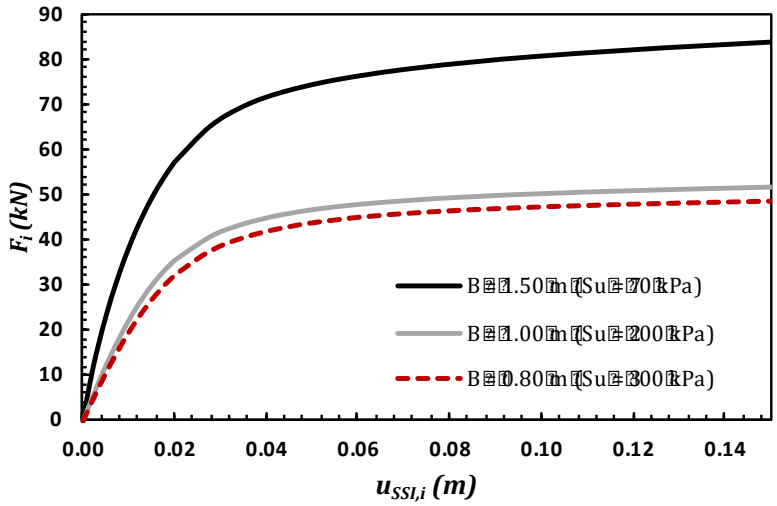

(a)

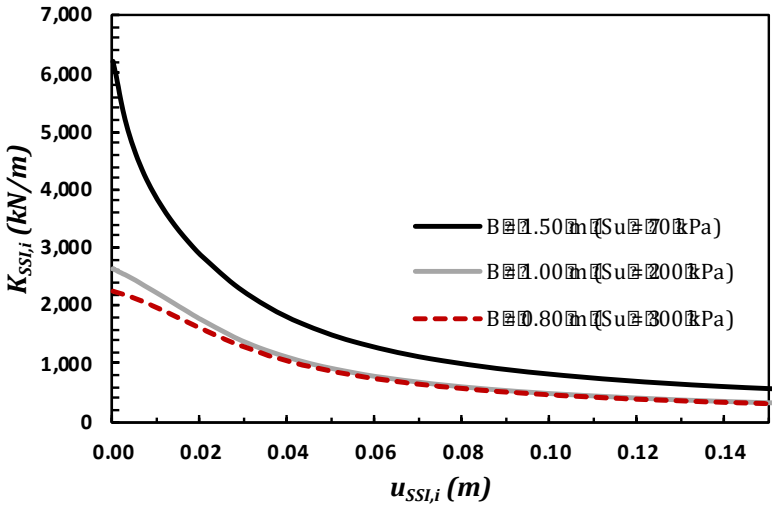

(b)

Figure 5.26: *(a) Reaction force (F) versus horizontal displacement at the top of the rigid column, and (b) Soil-Foundation Stiffness (k_{SSI}) horizontal displacement at the top of the rigid column.*

For the optimization process, a novel metaheuristic algorithm, harmony search algorithm (HS), is adopted. In this study, the optimization is formed according to the seismic design codes. The constraints and objective function are selected from the time-domain responses.

5.3.2.2 Statement of the Optimization Problem

The design of the proposed control strategy must be efficient and realistic at the same time. For this reason, proper constraints that refer to the structural dynamic responses and therefore the EKD components must be applied. The system is subjected to 30 Artificial Accelerograms generated according to section 3.3.2.1 of Chapter 3, with a mean PGA of *0.519g*. The structure's first floor drift is set as the objective function (mean of 30 maximum responses).
Furthermore, the given parameters of the system with the EKD, i.e. the additional mass m_D and the stability factors ε_{NS}, $\varepsilon_{PS,}$ and ε_R, as well as the limits of the free design variables sought in the optimization problem, f_0, k_{NS}, c_{PS} and c_{NS}, must be within reasonable technological capabilities in order for design to be realistic. In particular:

i. In the previous work of KDamper, the stability factor ε_{NS} that relates to the variation of the negative stiffness element k_{NS}, is taken as *5%*. In this study, a variation in all stiffness elements is considered, making the design of the proposed vibration absorption concept rather conservative. The stability factors ε_{PS} and ε_{NS} are selected equal to *10%*, and the stability factor that relates to the stiffness element k_R is selected equal to *25%*. The potential *25%* stiffness reduction was selected based on an initial linear analysis with the EKD implemented in the structure assuming rigid footing. In this way, the anticipated displacement of the column top was calculated and the expected reduction of the k_{SSI} stiffness due to this deformation was estimated (approximately *25%*, refer to Figure 5.26.b).
ii. The purpose of this design is to implement the proposed control strategy for seismic protection of building structures. Since EKD can be implemented between the floors of structures, there are no strict limitations regarding the additional mass. According to the previous work of KDamper implemented as an Absorption Base (KDAB) of multi-story building structures with the same characteristics, (Kapasakalis et al., 2019c), a *5%* additional mass is efficient and realistic.
iii. The negative stiffness element k_{NS}, in the proposed configuration of EKD, is realized with pre-compressed springs following the procedure described in the Proposed Configuration II of Chapter 3. Based on previous indicative designs of KDamper with pre-compressed springs by Antoniadis et al. (Antoniadis et al., 2018) and (Kapasakalis et al., 2019), for a total superstructure mass of *300 tn*, a realistic value of k_N is *-34171 kN/m*. In this work, the negative stiffness element absolute upper value is $|30000|$ *kN/m*.

iv. The damping coefficients maximum value is set equal to *600 kNs/m* for the whole configuration (multiple EKD devices can be implemented), therefore, common linear damping devices can be used.

v. The negative stiffness element stroke ($X_{S\text{-}D}$) is set as a constraint, with an upper limit value of *15 cm* which, based on previous work of (Kapasakalis et al., 2019), proves to be a realistic value for the design of the negative stiffness element with pre-compressed springs.

Finally, the limits of the free design variables are: 1) the nominal EKD frequency f_0 (*Hz*) [*0.15 1.5*], 2) the negative stiffness element k_{NS} (*kN/m*) [*-30000 -1*] and 3, 4) the damping coefficients c_{PS} and c_{NS} (*kNs/m*) [*1 600*].

5.3.2.3 Numerical Example 5 – *Case Study on a 4-Story Building Structure*

A numerical case study has been conducted considering a 4-storey typical residential building. The structural system has 4 dynamic DoFs represented by the relative displacements of the 4 storeys with respect to the ground. The elastic modulus of reinforced concrete (assuming long-term cracked conditions) is equal to E=26 GPa. The mass of the building is considered to be concentrated at the floor levels, with m_i=80000 kg denoting the mass of the 4 storeys ($i=1,\dots,4$), while the columns are assumed to be weightless. The superstructure's damping coefficients are mass and stiffness proportional (Rayleigh damping), with ζ_{Si}=0.02 ($i=1,\dots,4$).

The geometry of the model is presented in Figure 5.27 below. A *15x15 m* floor in plan-view has been considered with *0.3x0.3 m* square columns. Analysis for different foundation widths (B) and soil material properties has been undertaken and results for a single case are presented herein. Therefore, the material under investigation has an undrained shear strength equal to S_u=70 kPa and a G_0=53 MPa. The footing width (B) is considered as 1.50 *m* and a total FoS against vertical loading equal to 3.8 is calculated, hence ensuring the static stability of the system. For more details regarding the selection of the material properties refer to section 5.3.2.1 of this Chapter. The soil-structure interaction is regarded in the excitation analysis as explicitly detailed in section 5.3.2.1 of this Chapter and the parameters of the EKD are optimized based on the methodology described in section 5.3.2.2. A Matlab-based code is incorporated to model the structure and extended KDamper system as a series of masses and springs; linear and non-linear representing the structural elements and soil-foundations respectively. A number of artificial and real seismic excitations are subsequently applied and

the response of the structure is investigated. Results of the analysis are presented in Figure 5.28 and Tables 5.8 and 5.9 below.

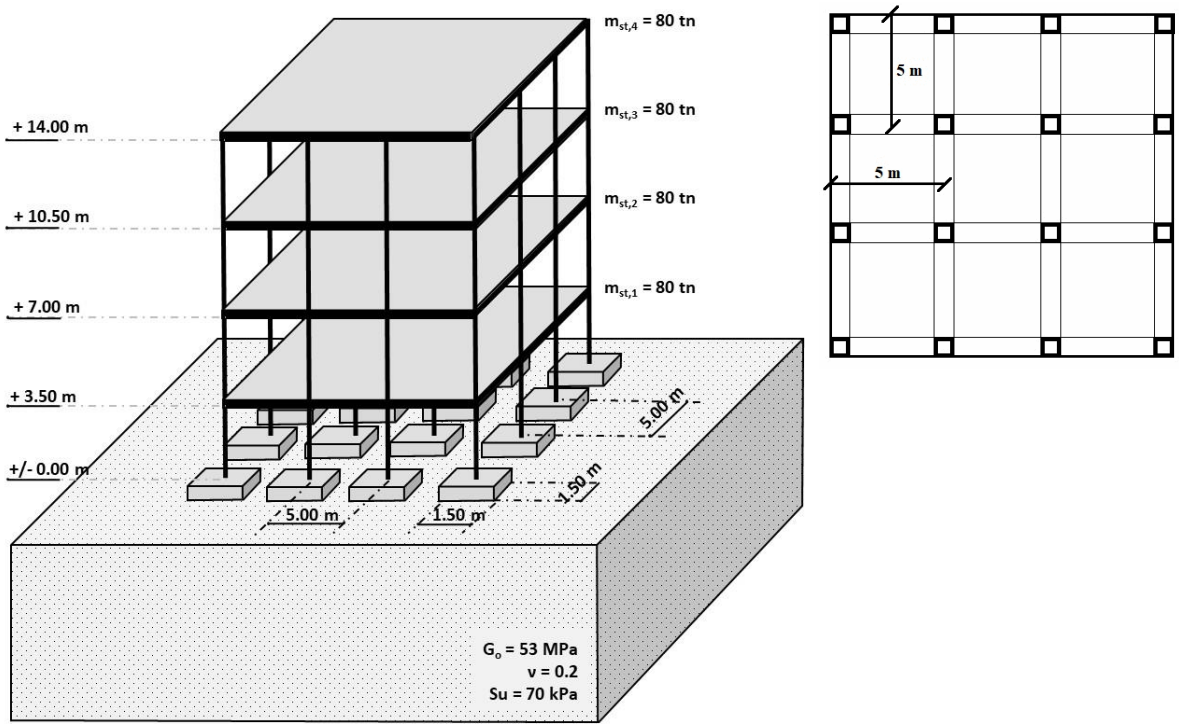

(a) (b)

Figure 5.27: *(a) Typical 4-storey residential building investigated as a case study, and (b) plan view of a typical floor of the building considered in this case study.*

Table 5.8: *Dynamic responses (mean of max values) of the four examined residential building systems (with fixed footings, with SSI footings, with KDamper and fixed footings, with KDamper and SSI footings) for all the selected artificial accelerograms.*

Structural System	$a_{S,4}$ (g)	$u_{S,1}$ (cm)	$u_{col,1}$ (cm)	$u_{SSI,1}$ (cm)	V_B (kN)
Building with fixed footings	1.18	3.91	3.91	-	2,540
Building with SSI footings	1.08	6.67	2.02	4.65	1,310
Building with KDamper & fixed footings	0.35	3.32	3.32	-	640
Building with KDamper & SSI footings	0.29	3.29	1.36	1.93	518

Table 5.9: *Dynamic responses (max values) of the four examined residential building systems (with fixed footings, with SSI footings, with KDamper and fixed footings, with KDamper and SSI footings) for a near fault earthquake record (L'Aquila, 2009, Mw = 6.3).*

Structural System	$a_{S,4}$ (g)	$u_{S,1}$ (cm)	$u_{col,1}$ (cm)	$u_{SSI,1}$ (cm)	V_B (kN)
Building with fixed footings	1.13	2.35	2.35	-	1,527
Building with SSI footings	0.89	5.72	1.85	3.88	1,204
Building with KDamper & fixed footings	0.29	3.60	3.60	-	745
Building with KDamper & SSI footings	0.29	4.50	1.61	2.90	400

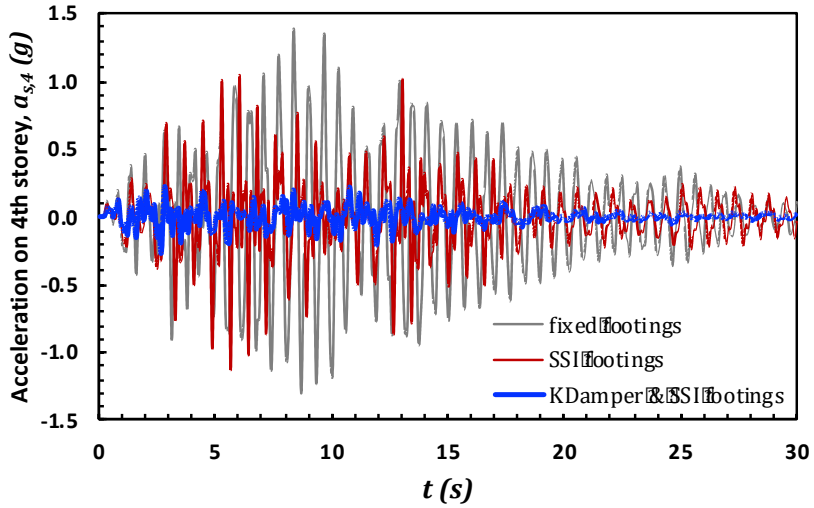

(a)

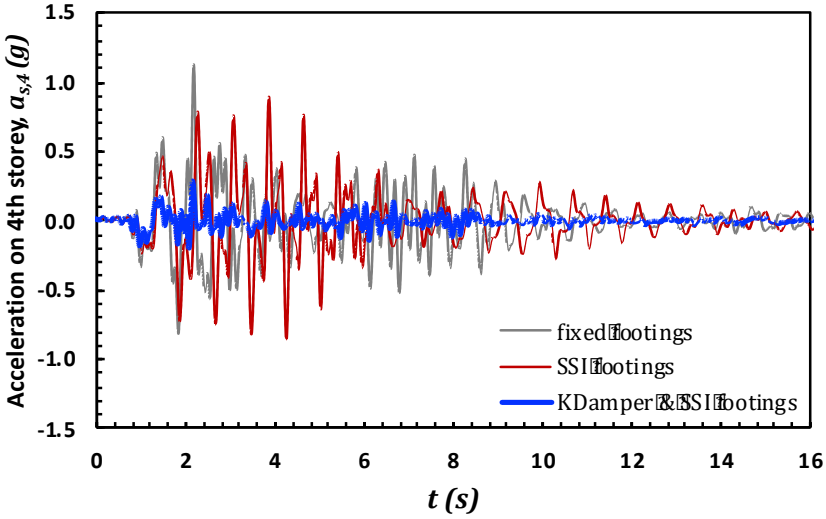

(b)

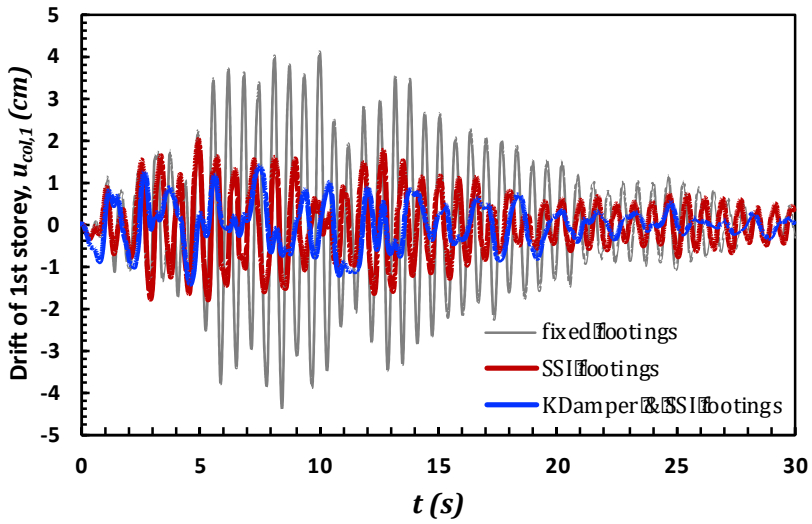
Drift of 1st storey, $u_{col,1}$ (cm)
t (s)
fixed footings
SSI footings
KDamper & SSI footings

(c)

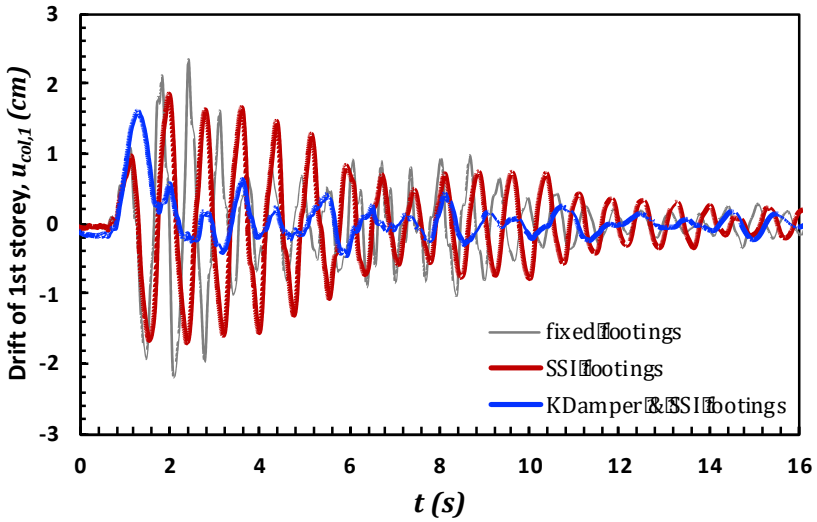
Drift of 1st storey, $u_{col,1}$ (cm)
t (s)
fixed footings
SSI footings
KDamper & SSI footings

(d)

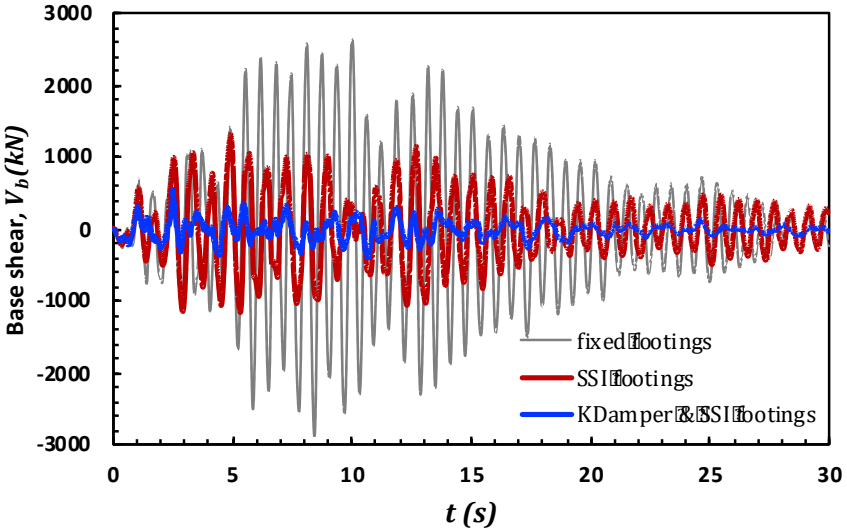
Base shear, V_b (kN)
t (s)
fixed footings
SSI footings
KDamper & SSI footings

(e)

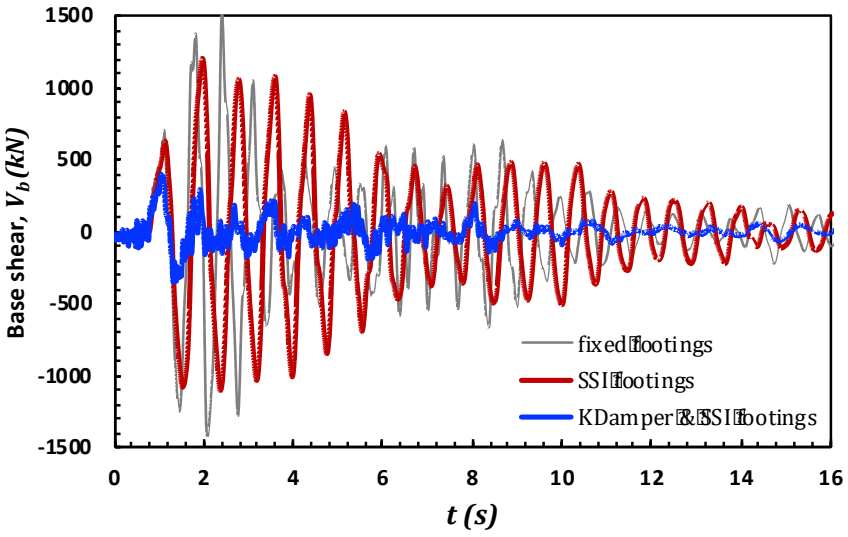

(f)

Figure 5.28: *Comparative results in terms of absolute acceleration of the top storey of the structure, horizontal displacement (drift) of the 1st floor, and base shear-force of the structure for one artificial accelerogram (a, c, e) and the L'Aquila earthquake record (b, d, f) respectively.*

A comparison between the response of the structural model considering a) fixed foundations, b) SSI effects by incorporating the non-linear stiffness of the soil and c) the EKD coupled with SSI effects is undertaken for one of the artificial accelerograms (matching the EC8 design spectrum) and a real earthquake excitation. It can be observed that, the application of the extended KDamper along with the SSI effects lead to the main following results:

1. The EKD together with the SSI effects appear to improve the structural response under a dynamic seismic excitation, indicating that the non-linearity of the overall system stiffness parameters does not lead to detuning of the damper;
2. A *40-70%* reduction of the absolute acceleration values of the building stories is achieved, hence remaining within the structural limits;
3. The base shear values appear to be significantly reduced in accordance with the absolute acceleration values;
4. The total horizontal displacement of the first floor is slightly reduced compared to the fixed footings. However, as indicated in Figure 5.29 below, due to the rotational and horizontal movement of the foundation the total displacement is distributed between the column and the footing (SSI) and consequently structural flexural displacements are reduced and remain within an acceptable region.

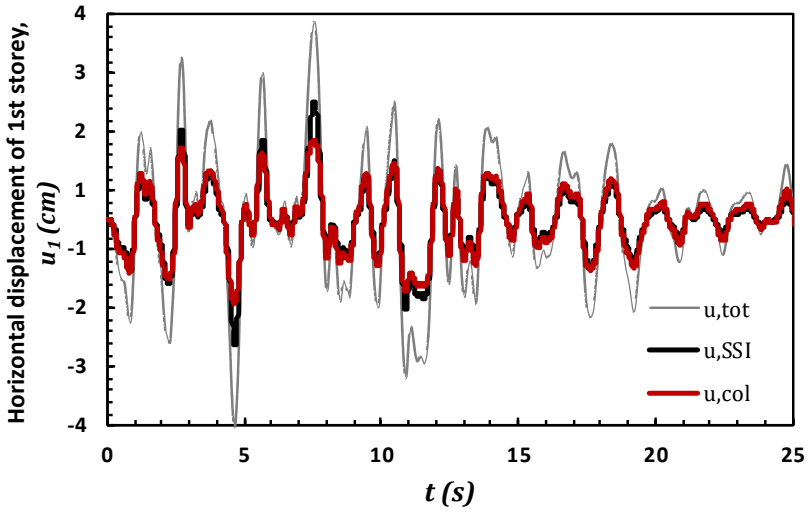

(a)

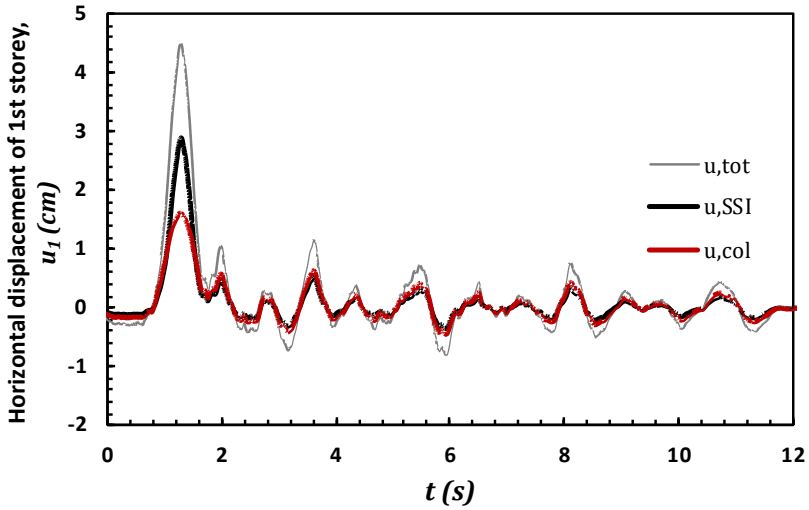

(b)

Figure 5.29: *Distribution of the first storey total horizontal displacement due to the flexural deformation of the column (drift) and deformation due to SSI effects (horizontal and rotational movement of the footing), for the case of an artificial accelerogram (a), and the L'Aquila record (b)*

As it can be observed in Figure 5.29, although the displacement of the first storey for the case of an artificial accelerogram (u_{tot}) reached *3.36 cm*, it was distributed both in the column, in the form of flexural deformation (u_{col}), and in the footing, in the form of predominantly rotational, and also translational displacement, due to the SSI effects (u_{SSI}). The maximum flexural deformation was a mere *1.37 cm*, which is almost three times lower than the flexural deformation that was demanded in the case of the building with no seismic protection. The 1st-

storey displacement is primarily undertaken by the SSI mechanism, meaning that during the shaking, the equivalent soil-foundation stiffness of a single footing *1.50 m x 1.50 m* has dropped below the structural column stiffness of a single column, equal to 4,000 kN/m. In general, the distribution of the stiffness in the column-footing-soil system governs the distribution of the deformation in these components. It should be highlighted that for the case of either wider surface footings, or for footings whose rotational and horizontal displacement have been kinematically constrained, as in the case of footings connected with strap beams, the equivalent soil-foundation stiffness of the system increases dramatically, and hence the displacement is not distributed among the column and the foundation. Thus, the total displacement is undertaken by the columns leading to additional loading of the structural elements.

5.4 Seismic Protection Configurations Based on Extended KDamper Equipped with Inerter

In this section, a stiff seismic base absorber (SBA) is proposed, that combines the extended KDamper concept (EKD) with an inerter. An inerter is first implemented, connecting directly the structure to the ground. This results to the decrease of the natural frequency and the seismic load of the structure, without the decrease of the structural stiffness. Parallel, an extension of the KDamper concept (EKD) is used, in order to increase the apparent damping behavior of the inerter. Section 5.4.1 presents the optimization problem from which the system parameters are selected. Proper limitations and constraints are imposed on the free design variables and main dynamic responses, respectively. The excitation input is selected according to section 3.3.2.1 of Chapter 3. The dynamic performance of a SDoF system controlled with the SBA is evaluated in the Numerical Example 6, with real earthquake records and a realistic displacement-dependent configuration, according to the Proposed Configuration II of Chapter 3. Numerical Example 7 presents the extension of the optimal design of the SBA in MDoF structural systems. A 3-story building structure is assumed in which the SBA is implemented in its base. The effectiveness of the SBA is observed based on a comparison with: 1) a conventional base isolated system (BI), 2) a highly damped BI system (BI-HD), 3) a conventional BI system equipped with an inerter device (BI-I) and 4) an extended KDamper concept (EKD) implemented in the base. Finally, an indicative design of the implemented SBA devices is presented, where the SBA components are realistically designed, and proves that the design of the SBA devices is realistic and within reasonable technological capabilities.

5.4.1 Statement of the Optimization Problem

The given parameters of the SBA are the additional mass m_D and the stability factors ε_{NS}, $\varepsilon_{PS,}$ and ε_R. The free design variables sough in the optimization problem are: 1) the nominal SBA frequency f_0, 2) the NS element value k_{NS}, 3, 4) the damping coefficients c_{NS} and c_{PS} and 5) the inerter coefficient, b. The structure relative to the base displacement is set as the objective function. In order for the proposed vibration control strategy to be efficient and realistic, the constraints that refer to the structural dynamic responses and the limits of the free design variables must be engineering-criteria based. In particular:

i. An acceleration filter (AF) is placed as a constraint for the structure absolute acceleration, expressed as a percentage of the mean PGA.
ii. The NS element stroke ($X_{S\text{-}D}$) is set as a constraint, with an upper limit that of *12 cm*, which based on the previous work of (Kapasakalis et al., 2019) proves to be a realistic value for the design of the negative stiffness element with pre-compressed springs.
iii. According to previous work of KDamper, an additional mass of *5%* is efficient. In an effort to make the device more realistic and easier to implement, m_D is selected as *0.1%* of the structure mass.
iv. The stability factors ε_{NS}, $\varepsilon_{PS,}$ and ε_R are selected equal to *10%*.
v. The damping coefficients c_{NS} and c_{PS} upper limit is *600 kNs/m*. Common linear damping devices can be used.
vi. The nominal SBA frequency f_0 varies in the range *[0.15 1.5]* (*Hz*).
vii. The NS element absolute maximum value is set as |*-15000*| *kN/m*, which based on previous indicative designs of the NS element realized with pre-compressed springs, (Antoniadis et al., 2018) and (Kapasakalis et al., 2019) (in Greek), for m_{tot}*=300 tn* is a realistic value (*50%* lower compared to (Kapasakaliset al., 2019)).

The addition of the inerter, that connects the structure directly to the base, aims to reduce the nominal frequency f_0 of the EKD. The inerter, b is expressed as a *%* of the structure mass, m_S. In order to observe its effectiveness to the system responses, 3 cases regarding the implementation of the inerter are considered. In the first case, only the EKD is considered (b_{max}*=0*). In the second and third cases, the SBA's maximum inerter coefficient is b_{max}*=1* (100*%*) and *2* (200*%*) respectively. Figure 5.30 presents these 3 optimized test cases. It is observed that the addition of the inerter manages to greatly reduce the structure relative

displacement and NS element stroke in all the range of the Acceleration Filter. The increase of the upper limit of *b* over than *1*, does not improve the dynamic structural behavior.

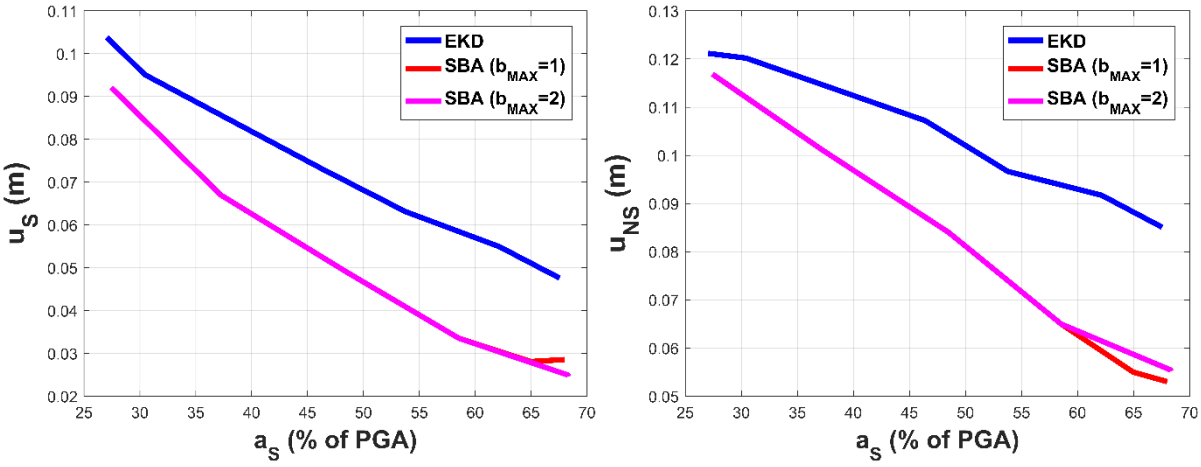

(a) (b)

Figure 5.30: *(a) Structure relative displacement, and (b) NS element stroke (mean of 30 max) over the structure absolute acceleration (% of the mean PGA) of the SBA with various values of the upper limit of the inerter.*

The performance of the SBA-*AF* is compared with the previous optimal design of KDamper, as presented in (Kapasakalis et al., 2019c). For this reason, two sets of parameters of each concept, that present similar results, in terms of the structure's dynamic responses, are selected and compared in Table 5.10. It is observed that the SBA (b_{max}=1) manages to reduce the structure relative displacement and the NS element stroke, at the same time, in all the range of the imposed acceleration filter (*AF*), as compare with the previously optimized KDamper presented in (Kapasakalis et al., 2019c) and the EKD with the same limitations and constraints as the SBA. Finally, the transfer functions of the SBA-30,50 and 70 are presented in Figure 5.31 and are compared with a highly damped base isolation system with a damping ratio of 20% (BI-HD), and a natural base frequency equal to 0.4 *Hz*. The maximum value of the structure acceleration Transfer Function H_{AS} of the SBA system, increases as the imposed acceleration filter increases, as well as the frequency content of the H_{AS}, as expected. The structure relative displacement Transfer Function H_{US}, is improved in all frequency range as the acceleration filter (*AF*) increases. The same applies in the SBA relative displacement Transfer Function H_{UD}. As compared to the BI-HD system, the H_{AS} has a smaller maximum value, however as the *AF* increases, also the frequency content increases, and the H_{US} is dramatically improved in all frequency range for all the values of the design *AF*.

Table 5.10. *Comparison of the KDamper and SBA system proposed in this section.*

#	Examined system	a_S (m/sec^2)	a_S (% *of* PGA)	u_S (m)	u_{NS} (m)	ε_i (%)
Set #1	KDamper	2.085	40.2	0.093	0.363	$\varepsilon_{NS}=5$
	SBA-30 ($b=0$) / EKD	1.579	30.4	0.0951	0.1202	$\varepsilon_{NS,PS,R}=10$
	SBA-30 ($b_{max}=1$)	1.934	37.3	0.0669	0.1011	$\varepsilon_{NS,PS,R}=10$
Set #2	KDamper	3.692	71.1	0.0379	0.163	$\varepsilon_N=5$
	SBA-70 ($b=0$) / EKD	3.225	62.1	0.0549	0.0917	$\varepsilon_{NS,PS,R}=10$
	SBA-70 ($b_{max}=1$)	3.372	65.0	0.0281	0.055	$\varepsilon_{NS,PS,R}=10$

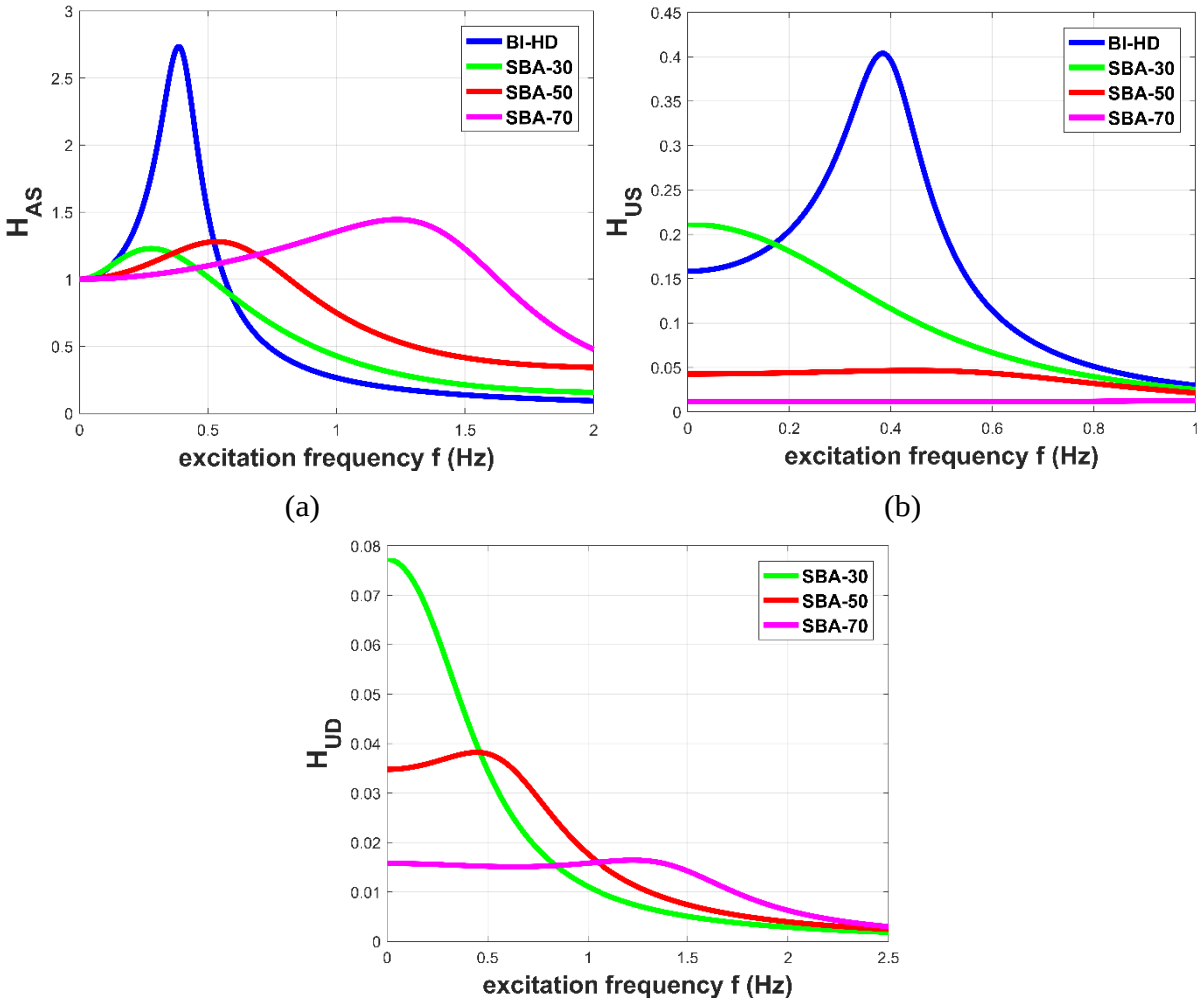

Figure 5.31: *Transfer Functions of the SBA-30, 50 and 70 systems compared with a highly damped base isolated one (BI-HD). (a) absolute acceleration H_{AS}, (b) relative displacement H_{US}, and (c) relative displacement H_{US}.*

5.4.2 Numerical Example 6 – *SDoF Dynamic Performance*

The effectiveness of the proposed base absorber (SBA) is examined also with real earthquake records, considering a realistic displacement-dependent non-linear configuration for the realization of the NS element, following the procedure described Proposed Configuration II of Chapter 3. The selection of the NS element's set-up requires the solution of a linear problem first in order to estimate the maximum absolute displacement values that are necessary for the design, as described in section 5.4.1 for the optimal SBA parameters. The real earthquake excitations selected in this section are the 12 near and 12 far fault earthquake records presented in section 5.2.1.2, Table 5.3.

In order to observe the efficiency of the SBA, it is compared with 2 base isolated systems. The first one is a conventional base isolated system with a damping ratio of 5% and will be referred hereafter as BI, the second one is a highly damped BI with an increased damping ratio of 20% and will be referred hereafter as BI-HD. The considered base isolated systems have both a base natural frequency equal to 0.4 *Hz*. Figure 5.32 presents the system dynamic responses of all the examined control systems and considered earthquake excitations.

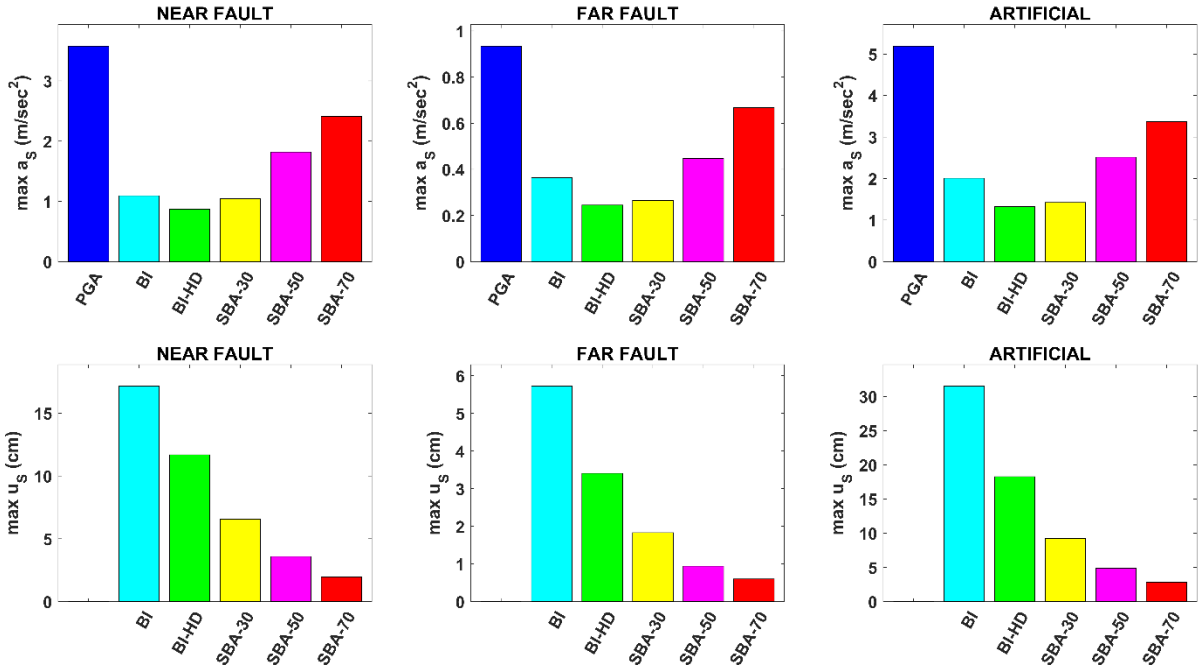

Figure 5.32: *Max values of the dynamic responses of the examined control systems (BI, BI-HD, SBA-AF) for all the artificial accelerograms (mean of 30 max), real near-fault earthquake records (mean of 12 max) and real far-fault earthquake records (mean of 12 max).*

Figure 5.33 presents comparative results between a conventional base isolated system (BI) and the SBA-30 system, considering linear NS and non-linear NS with the Proposed Configuration II proposed in Chapter 3, for the Loma Prieta earthquake excitation. The SBA retains the structure absolute acceleration at comparable levels with the BI, while the structure relative displacement is reduced by more than 60%. Finally, it is observed that the dynamic responses of the proposed displacement-dependent non-linear configurations are in a very good agreement to that of the initial linear system previously solved.

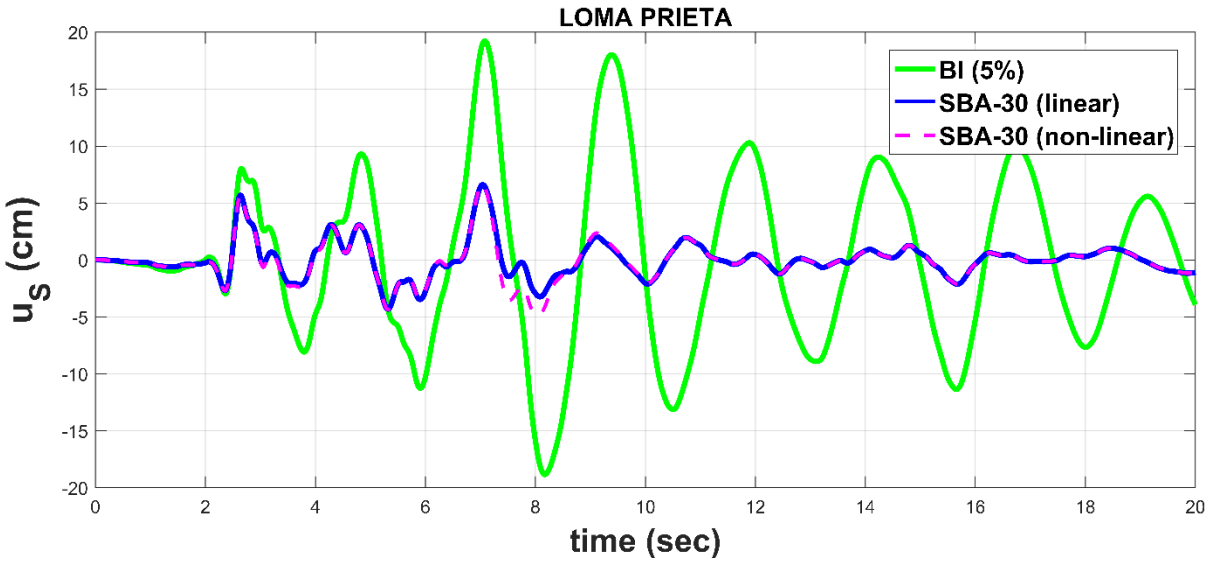

(a)

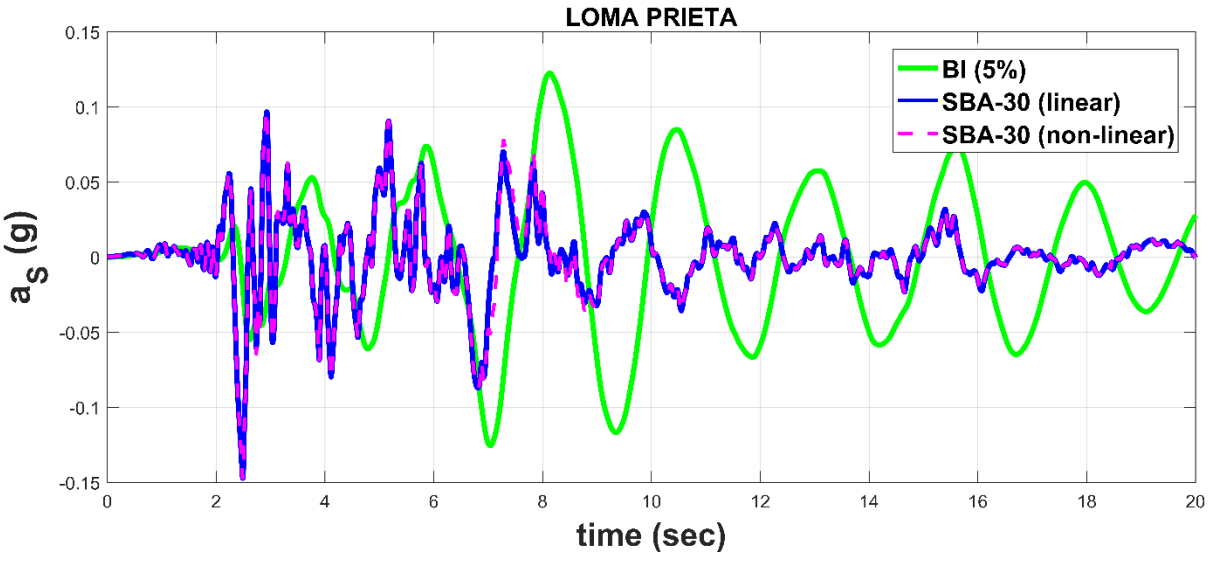

(b)

Figure 5.33: *Dynamic responses of the SBA-30 system, considering linear NS and non-linear NS, compared with a BI system, for the Loma Prieta earthquake excitation. (a) Structure relative displacement u_S, and (b) structure absolute acceleration a_S.*

The results of the non-linear system are proven to be equivalent to the initially solved linear one. In conclusion, the SDoF system controlled with SBA manages to retain the structure absolute acceleration at acceptable levels, while at the same time the structure relative displacement is significantly low.

5.4.3 Numerical Example 7 – *Preliminary Assessment of the Extended KDamper Equipped with Inerter Implemented in the Base of a 3-Story Building Structure and Detuning Phenomena*

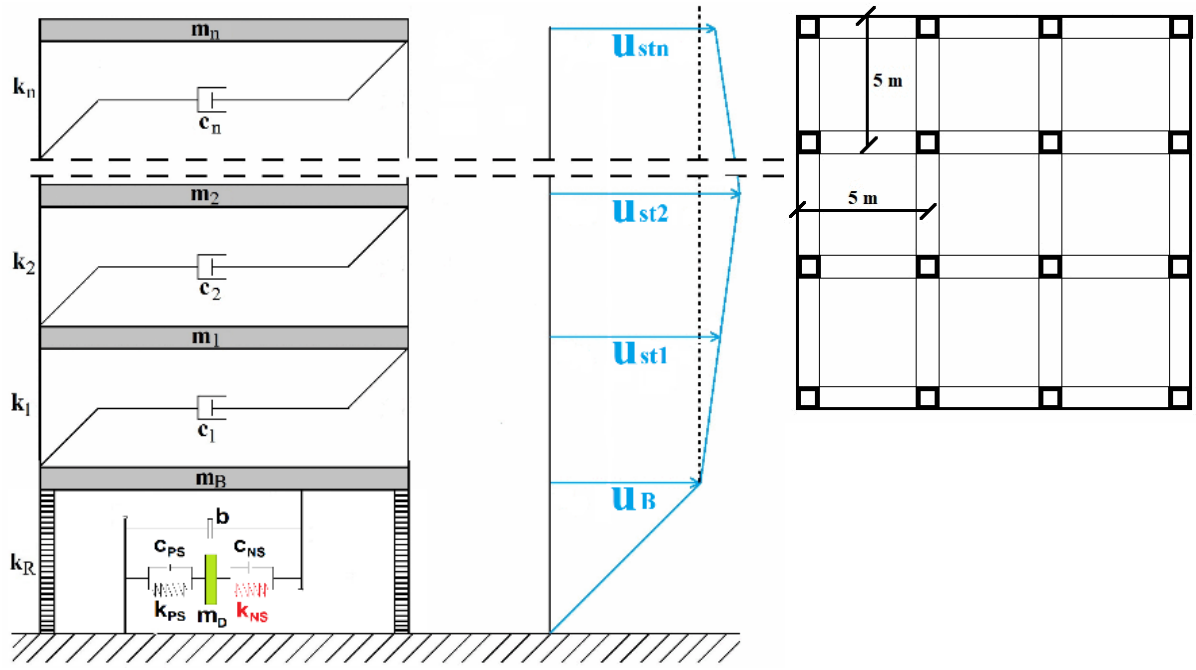

(a) (b)

Figure 5.34: *(a) Multi-story building with the proposed seismic base absorber system, SBA (sketch of the model), and (b) typical ground floor plan of the structure.*

In this numerical example, the proposed control strategy (SBA) is extended for possible implementation in MDoF structural systems. The optimal SBA parameters are selected according to the methodology proposed in section 5.4.1. In order to examine the efficiency of the SBA, the controlled system is subjected to artificial accelerograms and real earthquake records, and is compared with 3 cases of base isolated systems.

The proposed stiff seismic base absorber, SBA, is implemented in the bases of multi-story building structures, as illustrated in Figure 5.34.a. Regarding the modeling of the superstructure, it is assumed that: the dynamic DoFs are collected in the array $[u_{st}(t)]=[u_{st1}(t),$

$u_{st2}(t)$, …, $u_{stn}(t)]^T$, where u_{sti} represents the relative to the ground displacement of the i^{th} floor, the superstructure response is considered elastic and the SSI (soil structure interaction) effects are ignored. Taking into consideration the aforementioned assumptions, the equations of motion of the controlled system involve matrices with dimensions $(n+2) \times (n+2)$:

$$[M][\ddot{u}(t)]+[C][\dot{u}(t)]+[K][u(t)]=-[\tau]a_G(t) \tag{5.15}$$

A numerical case study has been conducted considering a 3-story typical residential building. The structural system's dynamic DoF are represented by the relative to the ground displacements of the 3-stories. The elastic modulus of reinforced concrete (assuming long-term cracked conditions) is equal to $E=26\ GPa$. The mass of the building is considered to be concentrated at the floor levels, with $m_i=80\ tn$ denoting the mass of the 3 stories, while the columns are assumed to be weightless. Rayleigh damping is assumed (mass and stiffness proportional) with $\zeta_{Si}=0.02$. A $15\times15\ m$ floor plan-view has been considered with $0.3\times0.3\ m$ square columns. According to performed modal analysis, the natural periods of the original structure are: $T_{Si}\ [sec] = [0.495, 0.177, 0.122]$. The mass of the base is equal to $60\ tn$ and the additional mass m_D is selected equal to 0.1% of the $m_{S,tot}$: $0.1\%\ m_{S,tot}=0.1\%(60+3\times80)=0.3\ tn$. The calculation of the matrices of mass [M], stiffness [K], and damping [C] of the initial 3-story structure, the procedure from which the SBA design is extended for implementation in MDoF structural systems, are presented in Appendix A2.

In order to observe the efficiency of the proposed system, SBA, the results of the controlled structure are compared to other seismically protected structures. In particular: 1) a conventional base isolated structure with ζ_B=5% and f_B=0.4 *Hz* (BI), 2) a highly damped base isolated structure with an increased damping ratio of 20% (BI-HD), 3) a conventional base isolated structure equipped with an inerter (BI-I) and 4) a controlled structure with the extended KDamper implemented at the base of the structure, without the inerter (EKD, SBA with b=0). Comparative results: a) of the top floor absolute acceleration, b) the total base shear, and c) the base relative displacement between the initial (IN), the conventional Base Isolated system (BI) and the SBA-*70*, are presented in Figure 5.35. The presented time histories relate to the Chi-Chi earthquake (1999). Figure 5.36 presents the system main dynamic responses of all the examined control systems and considered earthquake excitations. It is observed that the SBA-70 manages to greatly reduce the superstructure dynamic behavior, retaining the base displacement drastically low (few centimeters).

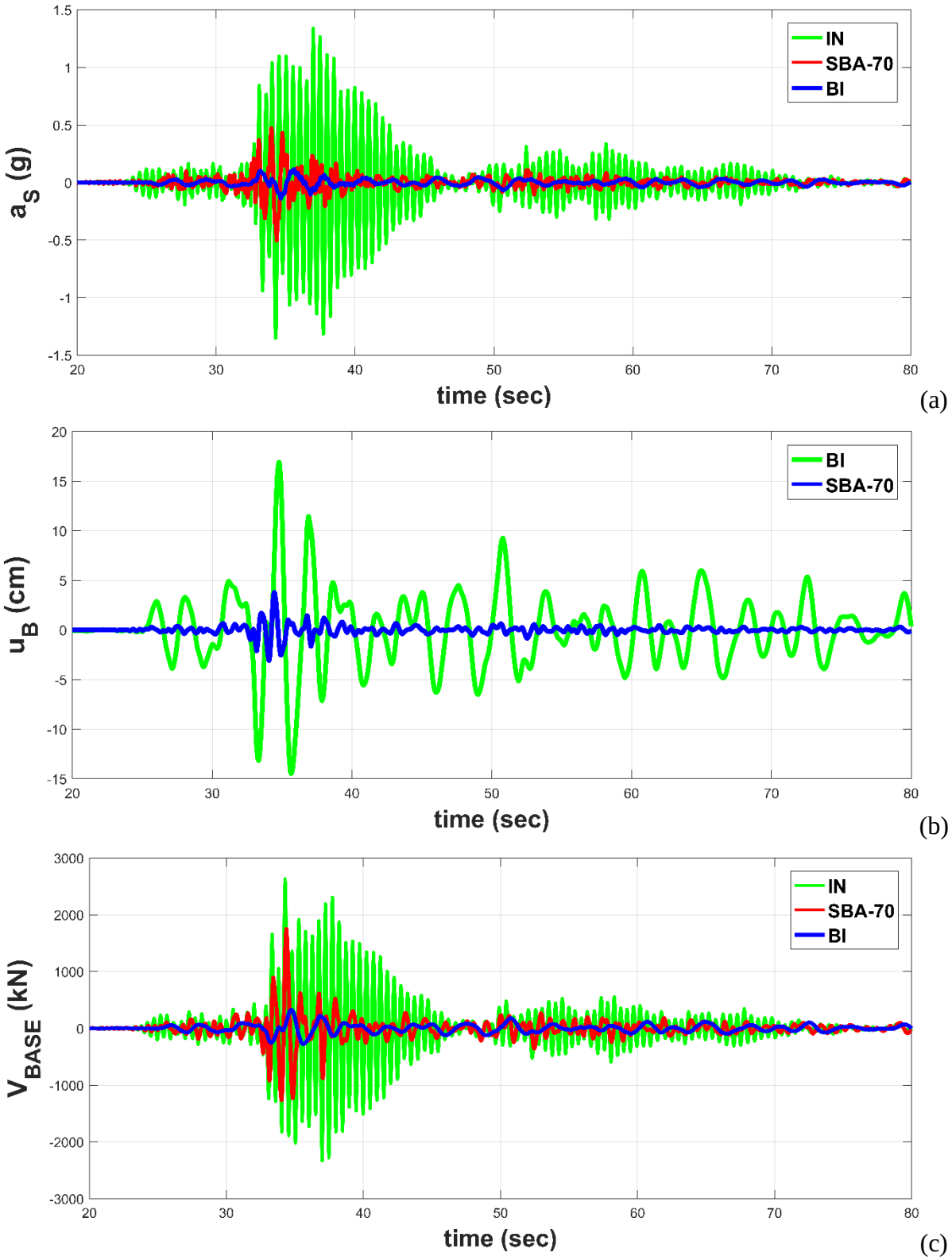

Figure 5.35: *Comparative results, in terms of: (a) top floor absolute acceleration (g), (b)base's relative displacement (cm),and (c) total base shear (kN), between the IN, BI, and the SBA-70, for the Chi-Chi earthquake record (1999).*

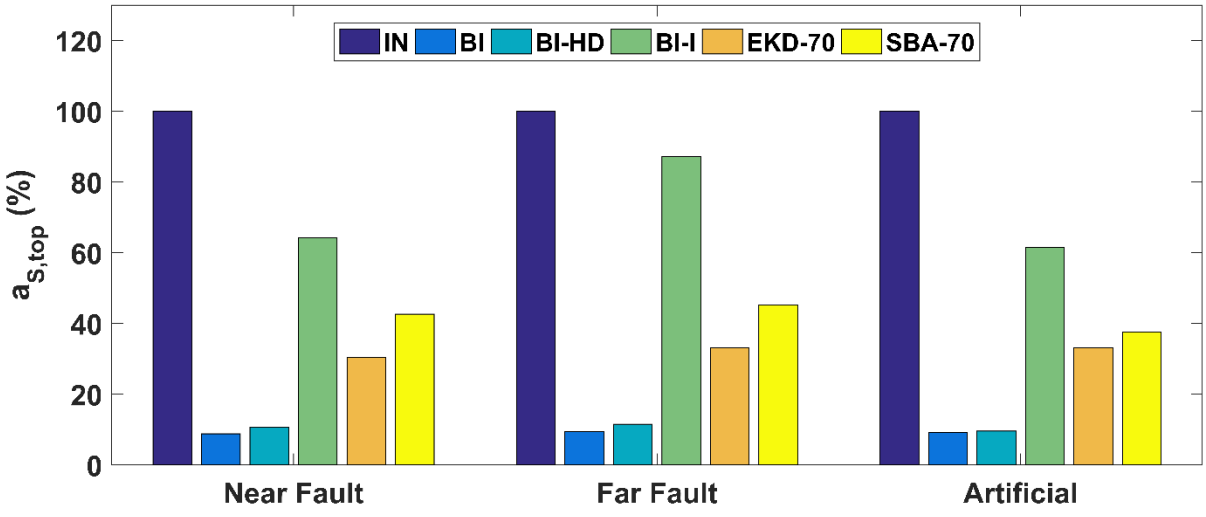
IN
BI
BI-HD
BI-I
EKD-70
SBA-70
$a_{S,top}$ (%)
120
100
80
60
40
20
0
Near Fault
Far Fault
Artificial

(a)

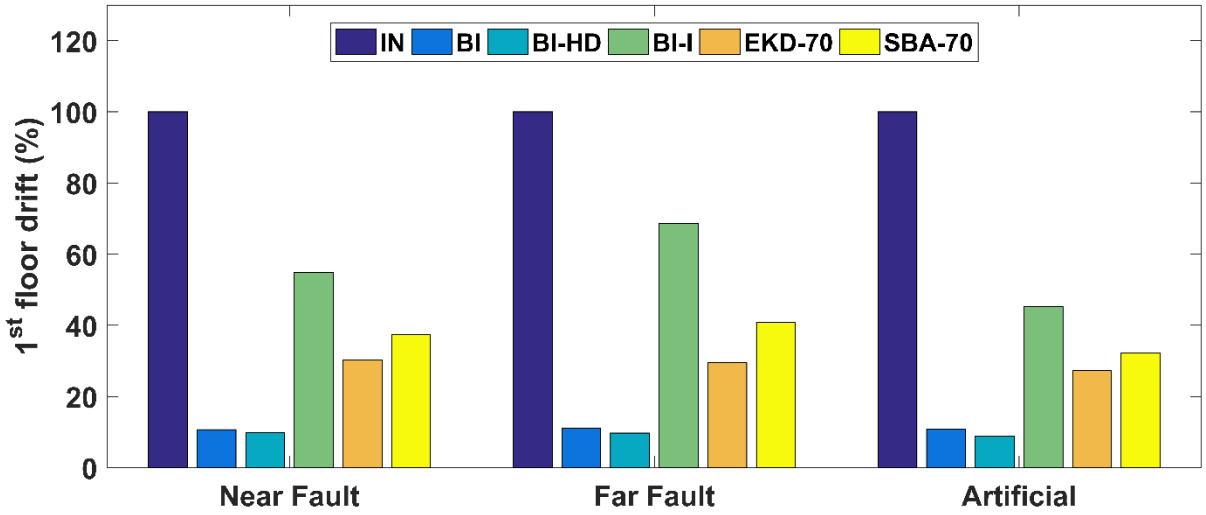
IN
BI
BI-HD
BI-I
EKD-70
SBA-70
1st floor drift (%)
120
100
80
60
40
20
0
Near Fault
Far Fault
Artificial

(b)

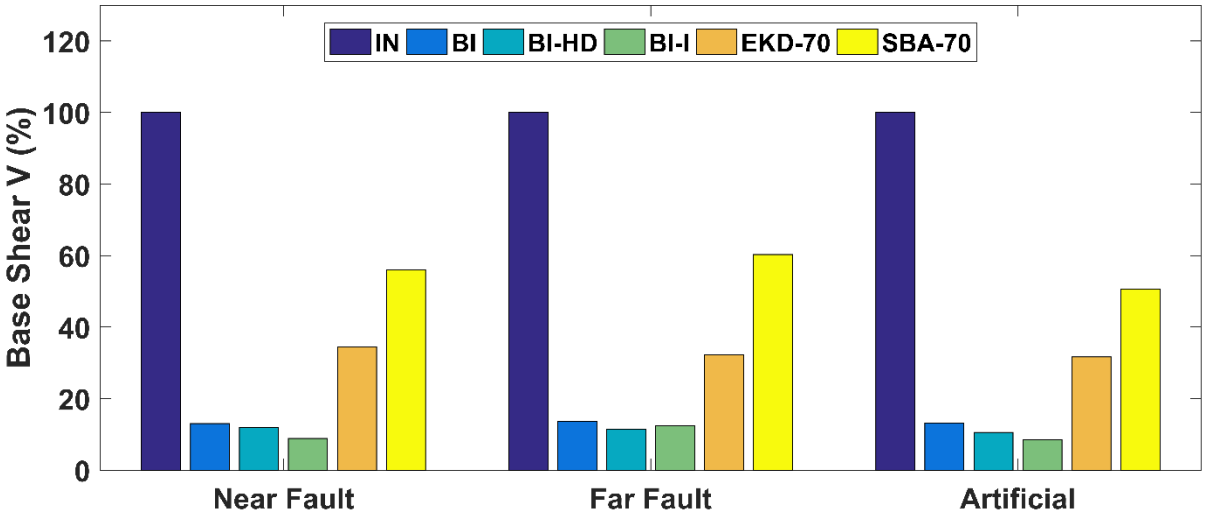
IN
BI
BI-HD
BI-I
EKD-70
SBA-70
Base Shear V (%)
120
100
80
60
40
20
0
Near Fault
Far Fault
Artificial

(c)

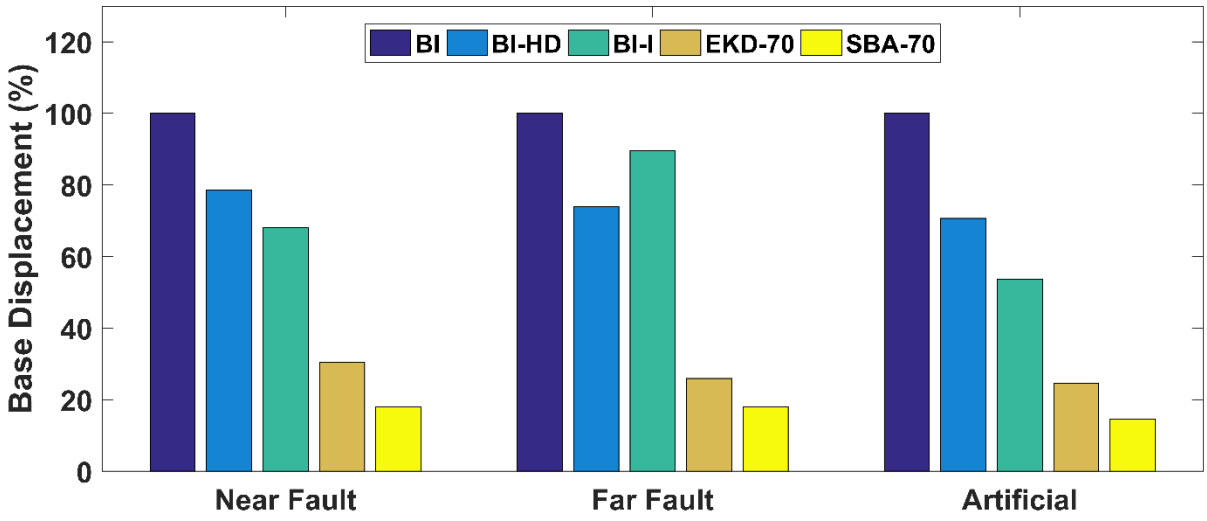

(d)

Figure 5.36: *Max values of the dynamic responses of the examined control systems (IN, BI, BI-HD, EKD-70, SBA-70) for all the artificial accelerograms (mean of 30 max), real near-fault earthquake records (mean of 12 max) and real far-fault earthquake records (mean of 12 max). (a) top-floor acceleration, (b) 1st floor drift, (c) base shear and (d) base displacement.*

Once the optimal SBA parameters of a SDoF system have been derived in Section 5.4.1, the validity of the optimal design procedure is here assessed for a multistory building. To this aim, a sensitivity analysis is performed in which the SBA parameters are slightly varied from their actual optimal values found in the above optimization problem, in an attempt to assess to what extent, the dynamic response varies (degrades) accordingly. Time history analyses are performed with all the 30 artificial accelerograms generated according to section 3.2.2.1. Given the dynamic properties of the seismically protected building, and considering the SBA-70 set of optimized parameters, a 50% variation (detuning) of the SBA free design variables is explored, i.e. the interval [0.5 – 1.5]f_0, k_N, c_{NS}, c_{PS}, b and the additional mass m_D. For variation of each of these elements, the results of 30 time-history analyses are then averaged to obtain the mean values of a few response indicators, including: 1) top floor absolute acceleration a_S, 2) top floor displacement u_{top}, 3) 1st floor inter-story drift, 4) base relative displacement u_B, 5) NS element stroke $u_{B\text{-}D}$ and 6) total base shear V_{BASE}. It is expected that as the SBA parameters depart from their optimal values, the effectiveness of the vibration control decreases accordingly. Relevant results, in terms of surface and contour plots of the top floor absolute acceleration a_S, 1st floor drift and base displacement u_B are illustrated in Figures 5.37.a, b and c, respectively.

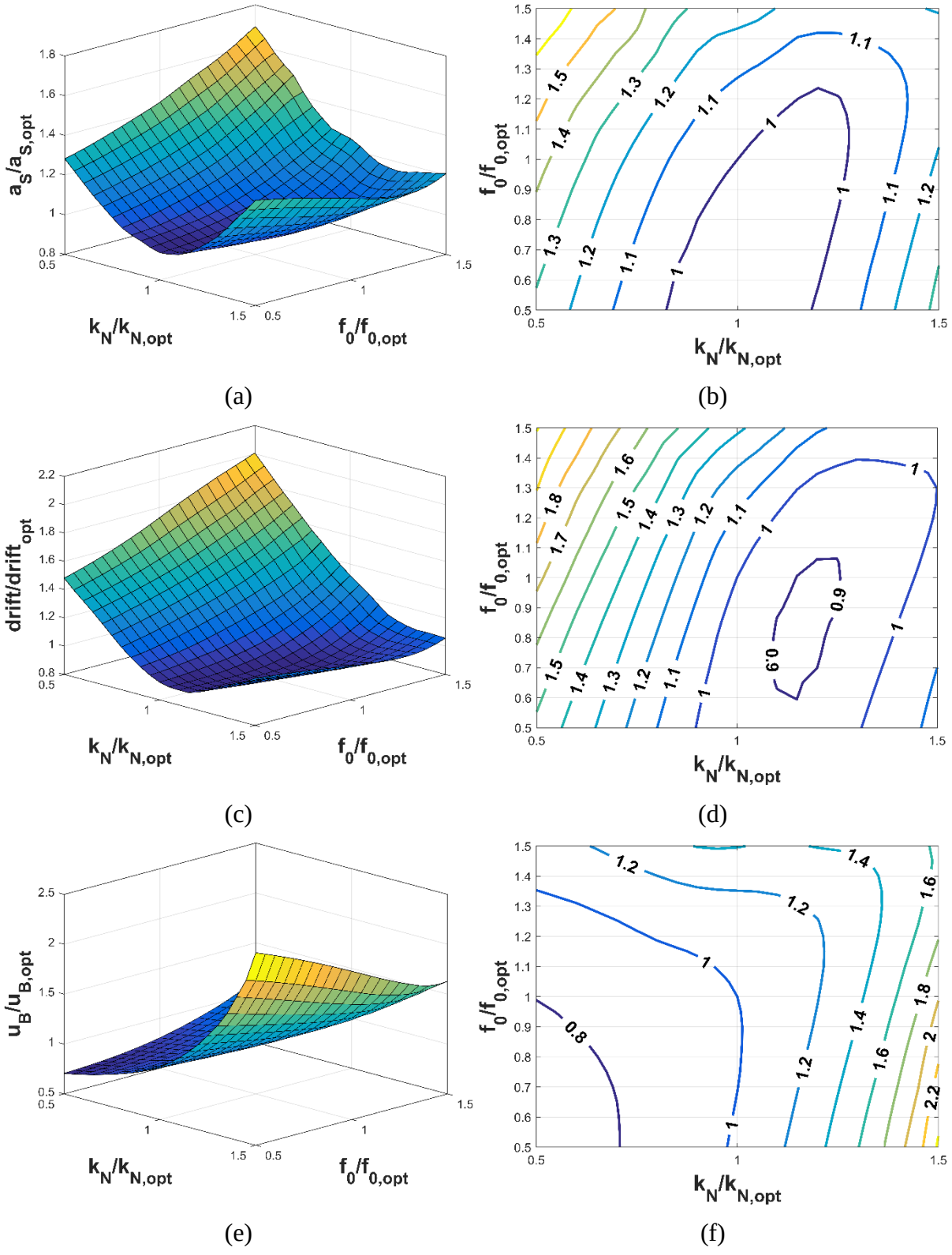

Figure 5.37: *Sensitivity analysis and detuning effects of the top floor absolute acceleration (a-b), 1st floor inter-story drift (c-d), and base relative displacement (e-f) by varying the free design variables of the SBA-70 set of optimized parameters, f_0 and k_N, from their optimal values by 50% each.*

It can be seen that the optimal SBA parameters based on the SDoF assumption lead to very accurate results for the system response in terms of displacements and accelerations. Indeed, the minimum top floor absolute acceleration a_S, 1st floor drift and base displacement u_B are attained almost where the SBA parameters match the optimal values f_0 and k_N obtained in section 5.4.1 (Figure 5.37). In Figure 5.38, the aforementioned response indicators are scrutinized by varying one SBA parameter one at a time, i.e. c_{NS}, c_{PS}, b, and m_D. It is observed that the detuning effects regarding the SBA parameters c_{PS} and m_D have no significant influence on the dynamic responses. On the other hand, variation of the c_{NS} influences mainly the NS element stroke and the base relative displacement and does not affect the superstructure response. The variation of b influences the top structure acceleration and displacement. However, variation of 50% of these parameters influences the responses by lower than 30%.

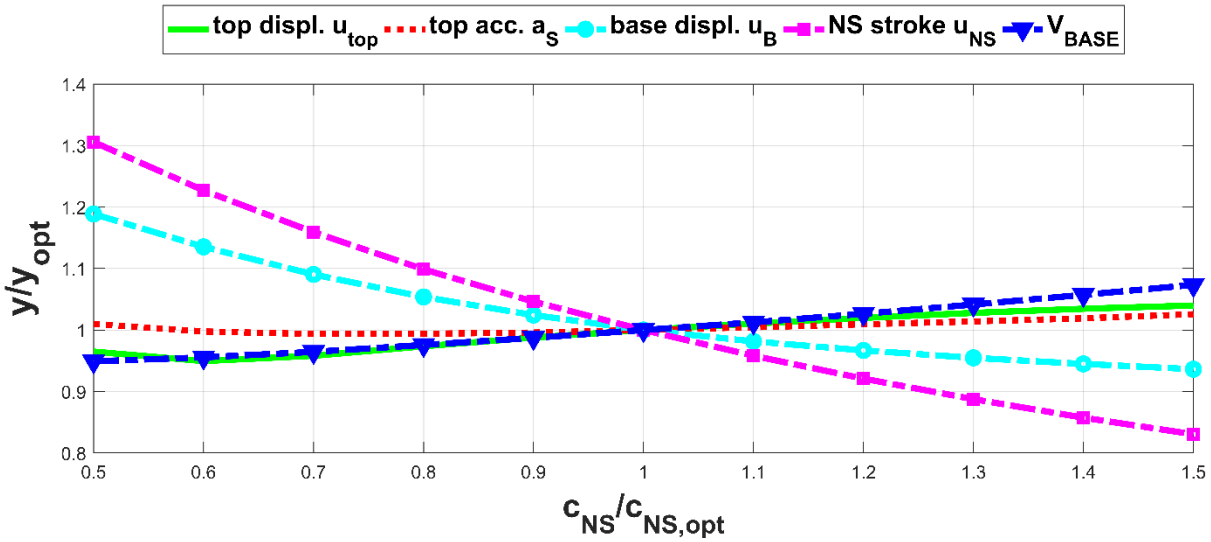

(a)

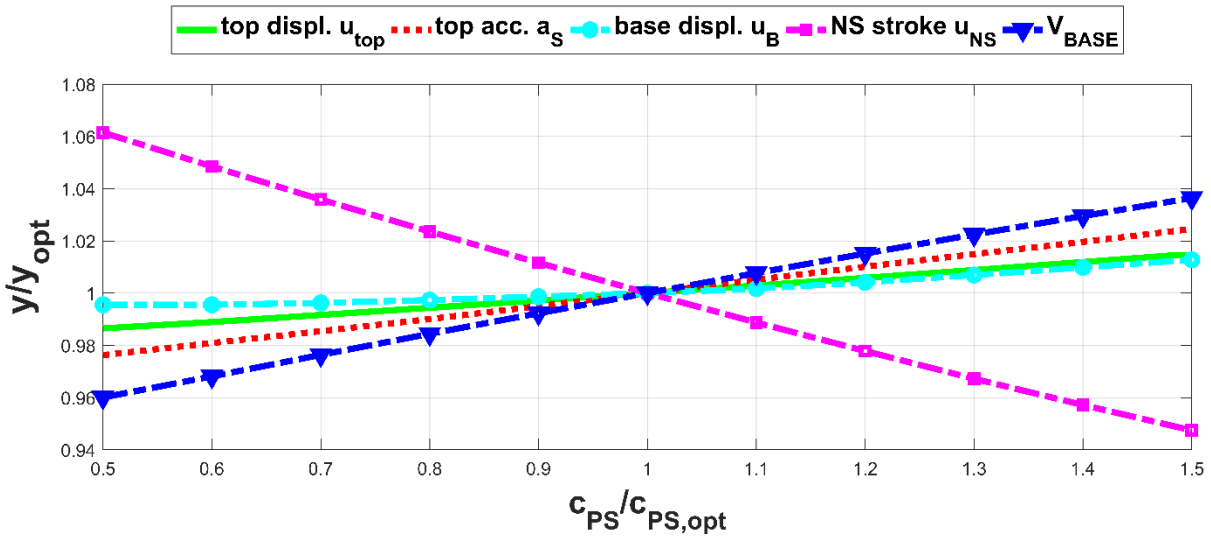

(b)

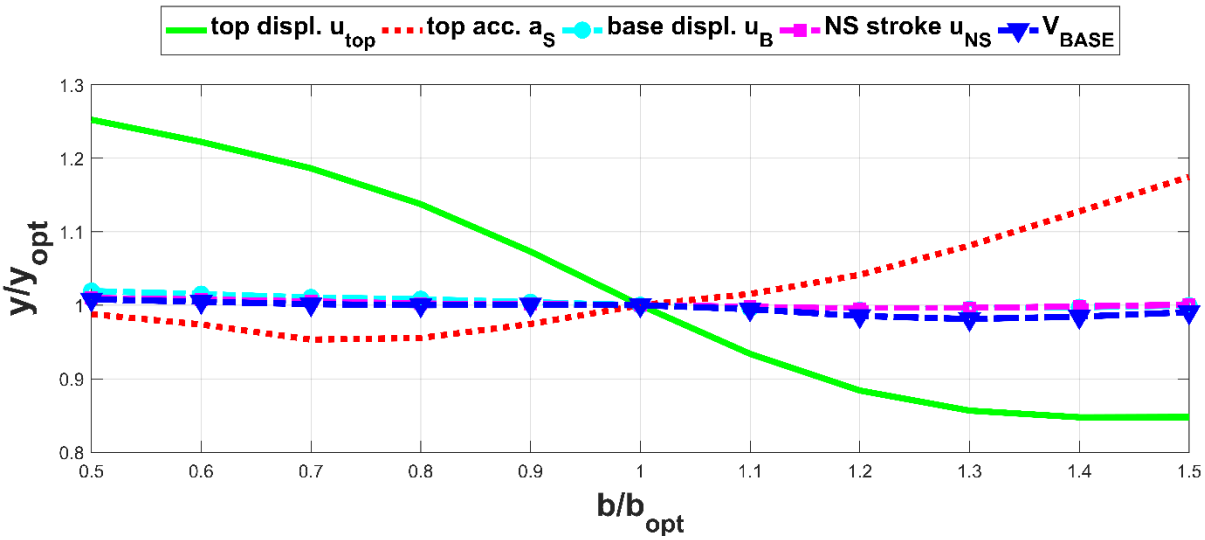

(c)

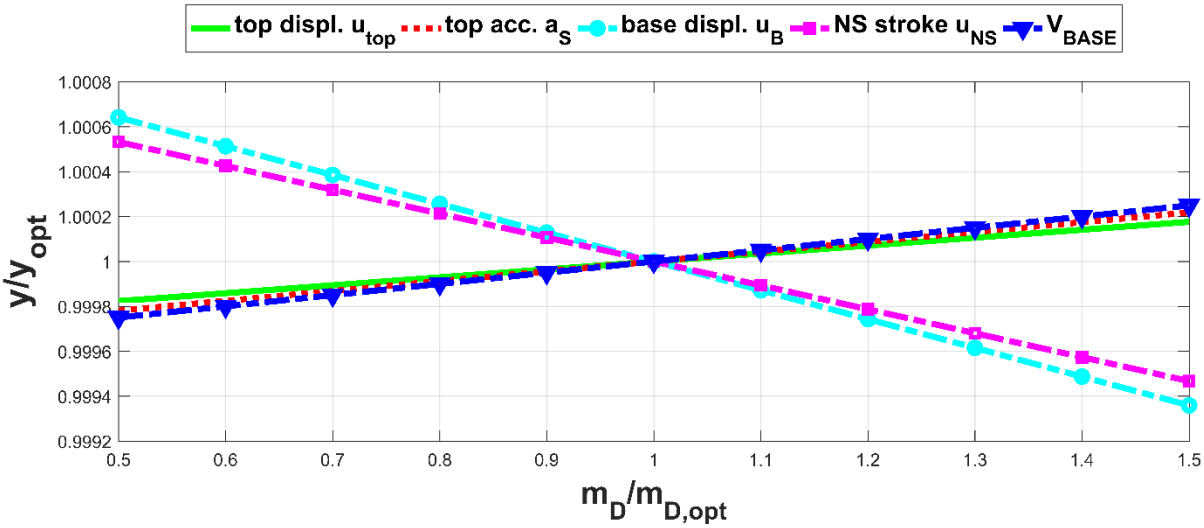

(d)

Figure 5.38: *Sensitivity analysis and detuning effect of five response indicators, u_{top}, a_S, u_B, u_{NS} and V_{BASE} by varying the SBA parameters: (a) c_{NS}, (b) c_{PS}, (c) b and (d) m_D.*

The selection of the NS element's set-up, as well as the positive stiffness elements, k_{PS} and k_R, the artificial dampers c_{NS} and c_{PS} and the additional mass m_D, require the solution of the linear problem first in order to estimate the maximum absolute dynamic responses that are necessary for the design. More specifically, the base relative displacement u_B relates to k_R, the NS element stroke $u_{B\text{-}D}$ relates to the NS element, the SBA relative displacement u_D relates to k_{PS}. The SBA-70 set of optimized parameters, implemented in a 3-story building structure with a total superstructure mass of 300 *tn*, is considered. The maximum values of the dynamic responses needed for the design is: $\max|u_B|$=0.0304 *m*, $\max|u_{B\text{-}D}|$= 0.055 *m* and $\max|u_D|$=0.0389

m. The parameters of the (total) SBA-70 components are presented in Table 5.11. The implementation is realized using 4 SBA devices.

Table 5.11. *SBA-70 set of optimized parameters.*

	f_0 (Hz) without b	f_0 (Hz) with b	k_{NS} (*kN/m*)	k_{PS} (*kN/m*)	k_R (*kN/m*)	c_{NS} (*kNs/m*)	c_{PS} (*kNs/m*)	b ($\%m_{tot}$)	m_D ($\%m_{tot}$)
SBA-70	1.5	1.07	-14287	24467	60996	564.2	394.1	97	0.1

Regarding the realization of the NS element, the proposed configuration presented in section 3.3.1.2 is followed, with 9 conventional steel spiral spring implemented per device. In Table 5.12, the NS element entire set-up is presented, regarding the proposed configuration of the NS element for each one of the four SBA devices, with k_{NS}=k_{NC}=(-14287/4)/9=-397 *kN/m*, *UB*=1.01, *LB*=0.9, $u_{B\text{-}D}$=*umax*=0.055 *m* and c_I=-0.05 (parameters regarding the NS element set up, (Antoniadis et al., 2018)).

Table 5.12. *NS element set-up for each SBA device.*

k_H (*kN/m*)	l_{HI} (*m*)	a (*m*)	d (*m*)	c_I
421.9	0.256	0.0758	0.26	-0.05

The artificial dampers are realized with four parallel damping elements implemented per device. The damping coefficients are low, c_{NS}=564.2/(4*4)=35.26 *kNs/m* and c_{PS}=394.1/(4*4)=24.63 *kNs/m*, therefore linear damping devices can be used, such as LD1110 from (Fluid Viscous Dampers | ITT Infrastructure) catalog.

The maximum design displacements for the stiffness elements k_{PS} and k_R is *3.89* and *3.04 cm* respectively. Furthermore, the stiffness of these elements for each of the 4 SBA devices is: k_{PS}=24467/4=6116.75 *kN/m* and k_R=60996/4=15249 *kN/m*. Therefore, the realization of the positive stiffness elements is possible in various ways, as for example, conventional steel spiral springs, simple elastomeric bearings (or any type of special bearings) or even conventional structural elements. For example, the realization of the k_{PS} and k_R with simple elastomeric bearings is possible with the SI-H550/56 and SI-H 1000/70 from the FIP Industriale elastomeric isolators catalog (Elastomeric isolators - Fip Industriale, n.d.), with a designed maximum deformation of 10.0 *cm*.

The additional mass of each of the 4 SBA devices is realized with concrete, having ρ_{mat}=2400 kg/m^3. Assuming planar square top view with a height of h_{SBA}=0.1 *m*, the resulting dimension of the additional mass is:

$$x_{add,mass} = \sqrt[2]{(m_D / No.Devices * h_{SBA}) / \rho_{mat}} = \sqrt[2]{(0.1\% * 300 / 4 * 0.1) / 2.4} = 56cm \qquad (5.16)$$

In conclusion, in this numerical example the SBA is implemented as a base absorption layer of a 3-story building structure, and is compared with various base-isolation related systems. Based on results obtained, the following concluding remarks can be made:

i. The SBA is realistically designed, as it foresees variation in all stiffness elements (10%) and assumes a small additional mass of 0.1%
ii. The optimal system parameters are selected based on engineering criteria with proper constraints and limitations to the system dynamic responses.
iii. Based on the performed sensitivity analysis, the SBA is not vulnerable to detuning.
iv. The superstructure dynamic behavior of the examined multi-story building controlled with SBA is greatly improved. More specifically, the floor accelerations and the inter-story drifts are significantly reduced, and at the same time, the base displacement is dramatically low, as compared to other base isolation approaches.
v. The small base displacement of the SBA with high *AF=70%* (acceleration filter), renders the implementation of the proposed device feasible using conventional structural elements, without the need of special type of bearings. As a consequence, retrofitting is possible.
vi. The design of the SBA devices is realistic and within reasonable technological capabilities.

5.5 Concluding Remarks

In this Chapter, alternative designs of the KDamper concept are investigated. The purpose of the proposed extensions of KDamper aim to further reduce the structural relative displacements required (base displacement and NS element stroke) to acquire the desired improvement in the superstructure dynamic behavior, as compared to the KDamper concept. Initially, the extension of KDamper (EKD) is introduced in section 5.2, along with the optimization procedure from which the EKD parameters are selected. Subsequently, the EKD is implemented for horizontal seismic protection of SDoF, as well as multi-story building structures. Based on the results obtained from the numerical examples, the EKD is efficient and realistically designed. Section

5.3 presents possible retrofitting options of the EKD for implementation in existing structures for horizontal seismic protection. Section 5.4 introduces a stiff base absorber (SBA) which is a combination of the extend KDamper concept with an inerter. The optimization problem for the design of the SBA is presented, and is then implemented in SDoF and MDoF structural systems. A comparison with other base isolation approaches is performed, and the detuning phenomena are observed via sensitivity analysis. Based on the dynamic analysis and the results obtained, the following concluding remarks can be made:

i. The performance of EKD is superior, as compared to the previously optimal KDamper concept, while it foresees variation in all stiffness elements.

ii. The evaluation of the optimization constraints and the limits of the free design variables is based on engineering criteria and render the implementation of the EKD feasible. As compared with previous indicative designs of KDamper, all the stiffness elements are designed to be at least *50%* lower. Furthermore, the negative stiffness element stroke is reduced by *50-67%*.

iii. Based on the performed sensitivity analysis, where the stiffness elements, the additional mass, and the artificial damper varied from their optimal values by 20, 50, and 50%, respectively, the EKD is not vulnerable to detuning.

iv. The EKD implemented in a SDOF system manages to retain the structure absolute acceleration at acceptable levels, while at the same time the structural relative displacement is significantly low, in the order of a few centimeters, 50-80% lower as compared to conventional and highly damped base isolation systems.

v. The 3-story building structure controlled with EKD, presents an improved dynamic behavior. More specifically, the floor accelerations and the inter-story drift are reduced *65-85%*, results comparable with the base isolated system (*90%* reductions). At the same time, the base displacement is greatly reduced (up to *75%*) as compared with the base isolated concepts, retained at very low levels (*5-9cm*).

vi. The small base displacement of the EKD with high Acceleration Filters (*70*, *80%*), render the implementation of the proposed device feasible using conventional structural elements, without the need of special type of bearings. Furthermore, the base shear of the whole proposed configuration as well as the base shear of the independent component k_R, is reduced, as compared with the initial system total base shear. As a consequence, retrofitting is possible.

vii. An alternative spectra driven approach for the selection of the EKD parameters, implemented in the base of a multi-story building structures is introduced. The superstructure dynamic performance is enhanced, and at the same time the proposed configuration is realistically designed. More specifically, The inter-story drifts are low (2-3 *cm*), 30-60% lower as compared to the initial 3-story building structure, the top floor absolute accelerations are reduced by 30-50%, the NS element stroke is retained at acceptable levels (5-10 *cm*), and the base relative displacements are in the order of a few centimetres (2-4 *cm*).

viii. The horizontal seismic protection of a multi-story building structure with distributed EKD devices is examined. An EKD is placed in each floor, significantly improving the structural dynamic performance. However, in the case of implementing one EKD only in the first floor, the dynamic performance of the structure is still greatly improved, as compared with the previous case.

ix. Another retrofitting option is examined, that foresees the implementation of the EKD in the first floor of a multi-story building structure, exploiting the soil-structure-interaction (SSI) effects. The EKD together with the SSI effects appear to improve the structural dynamic responses, as compared to the original uncontrolled structure. A *40-70%* reduction of the absolute acceleration values of the building stories is achieved, the base shear values appear to be significantly reduced in accordance with the absolute acceleration values, and the total horizontal displacement of the first floor is slightly reduced compared to the fixed footings. However, due to the rotational and horizontal movement of the foundation the total displacement is distributed between the column and the footing (SSI) and consequently structural flexural displacements are reduced and remain within an acceptable region.

x. The extension of KDamper equipped with an inerter (SBA system) is presented. The design of the SBA is realistic, as it foresees variation in all stiffness elements (10%) and assumes a small additional mass of 0.1%. Furthermore, the optimal system parameters are selected based on engineering criteria with proper constraints and limitations to the system dynamic responses.

xi. Based on the performed sensitivity analysis, the SBA is not vulnerable to detuning.

xii. The superstructure dynamic behavior of the examined multi-story building controlled with SBA is greatly improved. More specifically, the floor accelerations and the inter-

story drifts are significantly reduced, and at the same time, the base displacement is dramatically low, as compared to other base isolation approaches.

xiii. The small base displacement of the SBA with high *AF=70%* (acceleration filter), renders the implementation of the proposed device feasible using conventional structural elements, without the need of special type of bearings. As a consequence, retrofitting is possible.

Chapter **6**

Vertical Seismic Protection with Extended KDamper Designs

6.1 Introduction

In the latest years, many earthquake excitations whose vertical component of accelerations is almost 1*g* or more have been recorded. To protect building structures, as well as nonstructural components, such as fragile objects, precision equipment, and fine arts, from these strong ground motions, needs for not only horizontal vibration isolators but also vertical ones (Furukawa et al., 2013). Horizontal seismic isolators have been employed effectively, while vertical ones have not reached yet such a maturity level. For this reason, vertical seismic isolation of a base-isolated (BI) structure has gained the interest of researchers. Various kinds of vertical seismic isolation devices have been developed to mitigate earthquakes, such as the low shape factor (LSF) elastomeric bearings (Warn and Vu, 2012), air springs consisting of cylinders filled with nitrogen gas (MORISHITA et al., 2004; Tomizawa et al., n.d.), vertical flexibility (Vu et al., 2014), inertia-type (Lu et al., 2016), vertical-rocking isolation systems (Auad and Almazán, 2017), variable ellipse curve mechanisms (Asai et al., 2017), as well as three-dimensional ones (Zhou et al., 2016). However, these approaches have their own drawbacks. The LSF approach is used only for low-rise structures. Vertical air springs and vertical flexibility are so costly and hence not likely to be widely applied. Furthermore, in order to achieve the seismic isolation effect, a longer vertical isolation period implies a lower vertical stiffness, which will lead to larger static displacement of the mass. This hinders the development of vertical seismic isolation systems. In recent years, negative stiffness structures (NSS) and quasi-zero stiffness (QZS) systems have been developed to overcome this disadvantage (Le and Ahn, 2013; Seismic Response Analysis of an Isolated Structure with QZS under Near-Fault Vertical Earthquakes, n.d.; Zheng et al., 2016). Nevertheless, the new approaches applications are for the isolation of mechanical engineering only, and very limited researches focus on vertical seismic isolation.

In this chapter, a stiff vertical seismic absorber (VSA) that can control the vertical accelerations, while at the same time retain the static vertical deformations at acceptable levels is proposed. The VSA is a combination of an Extension of KDamper (EKD) with an Inerter. This idea is based on reducing the natural frequency of the system with the inerter and then control the structure accelerations with the extraordinary damping properties that the KDamper offers. This way, the VSA aims to reduce the structure vertical accelerations and at the same time retain the static deflections in reasonable ranges.

Section 2 of the current Chapter presents an overview of the conventional SDoF seismically/base isolated system, together with a concise presentation of the main disadvantage when considering vertical seismic isolation. Next, the proposed configuration of the VSA is presented. The Transfer Functions, response power spectral densities (PSD) and root mean square responses (RMS) of the system are introduced when considering vertical acceleration excitation. In section 3, the free design variables of the system are presented, along with the optimization procedure from which the optimal VSA parameters are selected. For the design to be efficient and realistic, proper engineering-criteria constraints and limitations are imposed in the system dynamic responses and free design variables, respectively. The optimized parameters of the VSA are presented and based on a comparison with a highly damped base isolated system, it is observed that the VSA significantly reduces the vertical accelerations as compared to the BI, especially at the high-frequency range, where small static settlements are allowed. Finally, in section 4, the SDoF nonlinear dynamic performance is evaluated with real earthquake records and the detuning phenomena are observed via sensitivity analysis.

6.2 Vertical Seismic Absorber (VSA) Based on Extended KDamper Equipped with Inerter

The fundamental principle of seismic isolation is to decrease the natural frequency of the system, *f*, below the predominant energy-containing frequencies of earthquake motions, and thus develop reduced peak accelerations. However, the application of such approaches may result in unsolvable problems, especially for vertical vibration isolation. The main reason is due to the conflict concerning the demand for isolation stiffness. More specifically, a vertical isolated system must have sufficient vertical rigidity to sustain the weight of the isolated object/system and retain the static vertical deflection in reasonable limits. On the other hand, the isolated system must also have enough flexibility to isolate the accelerations. The vertical static settlement of such an isolated system under its own weight is expressed:

$$X_{SVD} = \frac{mg}{k} = \frac{g}{(2\pi f)^2} \tag{6.1}$$

Figure 2.c presents graphically Equation (1) and clearly reflects the implicit constraints for low-frequency vibration isolation, especially in the vertical direction. It should be noted that X_{SVD} depends only on the acceleration of gravity g and on the natural frequency f.

6.2.1 Equations of Motion, Transfer Functions, Power Spectral Densities and Root Mean Square Responses

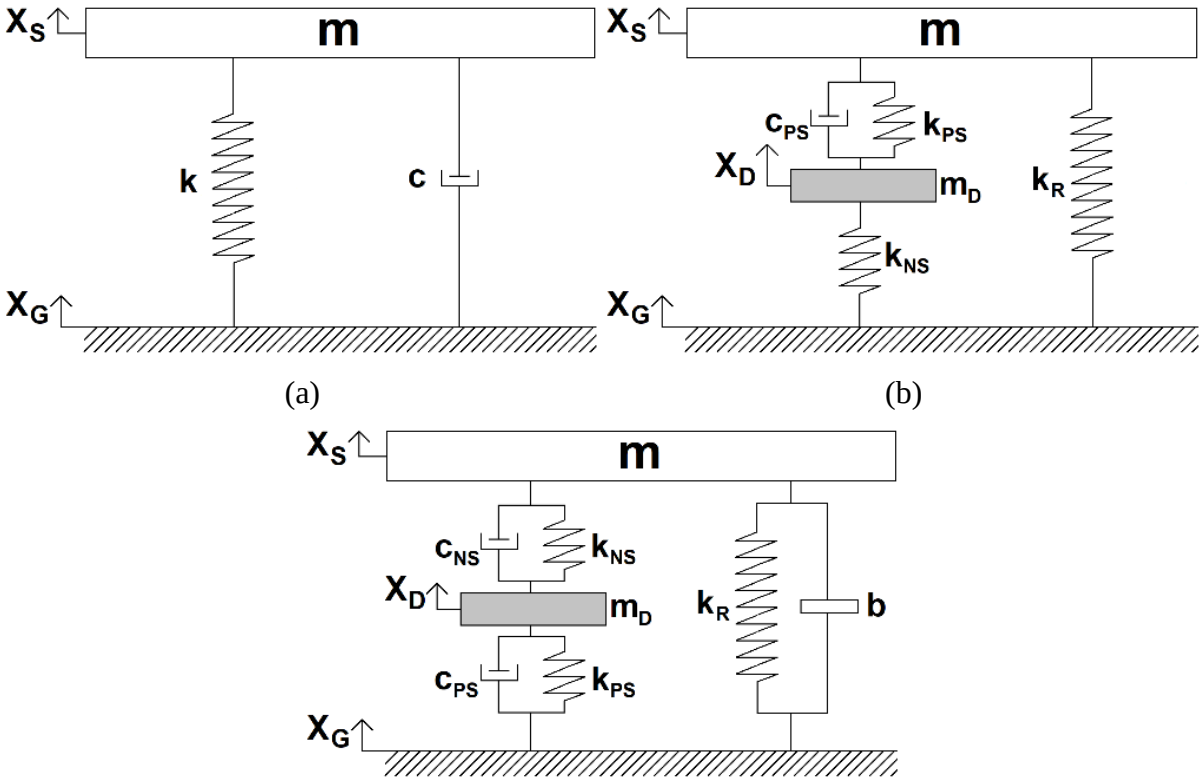

Figure 6.1: *Three vertical vibration control systems: (a) conventional BI; (b) KDamper; (c) proposed extension of KDamper equipped with inerter (VSA).*

A seismically/base isolated (BI) system in the vertical direction is presented in Figure 1.a. The equation of motion of this system is:

$$m\ddot{u}_S + c\dot{u}_S + ku_S = -m\ddot{X}_G \tag{6.2}$$

where $u_S=X_S-X_G$. In order to define the Transfer Functions of the SDoF BI system, we assume a harmonic base excitation in the form of:

$$\ddot{X}_G(t) = A_G \exp(j\omega t) \tag{6.3}$$

and a steady-state response of:

$$u_S(t) = \tilde{U}_S \exp(j\omega t) \tag{6.4}$$

where $\tilde{U}_S$ denotes the response complex amplitude. The equation of motion of the SDoF system becomes:

$$-\omega^2 m\tilde{U}_S + j\omega c\tilde{U}_S + k\tilde{U}_S = -mA_G \tag{6.5}$$

The Transfer Functions of the system considering a harmonic base excitation are:

$$\tilde{H}_{US} = \tilde{U}_S / A_G = -\tilde{H}^{-1} m_S \tag{6.6.a}$$

$$\tilde{H}_{AS} = \tilde{A}_S / A_G = (-\omega^2 \tilde{X}_S) / A_G = 1 - \omega^2 \tilde{H}_{US} \tag{6.6.b}$$

$$\tilde{H} = [-\omega^2 m + j\omega c + k] \tag{6.6.c}$$

The natural frequency and the damping ratio of the SDoF isolated system are defined as:

$$f = \sqrt{k/m}/(2\pi) \tag{6.7.a}$$

$$\zeta = c/(2\sqrt{mk}) \tag{6.7.b}$$

The KDamper, presented in Figure 1.b is essentially an extension of the conventional TMD, by the introduction of an appropriate negative stiffness (NS) element to the additional oscillating mass, increasing the system's effective damping (Antoniadis et al., 2018). This Chapter proposes a stiff vertical seismic absorber (VSA), as presented in Figure 1.c. The VSA is the combination of an extension of the KDamper (EKD) equipped with an inerter. More specifically, the NS element k_{NS} connects the structure mass with the additional mass, m_D, instead of the positive stiffness element k_{PS}, a damping coefficient is placed in parallel to each stiffness element, and an inerter is implemented between the structure and its base. This way,

the VSA aims to reduce the structure accelerations, retaining the natural frequency, *f*, and hence the X_{VSD}, at any desired level. The equations of motion of the VSA are:

$$(m+b)\ddot{u}_S + c_{NS}(\dot{u}_S - \dot{u}_D) + k_R u_S + k_{NS}(u_S - u_D) = -m\ddot{X}_G \quad (6.8.a)$$

$$m_D\ddot{u}_D - c_{NS}(\dot{u}_S - \dot{u}_D) + c_{PS}\dot{u}_D - k_{NS}(u_S - u_D) + k_{PS}u_D = -m_D\ddot{X}_G \quad (6.8.b)$$

where $u_D=X_D-X_G$. In order to define the Transfer Functions of the controlled system with the proposed vertical seismic absorber (VSA), we assume a harmonic base excitation in the form of Equation (6.3). The steady-state responses of the VSA system are:

$$u_S(t) = \tilde{U}_S \exp(j\omega t) \quad (6.9.a)$$

$$u_D(t) = \tilde{U}_D \exp(j\omega t) \quad (6.9.b)$$

where $\tilde{U}_S$ and $\tilde{U}_D$ denote the response complex amplitudes. The equations of motion (6.8) of the VSA, thus become:

$$-\omega^2(m+b)\tilde{U}_S + j\omega c_{NS}(\tilde{U}_S - \tilde{U}_D) + k_R\tilde{U}_S + k_{NS}(\tilde{U}_S - \tilde{U}_D) = -mA_G \quad (6.10.a)$$

$$-\omega^2 m_D\tilde{U}_D - j\omega c_{NS}(\tilde{U}_S - \tilde{U}_D) + j\omega c_{PS}\tilde{U}_D - k_{NS}(\tilde{U}_S - \tilde{U}_D) + k_{PS}\tilde{U}_D = -m_D A_G \quad (6.10.b)$$

and the resulting Transfer Function are:

$$\begin{bmatrix} \tilde{H}_{US} \\ \tilde{H}_{UD} \end{bmatrix} = \begin{bmatrix} \tilde{U}_S / A_G \\ \tilde{U}_D / A_G \end{bmatrix} = -\tilde{H}^{-1}\begin{bmatrix} m_S \\ m_D \end{bmatrix} \quad (6.11.a)$$

$$\tilde{H}_{AS} = \tilde{A}_S / A_G = 1 - \omega^2\tilde{H}_{US} \quad (6.11.b)$$

$$\tilde{H}_{AD} = \tilde{A}_D / A_G = 1 - \omega^2\tilde{H}_{UD} \quad (6.11.c)$$

$$\tilde{H} = \begin{bmatrix} -\omega^2(m+b) + j\omega c_{NS} + k_R + k_{NS} & -j\omega c_{NS} - k_{NS} \\ -j\omega c_{NS} - k_{NS} & -\omega^2 m_D + j\omega(c_{NS} + c_{PS}) + k_{NS} + k_{PS} \end{bmatrix} \quad (6.11.d)$$

The response Power Spectral Densities (PSDs) are derived:

$$S_{US} = H_{US}^2 S_A \quad (6.12.a)$$

$$S_{UD} = H_{UD}^2 S_A \quad (6.12.b)$$

$$S_{AS} = H_{AS}^2 S_A \tag{6.12.c}$$

$$S_{AD} = H_{AD}^2 S_A \tag{6.12.d}$$

where S_A is the ground motion excitation acceleration PSD. The root mean square (RMS) values of the responses are next defined as the root under the area of the PSD curve, as an indicator of the actual energy content of the response:

$$R_{US} = \sqrt{\int_{-\infty}^{+\infty} S_{US}(\omega)\,\mathrm{d}\,\omega} \tag{6.13.a}$$

$$R_{UD} = \sqrt{\int_{-\infty}^{+\infty} S_{UD}(\omega)\,\mathrm{d}\,\omega} \tag{6.13.b}$$

$$R_{AS} = \sqrt{\int_{-\infty}^{+\infty} S_{AS}(\omega)\,\mathrm{d}\,\omega} \tag{6.13.c}$$

$$R_{AD} = \sqrt{\int_{-\infty}^{+\infty} S_{AD}(\omega)\,\mathrm{d}\,\omega} \tag{6.13.d}$$

Finally, the following position concerning the VSA configuration are introduced:

$$m_D = \mu_D m \tag{6.14.a}$$

$$b = \mu_b m \tag{6.14.b}$$

$$\zeta_{NS} = c_{NS} / (2 m_D \omega_D) = c_{NS} / (2\sqrt{(k_{NS} + k_{PS}) m_D}) \tag{6.14.c}$$

$$\zeta_{PS} = c_{PS} / (2 m_D \omega_D) = c_{PS} / (2\sqrt{(k_{NS} + k_{PS}) m_D}) \tag{6.14.d}$$

$$\omega_D = \sqrt{\frac{k_{NS} + k_{PS}}{m_D}} \tag{6.14.e}$$

where μ_D, μ_b are the mass ratio of the additional mass m_D, and the inertance ratio of the inerter coefficient b, and ζ_{NS}, ζ_{PS} are the damping ratios of the artificial dampers c_{NS} and c_{PS}, respectively.

6.3 Optimal Design of VSA

In this section, a spectra driven approach is followed for the optimal design of the proposed VSA control system. As observed from similar approaches followed in Chapters 4 and 5, for the design of KDamper and extended KDamper configurations, respectively, a spectra driven approach for the design of a control system is accurate as verified in the time domain. The results will also be verified with time-history analyses in this section. The vertical excitation input is selected according to section 3.3.2.2 of Chapter 3. The free design variables are presented and an engineering optimization procedure if formed, based on engineering criteria, for a more realistic design. Finally, the system non-linear dynamic performance is evaluated following the Proposed Configuration I, presented in Chapter 3, regarding the realization of the NS element, and subjecting the system with real earthquake records, having a strong vertical component. Finally, the detuning phenomena are observed via sensitivity analysis.

6.3.1 Free Design Variables

As stated in section 2, an unsolvable problem when considering vertical seismic isolation is the static vertical deflections. In the case a rigid mass is mounted on a VSA, the static deflections of the system under its own weight are expressed as follows:

$$\left[F_g\right]_{(2\times1)} = \left[K\right]_{(2\times2)} \begin{bmatrix} X_{SVD} \\ X_{SVD,VSA} \end{bmatrix} \Rightarrow X_{SVD} = \left[\begin{bmatrix} k_R + k_{NS} & -k_{NS} \\ -k_{NS} & k_{NS} + k_{PS} \end{bmatrix}^{-1} \begin{bmatrix} mg \\ m_D g \end{bmatrix} \right](1,1) \tag{6.15}$$

This way, the static vertical deflections of the system are maintained at any desired level, and as a result, the static settlement of the rigid mass is considered a free design variable. However, variation in the absolute values of the stiffness elements may endanger the static stability of the system. To ensure that potential loss of the static stability is prevented, the possible variations of k_{NS}, $k_{PS,}$ and k_R should be taken into consideration in the design and optimization of the VSA. The stiffness parameters of the system may present significant fluctuations since almost all NS designs result from unstable non-linear configurations (Li et al., 2020). Consequently, an increase of the absolute value of k_{NS} and/or a decrease of the values of k_{PS} and k_R by a factor ε_{NS}, $\varepsilon_{PS,}$ and ε_R, respectively, may result in the system being unstable.

In the limit case that the determinant of the stiffness matrix is equal to zero, the VSA system is unstable:

$$\det[K]=0 \Rightarrow (1-\varepsilon_R)k_R+\frac{(1-\varepsilon_{PS})k_{PS}(1+\varepsilon_{NS})k_{NS}}{(1-\varepsilon_{PS})k_{PS}+(1+\varepsilon_{NS})k_{NS}}=0 \tag{6.16}$$

As a result, the stiffness elements k_{PS} and k_R, result from Equations (6.15, 6.16) as a function of the static deflection, X_{SVD}, and the value of k_{NS}. Finally, assuming that the structure mass m, the additional mass m_D, and the variations of the stiffness elements, ε_i are supposed known, the free design variables of the VSA system are:

1. The static vertical deflection X_{SVD};
2. The value of the NS element k_{NS};
3. The damping ratios ζ_{NS} and ζ_{PS};
4. The inertance ratio μ_b;

6.3.2 Statement of the Optimization Problem

The purpose of the VSA is to reduce the structure's vertical absolute accelerations. In order for the proposed vibration control strategy to be efficient and realistic at the same time, proper engineering-criteria constraints and limitations must be imposed in the dynamic responses and free design variables, respectively. In particular:

i. The RMS structure absolute acceleration, R_{AS}, is set as the objective function;
ii. The additional oscillating mass μ_D of the VSA is selected equal to *5%*;
iii. The variations of the stiffness elements, ε_{NS}, $\varepsilon_{PS,}$ and ε_R, are selected equal to *10%*;
iv. The upper limit of the damping ratios ζ_{NS} and ζ_{PS} is 0.4 and 0.2, respectively;
v. The inertance ratio μ_b maximum value is equal to 2;
vi. The NS element maximum (absolute) value is equal to *-100 N/m* per *kg* of structure mass, as presented in (Antoniadis et al., 2018);
vii. The RMS value of the negative stiffness (NS) element stroke $R_{US\text{-}D}$ is set as a constraint with an upper limit of $50\%X_{SVD}$;

6.3.3 Optimization Results

The vibrations of a rigid mass of m=1000 kg are to be controlled with the VSA configuration. The optimal parameters are selected according to the optimization procedure described in section 3.2, considering the variation of the static settlement X_{SVD} in the range of [1 5] (cm). The full set of the VSA set of parameters is presented in Table 6.1.

The Transfer Functions of the structure absolute acceleration H_{AS}, structure relative displacement H_{US}, and the VSA relative displacement H_{UD} are presented in Figure 6.2, and the respective response PSDs are presented in Figure 6.3. The Transfer Functions and response PSDs are plotted for different values of the design parameter X_{SVD}, in order to evaluate the sensitivity of the Transfer Functions and response PSDs to the parameter X_{SVD}.

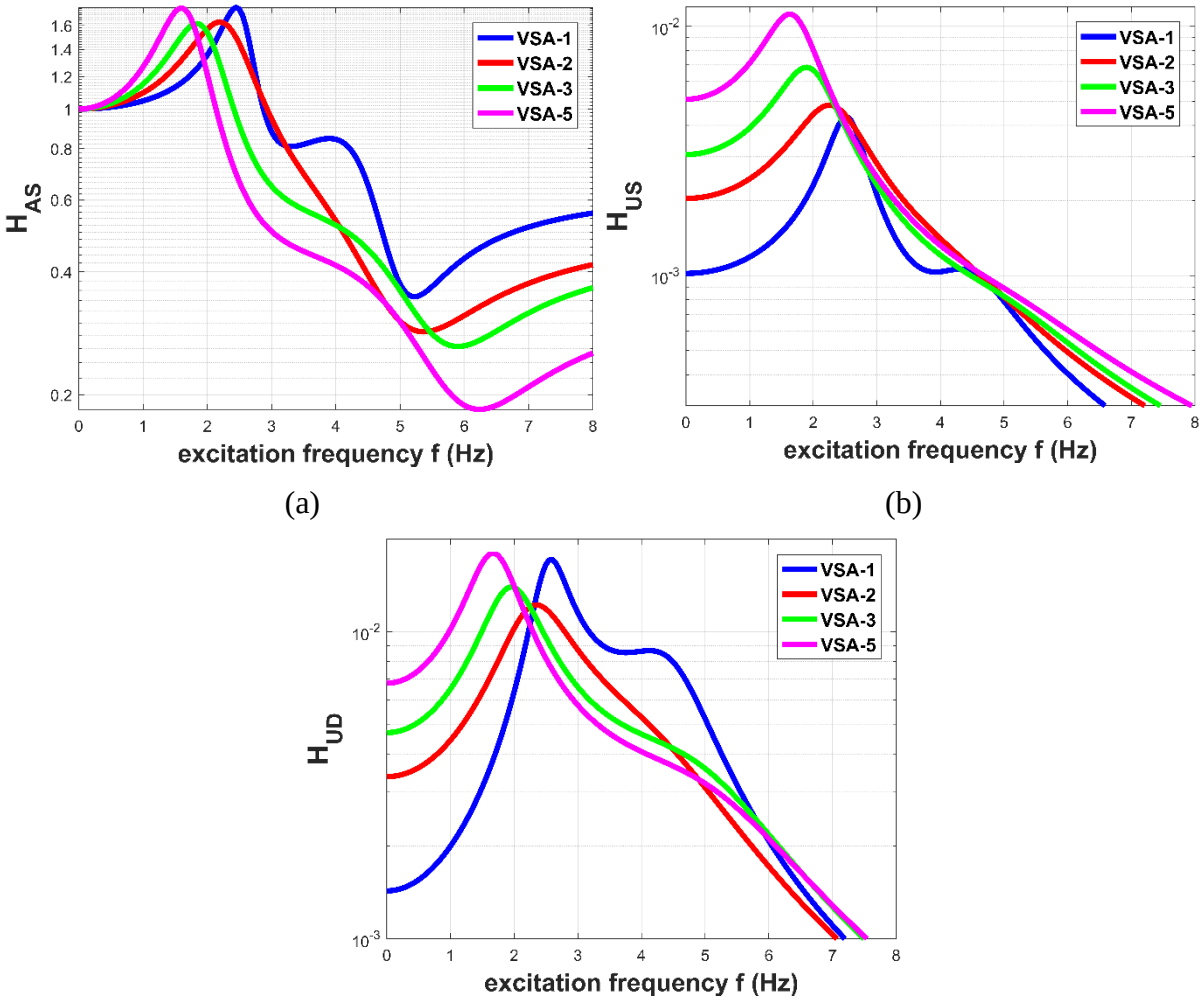

Figure 6.2: *Transfer Functions of the VSA system over the X_{SVD}: (a) Structure absolute acceleration H_{AS}; relative displacement H_{US}; VSA relative displacement H_{UD}.*

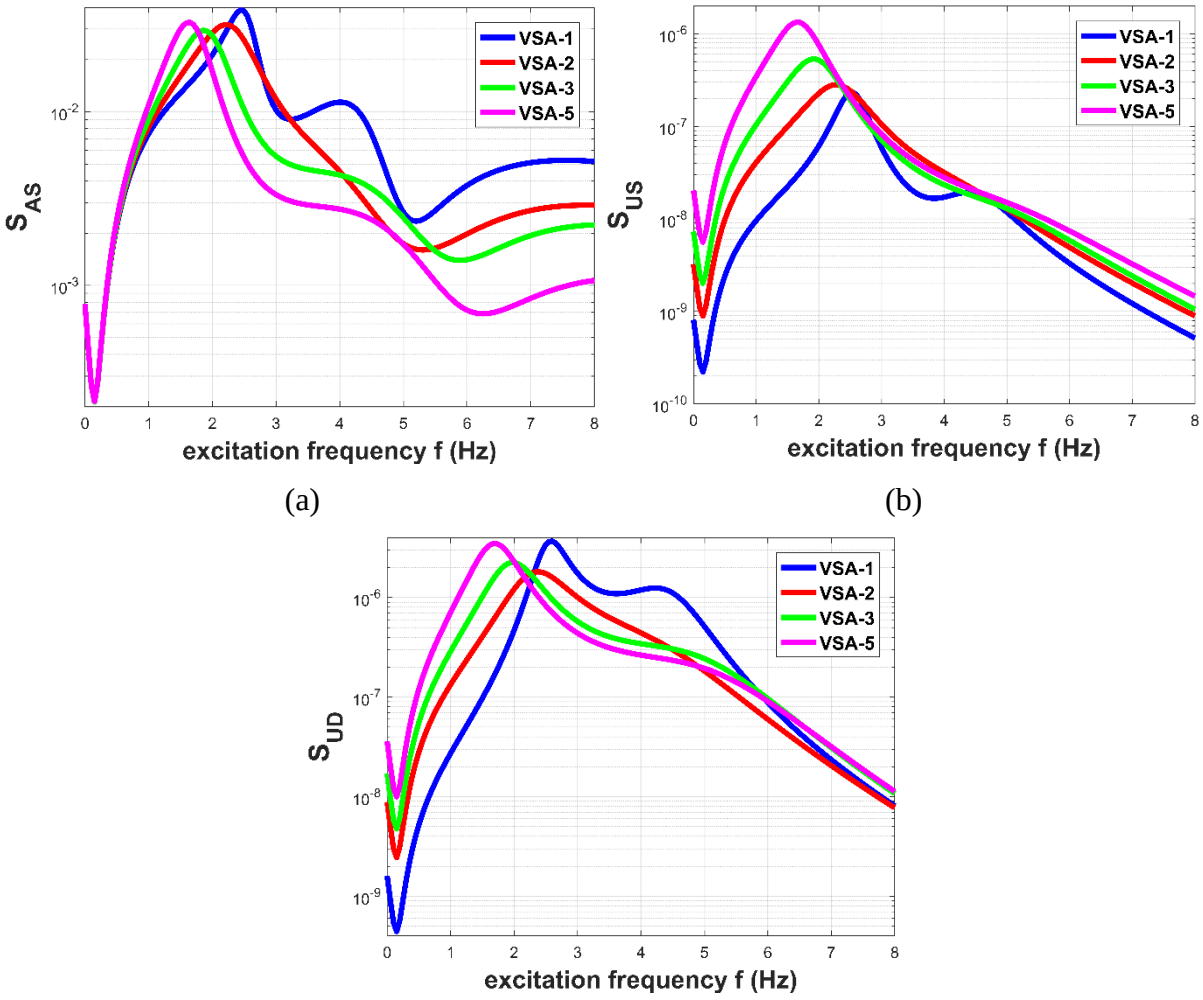

Figure 6.3: *Response PSDs considering the ground motion acceleration excitation PSD, S_A, described in section 4.1. (a) Structure absolute acceleration S_{AS}; structure relative displacement S_{US}; VSA relative displacement S_{UD}.*

The absolute acceleration Transfer Function H_{AS} and response PSD S_{AS} are not very much affected by the X_{SVD}. However, the values of the H_{AS} and S_{AS} don't decline due to the presence of the inerter coefficient b. The bigger the value of b, the less degradation of the acceleration in the high-frequency content. The structure relative displacement Transfer Function H_{US} and response PSD S_{US} are affected in the low-frequency range, as expected when considering different static vertical displacements X_{VSD}, and therefore different static vertical stiffness. The VSA relative displacement Transfer Function H_{UD} and response PSD S_{UD}, similar to the H_{US} and S_{US}, are affected in the low-frequency range due to the variation of the static design settlements X_{VSD}.

Table 6.1. *Full set of the VSA parameters in the range of the design static vertical deflections* X_{SVD}*=[1 5] (cm).*

VSA set	μ_D	μ_b	k_{NS} (*kN/m*)	k_{PS} (*kN/m*)	k_R (*kN/m*)	ζ_{NS} (*%*)	c_{NS} (*kNs/m*)	ζ_{PS} (*%*)	c_{PS} (*kNs/m*)
X_{SVD}=1 *cm*	0.05	1.85	-97.97	132.82	1216.5	6.9	0.182	16.5	0.436
X_{SVD}=2 *cm*	0.05	1.09	-95.15	137.88	742.94	27.6	0.806	17.7	0.518
X_{SVD}=3 *cm*	0.05	0.91	-97.93	151.15	575.02	36.7	1.197	0.3	0.01
X_{SVD}=4 *cm*	0.05	0.65	-85.95	136.44	456.65	37.85	1.203	7.3	0.233
X_{SVD}=5 *cm*	0.05	0.57	-86.96	144.88	399.00	32.14	1.094	5.9	0.200

To better observe the effectiveness of the VSA it is compared with a highly damped (ζ=15%) base isolated system (BI) with natural frequency, *f*, varying with respect to the design static vertical deflection parameter X_{SVD}. Finally, the dynamic response indicators are defined in Equation (6.17), and are plotted in Figure 6.4 with respect to the static vertical deflection X_{SVD}.

$$r_{AS,BI,X_{SVD}} = \frac{R_{AS,BI,X_{SVD}}}{\sqrt{\int S_A(\omega)\,\mathrm{d}\omega}\ (=PGA)} \tag{6.17.a}$$

$$r_{AS,VSA,X_{SVD}} = \frac{R_{AS,VSA,X_{SVD}}}{\sqrt{\int S_A(\omega)\,\mathrm{d}\omega}\ (=PGA)} \tag{6.17.b}$$

$$r_{US,BI,X_{SVD}} = \frac{R_{US,BI,X_{SVD}}}{R_{US,BI,X_{SVD}}(ref)} \tag{6.17.c}$$

$$r_{US,VSA,X_{SVD}} = \frac{R_{US,VSA,X_{SVD}}}{R_{US,VSA,X_{SVD}}(ref)} \tag{6.17.d}$$

$$r_{UD,VSA,X_{SVD}} = \frac{R_{UD,VSA,X_{SVD}}}{R_{UD,VSA,X_{SVD}}(ref)} \tag{6.17.e}$$

In order to confirm the accuracy of the spectra driven approach for the optimal selection of the VSA parameters, the results are evaluated in the time-domain. The equations of motion of the BI and VSA systems, respectively, are solved for all the 50 accelerograms of the database, generated according to the procedure described in section 3.3.2.2 of Chapter 3, using the Newmark-β method with linear acceleration. The mean of the maximum of the dynamic response's ratio are defined as:

$$v_{AS,BI,X_{SVD}} = \frac{V_{AS,BI,X_{SVD}}}{meanPGA(=0.417g)} \tag{6.18.a}$$

$$v_{US,BI,X_{SVD}} = \frac{V_{US,BI,X_{SVD}}}{V_{US,BI,X_{SVD}}(ref)} \tag{6.18.b}$$

$$v_{AS,VSA,X_{SVD}} = \frac{V_{AS,VSA,X_{SVD}}}{meanPGA(=0.417g)} \tag{6.18.c}$$

$$v_{US,VSA,X_{SVD}} = \frac{V_{US,VSA,X_{SVD}}}{V_{US,VSA,X_{SVD}}(ref)} \tag{6.18.d}$$

$$v_{UD,VSA,X_{SVD}} = \frac{V_{UD,VSA,X_{SVD}}}{V_{UD,VSA,X_{SVD}}(ref)} \tag{6.18.e}$$

where $V_{US,BI,Xsvd}$, $V_{AS,BI,Xsvd}$, $V_{US,VSA,Xsvd}$, $V_{AS,VSA,Xsvd}$, and $V_{UD,VSA,Xsvd}$ are the mean of the maximum systems dynamic responses with respect to the design static vertical displacements X_{SVD}, and $V_{US,BI,Xsvd}$ *(ref)*, $V_{US,VSA,Xsvd}$ *(ref)*, and $V_{UD,VSA,Xsvd}$*(ref)* pertain to the mean of maximum dynamic responses of the respective control system with a design static vertical deflection equal to 3 *cm*. The results are also plotted in Figure 6 (dotted lines), and clearly confirm that a spectral driven approach for the design of the proposed stiff vertical seismic absorber, VSA system is accurate.

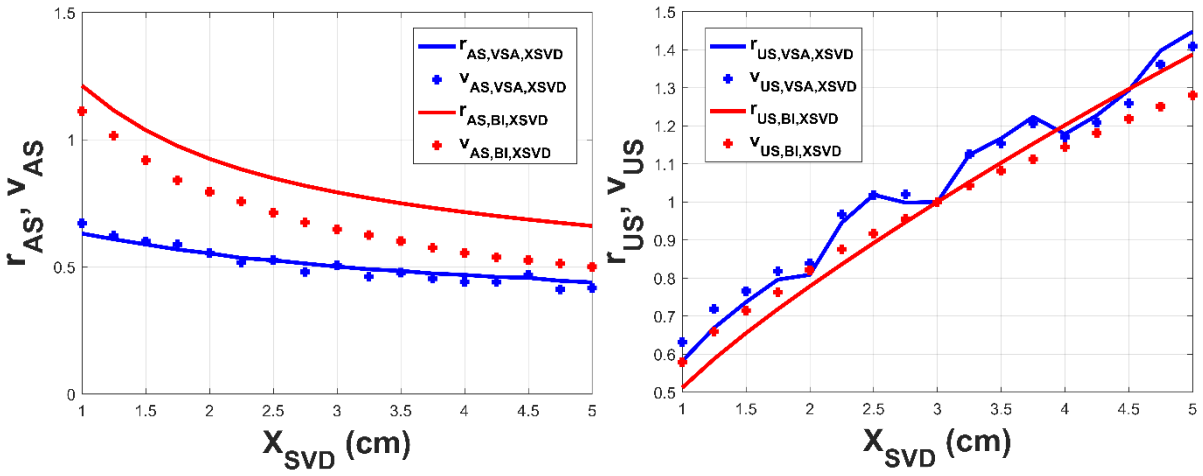

(a) (b)

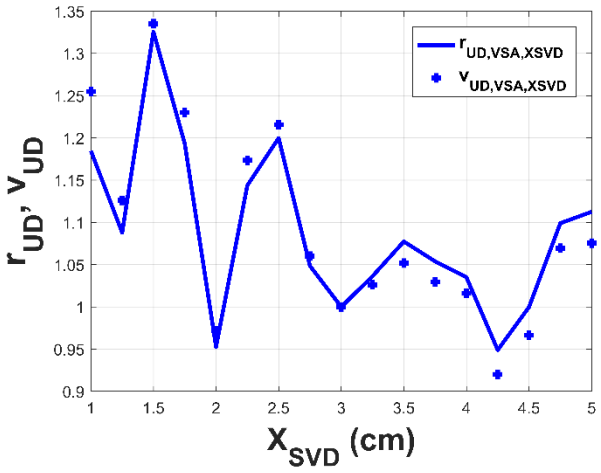

(c)

Figure 6.4: *Variation of: (a) the acceleration response indicator r_{AS}, (b) the structure relative displacement response indicator r_{US}, and (c) the VSA relative displacement response indicator r_{UD} over the X_{SVD}, of the VSA and BI systems, and verification with the mean responses in the time-domain, v_{AS}, v_{US}, and v_{UD}, respectively.*

6.3.4 Numerical Example 1 – *SDoF Nonlinear Dynamic Performance and Detuning Phenomena*

Real earthquake records are non-stationary, have random duration and peak ground acceleration, as well as a variety of frequency contents. Furthermore, almost all negative stiffness-based designs, result from nonlinear unstable configurations. As a result, it is of great importance that the effectiveness of the proposed vertical seismic absorber (VSA) to be examined with real earthquake records using a realistic displacement-dependent configuration regarding the realization of the NS element. The NS element is realized with the Proposed Configuration I of Chapter 3. The nonlinear equations of motion are solved using the Newmark-β method with linear accelerations.

Recently, strong motion records have been increasingly available online in the form of databases. A representative database is the (PEER Ground Motion Database - PEER Center, n.d.). Table 6.2 shows all the selected vertical earthquake motions from the PEER database, along with their respective information, and Figure 6.5 presents their frequency content. The selected motions are near-field with large Magnitudes (>5.5, Type 1) having various earthquake focal mechanisms. Near-field and far-field is denoted in this study according to a conservative threshold of 10 *km*.

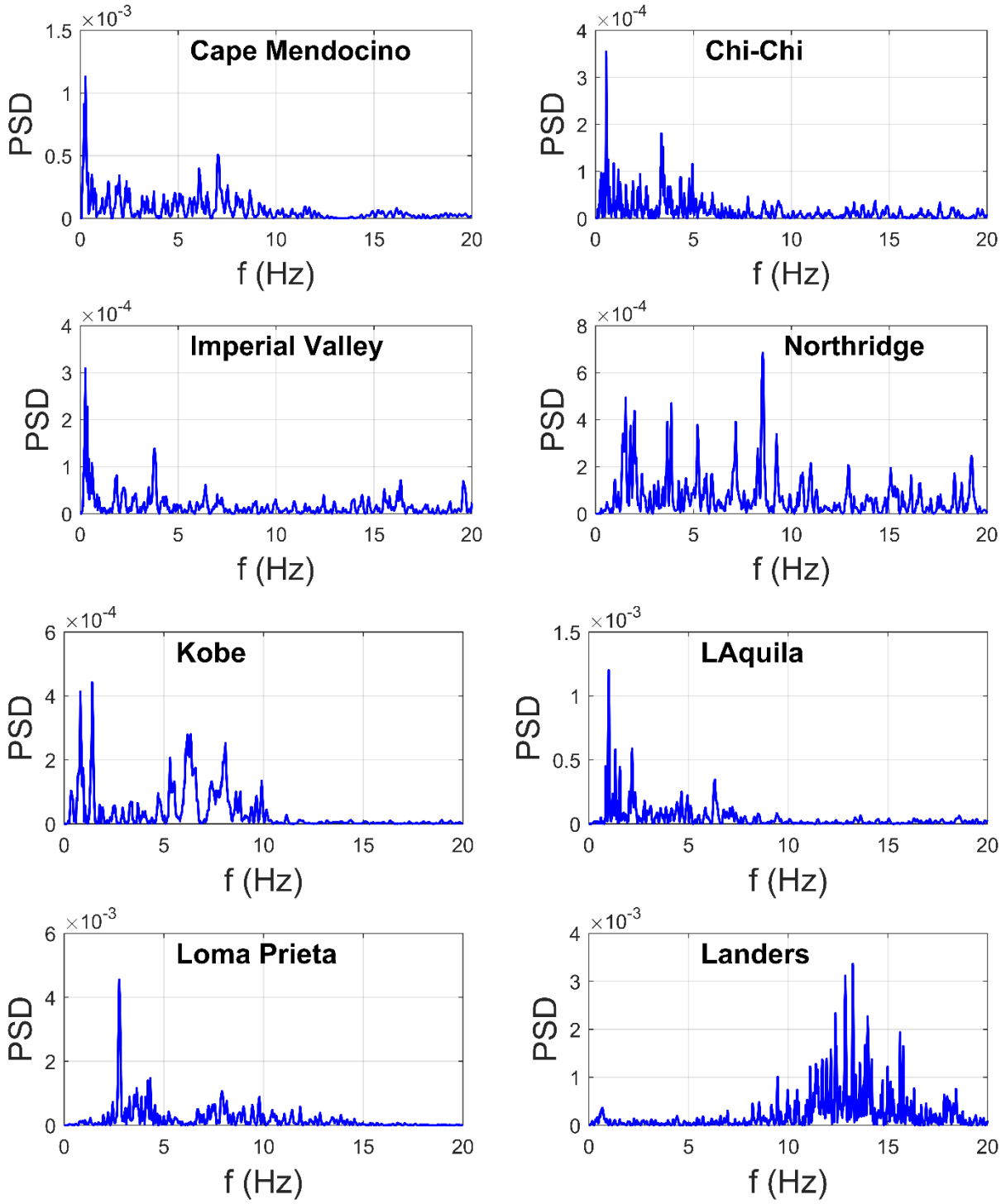

Figure 6.5: *Frequency content (Fourier spectrum) of the considered earthquake vertical ground motions.*

The proposed nonlinear configuration for the realization of the NS element follows the procedure described in (Antoniadis et al., 2018), where a mechanism with pre-compressed springs, manages to generate almost 'linear' negative stiffness. More specifically, the NS element, k_{NS}, is realized by a set of two linear horizontal springs with constants k_H, which

connect the oscillating additional mass, m_D, and the structure by an articulated mechanism. Further details regarding this configuration for the realization of the vertical NS element can be found in section 3.3.1.1 of Chapter 3.

Table 6.2. *Real (vertical) earthquake records selected in this Chapter.*

Earthquake	Date	Recording station	*Mw*	PGA (*g*)	R_{jb} (*km*)	dt (*sec*)	$Dur._{5\text{-}95}$ (*sec*)
Cape Mendocino	4/25/1992	Cape Mendocino	7.01	0.74	0.0	0.02	9.7
Chi-Chi	9/20/1999	CHY028	7.62	0.34	3.12	0.005	8.7
Imperial Valley	10/15/1979	El Centro Array #4	6.53	0.29	4.9	0.005	10.3
Northridge	1/17/1994	Simi Valley – Katherine Rd	6.69	0.40	0.0	0.01	6.7
Kobe	1/16/1995	Kobe University	6.9	0.45	0.9	0.01	7.0
L'Aquila	4/6/2009	L'Aquila -Parking	6.3	0.37	0.0	0.005	11.6
Loma Prieta	10/18/1989	BRAN	6.93	0.51	3.85	0.005	9.8
Landers	6/28/1992	Lucerne	7.28	0.82	2.19	0.005	13.8

In Table 6.3, the NS element entire set-up is presented, regarding the maximum (absolute) value of the k_{NS}, as the optimization tends to obtain this limit value in all the range of X_{SVD}. The parameter c_I is selected equal to -0.05, to achieve as far as possible linear behavior, and the value of u_0 is selected as u_0=0.1 *cm* so that an almost symmetric response around the equilibrium point is obtained.

Table 6.3. *NS element set-up regarding the maximum (absolute) value of* k_{NS}.

k_{NS} (*kN/m*)	k_H (*kN/m*)	*a* (*cm*)	*b* (*cm*)	l_{HI} (*cm*)	c_I	u_0 (*cm*)
-100	53.16	7.03	21.38	21.03	-0.05	0.1

The maximum structure absolute accelerations are collected in the bar plots reported in Figure 6.6. Note that the vertical axis scale is normalized with the acceleration response indicator v_{AS} (=a_S/PGA). The performances of the control system vary from case to case since are dependent on the frequency content of the earthquake. Overall, it emerges that the VSA is always effective in reducing the structure absolute acceleration, retaining the static vertical deflection X_{SVD} between 1-2 *cm*, where a BI with the same X_{SVD} is not always as effective. On

average, a reduction of 32.17% and 4.45% is attained regarding the VSA-1 and the BI-1 systems, and 40.85% and 24.25% for the VSA-2 and the BI-2 systems, respectively. In Figure 6.7, the maximum dynamic deflections are presented, and it is observed that the vii. constraint of section 3.2 is ineffective for only two out of the eight selected real earthquake motion, the Cape Mendocino and Loma Prieta records. It must be mentioned however, that the dynamic deflections are slightly higher that 50%X_{VSD}. The system dynamic responses relevant to the Chi-Chi and Loma Prieta earthquake records are illustrated in Figures 6.8-6.10.

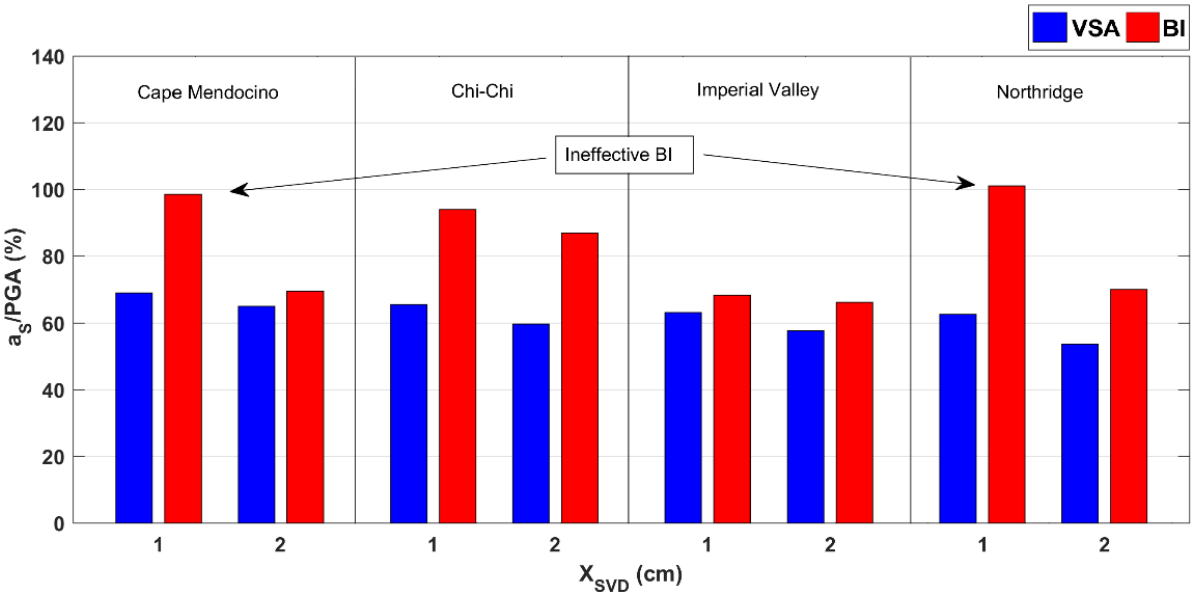

(a)

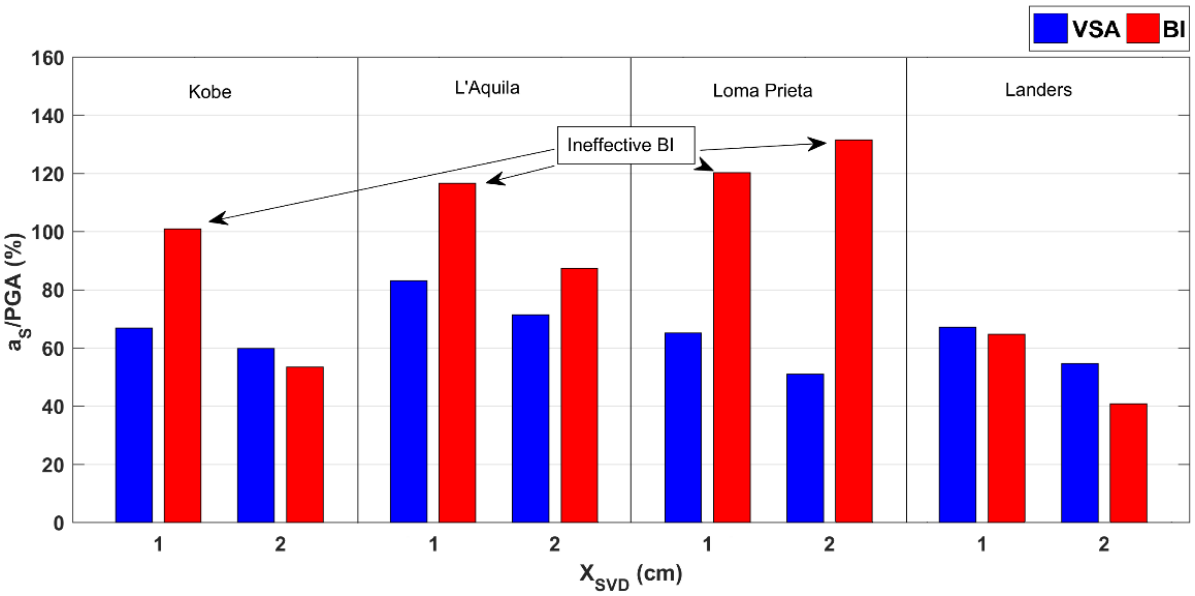

(b)

Figure 6.6: *Maximum structure absolute accelerations of all the considered real earthquake records, of the VSA and the BI systems.*

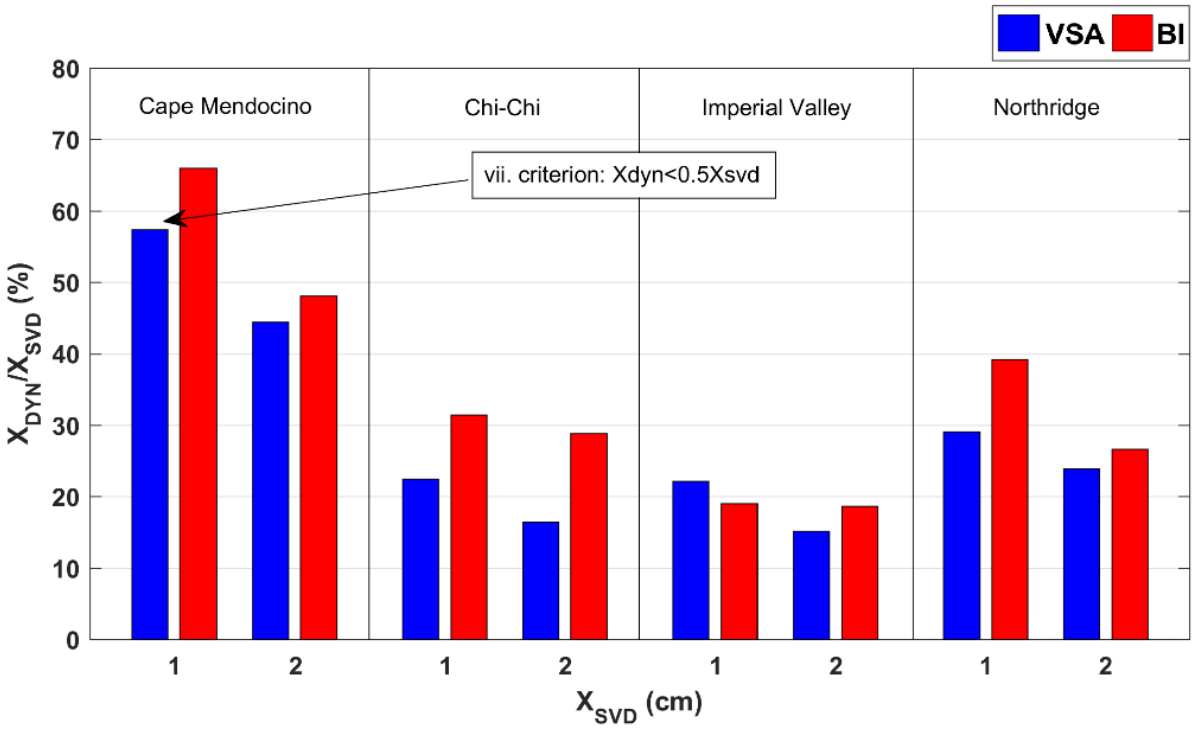

(a)

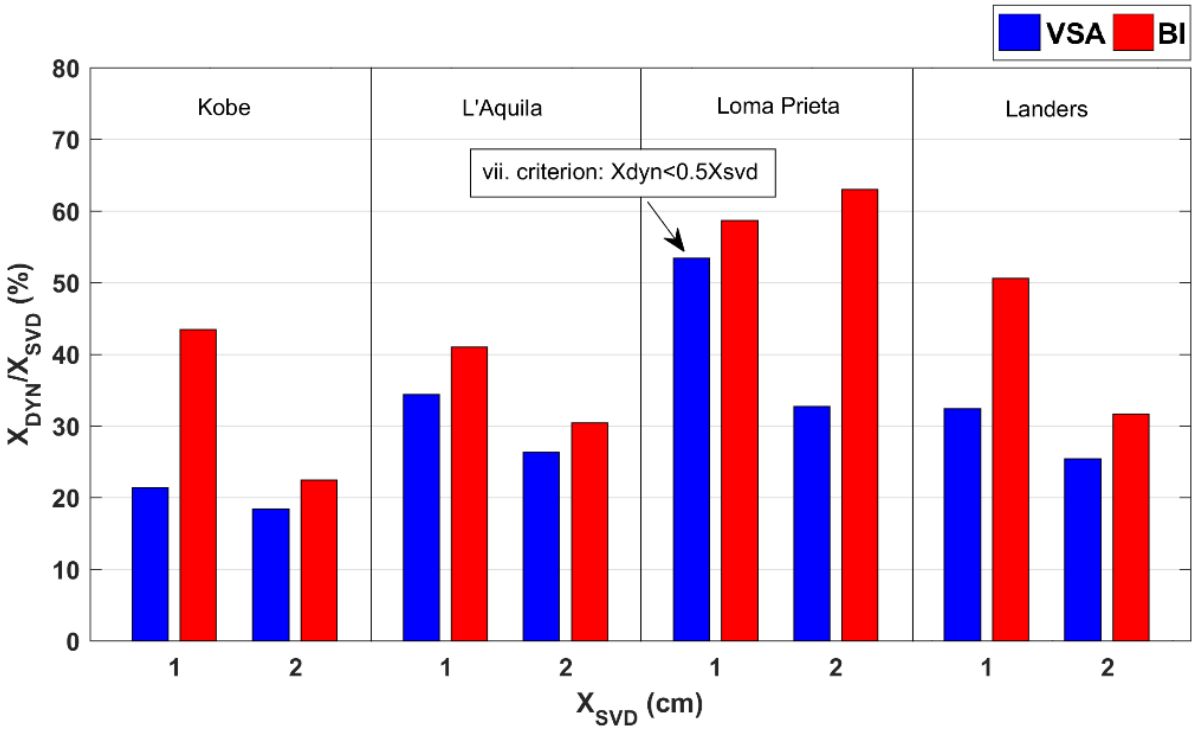

(b)

Figure 6.7: *Maximum structure dynamic deflections of all the considered real earthquake records, of the VSA and the BI systems.*

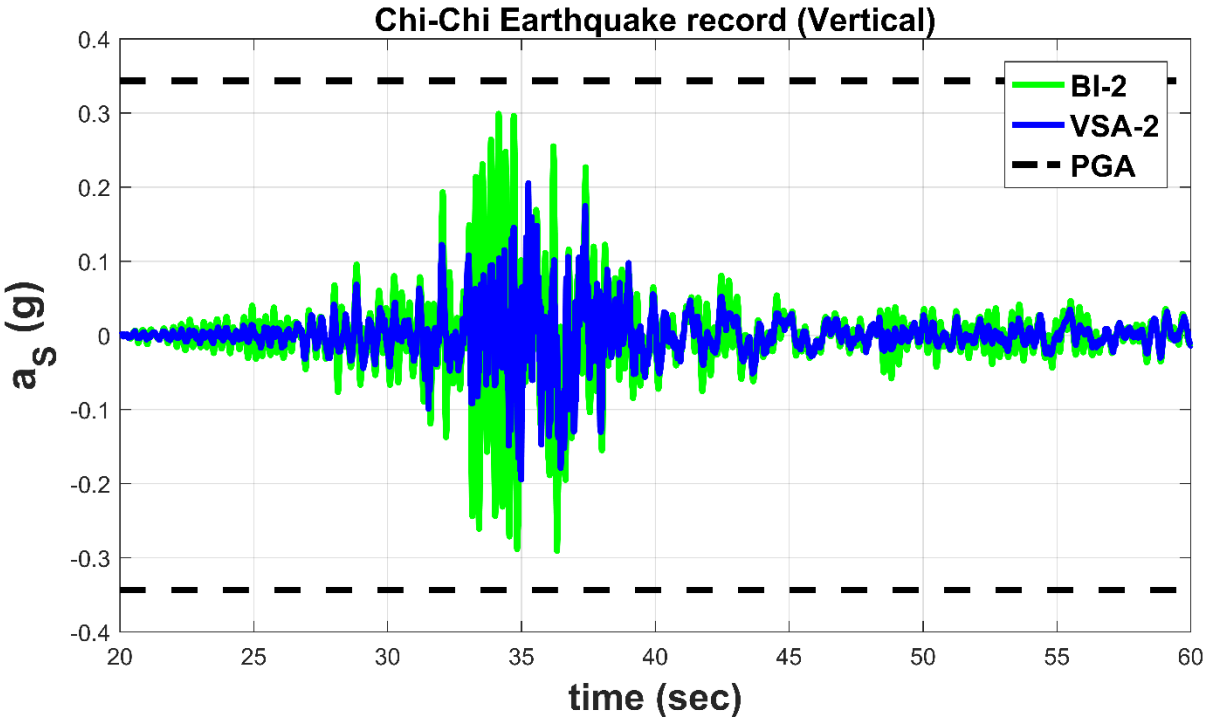

(a)

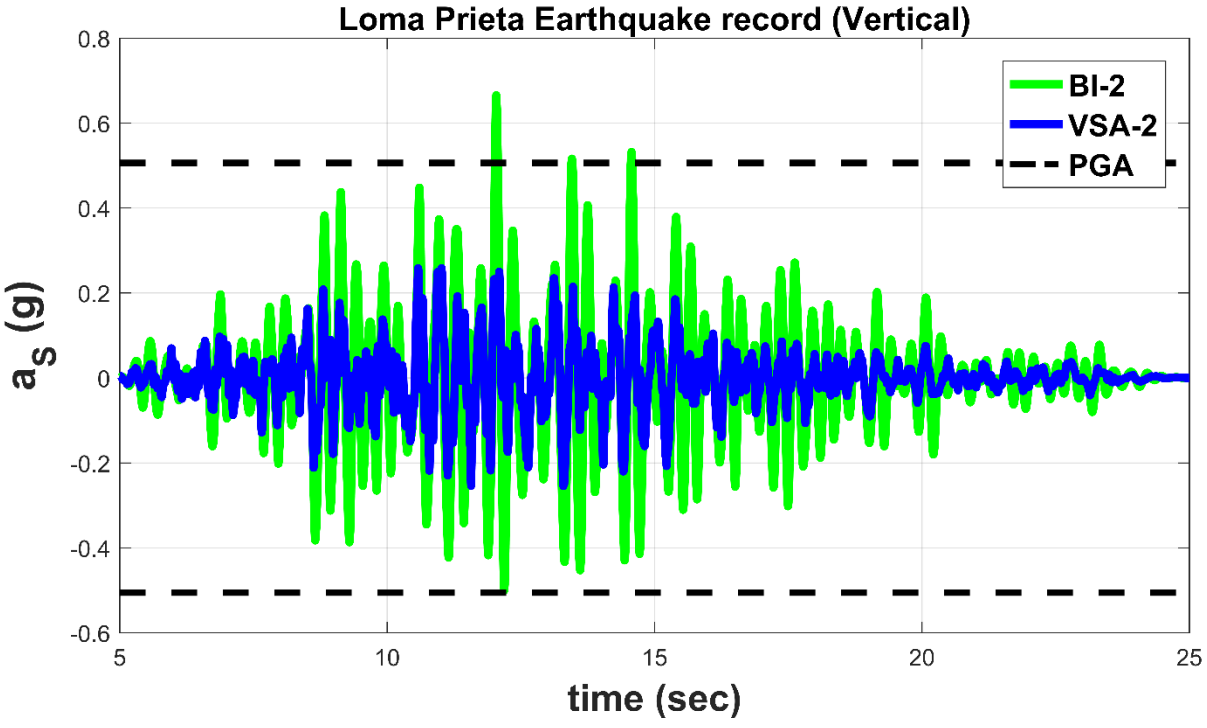

(b)

Figure 6.8: *Comparative results in terms of structure absolute accelerations, between the BI-2 and the VSA-2 systems, for the Chi-Chi and Loma Prieta earthquake excitations.*

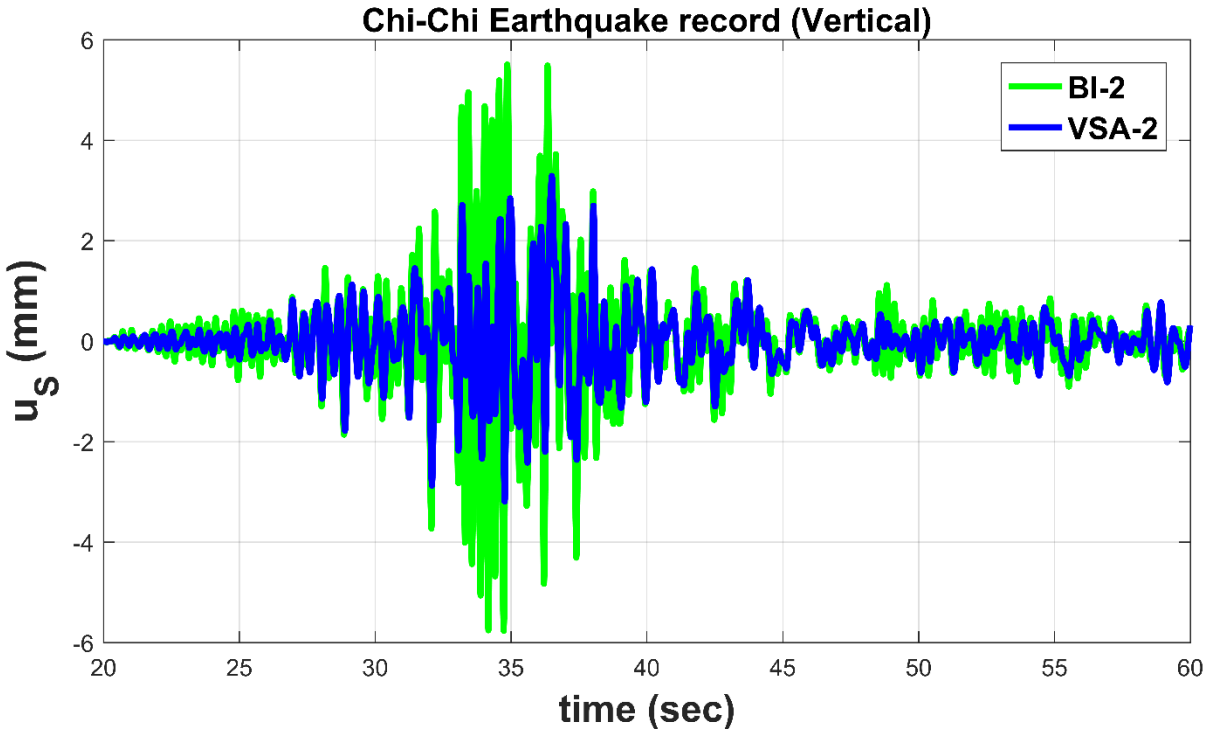

(a)

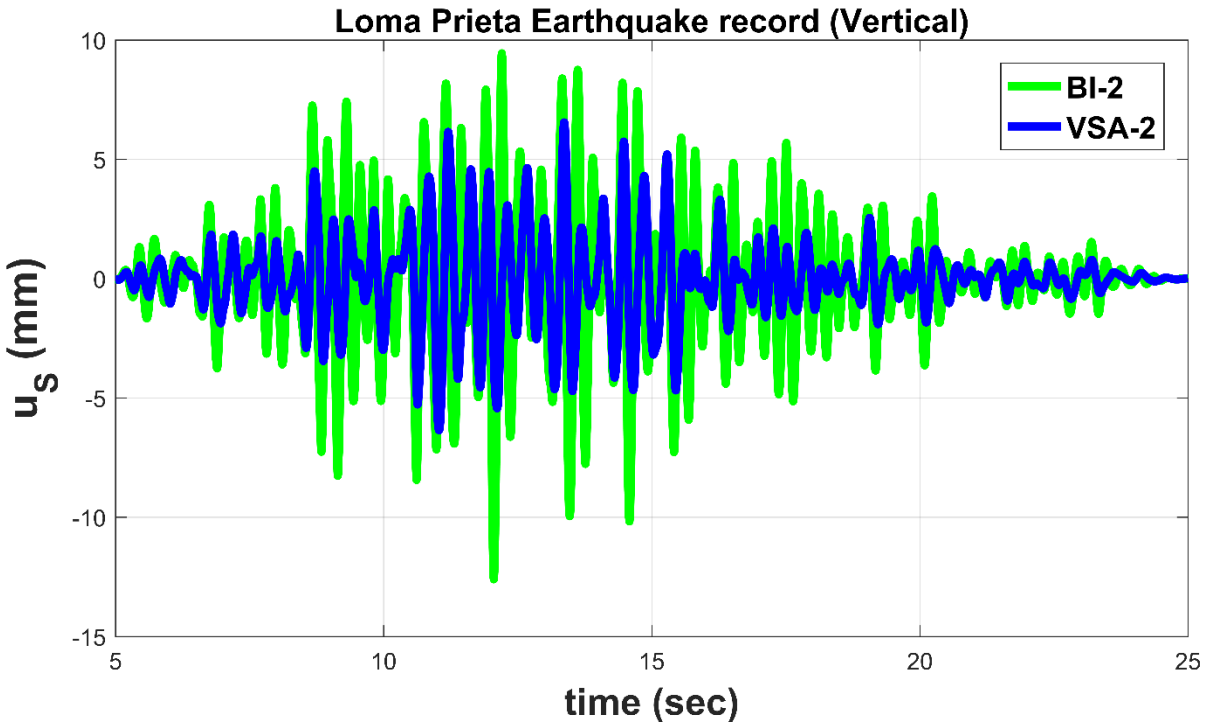

(b)

Figure 6.9: *Comparative results in terms of structure relative displacements, between the BI-2 and the VSA-2 systems, for the Chi-Chi and Loma Prieta earthquake excitations.*

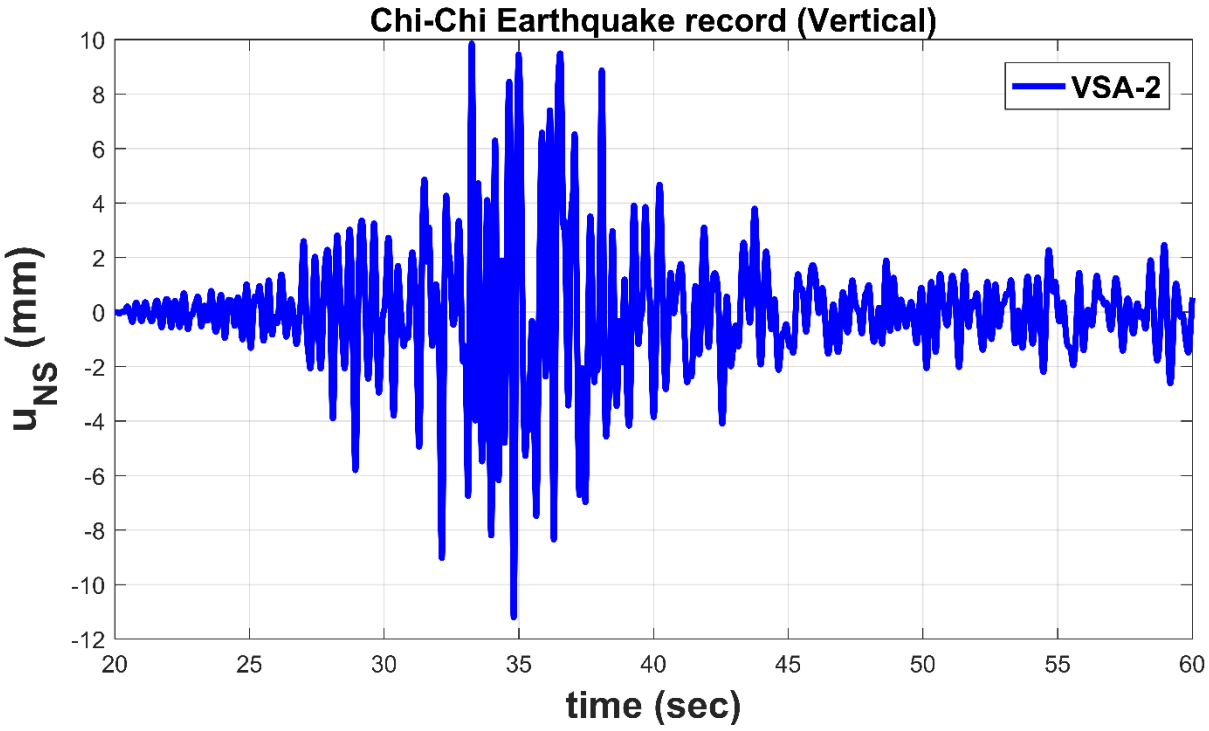

(a)

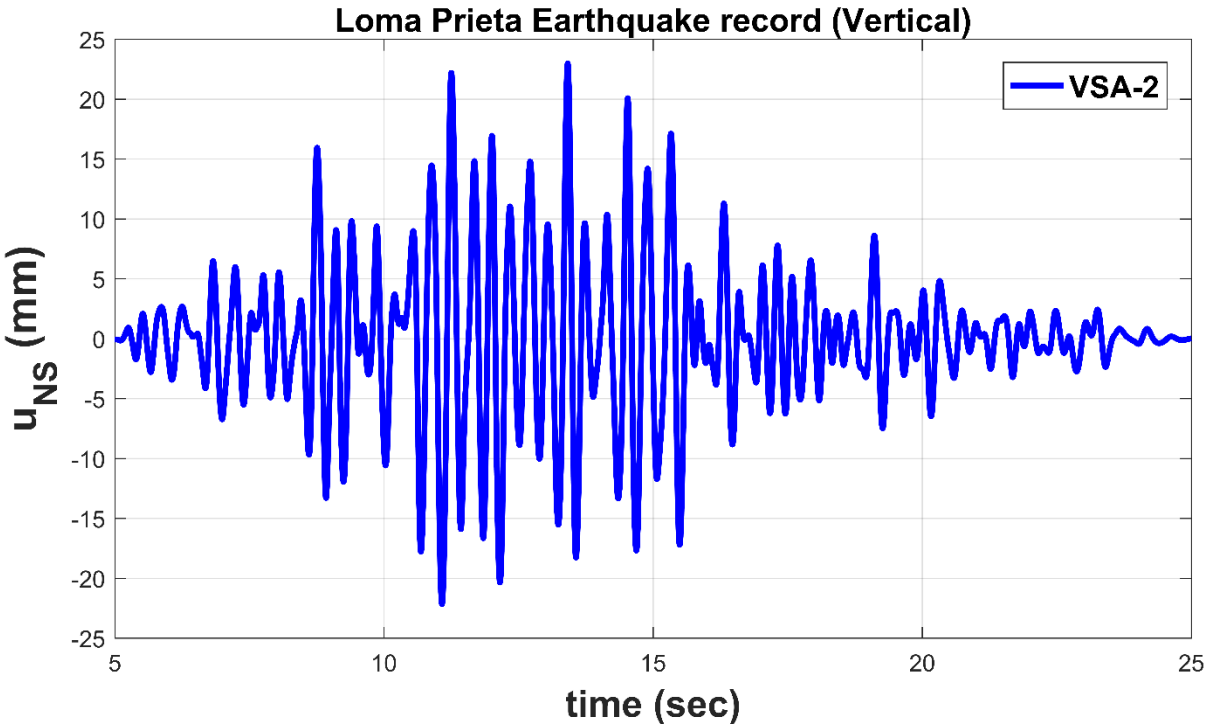

(b)

Figure 6.10: *VSA relative displacements dynamic responses of the VSA-2 system, for the Chi-Chi and Loma Prieta earthquake excitations.*

Once the optimal VSA parameters of a SDoF system have been derived in section 6.3.3 of this Chapter, the validity of the optimal design procedure is here assessed for the considered Numerical Example. To this aim, a sensitivity analysis is performed in which the VSA parameters are slightly varied from their actual optimal values found in the above optimization problem, in an attempt to assess to what extent, the dynamic response varies (degrades) accordingly. Time history analyses are performed with all the 50 artificial accelerograms generated according to section 3.3.2.2 of Chapter 3. Considering the VSA-1 set of optimized parameters, a 20% variation (detuning) of the VSA free design variables k_{NS} and b is explored, i.e. the interval [0.8 – 1.2] k_{NS} and b. For variation of each of these parameters, the results of the 50 time-history analyses are averaged to obtain the mean values of the structure absolute acceleration, and are illustrated in the surface and contour plots of Figure 6.11. It is expected that as the VSA parameters depart from their optimal values, the effectiveness of the vibration control decreases accordingly.

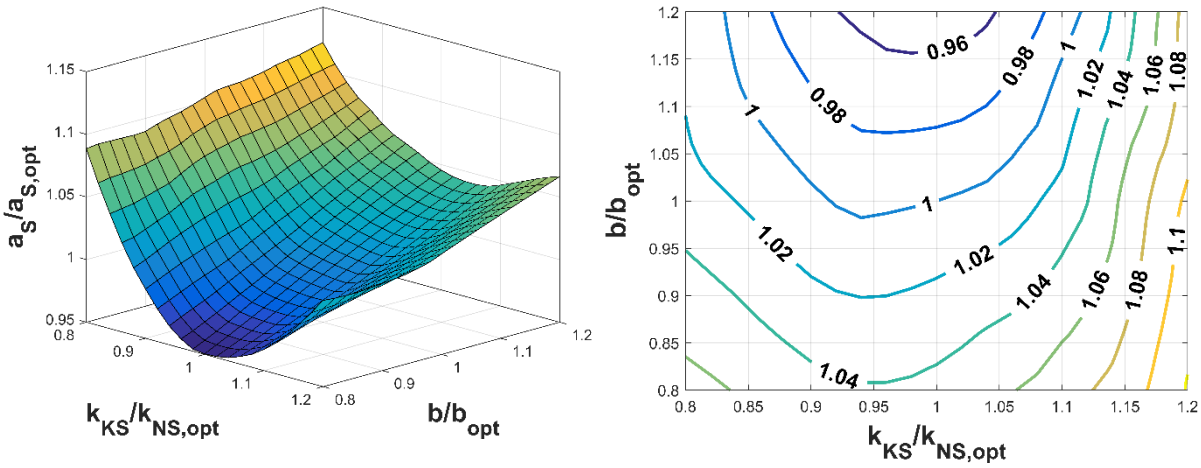

(a) (b)

Figure 6.11: *Sensitivity analysis and detuning effects of the structure absolute acceleration by varying (20%) the free design variables k_{NS} and b of the VSA-1 set of parameters from their optimal values.*

In Figure 6.12, the static vertical displacement X_{SVD} is scrutinized by varying (20%) the stiffness elements, i.e. k_{NS}, k_{PS}, and k_R, one at a time of the VSA-1 set of parameters. As expected, an increase of the NS element k_{NS}, or respectively a decrease of the positive stiffness element k_{PS}, greatly influences the static settlements. However, a variation of less than 15%, of any stiffness element, does not much affect the X_{SVD}. Finally, it is observed that the structure acceleration isn't vulnerable to detuning.

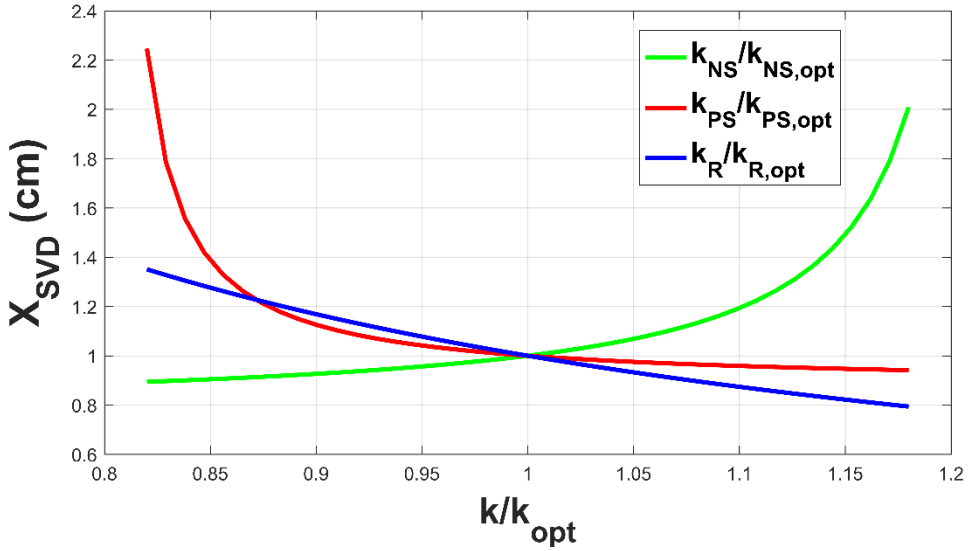

Figure 6.12: *Sensitivity analysis and detuning effect of the static settlement XSVD by varying the stiffness elements of the VSA, k_{NS}, k_{PS},* and *k_R.*

6.4 Concluding Remarks

In this Chapter a negative stiffness driven vertical seismic absorber (VSA) that combines an extension of the KDamper concept with an inerter is proposed. This idea is based on reducing the natural frequency of the system with the inerter and then control the structure accelerations with the extraordinary damping properties that the KDamper offers. To this aim a constraint engineering-criteria driven optimization procedure is followed, to ensure that the design of the VSA is efficient and realistic. The excitation input is a ground motion acceleration excitation PSD, generated from a database of artificial accelerograms designed to match the EC8 vertical spectrum. The performance of the VSA is examined also with real earthquake records and the NS element is realized with a displacement-dependent configuration. Finally, a comparison with the BI system is performed and the detuning phenomena are observed via sensitivity analysis. Based on the dynamic analysis and the results obtained, the following concluding remarks can be made:

1. The design of the VSA is realistic, as it employs small additional masses (5%) and ensures the static stability of the structure by foreseeing variation in all stiffness elements (10%), and follows an engineering-criteria driven optimization procedure;
2. The acceleration excitation input is selected according to the seismic design codes, following the procedure described in section 3.3.2.2 of Chapter 3;

3. The selection of the VSA parameters in the frequency-domain is accurate, as verified in the time-domain;
4. The dynamic performance of the VSA is assessed with real earthquake records using a realistic displacement-dependent configuration for the realization of the NS element, proposed in the Proposed Configuration I of Chapter 3, and is confirmed to be within the limits stated in the optimization procedure;
5. The VSA manages to greatly reduce the vertical accelerations (30-30%) and at the same time retains the static settlements in acceptable levels (1-2 *cm*), as compared to other conventional base isolation approaches (BI);
6. The detuning phenomena are observed via sensitivity analysis, and confirm that the VSA is not vulnerable to detuning;

Chapter 7

Vibration Mitigation Approaches for Wind Turbine Towers with KDamper – Based Designs

7.1 Introduction

As wind power continues its rapid growth worldwide, wind farms are likely to comprise a significant portion of the total production of wind energy, and may even become a sizable contributor to the total electricity production in some countries. The high-quality wind resource and the proximity to load centres make wind energy a compelling proposition. The installed Wind Turbines (WT) energy potential is currently estimated at 539GW, according to the WWEA (World Wind Energy Association, n.d.). An important part of the WT network is the offshore wind turbines (OWT). OWT are expected to increase significantly as European coasts and seas offer a large wind energy potential. The WWEA predicts that offshore wind farms of 150GW will operate in the EU by 2030, contributing 14% of the EU's total electricity consumption.

However, the above prediction is very ambitious. It is noted, that in 2018 the annual rate of WT installation reached the lowest rate (10.8%) since the start of their industrial growth. Moreover, in recent years, several failures have been recorded in existing WT. It is estimated that the structural failure (tower, foundation) of the installed WT amounts up to 10% (Li, 2018), significantly reducing their contribution to the energy network. These failures stem mainly from: i) WT collapse due to earthquake excitations, that cause structural failures due to high dynamic stress loading exciding structural strength, and ii) WT collapse due to wind loading, because of its continuous and cyclic nature, that causes failure due to structural fatigue. In addition, the structural and foundation costs are excessively high, reaching up to 17% for land based (onshore) and fixed bottom offshore WT, while when considering floating offshore WT the cost rises up to 40% (Mone et al., 2015; Morais et al., n.d.; Renewable Energy Agency, 2012).

From the above comments, and according to the International Energy Agency (Sustainable Development Scenario – World Energy Model – Analysis - IEA, n.d.), it emerges as top priority to enhance research to avoid WT structural failures. A way to extend the feasibility of Wind Turbine towers is by means of structural control. The application of vibration control system in a WT will result in a structural system with enhanced dynamic behavior under vibrating loading. It is classified as passive, active, hybrid, or semi-active control. Several researchers have been studying the use of structural control to help suppress the wind-induced vibrations experienced by Wind Turbine towers (Avila et al., 2016; Lackner and Rotea, 2011; Nigdeli and Bekdaş, 2017; Stewart and Lackner, 2014). The passive control methods are simple and reliable, as they do not require an external force, are easy to implement to reduce the structural vibration, and are widely used in WT technology for enhancing their effective damping. The purpose of the installation of such devises, for the control of WT, is to mitigate their dynamic responses, due to the fact that the vibrations caused the by aerodynamic loads are lasting and cause fatigue problems to the body of the tower, and to their foundation.

The concept of a resonant damper, like a Tuned Mass Damper (TMD) is among the approaches that have received the most attention in the literature. The principal of the TMD system (Frahm, 1911) is the degradation of the dynamic response of the system through energy transfer to a system of an additional mass, designed with optimum characteristics and adapted in a suitable position in the structure (Casciati and Giuliano, 2009; Soong and Dargush, 1997). The TMD system consist of an additional small mass and a positive stiffness element in combination with an artificial damper. The parameters that concern the design of such devices, are determined with the resonance of the frequency of the device with the fundamental eigenfrequency of the initial system. As a result, a great portion of the vibration energy of the structure, due to a vibratory excitation, is consumed by the additional mass of the device and then dissipated through the damper.

The Active Tuned Mass Damper (ATMD) is a hybrid devise consisting of a passive TMD supplemented by an actuator parallel to the spring and damper. It is a well-known concept in structural control and has been proved to yield enhanced damping performance compared to the passive TMD (Ankireddi and Yang, 1996; Ricciardelli et al., 2003). Semi-active TMDs are examined thoroughly recently, that introduce negative stiffness elements and negative stiffness tension adjusting mechanisms (Acar and Yilmaz, 2013; Casciati et al., 2012; Liao et al., 2011; Weber, 2014; Weber et al., 2011). The downside of such designs is that their performance is directly (or obliquely) depended by the accuracy of the actuators output, which over time can have an alternation in its performance by false estimation of the desirable function of the vibration absorption concept and eventually burden the structure.

In addition, various forms of Dynamic Vibration Absorbers (DVA) have been used, such as Tuned Liquid Column Damper (TCLD) and multiple TMDs. Some of the pioneering work concerning applications in wind turbines include the work by (Colwell and Basu, 2009) in which the damping effect of a TLCD installed in an offshore wind turbine has been investigated by assuming correlated wind and wave load conditions, whereas the potential of using a pair of TMDs simultaneously targeting the dominant fore-aft ad side-side modes has been demonstrated by (Lackner and Rotea, 2011). More recently, attention has focused on how to address the absence of aerodynamic damping in the side-side direction, when significant wind-wave misalignment is present, e.g. in the work by (Stewart and Lackner, 2014) where the beneficial of a TMD in reducing the tower base moment is demonstrated through numerical simulation, and in particular, a significant reduction in the side-side moment has been reported. The essential limitations of all the aforementioned TMD-related concepts, are related with the location and the selected mass of these devices. In order to be effective, a resonant damper like the TMD should be installed where the absolute motion of the targeted vibration mode is largest, which is at the top of the tower or inside the nacelle. Effective damping by a TMD is furthermore associated with a large damper mass, which constitutes a major limitation, since additional mass is highly undesirable at the top of the wind turbine.

In this Chapter, two alternative vibration absorption approaches for mitigation of the WT dynamic responses are considered. First, the nacelle is released from the WT tower (nacelle isolation concept), using a low stiffness connection. This option is based on the seismic isolation concept of structures. This way, the nacelle is no longer rigidly connected to the WT tower, but is connected with a low stiffness element (elastomeric bearings). In order to retain the relative displacements of the nacelle-WT tower, an energy dissipation mechanism is implemented to reduce the control the displacements. In the second option, the a KDamper (or an extension of it) is intervened between the nacelle and the WT tower. The KDamper, introduced in (Antoniadis et al., 2018), is essentially an extension of the classical TMD, by incorporating appropriate negative stiffness elements. Instead of increasing the additional mass, the vibration isolation capability of the KDamper can be increased by increasing the value of the negative stiffness element, overcoming the sensitivity problems of TMDs as the tuning is mainly controlled by the negative stiffness element's parameters. Thus, the KDamper always indicates better isolation properties than a TMD damper with the same additional mass. Although the KDamper incorporates a negative stiffness element, it is designed to be both statically and dynamically stable.

Section 7.2 presents the vibration mitigation approaches considered in this Chapter, along with the dynamic model of the WT tower. The developed model is an assemblage of prismatic

beam elements with sway degrees of freedom considered to be the dynamic degrees of freedom. In order to verify the validity and the efficiency of the developed formulation, a set of simplified analyses were conducted and the obtained results were compared with those obtained from the commercial software package SOFiSTiK (FEM Software for Structural Engineers | SOFiSTiK AG, n.d.) based on FEM. The aerodynamic load is taken into account by generating artificial basic wind velocities applying the corresponding regulations of EC1, Part1,4 (*EN 1991 - Wind actions*, 2010) and applying it at the WT following the procedure described in (Hansen, 2008). Section 7.3, presents the optimization procedure from which the optimal KDamper, and the extended versions of it, are obtained. The free design variables are presented, and proper limitations and constraints are imposed on the free design variables and the system main dynamic responses, respectively, based on the proposed engineering-criteria driven optimization procedure. The NS element is realistically designed according to the Proposed Configuration II of Chapter 3. Finally, in section 7.4 a numerical example is presented, where the effectiveness of the proposed KDamper-based vibration mitigation approaches is verified. Based on a comparison with a conventional TMD, and the proposed nacelle-isolation concept, the KDamper designs manage to significantly increase the effective damping, and thus mitigate the WT dynamic responses, with small additional masses and a realistically designed configuration.

7.2 Methodology and Modelling

In this section, the vibration mitigation approaches considered in this Chapter are presented. The developed dynamic model of the wind turbine tower is an assemblage of prismatic beam elements with sway degrees of freedom considered to be the dynamic degrees of freedom. The validity and the efficiency of the developed formulation is verified with simplifies analyses, based on a comparison with a commercial software package, based on FEM (FEM Software for Structural Engineers | SOFiSTiK AG, n.d.). Finally, the aerodynamic load is taken into account based on artificial wind basic velocities.

7.2.1 Vibration Mitigation Approaches

Figure 1 presents the dynamic vibration absorber design options considered in this Chapter. The first vibration mitigation approach is based on the classical Tuned Mass Damped (TMD).

Figure 7.1.b presents the schematic representation of the TMD concept implemented in wind turbines, where the additional mass (m_D) of the TMD is attached at the top of the wind turbine tower or inside the nacelle, using a positive stiffness element and a linear damper (k_D, c_D).

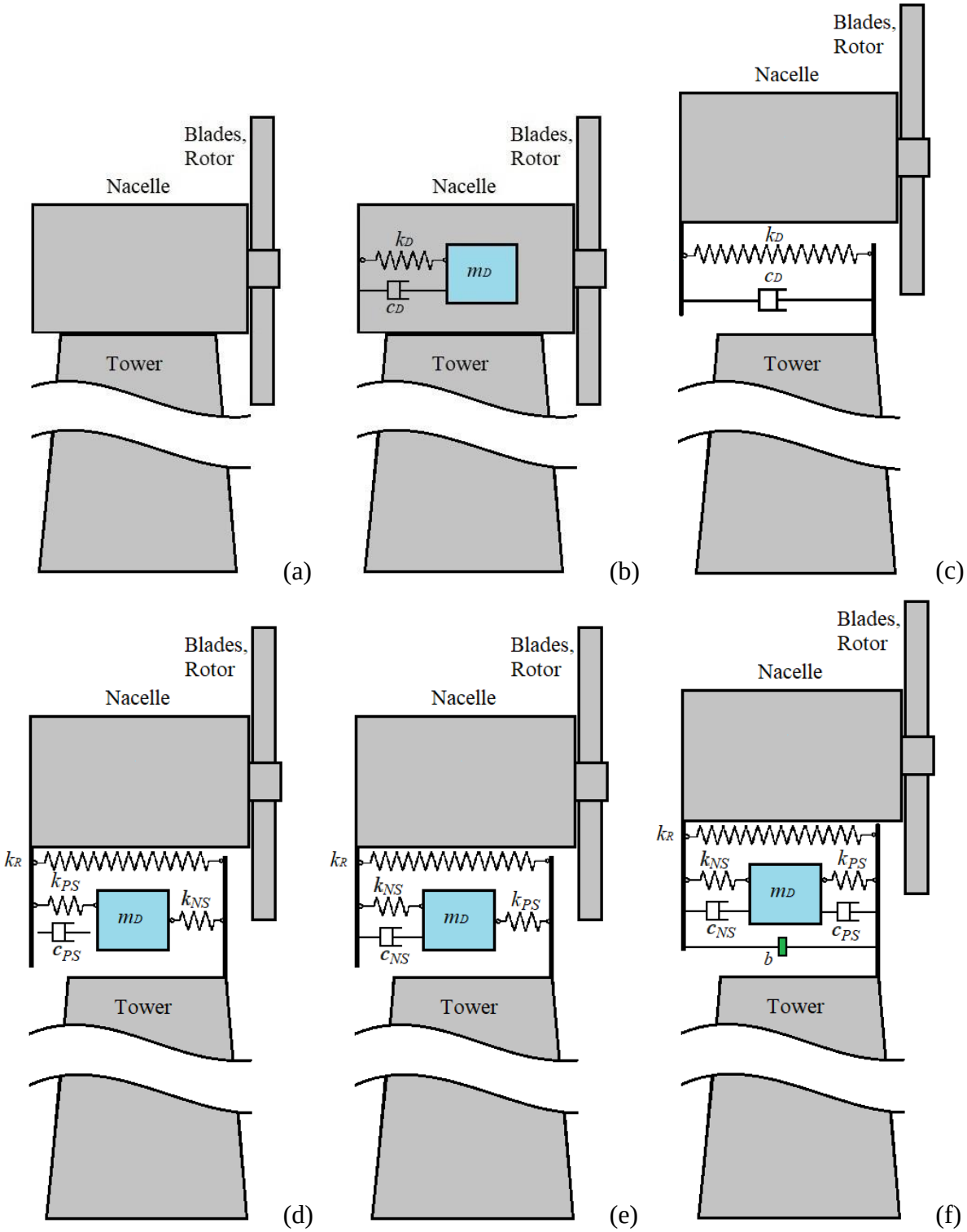

Figure 7.1: *Schematic representation of the vibration absorption concepts: (a) uncontrolled WT, (b) TMD, (c) nacelle-isolation, (d) KDamper, (e) EKD, and (f) EKDI.*

This concept is employed as a benchmark because it has received the most attention in the literature due to the simplicity of its implementation. The main drawback of this option is the need for large additional masses, in order for the TMD to achieve significant effective damping, as will be observed in the numerical results.

The second vibration absorption option is based on the TMD concept combined with the seismic isolation principle, where the superstructure is isolated from its base/foundation with a low stiffness connection. Figure 7.1.c presents the schematic representation of the proposed vibration absorption concept, where the mass that corresponds to the mechanical parts (nacelle, rotor and blades) is used as the additional mass of a TMD. Thus, the additional mass concentrated mass at the top of the tower is no longer connected rigidly to the steel tower, but is realized with a stiffness connection and a linear damper (k_D, c_D), as in the case of the classical TMD concepts. This system will be referred to hereafter as nacelle-isolation concept. The main drawback that is to be expected, is that in order to isolate the steel tower from the vibrations of the nacelle, large relative displacements between the nacelle and the steel tower are required, which may prohibit the good function of the wind turbine.

In an effort to combine the aforementioned vibration control options, exploiting their advantages without their respective drawbacks, the KDamper is employed, as presented in Figure 1.d. As in the case of the nacelle isolation concept, the additional mass of the nacelle, rotor and blades is no longer rigidly attached to the wind turbine tower but through the interference of a KDamper device. In this concept, the additional oscillating mass of the KDamper (m_D) is connected with the nacelle with a positive stiffness element and a linear damper (k_{PS}, c_{PS}), and with the steel tower with a negative stiffness (NS) element (k_{NS}), and the steel tower is connected with the nacelle with a stiffness connection (k_R). This way, the KDamper aims to isolate the vibrations of the nacelle form the steel tower, as in the case of the nacelle-isolation concept, retaining the relative displacements nacelle-tower within reasonable ranges. In addition, the KDamper aims to increase the effective damping of the wind turbine tower compared to the TMD with the same additional mass, as it has been proven that the KDamper always presents an improved dynamic behavior compared to the TMD. Finally, two extended version of the KDamper are presented in Figures 7.1.e, f. In the proposed extensions, the additional mass, m_D is connected with the nacelle with a NS element and an artificial damper (k_{NS}, c_{NS}), and with the steel tower with a positive stiffness element k_{PS}. The extended version of KDamper will be referred to hereafter as EKD. In Figure 7.1.f, the EKD is equipped with an inerter, that connects the top of the tower directly with the nacelle, and thus is parallel to the stiffness element k_R. The addition of the inerter aims to further reduce the vibrations of the WT tower retaining the relative displacement nacelle-WT tower within reasonable ranges.

7.2.2 Dynamic Model of the Wind Turbine

In this section, the NREL baseline 5-MW nacelle and rotor, supported by a steel tower of 120 *m* height is examined. This choice is made due to the fact that is widely used in the literature as a benchmark for vibration control of wind turbine towers. The key properties of the wind turbine and the steel tower are listed in Table 7.1 and Table 7.2 respectively.

Table 7.1: *Key properties of NREL baseline 5 MW wind turbine.*

Property	**Value**
Rating	5 *MW*
Rotor diameter	126 *m*
Hub diameter	3 *m*
Cut-in wind speed	3 *m/sec*
Rated wind speed	11.4 *m/sec*
Cut-out wind speed	25 *m/sec*
Cut-in rotor speed	6.9 *rpm*
Rated rotor speed	12.1 *rpm*
Nacelle mass	240,000 *kg*
Rotor mass	110,000 *kg*
Blade material	Glass-fibre
Blade length	61.5 *m*
Blade mass	17,740 *kg*
Blade CM (from blade root)	20.475 *m*
Blade damping ratio (all modes)	0.48%

Table 7.2: *Key properties of the considered steel tower.*

Property	**Value**
Height	120 *m*
Base diameter	8.43 *m*
Base steel thickness	0.048 *m*
Top diameter	3.87 *m*
Top steel thickness	0.025 *m*
Young's modulus	210 *GPa*
Steel density	8,500 kg/m^3

Total mass	798,640 *kg*
Location of CM (above base)	43.042 *m*
Tower damping ratio (all modes)	1%

The WT tower (Table 7.2) of variable tubular cross section the NREL baseline 5-MW nacelle and rotor (Quilligan et al., 2012) is examined. In order to take into account, the inertial forces applied by the mechanical parts (nacelle, rotor and blades), an additional concentrated mass $m_{top} = 403.22\ tn$ (Quilligan et al., 2012) is added at the top of the WT tower.

The wind turbine tower is modeled as an assemblage of beam elements with sway degrees of freedom considered to be the dynamic degrees of freedom. The theoretical development is based on the assumption that the cross-sectional dimension within the element remains the same, i.e. prismatic beam element. Additional assumptions made for the analytical formulation are: (i) the WT tower is considered to remain within the elastic limit under the aerodynamic loads, (ii) the effects of soil-structure-interaction (SSI) are not taken into consideration, and (iii) the axial DoFs are not considered in this formulation as the purpose of this work is to mitigate the dynamic responses of the WT tower due to horizontal aerodynamic loads, and thus is reasonable to neglect them. Figure 7.2 presents the lumped mass model of the WT tower.

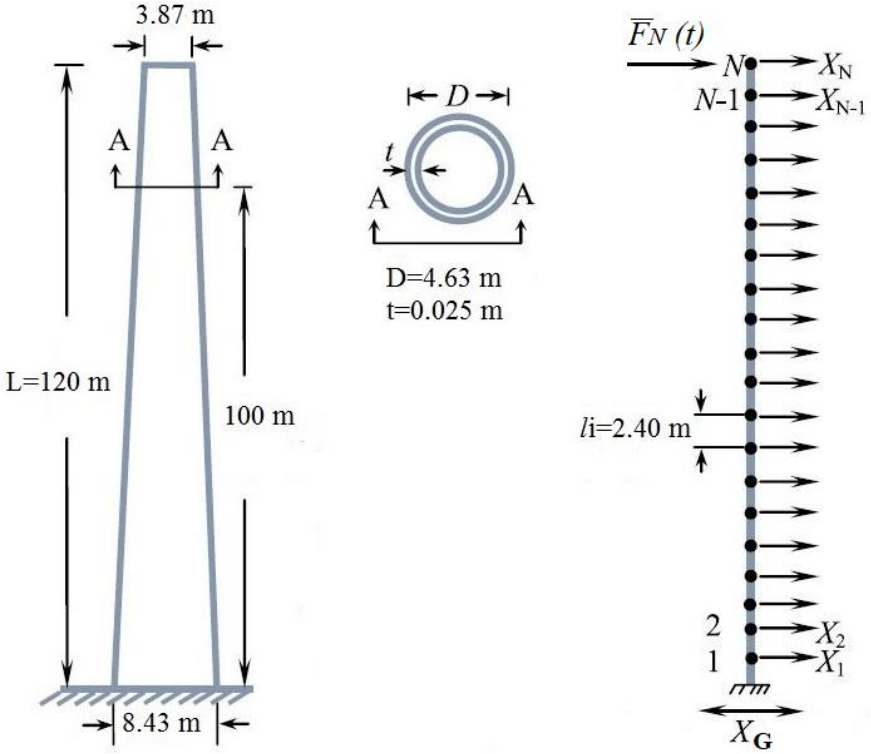

Figure 7.2: *Lumped mass model of the wind turbine tower, with the sway degrees of freedom taken as dynamic DoFs.*

This model is serviceable due to the fact that it can incorporate easily each of the considered vibration absorption concepts, presented in section 7.2.1, and therefore evaluate their optimized parameters for vibration absorption, via optimization. The equations of motion of the uncontrolled wind turbine, considering the equilibrium of forces at the location of each degree of freedom is expressed as follows:

$$[M_S]\{\ddot{X}_S\}+[C_S]\{\dot{X}_S\}+[K_S]\{X_S\}=[P_S]\pm[M_S]\ddot{X}_G \tag{7.1}$$

where $[M_S]$, $[C_S]$ and $[K_S]$ are the mass, damping and stiffness matrices of the original wind turbine tower, respectively of order ($N \times N$), N indicating the number of prismatic beam elements selected to model the wind turbine tower. The initial stiffness matrix is of order ($2N \times 2N$), as each beam element has two rotational and sway DoFs, respectively. The condensed stiffness matrix of the uncontrolled wind turbine tower is corresponding to the sway degrees of freedom, taken as the dynamic DoF, and thus is $[K_S]_{NxN}$. The damping matrix $[C_N]_{NxN}$ is not explicitly known but is obtained with the help of the Rayleigh's approach using the same damping ratio in all modes, *1*% (Quilligan et al., 2012). The unknown nodal displacements, relative to the base, are expressed as Xi, and are collected in the array $\{X_S\} = \{X_1,X_2,X_3,\ldots,X_N\}^T$. In this work, the number of beam elements selected for the model of the uncontrolled steel tower are equal to $N = 24$.

In order to verify the validity and the efficiency of the developed formulation, a set of simplified analyses were conducted and the obtained results were compared with those obtained form the commercial software package SOFiSTiK (FEM Software for Structural Engineers | SOFiSTiK AG, n.d.) based on FEM. More specifically, in Table 7.3, the first 5 eigenperiods of vibration, are presented using SOFiSTiK, and are compared with those obtained from a FEM solution employing 24 prismatic beam elements for the tower, while in Figure 7.3, the corresponding flexural modal shapes of the tower are illustrated. Furthermore, the response of each tower configuration is examined performing a simplified linear static analysis, applying a concentrated force $\bar{F}_N = 1353.258$ *kN* (starting value of the generated aerodynamic load presented in section 7.2.3) at the top of the tower. Table 7.3 presents the static deflections X_{top} at the top of the WT tower obtained from the developed model of the WT tower as compared with the aforementioned FEM solution, using SOFiSTiK software. It can be observed that the validity of the developed model of the WT tower is verified, as both the values of the WT eigenperiods and the static deflection of the top of the WT tower are in a very good agreement.

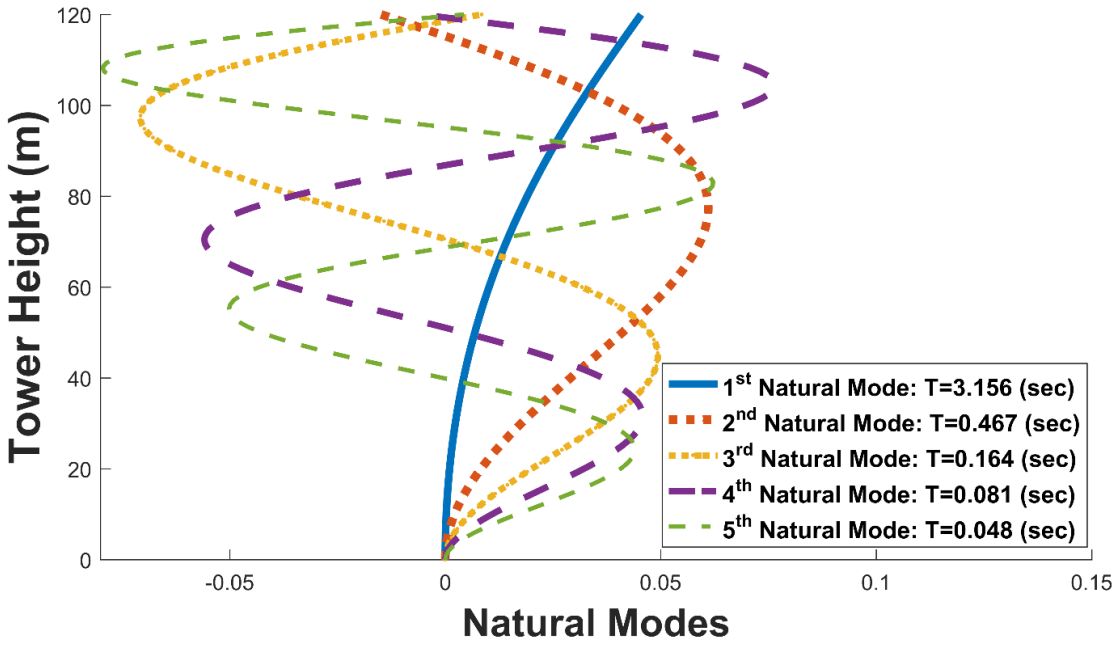

Figure 7.3: *First 4 natural modes and eigenperiods of the uncontrolled wind turbine.*

Table 7.3: *Eigenperiods of the WT tower, and static deflection at the top of the tower under static analysis.*

	Eigenperiods (*sec*)					Static deflection at the top of the tower X_{top} (*m*)
	T1	T2	T3	T4	T5	
Present Study	3.156	0.467	0.164	0.081	0.048	0.7063
SOFiSTiK	3.164	0.474	0.172	0.089	0.056	0.711

The governing equations of motion for the WT including the respective vibration mitigation concept to be considered are obtained by considering the equilibrium of forces at the location of each degree of freedom as follows:

$$[M]\{\ddot{X}\}+[C]\{\dot{X}\}+[K]\{X\}=[P]\pm[M]\ddot{X}_G \tag{7.2}$$

where [*M*], [*C*] and [*K*] are the mass, damping and stiffness matrices of the controlled wind turbine tower, respectively of order (*N*+*n*) *x* (*N*+*n*). As stated previously, *N* indicates the wind turbine's DoFs and *n* the extra DoFs of each of the vibration isolation option to be considered. Furthermore, $\{X\} = \{\{X_N\}, \{X_n\}\}^T$ are the unknown, relative to the base, nodal displacements. The matrices of mass [*M*], damping [*C*], and stiffness [*K*] are of order (*N*+*n*) *x* (*N*+*n*), and are expressed as follows:

$$[M]=\left[\begin{bmatrix}[M_S]_{N\times N} & [0]_{N\times n}\\ [0]_{n\times N} & [0]_{n\times n}\end{bmatrix}+\begin{bmatrix}[M_{n,a}]_{N\times N} & [0]_{N\times n}\\ [0]_{n\times N} & [M_{n,d}]_{n\times n}\end{bmatrix}\right]_{(N+n)\times(N+n)} \tag{7.3.a}$$

$$[K]=\left[\begin{bmatrix}[K_S]_{N\times N} & [0]_{N\times n}\\ [0]_{n\times N} & [0]_{n\times n}\end{bmatrix}+\begin{bmatrix}[K_{n,a}]_{N\times N} & -[K_{n,b}]_{N\times n}\\ -[K_{n,c}]_{n\times N} & [K_{n,d}]_{n\times n}\end{bmatrix}\right]_{(N+n)\times(N+n)} \tag{7.3.b}$$

$$[C]=\left[\begin{bmatrix}[C_S]_{N\times N} & [0]_{N\times n}\\ [0]_{n\times N} & [0]_{n\times n}\end{bmatrix}+\begin{bmatrix}[C_{n,a}]_{N\times N} & -[C_{n,b}]_{N\times n}\\ -[C_{n,c}]_{n\times N} & [C_{n,d}]_{n\times n}\end{bmatrix}\right]_{(N+n)\times(N+n)} \tag{7.3.c}$$

where the submatrices $[M_N]$, $[C_N]$, and $[K_N]$ are expressed corresponding to the degrees of freedom associated with the respective control system to be considered. The expressions of the additional matrices in Equations (7.3), that correspond to the employed vibration absorption concepts, are given in appendix A3.

7.2.3 Aerodynamic Loads

The loading due to the wind is taken into account as follows. The tower is considered to be subjected to the horizontal force $\overline{F}_N(t)$ due to the wind at its top, as presented in Figure 7.4.

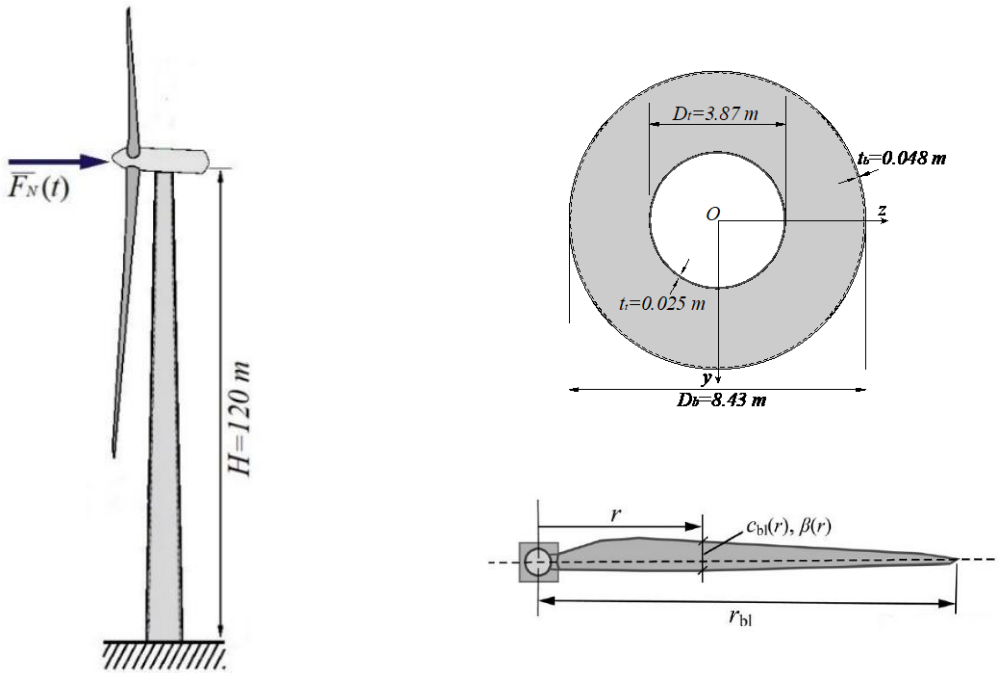

Figure 7.4: *Wind turbine tower of variable tubular cross section, and the turbine blade.*

Moreover, the horizontal force $F_N(r,t)$ acting as a position r (Figure 7.4) along the wind turbine blade can be obtained by the following relation (Hansen, 2008):

$$F_N(\mathrm{r},\mathrm{t}) = \frac{1}{2}\rho_{air} C_N(r) c_{bl}(r)(\overline{V}(t))^2 \tag{7.4}$$

where ρ_{air} = 1.225 x 10^{-3} tn/m^3 is the air density, and C_N (r) is the coefficient computed by the corresponding lift C_L (r) and drag C_D (r) coefficients. The values of the latter coefficients depend on the airfoil characteristics of the blades and their distribution with respect to the "angle of attack" of the wind velocity $\overline{V}(t)$ vector passing through the blade profile can be retrieved from. It is noted that $\overline{V}(t)$ is assumed to have a uniform spatial distribution over the actuator disc. c_{bl} (r), β (r) is the chord and the pitch angle of the blade profile varying along the blade length r (Figure 7.4), the distributions of which are obtained according to the blade type employed to equip the turbine. C_N (r) is given as:

$$C_N(\mathrm{r}) = C_L(r)\cos\varphi(\mathrm{r}) + C_D(r)\sin\varphi(r) \tag{7.5}$$

where φ (r) is the wind flow angle (Hansen, 2008). In order to evaluate φ (r) and consequently C_N (r), the blade element momentum theory incorporating Prandtl's tip loss factor and Glauert's correction (Hansen, 2008) is employed with an assumption of constant angular velocity of the blades Ω_{bl}. Subsequently, breaking $\overline{V}(t)$ down into a mean component V_{m} and a fluctuating component V (t), the corresponding mean and fluctuating components of $F_N(r,t)$ can be obtained as:

$$F_{Nm} = \frac{1}{2}\rho_{air} C_N(r) c_{bl}(r) V_m^2 \tag{7.6.a}$$

$$F_N(r,t) = \frac{1}{2}\rho_{air} C_N(r) c_{bl}(r)(2V_m V(t) + V(t)^2) \tag{7.6.b}$$

In this work, the mean velocity is obtained by employing a basic velocity at the altitude of 10 m, V_{b} and applying the corresponding regulations of EC1, Part1,4 (*EN 1991 - Wind actions*, 2010). Moreover, in order to take into account, the wind velocity fluctuation at the altitude of l_{t}, an artificial velocity time history is generated applying the procedures presented in (Jonkman, 2007; Koulatsou et al., 2013; M, 1998; Norske Veritas (Organization) and

Forskningscenter Risø., 2002) assuming a value of standard deviation σ. After having established $F_N(r,t)$, the total concentrated force exerted on the top of the tower can be computed as:

$$\overline{F}_N(t) = 3\int_0^{r_{bl}} \overline{F}_N(r,t)dr \tag{7.7}$$

Apart from the concentrated force applied on the top of the steel tower due to operation of the turbine, an additional distributed loading along the tower height is taken into account due to the fact that a portion of wind forced is exerted directly on the tower. The spatial and time distribution of this loading is obtained by employing the procedures of (*EN 1991 - Wind actions*, 2010) and of the studies (Koulatsou et al., 2013; M, 1998; Norske Veritas (Organization) and Forskningscenter Risø., 2002).

The basic wind velocity that is employed has corresponding standard deviation V_b = 27.0 m/s with σ = 3.30 m/s ($V_m(120m)$ = 39.93 *m/s*). The rotor is assumed to develop a constant angular velocity Ω_{bl} = 12.1 rpm, while all the necessary blade profile characteristics are retrieved from (Jonkman, 2007; Quilligan et al., 2012). Figure 7.5.a presents the mean wind velocity, and Figure 7.5.b the time history of the evaluated total forces $\overline{F}_N(t)$ for the aforementioned basic wind velocity (V_b = 27.0 m/s, σ = 3.30 m/s).

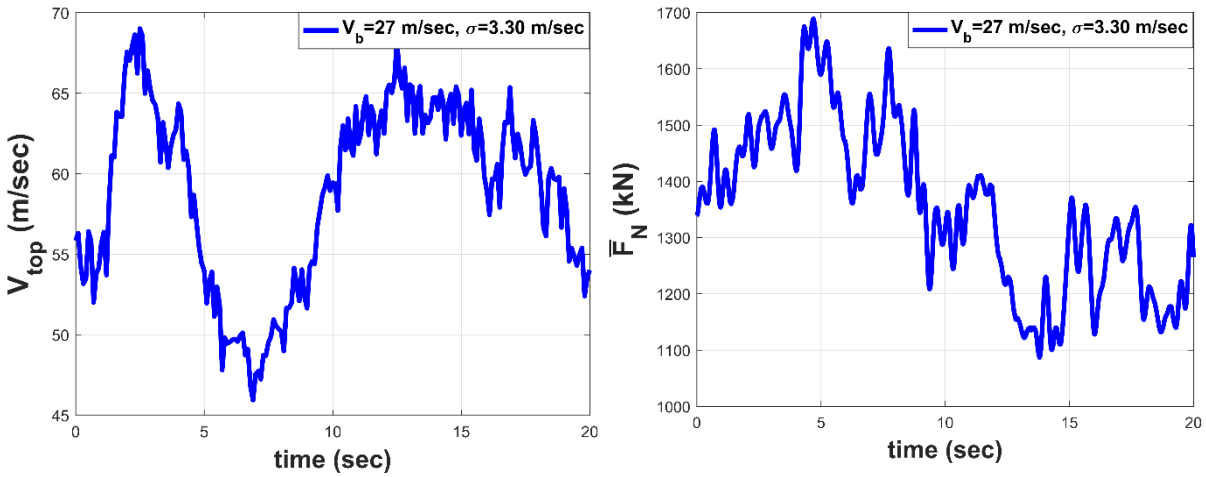

(a) (b)

Figure 7.5: *Basic wind speed V_b at the altitude of 10 m (a) and (b) time history of the total Force $\overline{F}_N(t)$ applied at the top of the wind turbine tower.*

7.3 Optimal Design of KDamper – Based Designs

In this section, an engineering-criteria driven optimization approach is followed for the selection of the proposed KDamper-based configuration parameters. The excitation input is generated according to section 7.2.3 of this Chapter. The free design variables of the devices implemented in between the nacelle and the wind turbine tower are presented, and proper limitations and constraints are imposed on the free design variables and the system main dynamic responses, respectively. The NS element is realistically designed according to the Proposed Configuration II of Chapter 3. The effectiveness of the proposed devices is evaluated by comparing its performance to a controlled system with a conventional TMD, and an alternative approach proposed in this Chapter, namely the nacelle-isolation concept presented in section 7.2.1 of this Chapter.

7.3.1 Free Design Variables

The Configurations of KDamper, extended KDamper (EKD), and EKD equipped with inerter are presented in section 2.3 of Chapter 2. The following positions concerning the KDamper concept are presented below:

$$\mu_D = m_D / m_{top} \tag{7.8.a}$$

$$k_D = k_{NS} + k_{PS} \tag{7.8.b}$$

$$\omega_D = 2\pi f_D = \sqrt{k_D / m_D} = \sqrt{\frac{k_{NS} + k_{PS}}{m_D}} \tag{7.8.c}$$

$$k_0 = k_R + \frac{k_{NS} k_{PS}}{k_{NS} + k_{PS}} \tag{7.8.d}$$

$$\omega_0 = 2\pi f_0 = \sqrt{k_0 / \left(m_D + m_{top}\right)} = \sqrt{\left(k_R + \frac{k_{NS} k_{PS}}{k_{NS} + k_{PS}}\right) / \left(m_D + m_{top}\right)} \tag{7.8.e}$$

$$\zeta_{PS} = c_{PS} / (2 m_D \omega_D) = c_{PS} / (2\sqrt{k_D m_D}) \tag{7.8.f}$$

where μ_D is the mass ratio of the KDamper additional mass. Based on the sensitivity analyses performed in section 5.2.1.2, the damping coefficient placed in parallel to the positive stiffness element k_{PS}, namely c_{PS}, does not significantly affects the dynamic performance of the extended

KDamper designs, EKD and EKDI, and therefore is not considered in this study. The positions concerning the extended KDamper designs, therefore are:

$$\mu_D = m_D / m_{top} \tag{7.9.a}$$

$$k_D = k_{NS} + k_{PS} \tag{7.9.b}$$

$$\omega_D = 2\pi f_D = \sqrt{k_D / m_D} = \sqrt{\frac{k_{NS} + k_{PS}}{m_D}} \tag{7.9.c}$$

$$k_0 = k_R + \frac{k_{NS} k_{PS}}{k_{NS} + k_{PS}} \tag{7.9.d}$$

$$\omega_0 = 2\pi f_0 = \sqrt{k_0 / \left(m_D + m_{top}\right)} = \sqrt{\left(k_R + \frac{k_{NS} k_{PS}}{k_{NS} + k_{PS}}\right) / \left(m_D + m_{top}\right)} \tag{7.9.e}$$

$$\zeta_{NS} = c_{NS} / (2 m_D \omega_D) = c_{NS} / (2\sqrt{k_D m_D}) \tag{7.9.f}$$

$$\mu_b = m_b / m_{top} \tag{7.9.g}$$

where μ_b is the inertance mass ratio. In order for the proposed configuration to be realistic, the design of the KDamper-based designs foresees variation in all the stiffness elements, as presented in section 5.2.1 of Chapter 5, to ensure that the system remain statically and dynamically stable:

$$(1-\varepsilon_R)k_R + \frac{(1-\varepsilon_{PS})k_{PS}(1+\varepsilon_{NS})k_{NS}}{(1-\varepsilon_{PS})k_{PS} + (1+\varepsilon_{NS})k_{NS}} = 0 \tag{7.10}$$

As a result, the stiffness elements k_{PS} and k_R, result from Equations (7.8.e, 7.9.e, 7.10) as a function of f_0, and k_{NS}. Therefore, assuming that the m_D, and the values of the stability factors ε_{NS}, ε_{PS}, and ε_R are supposed known, the free design variables sought in the optimization are:

1. the nominal frequency f_0;
2. the value of the negative stiffness (NS) element k_{NS};
3. the value of the damping coefficient c_{NS};
4. the value of the inerter b;

For the optimization process, the Harmony Search (HS) optimization algorithm is used, presented thoroughly in section 3.3.3 of Chapter 3.

7.3.2 Statement of the Optimization Problem

The purpose of the proposed vibration absorption configurations, based on the KDamper concept (KDamper, EKD and EKDI) is to enhance the dynamic performance of wind turbine towers, by increasing the effective damping, and thus mitigate their dynamic responses. For the design to be realistic and efficient, at the same time, proper engineering criteria constraints and limitation must be applied in the system dynamic responses and free design variables, respectively. In particular:

i. The top displacement of the WT tower u_{TOP} is set as the objective function.
ii. A geometric limitation is imposed, regarding the relative displacement between the additional oscillating mass of the KDamper designs (m_D) and the top of the WT tower, $u_{D,REL}=u_D - u_{TOP}$. The upper limit of $u_{D,REL}$ is set equal to 1.5 *m*, lower than half of the top diameter of the steel tower (3.84/2=1.92 *m*).
iii. Another geometrical limitation is the nacelle's relative displacement with respect to the top of the wind turbine tower, $u_{NAC,\,REL}=u_{NAC} - u_{TOP}$. In order to ensure the effective operation of the wind turbine, an upper limit of 0.5 *m* is placed in the $u_{NAC,\,REL.}$
iv. The additional mass of the KDamper-based designs should be within reasonable ranges, since large masses constitute a major limitation, and are highly undesirable at the top of the wind turbine. For this reason, various sets of optimized EKDI parameters are selected for different values of the mass ratio μ_D, in the range [0.1 0.5] *%*, more than one order of magnitude smaller compared to the TMD concept.
v. The nominal frequency f_0 varies in the range *[0.1 2.0]* (*Hz*).
vi. The upper limit of the inertance mass ratio μ_b is set equal to 0.5.
vii. The damping coefficients maximum value c_{PS} for the KDamper, and c_{NS} for the extended KDamper designs, is set equal to *1000 kNs/m*, which based on the work of KDamper is a realistic value for a superstructure mass 403.22 *tn*, which in this case is the concentrated mass at the top, m_{top}.
viii. The NS element is realized with the Proposed Configuration II of Chapter 3. The maximum (absolute) value is equal to *-50 kN/m* per *tn* of structure mass, 50% lower as compared to the study of (Antoniadis et al., 2018);

Finally, the limits of the free design variables are: a) the nominal frequency f_0 (*Hz*) [*0.1 2.0*], b) the negative stiffness element k_{NS} (*kN/m*) [*-20000 -1*], c) the damping coefficient c_{NS} and c_{PS} (*kNs/m*) [*1 1000*], and the inertance mass ratio μ_b [0 0.5].

7.3.3 Comparison Approaches

The considered comparison approaches selected to verify the effectiveness of the KDamper-based design concepts are the conventional TMD and the nacelle-isolation concept, presented thoroughly in section 7.2.1. The TMD system, consists of 3 elements, an additional mass, m_D, a positive stiffness e lement, k_D, and a linear damper, c_D. The following positions concerning the TMD design are introduced, considering implementation at the top of the WT tower or inside the nacelle, as presented in Figure 7.1.b:

$$\mu_D = m_D / m_{top} \tag{7.11.a}$$

$$\omega_D = 2\pi f_D = \sqrt{k_D / m_D} \tag{7.11.b}$$

$$\zeta_D = c_D / \left(2\omega_D m_D\right) = c_D / \left(2\sqrt{k_D m_D}\right) \tag{7.11.c}$$

where μ_D is the mass ratio of the additional mass of the TMD. The WT tower is a MDoF structural system, therefore the TMD design is not straightforward. The TMD tuning frequency is usually selected to be equal to the fundamental frequency, f_1, of the primary structure. In order to verify that this approach is indeed optimum for the implementation of the TMD to WT, the maximum top displacement over the TMD tuning frequency is illustrated in Figure 7.6, for various values of the TMD damping ratio, and the aerodynamic load presented previously. The mass ratio of TMD is selected for the considered analysis as 5%.

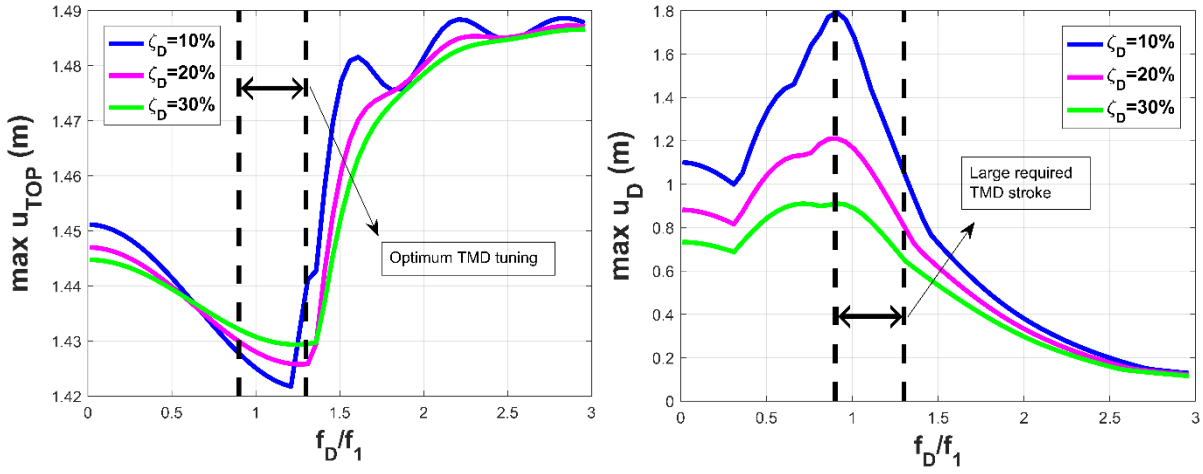

(a) (b)

Figure 7.6: *Optimum TMD tuning. (a) Maximum top tower displacement, and (b) TMD stroke, over the TMD nominal frequency ratio f_D/f_1, for various values of ζ_D.*

The optimum value of the TMD frequency is indeed near the fundamental frequency of the uncontrolled wind turbine tower, and more specifically in the range [0.9 1.3]f_1. The optimum value observed from Figure 7.6.a of the f_D is 1.25 f_1, and this value is adopted in this study for the optimum tuning of the TMD. It is observed from Figure 7.6.a that the damping ratio ζ_D of the TMD does not significantly affects the top tower displacement of the controlled system. However, from Figure 7.6.b, it is clear that the TMD stroke is directly affected by the ζ_D.

In order to optimally select the TMD damping ratio, ζ_D, the maximum top tower displacements and the TMD stroke are plotted in Figure 7.8, over the frequency ratio ζ_D, for various values of the TMD mass ratio μ_D. In this case, as stated previously, the TMD tuning frequency is selected to be equal to 1.25 f_1, and is equal to 0.396 *Hz*. It is observed that in the range of the TMD damping ratio [5 15] %, the maximum tower displacements are minimized. However, for greater values of ζ_D over 15%, the top displacement is not much affected. At the same time, from Figure 7.8.b it is observed that as ζ_D increased, the TMD stroke decreases, as expected. Therefore, the TMD damping ratio is selected equal to 30%, to mitigate the response of the wind turbine tower, and at the same time retain the TMD stroke as small as possible. This value of the damping ratio (ζ_D=30%) is usually high for a TMD with a large mass ratio up to μ_D=5%, but for the purpose of the comparison it can be adopted, as we are not interested in realistically designing the TMD, but to have a comparison basis.

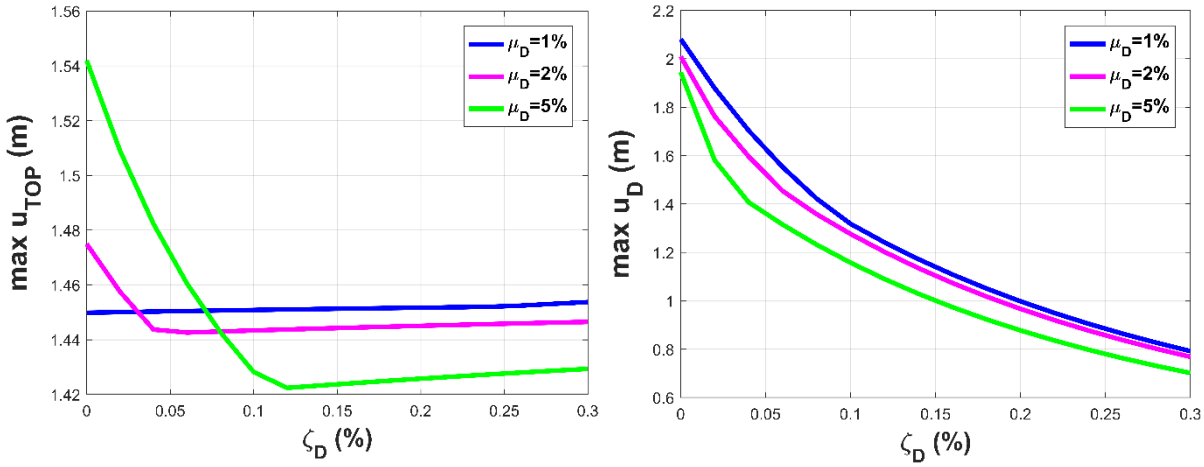

(a) (b)

Figure 7.7: *Selection of TMD damping ratio. (a) Maximum top tower displacement, and (b) TMD stroke, over the TMD damping ratio ζ_D, for various values of the TMD mass ratio μ_D.*

Figures 7.8.a, b present the effect of the mass ratio of the TMD, μ_D, to the system main dynamic responses, i.e. the top tower displacement, and the TMD stroke. In addition, the effect of the implementation of the TMD to the effective damping of the WT tower is examined. In order to calculate the exact value of the effective damping ratio ζ_{eff}, the system is subjected to a free vibration with initial conditions, that are according to the first modal eigenform of the uncontrolled WT tower. The initial condition of the TMD's DoF is selected to be equal to the one at the top tower. The value of ζ_{eff} is calculated according to the logarithmic rule:

$$\ln\left[\frac{X_N(t)}{X_N(t+T)}\right]=\frac{2\pi\zeta_{eff}}{\sqrt{1-\zeta_{eff}^2}} \tag{7.12}$$

where T is the time between two consecutive peaks of the dynamic response, and X_N is the top tower displacement. Figure 7.8.c presents the effect of μ_D to the effective damping ratio ζ_{eff}.

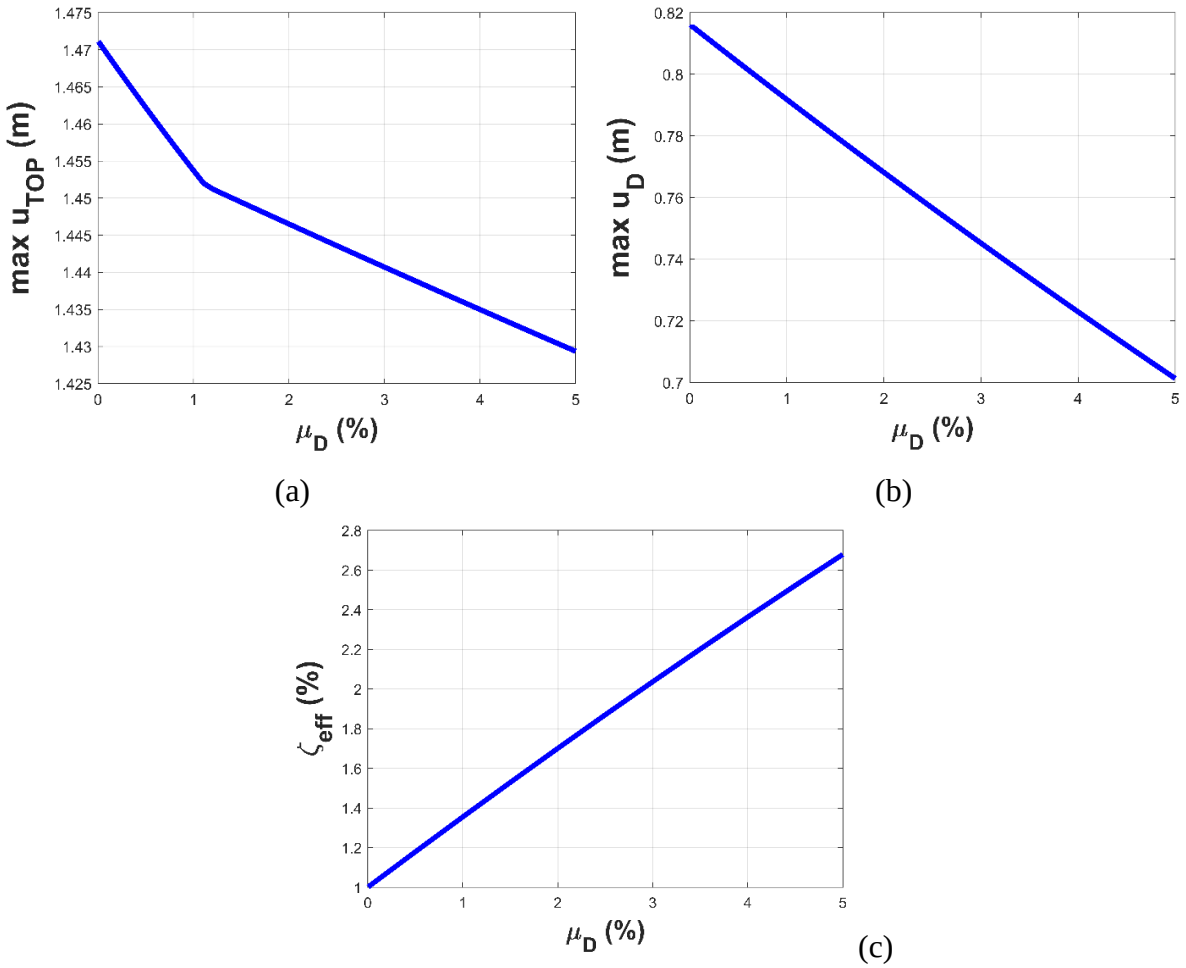

Figure 7.8: *Effect of the TMD mass ratio μ_D to: (a) the top tower displacement, (b) the TMD stroke, and (c) the effective damping of the controlled system.*

The increase of the additional mass ratio, μ_D, greatly affect the top tower dynamic response, as expected. It is observed that as the μ_D the effect to the top displacement decreases. Furthermore, the mass ratio affects linearly the improvement of the TMD stroke, and the increase of the effective damping of the controlled system.

Regarding the nacelle-isolation concept, the design parameters are the positive stiffness element k_D, and the artificial damper c_D. Based on the geometrical limitation presented for the KDamper-based designs, that the nacelle relative to the top of the tower displacement to be lower than 0.5 *m*, in order to have an equal comparison basis, the same constraint applies for the nacelle isolation concept. Furthermore, the maximum value of the c_D is set to be equal to 1000 *kNs/m*, as in the KDamper-based designs. Parametric analyses are conducted and plotted in Figure 7.9, in order to select the optimum system parameters, reported in Equations (7.13).

$$\omega_D = 2\pi f_D = \sqrt{k_D / m_{tot}} \tag{7.13.a}$$

$$\zeta_D = c_D / \left(2\omega_D m_D\right) = c_D / \left(2\sqrt{k_D m_{tot}}\right) \tag{7.13.b}$$

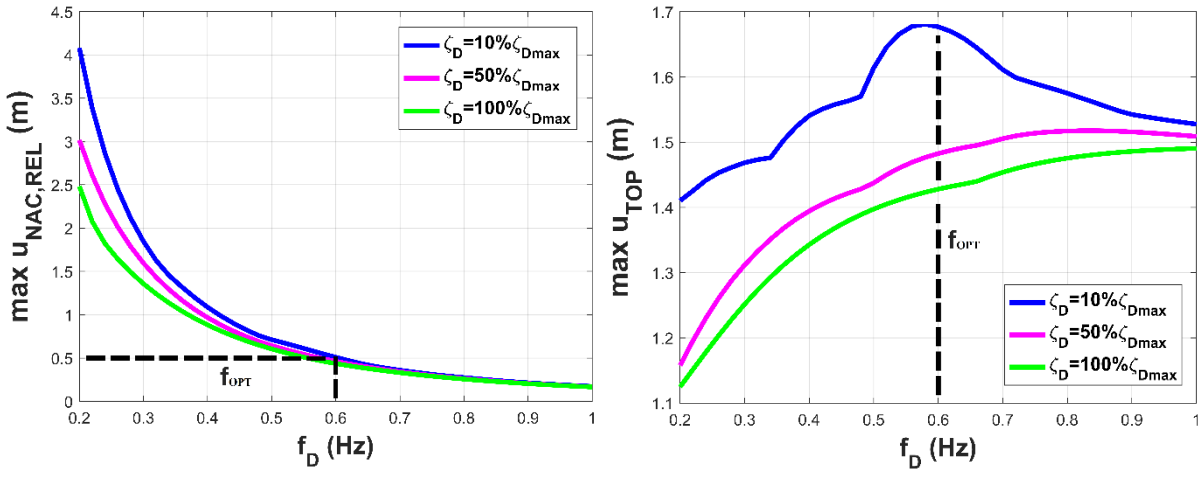

(a) (b)

Figure 7.9: *Design of the nacelle-isolation concept. (a) Selection of the tuning frequency, and (b) selection of the system damping ratio.*

In Figure 7.9.a, the nacelle relative to the top tower displacement, $u_{NAC,\,REL}$ is plotted over the tuning frequency f_D. It is observed that the tuning frequency of the nacelle-isolation concept is around 0.6 *Hz*, applying the constraint that the upper limit of the $u_{NAC,\,REL}$ is set to be equal to 0.5 *m*. The damping ratio ζ_D does not affect the $u_{NAC,\,REL}$, as observed in Figure 7.9.a, but significantly affects the top tower displacement, which is the minimization goal of all the proposed vibration control strategies. For this reason, the damping ratio is selected to be equal

to the upper limit ($c_{D,max}$=1000 *kNs/m*). The optimal system parameters of the nacelle-isolation concept therefore are f_D=0.556 *Hz* (limit case where $u_{NAC,\,REL}$=0.5 *m*), and ζ_D=35.5 %.

7.4 Numerical Example 1 – *NREL 5-MW Wind Turbine Dynamic Performance*

In this section, the KDamper-based designs are implemented for vibration control in the considered WT. The optimal system parameters are selected following the optimization procedure described previously in section 7.3.2 of this Chapter. The parameters of the KDamper, EKD, and EKDI system are presented in Tables 7.4-7.6, respectively.

Table 7.4: *KDamper components.*

μ_D (%)	f_0 (*Hz*)	k_{NS} (*kN/m*)	c_{PS} (*kNs/m*)	k_{PS} (*kN/m*)	k_R (*kN/m*)
0.1	0.547	-3558.16	993.13	6714.58	12343.34
0.2	0.557	-3492.81	966.73	6472.92	12538.02
0.3	0.547	-3674.95	931.00	7006.28	12514.36
0.4	0.550	-3371.66	831.60	6227.71	12181.48
0.5	0.548	-3504.47	989.40	6564.08	12326.82

Table 7.5: *Extended KDamper (EKD) components.*

μ_D (%)	f_0 (*Hz*)	k_{NS} (*kN/m*)	c_{NS} (*kNs/m*)	k_{PS} (*kN/m*)	k_R (*kN/m*)
0.1	0.541	-9501.00	986.08	32385.78	18103.61
0.2	0.532	-9335.64	968.12	32313.48	17638.61
0.3	0.532	-8822.59	996.64	28789.43	17240.72
0.4	0.532	-8758.40	963.99	28341.94	17201.80
0.5	0.523	-8668.35	993.72	28732.58	16783.15

Table 7.6: *Extended KDamper equipped with inerter (EKDI) components.*

μ_D (%)	f_0 (*Hz*)	k_{NS} (*kN/m*)	c_{NS} (*kNs/m*)	μ_b (%)	k_{PS} (*kN/m*)	k_R (*kN/m*)
0.1	0.551	-12543.61	997.34	0.498	58079.07	20829.40
0.2	0.545	-10395.09	986.69	0.496	38285.04	19015.52
0.3	0.544	-10380.34	960.28	0.497	38435.78	18938.34
0.4	0.538	-8995.40	939.73	0.493	29242.48	17618.43
0.5	0.540	-9086.47	996.11	0.497	29604.58	17772.91

The WT tower dynamic responses and effective damping are illustrated in Figure 7.10, over the KDamper-based design additional mass ratio, considering the optimized KDamper, EKD and EKDI vibration control configurations.

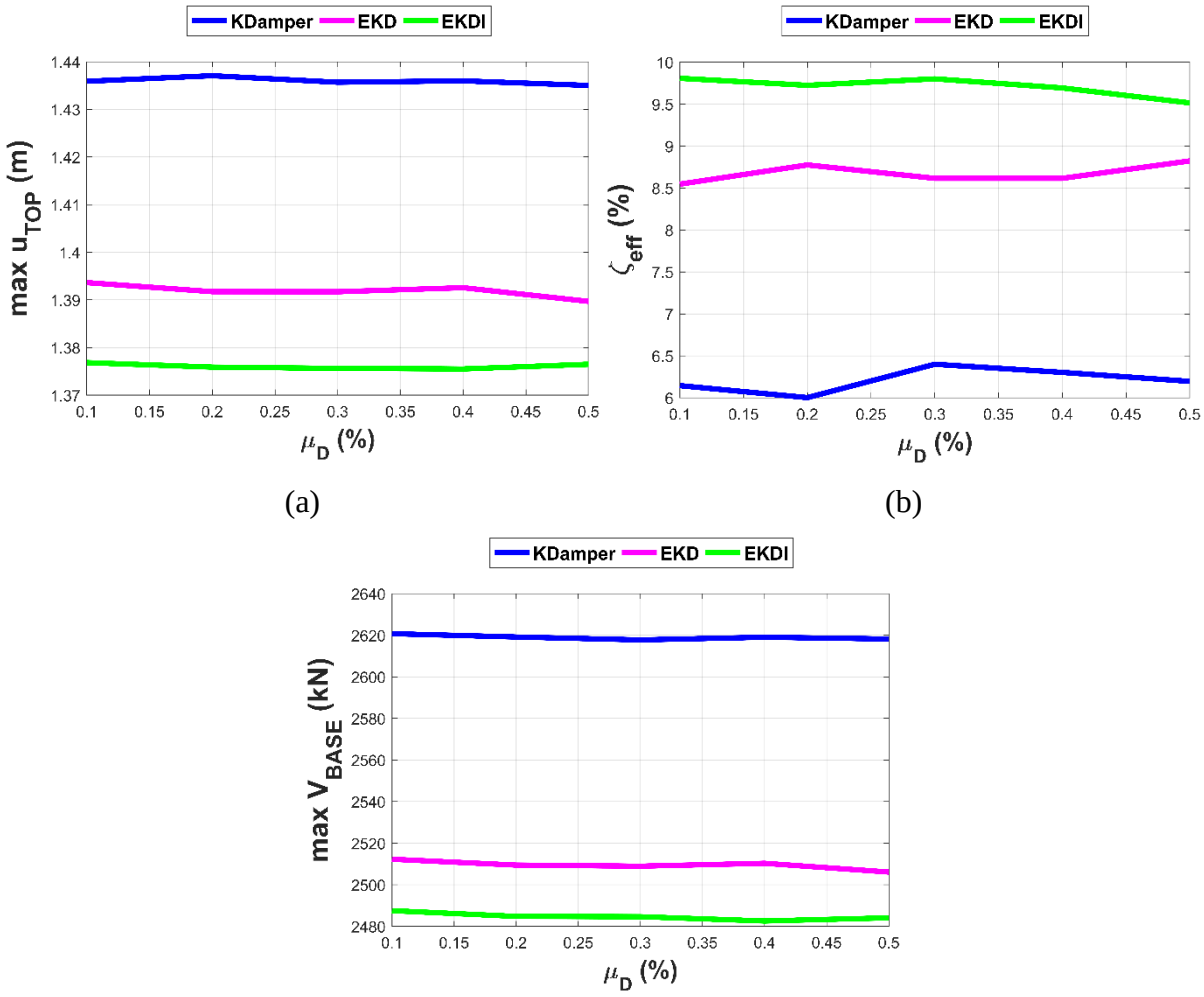

Figure 7.10: *Optimization results considering the KDamper-based designs, i.e. KDamper, EKD, and EKDI. (a) Top WT tower displacement, (b) new (effective) damping ratio of the controlled tower, and (c) base shear.*

In addition, the dynamic behavior of the nacelle is of great importance to the performance of the WT, and is greatly influenced by the nacelle's angle of deflection, angular velocity, and relative (to the base) velocity. The aforementioned response variables of the nacelle, of the controlled system with KDamper, EKD, and EKDI are illustrated in Figure 7.11, over the additional mass of the respective system. Finally, the relative displacement of the additional oscillating mass, m_D, and the NS element stroke of all the KDamper-based designs are plotted in Figure 7.12, over the additional mass ratio, μ_D.

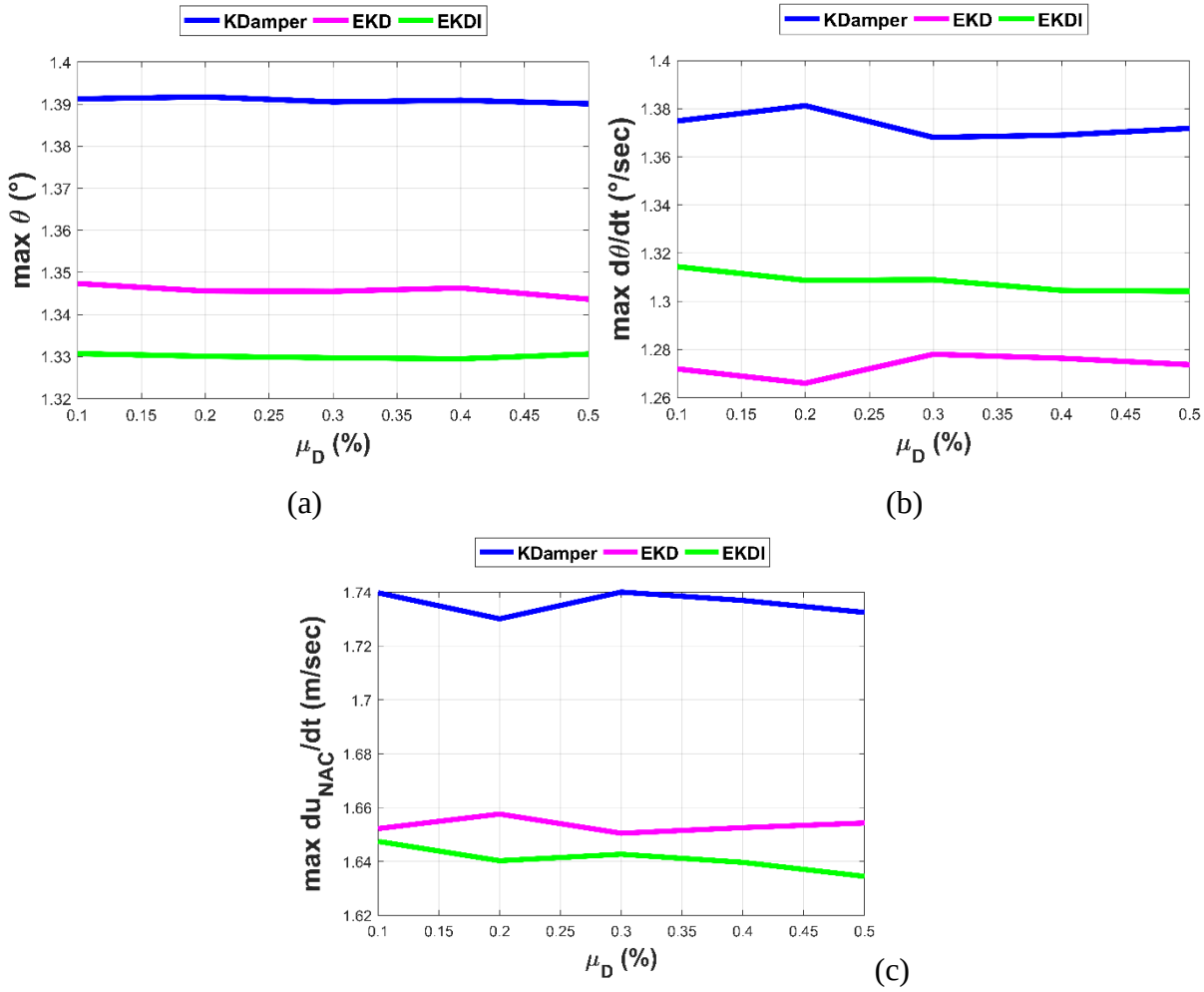

Figure 7.11: *Optimization results considering the KDamper-based designs, i.e. KDamper, EKD, and EKDI. Nacelle's (a)* angle of deflection, *(b)* angular velocity, *and (c)* relative (to the base) velocity.

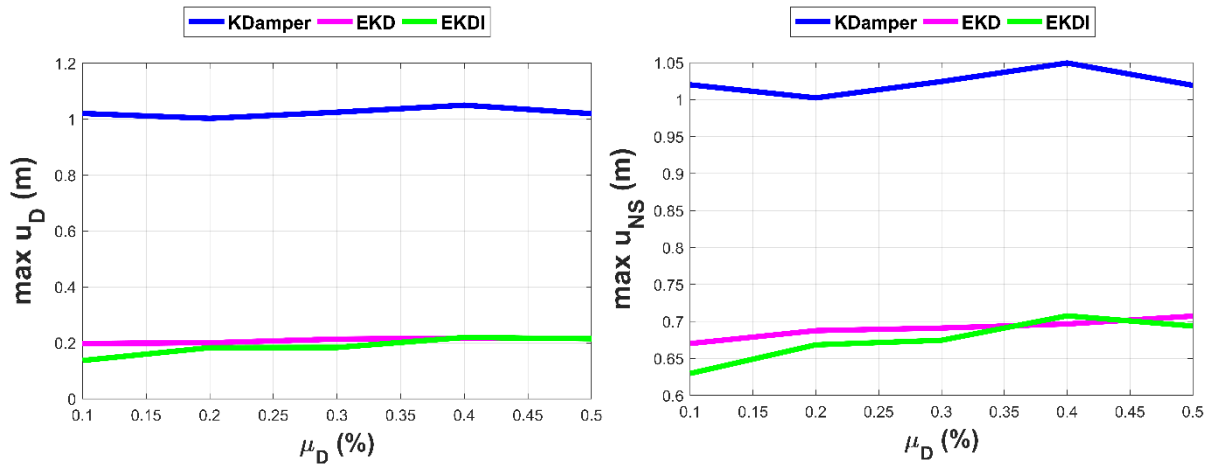

Figure 7.12: *Optimization results considering the KDamper-based designs, i.e. KDamper, EKD, and EKDI. (a) Device relative displacement, and (b) NS element stroke.*

In order to assess the effectiveness of the proposed absorbers, their performance is compared to a conventional TMD and the nacelle-isolation concept, presented in section 7.2.1, and optimized for the specific implementation in section 7.3. More specifically, the TMD system has a mass ratio of 5%, its nominal frequency is tuned to $1.25f_1$, where f_1 is the fundamental frequency of the primary WT, and its damping ratio is selected as 30%. The nacelle isolation concept is tuned to f_D=0.556 *Hz*, and the value of its artificial coefficients is equal to 1000 *kNs/m* (upper limit of the KDamper designs). The maximum values of the dynamic responses and the effective damping of all the considered vibration control systems are collected in Table 7.7. Regarding the KDamper-based designs, the results concerning the optimized sets of parameters with an additional mass ratio of 0.1% are presented.

Table 7.7: *Maximum values of the WT tower's effective damping ratio, dynamic responses of the WT tower and the respective control system, and the nacelle's response variables.*

	Control System					
	Initial WT	TMD (5%)	Nacelle-isolation	KDamper (0.1%)	EKD (0.1 %)	EKDI (0.1%)
u_{TOP} (m)	1.471	1.429	1.4167	1.436	1.394	1.377
ζ_{eff} $(\%)$	1	2.68	7.82	6.14	8.55	9.81
V_{BASE} (kN)	2677.6	2308.6	2547.1	2620.7	2512.3	2487.5
θ $(^\circ)$	1.424	1.391	1.368	1.391	1.347	1.331
$d\theta/dt$ $(^\circ/sec)$	1.484	1.451	1.238	1.375	1.272	1.314
du_{NAC}/dt (m/sec)	1.448	1.406	1.703	1.740	1.652	1.647
u_D (m)	-	0.701	0.500	1.020	0.198	0.136
u_{NS} (m)	-	-	-	1.020	0.670	0.629

The KDamper-based designs manage to greatly improve the dynamic behavior of the WT tower, more that the TMD and the nacelle-isolation concepts. The effective damping ratio of the WT tower increases up to 10% with the EKDI system with only 0.1% additional mass. The nacelle's dynamic response variables are also improved, with the exception of the nacelle's relative velocity, where a slight increase is observed. In addition, the extended versions of KDamper, i.e. EKD and EKDI, greatly reduce the NS element stroke and the oscillating mass of the proposed devices making the configuration design more realistic. The dynamic responses of the WT tower and the nacelle's response variables, considering the TMD, the nacelle-isolation, and the EKDI are illustrated in Figures 7.13 and 7.14, respectively.

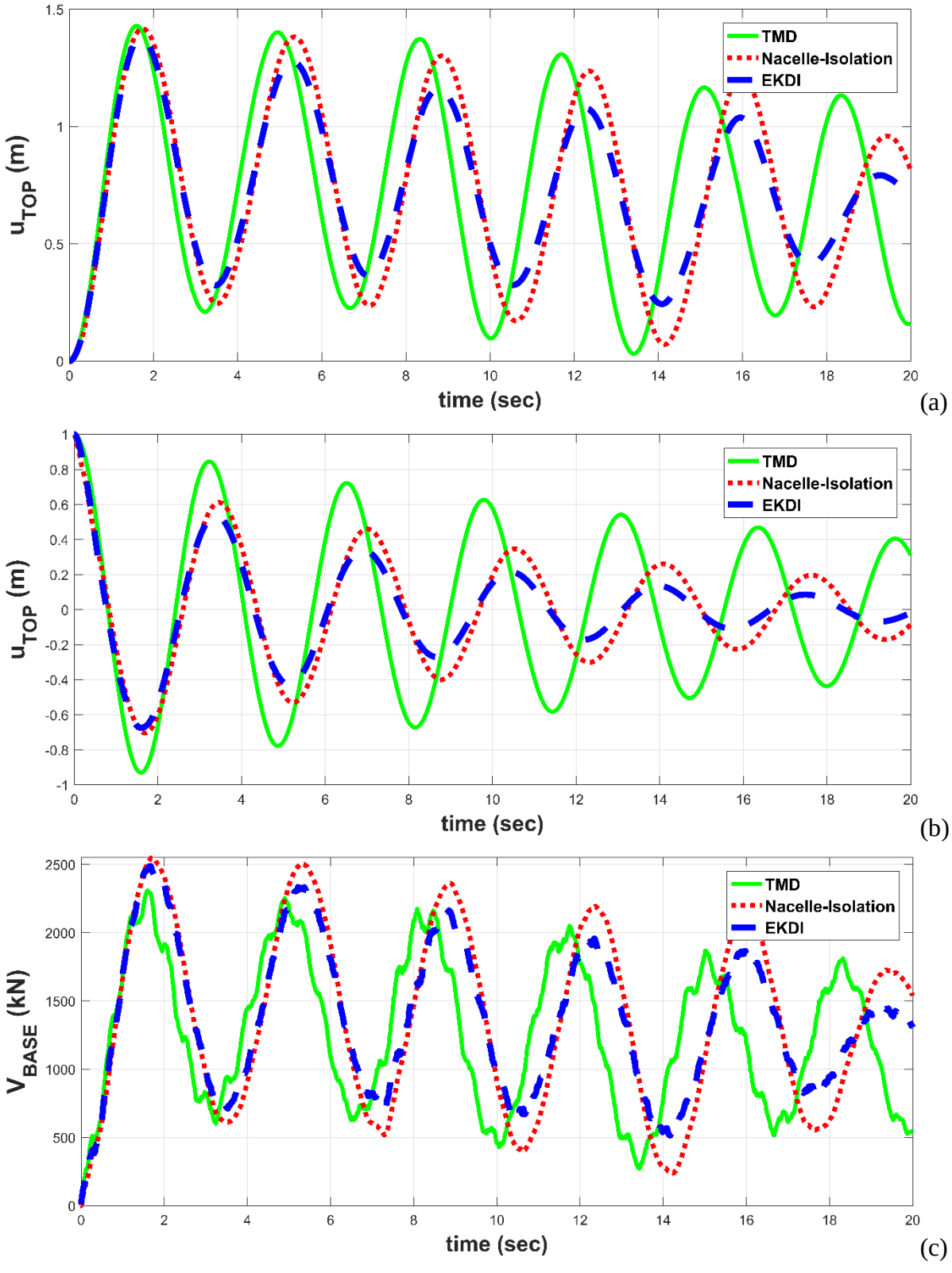

Figure 7.13: *Dynamic responses of the controlled WT: (a) top tower displacement due to the aerodynamic load, (b) top tower displacement considering a free vibration with initial conditions, and (c) base shear due to the aerodynamic load.*

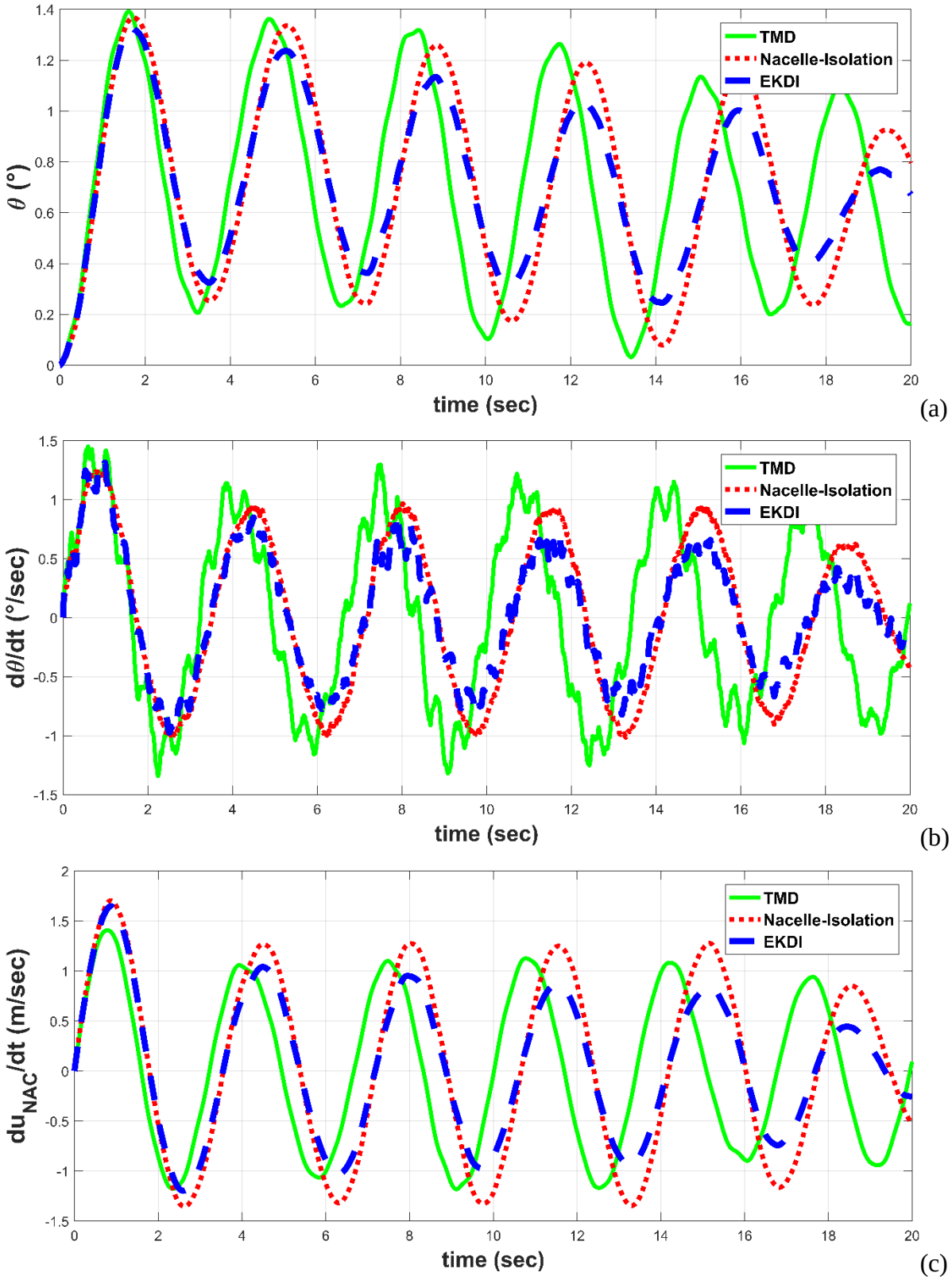

Figure 7.14: *Nacelle's response variables of the controlled WT: (a) angle of deflection, (b) angular velocity, and (c) relative (to the base) velocity, due to the aerodynamic load.*

Finally, the time history of the NS element stroke, and the relative displacement of the additional oscillating mass are illustrated in Figure 7.15 for all the KDamper-based designs.

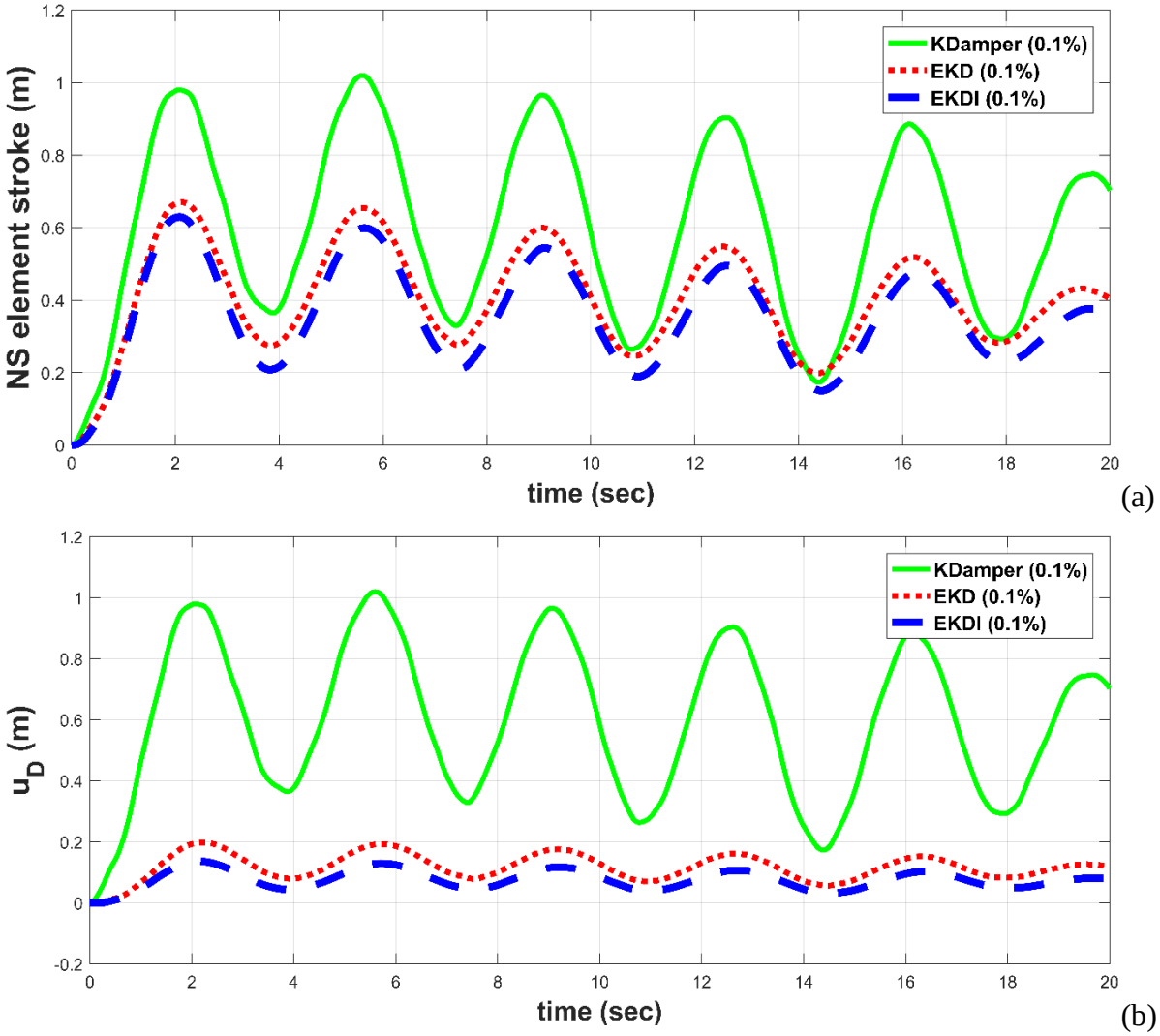

Figure 7.15: *KDamper-based designs responses: (a) NS element stroke, and (b) relative displacement of the oscillating mass with the top of the WT tower, due to the aerodynamic load.*

7.5 Concluding Remarks

In this Chapter, three dynamic vibration absorber options are examined for improving the WT tower dynamic behavior and increasing the effective damping, i.e. the conventional TMD, the nacelle-isolation concept, and three KDamper-based designs. A wind turbine of 5MW supported by a steel tower of 120 m was analyzed under a horizontal aerodynamic load due to

the wind. The vibration mitigation approaches are presented, along with the dynamic model of the WT tower. The developed model is an assemblage of prismatic beam elements, the validity of which is verified based on a comparison with a commercial software package on FEM. The aerodynamic load is taken into account by generating artificial basic wind velocities applying the corresponding regulations of EC1, Part1,4. The TMD and the nacelle-isolation concepts, are optimally design for the specific implementation for the protection of the WT tower. An engineering-criteria optimization procedure is followed for the design of the KDamper-based configurations. The NS element is realistically designed according to the Proposed Configuration II of Chapter 3. Based on a comparison with a conventional TMD, and the proposed nacelle-isolation concept, the KDamper designs manage to significantly increase the effective damping, and thus mitigate the WT dynamic responses, with small additional masses and a realistically designed configuration. Finally, the following conclusive comments can be made:

i. The dynamic model of the WT tower develop here is serviceable due to the fact that it can incorporate easily each of the considered vibration absorption concepts, and the validity of the proposed formulation is verified as compared with a commercial software package based on FEM.
ii. The increase of the effective damping of the WT tower is much greater with the implementation of the KDamper-based designs (6.14%, 8.55%, 9.81%), compared to that with a TMD (2.68%) with an additional mass of 5%, and the nacelle-isolation concept (7.82%).
iii. The KDamper-based configurations are much more effective than the conventional TMD approach, employing a small additional mass of only 0.1%, 50 times lower compared to the TMD's.
iv. Concerning the dynamic behavior of the WT tower the KDamper-based concepts provided the best results followed by the TMD concept and the nacelle-isolation concept. More specifically, the tower's top displacement is reduced 2.38%, 5.23% and 6.39% with the KDamper-based concepts (0.1% mass ratio), 2.86% with the TMD concept (5% mass ratio) and 3.69% with the nacelle-isolation concept and the shear force of the tower is reduced 2.12%, 6.17% and 7.10% with the KDamper-based concepts, 13.78% with the TMD concept and 4.87% with the nacelle-isolation concept.
v. The use of a TMD has a small influence on the nacelle's response variables. The KDamper-based concepts, and the nacelle-isolation concept improve all the response

variables of the nacelle, except for the maximum value of the nacelle's velocity which in the first peak of the dynamic response present a slight increase.

vi. The proposed extensions of KDamper manage to significantly decrease the NS element stroke, making the device's design more realistic.

vii. The addition of the inerter in the EKD configuration has a beneficial impact in the overall dynamic behavior of the WT.

According to the comments made above, the KDamper-based designs can provide a realistic alternative to the existing vibration absorption design options in WT towers, providing a great increase to the tower's damping as well as improving the dynamic performance both of the nacelle and the WT tower. The reliability and simplicity of the system are also advantages that render the device suitable for various technological implementations and competitive against other vibration absorption designs.

Chapter 8

Conclusions and Future Research

8.1 Concluding Remarks

In this doctoral dissertation, the mitigation of ambient vibrations in civil engineering structures employing advanced negative stiffness-based dynamic vibration absorbers is examined. The main issues investigated are the following:

- The optimal design of the proposed configurations, with respect to the limitations and constraints imposed by the considered application.
- Horizontal seismic protection of multi-story building structures.
- Vertical seismic protection of structural systems.
- The extension of wind turbine towers feasibility by increasing the effective damping of the wind turbine tower.

For the performance of the proposed dynamic vibration absorbers to be effective, realistic configurations have been formulated, and the provisions of the design codes are taken into consideration. Several case studies have been examined, where the performance of the proposed control systems is assessed, and compared with various vibration isolation approaches widely used in the literature. The main conclusions that can be drawn from this doctoral dissertation are:

i. The systematic design procedure of the KDamper concept leads to a performance that can inherently offer far better isolation and damping properties than the Tuned Mass Damper (TMD).

ii. The isolation and damping properties of the KDamper essentially result from the stiffness properties of the system, and thus further technological advantages can

emerge over the TMD, in terms of weight, complexity and reliability, without the need for compromises in the overall stiffness as in the case of the QZS configurations.

iii. The excitation input effectively follows the provisions of the design codes.

iv. The proposed spectra driven approaches for the selection of the KDamper nominal frequency are accurate, as verified in the time domain.

v. Indicative designs of KDamper, prove that the additional mass, artificial damper, and the stiffness elements are within reasonable technological capabilities.

vi. The results of the non-linear problem are in a very good agreement to the initial linear one, regarding the proposed configuration for the realization of the one-dimensional negative stiffness element.

vii. The KDamper can be effectively implemented in the bases of structures as a supplement to the conventional base isolation approaches, greatly reducing the base displacement demand.

viii. An alternative implementation of KDamper as a stiff base absorber can greatly enhance the superstructure dynamic behavior, retaining the base displacements in the order of a few centimeters.

ix. The performance of KDamper assessed with real earthquake records, confirms the effectiveness of KDamper implemented in SDoF, as well as, multi-story building structures.

x. An extended version of KDamper (EKD) is proposed, that foresees variation in all stiffness elements and employs small additional masses, as compared to KDamper.

xi. The design of the EKD is based on engineering criteria, and renders its implementation feasible. As compared to the KDamper, the effectiveness of the controlled system in enhanced, while the stiffness elements at 50% lower, and the negative stiffness element stroke is significantly reduced.

xii. Based on the performed sensitivity analysis, where the EKD components varied from their optimal values, the EKD in not vulnerable to detuning.

xiii. The EKD is effectively implemented as a base absorber of multi-story building structures, significantly improving their dynamic behavior. The superstructure dynamic responses are improved at comparable levels compared to a base isolated structure, while at the same time the base displacements are dramatically reduced.

xiv. The small base displacement of the EKD render the implementation of the proposed device feasible using conventional structural elements, without the need of special type of bearings.

xv. An alternative spectra driven approach for the realistic design of the EKD as a stiff base absorber of multi-story building structures is effective in improving the superstructure dynamic behavior, retaining small base displacements.

xvi. Retrofitting options for the implementation of the EKD in existing multi-story building structures is possible. The structural accelerations and interstory drifts are reduced, without reducing the stiffness of the primary structure or introducing large additional masses.

xvii. The proposed configuration for the realization of the EKD's negative stiffness element manages to generate 'linear' two-dimensional negative stiffness.

xviii. An extension of KDamper equipped with an inerter in presented as a stiff seismic base absorber (SBA), designed based on engineering criteria.

xix. The SBA is implemented in multi-story building structures, greatly improving their dynamic behavior. The floor accelerations and interstory drifts are significantly reduced, and the base displacements are dramatically low, as compared to other base isolation approaches, as well as to the KDamper and the EKD implemented as base absorbers.

xx. Based on the performed sensitivity analysis, the SBA is not vulnerable to detuning.

xxi. The small base displacement of the SBA, renders the implementation of the proposed device feasible using conventional structural elements, without the need of special type of bearings. As a consequence, retrofitting is possible.

xxii. The proposed vertical seismic absorber (VSA), designed based on the extended versions of KDamper is realistically designed in the frequency domain based on engineering criteria.

xxiii. The VSA manages to greatly reduce the vertical peak accelerations and at the same time retains the static settlements in acceptable levels, overcoming the disadvantages of the existing vertical isolation approaches.

xxiv. The performance of the VSA is assessed with real earthquake records using displacement-dependent configuration for the realization of the negative stiffness element.

xxv. The detuning phenomena are observed via sensitivity analysis, and confirm that the VSA is not vulnerable to detuning.

xxvi. The proposed dynamic vibration absorbers based on KDamper are realistically designed for implementation in Wind Turbines (WT), employing small additional masses.

xxvii. The dynamic model of the WT tower developed here is serviceable due to the fact that it can incorporate easily proposed concepts, the validity of which is verified as compared with a commercial software package based on FEM.

xxviii. The effective damping of the WT tower is significantly increased, and its dynamic performance is greatly improved, as compared with other vibration absorption approaches for WT widely used in the literature.

8.2 Future Research

This doctoral dissertation consists a contribution to the vibration absorption in Civil Engineering structures. The following are research directions that will further improve the present work and will provide even more realistic configurations for the protection of Civil Engineering structures due to ambient vibrations.

i. The inherent nonlinear nature of the negative stiffness force can be exploited to offer further potential advantages of the KDamper-based designs, such as robustness, broadband response and energy sinks.

ii. The investigation of alternative realistic configurations for the realization of the negative stiffness element using conventional structural elements capable of providing the necessary elastic forces when considering applications in Civil Engineering structures.

iii. The simulation of the examined applications in FEM commercial software packages using realistic constitutive models regarding the superstructure and the positive stiffness elements of the proposed dynamic vibration absorbers. This is noted as in the present dissertation linear models are considered for the modeling of all the examined applications, with the exception of the geometric nonlinearity regarding the negative stiffness element.

iv. The execution of experiments in realistic scaled structural systems with the implementation of the proposed dynamic vibration absorbers for seismic protection, using simple configurations with pre-compressed springs for realizing the negative stiffness element.

v. The implementation of the proposed dynamic vibration absorbers as possible realistic retrofitting options for existing building structures, taking into account the beneficial role of the soil-structure interaction effects.

vi. The realistic design of a three-dimensional passive dynamic vibration absorber for seismic protection in existing, as well as in new building structures.

vii. Increase the life-cycle of existing, as well as new wind turbines to avoid replacement costs in case of failure, and reduction of the tower dimensions, reducing the construction costs.

viii. Investigation of energy harvesting systems in combination with vibration control of wind turbine towers, due to wind and wave loading.

Appendix **A1**

KDamper Coefficients and Optimization Process

A1.1 Derivation of KDamper Stiffness Coefficients – Equations (3.4.a) – (3.4.c)

In this Appendix, the concise derivation of the KDamper stiffness coefficients, k_N, k_P, and k_R, presented in section 3.2 of Chapter 3, Equations (3.4.a-c) is presented. Precisely, the following steps are followed:

Starting from Equation (3.3.a):

$$\kappa = -\frac{k_N}{k_P + k_N} \Rightarrow k_N = -\kappa(k_P + k_N) \tag{A1.1}$$

$$\frac{k_N}{k} = -\kappa \frac{k_P + k_N}{k} \tag{A1.2}$$

From Equations (3.3.e, f) and considering that $k_D = k_P + k_N$, the following relations can be derived:

$$k_P + k_N = m_D \omega_D^2 \tag{A1.3.a}$$

$$k = m\omega_0^2 \tag{A1.3.b}$$

After substituting Equations (A1.3) to Equation (A1.2), the latter becomes:

$$\frac{k_N}{k} = -\kappa \frac{m_D \omega_D^2}{m\omega_0^2} \Rightarrow \frac{k_N}{k} = -\kappa \frac{m_D}{m} \left(\frac{\omega_D}{\omega_0} \right)^2 \tag{A1.4}$$

Taking into account Equations (3.3.b-c), Equation (A1.4) becomes:

$$\frac{k_N}{k} = -\kappa\mu\rho^2 \tag{A1.5}$$

namely, Equation (3.4.a).

Following the first two steps of the previously described procedure, Equation (A1.6) can be derived:

$$\frac{k_P + k_N}{k} = -\frac{1}{\kappa}\frac{k_N}{k} \Rightarrow \frac{k_P}{k} + \frac{k_N}{k} = -\frac{1}{\kappa}\frac{k_N}{k} \Rightarrow \frac{k_P}{k} = -\frac{1}{\kappa}\frac{k_N}{k} - \frac{k_N}{k} \tag{A1.6}$$

and after substituting Equation (A1.5), Equation (A1.6) becomes:

$$\frac{k_P}{k} = -\frac{1}{\kappa}\left(-\kappa\mu\rho^2\right) - \left(-\kappa\mu\rho^2\right) \Rightarrow \frac{k_P}{k} = \mu\rho^2 + \kappa\mu\rho^2 \tag{A1.7}$$

leading after manipulation to:

$$\frac{k_P}{k} = \left(1+\kappa\right)\mu\rho^2 \tag{A1.8}$$

namely, Equation (3.4.b).

Finally, combining Equations (2.23) and (3.3.a), the stiffness coefficient k_R is given by:

$$k_R = k + \kappa k_P \Rightarrow \frac{k_R}{k} = 1 + \kappa\frac{k_P}{k} \tag{A1.9}$$

which after substituting Equation (A1.8) to Equation (A1.9), the later becomes:

$$\frac{k_R}{k} = 1 + \kappa\left(1+\kappa\right)\mu\rho^2 \tag{A1.10}$$

namely, Equation (3.4.c).

A1.2 Optimization Coefficients *Ai, Bi, Ci, Di* Considering Optimal Displacement Response Under Base Acceleration Excitation

The coefficients *A*, *B*, *C*, and *D* presented in Equation (3.5) of section 3.2.1, Chapter 3 are obtained from the following relations:

$$A = A_2 q^2 + A_0 \tag{A1.11.a}$$

$$B = B_0 \rho q \tag{A1.11.b}$$

$$C = q^4 + C_2 q^2 + C_0 \tag{A1.11.c}$$

$$D = (D_2 q^2 + D_0)\rho q \tag{A1.11.d}$$

where A_i, B_i, C_i, and D_i are obtained from:

$$A_2 = A_{2\rho}\rho^2 + A_{20} \tag{A1.12.a}$$

$$A_0 = A_{0\rho}\rho^2 + A_{00} \tag{A1.12.b}$$

$$B_0 = B_{0\rho}\rho^2 + B_{00} \tag{A1.12.c}$$

$$C_2 = C_{2\rho}\rho^2 + C_{20} \tag{A1.12.d}$$

$$C_0 = C_{0\rho}\rho^2 + C_{00} \tag{A1.12.e}$$

$$D_2 = D_{2\rho}\rho^2 + D_{20} \tag{A1.12.f}$$

$$D_0 = D_{0\rho}\rho^2 + D_{00} \tag{A1.12.g}$$

$$A_\rho = (A_{0\rho}D_{2\rho} + A_{2\rho}D_{0\rho} + B_{0\rho}C_{2\rho})D_{20} - 2(A_{2\rho}D_{20} + A_{20}D_{2\rho} + B_{0\rho})D_{0\rho} \tag{A1.13.a}$$

$$B_{\rho A} = [(A_{0\rho}D_{20} + D_{2\rho}A_{00}) + (A_{2\rho}D_{00} + D_{0\rho}A_{20}) + (B_{0\rho}C_{20} + C_{2\rho}B_{00})]D_{20} \tag{A1.13.b}$$

$$B_{\rho B} = -2(A_{2\rho}D_{20} + A_{20}D_{2\rho} + B_{0\rho})D_{00} - 2(A_{20}D_{20} + B_{00})D_{0\rho} \tag{A1.13.c}$$

$$B_\rho = B_{\rho A} + B_{\rho B} \tag{A1.13.d}$$

$$C_\rho = (A_{00}D_{20} + A_{20}D_{00} + B_{00}C_{20})D_{20} - 2(A_{20}D_{20} + B_{00})D_{00} \tag{A1.13.e}$$

and the coefficients A_{ij}, B_{ij}, C_{ij}, and D_{ij} entering Equations (A1.12) and (A1.13) are defined in Table A1.1.

Table A1.1. *Coefficients in Equations (A1.12) and (A1.13).*

	A_{2i}	A_{0i}	B_{0i}	C_{2i}	C_{0i}	D_{2i}	D_{0i}
$i=\rho$	0	$1+(1+\kappa)\mu$	0	$-[1+(1+\kappa)^2\mu]$	0	0	$\kappa^2\mu$
$i=0$	-1	0	$1+\mu$	-1	1	$-(1+\mu)$	1

A1.3 Optimization Coefficients *Ai, Bi, Ci, Di* Considering Optimal Acceleration Response Under Base Acceleration Excitation

The coefficients *A*, *B*, *C*, and *D* presented in Equation (3.19) of section 3.2.2, Chapter 3 are obtained from the following relations:

$$A = A_2 q^2 + A_0 \tag{A1.14.a}$$

$$B = B_0 \rho q \tag{A1.14.b}$$

$$C = q^4 + C_2 q^2 + C_0 \tag{A1.14.c}$$

$$D = (D_2 q^2 + D_0)\rho q \tag{A1.14.d}$$

where A_i, B_i, C_i, and D_i are obtained from:

$$A_2 = A_{2\rho}\rho^2 + A_{20} \tag{A1.15.a}$$

$$A_0 = A_{0\rho}\rho^2 + A_{00} \tag{A1.15.b}$$

$$B_0 = B_{0\rho}\rho^2 + B_{00} \tag{A1.15.c}$$

$$C_2 = C_{2\rho}\rho^2 + C_{20} \tag{A1.15.d}$$

$$C_0 = C_{0\rho}\rho^2 + C_{00} \tag{A1.15.e}$$

$$D_2 = D_{2\rho}\rho^2 + D_{20} \tag{A1.15.f}$$

$$D_0 = D_{0\rho}\rho^2 + D_{00} \tag{A1.15.g}$$

$$A_\rho = (A_{0\rho}D_{2\rho} + A_{2\rho}D_{0\rho} + B_{0\rho}C_{2\rho})D_{20} - 2(A_{2\rho}D_{20} + A_{20}D_{2\rho} + B_{0\rho})D_{0\rho} \tag{A1.16.a}$$

$$B_{\rho A} = [(A_{0\rho}D_{20} + D_{2\rho}A_{00}) + (A_{2\rho}D_{00} + D_{0\rho}A_{20}) + (B_{0\rho}C_{20} + C_{2\rho}B_{00})]D_{20} \tag{A1.16.b}$$

$$B_{\rho B} = -2(A_{2\rho}D_{20} + A_{20}D_{2\rho} + B_{0\rho})D_{00} - 2(A_{20}D_{20} + B_{00})D_{0\rho} \tag{A1.16.c}$$

$$B_\rho = B_{\rho A} + B_{\rho B} \tag{A1.16.d}$$

$$C_\rho = (A_{00}D_{20} + A_{20}D_{00} + B_{00}C_{20})D_{20} - 2(A_{20}D_{20} + B_{00})D_{00} \quad \text{(A.16.e)}$$

and the coefficients A_{ij}, B_{ij}, C_{ij}, and D_{ij} entering Equations (A1.15) and (A1.16) are defined in Table A1.2.

Table A1.2. *Coefficients in Equations (A.15) and (A.16).*

	A_{2i}	A_{0i}	B_{0i}	C_{2i}	C_{0i}	D_{2i}	D_{0i}
$i=\rho$	$-\kappa(1+\kappa)\mu$	1	$\kappa^2\mu$	$-[1+(1+\kappa)^2\mu]$	1	0	$\kappa^2\mu$
$i=0$	-1	0	1	-1	0	$-(1+\mu)$	1

Appendix **A2**

Extension of KDamper – Based Designs to MDoF Structural Systems

A2.1 Introduction

In this Appendix, the KDamper-based configurations are extended for implementation to MDoF structural systems, and more specifically, multi-story building structures for horizontal seismic protection. Initially, the equations of motion of the uncontrolled building structures are presented, and subsequently, the employed vibration control system based on KDamper is introduced. A planar *n*-story structure is considered, and depicted in Figure A2.1, along with a typical ground floor plan of the structure.

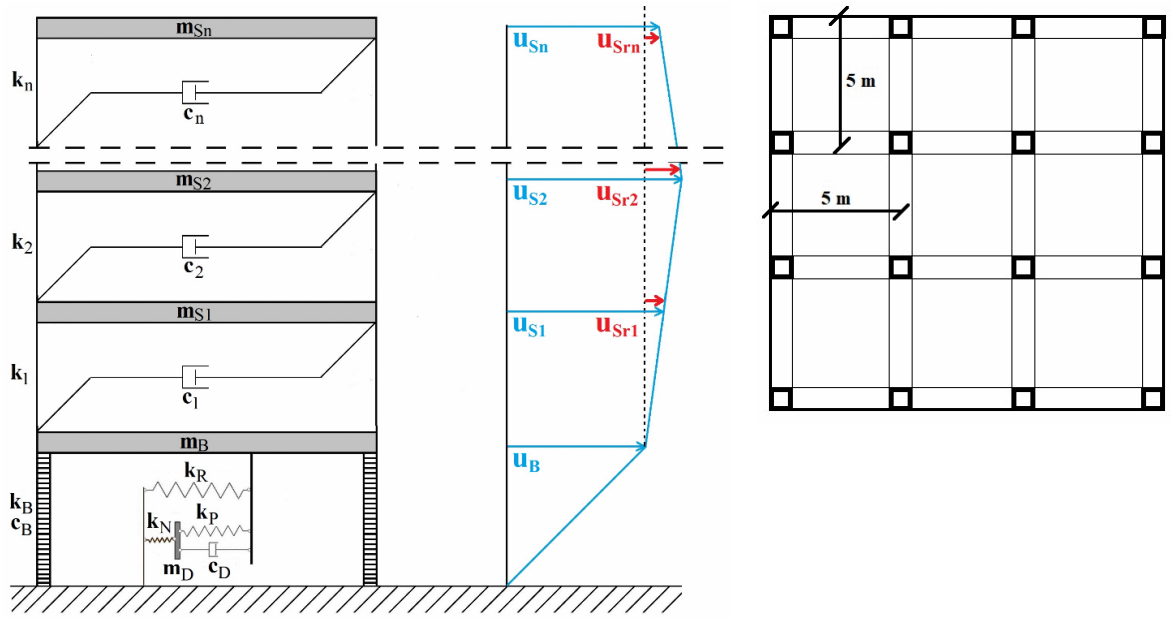

(a) (b)

Figure A3.1: *Examined n-story concrete building structure with the proposed absorption base system (KDAB), (a) sketch of the model and (b) typical ground floor plan of the structure.*

The assumptions made for the modeling of this structure are:

i. the total structure mass is concentrated at the floor levels;
ii. the slabs and grinders on the floors are rigid as compared to the columns;
iii. the columns are considered inextensible and weightless providing the lateral stiffness;
iv. the effect of soil-structure-interaction (SSI) is not taken into consideration;
v. the superstructure is considered to remain within the elastic limit during the analysis;

As a result, the superstructure has *n* dynamic DOFs, represented by the relative to the base displacements of the *n*-story masses m_{Sj} ($j=1,\ldots,n$), as presented in Figure 4.12.a,. The equation of motion, expressed in a matrix form are presented below:

$$[M][\ddot{u}(t)]+[C][\dot{u}(t)]+[K][u(t)]=-[\tau]a_G(t) \tag{A2.1}$$

The mass and stiffness matrices are of order $n\times n$, and are expressed as:

$$[M]=[M_S]_{n\times n}=\begin{bmatrix} m_1 & \cdots & 0 \\ \vdots & \ddots & \vdots \\ 0 & \cdots & m_n \end{bmatrix}_{n\times n} \tag{A2.2.a}$$

$$[K]=[K_S]_{n\times n}=\begin{bmatrix} k_1 & -k_1 & 0 & \cdots & 0 \\ -k_1 & k_1+k_2 & -k_2 & \cdots & 0 \\ 0 & -k_2 & k_2+k_3 & & \vdots \\ \vdots & \vdots & & \ddots & -k_{n-1} \\ 0 & 0 & \cdots & -k_{n-1} & k_{n-1}+k_n \end{bmatrix}_{n\times n} \tag{A2.2.b}$$

The damping coefficients of the superstructure are assumed to be mass and stiffness proportional (Rayleigh damping). The damping matrix is thus expressed as:

$$[C]=[C_S]_{n\times n}=[M_S]_{n\times n}[F]_{n\times n}\begin{bmatrix} 2\omega_1\xi_1 & \cdots & 0 \\ \vdots & \ddots & \vdots \\ 0 & \cdots & 2\omega_n\xi_n \end{bmatrix}_{n\times n}[F]^T_{n\times n}[M_S]^T_{n\times n} \tag{A2.3}$$

where $[F]$ is the eigenform matrix, ω_i is the ith eigenfrequency, and ξ_i is the damping ratio of the ith eigenform.

A2.2 KDamper – Based Configurations Implemented in the Bases of Multi – Story Building Structures

In this section, the KDamper-based designs are implemented as a seismic absorption layer of multi-story building structures. Therefore, a base floor is implemented, in which the proposed devices is intervened. As a result, the controlled structural system has two extra DoFs, one of the base's, and one that corresponds to the additional oscillating mass of the proposed absorber.

A2.2.1 KDamper Concept

The KDamper implemented in the bases on multi-story structures is presented in section 4.3.1.3 and 4.3.3.2-3 of Chapter 4. The equations of motion, Equation (A2.1), still hold, but now involve matrices with dimensions $(n+2) \times (n+2)$, which are defined as:

$$[M]_{(n+2)\times(n+2)} = \begin{bmatrix} [M_S]_{n\times n} & [0]_{n\times 1} & [0]_{n\times 1} \\ [0]_{1\times n} & m_B & 0 \\ [0]_{1\times n} & 0 & m_D \end{bmatrix}_{(n+2)\times(n+2)} \quad \text{(A2.4.a)}$$

$$[K]_{(n+2)\times(n+2)} = \begin{bmatrix} [K_S]_{n\times n} & [0]_{n\times 1} & [0]_{n\times 1} \\ [0]_{1\times n} & k_{PS}+k_R & -k_{PS} \\ [0]_{1\times n} & -k_{PS} & k_{PS}+k_{NS} \end{bmatrix}_{(n+2)\times(n+2)} \quad \text{(A2.4.b)}$$

$$[C]_{(n+2)\times(n+2)} = \begin{bmatrix} [C_S]_{n\times n} & [0]_{n\times 1} & [0]_{n\times 1} \\ [0]_{1\times n} & c_{PS} & -c_{PS} \\ [0]_{1\times n} & -c_{PS} & c_{PS} \end{bmatrix}_{(n+2)\times(n+2)} \quad \text{(A2.4.c)}$$

$$[u_{(t)}]_{(n+2)\times 1} = \begin{bmatrix} [u_{S(t)}] \\ u_{B(t)} \\ u_{D(t)} \end{bmatrix}_{(n+2)\times 1} \quad \text{(A2.4.d)}$$

$$[\tau]_{(n+2)\times 1} = \begin{bmatrix} [M][1]_{n\times 1} \\ m_B \\ m_D \end{bmatrix}_{(n+2)\times 1} \quad \text{(A2.4.e)}$$

$$m_D = \mu_D m_{S,tot} = \mu_D \left(m_B + \sum_{i=1}^{n} m_i \right) \quad \text{(A2.4.f)}$$

where the parameters of KDamper entering Equations (A2.4) are selected according to the optimization procedure described in the respective section of Chapter 4.

A2.2.2 Extended KDamper

The main difference would be the change of the system configuration where the positive stiffness spring (k_{PS}) connects the damper mass (m_D) to the base of the system while the negative stiffness element (k_{NS}), is attached between the damper mass (m_D) and the mass of the oscillator (m). Also, an additional artificial damper is adopted and placed in parallel with the negative stiffness element so that we end up having two dampers, namely c_{NS} and c_{PS}. The extended KDamper (EKD) implemented in the bases on multi-story structures is presented in section 5.2.1.3 and 5.2.2.2 of Chapter 5. The equations of motion, Equation (A2.1), still hold, but now involve matrices with dimensions $(n+2) \times (n+2)$, which are defined as:

$$[M]_{(n+2)\times(n+2)} = \begin{bmatrix} [M_S]_{n\times n} & [0]_{n\times 1} & [0]_{n\times 1} \\ [0]_{1\times n} & m_B & 0 \\ [0]_{1\times n} & 0 & m_D \end{bmatrix}_{(n+2)\times(n+2)} \tag{A2.5.a}$$

$$[K]_{(n+2)\times(n+2)} = \begin{bmatrix} [K_S]_{n\times n} & [0]_{n\times 1} & [0]_{n\times 1} \\ [0]_{1\times n} & k_{NS}+k_R & -k_{NS} \\ [0]_{1\times n} & -k_{NS} & k_{NS}+k_{PS} \end{bmatrix}_{(n+2)\times(n+2)} \tag{A2.5.b}$$

$$[C]_{(n+2)\times(n+2)} = \begin{bmatrix} [C_S]_{n\times n} & [0]_{n\times 1} & [0]_{n\times 1} \\ [0]_{1\times n} & c_{PS} & -c_{PS} \\ [0]_{1\times n} & -c_{PS} & c_{PS}+c_{NS} \end{bmatrix}_{(n+2)\times(n+2)} \tag{A2.5.c}$$

$$[u_{(t)}]_{(n+2)\times 1} = \begin{bmatrix} [u_{S(t)}] \\ u_{B(t)} \\ u_{D(t)} \end{bmatrix}_{(n+2)\times 1} \tag{A2.5.d}$$

$$[\tau]_{(n+2)\times 1} = \begin{bmatrix} [M][1]_{n\times 1} \\ m_B \\ m_D \end{bmatrix}_{(n+2)\times 1} \tag{A2.5.e}$$

$$m_D = \mu_D m_{S,tot} = \mu_D \left(m_B + \sum_{i=1}^{n} m_i \right) \tag{A2.5.f}$$

where the parameters of EKD entering Equations (A2.5) are selected according to the optimization procedure described in the respective section of Chapter 5.

A2.2.3 Extended KDamper Equipped with Inerter

This proposed configuration combines the extended version of KDamper with an inerter (EKDI). The inerter connects the structure (or superstructure) mass with the base/foundation. The EKDI implemented in the bases on multi-story structures is presented in section 5.4.3 of Chapter 5. The equations of motion, Equation (A2.1), still hold, but now involve matrices with dimensions $(n+2) \times (n+2)$, which are defined as:

$$[M]_{(n+2)\times(n+2)} = \begin{bmatrix} [M_S]_{n\times n} & [0]_{n\times 1} & [0]_{n\times 1} \\ [0]_{1\times n} & m_B + m_b & 0 \\ [0]_{1\times n} & 0 & m_D \end{bmatrix}_{(n+2)\times(n+2)} \quad \text{(A2.6.a)}$$

$$[K]_{(n+2)\times(n+2)} = \begin{bmatrix} [K_S]_{n\times n} & [0]_{n\times 1} & [0]_{n\times 1} \\ [0]_{1\times n} & k_{NS} + k_R & -k_{NS} \\ [0]_{1\times n} & -k_{NS} & k_{NS} + k_{PS} \end{bmatrix}_{(n+2)\times(n+2)} \quad \text{(A2.6.b)}$$

$$[C]_{(n+2)\times(n+2)} = \begin{bmatrix} [C_S]_{n\times n} & [0]_{n\times 1} & [0]_{n\times 1} \\ [0]_{1\times n} & c_{PS} & -c_{PS} \\ [0]_{1\times n} & -c_{PS} & c_{PS} + c_{NS} \end{bmatrix}_{(n+2)\times(n+2)} \quad \text{(A2.6.c)}$$

$$[u_{(t)}]_{(n+2)\times 1} = \begin{bmatrix} [u_{S(t)}] \\ u_{B(t)} \\ u_{D(t)} \end{bmatrix}_{(n+2)\times 1} \quad \text{(A2.6.d)}$$

$$[\tau]_{(n+2)\times 1} = \begin{bmatrix} [M][1]_{n\times 1} \\ m_B \\ m_D \end{bmatrix}_{(n+2)\times 1} \quad \text{(A2.6.e)}$$

$$m_D = \mu_D m_{S,tot} = \mu_D \left(m_B + \sum_{i=1}^{n} m_i \right) \quad \text{(A2.6.f)}$$

where the parameters of EKDI entering Equations (A2.6) are selected according to the optimization procedure described in the respective section of Chapter 5. It must be noted that the inerter coefficient does not enter the matrix that corresponds to the seismic load.

A2.3 Retrofitting Options for the Implementation of Extended KDamper in Multi – Story Building Structures

A2.3.1 Distributed EKD Devices

In this section, the implementation of the EKD for the seismic protection of multi-story building structures is presented, by distributing it between each floor. The schematic representation of this configuration is presented in section 5.3.1. The equations of motion, Equation (A2.1) still hold, and assuming that an EKD device is placed in between the i-1th and ith floor, the matrices entering Equation (A2.1) are expressed as follows:

$$[M]_{(n+1)\times(n+1)} = \begin{bmatrix} m_1 & & & \cdots & & 0 \\ & \ddots & & & & \\ & & m_{i-1} & & & \\ \vdots & & & m_D & & \vdots \\ & & & & m_i & \\ & & & & & \ddots \\ 0 & & & \cdots & & m_n \end{bmatrix}_{(n+1)\times(n+1)} \tag{A2.7.a}$$

$$[K]_{(n+1)\times(n+1)} = \begin{bmatrix} k_1 & -k_1 & & & \cdots & & & 0 \\ -k_1 & k_1+k_2 & \ddots & & & & & \\ & & & k_{i-2}+k_{i-1}+k_R+k_{NS} & -k_{NS} & -k_R & & \\ \vdots & & & -k_{NS} & k_{NS}+k_{PS} & -k_{PS} & & \vdots \\ & & & -k_R & k_{PS} & k_{i-1}+k_i+k_R+k_{PS} & \ddots & \\ & & & & & & k_{n-1}+k_n & -k_n \\ 0 & & & & \cdots & & -k_n & k_n \end{bmatrix}_{(n+1)\times(n+1)} \tag{A2.7.b}$$

$$[C]_{(n+1)\times(n+1)} = \begin{bmatrix} c_{11} & c_{12} & & & \cdots & & & 0 \\ c_{21} & c_{22} & \ddots & & & & & \\ & & & c_{i-1,i-1}+c_{NS} & -c_{NS} & c_{i-1,i} & & \\ \vdots & & & -c_{NS} & c_{ii}+c_{NS}+c_{PS} & -c_{PS} & & \vdots \\ & & & c_{i,i-1} & -c_{PS} & c_{ii}+c_{PS} & \ddots & \\ & & & & & & c_{n-1,n-1} & c_{n-1,n} \\ 0 & & & & \cdots & & c_{n,n-1} & c_{n,n} \end{bmatrix}_{(n+1)\times(n+1)} \tag{A2.7.c}$$

$$[u_{(t)}]_{(n+1)\times 1} = \begin{bmatrix} u_{S1(t)} & \cdots & u_{Si-1(t)} & u_{D(t)} & u_{Si(t)} & \cdots & u_{Sn(t)} \end{bmatrix}^T_{(n+1)\times 1} \tag{A2.7.d}$$

The same procedure can be followed in the case of implementing multiple divices between any floor-combination.

A2.3.2 Implementation of EKD in the First Floor Exploiting Soil Structure Interaction (SSI) Effects

In this section, the EKD is implemented as a seismic protection measure between the foundations and the first floor of a typical residential structure (Ground / 'Pilotis' level). The proposed configuration is presented in section 5.3.2 of Chapter 5. The equation of motion, Equation (A2.1) still hold, having matrices with dimension $(n+1) \times (n+1)$, which are defined as follows:

$$[M]_{(n+1)\times(n+1)} = \begin{bmatrix} [M_S]_{n\times n} & [0]_{n\times 1} \\ [0]_{1\times n} & m_D \end{bmatrix} \tag{A2.8.a}$$

$$[K]_{(n+1)\times(n+1)} = \begin{bmatrix} [K_S]_{n\times n} & [0]_{n\times 1} \\ [0]_{1\times n} & [0]_{1\times 1} \end{bmatrix} + \begin{bmatrix} [0]_{(n-1)\times(n-1)} & [0]_{(n-1)\times 1} & [0]_{(n-1)\times 1} \\ [0]_{1\times(n-1)} & k_{NS}+k_R-k_n & -k_{NS} \\ [0]_{1\times(n-1)} & -k_{NS} & k_{PS}+k_{NS} \end{bmatrix} \tag{A2.8.b}$$

$$[C]_{(n+1)\times(n+1)} = \begin{bmatrix} [C_S]_{n\times n} & [0]_{n\times 1} \\ [0]_{1\times n} & [0]_{1\times 1} \end{bmatrix} + \begin{bmatrix} [0]_{(n-1)\times(n-1)} & [0]_{(n-1)\times 1} & [0]_{(n-1)\times 1} \\ [0]_{1\times(n-1)} & c_{NS} & -c_{NS} \\ [0]_{1\times(n-1)} & -c_{NS} & c_{NS}+c_{PS} \end{bmatrix} \tag{A2.8.c}$$

$$[u_{(t)}]_{(n+1)\times 1} = \begin{bmatrix} [u_{s(t)}]_{n\times 1} \\ u_{D(t)} \end{bmatrix}_{(n+1)\times 1} \tag{A2.8.d}$$

where in this case the stiffness element k_R incorporating the SSI effects is expressed as:

$$k_R = \frac{k_{SSI}k_n}{k_{SSI}+k_n} \tag{A2.9}$$

Further information regarding the specific formulation are presented in section 5.3.2.

Appendix **A3**

Formation of the Submatrices of the Controlled Wind Turbine Tower

A3.1 Traditional TMD Oscillator

The TMD concept implemented in WT tower consists of an additional mass(m_D), attached at the top of the wind turbine tower or inside the nacelle, as presented in Figure 7.1.b, using a positive stiffness element and a linear damper (k_D, c_D). Thus, the controlled system has (N+1) dynamic DoFs, where N indicates the number of prismatic beam elements selected to model the WT tower. The modified matrices that enter the equations of motion of the controlled system, including the TMD, are presented in Equations (7.3). The submatrices that relate to the TMD are expressed as follows:

$$\left[M_{n,a}\right]_{N\times N} = \left[0\right]_{N\times N} \tag{A3.1.a}$$

$$\left[M_{n,b}\right]_{N\times 1} = \left[0\right]_{N\times 1} \tag{A3.1.b}$$

$$\left[M_{n,c}\right]_{1\times N} = \left[0\right]_{1\times N} \tag{A3.1.c}$$

$$\left[M_{n,d}\right]_{1\times 1} = \left[+m_D\right]_{1\times 1} \tag{A3.1.d}$$

where $m_D=\mu_D\, m_{tot}$ is the additional mass of the TMD. The submatrices entering the control stiffness matrix, Equation (7.3.b), are expressed as:

$$\left[K_{n,a}\right]_{N\times N} = \begin{bmatrix} 0 & \cdots & 0 \\ \vdots & \ddots & \vdots \\ 0 & \cdots & +k_D \end{bmatrix}_{N\times N} \tag{A3.2.a}$$

$$\left[K_{n,b}\right]_{N\times 1} = \left[0 \quad \cdots \quad -k_D\right]^T_{1\times N} \tag{A3.2.b}$$

$$\left[K_{n,c}\right]_{1\times N} = \left[0 \quad \cdots \quad -k_D\right]_{1\times N} \tag{A3.2.c}$$

$$\left[K_{n,d}\right]_{1\times 1} = \left[+k_D\right]_{1\times 1} \tag{A3.2.d}$$

where k_D is the positive stiffness element, calculated using Equation (7.11.b) having defined the tuning frequency f_D. The submatrices entering the control damping matrix, Equation (7.3.c), are expressed as:

$$\left[C_{n,a}\right]_{N\times N} = \begin{bmatrix} 0 & \cdots & 0 \\ \vdots & \ddots & \vdots \\ 0 & \cdots & +c_D \end{bmatrix}_{N\times N} \tag{A3.3.a}$$

$$\left[C_{n,b}\right]_{N\times 1} = \left[0 \quad \cdots \quad -c_D\right]^T_{1\times N} \tag{A3.3.b}$$

$$\left[C_{n,c}\right]_{1\times N} = \left[0 \quad \cdots \quad -c_D\right]_{1\times N} \tag{A3.3.c}$$

$$\left[C_{n,d}\right]_{1\times 1} = \left[+c_D\right]_{1\times 1} \tag{A3.3.d}$$

where c_D results from Equation (7.11.c).

A3.2 Nacelle-Isolation Concept

In the nacelle-isolation concept, the nacelle is used as the additional mass of a TMD, as illustrated in Figure 7.1.c. Thus, the additional mass concentrated at the top of the tower is no longer connected rigidly to the steel tower, but is realized with a stiffness connection and a linear damper (k_D, c_D), as in the case of the classical TMD concept. The controlled system has (N+1) dynamic DoFs, and the modified matrices that enter the equations of motion of the controlled system (nacelle-isolation) are presented in Equations (7.3). The submatrices that relate to the proposed vibration absorption concept are expressed as follows:

$$\left[M_{n,a}\right]_{N\times N} = \begin{bmatrix} 0 & \cdots & 0 \\ \vdots & \ddots & \vdots \\ 0 & \cdots & -m_{top} \end{bmatrix}_{N\times N} \tag{A3.4.a}$$

$$\left[M_{n,b}\right]_{N\times 1} = \left[0\right]_{N\times 1} \tag{A3.4.b}$$

$$\left[M_{n,c}\right]_{1\times N} = \left[0\right]_{1\times N} \tag{A3.4.c}$$

$$\left[M_{n,d}\right]_{1\times 1} = \left[+m_{top}\right]_{1\times 1} \tag{A3.4.d}$$

where m_{tot} corresponds to the mechanical parts (nacelle, rotor and blades). The submatrices entering the control stiffness matrix, Equation (7.3.b), are expressed as:

$$\left[K_{n,a}\right]_{N\times N} = \begin{bmatrix} 0 & \cdots & 0 \\ \vdots & \ddots & \vdots \\ 0 & \cdots & +k_D \end{bmatrix}_{N\times N} \tag{A3.5.a}$$

$$\left[K_{n,b}\right]_{N\times 1} = \left[0 \quad \cdots \quad -k_D\right]^T_{1\times N} \tag{A3.5.b}$$

$$\left[K_{n,c}\right]_{1\times N} = \left[0 \quad \cdots \quad -k_D\right]_{1\times N} \tag{A3.5.c}$$

$$\left[K_{n,d}\right]_{1\times 1} = \left[+k_D\right]_{1\times 1} \tag{A3.5.d}$$

where k_D is the positive stiffness element, that connects the concentrated mass at the top, m_{top}, with the top of the WT tower, calculated using Equation (7.13.b) having defined the tuning frequency f_D. The submatrices entering the control damping matrix, Equation (7.3.c), are expressed as:

$$\left[C_{n,a}\right]_{N\times N} = \begin{bmatrix} 0 & \cdots & 0 \\ \vdots & \ddots & \vdots \\ 0 & \cdots & +c_D \end{bmatrix}_{N\times N} \tag{A3.6.a}$$

$$\left[C_{n,b}\right]_{Nx1} = \left[0 \quad \cdots \quad -c_D\right]^T_{1\times N} \tag{A3.6.b}$$

$$\left[C_{n,c}\right]_{1\times N} = \left[0 \quad \cdots \quad -c_D\right]_{1\times N} \tag{A3.6.c}$$

$$\left[C_{n,d}\right]_{1\times 1} = \left[+c_D\right]_{1\times 1} \tag{A3.6.d}$$

where c_D results from Equation (7.13.b).

A3.3 KDamper-Based Designs

In the proposed KDamper-based designs, the additional mass of the nacelle is not rigidly connected to the top of the WT tower, as in the case of the nacelle-isolation concept, but a KDamper-based device is intervened. When considering a KDamper (Figure 7.1.d), the additional oscillating mass is connected with the nacelle with a positive stiffness element and a linear damper (k_{PS}, c_{PS}), and with the steel tower with a negative stiffness (NS) element (k_{NS}), and the steel tower is connected with the nacelle with a stiffness connection (k_R). The controlled system has (N+2) dynamic DoFs, and the modified matrices that enter the equations of motion of the controlled system (KDamper concept) are presented in Equations (7.3). The submatrices that relate to the proposed vibration absorption concept are expressed as follows:

$$\left[M_{n,a}\right]_{N\times N}=\begin{bmatrix}0 & \cdots & 0\\ \vdots & \ddots & \vdots\\ 0 & \cdots & -m_{top}\end{bmatrix}_{N\times N} \tag{A3.7.a}$$

$$\left[M_{n,b}\right]_{N\times 2}=\left[0\right]_{N\times 2} \tag{A3.7.b}$$

$$\left[M_{n,c}\right]_{2\times N}=\left[0\right]_{2\times N} \tag{A3.7.c}$$

$$\left[M_{n,d}\right]_{2\times 2}=\begin{bmatrix}+m_D & 0\\ 0 & +m_{top}\end{bmatrix}_{2\times 2} \tag{A3.7.d}$$

where $m_D=\mu_D\, m_{tot}$ is the additional mass of the KDamper, and m_{tot} corresponds to the mechanical parts (nacelle, rotor and blades). The submatrices entering the control stiffness matrix, Equation (7.3.b), are expressed as:

$$\left[K_{n,a}\right]_{N\times N}=\begin{bmatrix}0 & \cdots & 0\\ \vdots & \ddots & \vdots\\ 0 & \cdots & +(k_R+k_{NS})\end{bmatrix}_{N\times N} \tag{A3.8.a}$$

$$\left[K_{n,b}\right]_{N\times 1}=\begin{bmatrix}0 & \cdots & -k_{NS}\\ 0 & \cdots & -k_R\end{bmatrix}^T_{2\times N} \tag{A3.8.b}$$

$$\left[K_{n,c}\right]_{N\times 2}=\begin{bmatrix}0 & \cdots & -k_{NS}\\ 0 & \cdots & -k_R\end{bmatrix}_{2\times N} \tag{A3.8.c}$$

$$\left[K_{n,d}\right]_{2\times2}=\begin{bmatrix}+\left(k_{PS}+k_{NS}\right) & -k_{PS}\\ -k_{PS} & k_R+k_{PS}\end{bmatrix}_{2\times2} \tag{A3.8.d}$$

where the stiffness elements k_{PS}, k_{NS}, and k_R result from the optimization procedure described in section 7.3.2 of Chapter 7. The submatrices entering the control damping matrix, Equation (7.3.c), are expressed as:

$$\left[C_{n,a}\right]_{N\times N}=\left[0\right]_{N\times N} \tag{A3.9.a}$$

$$\left[C_{n,b}\right]_{Nx2}=\left[0\right]^T_{2\times N} \tag{A3.9.b}$$

$$\left[C_{n,c}\right]_{2\times N}=\left[0\right]_{2\times N} \tag{A3.9.c}$$

$$\left[C_{n,d}\right]_{2\times2}=\begin{bmatrix}+c_{PS} & -c_{PS}\\ -c_{PS} & +c_{PS}\end{bmatrix}_{2\times2} \tag{A3.9.d}$$

and c_{PS} results from the optimization problem stated in section 7.3.2 of Chapter 7.

Regarding the extended version of KDamper (EKD), presented in Figure 7.1.e, the additional mass, m_D is connected with the nacelle with a NS element and an artificial damper (k_{NS}, c_{NS}), and with the steel tower with a positive stiffness element k_{PS}. Again, the controlled system has (N+2) dynamic DoFs, and the modified matrices that enter the equations of motion of the controlled system (EKD configuration) are presented in Equations (7.3). The submatrices that relate to the proposed vibration absorption concept are expressed as follows:

$$\left[M_{n,a}\right]_{N\times N}=\begin{bmatrix}0 & \cdots & 0\\ \vdots & \ddots & \vdots\\ 0 & \cdots & -m_{top}\end{bmatrix}_{N\times N} \tag{A3.10.a}$$

$$\left[M_{n,b}\right]_{N\times2}=\left[0\right]_{N\times2} \tag{A3.10.b}$$

$$\left[M_{n,c}\right]_{2\times N}=\left[0\right]_{2\times N} \tag{A3.10.c}$$

$$\left[M_{n,d}\right]_{2\times2}=\begin{bmatrix}+m_D & 0\\ 0 & +m_{top}\end{bmatrix}_{2\times2} \tag{A3.10.d}$$

where $m_D=\mu_D\, m_{tot}$ is the additional mass of the KDamper, and m_{tot} corresponds to the mechanical parts (nacelle, rotor and blades). The submatrices entering the control stiffness matrix, Equation (7.3.b), are expressed as:

$$\left[K_{n,a}\right]_{N\times N}=\begin{bmatrix}0 & \cdots & 0\\ \vdots & \ddots & \vdots\\ 0 & \cdots & +(k_R+k_{PS})\end{bmatrix}_{N\times N} \tag{A3.11.a}$$

$$\left[K_{n,b}\right]_{N\times 1}=\begin{bmatrix}0 & \cdots & -k_{PS}\\ 0 & \cdots & -k_R\end{bmatrix}^T_{2\times N} \tag{A3.11.b}$$

$$\left[K_{n,c}\right]_{N\times 2}=\begin{bmatrix}0 & \cdots & -k_{PS}\\ 0 & \cdots & -k_R\end{bmatrix}_{2\times N} \tag{A3.11.c}$$

$$\left[K_{n,d}\right]_{2\times 2}=\begin{bmatrix}+\left(k_{NS}+k_{PS}\right) & -k_{NS}\\ -k_{NS} & k_R+k_{NS}\end{bmatrix}_{2\times 2} \tag{A3.11.d}$$

where the stiffness elements k_{PS}, k_{NS}, and k_R result from the optimization procedure described in section 7.3.2 of Chapter 7. The submatrices entering the control damping matrix, Equation (7.3.c), are expressed as:

$$\left[C_{n,a}\right]_{N\times N}=\left[0\right]_{N\times N} \tag{A3.12.a}$$

$$\left[C_{n,b}\right]_{Nx2}=\left[0\right]^T_{2\times N} \tag{A3.12.b}$$

$$\left[C_{n,c}\right]_{2\times N}=\left[0\right]_{2\times N} \tag{A3.12.c}$$

$$\left[C_{n,d}\right]_{2\times 2}=\begin{bmatrix}+c_{NS} & -c_{NS}\\ -c_{NS} & +c_{NS}\end{bmatrix}_{2\times 2} \tag{A3.12.d}$$

and c_{NS} results from the optimization problem stated in section 7.3.2 of Chapter 7.

In the extended version of KDamper equipped with an inerter (EKDI), presented in Figure 7.1.f, an inerter coefficient connects the top of the tower directly with the nacelle, and thus is parallel to the stiffness element k_R. As in the case of the EKD, the controlled system has (N+2) dynamic DoFs, and the modified matrices that enter the equations of motion of the controlled system (EKDI configuration) are presented in Equations (7.3). Since the only difference with the EKD concept is the addition of the inerter, only the submatrices that concern the mass matrix [M] will be presented:

$$\left[M_{n,a}\right]_{N\times N}=\begin{bmatrix}0 & \cdots & 0\\ \vdots & \ddots & \vdots\\ 0 & \cdots & -m_{top}+m_b\end{bmatrix}_{N\times N} \tag{A3.13.a}$$

$$\left[M_{n,b}\right]_{N\times 2}=\left[0\right]_{N\times 2} \tag{A3.13.b}$$

$$\left[M_{n,c}\right]_{2\times N}=\left[0\right]_{2\times N} \tag{A3.13.c}$$

$$\left[M_{n,d}\right]_{2\times 2}=\begin{bmatrix}+m_D & -m_b\\ -m_b & +\left(m_{top}+m_b\right)\end{bmatrix}_{2\times 2} \tag{A3.13.d}$$

References

Acar MA and Yilmaz C (2013) Design of an adaptive-passive dynamic vibration absorber composed of a string-mass system equipped with negative stiffness tension adjusting mechanism. *Journal of Sound and Vibration* 332(2): 231–245. DOI: 10.1016/j.jsv.2012.09.007.

Anagnostopoulos SA and Spiliopoulos K V. (1992) An investigation of earthquake induced pounding between adjacent buildings. *Earthquake Engineering & Structural Dynamics* 21(4): 289–302. DOI: 10.1002/eqe.4290210402.

Anastasopoulos I, Gazetas G, Loli M, et al. (2010) Soil failure can be used for seismic protection of structures. *Bulletin of Earthquake Engineering* 8(2). Springer: 309–326. DOI: 10.1007/s10518-009-9145-2.

Anastasopoulos I, Gelagoti F, Kourkoulis R, et al. (2012) Simplified constitutive model for simulation of cyclic response of shallow foundations: Validation against laboratory tests. *Journal of Geotechnical and Geoenvironmental Engineering* 137(12). American Society of Civil Engineers (ASCE): 1154–1168. DOI: 10.1061/(ASCE)GT.1943-5606.0000534.

Ankireddi S and Yang HTY (1996) Simple ATMD control methodology for tall buildings subject to wind loads. *Journal of Structural Engineering* 122(1). ASCE - American Society of Civil Engineers: 83–91. DOI: 10.1061/(ASCE)0733-9445(1996)122:1(83).

Antoniadis I, Chronopoulos D, Spitas V, et al. (2015) Hyper-damping properties of a stiff and stable linear oscillator with a negative stiffness element. *Journal of Sound and Vibration*. DOI: 10.1016/j.jsv.2015.02.028.

Antoniadis I, Kapasakalis K and Sapountzakis E (2019) Advanced Negative Stiffness Absorbers for the Seismic Protection of Structures. In: *Proceedings of the International Conference on Key Enabling Technologies 2019 (KEYTECH2019)*, 2019. DOI: https://doi.org/10.1063/1.5123704.

Antoniadis IA, Kanarachos SA, Gryllias K, et al. (2018) KDamping: A stiffness based vibration absorption concept. *JVC/Journal of Vibration and Control* 24(3): 588–606. DOI: 10.1177/1077546316646514.

Antoniadis I, Kapasakalis K and Sapountzakis E (2019) Isolation or Damping? A Soil-dependent approach based on the KDamper concept. In: *Proceedings of the 2nd International Conference on Natural Hazards & Infrastructure (ICONHIC 2019)*, 2019.

Asai T, Araki Y, Kimura K, et al. (2017) Adjustable vertical vibration isolator with a variable ellipse curve mechanism. *Earthquake Engineering & Structural Dynamics* 46(8). John Wiley and Sons Ltd: 1345–1366. DOI: 10.1002/eqe.2859.

Attary N, Symans M and Nagarajaiah S (2017) Development of a rotation-based negative stiffness device for seismic protection of structures. *Journal of Vibration and Control* 23(5). SAGE Publications Inc.: 853–867. DOI: 10.1177/1077546315585435.

Auad GA and Almazán JL (2017) Non linear vertical-rocking isolation system: Application to legged wine storage tanks. *Engineering Structures* 152. Elsevier Ltd: 790–803. DOI: 10.1016/j.engstruct.2017.09.061.

Avila S, Shzu M, Morais M, et al. (2016) Numerical Modeling of the Dynamic Behavior of a Wind Turbine Tower. *Advances in Vibration Engineering* 4.

Baravelli E and Ruzzene M (2013) Internally resonating lattices for bandgap generation and low-frequency vibration control. *Journal of Sound and Vibration* 332(25). Academic Press: 6562–6579. DOI: 10.1016/j.jsv.2013.08.014.

Bollano P, Kapasakalis K, Sapountzakis E, et al. (2019) Design and Optimization of the KDamper Concept for Seismic Protection of Bridges. In: *Proceedings of the 14th International Conference on Vibration Problems (ICOVP 2019)*, 2019.

Brzeski P, Kapitaniak T and Perlikowski P (2015) Novel type of tuned mass damper with inerter which enables changes of inertance. *Journal of Sound and Vibration* 349. Academic Press: 56–66. DOI: 10.1016/j.jsv.2015.03.035.

Cacciola P and D'Amico L (2015) Response-Spectrum-Compatible Ground Motion Processes. In: *Encyclopedia of Earthquake Engineering*, pp. 1–27. DOI: 10.1007/978-3-642-36197-5_325-1.

Carrella A, Brennan MJ and Waters TP (2007) Static analysis of a passive vibration isolator with quasi-zero-stiffness characteristic. *Journal of Sound and Vibration* 301(3–5): 678–689. DOI: 10.1016/j.jsv.2006.10.011.

Casciati F and Giuliano F (2009) Performance of Multi-TMD in the Towers of Suspension Bridges. *Journal of Vibration and Control* 15(6). SAGE PublicationsSage UK: London, England: 821–847. DOI: 10.1177/1077546308091455.

Casciati F, Rodellar J and Yildirim U (2012) Active and semi-active control of structures – theory and applications: A review of recent advances. *Journal of Intelligent Material Systems and Structures* 23(11). SAGE PublicationsSage UK: London, England: 1181–1195. DOI: 10.1177/1045389X12445029.

Chen J-L and Georgakis CT (2015) Spherical tuned liquid damper for vibration control in wind turbines. *Journal of Vibration and Control* 21(10). SAGE Publications Inc.: 1875–1885. DOI: 10.1177/1077546313495911.

Chen MZQ and Smith MC (2009) Restricted complexity network realizations for passive mechanical control. *IEEE Transactions on Automatic Control* 54(10): 2290–2301. DOI: 10.1109/TAC.2009.2028953.

Chen MZQ, Papageorgiou C, Scheibe F, et al. (2009) The missing mechanical circuit element. *IEEE Circuits and Systems Magazine* 9(1): 10–26. DOI: 10.1109/MCAS.2008.931738.

Chronopoulos D, Antoniadis I, Collet M, et al. (2015) Enhancement of wave damping within metamaterials having embedded negative stiffness inclusions. *Wave Motion* 58. Elsevier B.V.: 165–179. DOI: 10.1016/j.wavemoti.2015.05.005.

Chung LL, Wu LY, Huang HH, et al. (2009) Optimal design theories of tuned mass dampers with nonlinear viscous damping. *Earthquake Engineering and Engineering Vibration* 8(4). Institute of Engineering Mechanics (IEM): 547–560. DOI: 10.1007/s11803-009-9115-3.

Colwell S and Basu B (2009) Tuned liquid column dampers in offshore wind turbines for structural control. *Engineering Structures* 31(2): 358–368. DOI: 10.1016/j.engstruct.2008.09.001.

Correa DM, Klatt T, Cortes S, et al. (2015) Negative stiffness honeycombs for recoverable shock isolation. *Rapid Prototyping Journal* 21(2). Emerald Group Publishing Ltd.: 193–200. DOI: 10.1108/RPJ-12-2014-0182.

De Domenico D and Ricciardi G (2018a) An enhanced base isolation system equipped with optimal tuned mass damper inerter (TMDI). *Earthquake Engineering and Structural Dynamics*. DOI: 10.1002/eqe.3011.

De Domenico D and Ricciardi G (2018b) An enhanced base isolation system equipped with optimal tuned mass damper inerter (TMDI). *Earthquake Engineering & Structural Dynamics* 47(5): 1169–1192. DOI: 10.1002/eqe.3011.

De Angelis M, Giaralis A, Petrini F, et al. (2019) Optimal tuning and assessment of inertial dampers with grounded inerter for vibration control of seismically excited base-isolated systems. *Engineering Structures* 196. Elsevier Ltd: 109250. DOI: 10.1016/j.engstruct.2019.05.091.

De Domenico D, Impollonia N and Ricciardi G (2018) Soil-dependent optimum design of a new passive vibration control system combining seismic base isolation with tuned inerter damper. *Soil Dynamics and Earthquake Engineering*. DOI: 10.1016/j.soildyn.2017.11.023.

Debnath N, Deb SK and Dutta A (2016) Multi-modal vibration control of truss bridges with tuned mass dampers under general loading. *JVC/Journal of Vibration and Control* 22(20): 4121–4140. DOI: 10.1177/1077546315571172.

Den Hartog JP (1956) *Mechanical Vibrations*. *McGraw-Hill, New York*. 4th ed. New York. DOI: 10.1038/161503c0.

DeSalvo R (2007) Passive, Nonlinear, Mechanical Structures for Seismic Attenuation. *Journal of Computational and Nonlinear Dynamics* 2(4): 290. DOI: 10.1115/1.2754305.

Dong L and Lakes R (2013) Advanced damper with high stiffness and high hysteresis damping based on negative structural stiffness. *International Journal of Solids and Structures* 50(14–15). Pergamon: 2416–2423. DOI: 10.1016/j.ijsolstr.2013.03.018.

Dyskin A V. and Pasternak E (2012) Mechanical effect of rotating non-spherical particles on failure in compression. In: *Philosophical Magazine*, 1 October 2012, pp. 3451–3473. Taylor & Francis Group . DOI: 10.1080/14786435.2012.704421.

Elastomeric isolators - Fip Industriale (n.d.). Available at: https://www.fipindustriale.it/index.php?area=106&menu=67&lingua=1 (accessed 22 January 2020).

EN 1991-1-4: Eurocode 1: Actions on structures - Part 1-4: General actions - Wind actions (2010).

EN 1998-1: Eurocode 8: Design of structures for earthquake resistance – Part 1: General rules, seismic actions and rules for buildings (2004).

Farag MMN, Mehanny SSF and Bakhoum MM (2015) Establishing optimal gap size for precast beam bridges with a buffer-gap-elastomeric bearings system. *Earthquake and Structures* 9(1): 195–219. DOI: 10.12989/eas.2015.9.1.195.

FEM, BIM and CAD Software for Structural Engineers | SOFiSTiK AG (n.d.). Available at: https://www.sofistik.com/?__hstc=136929903.778d8a8e3515c0a0f7da049d7f27258a.1587748377743.1587748377743.1587748377743.1&__hssc=136929903.2.1587748377744&__hsfp=4014916924 (accessed 24 April 2020).

Fluid Viscous Dampers | Seismic Dampers | ITT Infrastructure | ITT Enidine (n.d.). Available at: https://www.itt-infrastructure.com/en-US/Products/Viscous-Dampers/ (accessed 22 January 2020).

Frahm H (1911) Device for damping of bodies. *U.S. Patent*. US patent #989958.

Furukawa S, Sato E, Shi Y, et al. (2013) Full-scale shaking table test of a base-isolated medical facility subjected to vertical motions. *Earthquake Engineering & Structural Dynamics* 42(13). John Wiley and Sons Ltd: 1931–1949. DOI: 10.1002/eqe.2305.

Gajan S, Kutter BL, Phalen JD, et al. (2005) Centrifuge modeling of load-deformation behavior of rocking shallow foundations. *Soil Dynamics and Earthquake Engineering* 25(7–10): 773–783. DOI: 10.1016/j.soildyn.2004.11.019.

Gang W, Kehai W, Panpan Z, et al. (2018) Effect of mechanical degradation of laminated elastomeric bearings and shear keys upon seismic behaviors of small-to-medium-span highway bridges in transverse direction. *Earthquake Engineering and Engineering Vibration* 17(1). Institute of Engineering Mechanics (IEM): 205–220. DOI: 10.1007/s11803-018-0435-z.

Geem ZW (2008) Novel derivative of harmony search algorithm for discrete design variables. *Applied Mathematics and Computation* 199(1): 223–230. DOI: 10.1016/j.amc.2007.09.049.

Geem ZW, Kim JH and Loganathan G V. (2002) Harmony search optimization: Application to pipe network design. *International Journal of Modelling and Simulation* 22(2). Int. Assoc. of Science and Technology for Development: 125–133. DOI: 10.1080/02286203.2002.11442233.

Gerolymos N GG (2005) Nonlinear Lateral Response of Caisson Foundations. In: *1st Greece-Japan Workshop on Seismic Design, Observation, Retrofit of Foundations,Athens, Greece*, 2005, p. 125.

Giaralis A and Spanos PD (2012) Derivation of response spectrum compatible non-stationary stochastic processes relying on Monte Carlo-based peak factor estimation. *Earthquake and Structures* 3(3–4): 581–609. DOI: doi: 10.12989/EAS.2012.3.3_4.581.

Giaralis A and Taflanidis AA (2018) Optimal tuned mass-damper-inerter (TMDI) design for seismically excited MDOF structures with model uncertainties based on reliability criteria. *Structural Control and Health Monitoring*. DOI: 10.1002/stc.2082.

Goldberg DE and Holland JH (1988) Genetic Algorithms and Machine Learning. *Machine Learning*. DOI: 10.1023/A:1022602019183.

Han B and Li C (2006) Seismic response of controlled structures with active multiple tuned mass dampers. *Earthquake Engineering and Engineering Vibration* 5(2): 205–213. DOI: 10.1007/s11803-006-0657-3.

Hansen MOL (2008) *Aerodynamics of Wind Turbines*. Earthscan.

Hashimoto T, Fujita K, Tsuji M, et al. (2015) Innovative base-isolated building with large mass-ratio TMD at basement for greater earthquake resilience. *Future Cities and Environment*. DOI: 10.1186/s40984-015-0007-6.

Haskett T, Breukelman B, Robinson J, et al. (2004) Tuned mass dampers under excessive structural excitation. *Report of the Motioneering Inc*. Available at: http://www.waterfordmgmt.com/school/Articles/tmd article.pdf.

Holland JH (1975) *Adaptation in Natural and Artificial Systems : An Introductory Analysis with Applications to Biology, Control, and Artificial Intelligence*. *Ann Arbor University of Michigan Press 1975*. University of Michigan Press. Available at: http://mitpress.mit.edu/catalog/item/default.asp?ttype=2&tid=8929 (accessed 2 April 2020).

Ibrahim RA (2008) Recent advances in nonlinear passive vibration isolators. *Journal of Sound and Vibration* 314(3–5): 371–452. DOI: 10.1016/j.jsv.2008.01.014.

Iemura H and Pradono MH (2009) Advances in the development of pseudo-negative-stiffness dampers for seismic response control. *Structural Control and Health Monitoring* 16(7–8): 784–799. DOI: 10.1002/stc.345.

Jaglinski T, Kochmann D, Stone D, et al. (2007) Composite materials with viscoelastic stiffness greater than diamond. *Science* 315(5812): 620–622. DOI: 10.1126/science.1135837.

Jonkman JM (2007) *Dynamics Modeling and Loads Analysis of an Offshore Floating Wind Turbine. Technical Report No. NREL/TP-500-41958*. Available at: http://www.osti.gov/bridge (accessed 22 April 2020).

Kapasakalis K, Sapountzakis E and Antoniadis I (2017) Implementation of the KDamper Concept to Wind Turbine Towers. In: *Proceedings of the 6th International Conference on Computational Methods in Structural Dynamics and Earthquake Engineering*

(COMPDYN 2017), 2017.

Kapasakalis K, Sapountzakis E and Antoniadis I (2018a) Kdamper concept in seismic isolation of building structures with soil structure interaction. In: *Proceedings of the 13th International Conference on Computational Structures Technology (CST2018)*, 2018.

Kapasakalis K, Sapountzakis E and Antoniadis I (2018b) KDamper Concept in Seismic Isolation of Multi Storey Building Structures. In: *Proceedings of the 9th GRACM International Congress on Computational Mechanics (9GRACM 2018)*, 2018.

Kapasakalis K, Sapountzakis E and Antoniadis I (2018c) Optimal Design of the KDamper Concept for Structures on Compliant Supports. In: *Proceedings of the 16th European Conference on Earthquake Engineering (16ECEE 2018)*, 2018.

Kapasakalis K, Antoniadis I and Sapountzakis E (2019a) Control of Multi Storey Building Structures with a New Passive Vibration Control System Com-bining Base Isolation with KDamper. In: *Proceedings of the 7th International Conference on Computational Methods in Structural Dynamics and Earthquake Engineering (COMPDYN 2019)*, 2019.

Kapasakalis K, Alamir C, Antoniadis I, et al. (2019) Frequency Base Design of the KDamper Concept for Seismic Isolation of Bridges. In: *Proceedings of the 14th International Conference on Vibration Problems (ICOVP 2019)*, 2019.

Kapasakalis K, Antoniadis I and Sapountzakis E (2019b) Implementation of the KDamper Concept for Base Isolation to a Typical Concrete Building Structure. In: *Proceedings of the 12th International Congress on Mechanics (12HSTAM2019)*, 2019.

Kapasakalis K, Antoniadis I and Sapountzaki A (2019) Implementation of the KDamper Concept for Seismic Protection of Bridges. In: *Proceedings of the 14th International Conference on Vibration Problems (ICOVP 2019)*, 2019.

Kapasakalis K, Antoniadis I and Sapountzakis E (2019c) KDamper Concept for Base Isolation and Damping of High-Rise Building Structures. In: *Proceedings of the 14th International Conference on Vibration Problems (ICOVP 2019)*, 2019.

Kapasakalis K, Antoniadis I and Sapountzakis E (2019d) Novel Vibration Absorption Systems with Negative Stiffness Elements for the Seismic Protection of Structures. In: *4th National Conference on Earthquake Engineering and Engineering Seismology (Hellenic Association for Earthquake Engineering - HAEE / ETAM)*, 2019.

Kapasakalis K, Antoniadis I and Sapountzakis E (2019e) Performance Assessment of the KDamper as a Seismic Absorption Base. *Structural Control and Health Monitoring*. DOI: 10.1002/stc.2482.

Kelly JM (1999) The role of damping in seismic isolation. *Earthquake Engineering and Structural Dynamics* 28(1): 3–20.

Koulatsou K, Petrini F, Vernardos S, et al. (2013) *Artificial Time Histories of Wind ActionsFor Structural Analysis of Wind Turbines*. *BCCCE*.

Lackner MA and Rotea MA (2011) Passive structural control of offshore wind turbines. *Wind Energy* 14(3). John Wiley & Sons, Ltd: 373–388. DOI: 10.1002/we.426.

Lakes R, Rosakis P and Ruina A (1993) Microbuckling instability in elastomeric cellular solids. *Journal of Materials Science* 28(17). Kluwer Academic Publishers: 4667–4672. DOI: 10.1007/BF00414256.

Lakes RS (2001) Extreme damping in composite materials with a negative stiffness phase. *Physical Review Letters* 86(13): 2897–2900. DOI: 10.1103/PhysRevLett.86.2897.

Lazar IF, Neild SA and Wagg DJ (2014) Using an inerter-based device for structural vibration suppression. *Earthquake Engineering and Structural Dynamics*. DOI: 10.1002/eqe.2390.

Le TD and Ahn KK (2011) A vibration isolation system in low frequency excitation region using negative stiffness structure for vehicle seat. *Journal of Sound and Vibration* 330(26). Academic Press: 6311–6335. DOI: 10.1016/j.jsv.2011.07.039.

Le TD and Ahn KK (2013) Experimental investigation of a vibration isolation system using negative stiffness structure. *International Journal of Mechanical Sciences* 70. Pergamon: 99–112. DOI: 10.1016/j.ijmecsci.2013.02.009.

Lee CM and Goverdovskiy VN (2012) A multi-stage high-speed railroad vibration isolation system with 'negative' stiffness. *Journal of Sound and Vibration* 331(4). Academic Press: 914–921. DOI: 10.1016/j.jsv.2011.09.014.

Lee CM, Goverdovskiy VN and Temnikov AI (2007) Design of springs with 'negative' stiffness to improve vehicle driver vibration isolation. *Journal of Sound and Vibration* 302(4–5). Academic Press: 865–874. DOI: 10.1016/j.jsv.2006.12.024.

Lee KS and Geem ZW (2004) A new structural optimization method based on the harmony search algorithm. *Computers and Structures* 82(9–10). Pergamon: 781–798. DOI: 10.1016/j.compstruc.2004.01.002.

Lee KS and Geem ZW (2005) A new meta-heuristic algorithm for continuous engineering optimization: Harmony search theory and practice. *Computer Methods in Applied Mechanics and Engineering* 194(36–38): 3902–3933. DOI: 10.1016/j.cma.2004.09.007.

Lee KS, Geem ZW, Lee SHO, et al. (2005) The harmony search heuristic algorithm for discrete structural optimization. *Engineering Optimization* 37(7): 663–684. DOI: 10.1080/03052150500211895.

Li H, Li Y and Li J (2020) Negative stiffness devices for vibration isolation applications: A review. *Advances in Structural Engineering*. SAGE Publications Inc.: 136943321990031. DOI: 10.1177/1369433219900311.

Li Y (2018) Research and Development of the Wind Turbine Reliability. *International Journal of Mechanical Engineering and Applications* 6(2). Science Publishing Group: 35. DOI: 10.11648/j.ijmea.20180602.14.

Liao GJ, Gong XL, Kang CJ, et al. (2011) The design of an active–adaptive tuned vibration absorber based on magnetorheological elastomer and its vibration attenuation performance. *Smart Materials and Structures* 20(7). IOP Publishing: 075015. DOI: 10.1088/0964-1726/20/7/075015.

Loli M, Knappett JA, Brown MJ, et al. (2014) Centrifuge modeling of rocking-isolated inelastic

RC bridge piers. *Earthquake Engineering and Structural Dynamics* 43(15). John Wiley and Sons Ltd: 2341–2359. DOI: 10.1002/eqe.2451.

Lu LY, Chen PR and Pong KW (2016) Theory and experiment of an inertia-type vertical isolation system for seismic protection of equipment. *Journal of Sound and Vibration* 366. Academic Press: 44–61. DOI: 10.1016/j.jsv.2015.12.009.

Luft RW (1979) Optimal Tuned Mass Dampers for Buildings. *Journal of the Structural Division* 105(12). ASCE: 2766–2772. Available at: https://cedb.asce.org/CEDBsearch/record.jsp?dockey=0005281 (accessed 10 May 2019).

M DP (1998) Digital Simulation of Wind Field Velocity. *Journal of Winf Engineering and Industrial Aerodynamics* (74–76): 91–109.

Mayet J and Ulbrich H (2015) First-order optimal linear and nonlinear detuning of centrifugal pendulum vibration absorbers. *Journal of Sound and Vibration* 335. Academic Press: 34–54. DOI: 10.1016/j.jsv.2014.09.017.

McNamara RJ (1977) Tuned Mass Dampers for Buildings. *Journal of the Structural Division* 103(9). ASCE: 1785–1798.

Michelis P and Spitas V (2010) Numerical and experimental analysis of a triangular auxetic core made of CFR-PEEK using the Directionally Reinforced Integrated Single-yarn (DIRIS) architecture. *Composites Science and Technology* 70(7): 1064–1071. DOI: 10.1016/j.compscitech.2010.01.013.

Molyneaux W (1957) *Supports for Vibration Isolation*. G. Britain: ARC/CP-322, Aer Res Council.

Mone C, Hand M, Bolinger M, et al. (2015) *2015 Cost of Wind Energy Review*. Available at: www.nrel.gov/publications. (accessed 22 April 2020).

Morais M, Barcelos M, Avila S, et al. (n.d.) Dynamic behavior analysis of Wind Turbine towers.

MORISHITA M, INOUE K and FUJITA T (2004) DEVELOPMENT OF THREE-DIMENSIONAL SEISMIC ISOLATION SYSTEMS FOR FAST REACTOR APPLICATION. *Journal of JAEE* 4(3). Japan Association for Earthquake Engineering: 305–310. DOI: 10.5610/jaee.4.3_305.

Naeim F and Kelly JM (1999) *Design of Seismic Isolated Structures : From Theory to Practice*. John Wiley. Available at: https://www.wiley.com/en-us/Design+of+Seismic+Isolated+Structures%3A+From+Theory+to+Practice-p-9780471149217 (accessed 12 May 2019).

Nagarajaiah S, Pasala DTR, Reinhorn A, et al. (2013) Adaptive Negative Stiffness: A New Structural Modification Approach for Seismic Protection. *Advanced Materials Research* 639–640: 54–66. DOI: 10.4028/www.scientific.net/amr.639-640.54.

Nigdeli SM and Bekdaş G (2017) Optimum tuned mass damper design in frequency domain for structures. *KSCE Journal of Civil Engineering* 21(3). Springer Verlag: 912–922. DOI: 10.1007/s12205-016-0829-2.

Nigdeli SM, Bekdaş G and Alhan C (2014) Optimization of seismic isolation systems via harmony search. *Engineering Optimization* 46(11). Taylor and Francis Ltd.: 1553–1569. DOI: 10.1080/0305215X.2013.854352.

Norske Veritas (Organization) and Forskningscenter Risø. (2002) *Guidelines for Design of Wind Turbines.* 2nd ed. Copenhagen ;[Roskilde Denmark]: Det Norske Veritas.

Paolucci R, Shirato M and Yilmaz MT (2008) Seismic behaviour of shallow foundations: Shaking table experimentsvs numerical modelling. *Earthquake Engineering & Structural Dynamics* 37(4). John Wiley and Sons Ltd: 577–595. DOI: 10.1002/eqe.773.

Pasala DTR, Sarlis AA, Nagarajaiah S, et al. (2013) Adaptive Negative Stiffness: New Structural Modification Approach for Seismic Protection. *Journal of Structural Engineering* 139(7): 1112–1123. DOI: 10.1061/(ASCE)ST.1943-541X.0000615.

PEER Ground Motion Database - PEER Center (n.d.). Available at: https://ngawest2.berkeley.edu/ (accessed 20 March 2020).

Peng T, Yu X, Wang Z, et al. (2012) Study of the seismic performance of expansion double spherical seismic isolation bearings for continuous girder bridges. *Journal of Earthquake Engineering and Engineering Vibration* 11(2): 163–172. DOI: 10.1007/s11803-012-0107-3.

Pietrosanti D, De Angelis M and Basili M (2017) Optimal design and performance evaluation of systems with Tuned Mass Damper Inerter (TMDI). *Earthquake Engineering & Structural Dynamics* 46(8). John Wiley and Sons Ltd: 1367–1388. DOI: 10.1002/eqe.2861.

Platus DL and L.Platus D (1992) Negative-stiffness-mechanism vibration isolation systems. In: *Proc. of SPIE*, 1992, pp. 44–54. Available at: papers2://publication/uuid/CE69D582-256D-427E-AA2A-EFD72BBF5C9E.

Qin L, Yan W and Li Y (2009) Design of frictional pendulum TMD and its wind control effectiveness. *Journal of Earthquake Engineering and Engineering Vibration* 29(5): 153–157.

Quilligan A, O'Connor A and Pakrashi V (2012) Fragility analysis of steel and concrete wind turbine towers. *Engineering Structures* 36: 270–282. DOI: 10.1016/j.engstruct.2011.12.013.

Radu A, Lazar IF and Neild SA (2019) Performance-based seismic design of tuned inerter dampers. *Structural Control and Health Monitoring* 26(5). John Wiley and Sons Ltd: e2346. DOI: 10.1002/stc.2346.

Rafieipour MH, Ghorbani-Tanha AK, Rahimian M, et al. (2014) A novel semi-active TMD with folding variable stiffness spring. *Earthquake Engineering and Engineering Vibration* 13(3). Institute of Engineering Mechanics (IEM): 509–518. DOI: 10.1007/s11803-014-0258-5.

Ramezani M, Bathaei A and Ghorbani-Tanha AK (2018) Application of artificial neural networks in optimal tuning of tuned mass dampers implemented in high-rise buildings subjected to wind load. *Earthquake Engineering and Engineering Vibration* 17(4).

Institute of Engineering Mechanics (IEM): 903–915. DOI: 10.1007/s11803-018-0483-4.

Renewable Energy Agency I (2012) *RENEWABLE ENERGY TECHNOLOGIES: COST ANALYSIS SERIES Volume 1: Power Sector Acknowledgement*. Available at: www.irena.org/Publications (accessed 22 April 2020).

Ricciardelli F, Pizzimenti AD and Mattei M (2003) Passive and active mass damper control of the response of tall buildings to wind gustiness. *Engineering Structures* 25(9). Elsevier BV: 1199–1209. DOI: 10.1016/S0141-0296(03)00068-3.

Robertson WS, Kidner MRF, Cazzolato BS, et al. (2009) Theoretical design parameters for a quasi-zero stiffness magnetic spring for vibration isolation. *Journal of Sound and Vibration* 326(1–2): 88–103. DOI: 10.1016/j.jsv.2009.04.015.

Saka MP (2009) Optimum design of steel sway frames to BS5950 using harmony search algorithm. *Journal of Constructional Steel Research* 65(1): 36–43. DOI: 10.1016/j.jcsr.2008.02.005.

Saka MP and Erdal F (2009) Harmony search based algorithm for the optimum design of grillage systems to LRFD-AISC. *Structural and Multidisciplinary Optimization* 38(1): 25–41. DOI: 10.1007/s00158-008-0263-2.

Sapountzakis E, Kapasakalis K and Antoniadis I (2019) Negative Stiffness Elements in Seismic Isolation of Bridges. In: *Proceedings of the 2nd International Conference on Natural Hazards & Infrastructure (ICONHIC 2019)*, 2019.

Saravanos DA, Chortis DI, Varelis DS, et al. (2013) Linearized Frequencies and Damping in Composite Laminated Beams Subject to Buckling. *Article in Journal of Vibration and Acoustics*. DOI: 10.1115/1.4023051.

Sarlis AA, Pasala DTR, Constantinou MC, et al. (2012) Negative Stiffness Device for Seismic Protection of Structures. In: *Journal of Structural Engineering*. Corfu,Greece, pp. 1124–1133. DOI: 10.1061/(asce)st.1943-541x.0000616.

Seismic Response Analysis of an Isolated Structure with QZS under Near-Fault Vertical Earthquakes (n.d.). Available at: https://www.hindawi.com/journals/sv/2018/9149721/ (accessed 13 April 2020).

Seismosoft [2018] (2018) SeismoArtif - A computer program for generating artificial earthquake accelerograms matched to a specific target response spectrum. Available at: http://www.seismosoft.com.

Shen Y, Peng H, Li X, et al. (2017) Analytically optimal parameters of dynamic vibration absorber with negative stiffness. *Mechanical Systems and Signal Processing*. DOI: 10.1016/j.ymssp.2016.08.018.

Smith Malcolm C. (2002) Synthesis of mechanical networks: The inerter. *IEEE Transactions on Automatic Control*. DOI: 10.1109/TAC.2002.803532.

Smith Malcolm C (2002) Synthesis of Mechanical Networks: The Inerter. *IEEE TRANSACTIONS ON AUTOMATIC CONTROL* 47(10). DOI: 10.1109/TAC.2002.803532.

Soong TT and Dargush GF (1997) *Passive Energy Dissipation Systems in Structural Engineering*. Wiley.

Spitas V, Spitas C and Michelis P (2013) Modeling of the elastic damping response of a carbon nanotube-polymer nanocomposite in the stress-strain domain using an elastic energy release approach based on stick-slip. *Mechanics of Advanced Materials and Structures* 20(10): 791–800. DOI: 10.1080/15376494.2012.677100.

Stewart G and Lackner M (2014) The impact of passive tuned mass dampers and wind–wave misalignment on offshore wind turbine loads. *Engineering Structures* 73.

Sun H, Zuo L, Wang X, et al. (2019) Exact H_2 optimal solutions to inerter-based isolation systems for building structures. *Structural Control and Health Monitoring* 26(6). John Wiley and Sons Ltd: e2357. DOI: 10.1002/stc.2357.

Sun T, Lai Z, Nagarajaiah S, et al. (2017) Negative stiffness device for seismic protection of smart base isolated benchmark building. *Structural Control and Health Monitoring*. DOI: 10.1002/stc.1968.

Sustainable Development Scenario – World Energy Model – Analysis - IEA (n.d.). Available at: https://www.iea.org/reports/world-energy-model/sustainable-development-scenario (accessed 24 April 2020).

Symans MD, Charney FA, Whittaker AS, et al. (2007) Energy Dissipation Systems for Seismic Applications: Current Practice and Recent Developments. *Journal of Structural Engineering* 134(1): 3–21. DOI: 10.1061/(asce)0733-9445(2008)134:1(3).

Takewaki I, Murakami S, Yoshitomi S, et al. (2012) Fundamental mechanism of earthquake response reduction in building structures with inertial dampers. *Structural Control and Health Monitoring* 19(6). John Wiley & Sons, Ltd: 590–608. DOI: 10.1002/stc.457.

Taniguchi T, Der Kiureghian A and Melkumyan M (2008) Effect of tuned mass damper on displacement demand of base-isolated structures. *Engineering Structures* 30(12): 3478–3488. DOI: 10.1016/j.engstruct.2008.05.027.

Tomizawa T, Takahashi O, Aida H, et al. (n.d.) *Vibration test in a Building named 'Chisuikan' using Three-dimensional Seismic Isolation System.*

Virgin LN, Santillan ST and Plaut RH (2008) Vibration isolation using extreme geometric nonlinearity. *Journal of Sound and Vibration* 315(3): 721–731. DOI: 10.1016/j.jsv.2007.12.025.

Virk K, Monti A, Trehard T, et al. (2013) SILICOMB PEEK Kirigami cellular structures: mechanical response and energy dissipation through zero and negative stiffness. *Smart Materials and Structures* 22(8). IOP Publishing: 084014. DOI: 10.1088/0964-1726/22/8/084014.

Vu B, Unal M, Warn GP, et al. (2014) A distributed flexibility and damping strategy to control vertical accelerations in base-isolated buildings. *Structural Control and Health Monitoring* 21(4). John Wiley and Sons Ltd: 503–521. DOI: 10.1002/stc.1580.

Wang C, Zhao J, Zhu L, et al. (2016) Effects of vertical excitation on the seismic performance

of a seismically isolated bridge with sliding friction bearings. *Earthquake Engineering and Engineering Vibration* 15(1). Institute of Engineering Mechanics (IEM): 187–196. DOI: 10.1007/s11803-016-0315-3.

Wang F-C and Wu S-Y (2016) Vibration control of an optical table employing mechatronic inerter networks. *Journal of Vibration and Control* 22(1). SAGE Publications Inc.: 224–234. DOI: 10.1177/1077546314528365.

Wang FC, Hsieh MR and Chen HJ (2012) Stability and performance analysis of a full-train system with inerters. *Vehicle System Dynamics* 50(4). Taylor & Francis : 545–571. DOI: 10.1080/00423114.2011.606368.

Wang M, Sun F fei, Yang J qi, et al. (2019) Seismic protection of SDOF systems with a negative stiffness amplifying damper. *Engineering Structures*. DOI: 10.1016/j.engstruct.2019.03.110.

Wang M, Sun F and Nagarajaiah S (2019) Simplified optimal design of MDOF structures with negative stiffness amplifying dampers based on effective damping. *The Structural Design of Tall and Special Buildings*. Wiley. DOI: 10.1002/tal.1664.

Wang X, Gao XZ and Ovaska SJ (2009) Fusion of clonal selection algorithm and harmony search method in optimisation of fuzzy classification systems. *International Journal of Bio-Inspired Computation* 1(1–2): 80–88. DOI: 10.1504/IJBIC.2009.022776.

Wang Z, Chen Z and Wang J (2012) Feasibility study of a large-scale tuned mass damper with eddy current damping mechanism. *Journal of Earthquake Engineering and Engineering Vibration* 11(3): 391–401. DOI: 10.1007/s11803-012-0129-x.

Warn GP and Vu B (2012) Exploring the Low Shape Factor Concept to Achieve Three-Dimensional Seismic Isolation. In: *20th Analysis and Computation Specialty Conference*, Reston, VA, 29 March 2012, pp. 1–11. American Society of Civil Engineers. DOI: 10.1061/9780784412374.001.

Weber B and Feltrin G (2010) Assessment of long-term behavior of tuned mass dampers by system identification. *Engineering Structures* 32(11): 3670–3682. DOI: 10.1016/j.engstruct.2010.08.011.

Weber F (2014) Optimal semi-active vibration absorber for harmonic excitation based on controlled semi-active damper. *Smart Materials and Structures* 23(9). IOP Publishing: 095033. DOI: 10.1088/0964-1726/23/9/095033.

Weber F, Boston C and Maślanka M (2011) An adaptive tuned mass damper based on the emulation of positive and negative stiffness with an MR damper. *Smart Materials and Structures* 20(1). IOP Publishing: 015012. DOI: 10.1088/0964-1726/20/1/015012.

Wind Power Capacity reaches 546 GW, 60 GW added in 2017 – World Wind Energy Association (n.d.). Available at: https://wwindea.org/blog/2018/02/12/2017-statistics/ (accessed 22 April 2020).

Winterflood J, Blair D. and Slagmolen B (2002) High performance vibration isolation using springs in Euler column buckling mode. *Physics Letters A* 300(2–3): 122–130. DOI: 10.1016/S0375-9601(02)00258-X.

Wojnar CS and Kochmann DM (2014) A negative-stiffness phase in elastic composites can produce stable extreme effective dynamic but not static stiffness. *Philosophical Magazine* 94(6). Taylor & Francis: 532–555. DOI: 10.1080/14786435.2013.857795.

Xiang P and Nishitani A (2014) Optimum design for more effective tuned mass damper system and its application to base-isolated buildings. *Structural Control and Health Monitoring* 21(1): 98–114. DOI: 10.1002/stc.1556.

Yang R, Zhou X and Liu X (2002) Seismic structural control using semi-active tuned mass dampers. *Earthquake Engineering and Engineering Vibration* 1(1). Institute of Engineering Mechanics (IEM): 111–118. DOI: 10.1007/s11803-002-0014-0.

Zheng Y, Zhang X, Luo Y, et al. (2016) Design and experiment of a high-static-low-dynamic stiffness isolator using a negative stiffness magnetic spring. *Journal of Sound and Vibration* 360. Academic Press: 31–52. DOI: 10.1016/j.jsv.2015.09.019.

Zhou J, Xu D and Bishop S (2015) A torsion quasi-zero stiffness vibration isolator. *Journal of Sound and Vibration* 338. Academic Press: 121–133. DOI: 10.1016/j.jsv.2014.10.027.

Zhou N and Liu K (2010) A tunable high-static-low-dynamic stiffness vibration isolator. *Journal of Sound and Vibration* 329(9). Academic Press: 1254–1273. DOI: 10.1016/j.jsv.2009.11.001.

Zhou Z, Wong J and Mahin S (2016) Potentiality of Using Vertical and Three-Dimensional Isolation Systems in Nuclear Structures. *Nuclear Engineering and Technology* 48(5). Korean Nuclear Society: 1237–1251. DOI: 10.1016/j.net.2016.03.005.

Zong Woo Geem, Joong Hoon Kim and Loganathan GV (2001a) A New Heuristic Optimization Algorithm: Harmony Search. *SIMULATION* 76(2): 60–68. DOI: 10.1177/003754970107600201.

Zong Woo Geem, Joong Hoon Kim and Loganathan GV (2001b) A New Heuristic Optimization Algorithm: Harmony Search. *SIMULATION* 76(2). Sage PublicationsSage CA: Thousand Oaks, CA: 60–68. DOI: 10.1177/003754970107600201.